PALACKY UNIVERSITY OLOMOUC

Faculty of Science

Department of Biochemistry

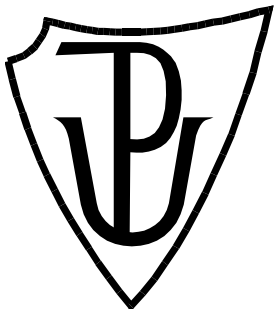

Enzymes linked to degradation pathway of cytokinins in maize

Ph.D. THESIS

Author:	**Mgr. RADKA KONČITÍKOVÁ**
Study programme:	P1416 Biochemistry
Studijní branch:	Biochemistry
Form of study:	Full-time
Supervisor:	**Mgr. David Kopečný, Ph.D.**
Year:	2015

I declare that the Ph.D. thesis is based on my own research carried out at the Department of Biochemistry, Faculty of Science, Palacky University, Olomouc in the period September 2010 – September 2015. Co-authors agree with the inclusion of published results. All sources cited in this work are listed in the “Reference“ section.

Olomouc ……. …….

Radka Končitíková

Acknowledgments

I am very grateful to **David Kopečný** for supervising my Ph.D. thesis and for his advices.

Special mention belongs to:

Marek Šebela (Department of Protein Biochemistry and Proteomics Centre of the Region Haná for Biotechnological and Agricultural Research, Faculty of Science, Palacký University in Olomouc) for his advices and help in fields of biochemistry and enzymology.

Martina Kopečná (Department of Protein Biochemistry and Proteomics Centre of the Region Haná for Biotechnological and Agricultural Research, Faculty of Science, Palacký University in Olomouc) for the help with cloning experiments.

Pierre Briozzo (INRA/AgroParisTech Versailles, France) for the insight to the fiels of protein crystallography.

Abstract

The presented Ph.D. thesis is focused on characterization of enzymes, which could be linked to degradation pathway of cytokinins in maize. Cytokinins are plant hormones, which play an important role in many developmental processes like regulation of cell proliferation and differentiation in root and shoot apical meristems, differentiation of plastids etc. Cytokinins negatively control root elongation and branching and the main naturally occurring cytokinins are N^6-prenylated adenine/adenosine derivatives, such as N^6-(Δ^2-isopentenyl)adenine (iP) and zeatin (Z) and their ribosides iPR and ZR. Cytokinin oxidase/dehydrogenase (CKO/CKX, EC 1.5.99.12) catalyzes irreversible degradation of above cytokinins to the corresponding adenine or adenosine and aldehyde.

The first aim of the work was to better understand substrate specificity differences among CKO isoforms and to search for more complex inhibitors. In consequence, new structures of CKO2 and CKO4a from maize as well as the binding mode of cytokinin ribosides were analyzed. New thidiazuron-derived inhibitors were tested and their binding was analyzed by X-ray crystallography. The importance of CKO glycosylation for the enzyme stability was studied using CKO1 from maize. The second aim of this work was to search for enzymes involved in possible interconversion of CKO reaction products. The search was focused on a superfamily of aldehyde dehydrogenases (ALDHs), which could metabolize the released aldehyde, and also on a family of nucleoside-N-ribohydrolases (NRH, EC 3.2.2.1), which could catalyze the interconversion of adenosine to adenine as well as the interconversion of cytokinin ribosides to bases.

Aldehydes are toxic, cancerogenic and mutagenic at higher concentrations and ALDHs are responsible for oxidation of biogenic aldehydes as well as for cell detoxification of aldehydes generated during lipid peroxidation. So far, 13 ALDH families have been described in plants. To get insight into their function, 10 maize genes covering three ALDH families (family 2, 7 and 10) were analyzed. Crystal structures of representatives of these three families were solved and their kinetics was characterized. It was found that ALDH2 family isoforms are able to oxidize aldehydes released from CKO reaction. NRHs catalyze a hydrolysis of nucleosides to nucleobase and ribose and the study was focused on purine nucleoside N-ribohydrolase, namely NRH3 from maize (ZmNRH3). Kinetic and structural study was performed and it was found that both adenosine and iPR/ZR can be metabolized to corresponding bases adenine and iP/Z.

Abstrakt

Předkládaná disertační práce je zaměřena na charakterizaci enzymů, které by mohly být spojeny s degradací cytokininů v kukuřici. Cytokininy jsou rostlinné hormony, které hrají důležitou roli v mnoha vývojových procesech, jako je regulace buněčného dělení a vývoje kořene a prýtu, diferenciace plastidů atd. Cytokininy často kooperují s dalšími rostlinými hormony, zejména auxiny. Přirozeně se vyskytující cytokininy jsou N^6-prenylované deriváty adeninu / adenosinu, jako N^6- (Δ^2-isopentenyl) adeninu (iP) a zeatin (Z) a jejich ribosidy iPR a ZR. Cytokininoxidasa / dehydrogenasa (CKO / CKX, EC 1.5.99.12) katalyzuje ireverzibilní degradaci cytokininů na adeninu nebo adenosinu a odpovídající aldehyd.

Prvním cílem práce bylo lépe popsat rozdíly v substrátové specificitě mezi jednotlivými isoformami CKO a najít účinnější inhibitory. V důsledku toho, byly analyzovány nové struktury CKO2 a CKO4a z kukuřice, stejně jako vazebný způsob cytokininových ribosidů. Byly testovány nové inhibitory odvozené od thidiazuronu a pomocí rentgenové krystalografie analyzována jejich vazba. Vliv glykosylace na stabilitu enzymu byl studován na CKO1 z kukuřice. Druhým cílem této práce bylo hledání enzymů podílejících se na možné interkonverzi reakčních produktů metabolismu cytokininů. Hledání bylo zaměřeno na nadrodinu aldehyddehydrogenas (ALDHs), které by mohly metabolizovat uvolněný aldehyd, a také na rodiny nukleosid-N-ribohydrolas (NRH, EC 3.2.2.1), které mohou katalyzovat vzájemnou přeměnu adenosinu na adenin, stejně jako interkonverzi cytokininových ribosidů na odpovídající báze.

Aldehydy jsou při vyšších koncentracích toxické, kancerogenní a mutagenní. ALDHs jsou zodpovědné za oxidaci biogenních aldehydů, podobně i za detoxifikaci aldehydů vznikajících při peroxidaci lipidů. Dosud bylo popsáno 13 ALDH rodin v rostlinách. Pro bližší pochopení jejich funkcí, bylo analyzováno 10 kukuřičný genů ze tří ALDH rodin (rodina 2, 7 a 10). Byly řešeny krystalové struktury zástupců těchto tří rodin, a také charakterizovány jejich kinetické vlastnosti. Bylo zjištěno, že izoenzymy z ALDH2 rodiny jsou schopny oxidovat aldehydy produkované CKO. NRHs katalyzují hydrolýzu nukleosidů na odpovídající báze a ribózu. Byly studovány purinové nukleosid N-ribohydrolasy, a to NRH3 z kukuřice (ZmNRH3). Na základě provedených kinetických a strukturální studií bylo zjištěno, že jak adenosin tak i iPR / ZR mohou být metabolizovány na odpovídající báze adenin a iP / Z.

Abbreviations

a	Enzymatic activity
Å	Angstrom
A	Absorbance
ABAL	4-aminobutyraldehyde
ALDH	aldehyde dehydrogenase
ALDH	gene encoding aldehyde dehydrogenase
AMADH	amino aldehyde dehydrogenase
APAL	3-aminopropionaldehyde
ASAL	L-aminoadipate-semialdehyde
BAL	betaine aldehyde
Benz-AL	benzaldehyde
C2-AL	acetaldehyde
C3-AL	propionaldehyde
C4-AL	butyraldehyde
C5-AL	valeraldehyde
C6-AL	capronaldehyde
C7-AL	heptanal
C8-AL	octanal
C9-AL	nonanal
Ck	Cytokinin
CKO	cytokinin oxidase/dehydrogenase
CPAL	3-cyanopropionaldehyde
CPPU	*N*-(2-chloro-4-pyridyl)-*N´*-phenyl urea
DAP	days after pollination
DCPIP	2,6-dichlorophenol indophenol
deamino-NAD^+	deamino nicotinamide adenine dinucleotide
DNA	Deoxyribonucleic acid
ε	Molar absorption coefficient
E.coli	Escherichia coli
E.C.	Enzyme commission number
Ef1α	Elongation factor 1-alpha
FAD	Flavin adenine dinucleotide
FMN	Flavin adenine mononucleotide
GABA	ɤ-aminobutyric acid
GBAL	4-guanidinobutyraldehyde
GPAL	3-guanidinopropionaldehyde
hCinn-AL	Hydrocinnamic aldehyde
iP	Isopentenyladenine
iP-AL	3-methyl-2-butenal
iPR	Isopentenyladenosine
iP9G	Isopentenyladenosine-N^9-glucoside
iPTG	Isopropyl-β-thiogalactopyranoside
isoC5-AL	isovaleraldehyde
k_{cat}	turnover number
K_m	Michaelis constant
L492A	mutation Leu492 to Ala of CKO1
mAnis-AL	m-Anisaldehyde
MALDI	Matrix-assisted laser desorption/ionozation
MASAL	adipic semialdehyde methylester
NAD^+	β-nicotinamide adenine dinucleotide
$NADP^+$	β-nicotinamide adenine dinucleotide phosphate
NRH	nucleoside N-ribohydrolase
NQ	1,4-Naphtoquinone
oAnis-AL	o-Anisaldehyde
PEG	polyethylene glycol
pAnis-AL	p-Anisaldehyde
PCAL	pyridine carboxaldehyde
Phac-AL	Phenylacetaldehyde
p*I*	Isoelectric point
PMS	Phenazine methosuphate
PpNRH	nucleoside N-ribohydrolase from *Physcomitrella patens*
Q_0	Coenzyme Q_0
qPCR	quantitative PCR
Q-TOF	quadrupole-time-of-flight mass analyzer
Thio-NAD^+	thionicotinamide adenine dinucleotide;
TMABAL	*N*,*N*,*N*-trimethyl-4-aminobutyraldehyde;
TMAPAL	*N*,*N*,*N*-trimethyl-3-aminopropionaldehyde
V_{max}	Limit (maximal) reaction velocity
WT	wild type
Y.lipolytica	Yarrowia lipolytica
*t*Z	*trans*-Zeatin
*c*Z	*cis*-Zeatin
ZmNRH	nucleoside N-ribohydrolase from *Zea mays*
2AP	2-acetyl-1-pyrroline

Aims of the work

1) Literature review on the degradation pathway of cytokinins focused on cytokinin oxidase/dehydrogenases, aldehyde dehydrogenases and nucleoside-N-ribohydrolases

2) Cloning of maize *aldehyde dehydrogenase* and *nucleoside-N-ribohydrolasegene* genes, their expression and protein purification

3) Characterization of molecular and kinetic properties with substrates and inhibitors

4) Crystallization studies

5) Gene expression studies in maize

Contents

1 Preface

This work deals with characterization of three enzyme families from *Zea mays*: cytokinin oxidase/dehydrogenase (ZmCKO), aldehyde dehydrogenase (ALDH) and nucleosid *N*-ribohydrolase (NRH). CKOs are involved in plant hormone (cytokinins) metabolism, ALDHs detoxify plants by oxidizing aldehydes to corresponding acids and NRHs are associated with the metabolism of purines and pyrimidine and hydrolyze nucleosides to corresponding bases and ribose. "Literature review" and "Results and Discussion" are divided into three main chapters dealing with CKO, ALDH and NRH. Each main chapter is divided into sections dealing with characterization, metabolism, and crystal structures. The first part of "Results and Discussion" summarizes results obtained from CKO study including investigation of reaction mechanism, crystallization and determination of structures of three CKO isoenzymes from maize. The second part is linked to the characterization of maize ALDH2, ALDH7 and ALDH10 families including investigation of kinetics and their crystal structures. Part 3 is related especially to kinetic study on NRH. The last part deals with gene expression analysis of 6 genes of ALDH2 family, 1 gene of ALDH7 family, 3 genes of ALDH10 family and 5 genes of NRH from maize.

The Ph.D. thesis has been done at the Departement of Biochemistry and Department of Protein Biochemistry and Proteomics of the Centre of the Region Haná for Biotechnological and Agricultural Research (Palacký University in Olomouc) under supervision of Mgr. David Kopečný Ph.D. and Prof. Marek Šebela. Some experiments were done in the Laboratorie Dynamique et structure des corps lipidiques (Institut Jean-Pierre Bourgin, INRA Versailles, France) and X-ray data were collected at the SOLEIL Synchrotron, (Saint-Aubin, France).

2 Introduction

In this work, I focused on characterization of enzymes, which take a part in cytokinin metabolism. I have studied cytokinin oxidase/dehydrogenase (CKO/CKX, EC 1.5.99.12) and I have been looking for an interconnection between CKO and specific aldehyde dehydrogenase (ALDH, EC 1.1.1.70) and nucleoside-N-ribohydrolase (NRH, EC 3.2.2.1) both possibly involved in metabolism of cytokinins as shown on Figure 1.

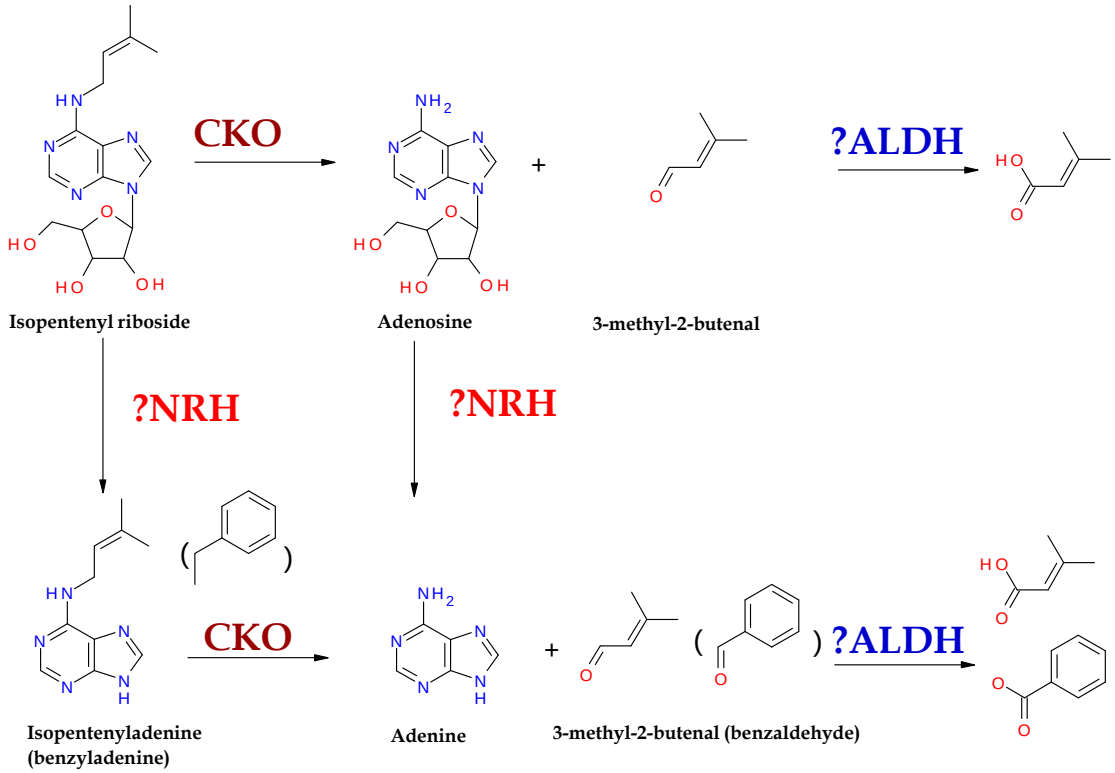

Figure 1. A scheme of CKO reaction with possible involvement of ALDH and NRH.

Cytokinins are a group of growth regulators that are involved in the control of important physiological functions in the plant organism by stimulating cell division, germination, differentiation of plastids and chlorophyll lateral bud dormancy, stimulate branching stem, seed production, increased resistance to pathogens and resistance conditions environment to senescence (Skoog, 1970; Gan and Amasino, 1995; Procházka, 1997; Inoue *et al*., 2001; Mok and Mok, 1; Fukuda, 2004; Kim *et al.*, 1995; Mahonen *et al.*, 2006; Tanaka *et al.*, 2006). CKO produces 3-methyl-buten-2-al but it is not clear what exactly is happening with this aldehyde after degradation of isoprenoid cytokinins. ALDHs are important and indispensable plant enzymes because they participate in degradation of aldehydes which are toxic, cancerogenic and mutagenic at higher concentrations. In plants, 13 families have been described up to now. In our laboratory, 3of 10 families in maize were characterized, namely families 2, 7 and 10. Crystal

structures of representatives of these families were solved and their kinetics was characterized as well NRHs are able to hydrolyze nucleosides and are classified according their preferences to nucleobase. I focused on purine nucleoside preferring NRH, namelyNRH3 from maize (ZmNRH3). This NRH is similar to NRH1 from *Physcomitrella patens* (PpNRH1). Maize (corn) was chosen as a model plant because it important representative of cereal crops and there are many studies related to cytokinin metabolism and ALDH.

The maize plant is usually 2.5 m in height (Karl, 2013). The stem is often composed of 20 internodes of 18 cm length (Stevenson and Goodman, 1972; Wellhausen, 1952). A leaf grows from each node. Ears evolve above a few of the leaves in the midsection of the plant (Kempton, 1924). They are female inflorescences, generally called husks. The male inflorescence, so called tassels, is located in the apex of the stem. Anthers on the tassels release pollen when tassels are mature. Silks (elongated stigmas) come out the whorl of husk leaves at the end of the ear. If a carpel (at the end of each ear) is fertilized by pollen, it may be developed into a kernel. The grains hold in regular rows around a white, pithy substance, forming the ear. An ear commonly carries 600 kernels (Grobman, 1961). Corn is an important model organism used in genetics and developmental biology.

In developed countries, maize is grown mainly for cattle feed, either in the form of grain or silage or as a raw material for the processing industry. Its direct consumption as food is marginal, although growing in importance of sweet corn as vegetables. In the food industry is used as a source of corn oil, starch, glucose, fructose syrup and bioethanol. Maize-germ oil is one of the better food oils and it is a valuable source of vitamin E. It is also envisaged for the use in production of biodegradable plastics and proteins for medical purposes. In Latin America and in Africa, maize is mostly consumed as main source of calories for the rural population. In Asia, its use as human food and as a livestock feed is roughly balanced. In Mexico, maize is an integral part of the culture and is present in almost all foods. Dry stems are used as building material for fences and roofing sheets for making mats, etc.

3 Literature review

3.1 Cytokinin metabolism

Enzyme, which is responsible for cytokinins degradation, is known as cytokinin oxidase/dehydrogenase (abbreviated as CKO or CKX, Figure 3, Chatfield and Armstrong 1987). CKO belongs to the group of oxidoreductases that contain a flavin cofactor (Fraaije *et al*., 1998). After it was shown that other compounds with reducing properties may act as a more efficient electron acceptors than oxygen, the enzyme was reclassified to cytokinin dehydrogenase in 2001 (EC 1.5.99.12; Morris *et al*., 1999; Galuszka *et al*. 2001). However, such a name is inaccurate because it excludes oxygen as the electron acceptor and the reaction simply occurs in both modes (Figure 2).

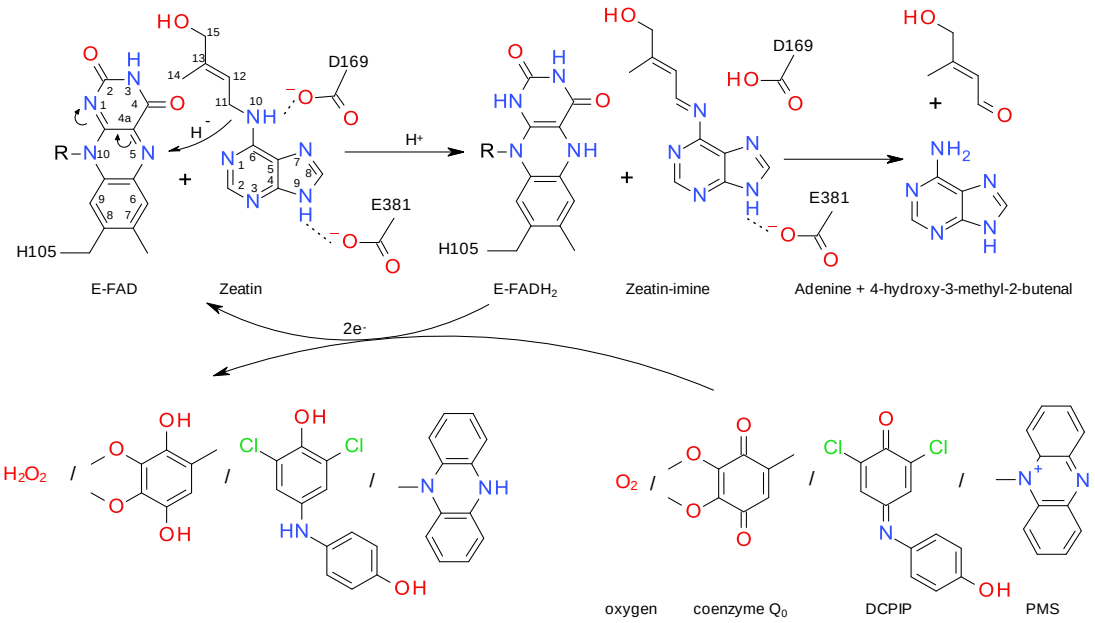

Figure 2. A mechanism of CKO reaction with zeatin as a substrate. During the reductive half reaction, zeatin is oxidized to an imine intermediate. D169 (ZmCKO1 numbering) polarizes the secondary amino group of the substrate and facilitates the transfer of a proton and two electrons from the substrate to N5 atom of the FAD cofactor. E381 forms a hydrogen bond with the N9 atom of the substrate. The resulting imine undergoes hydrolysis to the corresponding aldehyde and adenine. Reduced FAD cofactor is reoxidized either by oxygen with a subsequent release of H_2O_2 (oxidase mode) or by some other electron acceptor such as Q_0, DCPIP or PMS (dehydrogenase mode).

Cytokinins are inactivated by cleaving their isoprenyl or benzyl side-chain. FAD cofactor is reduced by two electrons transferred from substrate. An imine intermediate is formed and is further hydrolyzed to adenine and corresponding aldehyde (Mok and Mok 2001). $FADH_2$ is reoxidized by oxygen, which leads to production H_2O_2 (Kopečný *et al*., 2005) or other electron acceptor as for example by quinone (Frébortová *et al*., 2004). Flavin reduction is very fast but the reaction rate depends on the type and concentration of the used electron acceptor. If the flavin is reoxidized by molecular oxygen then the reaction rate reaches 0.5 s^{-1}. In case that

highly efficient electron acceptor (as DCPIP or PMS) is used, the enzyme is able to degrade

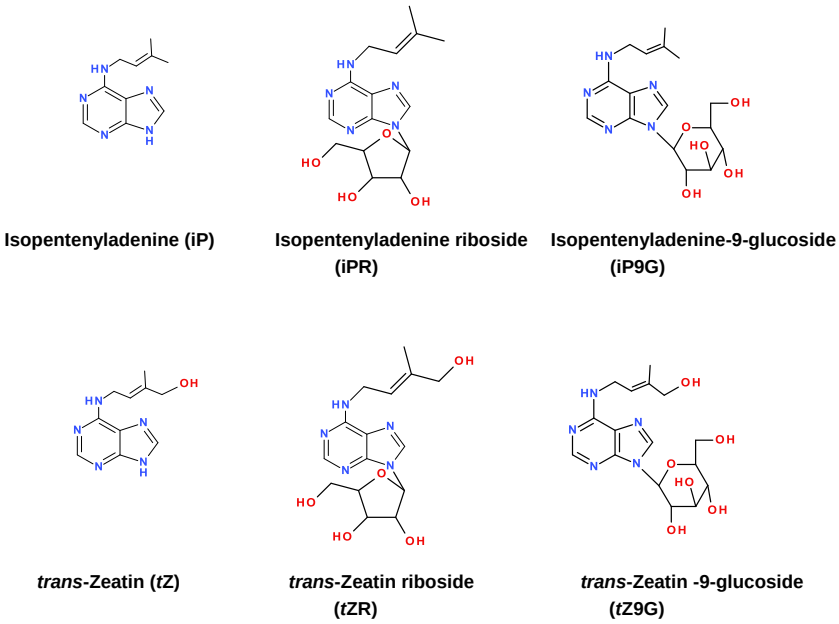

Figure 3. Isopreniod and aromatic cytokinis.

cytokinins at the reaction rate of $1000s^{-1}$ (Frébortová *et al.*, 2004). A whole range of compounds have been tested as potential electron acceptors including caffeic acid, *p*-quinones, analogs of ubiquinone, coenzymes Q_0 (K_m = 210 μM) a Q_1, 1,4-naftoquinone (K_m =11 μM), phenazine methosulphate (PMS), 2,6- dichlorophenol indophenol (DCPIP, K_m = 36 μM for ZmCKO1; Bilyeu *et al.*, 2001; Frébort *et al.*, 2002, Frébortová *et al.*, 2004). DCPIP is effective as electron acceptor in the neutral and slightly basic pH (7-9) while quinones are be predisposed to spontaneous oxidative side reactions in basic pH and thus they work at slightly acidic pH. CKOs are able to degrade aromatic cytokinins. Reaction rates are however rather low with no significant difference if using oxygen, Q_0 or DCPIP as the electron acceptor (Frébortová *et al.*, 2004). Precursor of natural electron acceptor could be 2,4-dihydroxy-7-methoxy-1,4-benzoxazin-3-on (DIMBOA) after reaction with polyphenol oxidase or peroxidase. DIMBOA is cleaved to 4-nitrosoresorcinol 1-monomethyl ether (coniferron). Coniferron is functional electron acceptor but the affinity and reaction rates with CKO are very low compared with artificial acceptors DCPIP or PMS. Effective acceptor forms upon subsequent oxidation of connifferon by laccase and peroxidase to conifferon radical, which further forms a polymer. Process of polymerization is inhibited in presence of CKO. Increased cytokinin levels in plant tissues are followed by increased levels of laccase and peroxidase, which might be involved in the synthesis of radicals suitable as CKO electron acceptors (Frébortová *et al.*, 2010).

3.1.1 Structure of ZmCKO1

ZmCKO1 (PDB 1W1Q, Malito *et al.*, 2004) is the best studied enzyme from CKO family. It is monomeric and glycosylated flavoenzyme. It comprises two domains, namely a FAD binding domain (residues 1 – 244 and 492 – 534) and a substrate binding domain (residues 245 – 491) which is very similar to other flavin oxidoreductases (Fraaije *et al.*, 1998). Isoalloxazine ring of FAD has a planar conformation and covalently bound to H105 via methyl-group in position 8 (Figure. 6.). This H105 residue belongs to a GHS motif conserved among all CKOs. Covalent flavin binding facilitates reduction catalysis and increase oxidative power flavin (Fraaije *et al.*, 1999). Mutations leading to removal of covalent FAD generally results in a reduction in redox potential and the speed of flavin reduction. Therefore, it can be assumed that the covalent binding of the FAD in CKO facilitates the reduction of FAD during catalysis.

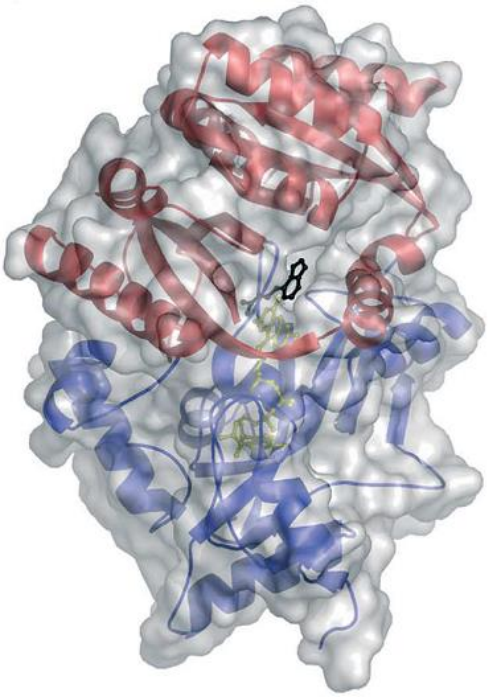

Figure 4. Structure of ZmCKO1. FAD binding domain (residues 40-244 a 492-534) colored in blue and substrate binding domain colored in red (residues 245-491). FAD is marked yellow and bound substrate iP is colored in black (Malito *et al.*, 2004).

3.1.2 The interaction of CKO with the substrate

Substrate binds to CKO on the lock and key principle. The side chain of substrate is anchored in the inner ellipsoidal cavity over isoalloxazine plane of FAD and interacts with D169 via H-bond and with W397 and L458 and several other residues via nonpolar interactions. This part of the active site is inaccessible to solvent molecules. Adenine ring is located in the funnel-shaped solvent accessible area, which is close to the surface of the protein. Adenine is positioned between nonpolar residues V378 and P427 and its N9 atom interacts with E381 via a

hydrogen bond. The important amino acid in the active site is D169, which via a hydrogen bond polarizes NH group of the substrate and facilitates transfer of proton and two electrons from the C11 atom of the substrate and N5 atom FAD (Figure 2. and 5; Malito *et al*., 2004). D169 is located in a highly conserved FAD-binding domain and is present in all CKO protein sequences (Popelková *et al*., 2004). This aspartate interacts through hydrogen bond to E288. This interaction stabilizes the neutral amino group of the substrate (Malito *et al*., 2004). E288 is not situated in any domain preserved, but the residue is present in all CKO sequences.

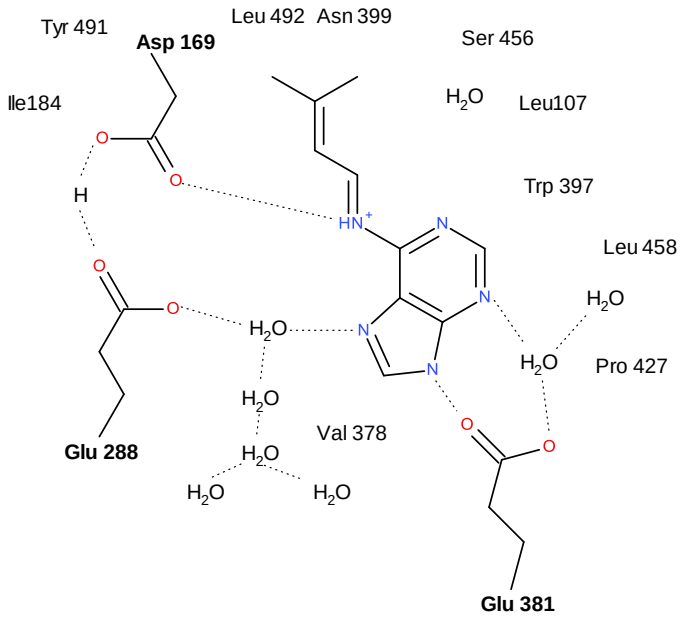

Figure 5. Schematic representation of the ZmCKO1 active site and formation of hydrogen bonds between substrate and Glu381 and Asp169 (Malito *et al*., 2004).

3.1.3 The composition of the active site in CKOs

Structure of ZmCKO1 (57.3 kDa) is similar to AtCKO7 (58.4 kDa, Bae *et al*., 2008). The active sites are highly conserved and contain a pair of amino acids Asp and Glu. W397, N399, L492 and L458 residues in ZmCKO1 are replaced by W382, N384, L480 and L447 in AtCKO7 structure. Glu381 at the entrance into the active site of ZmCKO1 (Figure 6) is replaced by serine residue at AtCKO7. Amino acids V378 and P427 are present at the entrance to the active site of both CKOs (Figure 6). Nonconserved residues Ser456 and Ile429 (in ZmCKO1) are replaced A441 and L413 (in AtCKO7) (Malito *et al*., 2004).

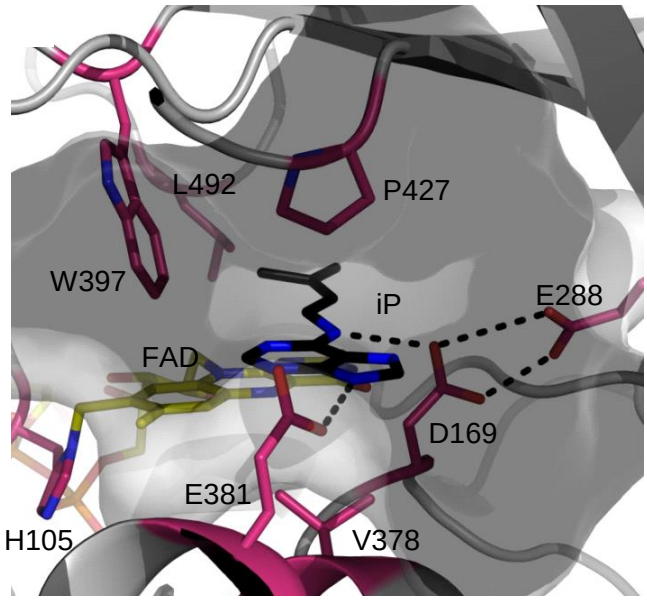

Figure 6. View of the active site of ZmCKO1. Residues surrounding bound substrate are labelled.

3.1.4 Inhibitors of CKOs

3.1.4.1 Substrate analogs and suicide substrates

An inhibitor N^6-isopentenyl-*N*-methylaminopurin ((methyl-iP), which is a substrate analogue, was described only in 1995 (Wang a Letham, 1995). Substrate analogs with adenine substituted at the position C2 and N9 behave as inhibitors CKO and they are able to inhibit CKO at 10^{-4} to 10^{-5} M concentrations (Galuszka *et al.*, 2001). Substrate analogs with a halogen atom, acetylenic or allenic group in β-the position belong among the so-called suicide substrates. These are defined as compounds similar to the substrate or product of the enzyme and they are catalytically converted to a reactive form, which is covalently bound to the active site of the enzyme and thereby inactivates it (Walsh, 1982). Derivatives of N^6-(buta-2,3-dienyl)adenine (HA-8) a N^6-(penta-2,3-dienyl)adenine (HA-1) belong to this group of CKO inhibitors (Suttle and Mornet, 2005). HA-8 is a close analog of the natural substrate iP. In comparison with iP, the side chain of HA-8 lacks the branched methyl group. Unlike HA-8, HA-1 contains an additional methyl group at the end allenic side chain. Oxidative degradation of cytokinin substrates CKO involves the formation of imine intermediate. It was confirmed that the HA-8 and HA-1 are bind covalently to the C4 atom of FAD cofactor in the form of a reactive imine, thus inactivating the CKO (Figure 7, Kopečný *et al.*, 2008). Due to the high similarity with preferred substrate iP, HA-8 may be considered the most effective inhibitor of ZmCKO1. The enzyme can be protected from inactivation by adding natural substrate or by a competitive inhibitor. Due to the irreversibility of inactivation and specificity of such substances can have many benefits for physiological studies (Kopečný *et al*. 2008). Several 6-anilinpurine derivatives were studied as effective inhibitors of CKO from *A. thaliana* (AtCKO2). A

substitution at phenyl ring and a substitution on C2 atom of the purine ring affect the inhibitory strength (Zatloukal *et al*; 2008). The benzyl group may be replaced by a phenyl group without significant loss of the activity against CKO.

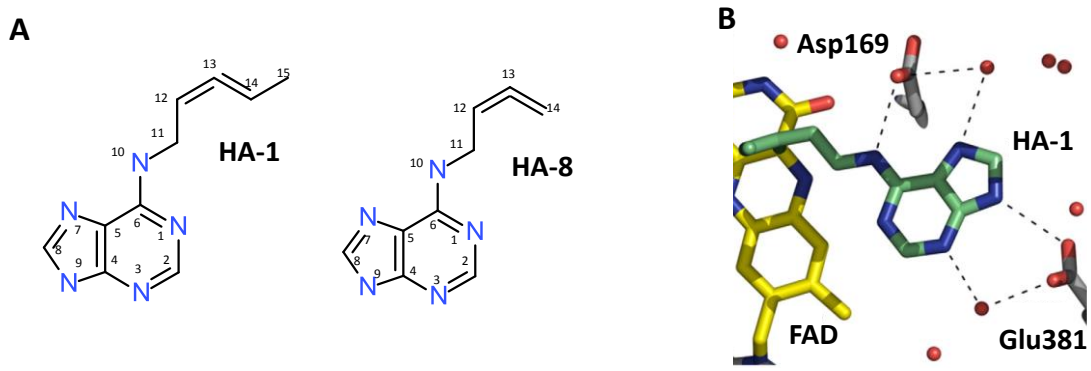

Figure 7. Mechanism-based inhibitors of CKOs. (A) N^6-adenine derivatives with allenic side chains – HA-1 and HA-8. (B) Crystal structure of ZmCKO1 inactivated by HA-1.Hydrogen-bonding interactions of the allenic inhibitor HA-1 at the active site of ZmCKO1 (Kopečný *et al.*, 2008).

Two derivatives 2-chloro-6-(3-mehoxyphenylamino) purine a 2-fluoro-6-(3-methoxyphenylamino) purine were developed as more effective inhibitors. While mono-substituted derivatives have similar IC_{50} as TDZ (20 – 30 μM), di-substituted substances have IC_{50} values much lower (1 – 2 μM). When a methoxy group on the phenyl ring is present, decreasing inhibitory strength was observed in the following order: meta > para ≥ ortho. When C2 substituents are present the inhibitory strength decreases as follows: F > Cl > NO_2 > NH_2 > SCH_3 (Zatloukal *et al*; 2008). Similar effects have been reported among derivatives of natural cytokinins containing fluorine (Matsubara, 1990; Doležal *et al*., 2007).

3.1.4.2 Urea derivatives as inhibitors of CKO

Synthetic cytokinins *N*-(2-chloro-pyridin-4-yl)-*N*′-phenyl urea (CPPU), 1-benzyl-3-(2-chloropyridin-4-yl)urea (CPBU) or *N*-(1,2,3-thidiazol-yl)-*N*′-phenyl urea (TDZ) and their derivates are well known as inhibitors of CKO (Laloue *et al.*, 1989; Burch *et al*., 1989; Hare *et al.*, 1994). The ability of CPPU, TDZ and their derivatives to replace cytokinins was demonstrated in a number of bioassays (Bruce *et al*., 1966; Mok *et al*., 1982; Isogai, 1981; Shudo, 1994). For a long time it was assumed that they are highly active due to inhibition of CKO and leading to elevated levels of endogenous cytokinins. But it was proven that the plant cytokinin receptors AHK4 and AHK3 are able to bind these urea derivatives such as TDZ (Spíchal *et al.*, 2004).

In the oxidase mode, CKO inhibition by CPPU and TDZ appears as a noncompetitive or competitive (Laloue *et al.*, 1989; Burch *et al*., 1989; Hare *et al.*, 1994). In the dehydrogenase mode, the inhibition is described as competitive to substrate (Bilyeu *et al.*, 2001) and

noncompetitive to the electron-acceptor (Frébortová *et al.*, 2004). K_i values are in 10^{-6} M. Binding of two urea derivatives *N*-(2-chloro-pyridin-4-yl)-*N´*-fenyl urea (CPPU) and *N*-(2-chloro-pyridin-4-yl)-*N´*-benzyl urea (CPBU) in ZmCKO1 was recently analyzed (Figure 8, Kopečný *et al.*, 2010, PDB accession codes 2QKN and 2QPM). Both compounds non-covalently bind to the active site above flavin plane and behave as competitive inhibitors (K_i ~ 10^{-6} M). CPPU binding to the active site allows two possible orientations with almost planar conformation, whereas the conformation of CPBU is not planar. Pyridyl ring is located above the FAD cofactor and benzyl ring protrudes above the plane outward from the active site.

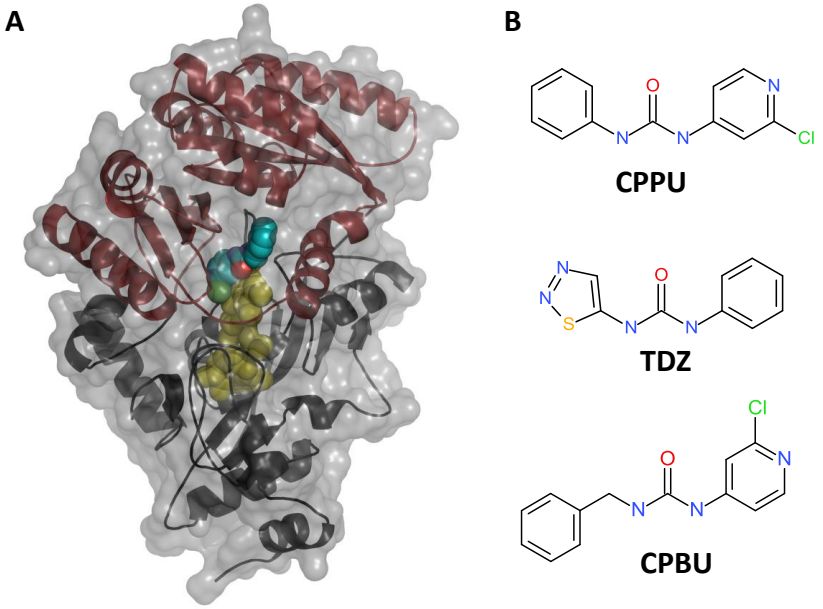

Figure 8. The structure of ZmCKO1 with the inhibitor CPBU inside the active site. FAD-binding domain is shown in black, brown substrate binding domain and the FAD cofactor is marked in yellow. CPBU (C atoms shown in blue, red, oxygen atom, chlorine atom green) is bound at the active site and its pyridinyl ring is positioned over the flavin while the benzyl ring extends to the surface (PDB 2QPM) (B) Urea derivatives inhibitors of CKOs: CPPU, CPBU and TDZ.

3.2 ALDHs

ALDHs catalyze $NAD(P)^+$-dependent oxidation of aldehydes to the corresponding carboxylic acid and NAD(P)H. These enzymes are present in many physiological metabolic pathways – carnitine biosynthesis, glycolysis, gluconeogenesis, amino acid metabolism (Marchitti *et al*., 2008; Sophos and Vasiliou 2003; Tylichová *et al*., 2010). They also participate in the detoxification of aldehydes generated during oxidative stress or during the metabolism of xenobiotics. ALDH enzymes play crucial role as "aldehyde scavengers" (Brocker *et al*., 2012) by oxidizing aldehydes which are toxic in higher concentrations. Aldehydes like 4-

hydroxynonenal, 4-oxononenal and malondialdehyde originate from lipid peroxidation and act as electrophiles and thus easily build adducts with nucleic acids and proteins. Experiments performed on plants have shown that upregulation of *ALDH* is often a response to environmental stresses (Barclay and McKersie, 1994; Kirch *et al*., 2001) such as drought, salinity etc. Depletion of water causes a change in osmotic pressure on the membrane, thereby pushing the water out of the cell. One of the ways to prevent osmotic stress is the generation of osmoprotectants by ALDHs (Fong *et al*., 2006).

3.2.1 Plant ALDH families

Up to date, ALDHs have been classified into 26 distinct families throughout all taxa. These families are numbered according to the criteria established by the ALDH Gene Nomenclature Committee (AGNC) (Vasiliou *et al*., 1999). ALDHs with amino acid sequences that are identical by more than 40% to previously identified ALDH sequences comprise a family, while those with sequence identity over 60% comprise a subfamily. ALDHs with sequence identity below 40%represent a new family. Among the 26 ALDH families, 13 families (ALDH2, ALDH3, ALDH5, ALDH6, ALDH7, ALDH10, ALDH11, ALDH12, ALDH18, ALDH21, ALDH22, ALDH23 and ALDH24) are found in plants (Zhang *et al*., 2012). Several ALDH families are conserved among animals and plants. (Brocker *et al*., 2012).Plant ALDHs are presented in many subcellular compartments including mitochondria, plastids, peroxisomes, microsomes and cytosol (Missihoun *et al*., 2011; Mitsuya *et al*., 2009). Most of the analyses on plant ALDHs have been performed in model species such as Arabidopsis (Kirch *et al*., 2004) and rice (Gao and Han, 2009).

Maize ALDH gene superfamily is one of the most expanded with 23 gene copies (Figure 9 and Table 1) compared with 20 genes in rice (Brocker *et al* 2013), 21 genes in moss *Physcomitrella patens* (Wood and Duff, 2009), 7 genes in algae *Volvox carteri* (Wood and Duff, 2009), and 14 genes in *Arabidopsis thaliana* (Kirch *et al*., 2004), 25 genes in *Vitis vinifera* (Zhang *et al*., 2012), 26 genes in *Populus trichocarpa* (Brocker *et al*., 2012), 24 gene copies in *Selaginela moelindorffii* (Brocker *et al*., 2012) and 19 genes in *Sorghum bicolor* (Brocker *et al*., 2012).

Maize genome comprises 3 genes coding for members of ALDH10 family (Table 1). Family 2 is represented by 6 genes and family 3 by 5 genes. These families are the largest ALDH families found in maize genome. ALDH5 comprises 2 genes and family 18 is composed by 3 genes. Families 6, 7, 11 and 22 are formed by a single gene. Families 21 and 23 are absent in maize. These two families were discovered only in *Physcomitrella patens*. Similarly, family 24 was found only in *Chlamydomonas reinhardtii* genome (Brocker *et al*., 2012).

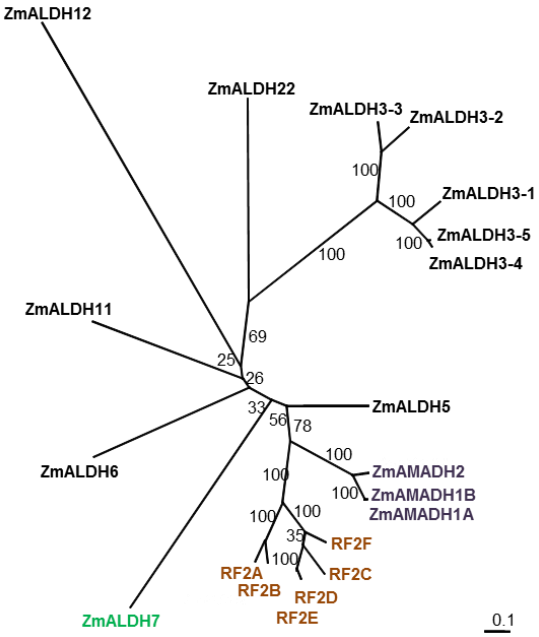

Figure 9. Phylogenetic analysis in maize (Zea mays). Amino acid sequence alignment was performed using the CLUSTAL W and the unrooted phylogenetic tree was built using the Neighbour-Joining algorithm. Analyzed ALDH families are colored.

Table 1. Maize ALDH superfamily: unified nomenclature and gene information (Brocker *et al.*, 2013)

Family	Gene name	NCBI gene ID	Other names	NCBI protein ID
Family 2	*ZmALDH2B2*	732806	RF2A	NP_001105981.1
	ZmALDH2B5	542567	RF2B	NP_001105576.1
	ZmALDH2C1	541913	RF2C	NP_001105046.1
	ZmALDH2C2	541914	RF2E	NP_001105047.1
	ZmALDH2C4	No entry	RF2D	No entry
	ZmALDH2C5	No entry	RF2F	No entry
Family 3	*ZmALDH3E1*	100280692	Aldehyde dehydrogenase	NP_001147083.1
	ZmALDH3E2	100284774	Aldehyde dehydrogenase	NP_001151141.1
	ZmALDH3H1	100285809	Aldehyde dehydrogenase(NADP+)	NP_001152171.1
	ZmALDH3H2	100281700	Aldehyde dehydrogenase (NADP+)	NP_001148092.1
	ZmALDH3H3	100382449	Aldehyde dehydrogenase(NADP+)	NP_001168661.1
Family 5	*ZmALDH5F1*	100280779	Succinate semialdehyde dehydrogenase	NP_001147173.1
	ZmALDH5F2	100284047	Succinate semialdehyde dehydrogenase	NP_001150417.1
Family 6	*ZmALDH6B1*	10027311	Methylmalonate semi-aldehyde dehydrogenase	NP_001142146.1
Family 7	*ZmALDH7B6*	100282748	Antiquitin	NP_001149126.1
Family 10	*ZmALDH10A5*	541949	Amino aldehyde dehydrogenase 2	ACS74868.1
	ZmALDH10A8	100302679	Amino aldehyde dehydrogenase 1a	ACS74867.1
	ZmALDH10A9	No entry	Amino aldehyde dehydrogenase 1b	AEP68091.1
Family 11	*ZmALDH11A3*	542583	NADH-dependent glyceraldehyde - 3-phosphate dehydrogenase	NP_001105589.1
Family 12	*ZmALDH12A1*	No entry	Delta-1-pyrroline-5-carboxylate dehydrogenase	AAL70108.1

Family 18	*ZmALDH18B2*	100280719	Delta-1-pyrroline-5-carboxylate synthetase	NP_001147111.1
	ZmALDH18B1	No entry	Delta-1-pyrroline-5-carboxylate synthetase	ACR33941.1
Family 22	*ZmALDH22A1*	100125658	Aldehyde dehydrogenase	NP_001106059.1

3.2.1.1 ALDH2

Family 2 ALDHs are mitochondrial or cytosolic homotetramers, which have been extensively studied not only in plants (Yoshida *et al.*, 1998, Navarro-Aviño *et al.*, 1999, Marchitti *et al.*, 2008). Plant ALDH2 isoforms have been studied in maize (*Zea mays*), rice (*Oryza sativa*) and Arabidopsis thaliana (Skibbe *et al.*, 2002, Liu *et al.*, 2002 Nakazono *et al.*, 2000). Mitochondrial enzyme from rice (OsALDH2) is responsible for the efficient detoxification of acetaldehyde after the flooding and ethanol fermentation (Wei *et al.*, 2009). Metabolism of acetaldehyde generates acetate, which is consecutively used for CoA synthesis *via* acetyl-CoA synthase, often described as the „pyruvate dehydrogenase pathway“(Figure 10.)

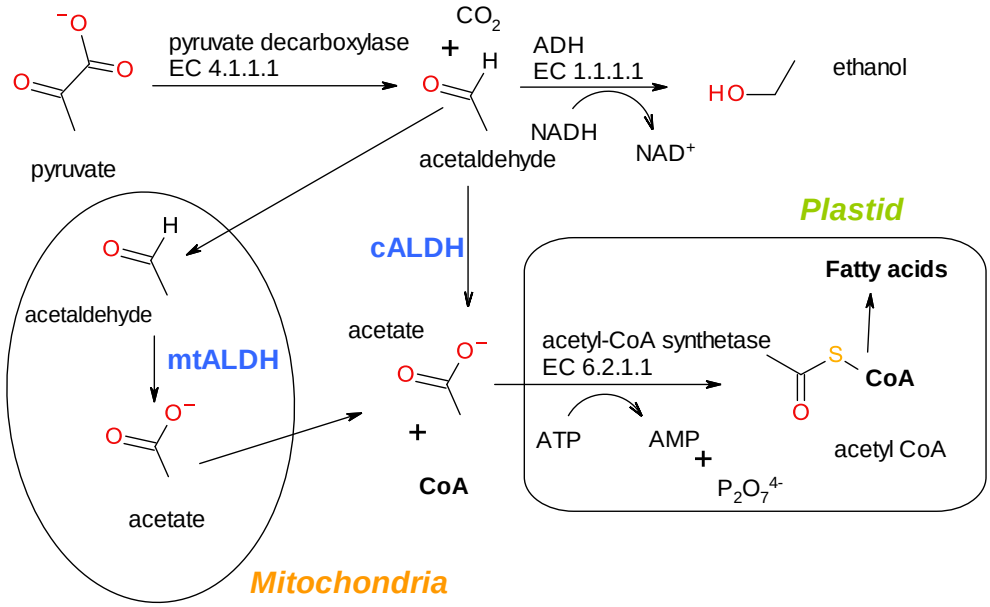

Figure 10. The oxidation of acetaldehyde to acetate in *Arabidopsis thaliana*. The Pyruvate dehydrogenase and pyruvate decarboxylase bypass pathways. ALDHs are involved in the flux from ethanol to fatty acids. (Wei *et al.*, 2009)

In *Arabidopsis*, two *ALDH2* genes (*ALDH2B7* and *ALDH2B4*) code for isoforms with 75% similarity that accumulate in mitochondria. Only ALDH2B4 was shown to predominantly participate in acetaldehyde metabolism (Wei *et al* 2009). ALDH2B4 homologue in Chinese wild grapevine anticipates a mildew infection (Wen *et al.*, 2012). Nevertheless, the protection mechanism against pathogen infection is not well understood.

A great progress in understanding the role of mitochondrial ALDH2 is linked to a discovery of *rf2a* (**r**estoration of **f**ertility) gene in maize, which codes for a mitochondrial ALDH (Liu *et al*., 2002) and its mutation is responsible for cytoplasmic male sterility (CMS). In general, male sterility is the failure of plants to produce functional anthers, pollen, or male gametes. Texas CMS maize is predisposed to the southern corn leaf blight disease caused by *Cochliobolus heterostrophus*, which produces a T-toxin (Hooker *et al*., 1970; Yoder, 1973). The *rf2a* is important for normal anther development in plants with normal cytoplasm (Liu *et al*., 2001). RF2A, but not RF2B, accumulates to high levels in the tapetal cells of anthers (Liu and Schnable, 2002) and the anther development halts in the lower florets of plants, which are homozygous for mutation in *rf2a* (Liu *et al*., 2001).

Cytoplasm of some plant expresses novel mitochondrial genes that cause male sterility. Nuclear genes that disrupt the accumulation of the corresponding mitochondrial gene products can restore fertility to such plants. CMS has been revealed in more than 150 plant species (Shnable and Wise 1998) and male sterility in maize is caused by a Texas cytoplasm-specific mitochondrial gene *urf13* – which codes for a URF13 protein (13 kDa; Wise *et al*., 1987). The mechanism of URF13 which causes male sterility and complete function of male sterility restorer RF2A are not known. Only combined action of *rf1* and *rf2a* nuclear genes restores fertility to Texas CMS maize lines (Schnable *et al*., 1998; Wise *et al*., 1999). *Rf1* gene alters the expression of *urf13* thereby reducing the accumulation of URF13 (Dewey *et al*., 1987; Rocheford *et al*., 1989) while *rf2a* differs from typical nuclear restorers in that it does not alter the accumulation of the mitochondrial protein URF13 necessary for T cytoplasm–induced male sterility. The maize RF2A is the most well characterized RF gene so far even though many mitochondrial genes associated with cytoplasmic male sterility have been described (Schnable *et al*., 1998; Wise *et al*., 1999). Maize mtALDHs RF2A and RF2B are capable to oxidize a broad range of aldehydes (Liu and Schnable, 2002). RF2A preferably oxidizes a wide range of aliphatic and aromatic aldehydes whereas RF2B prefers shorter aliphatic aldehydes (Liu and Schnable, 2002). In general, mtALDHs are longer by about 50 amino acids than cytosolic ALDHs because they carry an N-terminal targeting peptide (Perozich *et al*., 1999).

There is an assumption that ALDH2 isoforms are involved in phenylpropanoid pathway *as REF1* gene, which codes for ALDH2 in Arabidopsis, plays a significant role in the synthesis of ferulic acid and sinapic acid (Figure 11). Esters of ferulic acid accumulate in a wide range of plants. REF1 from *Arabidopsis* shares 76 % sequence similarity with maize RF2C and RF2D (Skibbe *et al*., 2002) and 79 % similarity with ALDH2C1 from *O. sativa* (Li *et al*., 2001), which could indicate that RF2C, RF2D and ALDH2C1 from *O. sativa* are involved in the biosynthesis of ferulic acid too. REF1, RF2C and RF2D are localized to the cytosol together with other enzymes of the phenylpropanoid pathway. RFA2 has a relatively high K_{cat}/K_m ratio for cinnamaldehyde (Liu and Schnable, 2002).

Ferulic acid derivatives play an important role in cross-linking of cell wall-bond polysaccharides to lignin in monocots (Grabber *et al*., 2000, 2002). Determination of ALDHs as enzymes required for ferulic acid but not lignin biosynthesis offers an opportunity to modify phenylpropanoid content of plant cell walls, which could has effect on digestibility of forages and quality of vegetables (Garcia-Conesa *et al*., 1997). Nair *at al*, 2004 analyzed enzyme extract from dicotyledonous (*A. thaliana, N. tabacum, and Raphanus sativus* [radish]) and monocotyledonous (*Z. mays*) plants as well as a gymnosperm (*Pinus strobus* [pine]) and a pteridophyte (*Ceratopteris richardii*) to determine the ability to synthesize ferulic and sinapic acids from coniferaldehyde and sinapaldehyde. Coniferyl aldehyde dehydrogenase and sinapaldehyde dehydrogenase activity were confirmed in all tested plants. In vitro enzyme assays reveal that activity of these two ALDH vary among species. The plant ALDH2 family is relatively miscellaneous and involves four subfamilies. It is possible that this expansion is caused by the development of basal land plants into basal vascular plants (Brocker *et al*., 2012).

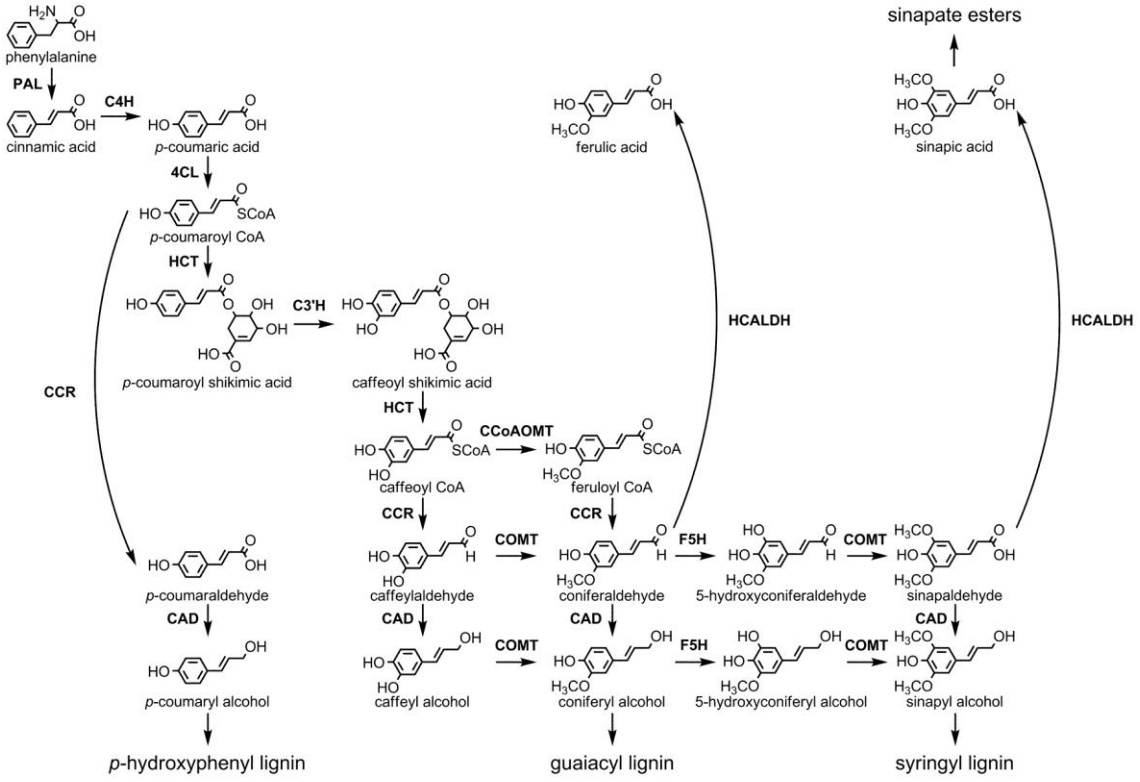

Figure 11. Phenylpropanoid pathway in *A. thaliana* showing the biosynthesis of ferulate, sinapate, and lignin precursors from Phe. The discovery of REF1 protein reverses the model of lignin production flux. According to this model, ferulate and sinapate are not precursors of coniferaldehyde and sinapaldehyde but the oxidation products of these aldehydes. The enzymes and their abbreviations are caffeoyl CoA O-methyltransferase (CCoAOMT), cinnamate 4-hydroxylase (C4H), hydroxycinnamyl alcohol dehydrogenase (CAD), hydroxycinnamoyl CoA reductase (CCR), p-coumaroyl shikimate/ quinate 39-hydroxylase (C39H), 4-coumarate CoA ligase (4CL), ferulate 5-hydroxylase (F5H), hydroxycinnamoyl CoA:shikimate/quinate hydroxycinnamoyltransferase (CST), Phe ammonia-lyase

(PAL), caffeic acid/5-hydroxyferulic acid O-methyltransferase (COMT), and sinapyl alcohol dehydrogenase (SAD) (Nair *et al*., 2004).

3.2.1.2 ALDH7

ALDHs from family 7 are known as antiquitins, α-aminoadipic semialdehyde dehydrogenases or Δ^1-piperideine-6-carboxylate dehydrogenases (P6CDH). The *ALDH7* gene family is one of the most conserved ALDH families across species and sequence identity of about 60% is observed on protein level among its members. These enzymes are involved in the lysine catabolism (Figure 12) and oxidize α-aminoadipic semialdehyde to the corresponding acid (Brocker *et al*., 2010). The expression of *ALDH7* takes part in the protection against hyperosmotic stress and seed maturation (Kirch *et al*., 2005) in plant such as garden pea (Guerrero *et al*. 1990), apple (Yamada *et al*. 1999), *Tortula ruralis* (Chen *et al*. 2002), brassica (Stroeher *et al*. 1995), sorghum (Buchanan *et al*. 2005) and Arabidopsis (Kirch *et al*. 2005).

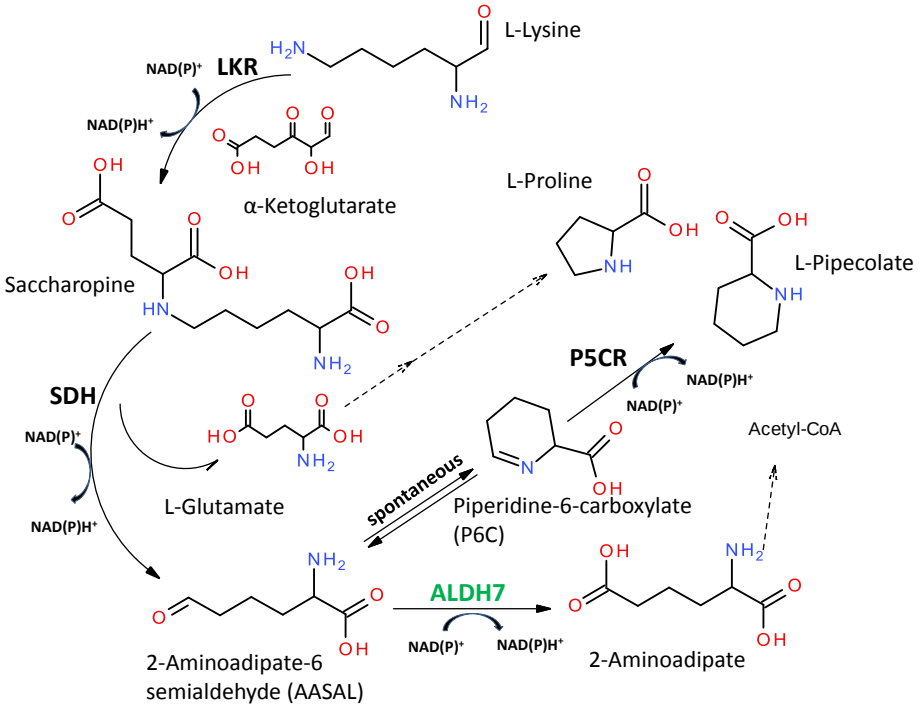

Figure 12. The saccharopine pathway. Involvement of ALDH7 in the L-lysine degradation in plants, mammals and bacteria. Indicated enzymes are lysineketoglutarate reductase (LKR); saccharopine dehydrogenase (SDH), pyrroline-5-carboxylate reductase (P5CR) (Arruda *et al*., 2000).

ALDH7 in rice (OsALDH7) participates in seed maturation and maintaining seed viability during storage (Shen *et al*., 2012, Shin *et al*., 2009). A mutation in *OsALDH7* gene leads to accumulation of a yellow pigment in endosperm, which was later identified as mixture of oryzamutaic acids A-J (Figure 13, Nakano *et al*., 2009), which are apparently products of

Millard reaction. Expression of *OsALDH7* is induced by various osmotic stresses such as dehydration, salinity and ABA, especially in leaf (Gao and Han 2009; Shin *et al*. 2009). OsALDH7 is capable to oxidize malondialdehyde, acetaldehyde and glyceraldehyde, which confirms the detoxification function during oxidative stress (Shin *et al*., 2009).

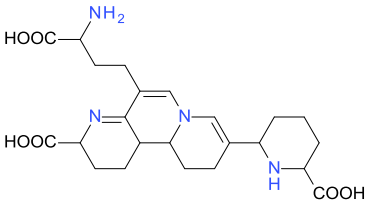

Figure 13. Oryzamutaic acid A

Drought tolerance, an important ability among the plant kingdom, is extensively studied for understanding molecular and biochemical mechanisms. The first plant ALDH7 was intitially described in the green garden pea as a“26g protein” involved the the regulation of turgor pressure (Guerrero *et al*., 1990). ALDH7 gene expression is induced upon dperivation of water or exposure to high salinity in *Tortula ruralis* and *Arabidopsis* (Guerrero *et al*., 1990; Chen *et al*., 2002). *Tortula ruralis* ALDH7 shares 60 % identity to human ALDH7 and 74 % identity to ALDH7 from pea (*Pisum sativum*; Kirch *et al*., 2004). In. Strong expression of *AtALDH7* is induced by low temperature, shock or high concentration of abscisic acid, UV-C radiation, abiotic stress (Wood *et al*., 2002) and aldehydes from lipid peroxidation (Kotchoni *et al*. 2006). The overexpression of soybean ALDH7 in Arabidopsis or tobacco also increases the plant tolerance to stresses (Rodrigues *et al*. 2006).

ALDH7 plays an important role in the regulation of the lysine catabolism. Lysine is produced *via* aspartic acid pathway and degraded through aminoadipic acid pathway in higher eukaryotes. However, yeast uses the aminoadipic acid pathway for lysine synthesis and degradation (Arruda *et al*. 2000; Zhu *et al*. 2000). An overexpression of yeast ALDH7 leads to lowered lysine concentration (Shen *et al*., 2012). A mutation in human ALDH7A1 causes the pyridoxine dependent epilepsy (PDE-pyridoxine-dependent seizures, Gallagher *et al*., 2009; Mills *et al*., 2006). It leads to the accumulation of α-aminoadipic semialdehyde in the urine, plasma and cerebrospinal liquor. An increase of α-aminoadipic semialdehyde (AASAL) level causes an atrophy of the brain due to high toxicity of this aldehyde (Brocker *et al*., 2010).

The AASAL is in the equilibrium with its cyclic Schiff base piperideine-6-carboxylate (P6C). Slow or aborted lysine degradation will cause an accumulation of α-aminoadipic semialdehyde and thus also P6C. The P6C is capable to interact with pyridoxal 5´- phosphate (PLP, Figure 14) by Knoevenagel´ condensation. PLP is an essential cofactor of many enzymatic reactions including the metabolism of neurotransmitters (Mills *et al*., 2006).

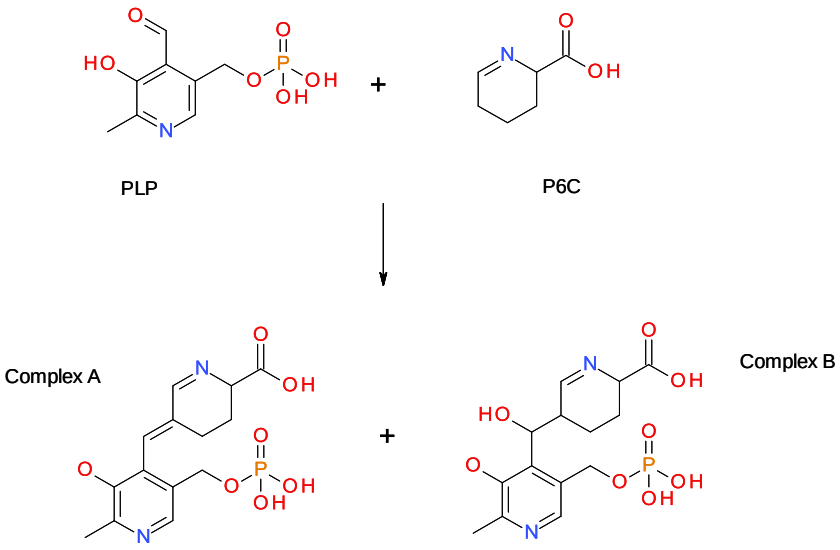

Figure 14. Knoevenagel condensation of PLP and P6C. Presence of condensation products was affirmed be tandem mass spectrometry (Mills *et al*., 2006).

3.2.1.3 ALDH10

ALDH10 family members are known as aminoaldehyde dehydrogenases (AMADHs, EC 1.2.1.19), 4-aminobutyraldehyde dehydrogenases, 4-guanidinobutyraldehyde dehydrogenases (EC 1.2.1.54) and betaine aldehyde dehydrogenases (BADH; EC 1.2.1.8). ALDH10 family has been studied due to connection with polyamine metabolism, degradation of toxic and reactive ω-aminoaldehydes, such as 3-aminopropionaldehyde (APAL) or 4-aminobutyraldehyde (ABAL), which originate from different metabolic pathways (Figure 15). Oxidation of these aldehydes leads to formation of nontoxic compounds, such as β-alanine and γ-aminobutyric acid (GABA). Plant AMADHs share 70-80% sequence identity.

Study on plant AMADHs has become attractive for economic reasons. The mutation in rice *AMADH* gene leads to accumulation of 2-acetyl-Δ^1-pyrroline, which is responsible for a fragrance of several rice varieties, such as Jasmine and Basmati. It is due to accumulation of Δ^1-pyrroline, which is a cyclic form of ABAL and which is further acetylated. The same mutation has been described in soybean as well (Arikit *et al*., 2011; Bradbury *et al*., 2008).Extensive studies on AMADHs have been performed to analyze the production of osmoprotectant glycine betaine (GB, Figure 16). Plants can be divided into two groups: GB-accumulating plants and GB non-accumulating plants. Both groups contain *ALDH10* gene in their genomes.

In general, osmoprotectants are highly soluble compounds with physiological pH, non-toxic in higher concentrations, capable to stabilize membranes and proteins in hypertonic environment and in extreme temperature conditions, increase the osmotic pressure in the

cytoplasm. Therefore, osmoprotectants play an important role in the adaptation to various adverse conditions.

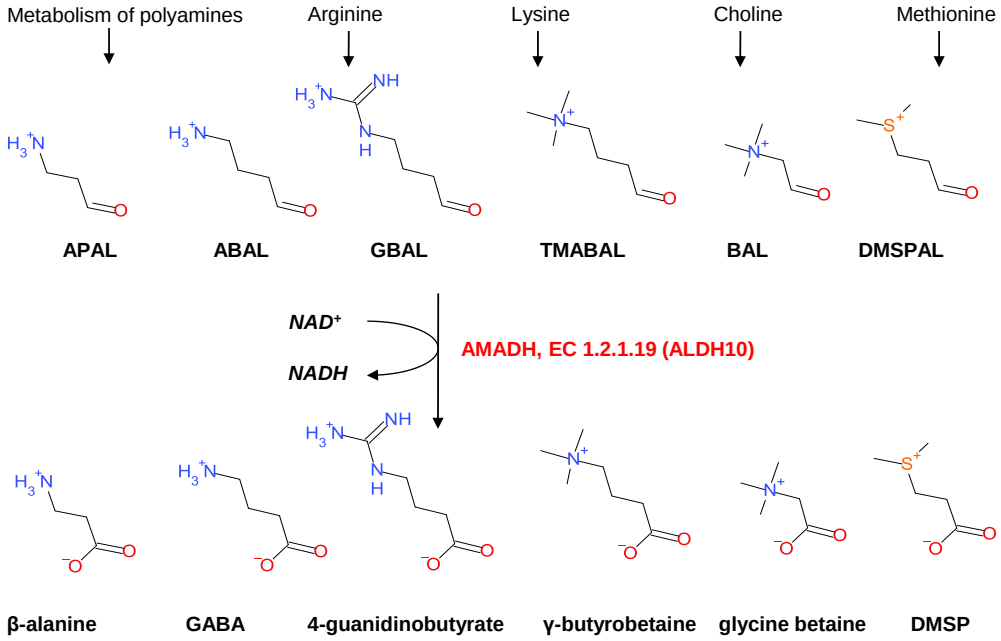

Figure 15. Overview of substrates oxidized by AMADHs (enzymes from. 3-Aminopropionaldehyde (APAL) is converted to β-alanine, 4-aminobutyraldehyde (ABAL) to γ-aminobutyric acid (GABA), 4-guanidinobutyraldehyde (GBAL) to 4-guanidinobutyrate, *N*,*N*,*N*-trimethyl-4-aminobutyraldehyde (TMABAL) to γ-butyrobetaine, betaine aldehyde (BAL) to glycine betaine and 3-dimethylsulfoniopropionaldehyde (DMSPAL) to DMSP (Kopečný et. al 2011).

As the most effective osmoprotectants are known betaines and derived compounds such as polyols, sugars and proline (Yancey, 1994). GB plays crucial role as a major cellular osmolyte and is involved in stabilization of protein structures as a molecular chaperone (Allakhverdiev *et al*., 2007). GB biosynthesis occurs in chloroplasts (Kotchoni *et al*., 2003). Many ALDH10 isoforms preferentially oxidize ω-aminoaldehydes rather than BAL (Bradbury *et al*., 2008; Missihoun *et al*., 2011; Tylichová *et al*., 2010; Wei *et al*., 2009).

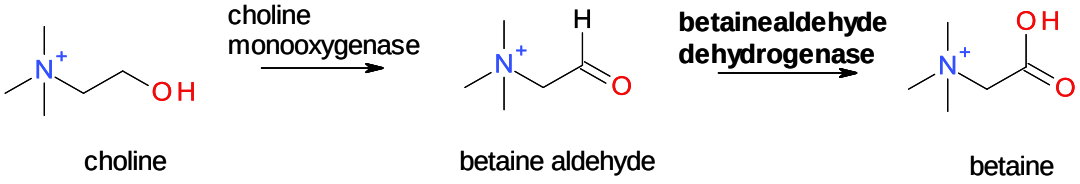

Figure 16. Oxidation of choline. Glycine betaine is synthesized in two steps. First, the oxidation of choline mediates choline monooxygenase (CMO) containing Fe-S cluster Rieske type. The second step is catalyzed by BADH (Trossat *et al*., 1997).

However, high activity with BAL has been described for ALDH10 from *Avicena marina*, *Amaranthus hypochondriacus* and *Spinacia oleracea* (Hibino *et al*., 2001; Incharoensakdi *et al*., 2002; Valenzuela-Soto and Munoz-Clares 1993). Therefore, ALDH10 family can be divided

into low and high BADH activity plants (Brocker *et al*., 2012). Munoz-Clares *et al*., 2014 published that alanine or cysteine residues at position 441 in spinach ALDH10 (SoBADH) play a crucial role in BAL oxidation. Isoenzymes with isoleucine at this position do not exhibit the activity with BAL. Phylogenetic analysis confirmed that A441- and C441-type isoenzymes evolved from the I441-type. A441 isoenzyme were found mostly in eudicots while C441 isoenzymes in monocots. Most of plant AMADHs are targeted to peroxisomes as they carry the C-terminal peroxisomal targeting signal S(A)KL, especially I441-type (Reuman *et al*., 2007; Nakamura *et al*., 1997) while all A441- and majority of C441-type ALDH10 isoenzymes lack the signal sequence (Munoz-Clares *et al*., 2014).

3.2.2 Catalytic mechanism of ALDHs

Catalytic mechanism is described on Figure 17 and follows the sequential binding model (Wymore *et al*., 2004; Perez-Miller *et al*., 2003). Essential residues in the active site such as Asn, Cys and Glu, are highly conserved within the whole subfamily. These three residues build the active site at the bottom part of substrate channel.

NAD^+ is bound to the coenzyme binding pocket before the aldehyde can be bound. A sulfur atom from a catalytic cysteine makes a nucleophilic attack on the carbonyl carbon of the aldehyde, resulting in a thiohemiacetal formation followed by a hydride transfer to the A-side of the nicotinamide ring (C4 atom) of NAD^+ (Jones *et al*., 1987). Asn residue stabilizes emerging thiohemiacetal (Steimmetz *et al*., 1997; Farres *et al*., 1995; Gonzalez-Segura *et al*., 2013). The water molecule is activated by a conserved glutamate residue leading to an attack on the acyl-sulfur bond of the thioester (Wang *et al*., 1995), subsequent the release of the product – corresponding acid, before NADH (Perez-Miller and Hurley, 2003; Sheikh *et al*., 1997; Wang *et al*., 1995; Gonzalez-Segura *et al*., 2013). Perez-Miller and Hurley (2003) pointed that there is a second possibility in reaction scheme so that NADH is released before the acid, which is the opposite of the scheme published by Wymore *et al* (2004).

3.2.3 Structure of ALDHs and NAD^+ binding domain

ALDHs are known as homotetramers or homodimers depending on the family. Plant ALDH10 family members are dimers including AMADHs from *Pisum sativum*, PsAMADH1 (PDB ID: 3IWK), PsAMADH2 (PDB ID: 3IWJ; Tylichová *et al*., 2010); BADH from *Spinacia oleracea*, SoBADH (PDB ID: 4A0M; Díaz-Sanchez *et al.*, 2012). On the contrary other AMADHs/BADHs like for example from *Agrobacterium tumefaciens* (PDB ID: 3R31; Agarwal *et al.*, to be published), from cod *Gadus callarias* (PDB ID: 1A4S; Johansson *et al.*, 1998) from *E.coli* (PBD ID: 1WNB; Gruez *et al.*, 2004) and *Pseudomonas aeruginosa* (PDB ID: 2WME; Gonzalez-Segura *et al.*, 2009) are homotetramers. All known structures of ALDH2 and ALDH7

family members were described as homotetramers including human ALDH2 (PDB ID: 1O02; Perez-Miller and Hurley, 2003) or bovine ALDH2 (PDB ID: 1AG8; Steinmetz *et al*., 1997),

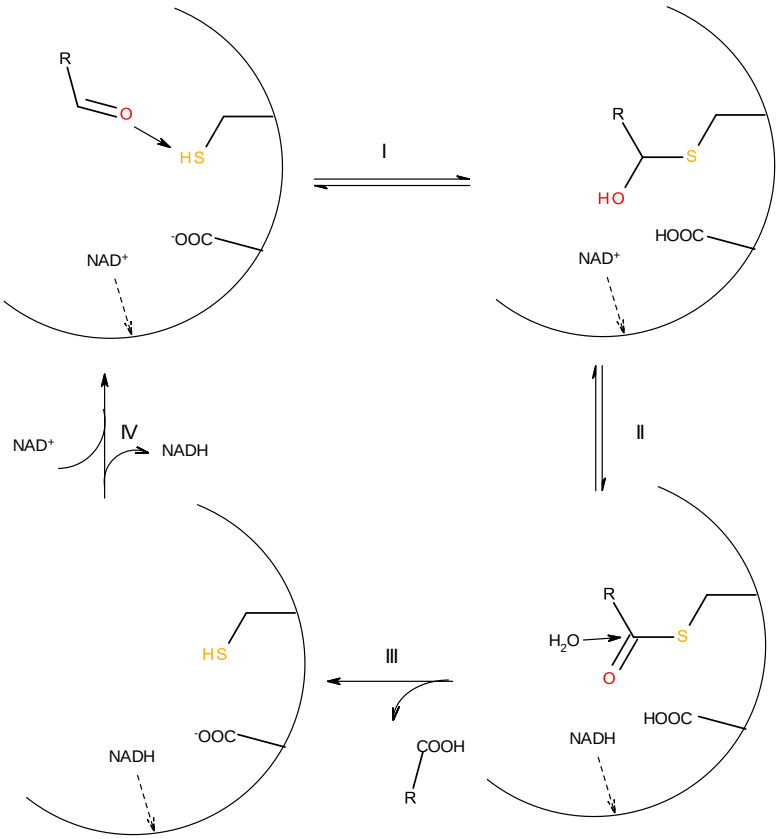

Figure 17. General mechanism for the ALDH reaction (Wymore *et al*., 2004; Tylichová *et al*., 2011). A schematic drawing of the enzyme active site is presented with the highlighted catalytic cysteine residue, which binds an aldehyde substrate. Dashed arrow illustrates the NAD^+/NADH binding. The general base is represented by carboxylate group belonging to the glutamate residue. Reaction I: Nucleophilic activation and attack on the substrate by the catalytic cysteine to yield a thiohemiacetal intermediate. Reaction II. Hydride transfer from the intermediate to NAD^+ and formation of NADH and thioester intermediate. There are two possibilities for last two steps. Reaction III: Hydrolysis of the thioester with release of the corresponding carboxylic acid followed by NADH in Reaction IV (Wymore *et al*., 2004). Second possibility includes the release of the NADH first (reaction III) followed by the carboxylic acid (reaction IV, Perez-Miller and Hurley, 2003).

seabream ALDH7 (PDB ID: 2JG7; Tang *et al*., 2008) and human ALDH7 (PDB ID: 2J6L; Brocker *et al*., 2010).

The structural motif called a "Rossmann fold" is present in proteins, which bind nucleotides (enzyme cofactors FAD, NAD^+ and $NADP^+$) including ALDHs. Each single subunit is composed of a coenzyme binding domain, a catalytic domain and an oligomerization domain (Figure 18A). The structure is built of up to seven mainly parallel beta strands and the first two strands are linked by α-helix (Rao and Rossmamn, 1973). The coenzyme specificity of ALDHs is mostly affected by a residue at position 195 (Figure 18B, human ALDH2 numbering) and NAD^+ is preferred with glutamate or proline residue at this position. Side chains of these residues electrostatically and sterically prevent binding of the 2´-phosphate group of $NADP^+$.

Presence of small neutral residues at position 244 allows for $NADP^+$ binding even if ALDH carries E195. Side chain of K192 makes a hydrogen bond to an oxygen atom of ribose's 2´-OH group of NAD^+. Residues with shorter side chains leave room for binding the 2´-phosphate group of $NADP^+$. Enzymes carrying different residue at position 195 like Thr, Ser or Gln exhibit sometimes lower K_m values with $NADP^+$ than with NAD^+ (Perozich *et al*., 2000; González-Segura *et al*., 2013). NAD^+ may be replaced by $NADP^+$ in many cases but not equivalently as is shown for PsAMADH1 (Šebela *et al*., 2000). Coenzyme preference of ALDHs is not affected only by coenzyme's binding site composition. An important role plays also subcellular localization and the necessity of NADH or NADPH in other metabolic processes (Velasco-Garcia *et al*., 2000).

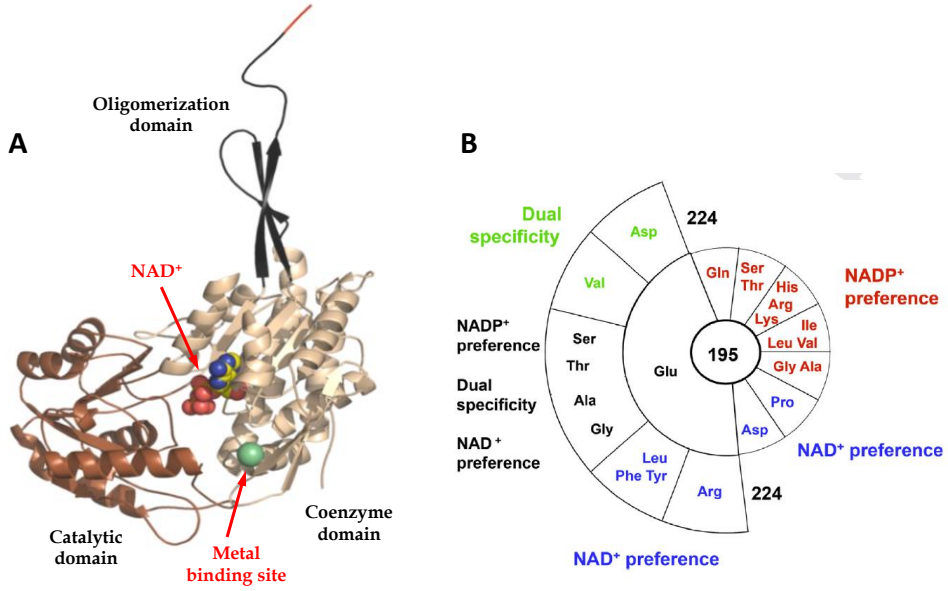

Figure 18. General composition of ALDH monomer (A) and schematic representation of the possible coenzyme preference of ALDHs (B). The inner circle includes the different residues at position 195; the outer semicircle includes the possible residues at position 224 in the enzymes that have E195 Adopted from González-Segura *et al* (2015).

Crystal structures of PsAMADH1 and PsAMADH2 (Tylichová *et al*., 2010) show that the catalytic C294 residue is located between the NAD^+ and the substrate binding sites. N162 and E260 residues are involved in catalysis. C294 and N162 are important form the oxyanion hole, which stabilizes thiohemiacetal and thiacyl intemediates produced during the enzyme reaction (Steinmetz *et al.,* 1997). The substrate channels of both pea isoenzymes are comparable in shape and size. The channel of PsAMADH1 is about 5‑8 Å wide and 14 Å deep. It comprises residues A109, D113, P452 and S453 at the entrance and by the side chains of D110, N162, Y163, L166, M167, W170, F284, F288, I293, C294, S295, Q451 and W459 in the interior. PsAMADH2 substrate channel differs only in three residues, A/W109, F/W288 and S/C453. However, substrate preference is similar for both (Tylichová *et al.*, 2010).

3.3 NRH

3.3.1 Nucleoside N-ribohydrolases

Purine and pyrimidine metabolism is essential for growth and development because nucleotides represent the building blocks of nucleic acids, major energy carrier components, essential coenzymes such as NAD^+ and alkaloid precursors and cytokinins. One of key enzymes associated with the catabolism of purines and pyrimidines (Figure 19) is a nucleoside-N-ribohydrolase (NRH), also called simply a nucleosidase (NH). It catalyzes the hydrolytic cleavage of nucleosides to corresponding bases and ribose (Figure 20A) *via* oxocarbenium intermediate. (Horenstein and Schramm, 1993)

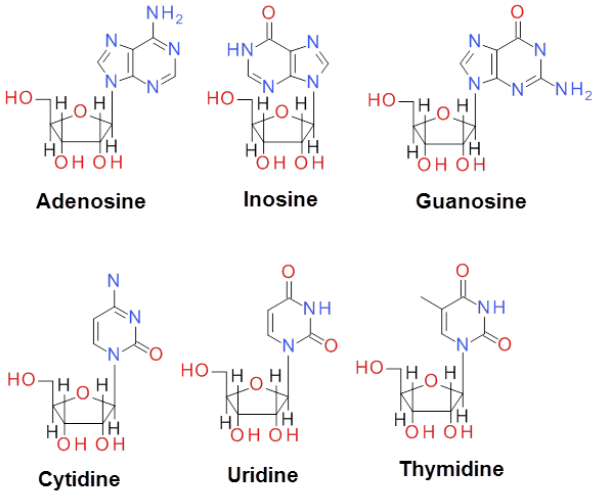

Figure 19. Purine and pyrimidine nucleosides.

NRH are widespread in nature, they are contained in bacteria (Petersen and Møller, 2001), yeast (Kurtz *et al.*, 2002), protozoans (Parkin, 1996) and in mesozoans (Versées *et al.*, 2003). Genes coding for NRH containing characteristic motif are also present in plants (Jung *et al.*, 2009) and insects (Ribeiro and Valenzuela, 2003). On the contrary, in mammals no NRHs have been found (Parkin *et al.*, 1991). NRHs have been well characterized in parasitic microorganisms as for example from *Trypanosoma*, *Leishmania*, and *Crithidia* but there is only little knowledge of their contribution in plant metabolism. These organisms rely on purine recycling (salvage pathway) because unlike most organisms they do not have the ability to synthesize *de novo* purine nucleotides. Thus, they take purine bases and nucleosides from their hosts and convert them to respective nucleotides. Parasitic NRHs have been extensively studied as a potential drug targets (Shi *et al*., 1999).

The enzymes responsible for the metabolism of nucleosides vary depending on the organism. In bacteria, ribonucleosides are predominantly metabolized by nucleoside

phosphorylases. The enzyme cleaves a nucleoside by phosphorylating the ribose-to the free base and ribose-1-phosphate. Uridine phosphorylase encoded by *udp* gene (Zalkin and Nygaard, 1996) is specific for uridine, while purine nucleoside phosphorylase, encoded by *deoD* gene (Zalkin and Nygaard, 1996), is able to catalyze the scission of all purine nucleosides except for xanthosine, which is metabolized by a xanthosine phosphorylase encoded by *xapA* gene. On the other hand, NRHs encoded by *rihA*, *rihB* and *rihC* genes have only secondary role in *E. coli* (Petersen and Moller, 2001).

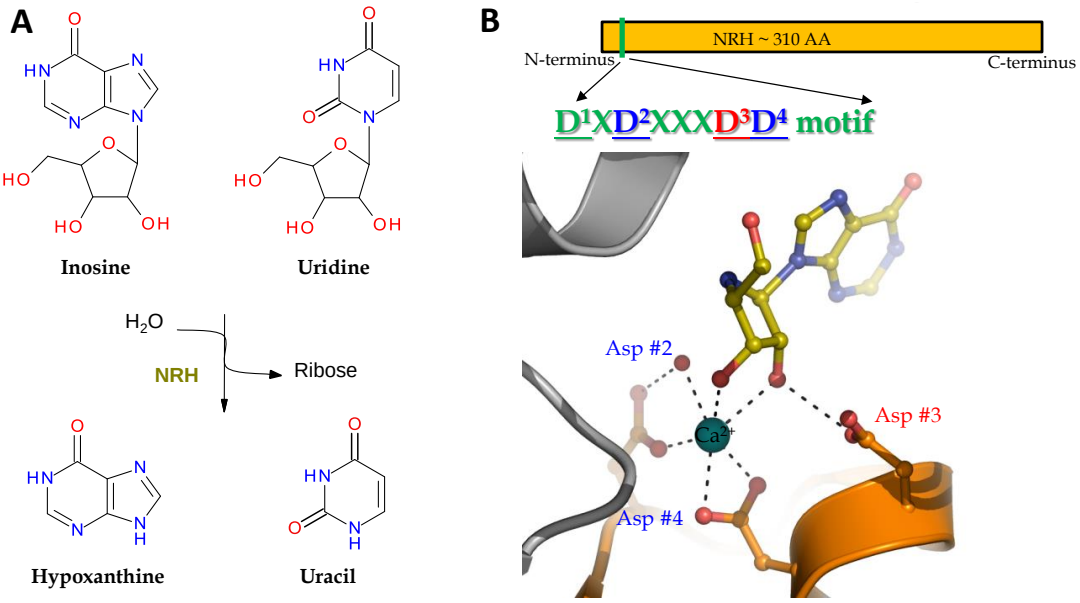

Figure 20. (A) A scheme of NRH reaction. NRHs hydrolyze *N*-glycosidic bond between the nucleobase and ribose. **(B) Active site contains 4 conserved aspartate residues.** Aspartate residues involved in calcium ion coordination are highlighted in blue and the aspartate residue binding 2-OH group of ribose is highlighted in red.

Plants contain ribosides and principle they can be either recycled or degraded. NRHs play a key role in these processes. Plant NRHs are localized in the cytosol. The distinctive feature of NRHs is the aspartate cluster sequence DXDXXXDD (Figure 20B), which is located near the N -terminus and forms the active site (Versées and Steyaert, 2003). NRHs have Ca^{2+} ion in the active site coordinated to two aspartate residues from DXDXXXDD motif. The active site is highly specific for the ribose and the substrate binds *via* the ribosyl end to calcium ion and aspartate residue (Verseés *et al.*, 2001).

NRHs are classified into four classes based on their substrate specificity: nonspecific NRHs (Shi *et al.* 1999), NRH that preferred by inosine and uridine (IU - NRHs) (Parkin *et al.*, 1991) and inosine and guanosine (IG-NRHs) (Estupiñán and Schramm, 1994) and purine-specific NRHs (Parkin *et al*, 1996) (IAG - NRHs). Dependence of nucleosidase activity on pH was determined for some of NRHs. NRH from *T. brucei* might be mentioned as an example (Parkin, 1996).

The pH profile for the inosine shows that three protonated groups contribute to full catalytic activity IAG - NRH. The loss of the proton from the most acidic group decreases V_{lim} ten times at pH 6.8 while the loss of two protons causes a complete inactivation of the IAG-NRH near pH 8.8. V_{lim} / K_m ratio shows that the catalytic activity does not change in the range of pH from 5 to 8.

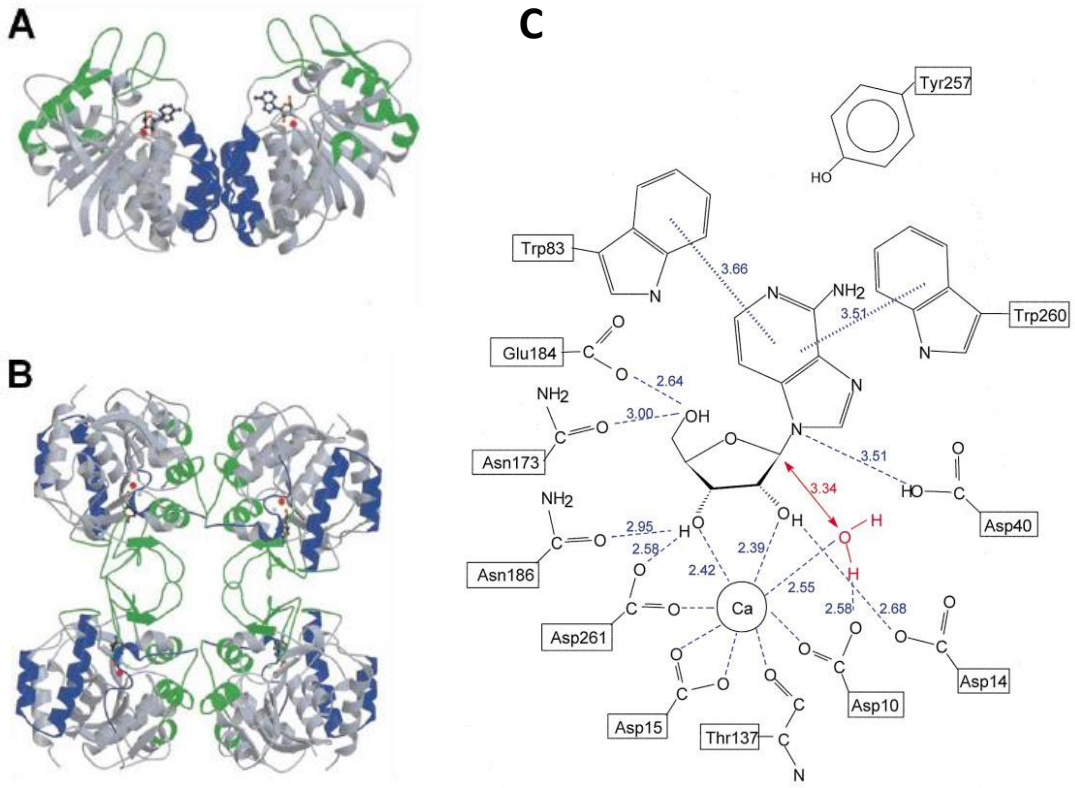

Figure 21. Comparison of quaternary structures of NRHs. (**A**) **A dimeric structure of IAG -NRH from *T. vivax*.** Those α-helices involved in subunit interactions are indicated in blue. (**B**) **Tetramer of IU-NRH from *C. fasciculata.*** The secondary structure elements involved in subunit interactions are colored in green (**C**) **Interactions in the active site of IAG-NRH from *T. vivax***. The catalytic molecule of water is indicated in red. Interactions with substrate base and residues are indicated by blue dotted lines (Verseés *et al.,* 2001).

Crystal structure of NRH is known for several microorganisms. *T. vivax* contains IAG - NRH, which has a dimeric structure (Verseés *et al.,* 2001; Figure. 21A). There are two independent active sites. The calcium ion is bound to to carboxyl group three aspartate residues at positions 10, 15 and 261 (first two aspartates belong to DXDXXXDD motif, Figure. 21C), the main chain oxygen of threonine 137, a water molecule and two –hydroxyl groups, which provides ribose of nucleoside substrate (Verseés *et al.,* 2001). IU-NRH from *C. fasciculata* has a tetrameric structure (Figure. 21B), (Degano *et al.* 1996). Tetrameric structures have also YbeK (Muzzolini *et al.,* 2006) and YeiK (Giabbai B. and Degano M., 2004) proteins from *E. coli.*

Novel insights into about catalytic mechanism provide two crystal structures of the purine-specific inosine-adenosine-guanosine NRH (IAG-NRH) and the pyrimidine-specific

cytidine-uridine NRH (CU-NRH) from archaeon *Sulfolobus solfataricus*. Both isoenzymes are tetrameric. CU-NRH carries Na^+ instead of Ca^{2+} cation in the active site (Minici *et al*., 2012).

3.3.2 Kinetic properties of NRH

NRH from *Trypanosoma brucei* (Parkin, 1996) prefer mainly inosine, adenosine and guanosine (IAG - NRH). Inosine is the best naturally occurring substrate with K_m value of 18 μM and k_{cat} of 34 s^{-1}. Similar K_m values were found for adenosine (K_m ~ 15 μM, k_{cat} ~ 18 s^{-1}) and for guanosine (K_m ~ 46 μM, k_{cat} ~ 38 s^{-1}). The rate of hydrolysis of pyrimidine ribosides uridine and cytidine was significantly lower (Parkin et al., 1996). Results obtained for *Trypanosoma vivax* showed that the best substrate was inosine (K_m ~ 5.4 μM, k_{cat} ~ 5.2 s^{-1}) followed by adenosine (K_m ~ 8.5 μM, k_{cat} ~ 1.5 s^{-1}) and guanosine (K_m ~ 3.8 μM, k_{cat} ~ 1.9 s^{-1}; Verseés *et al.*, 2001).

NRH from *L. major* has also been described. This enzyme belongs to IU-NRH class; the best substrate is uridine (K_m = 32 μM, k_{cat} = 234 s^{-1}) and inosine (K_m 445 μM, k_{cat} = 119 s^{-1}; Shi *et al.*, 1999). Two isoenzymes were found in *C. fasciculata*. IU-NRH hydrolyses inosine (K_m = 380 μM, k_{cat} = 28 s^{-1}) and uridine (K_m = 1220 μM, k_{cat} = 143 s^{-1}); the second one IG-NRH prefers inosine (K_m = 16 μM, k_{cat} = 88 s^{-1}) and guanidine (K_m = 77 μM, k_{cat} = 216 s^{-1}; Degano *et al.* 1996). IAG-NRH and CU-NRH were found in archea *S solfataricus.* The first one is similar to *T. vivax* and *T. brucei* and prefers inosine (K_m = 340 μM, k_{cat} = 12 s^{-1}), adenosine (K_m = 60 μM, k_{cat} = 1.9 s^{-1}) and guanosine (K_m = 160 μM, k_{cat} = 14.5 s^{-1}). Contrary, the latter prefers cytidine (K_m = 970 μM, k_{cat} = 9.8 s^{-1}) and uridine (K_m = 310 μM, k_{cat} = 1.8 s^{-1}) (Minici et al., 2012).

Two other NRHs were characterized from *E. coli* namely YeiK (Giabbai and Degano, 2004) and YbeK (Muzzolini *et al.*, 2006). Yeik protein was characterized as a pyrimidine riboside specific NRH. Catalytic efficiency of Yeik for inosine, adenosine and guanosine was more than a thousand times smaller than that for uridine (K_m of 142 μM, k_{cat} ~ 4.7 s^{-1}) and cytidine (K_m of 532μM, k_{cat} ~ 11.6 s^{-1}; Giabbai B. and Degano M., 2004). Conversely, YbeK protein belongs to the pyrimidine riboside specific NRHs. This enzyme hydrolyzes pyrimidine nucleosides 100-10000 times more efficiently than purine nucleosides mainly due to low K_m value of 83 μM for uridine (Muzzolini *et al.*, 2006).

Nucleosidase activity has been demonstrated in many plants such as wheat (K_m of 3.2 and 11.5 μM, V_{max} ~ 0.45 and 0.23mmol.s^{-1} mg^1 for AMP; Chen and Kristopeit, 1981), barley (adenosine nucleosidase, K_m of 0.8-2.3μM, Guranowski and Schneider, 1977), tomatoe (Burch and Stuchbury, 1986), *Camellia sinensis* (three adenosine nucleosidases; Imagawa *et al.*, 1979) and coffee plant (adenosine nucleosidase, K_m ~ 6.3μM, V_{max} ~ 9.8nkat; Campos *et al.*, 2005). Recently, NRH family from *Arabidopsis thaliana* (AtNRH1 and 2) has been characterized (Jung

et al. 2009 and 2011). AtNRH1 plays a major role in catabolism of purines and pyrimidines; AtNRH2 operates in the later stage of aging and hydrolyses inosine. (NRH from *Arabidopsis thaliana* (AtNRH1) (Jung *et al.,* 2009) prefers particularly uridine (K_m value of 0.8 mM and the value V_{lim} of 0.004 mmol s^{-1} mg^{-1}). Rate of hydrolysis of adenosine and inosine was much lower compared with uridine (V_{lim} for inosine was 0.0002 mmol s^{-1} mg^{-1}, and for adenosine only 7.7 x 10^{-6} mmol s^{-1} mg^{-1}).

4 Methods

4.1 Cloning, expression and purification

4.1.1 Maize ALDHs

The total RNA from apical meristems of 5-day-old maize seedlings (*Zea mays* var. *saccharata*) and pea seedlings (*Pisum sativum*) was extracted using the Plant RNA Isolation Aid solutions from Ambion (Austin, USA). The cDNA was synthesized using Superscript II reverse transcriptase (Invitrogen). ORFs were amplified using AccuPrime™ Pfx using gene specific primers shown in Table 2. The amplified sequences were double digested and ligated into a pCDFDuet vector (Novagen, La Jolla, CA), transformed into NEB 5 alpha *E. coli* cells (New England Biolabs, Hitchin, UK) and sequenced. Sequence data can be found in the EMBL/GenBank data libraries under accession numbers KJ004509 for ZmALDH7, KJ004510 for RF2A, KJ004511 for RF2B, KJ004512 for RF2C, KM225857 for RF2D, KM225858 for RF2E and KJ004513 for RF2F. Correct plasmids were transformed into T7 express *E. coli* cells (New England Biolabs, Hitchin, UK) for expression of N-terminal 6xHis-tagged ALDH proteins. The cells were grown in LB medium at 37 °C to an OD_{600} 0.6, then the temperature was reduced to 20 °C and gene expression was induced with 0.5 mM isopropyl-β-thiogalactopyranoside and cells were grown at 200 rpm overnight.

Table 2. Primer pairs used for the cloning of ALDHs. FP stands for forward primer, RP for reverse primer.

Gene	Primer pair
ZmALDH7	FP: 5'-CTAGAATTCGATGGGGGCCTTCGCGAAGGAG-3'
	RP: 5'-GCGCTCGAGTTAACCAAAATTGATTCCCTGGGCT-3'
PsALDH7	FP: 5'-CATGAATTCGGGTTCTGATAGCAACAATTTGGGAT-3'
	RP: 5'-AGTCTCGAGTTAGCCAAAGTTAATTCCCTGA-3'
RF2A	FP: 5'- CTCGGCTCGGAGGGCCGCGTCCTCG-3'
	RP: 5'-ATAGGTACCCTACAACCACGCGGCGTTC-3'
RF2B	FP: 5'-CAGGGATCCTGCTGCAACCGTGAGGAGGGCT-3'
	RP: 5'-ATACATATGTTACAGCCATGCGGGGTTCT-3'
RF2C	FP: 5'-CAGGAATTCTGCGACTGCGAACGGGAGCAGC-3'
	RP: 5'-ATACATATGTCAGAGCCATGGAGTGTTGTACAG-3'
RF2D	FP: 5'-CCTATGGCGAGCAACGGCTG-3'
	RP: 5'-ATACATATGTCAGTACCATGGCGAGTCCG-3'
RF2E	FP: 5'-CATGGATCCGATGGCGAGCAACGGCAACGG-3'
	RP: 5'-CATCTCGAGTCAGTACCACAGCGAGTCCGGGAGC-3'
RF2F	FP: 5'-ATTGAATTCGATGGTGAGCGAGAGCAAC-3'
	RP: 5'-ATAGGTACCAATTAAAGAGAATCAGATCCA-3'
ZmNRH3	FP: 5′-CGAGAATTCCAAGATCATCATTGACACG-3′
	RP: 5′-ATACATATGTCACGGCTTGGTGACGAGCTCC-3′

4.1.2 NRH3 from maize

Total RNA for reverse transcription was isolated from 5-day old maize seedlings (*Zea mays* var. *saccharata*) using the Plant RNA Isolation Aid solutions from Ambion (Austin, USA). The RNA was treated twice with the TURBO DNase-free kit (Ambion). The cDNA was then synthesized using the Superscript II RT (Invitrogen, Carlsbad, USA) and the RevertAid H Minus RT (Fermentas, Vilnius, Lithuania). *ZmNRH3* ORF (948 bp) was amplified using AccuPrime™ Pfx (the primers used are shown in Table 2) and submitted to GenBank (HQ825162). The plasmids were transformed into T7 express cells (New England Biolabs, Hitchin, UK). Protein expression was induced with 0.5 mM isopropyl-β-thiogalactopyranoside (IPTG), after which the cultures were incubated at 20 °C overnight.

4.1.3 Purification of ALDHs and NRHs

The cells were re-suspended in buffer A (50 mM Tris-HCl buffer, pH 8.0, 10 mM imidazole and 500 mM NaCl with protease inhibitor cocktail and disrupted on a cell lyser (One Shot model, Constant systems, UK). The lysate was cleared by centrifugation at 20,000 *g* at 4 °C for 30 min. The supernatant was filtered through a 0.22-µm membrane (Millipore) and purified on a HisPur cobalt spin columns (Thermo Fisher Scientific, Waltham, MA, USA) equilibrated with 20 mM Tris-HCl buffer pH 8.0, containing 100 mM NaCl, 10 mM imidazole and 5% glycerol. Elution was performed using 250 mM imidazole in the same buffer. Fractions containing ALDH or NRH were pooled and were further purified on a Superdex 200 HR 10/300 column (GE Healthcare), using 50 mM Tris-HCl buffer, pH 8.0, 150 mM NaCl. Fractions were analyzed by SDS-PAGE, and those containing pure and active enzyme were pooled, concentrated using Amicon Ultra-4 centrifugal filter units (10kDa, Millipore) and stored at -20 °C. The identity of the purified proteins was confirmed by peptide mass fingerprinting on a Microflex LRF20 MALDI-TOF mass spectrometer (Bruker Daltonik, Bremen, Germany) after SDS-PAGE and in-gel digestion (Šebela *et al*., 2006). The complete purification from a 400-mL culture yielded about 10 mg of recombinant ALDHs.

4.1.4 CKO1 from maize

ZmCKO1 was produced by recombinant expression in *Y. lipolytica* (secretion into the culture medium) and subsequent chromatographic purification form the supernatant of 5-day-old cultures grown in PPB medium (20 g l^{-1} sucrose, 1.32 g l^{-1} yeast extract, 1.32 g l^{-1} NH_4Cl, 0.32 g l^{-1} KH_2PO_4, 0.13 g l^{-1} $MgSO_4$ and 0.33 mg l^{-1} thiamine in 50 mM phosphate buffer, pH 6.8) as previously described (Kopečný *et al*., 2005).

4.2 Kinetic measurements

4.2.1 Substrates

Elementary aliphatic aldehydes, pyridine carboxaldehydes, BAL chloride together with APAL and ABAL diethylacetals were purchased from Sigma-Aldrich Chemie (Steinheim, Germany). DMSPAL and diethylacetals of 4-amino-2-hydroxybutyraldehyde (AHBAL), 4-guanidinobutyraldehyde (GBAL), 4-guanidino-2-hydroxybutyraldehyde (GHBAL) and 3-guanidinopropionaldehyde (GPAL) were all synthetic preparations (Šebela *et al*., 2006). Diethyl acetal iodides of *N*,*N*,*N*-trimethyl-3-aminopropionaldehyde (TMAPAL) and TMABAL were synthesized according to a protocol described for the latter compound (Šebela *et al*., 2000). 3-Acetamidopropionaldehyde (ACAPAL) diethylacetal was synthesized as described (Vaz *et al*., 2000). If necessary, free aminoaldehydes were prepared by heating their acetals in a plugged test tube with 0.2 M HCl for 10 min (Trossat *et al*., 1997). NAD^+ and NAD^+ analogs were purchased from Sigma-Aldrich. Purine and pyrimidine ribosides were purchased from Sigma-Aldrich Chemie (Steinheim, Germany). Cytokinin substrates were obtained from OlChemIm (Olomouc, Czech Republic)

Kinetic constants were determined GraphPad Prism 5.0 data analysis software (GraphPad Software, Inc., La Jolla, CA, USA). In those cases where no substrate inhibition was observed, the data were fitted to the Michaelis-Menten equation. The data were analyzed by a nonlinear regression using the Michaelis-Menten equation that includes terms in the numerator and denominator to account for partial substrate inhibition (Holt *et al*., 2007),

$V = V_{lim} . [S]/(K_m .(1/1+ \beta. [S]/K_i)) + [S].((1+ [S]/K_i)/1 + \beta. [S]/K_i))$

where v represents the determined initial velocity, V_{lim} is the maximal velocity, [S] is the concentration of the substrate, K_m is the substrate concentration at half-maximal velocity, K_i is the substrate inhibition constant, and β is the factor that describes the effect of substrate inhibition on V_{max}.

4.2.2 Activity measurement of ALDH10 family (AMADH)

Activity was measured spectrophotometrically by monitoring the formation of NADH (ε_{340} = 6.62 mM^{-1} cm^{-1}) at 37 °C. The reaction mixture in a cuvette contained 0.15 M Tris-HCl buffer, pH 9.0, 1 mM NAD^+ and enzyme. The enzyme reaction was started by the addition of APAL (or another aminoaldehyde) at a final 1 mM concentration. Accurate aldehyde concentration was verified spectrophotometrically by the complete conversion of supposed 20 μM aldehyde using excess of enzyme and supposed release of 20 μM NADH. This amount corresponds to the absorbance change of 0.1324. Proteins were determined by Bradford method.

4.2.3 Activity measurement of ALDH2 family

Activity was measured by monitoring the NADH formation (ε_{340} = 6.62 mM^{-1} cm^{-1}) at 37 °C on UV-Vis spectrophotometer 8453 (Agilent, Santa Clara, CA, USA). The reaction mixture in a cuvette contained 100 mM Tris-HCl buffer, pH 8.0, 0.5 mM NAD^+ and ALDH2. The enzyme reaction was started by the addition of hexanal or other aldehyde at a final 1 mM concentration. Accurate aldehyde concentration was again verified as above. Proteins were determined by Bradford method.

4.2.4 Activity measurement of ALDH7 family

Activity was measured by monitoring the NADH formation (ε_{340} = 6.62 mM^{-1} cm^{-1}) at 37 °C on UV-Vis spectrophotometer 8453 (Agilent, Santa Clara, CA, USA). The reaction mixture in a cuvette contained 100 mM sodium pyrophosphate buffer, pH 8.0, 2.0 mM NAD^+ and appropriate amounts of ALDH7 enzyme. The enzyme reaction was started by the addition of AASAL or other aldehyde at a final 1.5 mM concentration. Accurate aldehyde concentration was again verified as above. Proteins were determined by Bradford method.

4.2.5 NAD^+ analogs and pH optima

The following absorption maxima and extinction coefficients of reduced forms of these analogs were used for calculations: NADPH (ε_{340} = 6.62 mM^{-1} cm^{-1}), thio-NADH (ε_{400} = 11.9 $mM^{-1}cm^{-1}$), 3-pyridinealdehyde-NADH (ε_{358} = 9.3 $mM^{-1}cm^{-1}$), 3-acetylpyridine-NADH (ε_{363} = 9.1 $mM^{-1}cm^{-1}$), deamino NADH (ε_{338} = 6.2 $mM^{-1}cm^{-1}$). NAD^+ analogs were assayed at 0.5mM concentration with 1 mM APAL as described previously for AMADH (Tylichová *et al.*, 2010), at 1 mM analog concentration and 1 mM AASAL for ALDH7 and 1 mM hexanal for ALDH2. 150 mM Tris-HCl buffers in the pH range from 7.0 to 9.0 and 150 mM glycine-NaOH buffers in the pH range from 8.8 to 10.6 or Britton-Robinson buffers from 5.6 to 9.6 were used to determine pH optima using 1 mM APAL and 0.5 mM NAD^+ for AMADH; 2 mM NAD^+ and 1 mM AASAL for ALDH7; 1 mM NAD^+ and 1 mM hexanal for ALDH2.

4.2.6 Activity measurement of NRH

The NRH activity was measured spectrophotometrically at 30 °C according to a method described by Parkin (1996). The reaction was performed in 200 mM Tris-HCl buffer, pH 7.5, 400 mM KCl, 1 mM DTT, 200 μM riboside substrate and enzyme. Kinetic constants were determined by monitoring the absorption decrease of adenosine ($\Delta\varepsilon_{276}$ = -1.4 mM^{-1} cm^{-1}), inosine ($\Delta\varepsilon_{280}$ = -0.92 mM^{-1} cm^{-1}), uridine ($\Delta\varepsilon_{280}$ = -1.8 mM^{-1} cm^{-1}), cytidine ($\Delta\varepsilon_{280}$ = -3.42 mM^{-1} cm^{-1}) and thymidine ($\Delta\varepsilon_{265}$ = -1.7 mM^{-1} cm^{-1}) (Parkin, 1996). The differential extinction coefficients for xanthosine and guanosine were determined to be $\Delta\varepsilon_{248}$ = -3.7 mM^{-1} cm^{-1} and

$\Delta\varepsilon_{253}$ = -4.1 mM^{-1} cm^{-1}, respectively. Similarly, $\Delta\varepsilon_{289}$ values of -1.37 mM^{-1} cm^{-1} and -1.48 mM^{-1} cm^{-1} were determined for iPR and trans-zeatin riboside (*t*ZR), respectively. Proteins were determined by Bradford method.

4.2.7 CKO activity measurement

CKO activity was measured by DCPIP method (Bilyeu *et al*., 2001). The reaction was performed in a total volume of 1 ml at 30 ° C and contained 100 mM phosphate buffer, pH 7.0, 1 mM EDTA, 50 μM DCPIP, beef serum albumin (BSA, 1 mg mL^{-1}) and enzyme. The reaction was started adding the cytokinin substrate (iP) in the range of 1-100 μM. DCPIP reduction rate was monitored at 600 nm at 10 second intervals after addition of substrate. iP was dissolved in DMSO as a 100 mM stock solution. Accurate determination of iP concentration was performed spectrophotometrically using the extinction coefficient of ε_{270nm} = 19400 $M^{-1}cm^{-1}$. Aminophenol method (Frébort *et al*., 2002) was used for measurements with different electron acceptors. The method is based on the interaction of released aldehyde 3-methyl-2-butenal with 4-aminophenol under acidic conditions. Schiff base is formed and absorbs at 352 nm. The reaction mixture contained the enzyme on a suitable concentration, substrate (iP) and electron acceptors (0.5 mM DCPIP, 0.5 mM coenzyme Q_0, 0.5 mM 1,4-naphthoquinone and PMS) in 0.4M Tris-HCl buffer, pH8.5, for DCPIP and PMS or 0.4 M imidazole, pH 6.5, for Q_0 and 1,4-naphthoquinone. The mixture was incubated at 37 ° C for 30-50 minutes and then the reaction was stopped by adding 0.3 ml of 40% trichloroacetic acid. The mixture was centrifuged at 12000 g, for 5 min and then 0.2 ml of 2% of 4-aminophenol was added and spectra were measured at 352 nm. Protein content was estimated using a colorimetric assay with bicinchoninic acid; BSA served as a standard (Smith *et al*., 1985).

4.3 Enzymatic deglycosylation of ZmCKO1

Recombinant endoglycosidase H from *Streptomyces plicatus* was obtained from Sigma-Aldrich for deglycosylation experiments. The enzyme is supplied as a buffered aqueous solution. A total volume of 150 μl in the vial represents 1 activity unit, which is defined as an amount releasing N-glycans from 60 μmol of ribonuclease B per hour at 37 °C and pH 5.5. Three different protocols were followed in a comparative experiment: 1) the glycoprotein of 200 μg was denatured in 42.5 μl of 50 mM K-phosphate buffer, pH 5.5, containing 1% SDS and 60 mM 2-mercaptoethanol by heating at 100 °C for 5 min followed by the addition of 15% Triton X-100 (2.5 μl) and endoglycosidase H (1 μl–6.7 milliunits); the reaction mixture was then incubated at 37 °C for 3 h; 2) the same protocol was followed with omitting the denaturation step; the deglycosylation reaction proceeded at 37 °C for 3 h; 3) the denaturation step was

omitted as well; the deglycosylation reaction proceeded at 23 °C overnight. The deglycosylated samples were subjected to ultrafiltration on a 10-kDa Microcon centrifugal filter device (Millipore, Bedford, MA, USA) and the N-glycans recovered in the filtrate were purified on graphitized carbon essentially as described (Packer *et al*., 1998).

Thermostability of the enzyme was evaluated by monitoring the changes in activity upon incubating enzyme aliquots (in the assay buffer, pH7.0) at temperatures from 25 °C up to 70 °C for 30 min, followed by rapid cooling in water-ice bath.

4.4 SDS-PAGE

SDS-PAGE was performed using 4% stacking and 10% resolving polyacrylamide gels and the separated proteins were visualized by the Bio-Safe Coomasie Stain (Bio-Rad, Hercules, California, USA). The protein marker was the Protein Ladder 10-250 kDa (NEB). Eventually, in-gel tryptic digestion followed according to Shevchenko *et al*. 2006.

4.5 qPCR analysis

The total RNA from up to 2 week--old and 2 month-old maize plants was isolated using the RNAqueous kit and Plant RNA Isolation Aid solutions from Ambion (Austin, TX, USA) and treated twice by TURBO DNase-free kit (Ambion). First-strand cDNA was synthesized by RevertAid H Minus Moloney murine leukemia virus reverse transcriptase and oligo(dT) primers (Fermentas, Vilnius, Lithuania). RNA from every biological replicate was at least transcribed in two independent reactions. Diluted cDNA samples were used as templates in real-time PCRs containing TaqMan Gene Expression Master Mix (Applied Biosystems, USA), both primers at 300 nM concentrations and 250 nM TaqMan 6-FAM TAMRA probe on a StepOne-Plus Real-Time PCR System using a default program (Applied Biosystems). The TaqMan probes together with the corresponding primers were designed by Applied Biosystems customer service (Table 3). Plasmid DNA carrying ORF of respective maize *ALDH2*, *ALDH7* or *ALDH10* gene was used as a template for calibration curve to determine the PCR efficiencies of designed probes and primer pairs as well as to verify their specificity. Cycle threshold values were normalized with respect to elongation factor 1α and β-actin genes and amplification efficiency. Expression values were determined and statistically evaluated using the DataAssist v3.0 Software package (Life Technologies).

Table 3. Primer pairs used for the cloning of ALDHs and primer pairs with TaqMan probes used for qPCR. FP stands for forward primer, RP for reverse primer.

Gene	Primer pair
ZmALDH7	FP: 5'-TGTTCGCTGCTGTTGGTACAG-3'
	RP: 5'-CAACAAGCTGATCAAGGAAGGTT-3'
	Probe: 5´-FAM-CGCTGCACTACATGTCGTAGGCTGATTCTT-TAMRA-3'
RF2A	FP: 5'-CAGGACAGTGCCTGCAGATG-3'
	RP: 5'-TGCTGCTGCAGTGCTGAAC-3'
	Probe: 5'-FAM-CACAGGCTGTTGCCAGGTGTCCTTC-TAMRA-3'
RF2B	FP: 5'-TGTACGACGAGTTCGTGGAGAA-3'
	RP: 5'-ACTGGACGTACCGCAAGATCTT-3'
	Probe: 5'-FAM-CGTCGTCGGCGACCCCTTCA-TAMRA-3'
RF2C	FP: 5'-CTCCCGTCATCGTCTTCGA-3'
	RP: 5'-CTCGCCCTTGTTGGTGTAGGT-3'
	Probe: 5'-FAM-ACCTCGACATGGCCGTTAACCTCGT-TAMRA-3'
RF2D	FP: 5'-TGTGGTGGTACCGGAGATCA-3'
	RP: 5'-ATCAGCTTTGTCTGCCTCTGCTA-3'
	Probe: 5'-FAM-CGCCTCCGGCAAGACATTCGATAC -TAMRA-3'
RF2E	FP: 5'-CGCAGAACTGGAAGGTTGGA-3'
	RP: 5'-CCTCTCAAACTGGTCCTTGTCAA-3'
	Probe: 5'-FAM-TCACGAGCAACATGGGTCCGCA-TAMRA-3'
RF2F	FP: 5'-TCCGGAAGGGAAAGGCTACT-3'
	RP: 5'-CACATGACGGGTCCGAAGAT-3'
	Probe: 5'-FAM-TTCACCAACGTCAAGGAGGACATGATCA-TAMRA-3'
ZmAMADH1a	FP: 5'-CCAGAGGTTATCTGAGGAGATTGAC-3'
	RP: 5'-CCAAATCCACTGCGCTTGTT-3'
	Probe: 5'-FAM-TGGGTAAACTGCTCGCAACCCTGC-TAMRA-3'
ZmAMADH1b	FP: 5'-TGAGCGCTGCCAGAGATTATC-3'
	RP: 5'-AGCAGGGCTGTGAGCAGTTT-3'
	Probe: 5'-FAM-ATGCTGGAATTATCTGGG-TAMRA-3'
ZmAMADH2	FP: 5'-AGGTGTGAGCGCATTTCAAAG-3'
	RP: 5'-AAAACCGCTCCGCTTGTTC-3'
	Probe: 5'-FAM-TTCCCAACCATGCTTCGTTCAAGCTC-TAMRA-3'
β actin	FP: 5´-CGACAACCTGATGAAGATCCTTACT-3´
	FP: 5´-TCGCTCGGCAGTCGTA-3´
	Probe: 5´-GCAACGTAGGCAAGTTTTTCCTT-3´
EF1α	FP: 5'-TGATACCCACCAAGCCTATGGT-3'
	FP: 5'-AGACATTCTCCGCGTTTCCTCCCCT-3'
	Probe: 5'-CATGTCGCGGACAGCAAAC-3'

4.6 Size exclusion chromatography

Size exclusion chromatography was performed on a Superdex 200 HR (10/30) column or a Superdex 200 prep grade 26/600 column (GE Healthcare) linked to a BioLogic Duo Flow liquid chromatograph (Bio-Rad) to determine the molecular weight of studied enzymes. The column was equilibrated with 50 mM potassium phosphate buffer, pH 7.5 and containing 150 mM NaCl at a flow rate of 0.7 ml min^{-1}. Protein standards (MW-GF-1000) were from Sigma and contained seven proteins with Mr in the range from 29 to 2000 kDa.

4.7 Crystallization and data collection

Crystallization conditions were screened using commercial kits Classics, PEGs II, and JCSG I suites from Qiagen and Crystal screen I and II from Hampton Research in sitting-drops using a Cartesian nanodrop robot (Genomic Solutions) or in hanging drops during manual optimization procedure.

ZmAMADH1a with 5mM NAD^+ was crystallized over reservoirs containing 16% PEG 4000, 0.1 M HEPES, pH 7.5, and 10% isopropyl alcohol. Crystals were transferred to a cryoprotectant solution and flash-frozen in liquid nitrogen (Kopečný *et al*., 2013). Crystals of RF2C were obtained in hanging drops by mixing equal volumes of protein solution and a precipitant solution containing 30 % (*w/v*) PEG 400, 100 mM $CaCl_2$ and 100 mM sodium acetate pH 4.5. Crystals of RF2F were obtained by mixing equal volumes of protein solution and a precipitant solution containing 35% MPD, 100mM MES pH 6.5, 15% (*w/v*) PEG 4000. Crystals of ZmALDH7 were obtained by mixing equal volumes of protein solution and a precipitant solution containing 40 % MPD, 200 mM ammonium phosphate (Končitíková *et al*., 2015). ZmNRH3 crystals were obtained in hanging drops by mixing equal volumes of protein solution and a precipitant solution containing 50 mM Tris-HCl pH 8.0, 150 mM NaCl and 20% (*w/v*) PEG 2000 MME (Kopečná *et al*., 2013). Crystals of ZmCKO2 were grown in 100 mM sodium citrate pH 5.6, 20% 2-propanol and 20% PEG 4000. ZmCKO4a in the presence of 3 mM CPPU was crystallized in either 22% ethylene-glycol or 100 mM HEPES pH 7.5 and 50% MPD. ZmCKO4a was co-crystallized with a trifluoromethoxy derivative of TDZ 1-[1,2,3]thiadiazol-5-yl-3-(3-trifluoromethoxy-phenyl)-urea (3FMTDZ) in drops containing 100 mM HEPES pH 7.5, 80% MPD, 0.16 mM ZmCKO4 and 10 mM 3FMOTDZ in DMSO. Regarding UR15, the crystals of ZmCKO4 were grown in 22% ethylene-glycol and then they were infiltrated by 5 mM HETDZ in DMSO for 1 hour. Crystals were transferred to a cryoprotectant solution (the mother liquor supplemented with 25 % PEG 400 or glycerol) and flash frozen in liquid nitrogen. Diffraction data were collected at 100 K on the PROXIMA 1 and 2 beamlines (SOLEIL Synchrotron, Saint-Aubin, France). Diffraction intensities were integrated with the program XDS (Kabsch, 2010).

Diffraction data for ZmAMADH1a, RF2C, RF2F and ZmALDH7 were collected at resolutions of 1.95, 2.25, 2.40 and 2.80 Å, respectively. Diffraction data for the ZmNRH3 crystals were collected at resolutions of 2.49 Å. All structures were solved by molecular replacement with MOLREP (Vagin and Teplyakov 2010) or Phaser (Storoni *et al.*, 2004) using the monomer of human ALDH2 (PDB 1CW3 and 1O05) and of seabream ALDH7 (PDB 2JG7) as search models in case of RF2C, RF2F and ZmALDH7, using the coordinates of the YbeK monomer (PDB 1YOE) in case of ZmNRH3 and using the coordinates of ZmCKO1 (PDB 1W1O) in case of ZmCKO2 and ZmCKO4. The two different space group structures of ZmCKO2 (at 2.04 and 2.7 Å) and the two different space group structures of ZmCKO4 with CPPU (at 1.75 and 1.9 Å) were refined. Complexes of ZmCKO4-3FMOTDZ and ZmCKO4-HETDZ were both resolved at 2.05 Å resolution. All structures were refined using BUSTER-TNT with autoncs and TLS options (Blanc *et al*., 2004). Electron density maps were evaluated using COOT (Emsley and Cowtan, 2004). Molecular graphics images were generated using PYMOL (www.pymol.org).

5 Results and discussion

5.1 List of publications

Results are divided into 3 sections in line with aims of the work and with the enzyme group that was studied:

1. Cytokinin oxidase/dehydrogenase
    - Franc V, Šebela M, Řehulka P, **Končitíková R**, Lenobel R, Madzak C, Kopečný D. (2012) Analysis of N-glycosylation in maize cytokinin oxidase/dehydrogenase 1 using a manual microgradient chromatographic separation coupled offline to MALDI-TOF/TOF mass spectrometry. *J Proteomics* 75(13): 4027-37. [**5.07 Impact Factor**]
    - Kopečný D*, **Končitíková R***, Popelková H, Briozzo P, Vigouroux A, Šebela M, Kopečná M, Zalabák D, Frébort I, Moréra S. (2015) Kinetic and structural investigation of the cytokinin oxidase/dehydrogenase active site by site directed-mutagenesis. *authors contributed equally to this work. Manuscript
    - Nisler J, **Končitíková R,** Zatloukal M, Kopečný D, Bazgier V, Berka K, Zalabák D, Briozzo P, Strnad M, Spíchal L (2015) Novel thidiazuron-derived inhibitors of cytokinin oxidase/dehydrogenase. Manuscript

2. Aldehyde dehydrogenase
    - **Končitíková R,** Vigouroux A, Kopečná M, Andree T, Bartoš J, Šebela M, Moréra S, Kopečný D (2015) Role and structural characterization of plant aldehyde dehydrogenases from family 2 and family 7. *Biochem J.* 468(1): 109-23. [**4.78 Impact Factor**]
    - Kopečný D*, **Končitíková R***, Tylichová M, Vigouroux A, Moskalíková H, Soural M, Šebela M, Moréra S. (2013) Plant ALDH10 family: identifying critical residues for substrate specificity and trapping a thiohemiacetal intermediate. *J Biol. Chem*. 288(13): 9491-507. [**4.60 Impact Factor**] *authors contributed equally to this work

3. Nucleoside-N-ribohydrolase
    - Kopečná M, Blaschke H, Kopečný D, Vigouroux A, **Končitíková R**, Novák O, Kotland O, Strnad M, Moréra S, von Schwartzenberg K. (2013) Structure and function of nucleoside hydrolases from Physcomitrella patens and maize catalyzing the hydrolysis of purine, pyrimidine, and cytokinin ribosides. *Plant Physiol*. 163(4): 1568-83. [**7.39 Impact Factor**]

5.2 Cytokinin oxidase/ dehydrogenase

5.2.1 Role of glycosylation in ZmCKO1

The results of this chapter are published in Franc *et al*., 2012. My contribution in this publication was a purification and preparation of the deglycosylated recombinant ZmCKO1 and all kinetics experiment.

Amino acid sequences of several CKOs clearly demonstrate the presence of one to eight *N*-glycosylation sites (Schmulling *et al*., 2003). The glycosylation of ZmCKO1 was also proved by electrophoretic migration and estimated molecular mass was significantly higher than expected from sequence-based calculations (Houba-Hérin *et al*., 1999; Morris *et al*., 1999; Kopečný *et al*., 2005). According to published crystal structures, six of predicted *N*-glycosylation sites comprising N63, N89, N134, N294, N323 and N338 residues may be occupied by glycans (Kopečný *et al*., 2010; Malito *et al*., 2004). Effect of glycosylation was investigated by activity assays with N^6-isopentenyladenine (iP) as a substrate. Figure 22 represents a comparison between the glycosylated and deglycosylated ZmCKO1 in terms of saturation curves and thermostability. Although determined K_m values were similar for both variants, there is no visible substrate inhibition for the deglycosylated ZmCKO1. Deglycosylation treatment might obviously cause a mild structural change at the entrance of the active site.

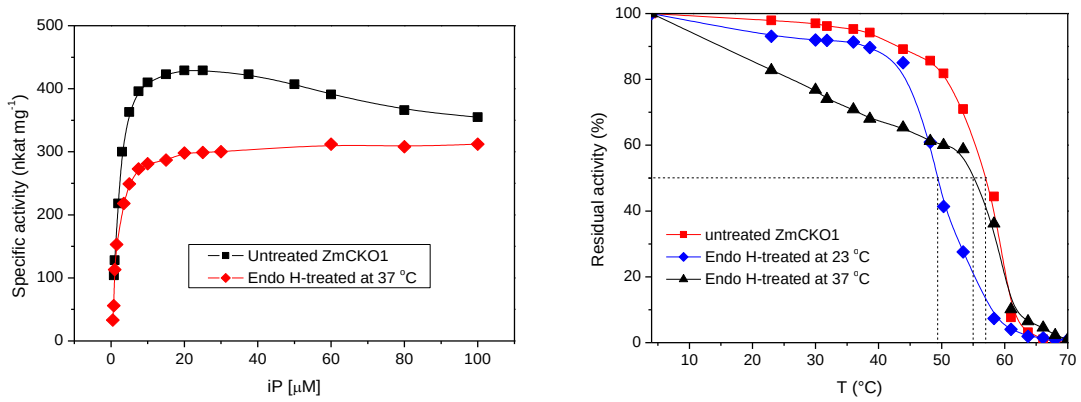

Figure 22. Left panel: Michaelis-Menten kinetics of the glycosylated (black colored curve) and the deglycosylated (colored red) ZmCKO1. Right panel: Thermostability of glycosylated (colored in red) and endoglycosidase H-treated ZmCKO1 (black and blue colored).

The thermostability of ZmCKO1 was analyzed by incubating aliquots at the temperature form 25 °C to 70 °C. The observed T_{50} value was 57 °C for untreated enzyme. After the deglycosylation step at 23 °C overnight, T_{50} value changed to 49 °C. Non-typical sigmoid curve was ascertained for recombinant ZmCKO1 deglycosylated at 37°C overnight with T_{50} value of

55 °C. Nevertheless, there is a significantly weaker activity between 20 - 50 °C in comparison with untreated enzyme. The kinetic experiments illustrate that the loss of N-glycosylation resulted in a destabilization of ZmCKO1 tertiary structure without any strong effect on the enzyme activity.

5.2.2 Role of E381 - structures of ZmCKO2 and ZmCKO4a

The results of this chapter are part of submitted manuscript Kopečný *et al*. My contribution in this publication was a crystallization of ZmCKO2 and ZmCKO4a together with kinetic measurements of the isoforms and ZmCKO1 mutants.

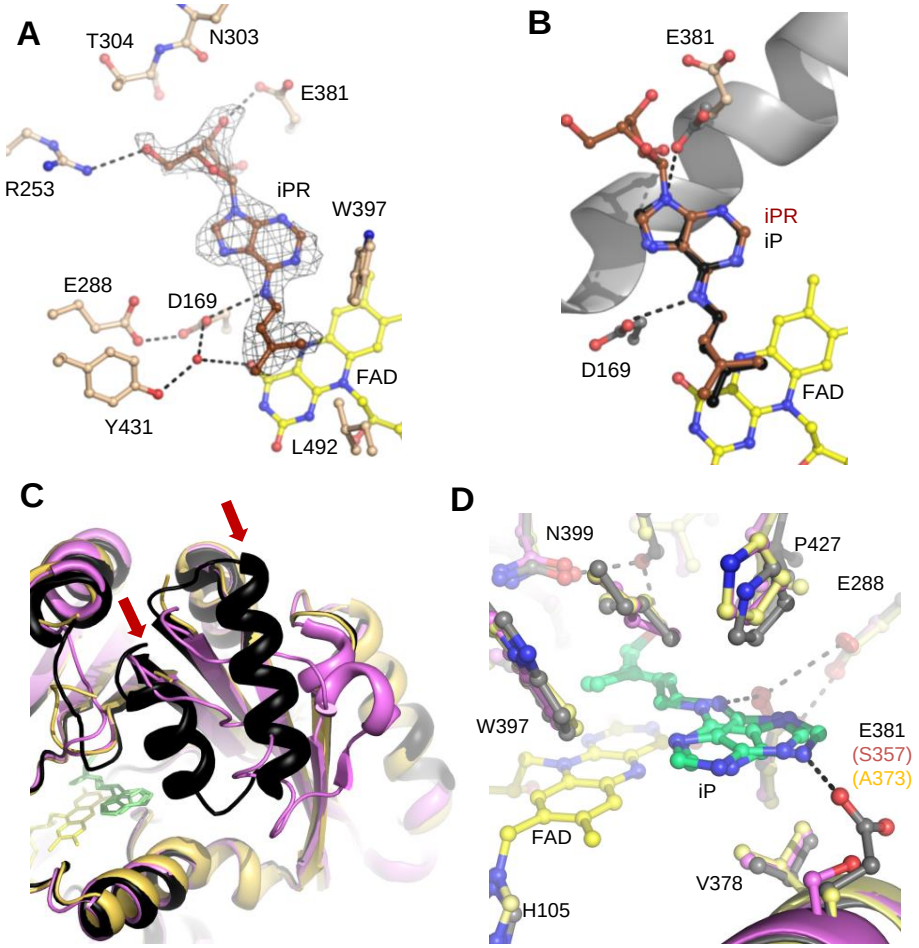

Figure 23. Binding of cytokinin ribosides in ZmCKO1 active site (A) WT ZmCKO1 structure. iPR (in brown) is shown in its Fo-Fc omit map contoured at 2.5 σ. Side-chain residues are in grey and labeled. FAD cofactor is shown in yellow and hydrogen bonds as dashed lines **(B)** Superposition of bound cytokinin base (iP, PDB 1W1Q, 15) and cytokinin riboside (iPR, PDB 3S1C, manuscript CKO) over the FAD cofactor. E381 in both structures is indicated by the respective color corresponding to the color of cytokinin substrate. **(C) Superposition of substrate binding domains between ZmCKO1 (in black), ZmCKO2 (in magenta) and ZmCKO4a (in sand yellow).** The helix-loop-helix region from residues 294 to 325 in ZmCKO1 (shown with red arrows) adopts a different conformation in ZmCKO2 and is disordered in ZmCKO4. **(D) Comparison of residues located at the active-site entrance in ZmCKO1 (in black), ZmCKO2 (in magenta) and ZmCKO4a (in sand yellow).**

Nonconserved residue E381 is present in half of known CKO sequences and participates in binding of the N9 atom of the cytokinin substrate. Presence of E381 residue in WT leads in higher K_m values for cytokinin ribosides and nearly no activity with cytokinin glucosides (iP9G and *t*Z9G). E381A and E381S mutants are highly active with all tested substrates including cytokinin glucosides such as N^6-isopentenyladenine-9-glucoside (iP9G) and *trans*-zeatin-9-glucoside (*t*Z9G). Crystal structures in complex with iPR could help to understand the contribution of E381 in cytokinin riboside binding (Figure 23A, 23B).

The isopentenyladenine moiety of the bound iPR superimposes the bound iP but due to the presence of the ribose, the side chain of E381, which can no longer form a hydrogen bond with the free N9 atom of the adenine ring, moves away and thus liberates room for the ribose. It should be noted that the E381 side chain is not well defined in the electron density map and is thus highly mobile. However, we can infer an interaction between the ribose and the E381 side chain. The ribose 5-hydroxyl group interacts with the R253 side chain and both 3- and 5-OH groups are in close contact with the main chain carbonyl of N303 and T304 (between 3.4-3.8 Å). Replacement of E381 by a serine and an alanine results in an enlargement of the entrance of the active site and allows binding bulkier substrates including cytokinin ribosides and glucosides. As evidenced K_m values of both E381 variant for iP9G, which are four times lower compared with WT. Therefore, a kinetic analysis was performed with four ZmCKO isoforms - ZmCKO2 and 3 having a serine and ZmCKO4a and ZmCKO4b possessing an alanine at the equivalent position of E381. All four ZmCKO isoforms exhibit similar K_m values for tested substrates as E381A/S mutants and show higher activities with cytokinin glucosides compared with ZmCKO1 (Figure 24).

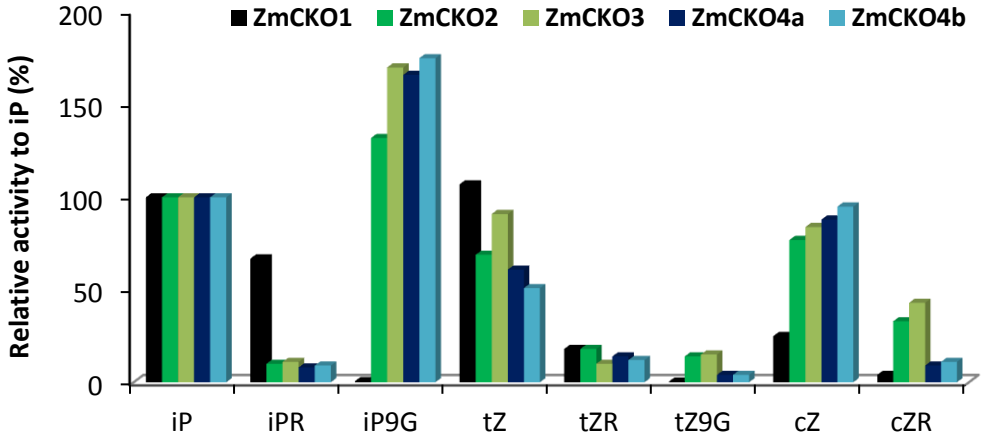

Figure 24. Relative activities of five maize CKOs with natural substrates. Relative activities were obtained with 30 μM substrates and DCPIP as an electron acceptor (29) in 100 mM phosphate buffer, pH 7.0.

Crystal structures of ZmCKO4a and ZmCKO2 were solved, in two different space groups for each (Table 4 and Figure 23) to explain differences in substrate specificity including high rates with iP9G. The structures of ZmCKO2 and ZmCKO4a are very similar to that of ZmCKO1 with RMSD values of 1.2 Å (428 Cα atoms) and 1.1 Å (423 Cα atoms) respectively. The major difference concerns the residues region 294-325, composed of two helices and a loop, belonging to the substrate binding domain. This region, which is well defined in ZmCKO1 structure, is disordered in the high resolution structures of ZmCKO4a and ZmCKO2 and adopts a different conformation in the low resolution structure of ZmCKO2 (Figure 23A). The region delineating the substrate entrance comprises residues surrounding the ribose moiety of cytokinin substrate (N303 and T304 in ZmCKO1) and is most likely responsible for the kinetic differences between E381 variants and ZmCKO isoforms. Despite several attempts, we unfortunately did not succeed in obtaining a crystal structure of ZmCKO2 and ZmCKO4a in complex with iP9G. All known intracellular CKOs contain valine or serine at E381 position and some of them have recently been shown to oxidize iP9G and *t*Z9G in agreement with our data. Thus, the substrate specificity of CKOs appears related to their subcellular localization and corresponds to the presumed occurrence of particular cytokinin derivatives within intracellular compartments.

Table 4. Data collection and refinement statistics. Numbers in parentheses represent values in the highest resolution shell

	ZmCKO1 + iPR	**ZmCKO2**	**ZmCKO2**	**ZmCKO4a + CPPU**	**ZmCKO4a + CPPU**	**ZmCKO4a +** 3FMTDZ	**ZmCKO4a + UR15**
Space group	C2	$C222_1$	C2	$P4_32_12$	$C222_1$	$P4_32_12$	$P4_32_12$
Asymmetric unit	monomer	2 monomers	4 monomers	monomer	2 monomers	monomer	monomer
Unit cell (Å)							
a	251.0	75.7	183.2	74.5	112.7	79.7	74.5
b	50.6	181.9	76.7	74.5	112.6	79.7	74.5
c	51.4	197.0	201.0	208.3	203.0	203.7	208.1
α, β, γ (°)	90.0 (β=94.0)	90.0	90.0 (β=92.1)	90.0	90.0	90.0	90.0
Resolution (Å)	32.5-2.10	23.6-2.04	38.4-2.70	42.7-1.75	1.90	50.0-2.00	47.0-2.00
Completeness (%)	91.1 (97.5)	99.2 (95.1)	99.6 (98.9)	97.5 (98.9)	99.7 (98.6)	99.7 (98.6)	99.6 (97.6)
$I/\sigma(I)$	16.9 (4.7)	14.0 (1.6)	9.8 (1.6)	13.1 (1.3)	11.4 (1.4)	14.7 (1.4)	22.9 (1.6)
$CC_{1/2}$ [b]	5.8 (33.7)	8.6 (113.3)	11.1 (75.5)	7.1 (101)	13.0 (131)	99.9 (59.8)	100.0 (73.3)
R_{sym} (%)	-	99.9 (79.7)	99.5 (65.0)	99.9 (84.3)	99.8 (59.8)	8.6 (152.2)	7.8 (123.7)
R_{cryst} (%)	21.3	18.2	18.1	18.7	20.7	18.3	20.1
R_{free} (%)	25.2	20.4	20.6	20.7	21.8	20.8	22.4
RMSD bond lengths (Å)	0.01	0.01	0.01	0.01	0.01	0.010	0.010
RMSD bond angles (°)	1.08	1.07	1.10	1.00	1.00	0.99	1.02

5.2.3 Reaction mechanism

Previous X-ray analyses revealed that upon binding, substrates seal the tunnel that leads to the catalytic site, leaving no space for electron acceptor entry except for the oxygen (Malito *et al*., 2004) and discourage previously proposed mechanism involving the formation of a ternary complex based on the measurements of enzyme kinetics with Q_0 (Frébortová *et al*., 2004). When the ping-pong (double displacement) mechanism is considered, any electron

acceptor might access the $FADH_2$ through the substrate tunnel after the imine intermediate release.

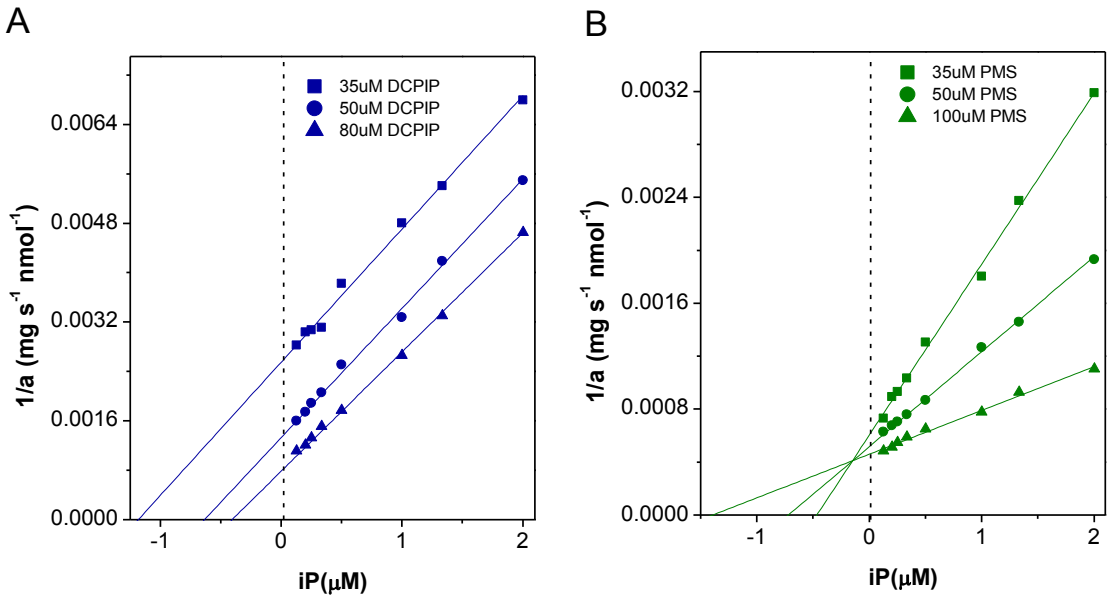

Figure 25. Double-reciprocal plots of ZmCKO1 activity with DCPIP (A) and PMS (B) and varying substrate concentration. Measurements were performed in triplicate in two independent runs with DCPIP and PMS as electron acceptors with varying concentration of iP (0.5-20 μM). Data were measured by aminophenol method (Frébort *et al.*, 2002) in 75 mM Tris-HCl, pH 8.0 (for DCPIP and PMS). In all cases, samples were measured at each concentration against the blank containing the electron acceptor at respective concentration.

We investigated the type of mechanism used for the two synthetic electron acceptors DCPIP and PMS. Initial rates were plotted as a function of concentrations of cytokinin and electron acceptor (Figure 25). Data clearly show that the DCPIP-catalyzed reaction follows a double displacement (ping-pong mechanism) while that with PMS follows a single displacement meaning that PMS forms a ternary complex with the enzyme and the cytokinin substrate. The difference in mechanisms may explain high versatility of PMS for various mutants (Kopečný *et al*., manuscript). The activity comparison between the WT and mutants is significant because use of both electron acceptors results in similar kinetic parameters for the same cytokinin substrates, even if the catalytic mechanism and binding mode of DCPIP and PMS seem different.

5.2.4 Novel thidiazuron-derived inhibitors of CKO

The results of this chapter are part of submitted manuscript Niesler *et al*. My contribution in this publication was a crystallization of ZmCKO4a with two inhibitors and kinetic measurements.

Two crystal structures of ZmCKO4a were solved in complex with two urea inhibitors derived from thidiazuron (1-phenyl-3-(1,2,3-thiadiazol-5-yl)urea, TDZ): 3-(1,2,3-thiadiazol-5-yl)-1-[3-(trifluoromethoxy)phenyl]urea (3FMTDZ) and 1-[2-(2-hydroxyethyl)phenyl]-3-(1,2,3-thiadiazol-5-yl)urea (HETDZ, Table 4, Figure 26D).

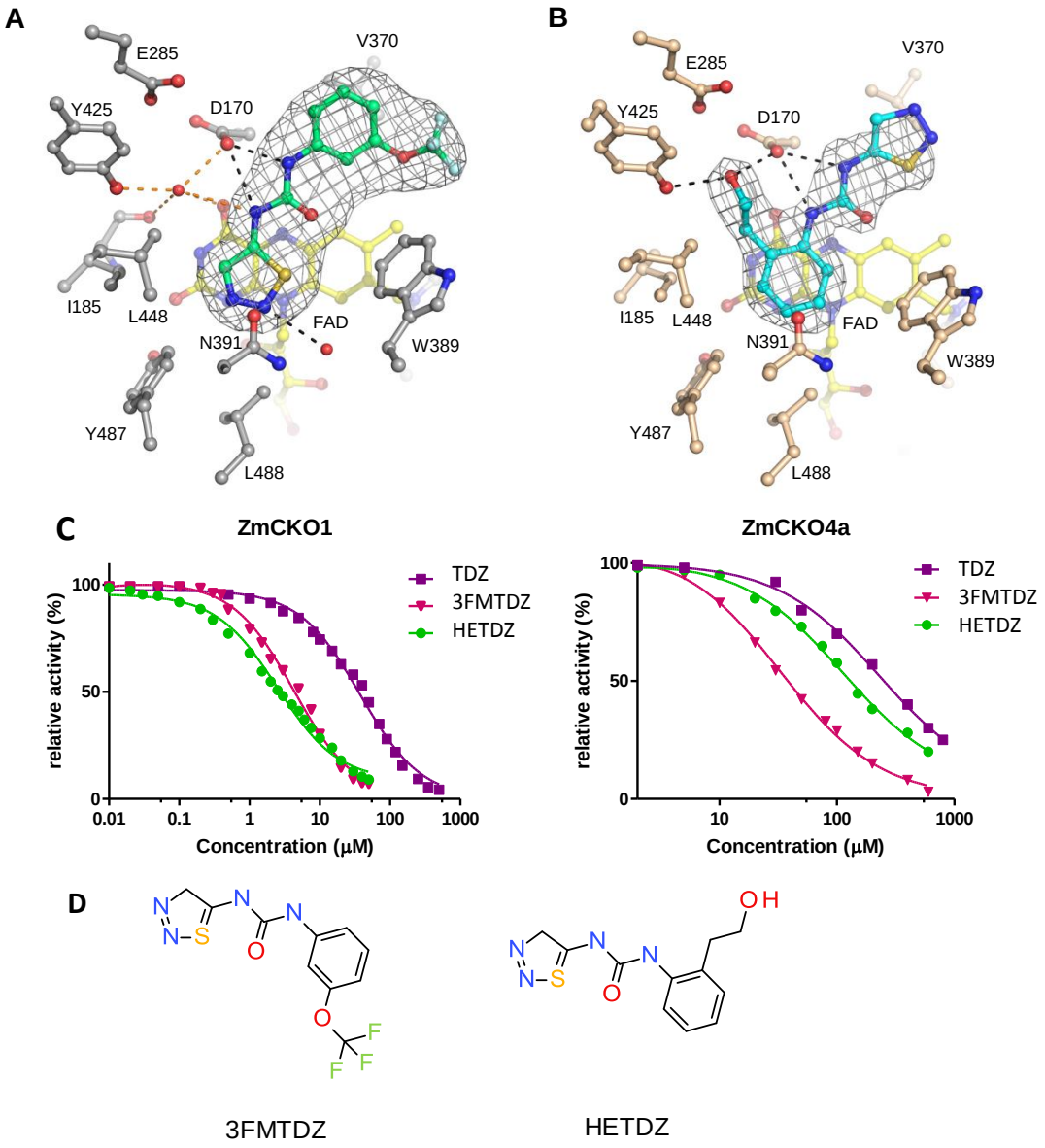

Figure 26. Binding of three urea inhibitors 3FMTDZ and HETDZ in the active site of ZmCKO4a. **(A)** Binding of 3FMTDZ. The inhibitor is green colored and shown in Fo-Fc omit map, contoured at 4.0 σ. **(B)** Binding of HETDZ. The inhibitor is blue colored and shown in Fo-Fc omit map, contoured at 3.0 **(C)** Inhbibiton effect of TDZ and two derivatives on ZmCKO1 and ZmCKO4a.(**D**) Two urea inhibitors derived from thidiazuron.

Crystal structure complexes reveal that HETDZ and 3FMTDZ bind in the active site in two different orientations. Their urea nitrogens are H-bonded to D170. The thiadiazolyl ring of 3FMTDZ is oriented inside over the flavin ring. One of the urea nitrogens creates an H-bond to

a water molecule close to D170 and one of two nitrogen atoms of thiadiazolyl ring is also bound to a water molecule close to N391. In contrast, the thiadiazolyl ring of HETDZ is oritented outside from the flavin ring and oxygen atom of the hydroxyethyl side chain of HETDZ makes an H-bond to oxygens of D170 and Y425 residues (Figure 26).

HETDZ and 3FMTDZ both inhibit maize CKO1 (IC_{50} of 48 μM for TDZ, 5 μM for 3FMTDZ and 2 μM for HETDZ) and maize CKO4a (IC_{50} of 200 μM for TDZ, 30 μM for 3FMTDZ and 120 μM for HETDZ better than TDZ itself (Niesler *et al*., manuscript) and represent new possible inhibitors for *in vivo* studies.

5.3 Characterization of maize ALDH2, 7 and 10 families

The results of this chapter are published in Kopečný *et al*., 2013 and Končitíková *et al*., 2015. My contribution in these publications was in cloning, expression, purification, kinetic measurments and crystallization of ZmAMADH1a, ZmALDH7 and all ZmALDH2 family members. I also performed qPCR measurements.

5.3.1 Gene models and phylogenetic analysis

The maize genome database (http://ensembl.gramene.org, AGPv3) indicates the existence of six putative *ALDH2* genes, one *ALDH7* gene and three *ALDH10* genes (Figure 8 and Table 5). In our work we described cloning of cDNAs of ten maize *ALDHs* using gene-specific primers to determine the gene models and obtain the corresponding recombinant proteins (Kopečný *et al*., 2015, Končitíková *et al*., 2015). The *ZmALDH7* gene consist of 14 exons and lies on chromosome 2. There are six *ZmALDH2* genes that are formed of 7 to 11 exons with the last three exons conserved except for *RF2E*, whose the last exon is separated into two by insertion of CACTA-like DNA transposon. Gene structures are similar to those described in rice and Arabidopsis (Gao and Han, 2009) with high variability in exon/intron number in middle part of the *ALDH2* genes. There are three *ZmALDH10* (*AMADH*) genes composed of 15 exons.

Both maize RF2A and RF2B belong to the ALDH2B subfamily consisting of mtALDH2 members including the snapdragon (*Antirrhinum majus*) benzaldehyde dehydrogenase (Long *et al.*, 2009), rice, tobacco and Arabidopsis mtALHDs (Nakazono *et al.*, 2000, op den Camp and Kuhlemeier, 1997, Skibbe *et al.*, 2002). RF2C, RF2D, RF2E and RF2F share about 70% sequence identity and belong to the ALDH2C subfamily composed of cytosolic ALDH2 members, together with Arabidopsis ALDH2C4 also named coniferaldehyde or sinapaldehyde dehydrogenase (Nair *et al.*, 2004). ZmALDH7 shares only 29 % sequence identity with ZmALDH2 members (Table 4). Poplar and soybean carry two or more *ALDH7* genes. Plant

AMADHs share around 70 – 80 % sequence identity. ZmAMADH1a and ZmAMADH1b share 95 % sequence identity. ZmAMDH2 shares 75 % identity with both ZmAMADH1a and -1b.

Table 5. Enzyme nomenclature and GenBank accession numbers of studied maize ALDH2, ALDH7 and ALDH10 family members. The alternative and systematic names follow previous publications dealing with nomenclature of plant ALDHs (Brocker *et al*., 2013, Šebela *et al*., 2000). Sequence identities (in %) of maize RF2C and maize ALDH7 with other ALDHs was calculated by Lalign (Huang and Miller, 1991).

Name	Alternative / systematic name	GenBank accession	Maize chromosome	Exon #	AA #	Sequence identity (%)	
						RF2C	ZmALDH7
RF2A	ZmALDH2-1 / ALDH2B2	KJ004510	9	11	549	59.1	29.5
RF2B	ZmALDH2-2 / ALDH2B5	KJ004511	4	9	550	60.2	28.2
RF2C	ZmALDH2-3 / ALDH2C1	KJ004512	3	7	502	--	27.5
RF2D	ZmALDH2-4 / ALDH2C2	KM225857	3	8	511	73.8	29.7
RF2E	ZmALDH2-5 / ALDH2C4	KM225858	8	10	501	71.1	29.1
RF2F	ZmALDH2-6 / ALDH2C5	KJ004513	6	8	519	70.2	29.4
ZmALDH7	ALDH7B6	KJ004509	2	14	509	27.5	--
ZmAMADH1a	ALDH10A8	GQ184593	4	15	505	40.1	29.6
ZmAMADH1b	ALDH10A9	JN635700	1	15	506	41.3	29.4
ZmAMADH2	ALDH10A5	GQ184594	10	15	506	40.5	29.4

5.3.2 Kinetic properties of ZmALDH2 family

Four maize cytosolic ALDH2 isoforms (RF2C, RF2D, RF2E and RF2F) were purified and their kinetic parameters measured using wide range of aldehydes at 1 mM concentration (Figure 27A). Specific activity values measured with 1.0 mM hexanal were 62 nkat mg^{-1} for RF2C, 12.2 nkat mg^{-1} for RF2D, 14.6 nkat mg^{-1} for RF2E and 8.9 nkat mg^{-1} for RF2F.

ALDH2C isoforms exhibit a broad substrate preference for aliphatic and aromatic aldehydes, especially for hexanal, benzaldehyde and *p*-anisaldehyde. AASAL, 3-aminopropionaldehyde (APAL) and 4-aminobutyraldehyde (ABAL), citral, glycolaldehyde belong to naturally occurring substrates, which were found as weak substrates (all below 10% rate compared with hexanal). According to the catalytic efficiency values (Končitíková *et al*., 2015) hexanal and cinnamaldehyde are the best substrates for RF2C (Table 6) while RF2D and RF2E preferentially oxidizes *p*-anisaldehyde and benzaldehyde and RF2F favors phenylacetaldehyde. A strong excess substrate inhibition is evident for especially aromatic aldehydes (Figure 27B) as for example for cinnamaldehyde with RF2C or phenylacetaldehyde with RF2F.

The specific activity of all ZmALDH2 isoforms is increasing with the length of linear carbon chain of aliphatic aldehyde up to six-carbon chain (hexanal). Much lower activities were described with heptanal and octanal (except for RF2C for octanal). A significant increase was

evident for nonanal – up to 50% activity compared with hexanal. Both *t*-2-hexenal and *t*-2-nonenal are weak substrates in comparison with the saturated analogues C6 and C9. Although *t*-2-nonenal represents one of the best substrate for RF2C isoform. Aliphatic C6 and C9 aldehydes and their unsaturated analogues belong to the green leaf volatiles.

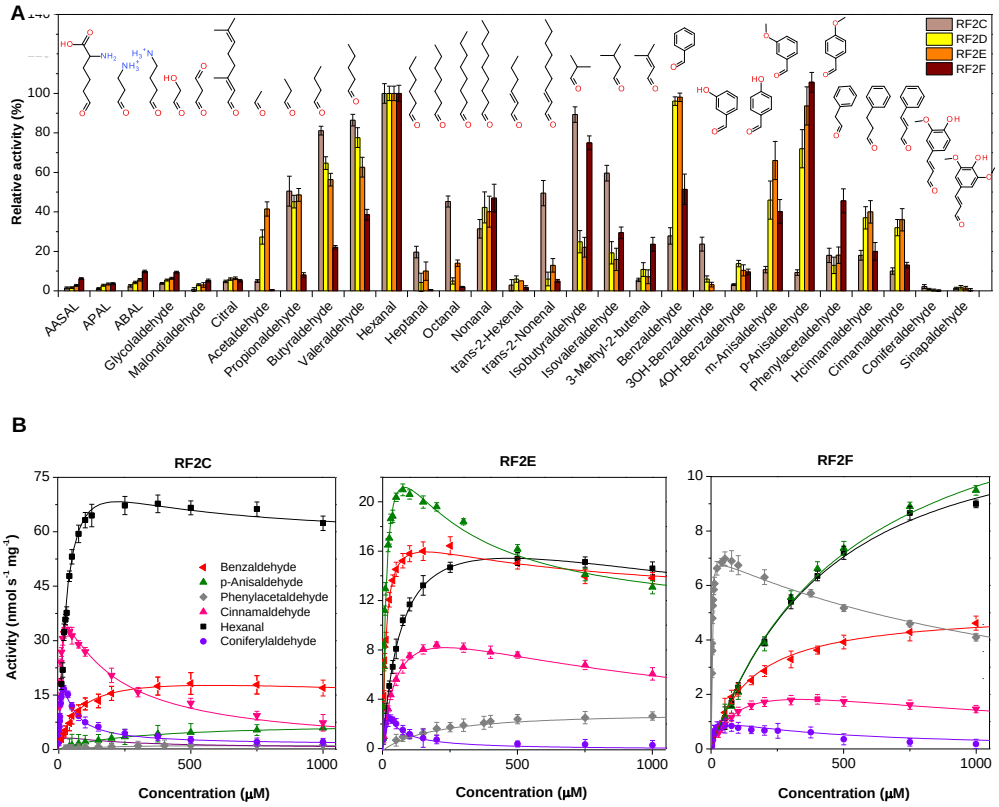

Figure 27. Screening of substrate specificity of maize ALDH2C isoforms. (A) Substrate specificity of four maize ALDH2 isoforms with aliphatic and aromatic aldehydes. Measurements were performed with 1 mM substrate in 0.15 M Tris-HCl buffer, pH 8.0 (for RF2C and RF2F) and pH 7.5 (for RF2D and RF2E), containing 1 mM NAD^+. The activity with hexanal was arbitrarily taken as 100%. Error bars stand for S.D. from four measurements. **(B)** Saturation curves for activity determination of maize RF2C, RF2E and RF2F. Data were measured as above and are shown for benzaldehyde, *p*-anisaldehyde, phenylacetaldehyde, cinammaldehyde, hexanal and coniferaldehyde.

They are responsible for an aroma of fruits and vegetable, moreover, they are produced as a response to wounding. These aliphatic aldehydes are derived from linolenic acid originated from lipoxygenase pathway (reviewed in Dudareva *et al.*, 2013). Branched aliphatic C4 and C5 aldehydes represent good substrate as well. All ALDH2 isoforms oxidize 3-methyl-2-butenal (isopentenal) originating from isoprenoid cytokinins degradation pathway (Kopečný *et al.*, 2005). The activity of this unsaturated aldehyde is between 8 - 25% compared to hexanal. Aromatic aldehydes such as benzaldehyde, *m*- and *p*-anisaldehyde, phenylacetaldehyde, cinnamaldehyde and hydrocinnamaldehyde display differences in ZmALDH2 isoforms activity. Nevertheless, they are good substrates. Aromatic aldehydes originate from phenylalanine *via* several pathways (reviewed in Dudareva *et al.*, 2013). Benzaldehyde is formed *via* the non-*β*-

oxidative pathway (Boatright *et al.*, 2004). Moreover, benzaldehyde is known as a product of oxidation of aromatic cytokinins by CKO. Coniferaldehyde and sinapaldehyde are produced *via* phenylpropanoid pathway. These two aldehydes are *in vivo* substrates for ALDH2C from Arabidopsis and oilseed rape (Nair *et al.*, 2004) and are also substrates for ZmALDH2 isoforms (Končitíková *et al.*, 2015).

5.3.3 Kinetic properties of ZmALDH7

The maize ALDH7 isoform preferentially oxidizes AASAL (Figure 28) as well as ALDH7 from pea (PsALDH7) and human (hALDH7). Specific activity measured with 1.0 mM AASAL was 45 nkat mg^{-1}. Substrate specificity study was performed using 1 mM substrates (Figure 26). K_m value of 90 μM for AASAL was measured with ZmALDH7 in agreement with previous studies on seabream ALDH7 (67 μM, Tang *et al.*, 2008) and on hALDH7 (169 μM, Brocker *et al.*, 2010). Methyl ester of adipic semialdehyde (MASAL) is oxidized with 5 % rate relative to that of AASAL. Natural *ω*-aminoaldehydes such as BAL, APAL, ABAL, 4-*N*-trimethylaminobutyraldehyde (TMABAL) and 4-guanidinobutyraldehyde (GBAL) are good substrates with up to 25 % rates relative to that of AASAL. Very weak activity was detected with aliphatic, aromatic aldehyde and succinic semialdehyde (SSAL). Very weak substrates are also *t*-2-hexenal, *t*-2-nonenal and malondialdehyde, which are products of lipid peroxidation (Figure 26, Končitíková *et al.*, 2015).

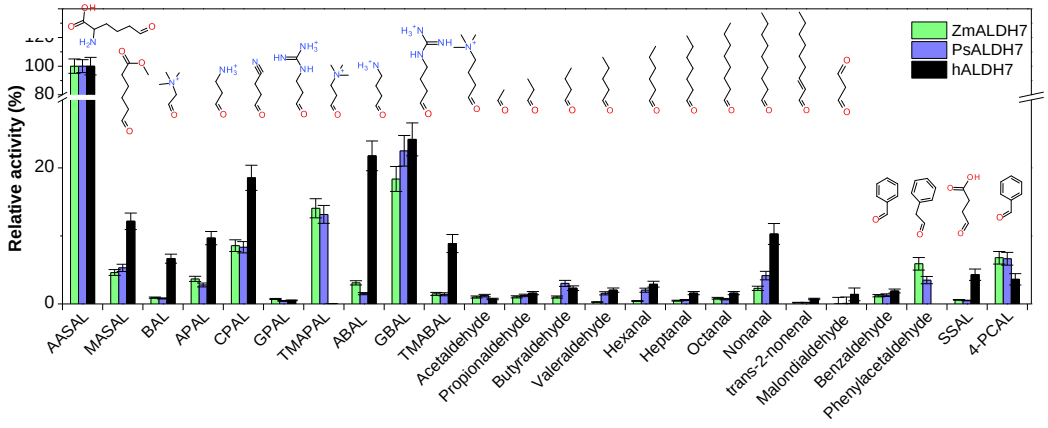

Figure 28. Screening of substrate specificity of ZmALDH7. (A) Substrate specificity of maize, pea and human ALDH7. The measurements were performed with 1 mM substrate in 0.1 M sodium pyrophosphate buffer, pH 8.0, containing 2.0 mM NAD^+. The activity with AASAL was arbitrarily taken as 100%. Error bars stand for S.D. Specific activity values measured with 1.0 mM AASAL as a substrate were 43.5, 57.5 and 3.8 nkat mg^{-1} for ZmALDH7, PsALDH7 and hALDH7, respectively.

Plant ADLH7 from rice and Arabidopsis have been shown to be localized in cytosol (Shin *et al.*, 2009, Kotchoni *et al.*, 2006) in agreement with the presence of the bifunctional lysine-ketoglutarate reductase/saccharopine dehydrogenase (LKR/SDH, Kemper *et al.*, 1999;

Zhu *et al.,* 2000), which catalyzes the first reaction of the lysine catabolism pathway (saccharopine pathway) leading to AASAL and glutamate. In contrast, hALDH7 was additionally found in mitochondria (Brocker *et al.*, 2010, Wong *et al.*, 2010) in line with the existence of two lysine catabolism pathways: the saccharopine pathway localized in mitochondria and the pipecolate pathway predominantly found in peroxisomal/cytosolic (reviewed in Hallen *et al.*, 2013).

BAL activity is important for hyperosmotic stress protection. BAL originates from choline and is oxidized to glycine betaine, which is an important osmolyte. It is clear that plant ALDH7 family is able to oxidize GBAL, APAL and ABAL (Table 6) results directly or after further conversion to osmoprotectants 4-guanidinobutyrate, β-alanine and γ-aminobutyric acid (GABA) in the cytosol. GBAL originates from arginine catabolism. 4-guanidinobutyrate, the product of the oxidation of GBAL, may be further hydrolyzed by ureohydrolase to urea and GABA.

Table 6. Kinetic parameters of maize ALDH7 and RF2C for selected substrates. All K_m and k_{cat} values are given in μM and s^{-1}, respectively.

Ligand	ZmALDH7			Ligand	RF2C		
	K_m μM	k_{cat} s^{-1}	k_{cat}/K_m $M^{-1}\ s^{-1}$		K_m μM	k_{cat} s^{-1}	k_{cat}/K_m $M^{-1}\ s^{-1}$
AASAL	97 ± 7	2.56 ± 0.043	**2.6 x 10^4**	Acetaldehyde	2419 ± 170	0.59 ± 0.02	2.4 x 10^2
MASAL	126 ± 21	0.09 ± 0.004	7.1 x 10^2	Hexanal	15 ± 1	4.54 ± 0.08	**3.0 x 10^5**
GBAL	2767 ± 146	1.43 ± 0.029	5.2 x 10^2	*t*-2-Hexenal	39 ± 5	0.35 ± 0.02	9.0 x 10^3
BAL	120 ± 3	0.03 ± 0.001	2.5 x 10^2	Nonanal	51 ± 5	1.63 ± 0.06	3.2 x 10^4
APAL	1280 ± 59	0.15 ± 0.002	1.1 x 10^2	*t*-2-Nonenal	19 ± 13	2.54 ± 0.30	1.3 x 10^5
ABAL	4371 ± 116	0.27 ± 0.005	6.3 x 10^1	Benzaldehyde	83 ± 9	1.21 ± 0.06	1.5 x 10^4
Hexanal	1805 ± 186	0.11 ± 0.005	6.1 x 10^1	Cinnamaldehyde	10 ± 1	2.95 ± 0.17	**3.0 x 10^5**
Nonanal	174 ± 14	0.07 ± 0.006	4.3 x 10^2	Coniferaldehyde	19 ± 3	2.65 ± 0.37	1.4 x 10^5

5.3.4 Kinetic properties of ZmALDH10 family

In a large screening study 1 mM aldehydes were used (Figure 29). All three maize AMADHs most readily oxidize natural aminoaldehydes APAL, ABAL and TMABAL as well as synthetic aminoaldehydes (Figure 29). Specific activity values measured with 1 mM APAL as a substrate 43 nkat mg^{-1} for ZmAMADH1a, 31 nkat mg^{-1} for ZmAMADH1b and 68 nkat mg^{-1} for ZmAMADH2. The highest reaction rates are achieved with APAL for all maize isoenzymes. Methyl and guanidine derivatives of APAL and ABAL are oxidized with 10 – 60% rates on average (relative to that of the best substrate). Hydroxylated derivatives as well as aliphatic aldehydes are oxidized more slowly. AASAL, the substrate of ALDH7 family is weak substrate, with 1 – 3 % rates on average. Only ZmAMADH1a exhibits a relatively high activity with BAL, comparable with ABAL oxidation (16% compared with APAL). For better understanding differences in BAL oxidation, ZmAMADH1a was chosen for a crystallographic study. AMADH/BADH oxidizes BAL to the osmoprotectant GB (Brouquisse *et al.*, 1989). High levels of GB have been detected in leaves of stressed diverse families of dicots and monocots,

including barley, wheat, and rye (Ishitani *et al*., 1993). Maize cultivars synthesize substantially lower levels of GB (Brunk *et al*., 1989).

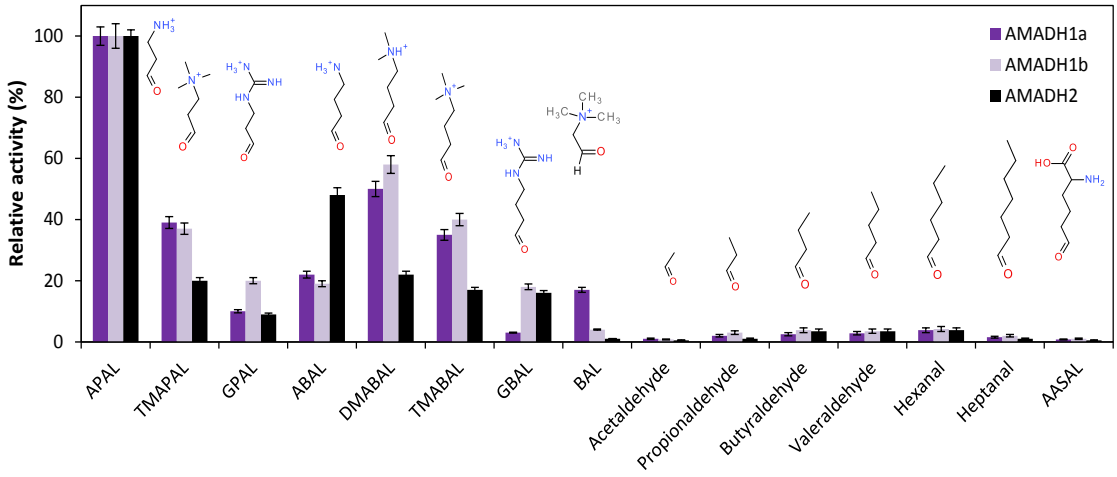

Figure 29. Substrate specificity of maize ALDH10 isoenzymes. The activity of each AMADH isoenzyme with the best substrate was arbitrarily taken as 100%. The measurements were performed with 1 mM substrates in 0.15 M Tris-HCl buffer, pH 9.0, containing 1 mM NAD^+. The following substrates were tested: APAL, N,N,N-trimethyl-3-aminopropionaldehyde (TMAPAL), 3-guanidinopropionaldehyde (GPAL), ABAL, TMABAL, GBAL, BAL, acetaldehyde (C2), propionaldehyde (C3), butyraldehyde (C4), valeraldehyde (C5), capronaldehyde (C6), enanthaldehyde (C7), and (AASAL).

5.3.5 Oligomerization status of studied ALDHs

Molecular weight of monomers of all ZmALDH2 is between 54 and 56kDa and those of three ZmAMADHs are ~ 55 kDa. Monomer of ZmALDH7 has the molecular weight of 54 kDa.

Table 7. Data collection and refinement statistics. Numbers in parentheses represent values in the highest resolution shell

	RF2C (ZmALDH2-3)	**RF2F (ZmALDH2-6)**	**ZmALDH7**	**ZmAMADH1a**
PDB code	4PXL	4PZ2	4PXN	4I8P
Space group	$P2_12_12$	$I4_1$	$I2_12_12_1$	C121
Asymmetric unit	1 dimer	1 tetramer	2 monomers	1 dimer
Oligomeric state	tetrameric	tetrameric	tetrameric	dimeric
Unit cell (Å)				
a	109.9	233.9	79.2	181.19
b	126.1	233.9	162.5	49.89
c	78.3	82.9	188.6	154.53
α, β, γ (°)	90.0	90.0	90.0	90.0 (β = 124.15)
Resolution (Å)	49.1-2.25	50.0-2.40	42.11-2.94	45.0-1.95
Completeness (%)	99.8 (99.0)	99.7 (98.3)	99.3 (95.7)	99.1 (98.2)
$I/\sigma(I)$	13.62 (2.1)	11.12 (1.2)	9.91 (1.8)	10.71 (2.29)
$CC_{1/2}$	-	99.7 (58.4)	99.6 (58.3)	
R_{svm} (%)	10.7 (78.9)	9.7 (155.7)	19.4 (153.3)	10.9 (62.2)
R_{crvst} (%)	17.1	19.0	18.8	17.6
R_{free} (%)	20.5	21.3	21.7	21.0
RMSD bond lengths (Å)	0.010	0.009	0.008	0.010
RMSD bond angles (°)	1.11	1.14	1.14	1.07

Using gel permeation chromatography, however, molecular masses of RF2C, RF2F and ZmALDH7 correspond to 214 kDa, 226 kDa and 181 kDa indicating that they are all tetramers

in solution. In case of ZmAMADHs, they all have molecular mass values between 106 and 115 kDa indicating that they are dimers in solution (Figure 30). The asymmetric unit of RF2F crystal is composed from a tetramer. RF2C and ZmALDH7 contain a dimer and two monomers.

Nevertheless, both RF2C and ZmALDH7 share tetrameric structures, which is in line with results from gel permeation chromatography. The asymmetric unit of ZmAMADH1a crystal is composed of the dimer again is in line with results from gel permeation chromatography.

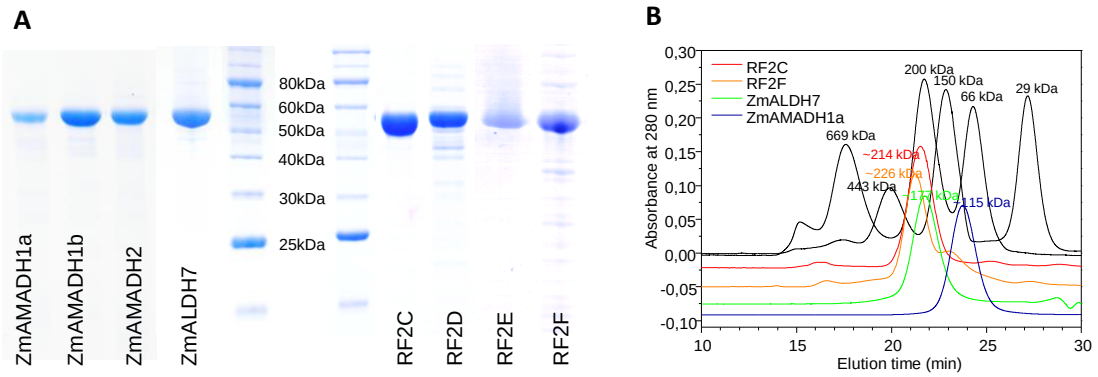

Figure 30. Molecular properties of plant ALDH2 and ALDH7 proteins. (A) Coomasie stained SDS-PAGE gels of recombinant ALDHs. Proteins are after partial His-tag affinity purification. The protein marker was the Protein Ladder 10-250 kDa (NEB). **(B)** Gel permeation chromatography of ZmALDHs. Gel permeation chromatography was performed on Superdex 200 HR 10/30 column (GE Healthcare). The column was equilibrated and run with 50 mM potassium phosphate buffer, pH 7.0, containing 150 mM NaCl at a flow rate of 0.7 ml min^{-1}. The molecular mass values were evaluated after calibration of the column with Gel filtration marker kit (Sigma-Aldrich). The elution profiles of ZmALDHs are shown in red, orange and green color and their calculated molecular mass values are indicated.

5.3.6 Overall fold of studied ALDHs

ZmAMADH1a, RF2C, RF2F and ZmALDH7 adopt the characteristic ALDH fold consisting of a coenzyme binding domain, a catalytic domain and an oligomerization domain. They all bind a conserved monovalent ion. The nature of the protein ligands and the distances of around 2.4 – 2.6 Å are typical for a bound sodium ion. This ion probably allows maintenance of the protein structural integrity and/or stabilizes the position of a loop involved in NAD^+ binding. The oligomerization domains connect both monomers by protruding over the surface of the neighboring subunits around substrate channel entrances while the NAD^+ binding sites reside on the opposite side of the dimer. The catalytic cysteine lies between the NAD^+ and the substrate binding sites.

Monomers of RF2C and RF2F are very similar to each other (average RMSD of 0.7 Å) and a structural comparison using PDBeFold (http://www.ebi.ac.uk/msd-srv/ssm/) shows that they both resemble the mitochondrial hALDH2 with the lowest RMSD of 0.80 – 0.85 Å for PDB codes 1O02, 1NZZ, 1NZX and others (Perez-Miller and Hurley, 2003; Figure 31). Both

RF2C and RF2F tetramers are very similar to hALDH2 tetramer with average RMSD values of 1.2 and 1.0 Å for 1940 Cα atoms, respectively. Subtle differences in the oligomerization arrangement can be observed. ZmALDH7 monomer is similar to that of human and seabream (PDB codes 2J6L and 2JG7) with RMSD of 0.72 and 0.74 Å, respectively.

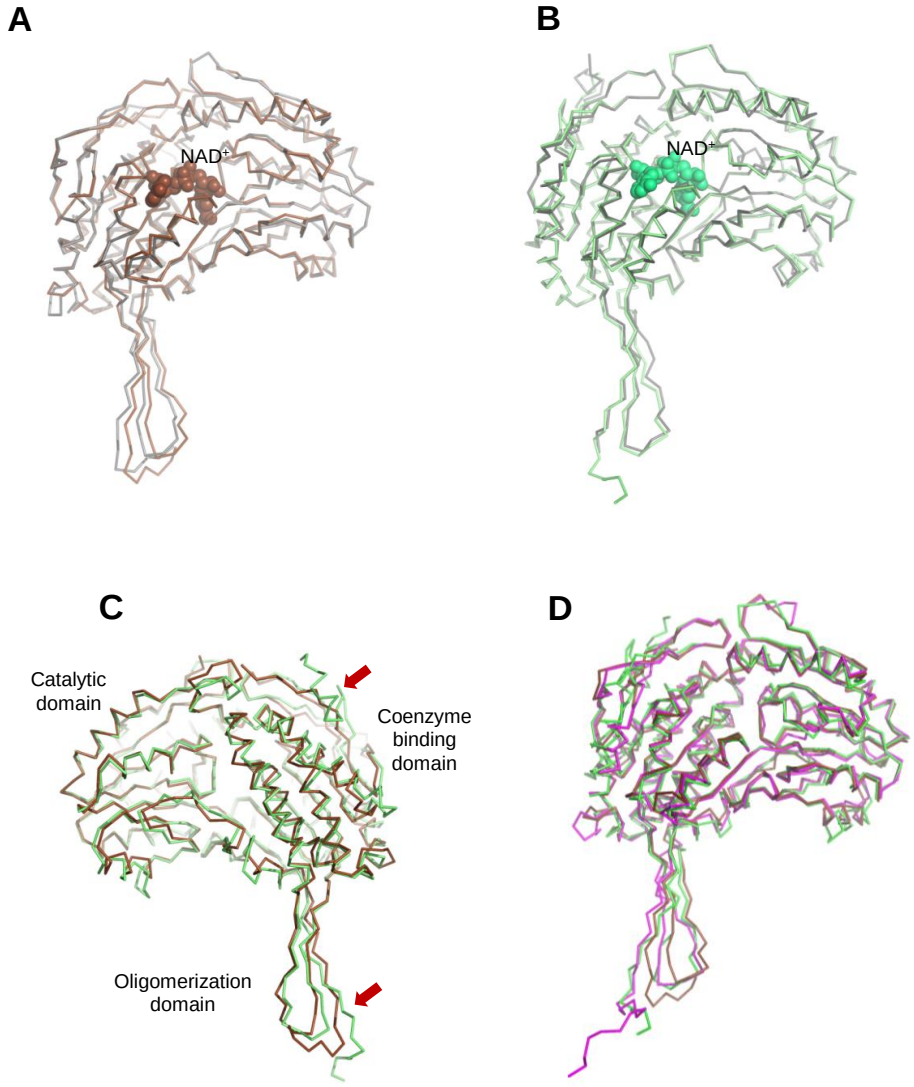

Figure 31. **ALDH fold in ZmALDHs**. **(A)** Superposition of ALDH2 monomers derived from crystal structures of maize RF2F (brown, this work) and hALDH2 (grey, PDB code 1NZX) with the coenzyme in plant ALDH2 shown in balls. **(B)** Superposition of ALDH7 monomers derived from crystal structures of ZmALDH7 (green, this work) and hALDH7 (grey, PDB code 2J6L) with the coenzyme in plant ALDH7 shown in balls. **(C)** Superposition of maize RF2F monomer (brown, this work) and ZmALDH7 monomer (green, this work). Monomers are rotated by 180° along the vertical axis compared with (A) and (B). Slight differences in the oligomerization domain and the presence of an N-terminal helix in maize ALDH7 are indicated by arrows. (**D)** Superposition of ALDH2 (brown), ALDH7 (green) and ALDH10 (violet) monomers.

The major difference between ZmADLH7 and ZmALDH2 monomers (RMSD of 1.3-1.4 Å for 465 Cα atoms) comes from a slight shift in the oligomerization domain and the presence of an N-terminal helix in ZmALDH7.

5.3.7 Substrate channels of studied ALDHs

Substantial differences are shown in a comparison of substrate channel residues in RF2C and RF2F (Figure 32A and 32B). Substrate binding site of RF2C is narrow and formed by an aromatic cluster composed of Y171, F178, F458, F460 and F466 and also by several mainly nonpolar residues including I302, V304, T174, M175 and T297. In contrast, that of RF2F is much wider due to the presence of V192 and M477 at the position of the two aromatic residues F178 and F460 in RF2C. Indeed, M477 side chain, which is shifted outwards by 3 Å, opens the cavity. Two more residues A316 and E495 (I302 and M478 in RF2C) also contribute to the substrate channel broadening. The cavity width of RF2F clearly correlates with high K_m values for various substrates most likely due to weaker nonpolar interactions except for phenylacetaldehyde.

RF2D and RF2E, which share 95 % sequence identity, do not differ in active site residues and thus have similar kinetic properties. A model of RF2E was made using RF2C structure as a template (Figure 32C). The substrate binding site of RF2E contains F459 (F460 in RF2C) making the cavity as narrow as in RF2C. Nevertheless, the cavity is slightly wider in the opposite direction due to the presence of L177 at the position of F178 in RF2C. Finally, only RF2C contains a threonine at the position 297 while the other three maize isoforms contain a phenylalanine at the equivalent position. This threonine, which occupies less space, might have a role in substrate binding plasticity and specificity by allowing the side chain of Y171 (equivalent to a phenylalanine in other maize isoforms) to move and facilitate substrate accommodation.

A sequence alignment of substrate channel residues in ALDH2C members (Figure 32D) reveals a high variability that allows various isoforms within one species oxidizing several different substrates from multiple pathways. Recently, maize *RF2C* gene was found to be induced in elongating internodes containing cells, which exhibit primary cell wall biosynthesis, compared to non-elongating internodes with cells depositing secondary cell wall material Nair *et al.*, 2004. In contrast, plant mtALDH2 isoforms including RF2A and RF2B share a conserved active site and are highly similar to hALDH2 (Figure 32D). Their sequences contain a triple cysteine motif including the catalytic cysteine. Although *in vivo* preferred substrate of hALDH2 is acetaldehyde, the enzyme has been shown to oxidize various aliphatic and aromatic aldehydes especially hexanal, phenylacetaldehyde or benzaldehyde (Klyosov, 1996). Likewise, RF2A, but not RF2B, is in addition to acetaldehyde also highly active with benzaldehyde and cinnamaldehyde (Liu and Schnable, 2002).

Comparison of ZmALDH7 with human and seabream ALDH7 illustrates that their active site residues are almost identical indicating that these enzymes have the same cellular role in plants, mammals or fish using AASAL as the preferred substrate. The three residues E120,

R300 and T302 located in the substrate binding site of ZmALDH7 are conserved and specific for ALDH7 family (Figure 33B). The role of E120 and R300 has been validated by mutagenesis studies on seabream ALDH7 and hALDH7 (Tang *et al.*, 2008, Chan *et al.*, 2011). E120 binds the α-amino group of AASAL while R300 its carboxylate group. The role of T302 has not been studied by mutagenesis yet.

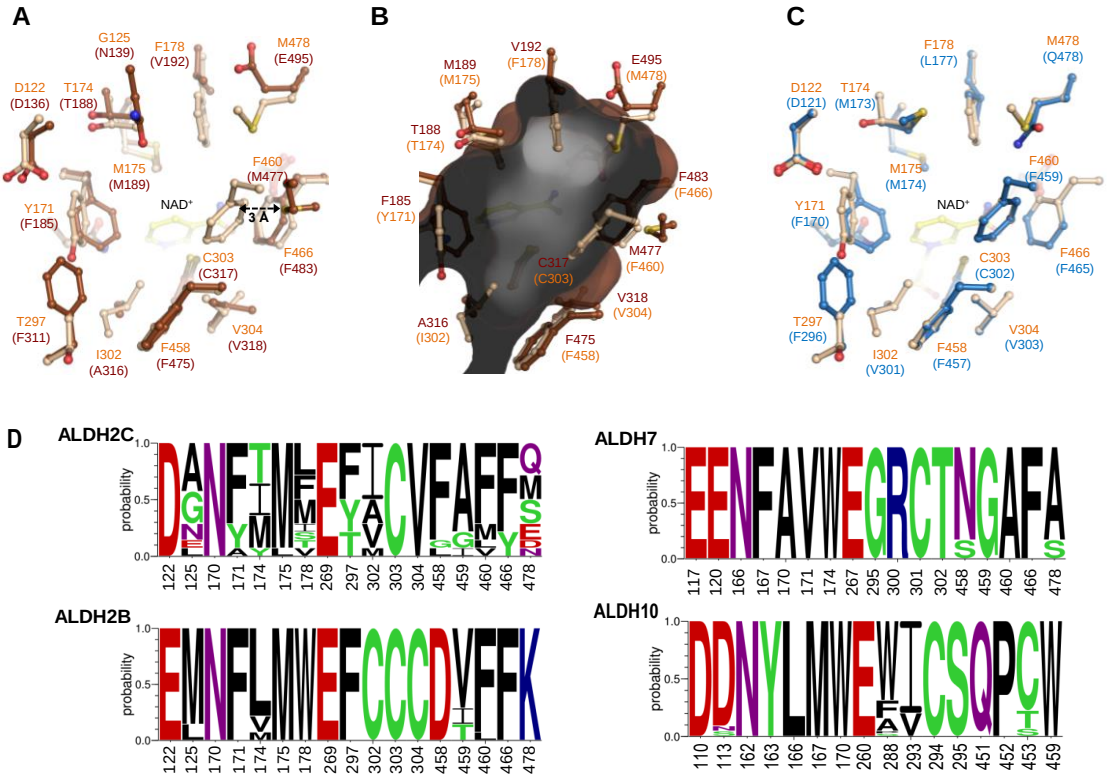

Figure 32. Composition of maize ALDH2 and ALDH7 active sites. (A) A view from the top on substrate channels of maize RF2C (light brown, this work) and RF2F (dark brown, this work). Residues of RF2C and RF2F are labelled in orange and shown in brackets respectively. **(B)** Transversal section of substrate channel of RF2F. The inner surface is grey colored (foreground is dark grey, background is light grey) and was calculated using Hollow with 0.7 Å grid spacing and a 1.2 Å interior probe. Labeled residues are colored in dark brown. Residues of RF2C (in light brown) are shown for comparison to indicate differences affecting diameter of the substrate channel. **(C)** Composition of the substrate channel in RF2E (blue). Model was done using SWISS-MODEL (http://swissmodel.expasy.org) and RF2C as a template. **(D)** Conservation of amino acid residues forming the substrate channel in ALDH2 and ALDH7 families. Residues are numbered according to maize RF2C for ALDH2C and ALDH2B subfamilies, maize ALDH7 for ALDH7 family and pea AMADH2 for ALDH10 family. Sequence logos were made using WebLogo server.

Manual modeling of ZmALDH7 active site reveals that this residue may interact with R300 in the binding of carboxylate side-chain of AASAL. According a kinetic analysis it is clear that AASAL and MASAL have similar K_m values. The major difference is in k_{cat} value, which is about two-fold lower for MASAL. Therefore we can conclude that to achieve a high reaction rate it is necessary to protonate an amino group of the substrate (and interaction with E120). Similarly for maintaining a high affinity to the substrate is important the presence of

carboxyl groups (interaction with R300 and T302), which prove high values of K_m for aminoaldehydes GBAL (~ 2.5 mM) and ABAL (~ 4.5 mM).

A comparison of the substrate channel residues in plant AMADHs show that almost all residues are evolutionarily highly conserved (Figure 30D). Noticeably, two residues at the positions 288 and 453 (PsAMADH numbering) are less preserved. W288 could be substituted by Ala, Phe or Ser and C453 by Ser or Thr residue. Based on the k_{cat}/K_m ratio, APAL is the best substrate for ZmAMADH1a and ZmAMADH1b as well as for PsAMADH2 (Tylichová *et al.*, 2010), which all possess W288 (W290 or W291 in ZmAMADH1s). ZmAMADH2, which contains an Ala at this position, prefers TMABAL as the best substrate accented by the increased K_m values for APAL and ABAL. PsAMADH1 containing a phenylalanine also prefers TMABAL (Tylichová *et al.*, 2010). The preference of TMABAL for W288-absent AMADHs appears either due to the increase in the substrate channel diameter and the loss of possible π-electron stacking interaction with the electrophilic protonated amino group of the substrate or indirectly by affecting the position of Y163 side chain (Y165 in ZmAMADH1a) (Figure 33).

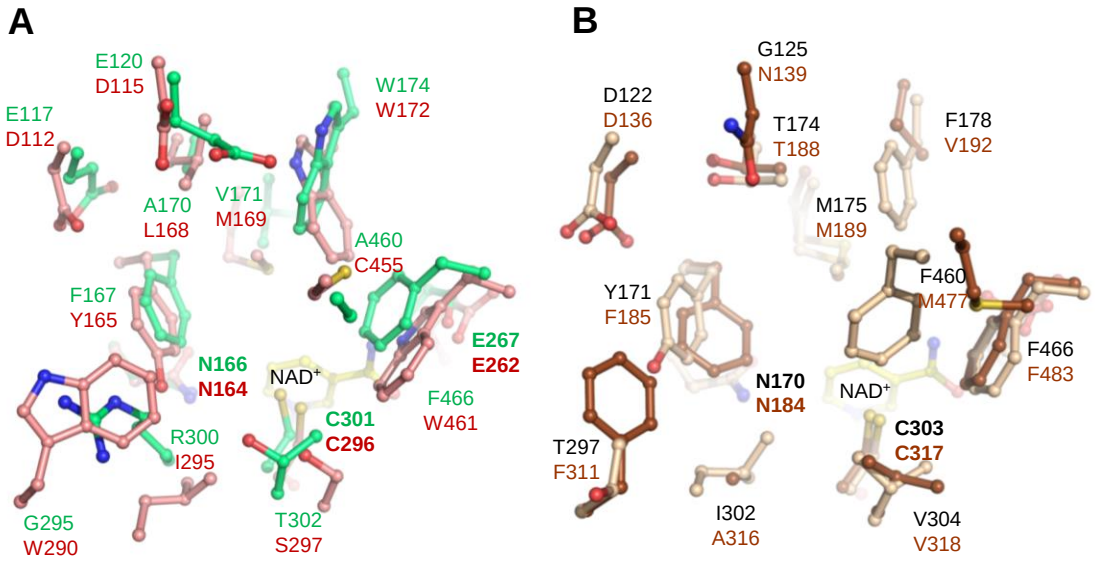

Figure 33. Comparison of ZmALDH10, ZmALDH7 and ZmALDH2 active sites. (A) Superposition of the substrate channels of ZmAMADH7 (green) and ZmAMADH1a (pink). **(B)** Superposition of substrate channels of maize RF2C (light brown) and RF2F (brown).

ZmAMADH1a shows a good activity with BAL (K_m of 14 μM and $k_{cat\ of}$ 0.6 s^1). Four strictly conserved residues Y165, W172, W290 and W461 in ZmAMADH1a appear to be able create cation- interactions with the trimethylammonium group of BAL, which becomes sandwiched between Y165 and W461 upon binding. The difference between the position of W461 in ZmAMADH1a and the equivalent tryptophans in the other plant AMADH structures SlAMADH1 and both PsAMADH1 and 2 is clear from their structural comparison. Indeed, its side chain is shifted by 1.6 Å (corresponding to a rotation of 23° along the Cβ-Cγ axis) away

from Y163 leading to an enlargement of the substrate channel favorable for binding of the bulky trimethylammonium group. I444 in PsAMADHs (I445 in SlAMADH1) prevents W459 from adopting the observed position in ZmAMADH1a due to a steric hindrance (Kopečný *et al.*, 2013). Interesting is also comparison of pH optima among studied families. While the optima for ALDH2 and ALDH7 reactions occur at pH between 7.0 and 8.0, oxidation of aminoaldehydes by ALDH10 occurs at much more basic pH.

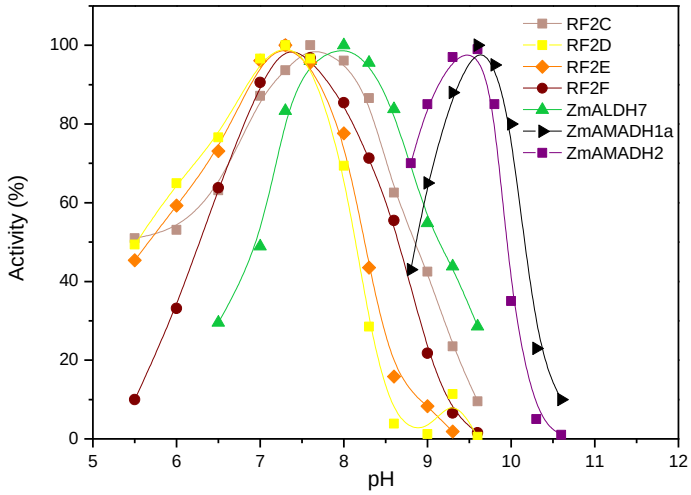

Figure 34. Comparison of pH optima of ZmALDH10, ZmALDH7 and ZmALDH2 isoforms. Data were measured with 1 mM APAL, 1 mM AASAL and 1 mM hexanal as a substrate and in glycine-NaOH buffers.

5.3.7.1 Coenzyme binding in studied ALDHs

In all ZmALDH2 monomers, a NAD^+ molecule is well defined in the electron density maps. In RF2F structure, the coenzyme adopts an extended conformation typically observed for oxidized NAD^+, and the catalytic cysteine C317 is oriented towards the substrate channel (attacking conformation). In RF2C structure, it adopts a contracted conformation most likely due to the high concentration of calcium ions present in the crystallization conditions. In ZmALDH7 monomer NAD^+ adopts the extended conformation with the catalytic C301.

The adenine moiety of NAD^+ inserted in a hydrophobic pocket flanked by two helices (αD and αE) makes no polar contact with the enzyme so that the free amino group is exposed to the solvent. Maize RF2C, RF2D, RF2E, RF2F and three ALDH10 isoforms exhibit similar K_m values for NAD^+ of ~ 10^{-5} μM, Farrés *et al.*, 1994, Tylichová *et al.*, 2010, Kopečný *et al.*, 2013) due to the identical interactions of both α and β-phosphates and the nicotinamide riboside (NiR) moiety of NAD^+ (Figure 35A). These enzymes are NAD^+ specific because they possess a conserved glutamate (E196 in RF2C) preventing the binding of the 2'-phosphate group of $NADP^+$. K_m values of 3.0, 1.5, 1.4 and 1.7 mM for $NADP^+$ with RF2C, RF2D, RF2E and RF2F respectively are ~ 20 - 70 times higher than those for NAD^+ and the reaction rates appear between 0.5 – 9.0 % of those with NAD^+.

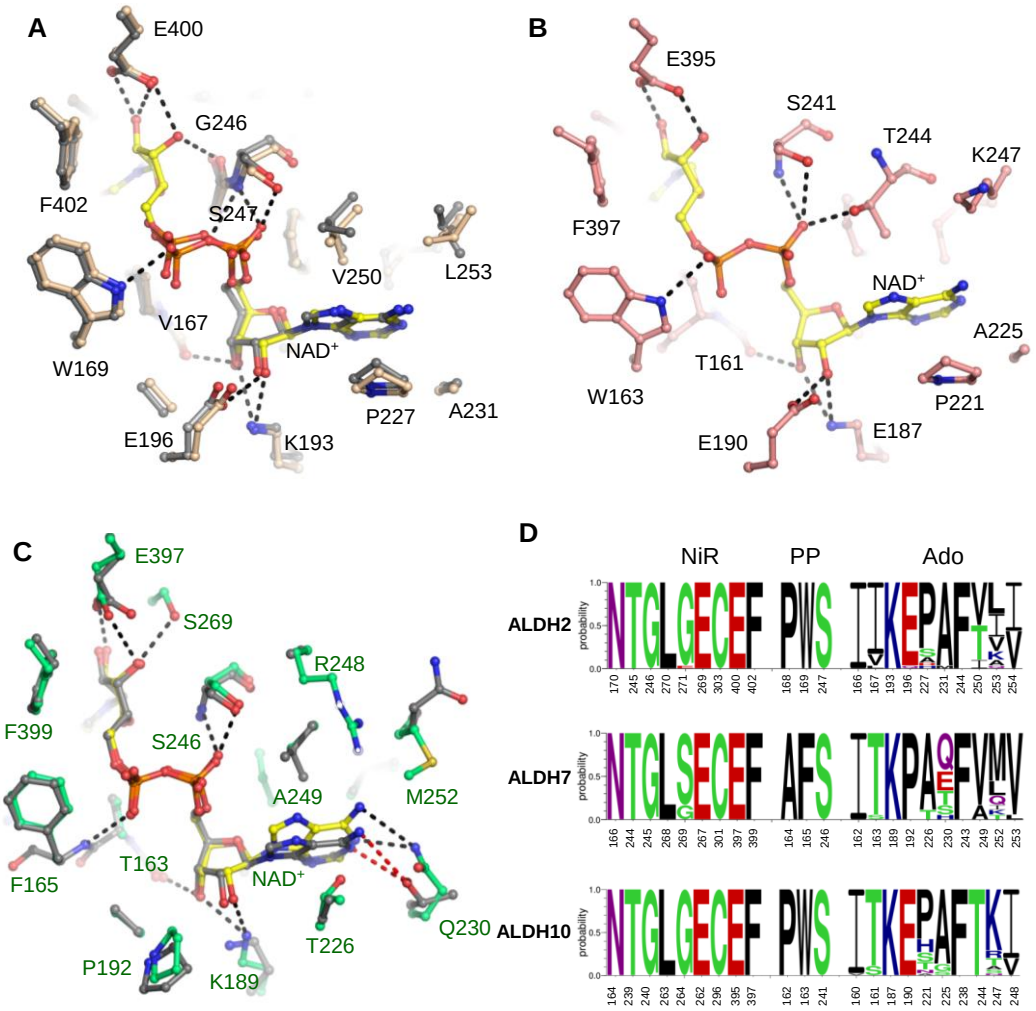

Figure 35. NAD$^+$ binding in ALDH2 and ALDH7 family. (A) Superposition of NAD$^+$ binding sites of maize RF2C (ZmALDH2-3, brown colour) and hALDH2 (grey colour, PDB code 1NZX). Residues are labeled and numbered accoring to RF2C sequence **(B)** NAD$^+$ binding site of ZmAMADH1a (pink color). Residues are labeled. **(C)** Superposition of NAD$^+$ binding sites of ZmALDH7 (green color) and hALDH7 (grey color, PDB code 2J6L). NAD$^+$ molecules are shown in yellow and atom-coded colors stick. Residues in vicinity of NAD$^+$ are labeled and numbered accoring to ZmALDH7 sequence. **(D)** Conservation of amino acid residues relevant for NAD$^+$ binding in ALDH2 and ALDH7 families. Residues are split into three clusters for NiR, diphosphate and Ado moiety of NAD$^+$ molecule. Sequence logos were made using WebLogo (http://weblogo.threeplusone.com).

The coenzyme binding site of ZmALDH7 is slightly different compared with ALDH2 family and hALDH7. Indeed, F165 in ZmALDH7 equivalent to F167 in hALDH7 is bound to the β-phosphate oxygen atom *via* its main chain NH atom restoring the direct interaction between the side chain of Trp residue and the β-phosphate in both ALDH2 and ALDH10 families (W169 and W163 in RF2C and ZmAMADH1a, Figure 35). S269 in ZmALDH7 (Gly in ZmALDH2) makes an additional interaction with the O3D atom of NiR moiety whereas hALDH7 and ALDH2 enzymes possess a glycine at the equivalent position. The conserved glutamate in ALDH2 (E196 in RF2C) and ALDH10 (E190 in ZmAMADH1a) which prevents binding of the 2'-phosphate group of NADP$^+$ (Tylichová *et al*., 2010) is replaced by a proline in ALDH7 family (P192 in ZmALDH7). This proline represents a steric hindrance for 2′-

phosphate of $NADP^+$ which is apparent from the K_m value of 16 mM (40 times higher than that for NAD^+). The major difference between ZmALDH7 and hALDH7/ALDH2 concerns the adenine position of NAD^+. Indeed, the adenine adopts a different position in ZmALDH7 due to the presence of T226 side chain (Ala in hALDH7 and Pro in ALDH2), which pushes the adenine ring up to 1 Å towards A249 (Figure 35C). The T226/A249 couple is present only in small subgroup of monocots including maize while most of ALDH7 family members carry a conserved alanine/valine couple (A227/V250 in hALDH7) at the corresponding positions. All above differences contribute by one order of magnitude to the higher K_m values for NAD^+ of ZmALDH7 compared with those of ALDH2 and ALDH10.

NAD^+ analogs including $NADP^+$ are less efficient coenzymes for all three ALDH families (Figure 36) and only deamino-NAD^+ can somehow replace NAD^+. 3-Pyridinealdehyde-NAD^+ is generally not accepted as a coenzyme and 3-acetylpyridine-NAD^+ functions well only for ALDH10 family.

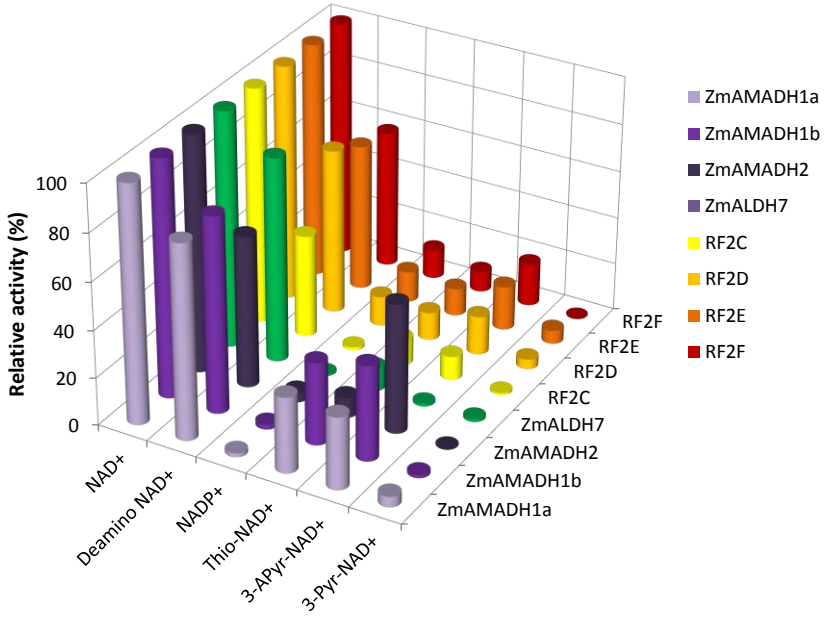

Figure 36. Relative activities of maize ALDHs with NAD^+ analogs. Coenzyme efficiency was measured with 0.5 mM NAD^+ analogs and using 1.0 mM substrates (1 mM APAL, 1 mM AASAL and 1 mM hexanal). The activity of each enzyme with NAD^+ was arbitrarily taken as 100%.

5.3.8 Expression of *ALDH2, ALDH7* and *ALDH10* genes in maize

The expression pattern of *ALDH2*, *ALDH7*, *AMADH* was analyzed in developing maize seedlings (stem, roots and leaves) during the first two weeks after germination (Figure 37). *RF2C* is highly expressed compared with the five other *ALDH2* genes with a strong and comparable transcript levels in leaves and roots but lower in stem. *RF2A* was preferentially expressed in leaves while *RF2B* in roots and less in leaves. Transcripts of *RF2D* and *RF2E* were the most abundant in roots, but almost absent in the stem, while *RF2F* transcripts appeared

especially in the stem of two-week-old seedlings. The highest levels of *ZmALDH7* transcripts were found in leaves. *ZmAMADH1a*, *ZmAMADH1b* and *ZmAMADH2* genes share a similar pattern of expression. All three genes transcripts were well detected in leaves and *ZmAMADH1b* is also well expressed in roots. However, *ZmAMADH2* gene is markedly less expressed than the other two *ZmAMADH* genes (Figure 37).

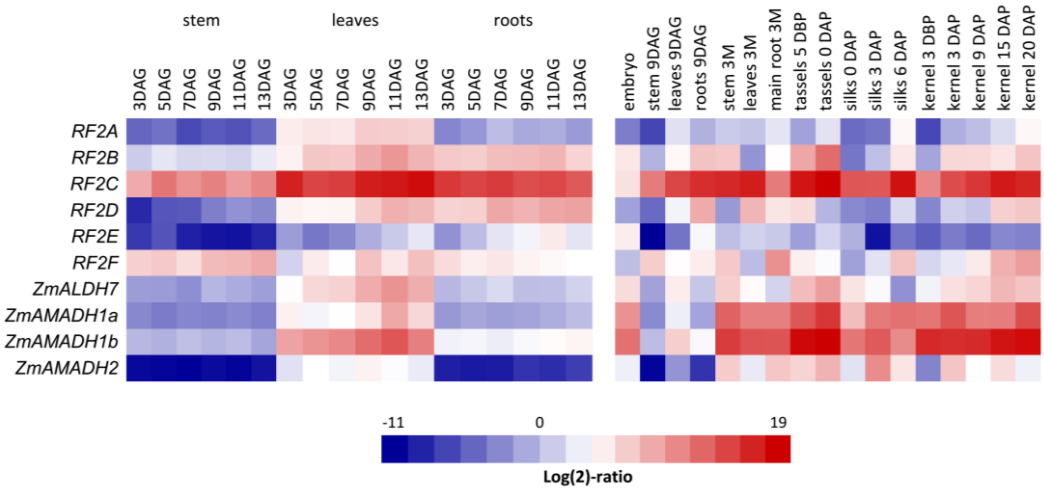

Figure 37. Expression profiles of *ZmALDH* genes. Gene expression was studied in stem, leaves and roots during 2 weeks after germination (left side) and in various organs during the lifespan of maize plants (right side). The heat map illustrates transcript levels detected in 1 ng of total RNA. All values are expressed as $\log_2$-ratios and are color-coded from blue to red (the lowest and highest detected transcript numbers, respectively). DAG, days after germination; DAP, days after pollination; DBP, days before pollination; M, months.

The pattern of gene expression in older plants, in tassels, silks and kernels was also analyzed. Again, *RF2C* is the most expressed *ALDH2* gene in maize. *RF2B*, *RF2C* and *ZmALDH7*, *ZmAMADH1a* and *ZmAMADH1b* are highly abundant in tassels at 5 DBP and 0 DAP suggesting their important role in pollen development. In silks, gene expression was lower compared with that in tassels. Relatively high levels of *RF2A*, *RF2B*, *RF2C* and *RF2F* transcripts appear in silks at 6 DAP. In kernel, we detected a strong expression of *RF2B* and *RF2C* followed by *RF2D* and *RF2F*. *RF2A* expression was highest in silks at 6 DAP and kernels at 20 DAP while those of *RF2B*, *RF2C* and *ZmALDH7* were strongest in tassels. The *RF2D* transcripts accumulated in mature leaves, while the *RF2E* gene was significantly expressed only in the embryo. The *FR2F* gene was strongly expressed in the stem and main root. The strong expression of *ZmALDH7* in kernel, tassels and silks correlates well with a strong expression of *LKR/SDH* gene observed in maize endosperm (Kemper *et al.*, 1999) and in Arabidopsis floral organs (Tang *et al.*, 1997) suggesting an active saccharopine pathway in developing seeds and in reproductive organs containing actively dividing cells. *ZmAMADH1a* (coding for the AMADH isoform with higher BADH activity) is highly expressed in young and mature leaves as well as in roots of younger plants. Z*mAMADH1b* is also highly expressed in silks at 0 days after pollination (DAP) and in kernel at 5 DAP. Both *ZmAMADH1* genes are well expressed in

tassels. These data indicate that AMADHs might be important for controlling ω-aminoaldehyde levels during early stages of the seed development.

Phenolamides (hydroxycinnamic acid amides) are accumulated in reproductive organs of many plants during stress or due to function as inducible defense against insect herbivory (Onkokesung et al., 2012). Moreover, they are also known as to contribute to cell-wall cross-linking (reviewed in Bassard et al., 2010; Gaquerel et al., 2014). The absence of phenolamides in the anthers was previously considered as a reason for the occurrence of male sterility in maize (Martin-Tanguy et al., 1982). Due to the changes in phenolamide biosynthesis might be the fertility restoration linked to *RF2A* gene expression, which is abundant in tapetal cells and important for the anther development (Liu *et al.*, 2001). Coniferaldehyde and sinapaldehyde are oxidized by other cALDH2 isoforms. Therefore, cALDH might be involved in the biosynthesis of phenolamides in various plant organs as well as during stress conditions

5.4 Purine riboside-preferring NRH from maize

The results of this chapter are published in Kopečná *et al*., 2013. My contribution in these publications was in cloning, expression, purification and kinetic measurements of ZmNRH3. I also performed qPCR measurements. These data are unpublished.

5.4.1 Substrate Specificity of ZmNRH3

The genome databases for the maize (www.maizesequence.org, v5b.60) indicate that it contains five *NRH* genes, respectively. The two paralogous genes *ZmNRH1a* and *ZmNRH1b* are localized on chromosomes 8 and 3, respectively. The two other paralogs, *ZmNRH2a* and *ZmNRH2b*, lie on chromosomes 4 and 1, respectively. The last *ZmNRH3* gene is localized on chromosome 2. In order to identify their function, I focused on analyzing ZmNRH3 isoform.

ZmNRH3 isoform was purified (Figure 36A) and kinetic parameters were measured using several ribosides (Figure 38B). The specific activity of ZmNRH3 with 200 mM xanthosine was 61 nkat mg^{-1}. ZmNRH3 prefers inosine and xanthosine as the best substrates while adenosine, uridine, cytidine, iPR and tZR are weaker substrates. ZmNRH3 displays similar substrate preferences together with PpNRH1 (Table 5, Kopečná et.al 2013). They both exhibit the highest catalytic efficiency with inosine and xanthosine. In line with our results and current system of classification, ZmNRH3 belongs to a nonspecific IU-NRH class with a preference towards purine ribosides (Parkin *et al*., 1991; Shi *et al*., 1999). Nevertheless, PpNRH1 and ZmNRH3 differ from a group of ZmNRH2a and 2b, PpNRH2 and AtNRH1, which all prefer uridine and xanthosine (Kopečná et.al 2013, Jung *et al*., 2009, 2011). This suggests at least two subclasses of IU-NRHs appear in plants. Inosine, xanthosine, and guanosine are involved in the purine catabolic pathway that starts with adenosine

monophosphate (Zrenner *et al*., 2006). The xanthine and hypoxanthine nucleobases are formed by the action of NRHs and are further processed by xanthine dehydrogenase to give uric acid. Adenosine and adenine are produced by the cytokinin degradation catalyzed by CKO (EC 1.5.99.12; Houba-Hérin *et al*., 1999).

Table 8. Substrate specificity of two NRHs from moss *P. patens* and maize. Relative reaction rates (%) were measured at 200 mM substrate concentration. Activities were measured in 200 mM Tris-HCl buffer (pH 7.5) containing 400 mM KCl and 1 mM DTT. The specific activities for PpNRH1 and ZmNRH3 with 200 mM xanthosine were 135 and 61 nkat mg^{-1}, respectively.

Substrate	Relative Rate (%)	
	PpNRH1	ZmNRH3
Inosine	87	100
Xanthosine	100	70
Adenosine	6.1	2
Guanosine	1.7	1.5
Uridine	5.7	5
Cytidine	0.1	0.1
iPR	0.1	1.4
tZR	0.1	1.5

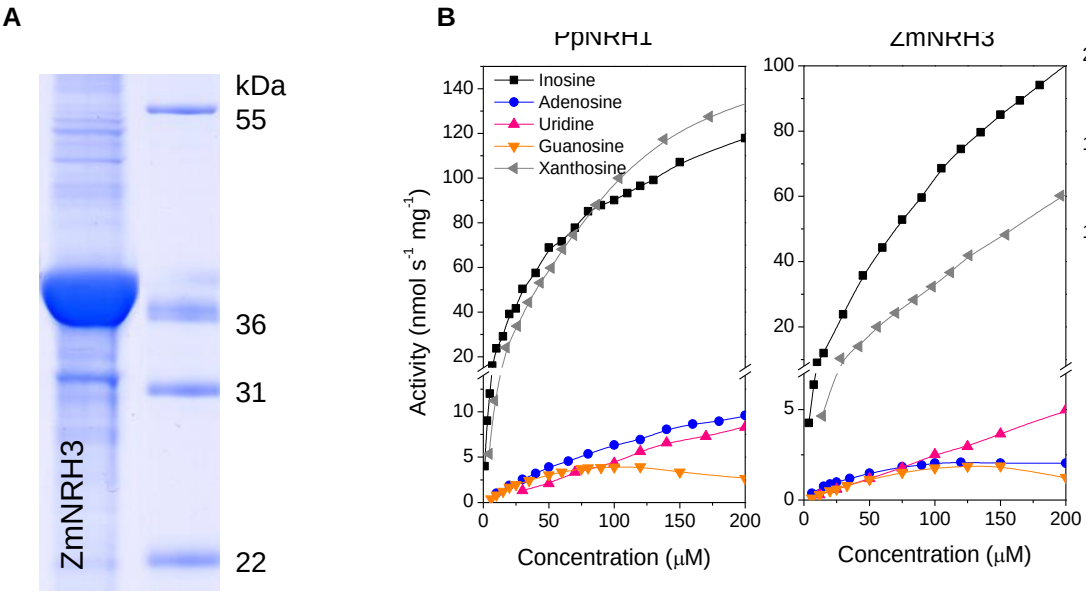

Figure 38. (A) Coomasie stained SDS-PAGE gels of recombinant ZmNRH3. Protein is after partial His-tag affinity purification. **(B) Saturation curves of purine riboside preferring NRHs - PpNRH1 and ZmNRH3**. Data were measured with five substrates (inosine, xanthosine, adenosine, guanosine, and uridine) in 200 mM Tris-HCl buffer (pH 7.5) containing 400 mM KCl and 2 mM DTT.

5.4.2 Substrate binding in ZmNRH3

The asymmetric unit of the ZmNRH3 crystal includes one dimer and according to the results from gel filtration chromatography the active form in solution is a dimer (Kopečná *et al*., 2013). The similar findings were obtained also for PpNRH1. PpNRH1 and ZmNRH3 crystal structures are the first reported crystal structures for plant NRHs (Figure 39A). PpNRH1 and ZmNRH3 monomers and dimers share high similarity to each other, with average RMSD values

of 0.9 and 1.2 Å for all Ca atoms, respectively. Each monomer is composed from a typical NRH fold containing 12 β-strands and 13 α-helices.

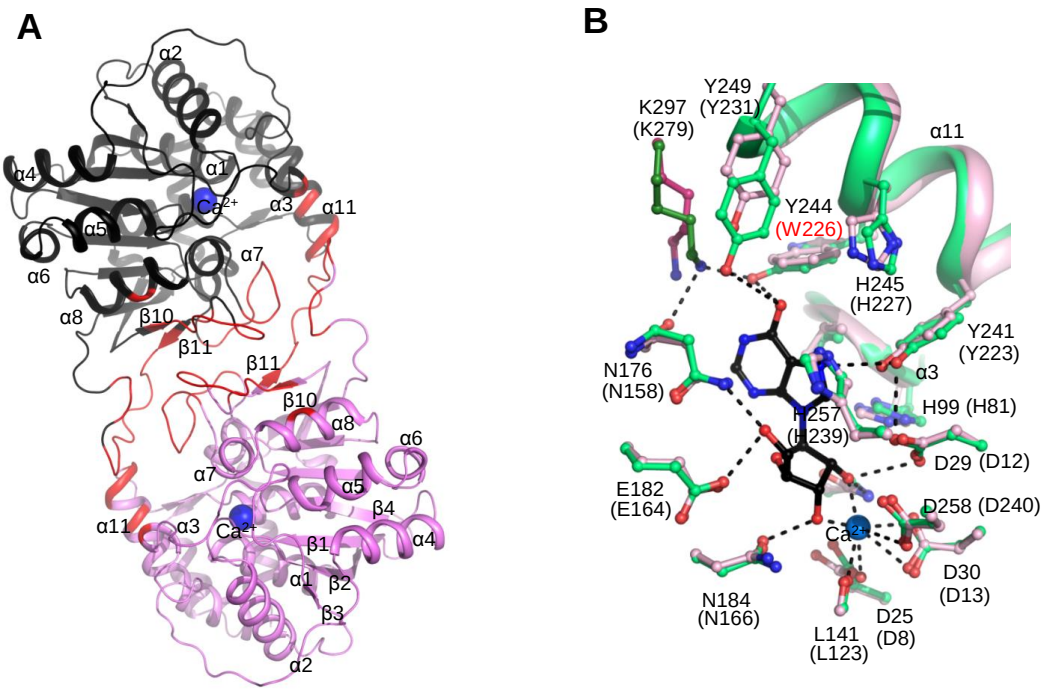

Figure 39. (A) Dimeric structure of plant NRH. One subunit is colored in black and the other in violet. The calcium ion in the active site is shown as a blue sphere. Inter-subunit contacts are shown in red. **(B) Substrate binding sites of PpNRH1 (in green) and ZmNRH3 (in pink).** A molecule of inosine (in black) was docked into the active site. Amino acid residues are labeled and H-bonds and calcium ion coordination are shown as dashed lines. Differences in the sequences of the two NRHs are red labeled

A conserved Ca^{2+} ion in the active site is tightly bound to the D8, D13 and D240 and to the main-chain carbonyl group of L123 in ZmNRH3 (Figure 39B). Its octahedral coordination can be completed either by three water molecules or by a catalytic water molecule and the 2′- and 3′-hydroxyl groups of the substrate ribose moiety. The catalytic water molecule in turn interacts with the catalytic base, which is believed to increase the nucleophilicity of the water molecule attacking the C1′-N9 bond of the substrate. The calcium ion is believed to lower the pK_a of the catalytic water molecule prior to proton transfer to the active site base (Degano *et al.*, 1998). The structure of YeiK in complex with inosine (PDB 3B9X) was used for modeling a substrate position in the active site of ZmNRH3 by structural superposition. The ribose moiety is tightly bound to conserved residues among NRHs family corresponding to N158, E164, D240, N166, D12, D13 and N37 in ZmNRH3. In contrast, the nucleobase is surrounded by more variable residues: V82 and H81 from helix α3, by the aromatic residues Y223, W226, H227 and Y231 from helix α11, by H239 in helix α12, by N158 in the β5-α7 loop and by the adjacent side chain of K279, which protrudes into the active site from the other subunit. A structural comparison of the substrate binding sites of PpNRH1 and ZmNRH3 (Figure 39B)

shows that only one residue is different around the nucleobase, tyrosine Y244 in PpNRH1 is replaced by a tryptophan in ZmNRH3.

5.5 Expression of *NRH* genes in maize

The expression pattern of *ZmNRHs* was analyzed in developing maize seedlings (stem, roots and leaves) during the first two weeks after germination (Figure 40). All *NRHs* genes were strongly expressed in young leaves and weakly in stem. The most abundant transcripts were those of *ZmNRH1a* and *ZmNRH3* in leaves and those of *ZmNRH1b* and *ZmNRH3* in roots. The lowest expression was observed for *ZmNRH2b* in all samples. The pattern of gene expression in older plants, in tassels, silks and kernels was also analyzed (Figure 40). The expression of *NRHs* genes was detected higher in leaves and stem compared with roots. Strong expression was observed in tassels, silks and kernel. Conversely, the lowest expression was observed in embryo for all studied genes.

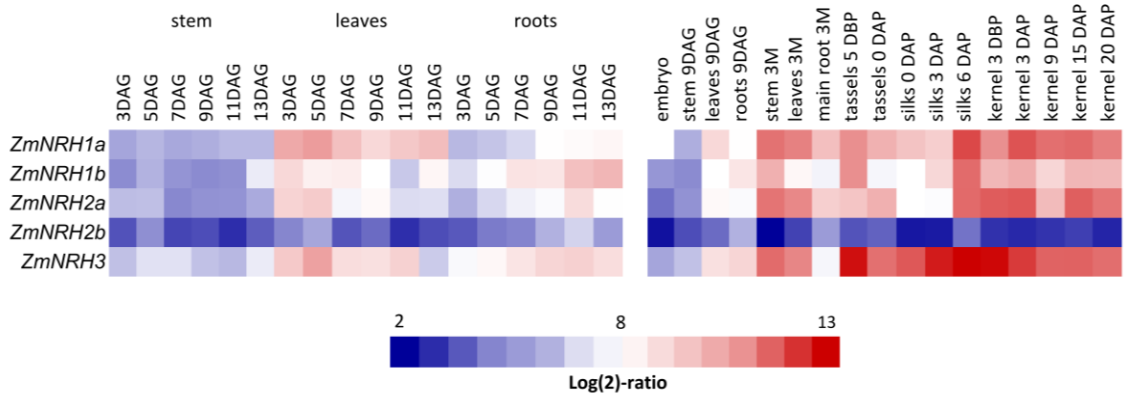

Figure 40. Expression profiles of *ZmNRHs* in maize. . Gene expression was studied in stem, leaves and roots during 2 weeks after germination (left side) and in various organs during the lifespan of maize plants (right side). The heat map illustrates transcript levels detected in 1 ng of total RNA. Total RNA was isolated from maize tissues from three independent biological replicates. As endogenous controls the elongation factor 1 and the *β*-actine genes were used.

.

6 Conclusions

The most important outputs of this work can be summarized as follows:

1. The glycosylation of ZmCKO1 is important for the enzyme stability.

2. New structures of ZmCKO2 and ZmCKO4a were solved and both their structures surprisingly lack two helices and a loop from substrate binding domain. This change leads to more open substrate cavity and allows for binding larger substrates like cytokinin glucosides. The change in substrate preferences is also linked to nonconserved residue E381, which is present in half of known CKO sequences and participates in binding of the N9 atom of the cytokinin substrate. Presence of E381 residue in ZmCKO1 (but not in ZmCKO2 and ZmCKO4a) leads in higher K_m values for cytokinin ribosides and nearly no activity with cytokinin glucosides (iP9G and *t*Z9G).

3. Inhibitory strength and binding mode of two new thidiazuron derivatives 3-(1,2,3-thiadiazol-5-yl)-1-[3-(trifluoromethoxy)phenyl]urea (3FMTDZ) and 1-[2-(2-hydroxyethyl)phenyl]-3-(1,2,3-thiadiazol-5-yl)urea (HETDZ) was analyzed. Crystal structures reveal that they bind in the active site in two mutually opposite orientations - thiadiazolyl ring of 3FMTDZ is positioned over the isoalloxazine ring of FAD while that of HETDZ is in opposite orientation and points to entrance of the active site. The inhibitors are easy to synthetize; they are stronger inhibitors than thidiazuron itself and inhibit CKO in competitive manner.

4. Kinetic and structural studies were perfomed on maize ALDH2, ALDH7 and ALDH10 isoforms. Interestingly, ALDH2 and ALDH7 are tetrameric but ALDH10 is dimeric. While the active sites of ALDH7 and ALDH10 are quite conserved and determine the substrate specificity towards particular aldehydes, those of ALDH2 isoforms are highly variable and oxidize wide range of aliphatic and aromatic aldehydes including aldehydes released by CKO reaction and aldehydes released during the lipid peroxidation.

5. Kinetic and structural study was perofmed on maize NRH family especially on purine riboside-preferring ZmNRH3. The enzyme is dimeric and is able to hydrolyze adenosine and cytokinin ribosides in addition to preffered substrates inosine and xanthosine.

6. ALDH2 and NRH isoforms studied in this work are localized in cytosol as well as one of CKO isoforms indicating that a mutual interconnection of these pathways is possible (Figure 41).

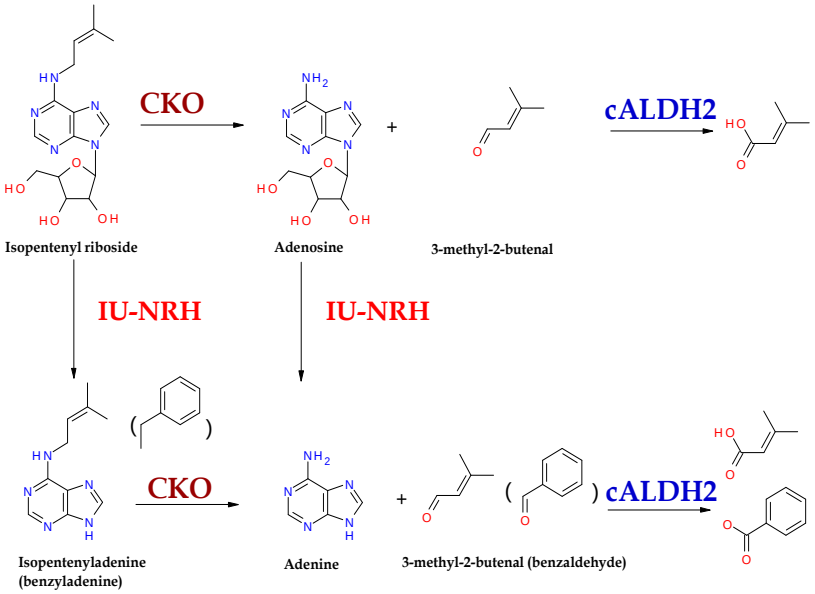

Figure 41. A scheme of possible reactions related to CKO. The scheme illustrates possible reactions in cytosol linked to action of cytosolic CKO including involvement of cytosolic ALDH2 and IU-NRHs

7 Abstracts from conferences

Končitíková R, Kopečná M, Vigouroux A, Moréra S, Šebela M, Kopečný D. Structure-function study on plant aldehyde dehydrogenases from family 2 and family 7. 13th Discussions in Structural Biology, Academic and University Center, Nové Hrady, March 19-21, 2015. ***Poster by R. Končitíková***. Abstract in: Materials Structure in Chemistry, Biology, Physics and Technology, Bulletin of the Czech and Slovak Crystallographic Association 2015, 22 (1):41.

Končitíková R, Kopečná M, Moréra S, Vigouroux A, Šebela M, Kopečný D. Structure-function study on enzymes linked to cytokinin metabolism - aldehyde dehydrogenases and nucleoside N-ribohydrolases. 12th Discussions in Structural Biology, Academic and University Center, Nové Hrady, March 13-15, 2014. ***Poster by R. Končitíková***. Abstract in: Materials Structure in Chemistry, Biology, Physics and Technology, Bulletin of the Czech and Slovak Crystallographic Association 2014, 21 (1):37.

Končitíková R, Kopečná M, Kopečný D, Moréra S, Vigouroux A, Frömmel J, Šebela M. Structural characterization of two maize aldehyde dehydrogenases from family 2. 11th Discussions in Structural Biology, Academic and University Center, Nové Hrady, March 14-16, 2013. ***Poster by R. Končitíková***. Abstract in: Materials Structure in Chemistry, Biology, Physics and Technology, Bulletin of the Czech and Slovak Crystallographic Association 2013, 20 (1): 31.

Končitíková R, Tylichová M, Kopečný D, Moréra S, Vigouroux A, Frömmel J, Šebela M. Maize aledyhe dehydrogenases from the family 7 and 10. 10th Discussions in Structural Biology, Academic and University Center, Nové Hrady, March 24-26, 2012. ***Lecture by R. Končitíková***. Abstract in: Materials Structure in Chemistry, Biology, Physics and Technology, Bulletin of the Czech and Slovak Crystallographic Association 2012, 19 (1): 24.

Šebela M, **Končitíková R**, Lenobel R, Franc V, Řehulka P, Tylichová M, Kopečný D, Madzak C. Analysis of N-glycosylation in maize cytokinin oxidase/dehydrogenase 1 using a manual micro gradient chromatographic separation coupled offline to MALDI-TOF/TOF mass spektrometry. Cytokinin metabolism, signaling and function, Freie Universität Berlin, Dahlem Centre of Plant Sciences (DCPS), July 6-8, 2012. ***Poster by R. Končitíková***.

Šebela M, **Končitíková R**, Lenobel R, Franc V, Řehulka P, Tylichová M, Kopečný D. Structural and functional study on the glycosylation in maize cytokinin oxidase/dehydrogenase 1. 9th Discussions in Structural Biology, Academic and University Center, Nové Hrady, March 24-26, 2011. ***Lecture L10 by M. Šebela***. Abstract in: Materials Structure in Chemistry, Biology, Physics and Technology, Bulletin of the Czech and Slovak Crystallographic Association 2011, 18 (1):19.

Šebela M, **Končitíková R**, Lenobel R, Franc V, Řehulka P, Tylichová M, Kopečný D. Mass spectrometric analysis of N-glycosylation in maize cytokinin oxidase/dehydrogenase 1. 5th Central and Eastern European Proteomic Conference, September 19-22, Conference Centre U Hájků, Prague, Czech Republic. ***Poster W-5 by R. Končitíková***. Abstract in: Book of Abstracts, p. 87.

Kopečný D, Tylichová M, Andree T, **Končitíková R**, Šebela M. Biochemical characterization of a recombinant plant aldehyde dehydrogenase 7 from *Pisum sativum* and *Zea mays*. 36th FEBS Congress, Biochemistry for Tomorrow's Medicine, Lingotto Conference Center, Torino, Italy, June 25-30, 2011. ***Poster P18.13 by D. Kopečný***. Abstract in: *FEBS J.* **278** (Suppl. 1), 315.

Šebela M, **Končitíková R**, Lenobel R, Franc V, Řehulka P, Tylichová M, Kopečný D. Structural and functional study on the glycosylation in maize cytokinin oxidase/dehydrogenase 1. 36th FEBS Congress, Biochemistry for Tomorrow's Medicine, Lingotto Conference Center, Torino, Italy, June 25-30, 2011. ***Poster P18.25 by M. Šebela***. Abstract in: *FEBS J.* **278** (Suppl. 1), 319.

8 References

Allakhverdiev, S.I., Los, D.A., Mohanty, P., Nishiyama, Y. and Murata, N. (2007) Glycinebetaine alleviates the inhibitory effect of moderate heat stress on the repair of photosystem II during photoinhibition. *Biochim Biophys Acta*. **1767**(12), 1363-71.

Arikit, S., Yoshihashi, T., Wanchana, S., Uyen, T. T., Huong, N. T., Wongpornchai, S., and Vanavichit, A. (2011) Deficiency in the amino aldehyde dehydrogenase encoded by GmAMADH2, the homologue of rice Os2AP, enhances 2-acetyl-1-pyrroline biosynthesis in soybeans (*Glycine max* L.). *Plant Biotechnol. J.* **9**, 75–87.

Arruda, P., Kemper, E.L., Papes, F. and Leite, A. (2000) Regulation of lysine catabolism in higher plants. *Trends Plant Sci.* **5**, 324–330.

Bae, E., Bingman, C.A., Bitto, E., Aceti, D.J. and Phillips, G.N. (2008) Crystal structure of Arabidopsis thaliana cytokinin dehydrogenase. *Proteins*.**7**, 303-306.

Barclay, K.D. and Mckersie, B.D. (1994) Peroxidation reactions in plant membranes – effects of free fatty acids. *Lipids.* **29**, 877-882.

Bassard, J.E., Ullmann, P., Bernier, F. and Werck-Reichhart, D. (2010) Phenolamides: bridging polyamines to the phenolic metabolism. *Phytochemistry*. **71**(16), 1808-24.

Bilyeu, K.D., Cole, J.L., Laskey, J.G., Riekhof, W.R., Esparza, T.J., Kramer, M.D. and Morris, R.O. (2001) Molecular and biochemical characterization of a cytokinin oxidase from maize. *Plant Physiol.* **125**, 378-386.

Blanc, E., Roversi, P., Vonrhein, C., Flensburg, C., Lea, S.M. and Bricogne, G. (2004) Refinement of severely incomplete structures with maximum likelihood in BUSTER-TNT, *Acta Crystallogr., Sect. D. Biol. Crystallogr.* **60**, 2210-2221.

Boatright, J., Negre, F., Chen, X., Kish, C. M., Wood, B., Peel, G., Orlova, I., Gang, D., Rhodes, D. and Dudareva, N. (2004) Understanding in vivo benzenoid metabolism in petunia petal tissue. *Plant Physiol*. **135**, 1993–2011.

Bradbury, L. M., Gillies, S. A., Brushett, D. J., Waters, D. L., and Henry, R. J. (2008) Inactivation of an aminoaldehyde dehydrogenase is responsible forfragrance in rice. *Plant Mol. Biol*. **68**, 439–449.

Brocker, Ch., Lassen, N., Estey, T., Pappa, A., Cantore, M., Orlova, V.V., Chavakis, T., Kavanagh, K.L., Oppermann, U. and Vasiliou. V. (2010) Aldehyde dehydrogenase 7A1 (ALDH7A1) is a novel enzyme involved in cellular defense against hyperosmotic stress. *Journal of Biological Chemistry*. **285**, 18452-18463.

Brocker, C., Thompson, D.C. and Vasiliou, V. (2012) The role of hyperosmotic stress in inflammation and disease. *Biomol Concepts*. **3**(4), 345-364.

Brocker, C., Vasiliou, M., Carpenter, S., Carpenter, C., Zhang, Y., Wang, X., Kotchoni, S.O., Wood, A.J., Kirch, H.H., Kopečný, D., Nebert, D.W, and Vasiliou, V. (2013) Aldehyde dehydrogenase (ALDH) superfamily in plants: gene nomenclature and comparative genomics. *Planta.* **237**, 189-210.

Brouquisse, R., Weigel, P., Rhodes, D., Yocum, C. F., and Hanson, A. D. (1989) Evidence for a ferredoxin-dependent choline monooxygenase from spinach chloroplast stroma.*Plant Physiol.* **90**, 322–329

Bruce, M.I. and Zwar, J.A. (1966) Cytokinin activity of some substituted ureas and thioureas. *Proc R Soc Lond B Biol Sci.* **165**, 245–265.

Brunk, D. G., Rich, P. J., and Rhodes, D. (1989) Genotypic variation forglycinebetaine among public inbreds of maize. *Plant Physiol*. **91**, 1122–1125.

Buchanan, C.D., Lim, S., Salzman, R.A., Kagiampakis, I., Morishige, D.T., Weers, B.D., Klein, R.R., Pratt, L.H., Cordonnier-Pratt, M.M., Klein, P.E. and Mullet, J.E. (2005) Sorghum bicolor's transcriptome response to dehydration, high salinity and ABA. *Plant Mol Biol*. **58**, 699–720.

Burch, L.R. and Stuchbury, T. (1987) Activity and distribution of enzymes that interconvert purine bases, ribosides and ribotides in the tomato plant and possible implications for cytokinin metabolism. Physiologia Plantarum. **69**. 283-288.

Burch, L. R. and Horgan, R. (1989) The purification of cytokinin oxidase from *Zea mays* kernels. *Phytochemistry.* **28**, 1313–1319.

op den Camp, R.G. and Kuhlemeier, C. (1997) Aldehyde dehydrogenase in tobacco pollen. *Plant Mol Biol.* **35**, 355-365.

Campos, A., Rijo-Johansen, M.J., Carneiro, M.F. and Fevereiro, P. (2005) Purification and characterisation of adenosine nucleosidase from Coffea arabica young leaves. *Phytochemistry.* **66**, 147–151.

Degano, M., Gopaul, D.N., Scapin, G., Schramm, V.L. and Sacchettini, J.C. (1996) Three-dimensional structure of the inosine-uridine nucleoside N-ribohydrolase from *Crithidia fasciculata*. *Biochemistry*. **35**, 5971–5981.

Degano M, Almo SC, Sacchettini JC, Schramm VL (1998) Trypanosomal nucleoside hydrolase: a novel mechanism from the structure with a transition-state inhibitor. *Biochemistry* **37**: 6277–6285.

Dewey, R.E., Timothy, D.H. and Levings, C.S. (1987) A mitochondrial protein associated with cytoplasmic male sterility in the T cytoplasm of maize. *Proc Natl Acad Sci U S A*. **84**(15), 5374-8.

Díaz-Sanchez, A., Gonzalez-Segura, L., Mujica-Jimenez, C., Rudino-Pinera, E., Montiel, C., Martinez-Castilla, L.P. and Munoz-Clares, R.A. (2012) Amino Acid Residues Critical for the Specificity for Betaine Aldehyde of the Plant ALDH10 Isoenzyme Involved in the Synthesis of Glycine Betaine. *Plant Physiology*. **158**, 1570–1582.

Doležal, K., Popa, I., Hauserova, E., Spichal, L., Chakrabarty, K., Novak, O., Kryštof, V., Voller, J., Holub, J. and Strnad, M. (2007). Preparation, biological activity and endogenous occurrence of N(6)-benzyladenosines. *Bioorg. Med. Chem*. **15**, 3737–3747.

Dudareva, N., Klempien, A., Muhlemann, J.K. and Kaplan, I. (2013) Biosynthesis, function and metabolic engineering of plant volatile organic compounds. *New phytologist*. **198**, 16-32.

Emsley P. and Cowtan K. (2004). Coot: model-building tools for molecular graphics.*Acta Crystallogr. Sect.D-Biol.Crystallogr*. **60**, 2126-2132.

Estupiñán, B. and Schramm, V.L. (1994) Guanosine-inosine-preferring nukleoside N-glycohydrolase from *Crithidia fasciculata*. *J Biol Chem*. **269**, 23068–23073.

Farrés, J., Wang, X., Takahashi, K., Cunningham, S.J., Wang, T.T. and Weiner, H. (1994) Effects of changing glutamate 487 to lysine in rat and human liver mitochondrial aldehyde dehydrogenase. A model to study human (Oriental type) class 2 aldehyde dehydrogenase. *J. Biol. Chem.* **269**, 13854-13860.

Fraaije, M.W., Benen, J.A.E., Visser, J., van Berkel, W.J.H. and Mattevi, A. (1998) A novel oxidoreductase family sharing a conserved FAD-binding domain, *Trends Biochem. Sci.* **23**, 206–207.

Fraaije, M.W., van den Heuvel, R.H., van Berkel, W.J. and Mattevi, A. (1999) Covalent flavinylation is essential for efficient redox catalysis in vanillyl-alcohol oxidase. *J Biol. Chem.* **274**, 35514-35520.

Frébort, I., Šebela, M., Galuszka, P., Werner, T., Schmülling, T. and Peč, P. (2002) Cytokinin oxidase/cytokinin dehydrogenase assay: optimized procedures and applications, *Anal. Biochem.* **306**, 1-7.

Frébortová, J., Fraaije, M.W., Galuszka, P., Šebela, M., Peč, P., Hrbáč, J., Novák, O., Bilyeu, K.D., English, J.T. and Frébort, I. (2004) Catalytic reaction of cytokinin dehydrogenase: preference for quinones as electron acceptors, *Biochem. J.* **380**, 121-130.

Frébortová, J., Novák, O., Frébort, I., Jorda, R. (2010) Degradation of cytokinins by maize cytokinin dehydrogenase is mediated by free radicals generated by enzymatic oxidation of natural benzoxazinones. *Plant J.* **61**, 467-481.

Fong, W.P., Cheng, C.H.K., Tang, W.K. (2006) Antikvitin, a relatively unexplored member in the superfamily of aldehyde dehydrogenases with diversified physiological functions. *Cellular and Molecular Life Sciences*. **63**, 2881-2885.

Fukuda, H., (2004) Signals that control plant vascular cell defferentiation. *Nature Reviews Molecular Cell Biology*. **5**, 379-391.

Gallagher, R.C., van Hove, J.L., Scharer, G., Hyland, K., Plecko, B., Waters, P.J., Mercimek-Mahmotoglu, S., Stockler-Ipsiroglu, S., Salomons, G.S., Rosenberg, E.H., Struys, E.A. and Jakobs, C. (2009) Folinic acid-responsive seizures are identical to pyridoxine-dependent epilepsy. *Annals of Neurology*. **65**, 550-556.

Galuszka, P., Frébort, I., Šebela, M., Sauer, P., Jacobsen, S. and Peč, P (2001) Cytokinin oxidase or dehydrogenase? Mechanism of the cytokinin degradation in plants. *Eur. J. Biochem.* **268**, 450–461.

Gan, S. and Amasino, R.M. (1995) Inhibition of leaf senescence by autoregulated production of cytokinin. *Science*. **270**, 1986-1988.

Gao, C.X. and Han, B. (2009) Evolutionary and expression study of the aldehyde dehydrogenase (ALDH) gene superfamily in rice (Oryza sativa). *Gene*. **431**, 86–94.

Gaquerel, E., Gulati, J. and Baldwin, I.T. (2014) Revealing insect herbivory-induced phenolamide metabolism: from single genes to metabolic network plasticity analysis. *Plant J*. **79**(4), 679-92.

Giabbai, B. and Degano, M. (2004) Crystal structure to 1.7 a of the Escherichia coli pyrimidine nucleoside hydrolase YeiK, a novel candidate for cancer gene therapy. *Structure*. **12**, 739–749.

Gonzalez-Segura, L., Rudino-Pinera, E., Munoz-Clares, R.A. and Horjales, E. (2009) The crystal structure of a ternary complex of betaine aldehyde dehydrogenase from Pseudomonas aeruginosa Providesnew insight into the reaction mechanism and shows a novel binding mode of the 2'-phosphate of NADP+ and a novelcation binding site. *J.Mol.Biol.* **385**, 542.

González-Segura, L., Ho, K.K., Perez-Miller, S., Weiner, H. and Hurley, T.D. (2013) Catalytic contribution of threonine 244 in human ALDH2. *Chem Biol Interact.* 202(1-3), 32-40.

Grabber, J.H., Ralph, J. and Hatfield, R.D. (2002) Model studies of ferulate-coniferyl alcohol cross-product formation in primary maize walls: implications for lignification in grasses. *J Agric Food Chem.* **50**(21), 6008-16.

Grabber, J.H., Ralph, J. and Hatfield, R.D. (2000) Cross-linking of maize walls by ferulate dimerization and incorporation into lignin. *J Agric Food Chem*. **48**(12):6106-13.

Grobman, Alexander (1961). *Races of Maize in Peru*.

Gruez, A., Roig-Zamboni, V., Grisel, S., Salomoni, A., Valencia, C., Campanacci, V., Tegoni, M. and Cambillau, C. (2004) Crystal structure and kinetics identify Escherichia coli YdcW gene product as a medium-chain aldehyde dehydrogenase. *J.Mol.Biol.* **343,** 29-41.

Guranowski, A. and Schneider, Z. (1977) Purification and characterization of adenosine nucleosidase from barley leaves. *Biochim Biophys Acta.* **482**, 145–158.

Guerrero, F.D., Jones, J.T. and Mullet, J.E. (1990) Turgor-responsive gene transcription and RNA levels increase rapidly when pea shoots are wilted. Sequence and expression of three inducible genes. *Plant Molecular Biology*. **15**, 11-26.

Hallen, A., Jamie, J.F. and Cooper, A.J. (2013) Lysine metabolism in mammalian brain: an update on the importance of recent discoveries. *Amino Acids.* **45**(6), 1249-72.

Hare, P.D. and van Staden, J. (1994) Cytokinin oxidase: Biochemical features and physiological significance. *Physiol. Plant*. **91**, 128-136.

Hibino, T., Meng, Y.L., Kawamitsu, Y., Uehara, N., Matsuda, N., Tanaka, Y., Ishikawa, H., Baba, S., Takabe, T., Wada, K., Ishii, T. and Takabe, T. (2001) Molecular cloning and functional characterization of two kinds of betaine-aldehyde dehydrogenase in betaine-accumulating mangrove Avicennia marina (Forsk.) Vierh. *Plant Mol Biol*. **45**(3), 353-63.

Holt, A., Degenhardt, O. S., Berry, P. D., Kapty, J. S., Mithani, S., Smith, D. J., and Di Paolo, M. L. (2007) The effects of buffer cations on interactions between mammalian copper-containing amine oxidases and their substrates. *J. Neural Transm.* **114**, 733–741.

Hooker, A., Smith, D., Lim, S. and Beckett, J. (1970) Reaction of corn seedling with male-sterile cytoplasm to *Helminthosporium maydis*, *Plant Dis. Rep.* **54**, 708-712.

Houba-Hérin, N., Pethe, C., d'Alayer, J. and Laloue, M (1999) Cytokinin oxidase from *Zea mays*: purification, cDNA cloning and expression in moss protoplasts, *Plant J.* **17**, 615–626.

Horenstein, B.A. and Schramm, V.L. (1993) Electronic nature of the transition state for nucleoside hydrolase. A blueprint for inhibitor design. *Biochemistry*. **32**, 7089-7097.

Huang and Miller (1991) The lalign program implements the algorithm of, published in *Adv. Appl. Math.* **12**, 337-357.

Chatfield, J.M. and Armstrong, D.J. (1987) Cytokinin oxidase from *Phaseolus vulgaris* callus tissue. Enhanced *invitro* activity of the enzyme in the presence of copper-imidazole complexes. *Plant Physiol.* **84**, 726-731.

Chan, C.L., Judy, W.Y., Wong, C.-P., Michel, K.L., Chan, W.-P., (2011) Human antiquitin: Structural and functional studies. *Chemico-Biological Interactions.* **191** (2011), 165–170.

Chen, C.M. and Kristopeit, S.M. (1981) Metabolism of cytokinin: deribosylation of cytokinin ribonucleoside by adenosine nucleosidase from wheat germ cells. *Plant Physiol*. **68**, 1020–1023.

Chen, X., Zeng, Q.i.n.and Wood, A.J. (2002) The stress-responsive *Tortula ruralis* gene ALDH21A1 describes a novel eukaryotic aldehyde dehydrogenase protein family. *Journal of Plant Physiology*. **159**, 677-684.

Imagawa, H., Yamano, H. and Inouem, K. (1979) Purification and properties of adenosime nucleosidases form tea leaves. *Agricul. Biol. Chem*. **43**, 2337-2342.

Incharoensakdi, A., Hibino, T. and Takabe, T. (2005) Glu 103 Gln site-directed mutation causes an alteration in physical properties of spinach betaine aldehyde dehydrogenase. *J Biochem Mol Biol Biophys*. **6**(4):243-8.

Inoue, T., Higuchi, M., Hashimoto, Y., Seki, M., Kobayashi, M., Kato, T., Tabata, S., Shinozaki, K. and Kakimoto, T. (2001) Identification of CRE1 as a cytokinin receptor from *Arabidopsis*. *Nature.* **409**, 1060–1063.

Ishitani, M., Arakawa, K., Mizuno, K., Kishitani, S., and Takabe, T. (1993) Betaine aldehyde dehydrogenase in the Gramineae. Levels in leaves of both betaine-accumulating and non-accumulating cereal plants. *Plant Cell Physiol*. **34**, 493–495.

Isogai, Y. (1981) Cytokinin activities of N-phenyl-N′-(4-pyridyl)ureas, In *Metabolismand Molecular Activities of Cytokinins*, Péaud-Lenoël, C. and Guern, J., (Eds.), Springer-Verlag, Berlin, 115-128.

Johansson, K., El-Ahmad, M., Ramaswamy, S., Hjelmqvist, L., Jornvall, H. and Eklund, H. (1998) Structure of betaine aldehyde dehydrogenase at 2.1 A resolution. *Protein Sci*. **7**, 2106-2117.

Jones, K.H., Lindahl, R., Baker, D.C., Timkovich, R. (1987) Hydride transfer stereospecificity of rat liver aldehyde dehydrogenases. *J Biol Chem.* **262**(23)**,** 10911-3.

Jung, B., Flörchinger, M., Kunz, H.H., Traub, M., Wartenberg, R., Jeblick, W., Neuhaus, H-E. and Möhlmann, T. (2009) Uridine-ribohydrolase is a key regulator in the uridine degradation pathway of Arabidopsis. *Plant Cell*. **21**, 876–891.

Jung, B., Hoffmann, C. and Möhlmann, T. (2011) Arabidopsis nucleoside hydrolases involved in intracellular and extracellular degradation of purines. *Plant J.* **65**, 703–711.

Kabsch, W. (2010) XDS. Acta Crystallogr D Biol Crystallogr. **66**, 125-132.

Kemper**,** E.L**.**, Neto**,** G.C**.**, Papes**,** F**.**, Moraes**,** K.C**.**, Leite**,** A**. and** Arruda**,** P. **(1999)** The role of opaque2 in the control of lysine-degrading activities in developing maize endosperm. *Plant Cell.* 11(10)**,** 1981-94**.**

Kempton, J. H. (1924). Jala Maize. A Giant Variety from Mexico.*J Hered*. **15** (8), 337–344.

Rocheford, T.R., Kennell, J.C. and Pring, D.R. (1989) Genetic analysis of nuclear control of T-urf13/orf221 transcription in T cytoplasm maize. *Theor Appl Genet*. **84**(7-8):891-8.

Karl, J.R. (2013). The maximum leaf quantity of the maize subspecies (PDF). *The Maize Genetics Cooperation Newsletter*. 86, 4. ISSN 1090-4573.

Kim, J., Fuller, J.H., Kursk, V., Cunane, L., Chen, Z.W., Mathews, F.S. and McIntire, W.S. (1995) The cytochrome subunit is necessary for covalent FAD attachment to the flavoprotein subunit of p-cresol methylhydroxylase. *J. Biol. Chem.* **270**, 31202-31209.

Kirch, H.H., Nair, A. and Bartels, D. (2001) Novel ABA-and dehydration-inducible aldehyde dehydrogenase genes isolated from the resurrection plant *Craterostigma plantagineum* and *Arabidopsis thaliana*. *Plant Journal*. **28**, 544-554.

Kirch, H.H., Bartels, D., Wei, Y.L., Schnable, P.S. and Wood, A.J. (2004) The ALDH gene superfamily of Arabidopsis. *Trends Plant Sci.* **9**, 371–377.

Kirch, H.H., Schlingensiepen, S., Kotchoni, S., Sunkar, R. and Bartels, D. (2005) Detailed expression analysis of selected genes of the aldehyde dehydrogenase (ALDH) gene superfamily in Arabidopsis thaliana. *Plant Mol Biol.* **57**, 315–332.

Klyosov, A.A. (1996) Kinetics and specificity of human liver aldehyde dehydrogenases toward aliphatic, aromatic, and fused polycyclic aldehydes. *Biochemistry.* **35,** 4457-4467.

Končitíková, R., Vigouroux, A., Kopečná, M., Andree, T., Bartoš, J., Šebela, M., Moréra, S. and Kopečný, D. (2015) Role and structural characterization of plant aldehyde dehydrogenases from family 2 and family 7. *Biochem J.* **468**(1): 109-23.

Kopečný, D., Pethe, C., Šebela, M., Houba-Hérin, N., Madzak, C., Majira, A. and Laloue, M. (2005) High-level expression and characterization of *Zea mays* cytokinin oxidase/dehydrogenase in *Yarrowia lipolytica*, *Biochimie.* **87**, 1011-1022.

Kopečný, D., Šebela, M., Briozzo, P., Spíchal, L., Houba-Hérin, N., Mašek, V., Joly, N., Madzak, C., Anzenbacher, P. and Laloue, M. (2008). Mechanism-based inhibitors of cytokinin oxidase/dehydrogenase attack FAD cofactor. *J.Mol.Biol*. **380**, 886-899.

Kopečný, D., Briozzo, P., Popelková, H., Šebela, M., Končitíková, R., Spíchal, L., Nisler, J., Madzak, C., Frébort, I., Laloue, M. and Houba-Hérin, N. (2010) Phenyl- and benzylurea cytokinins as competitive inhibitors of cytokinin oxidase/dehydrogenase: a structural study. *Biochimie.* **92**, 1052-1062.

Kopečný, D., Tylichová, M., Snegaroff, J., Popelková, H., and Šebela, M. (2011) Carboxylate and aromatic active-site residues are determinants of high-affinity binding of _-aminoaldehydes to plant aminoaldehyde dehydrogenases. *FEBS J.* **278**, 3130–3139.

Kopečný, D., Končitíková, R., Tylichová, M., Vigouroux, A., Moskalíková, H., Soural, M., Šebela, M. and Moréra, S. (2013) Plant ALDH10 family: identifying critical residues for substrate specificity and trapping a thiohemiacetal intermediate. *J Biol. Chem*. **288**(13), 9491-507.

Kopečná, M., Blaschke, H., Kopečný, D., Vigouroux, A., Končitíková, R., Novák, O., Kotland, O., Strnad, M., Moréra, S. and von Schwartzenberg, K. (2013) Structure and function of nucleoside

hydrolases from Physcomitrella patens and maize catalyzing the hydrolysis of purine, pyrimidine, and cytokinin ribosides. *Plant Physiol*. **163**(4): 1568-83.

Kotchoni, S.O. and Bartels, D. (2003) Water stress induces the up-regulation of a specific set of genes in plants: aldehyde dehydrogenases as an example. *Bulgarian Journal of Plant Physiology*. 37-51.

Kotchoni, S.O., Kuhns, C., Ditzer, A., Kirch, H.H. and Bartels, D. (2006) Overexpression of different aldehyde dehydrogenase genes in Arabidopsis thaliana confers tolerance to abiotic stress and protects plants against lipid peroxidation and oxidative stress. *Plant Cell Environ.* **29**, 1033–1048.

Kurtz, J.E., Exinger, F., Erbs, P. and Jund, R. (2002) The URH1 uridine ribohydrolase of Saccharomyces cerevisiae. *Curr Genet.* **41**(3), 132-41.

Laemmli, UK. (1970) Cleavage of structural proteins during the assembly of the head of bacteriophage T4. *Nature*. **227**, 680–5.

Laloue, M. and Fox, J.E. (1989) Cytokinin oxidase from wheat. Partial purification and general properties, *Plant Physiol.* **90**, 899–906.

Liu, F., Cui, X., Horner, H.T., Weiner, H., Schnable, P.S. (2001) Mitochondrial aldehyde dehydrogenase activity is required for male fertility in maize. *Plant Cell.* **13**, 1063-1078.

Liu F. and Schnable P.S. (2002) Functional specialization of maize mitochondrial aldehyde dehydrogenases. *Plant Physiology*. **130**, 1657-1674.

Long, M.C., Nagegowda, D.A., Kaminaga, Y., Ho, K.K., Kish, C.M., Schnepp, J., Sherman, D., Weiner, H., Rhodes, D., Dudareva, N. (2009) Involvement of snapdragon benzaldehyde dehydrogenase in benzoic acid biosynthesis. *Plant J.* **59**, 256–265.

Mähönen, A.P., Bishopp, A., Higuchi, M., Nieminen, K.M., Kinoshita, K., Tormakangas, K., Ikeda, Y., Oka, A., Kakimoto, T. and Helariutta, Y. (2006) Cytokinin signaling and its inhibitor AHP6 regulate cell fate during vascular development. *Science.* **311**, 94-98.

Malito, E., Coda, A., Bilyeu, K.D., Fraaije, M.W. and Mattevi A. (2004) Structures of Michaelis and product complexes of plant cytokinin dehydrogenase: implications for flavoenzyme catalysis, *J. Mol. Biol.* **341**, 1237-1249.

Martin-Tanguy, J., Perdrizet, E., Prevost, J. and Martic, C. (1982) Hydroxycinnamic acid amides in fertile and cytoplasmic male sterile lines of maize. *Phytochemistry*. **21**, 1939.

Marchitti, S. A., Brocker, C., Stagos, D., and Vasiliou, V. (2008) Non-P450 aldehyde oxidizing enzymes: the aldehyde dehydrogenase superfamily. *Expert Opin. Drug Metab. Toxicol.* **4**, 697–720.

Matsubara, S. (1990) Structure-activity relationships of cytokinins. *Crit. Rev. Plant Sci*. **9**, 17–57.

Mills, P.B., Struys, E., Jakobs, C., Plecko, B., Baxter, P., Baumgartner, M., Willemsen, M.A.A.P., Omran, H., Tacke, U., Uhlenberg, B., Weschke, B. and Clayton, P.T. (2006) Mutations in antiquitin in individuals with pyridoxine-dependent seizures. *Nature Medicine*. **12**, 307-309.

Minici, C., Cacciapuoti, G., De Leo, E., Porcelli, M. and Degano, M. (2012) New determinants in the catalytic mechanism of nucleoside hydrolases from the structures of two isozymes from *Sulfolobus solfataricus*. *Biochemistry*. **51**(22):4590-9.

Missihoun, T. D., Schmitz, J., Klug, R., Kirch, H. H., and Bartels, D. (2011) Betaine aldehyde dehydrogenase genes from *Arabidopsis* with different sub-cellular localization affect stress responses. *Planta.* **233**, 369 –382.

Mok, D. W. S. and Mok, M. C. (2001) Cytokinin metabolism and action. *Annu. Rev*. *Plant Physiol. Plant Mol. Biol*. **52**, 89–118.

Mok, M.C., Mok, D.W.S., Armstrong, D. J., Shudo, K., Isogai, Y. and Okamoto, T. (1982) Cytokinin activity of *N*-phenyl-*N´*-1,2,3-thiadiazol-5-ylurea (thidiazuron). *Phytochemistry.* **21**, 1509-1511.

Morris, R.O., Bilyeu, K.D., Laskey, J.G. and Cheikh, N.N. (1999) Isolation of a gene encoding a glycosylated cytokinin oxidase from maize, *Biochem. Biophys. Res. Commun.* **255**, 328-333.

Muñoz-Clares, R.A., Riveros-Rosas. H., Garza-Ramos, G., González-Segura, L., Mújica-Jiménez, C. and Julián-Sánchez, A. (2014) Exploring the evolutionary route of the acquisition of betaine aldehyde dehydrogenase activity by plant ALDH10 enzymes: implications for the synthesis of the osmoprotectant glycine betaine. *BMC Plant Biol.* **14,**149.

Muzzolini, L., Versées, W., Tornaghi, P., Van Holsbeke, E., Steyaert ,J. and Degano,M. (2006) New insights into the mechanism of nucleoside hydrolases from the crystal structure of the Escherichia coli YbeK protein bound to the reaction product. *Biochemistry*. **45**, 773–782.

Nakamura, T., Nomura, M., Mori, H., Jagendorf, A. T., Ueda, A., and Takabe, T. (2001) An isozyme of betaine aldehyde dehydrogenase in barley. *Plant Cell Physiol.* **42**, 1088–1092.

Nakamura, T., Yokota, S., Muramoto, Y., Tsutsui, K., Oguri, Y., Fukui, K. and Takabe, T. (1997) Expression of a betain aldehyde dehydrogenase gene in rice and possible localization of its protein in peroxisomes. *Plant J*. **11**, 1115-1120.

Nakano, H., Kosemura, S., Suzuki, T., Hirose, K., Kaji, R. and Sakai, M (2009) Oryzamutaic acid A, a novel yellow pigment from an Oryza sativa mutant with yellow endosperm. *Tetrahedron Lett.* **50**, 2003–2005.

Nakazono, M., Tsuji, H., Li, Y., Saisho, D., Arimura, S., Tsutsumi, N. and Hirai, A. (2000) Expression of a gene encoding mitochondrial aldehyde dehydrogenase in rice increases under submerged conditions. *Plany Physiology*. **124**, 587-598.

Nair, R.B., Bastress, K.L., Ruegger, M.O., Denault, J.W., Chapple, C. (2004) The Arabidopsis thaliana REDUCED EPIDERMAL FLUORESCENCE1 gene encodes an aldehyde dehydrogenase involved in ferulic acid and sinapic acid biosynthesis. *Plant Cell.* **16**, 544–554.

Navarro-Aviño, J.P., Prasad, R., Miralles, V.J., Benito, R.M. and Serrano, R. (1999) A proposal for nomenclature of aldehyde dehydrogenases in *Saccharomyces cerevisiae* and characterization of the stress-inducible ALD2 and ALD3 genes. *Yeast*. **15,** 829-842.

Onkokesung, N., Gaquerel, E., Kotkar, H., Kaur, H., Baldwin, I.T. and Galis, I. (2012) MYB8 controls inducible phenolamide levels by activating three novel hydroxycinnamoyl-coenzyme A:polyamine transferases in *Nicotiana attenuata*. Plant Physiol. **158**(1), 389-407.

Packer, N.H., Lawson, M.A., Jardine, D.R. and Redmond, J.W. (1998) A general approach to desalting oligosaccharides released from glycoproteins. *Glycoconj J*. **15**, 737–47.

Parkin, D.W. (1996) Purine-specific nucleoside N-ribohydrolase from *Trypanosoma brucei brucei*: purification, specificity, and kinetic mechanism. *J Biol Chem*. **271**: 21713–21719.

Parkin, D.W., Horenstein, B.A., Abdulah, D.R., Estupiñán, B. and Schramm, V.L. (1991) Nucleoside hydrolase from *Crithidia fasciculata*: metabolic role, purification, specificity, and kinetic mechanism. *J Biol Chem*. **266**, 20658–20665.

Perez-Miller, S.J. and Hurley, T.D. (2003) Coenzyme isomerization is integral to catalysis in aldehyde dehydrogenase. *Biochemistry.* **42**, 7100-710.

Perozich, J., Kuo, I., Wang, B.C., Boesch, J.S., Lindhal., R. and Hempel, J. (2000) Shifting the NAD/NADP preference in class 3 ALDH. *Eur. J. Biochem*. **267**, 238-249.

Petersen, C. and Møller, L.B. (2001) The RihA, RihB, and RihC ribonucleoside hydrolases of Escherichia coli. Substrate specificity, gene expression, and regulation. *J Biol Chem*. **276**(2):884-94.

Popelková, H., Fraaije, M.W., Novák, O., Frébortová, J., Bilyeu, K.D. and Frébort, I. (2006) Kinetic and chemical analyses of the cytokinin dehydrogenase-catalysed reaction: correlations with the crystal structure. *Biochem. J*. **398**, 113-124.

Procházka, S., Šebánek, J., a kolektiv (1997) Regulátory rostlinného růstu, pp. 63-77, Academia, Praha

Rao, S.T. and Rossmann, M.G. (1973) "Comparison of super-secondary structures in proteins". *Journal of Molecular Biology*. **76** (2), 241–56.

Reumann, S., Babujee, L., Ma, C., Wienkoop, S., Siemsen, T., Antonicelli, G. E., Rasche, N., Lu¨der, F., Weckwerth, W., and Jahn, O. (2007) Proteome analysis of *Arabidopsis* leaf peroxisomes reveals novel targeting peptides, metabolic pathways, and defense mechanisms. *Plant Cell.* **19**, 3170–3193.

Ribeiro, J.M. and Valenzuela, J.G. (2003) The salivary purine nucleosidase of the mosquito, Aedes aegypti. *Insect Biochem Mol Biol*. **33**(1), 13-22.

Rodrigues, S.M., Andrade, M.O., Gomes, A.P.S., DaMatta, F.M., Pereira, M.C.B. and Fontes, E.P.B. (2006) Arabidopsis and tabacco plants ectopically expressing the soybean antiquitin-like ALDH7 gene display enhanced tolerance to drought, salinity, and oxidative stress. *Journal of Experimental Botany*. **57**, 1909-1918.

Shen, Y., Zhang, Y., Yang, C., Lan, Y., Liu, L., Liu, S., Chen, Z., Ren, G. and Wan, J. (2012) Mutation of OsALDH7 causes a yellow-colored endosperm associated with accumulation of oryzamutaic acid A in rice. *Planta*. **235**(2), 433-41.

Shi, W., Schramm, V.L. and Almo, S.C. (1999) Nucleoside hydrolase from Leishmania major. Cloning, expression, catalytic properties, transition state inhibitors, and the 2.5-A- crystal structure. *J Biol Chem*. **274**, 21114-21120.

Shin, J.H., Kim, S.R. and An, G. (2009) Rice aldehyde dehydrogenase7 is needed for seed maturation and viability. *Plant Physiology.* **149**, 905-915.

Schnable, P.S. and Wise, R.P. (1998) The molecular basis of cytoplasmic male sterility and fertility restoration. *Trends Plant Sci*. **3**, 175-180.

Shevchenko, A., Tomas, H., Havliš, J., Olsen, J.V. and Mann, M. (2006) In-gel digestion for mass spectrometric characterization of proteins and proteomes. *Nat Protoc*.**1**, 2856–60.

Shudo, K. (1994) Chemistry of phenylurea cytokinins, In *Cytokinins: Chemistry, activity, and fiction*. Mok, D.W.S. and Mok, M.C. (Eds.), CRC Press, Boca Raton, 35-42

Skibbe, D.S., Liu, F., Wen, T-J., Yandeau, M.D., Cui, X., Cao, J., Simmons, C.R. and Schnable, P.S. (2002) Characterization of the aldehyde dehydrogenases gene families of Zea mays and Arabidopsis. *Plant Molecular Biology*. **48**, 751-764.

Skoog, F. and Armstrong, D.J. (1970) Cytokinins. *Annu Rev Plant Physiol.* **21**, 359–84.

Smith, P.K., Krohn, R.I., Hermanson, G.T., Mallia, A.K., Gartner, F.H., Provenzano, M.D., *et al*. (1985) Measurement of protein using bicinchoninic acid. *Anal Biochem*.v**150**, 76–85.

Sophos, N. A. and Vasiliou, V. (2003) Aldehyde dehydrogenase gene superfamily.The 2002 update. *Chem. Biol. Interact.* **143**, 5–22.

Spíchal, L., Rakova, N.Y., Riefler, M., Mizuno, T., Romanov, G.A., Strnad, M. and Schmülling, T. (2004) Two cytokinin receptors of *Arabidopsis thaliana*, CRE1/AHK4 and AHK3, differ in their ligand specificity in a bacterial assay. *Plant Cell Physiol.* **45**, 1299-1305.

Steinmetz, C.G., Xie, P., Weiner, H. and Hurley, D (1997) Structure of mitochondrial aldehyde dehydrogenase: the genetic component of ethanol aversion. *Structure*. **5**, 701-711.

Stevenson, J. C. and Goodman, M. M. (1972). Ecology of Exotic Races of Maize. I. Leaf Number and Tillering of 16 Races Under Four Temperatures and Two Photoperiods1. *Crop Science*. **12** (6), 864.

Storoni, L.C., McCoy, A.J. and Read, R.J. (2004) Likelihood-enhanced fast rotation functions. *Acta Crystallogr D Biol Crystallogr*. **60**, 432–438.

Stroeher, V.L., Boothe, J.G. and Good, A.G (1995) Molecular cloning and expression of a turgor-responsive gene in Brassica napus. *Plant Mol Biol*. **27**, 541–551.

Suttle, J.C. and Mornet, R. (2005) Mechanism-based irreversible inhibitors of cytokinin dehydrogenase.
J Plant Physiol. **162**(11), 1189-96.

Šebela, M., Štosová, T., Havlis, J., Wielsch, N., Thomas, H., Zdráhal, Z., and Shevchenko, A. (2006) Thermostable trypsin conjugates for highthroughput proteomics. Synthesis and performance evaluation. *Proteomics.* **6**, 2959–2963.

Šebela, M., Brauner, F., Radová, A., Jacobsen, S., Havliš, J., Galuszka, P., Peč, P. (2000) Characterisation of a homogeneous plant aminoaldehyde dehydrogenase. *Biochim Biophys Acta*. **1480**, 329-341.

Schmülling, T., Werner, T., Riefler, M., Krupková, E., Bartrina, Y. and Manns, I. (2003) Structure and function of cytokinin oxidase/dehydrogenase genes of maize, rice, Arabidopsis and other species. *J Plant Res*. **116**, 241–52.

Tang, G., Miron, D., Zhu-Shimoni, J.X. and Galili, G.(1997) Regulation of lysine catabolism through lysine-ketoglutarate reductase and saccharopine dehydrogenase inArabidopsis. *Plant Cell*. 9(8), 1305-16.

Tang, W.K., Wong, K.B., Lam, Y.M., Cha, S.S., Cheng, C.H.K. and Fong, W.P. (2008) The crystal structure of seabream antiquitin reveals the structural basis of its substrate specificity. *FEBS Lett.* **582**, 3090-3096.

Tanaka, M., Takei, K., Kojima, M., Sakakibara, H. and Mori, H.(2006) Auxin controls local cytokinin biosynthesis in the nodal stem in apical dominance. *Plant J*. **45**, 1028-1036.

Trossat, C., Rathinasabapathi, B. and Hanson, A.D. (1997) Transgenically expressed betaine aldehyde dehydrogenase efficiently catalyzes oxidation of dimethylsulfoniopropionaldehyde and [omega]-aminoaldehydes. *Plant Physiology*. **113**, 1457-1461.

Tylichová, M., Kopečný, D., Snégaroff, J. and Šebela, M. (2010) Aminoaldehyde dehydrogenases: has the time now come for new interesting discoveries? *Plant biology*. **396**, 870-882.

Tylichová, M., Kopečný, D., Moréra, S., Briozzo, P., Lenobel, R., Snégaroff, J. and Šebela, M. (2010) Structural and functional characterization of plant aminoaldehyde dehydrogenases from *Pisum sativum* with a broad specificity for natural and synthetic aminoaldehydes. *Journal of Molecular Biology*. **396**, 870-882.

Vagin, A. and Teplyakov, A. (2010) Molecular replacement with MOLREP. *Acta Crystallogr D Biol Crystallogr*. **66**(Pt 1):22-5.

Valenzuela-Soto, E.M. and Muñoz-Clares, R.A. (1994) Betaine-aldehyde dehydrogenase from leaves of Amaranthus hypochondriacus L. exhibits an Iso Ordered Bi Bi steady state mechanism. *J Biol Chem*. 268(32), 23818-23.

Vasiliou, V., Bairoch, A., Tipton, K.F. and Nebert, D.W. (1999) Eukaryotic aldehyde dehydrogenase (ALDH) genes: human polymorphisms, and recommended nomenclature based on divergent evolution and chromosomal mapping. *Pharmacogenet Genom.* **9**, 421–434.

Velasco-Garcia, R., Gonzalez-Segura, L. and Munoz-Clares, R.A. (2000) Steady-state kinetic mechanism of the ADP^+- and NAD^+-dependent reactions catalysed by betaine aldehyde dehydrogenase from Pseudomonas aeruginosa, *Biochem. J*. **352**, 675–683.

Walsh, C. (1982) Suicide substrates: mechanismbased enzyme inactivators. *Tetrahedron*. **38**, 871–909.

Garcia-Conesa MT, Plumb GW, Waldron KW, Ralph J, Williamson G. (1997) Ferulic acid dehydrodimers from wheat bran: isolation, purification and antioxidant properties of 8-O-4-diferulic acid. *Redox Rep*. **3**(5-6), 319-23.

Wang, J. and Letham, D.S (1995) Cytokinin oxidase-purification by affinity chromatography and activation by caffeic acid. *Plant Sci.* **112**, 161–166.

Wei, Y., Lin, M., Oliver, D.J., Schnable, P.S. (2009) The roles of aldehyde dehydrogenases (ALDHs) in the PDH bypass of Arabidopsis. *BMC Biochem.*, **10**:7.

Wen, Y., Wang, X., Xiao, S. and Wang, Y. (2012) Ectopic expression of VpALDH2B4, a novel aldehyde dehydrogenase gene from Chinese wild grapevine (Vitis pseudoreticulata), enhances resistance to mildew pathogens and salt stress in Arabidopsis. *Planta*. 236(2):525-39.

Versées, W., Decanniere, K., Pellé, R., Depoorter, J., Brosens, E., Parkin, D.W. and Steyaert, J. (2001) Structure and function of a novel purine specific nukleoside hydrolase from *Trypanosoma vivax*. *J Mol Biol.* **307**, 1363–1379.

Versées, W., Decanniere, K., Van Holsbeke, E., Devroede, N. and Steyaert, J. (2002) Enzyme-substrate interactions in the purine-specific nucleoside hydrolase from *Trypanosoma vivax*. *J Biol Chem*. **277**, 15938–15946.

Versées, W. and Steyaert, J. (2003) Catalysis by nucleoside hydrolases. *Curr Opin Struct Biol.* **13**, 731.

Wellhausen, Edwin John (1952). *Races of Maize in Mexico*.

Wise, R.P., Pring, D.R. and Gengenbach, B.G. (1987) Mutation to male fertility and toxin insensitivity in T-cytoplasm maize is associated with a frameshift in a mitochondrial open reading frame. *Proc Natl Acad Sci USA*. **84**, 2858-2862.

Wise, R.P., Bronson, C., Schnable, P.S. and Horner, H.T. (1999) T cytoplasmic male sterility of maize. *Adv Agron*. **65**,79-130.

Wood, A.J. and Krayesky, S. (2002) The role of aldehyde dehydrogenases (ALDHs) in plant stress tolerance. *In Biochemical and Molecular Responses of Plants to the Environment* (Wood A.J. ed.) pp. 1-14

Wood, A. and Duff, RJ. (2009) The aldehyde dehydrogenase (ALDH) gene superfamily of the moss Physcomitrella patens and the algae Chlamydomonas reinhardtii and Ostreococcus tauri. *The Bryologist*. **112**,1-11.

Wong, J.W., Chan, C.L., Tang, W.K., Cheng, C.H., Fong, W.P. (2010) Is antiquitin a mitochondrial enzyme? *J. Cell. Biochem.* **109**, 74-81.

Wymore, T., Hempel, J., Cho, S. S., Mackerell, A. D., Jr., Nicholas, H. B., Jr. and Deerfield, D. W. 2nd (2004) Molecular recognition of aldehydes by aldehyde dehydrogenase and mechanism of nucleophile activation. *Proteins.* **57**, 758–771.

Yamada, K., Mori, H. and Yamaki, S. (1999) Identification and cDNA cloning of a protein abundantly expressed during apple fruit development. *Plant Cell Physiol*. **40**, 198–204.

Yancey, P.H. (1994) Compatible and counteracting solutes: protecting cells from the Dead Sea to the deep sea. *Cellular and Molecular Physiology of Cell Volume Regulation*. Strange K. (ed.), *CRC press, Boca Raton*, pp. 81-109.

Yoder, O.C. and Scheffer, R.P. (1973) Effects of Helminthosporium carbonum Toxin on Nitrate Uptake and Reduction by Corn Tissues. Plant Physiol. 52(6)**,** 513-7.

Yoshida, A., Rzhetsky, A., Hsu, L.C. and Chang, Ch. (1998) Human aldehyde dehydrogenase gene family. *European Journal of Biochemistry*. **251**, 549-557.

Zalkin, H. and Nygaard, P. (1996) Biosynthesis of purine nucleotides. In *Escherichia coli* and *Salmonella:* Cellular and Molecular Biology. Neidhardt, F.C. (ed.). Washington, DC: ASM Press, pp. 561–579.

Zatloukal, M., Gemrotova, M., Doležal, K., Havlíček, L., Spíchal, L. and Strnad, M. (2008) Novel potent inhibitors of A. thaliana cytokinin oxidase/dehydrogenase. *Bioorg. Med. Chem*. **16**, 9268–9275.

Zrenner, R., Stitt, M., Sonnewald, U. and Boldt, R. (2006) Pyrimidine and purine biosynthesis and degradation in plants. *Annu Rev Plant Biol*. **57**, 805-36.

Zhang, Y., Mao, L., Wang, H., Brocker, C., Yin, X. *et al.* (2012) Genome-Wide Identification and Analysis of Grape Aldehyde Dehydrogenase (ALDH) Gene Superfamily. *PLoS ONE.* **7**(2), e32153.

Zhu, X., Tang, G. and Galili, G. (2000) The catabolic function of the alphaaminoadipic acid pathway in plants is associated with unidirectional activity of lysine-oxoglutarate reductase, but not saccharopine dehydrogenase. *Biochem J.* **351**, 215–220.

.

9 Articles

Article 1

Analysis of N-glycosylation in maize cytokinin oxidase/dehydrogenase 1 using a manual microgradient chromatographic separation coupled offline to MALDI-TOF/TOF mass spectrometry.

Franc V, Šebela M, Řehulka P, Končitíková R, Lenobel R, Madzak C, Kopečný D.

J Proteomics, 13, 4027-37 (2012)

JOURNAL OF PROTEOMICS 75 (2012) 4027–4037

Available online at www.sciencedirect.com

SciVerse ScienceDirect

www.elsevier.com/locate/jprot

Analysis of N-glycosylation in maize cytokinin oxidase/dehydrogenase 1 using a manual microgradient chromatographic separation coupled offline to MALDI-TOF/TOF mass spectrometry

Vojtěch Franc[a], *Marek Šebela*[a,b,*], *Pavel Řehulka*[c,**], *Radka Končitíková*[a], *René Lenobel*[a], *Catherine Madzak*[d], *David Kopečný*[a]

[a]*Department of Protein Biochemistry and Proteomics, Centre of the Region Haná for Biotechnological and Agricultural Research, Faculty of Science, Palacký University, Šlechtitelů 11, CZ-783 71 Olomouc, Czech Republic*

[b]*Department of Biochemistry, Faculty of Science, Palacký University, Šlechtitelů 11, CZ-783 71 Olomouc, Czech Republic*

[c]*Institute of Molecular Pathology, Faculty of Military Health Sciences, University of Defence, Třebešská 1575, CZ-500 01 Hradec Králové, Czech Republic*

[d]*INRA, UMR 1319 Micalis, Domaine de Vilvert, F-78352 Jouy-en-Josas, France*

ARTICLE INFO

Article history:
Received 24 February 2012
Accepted 8 May 2012
Available online 24 May 2012

Keywords:
Cytokinin oxidase/dehydrogenase
Endoglycosidase H
Glycan
N-glycosylation
Mass spectrometry
Yarrowia lipolytica

ABSTRACT

Cytokinin oxidase/dehydrogenase (CKO; EC 1.5.99.12) irreversibly degrades the plant hormones cytokinins. A recombinant maize isoenzyme 1 (ZmCKO1) produced in the yeast *Yarrowia lipolytica* was subjected to enzymatic deglycosylation by endoglycosidase H. Spectrophotometric assays showed that both activity and thermostability of the enzyme decreased after the treatment at non-denaturing conditions indicating the biological importance of ZmCKO1 glycosylation. The released N-glycans were purified with graphitized carbon sorbent and analyzed by MALDI-TOF MS. The structure of the measured high-mannose type N-glycans was confirmed by tandem mass spectrometry (MS/MS) on a Q-TOF instrument with electrospray ionization. Further experiments were focused on direct analysis of sugar binding. Peptides and glycopeptides purified from tryptic digests of recombinant ZmCKO1 were separated by reversed-phase chromatography using a manual microgradient device; the latter were then subjected to offline-coupled analysis on a MALDI-TOF/TOF instrument. Glycopeptide sequencing by MALDI-TOF/TOF MS/MS demonstrated N-glycosylation at Asn52, 63, 134, 294, 323 and 338. The bound glycans contained 3–14 mannose residues. Interestingly, Asn134 was found only partially glycosylated. Asn338 was the sole site to carry large glycan chains exceeding 25 mannose residues. This observation demonstrates that contrary to a previous belief, the heterologous expression in *Y. lipolytica* may lead to locally hyperglycosylated proteins.

Abbreviations: ACN, acetonitrile; CHCA, α-cyano-4-hydroxycinnamic acid; CID, collision-induced dissociation; CKO, cytokinin oxidase/dehydrogenase; ESI, electrospray ionization; MALDI-TOF, matrix-assisted laser desorption/ionization time-of-flight; MS, mass spectrometry; MS/MS, tandem mass spectrometry; Q-TOF, quadrupole time-of-flight; TFA, trifluoroacetic acid; ZmCKO1, isoenzyme 1 of maize (*Zea mays*) cytokinin oxidase/dehydrogenase.

* *Correspondence to:* M. Šebela, Department of Biochemistry, Faculty of Science, Palacký University, Šlechtitelů 11, CZ-783 71 Olomouc, Czech Republic. Tel.: +420 585634927; fax: +420 585634933.

** *Correspondence to:* P. Řehulka, Institute of Molecular Pathology, Faculty of Military Health Sciences, University of Defence, Třebešská 1575, CZ-500 01 Hradec Králové, Czech Republic. Tel.: +420 973255199.

E-mail addresses: marek.sebela@upol.cz (M. Šebela), rehulka@pmfhk.cz (P. Řehulka).

1874-3919/$ – see front matter © 2012 Elsevier B.V. All rights reserved.
doi:10.1016/j.jprot.2012.05.013

1. Introduction

The plant hormones cytokinins are substances which promote cell division and exert other important functions [1,2]. They have been shown to regulate diverse growth and developmental events such as seed germination, leaf expansion, *de novo* bud formation, release of buds from apical dominance, chloroplast formation and delay of senescence [3]. Naturally occurring cytokinins consist of an adenine/adenosine moiety carrying an N^6-isoprenoid or N^6-aromatic side chain [4]. Cytokinin-related processes are triggered by the activation of a multistep His-to-Asp phosphorelay cascade starting from the plasma membrane-localized histidine kinase receptors [5]. The content of endogenous cytokinins depends on the balance between *de novo* synthesis, import and export rates, interconversion of distinct forms, transient inactivation by conjugation and catabolic reactions resulting in a complete loss of biological activity [6]. Cytokinin biosynthesis is catalyzed by isopentenyltransferases [7,8], while inactivation involves either *N*- or *O*-conjugation [3] or irreversible oxidation by cytokinin oxidases/dehydrogenases (CKO or CKX; EC 1.5.99.12) [9].

An enzymatic activity capable of oxidative degradation of cytokinins was first demonstrated in cultured tobacco tissues [10]. Shortly afterwards, the enzyme was named "cytokinin oxidase", which reflected findings that it required oxygen for the catalytic reaction [11]. Substrate conversion in CKO reaction is achieved through the oxidative cleavage of its N^6-side chain resulting in the formation of adenine (or its corresponding derivative for N^9-substituted cytokinins [3]) and a side chain-derived aldehyde like for example 3-methyl-2-butenal from the substrate N^6-(Δ^2-isopentenyl)adenine [12]. Biochemical characterization of CKO was hampered for a long time by the lack of a homogeneous enzyme preparation. Due to a low concentration of CKO in plant tissues, purification of the native enzyme has often been demonstrated as an extremely difficult procedure requiring numerous chromatographic steps [9]. The breakthrough came with the cloning of a gene coding for the isoenzyme 1 of maize CKO (ZmCKO1) [13,14], which consequently allowed identification of related genes in other species and their expression in heterologous hosts. Recombinant ZmCKO1 itself was obtained in the yeasts *Pichia pastoris* [15] or *Yarrowia lipolytica* [16].

In most plants studied so far, CKOs are encoded by several genes resulting in the existence of isoenzymes [17]. The catalyzed reaction involves a two-electron (hydride) transfer from the substrate to FAD cofactor. A substrate-derived imine is produced, which is finally hydrolyzed to form the corresponding aldehyde and adenine/adenosine moieties [12]. $FADH_2$ reoxidation occurs after the reaction with oxygen (producing H_2O_2) or other electron acceptors such as quinones [4]. For that reason, the term "cytokinin oxidase/dehydrogenase" better reflects the nature of the enzyme. Monomeric CKOs belong to the group of FAD-containing oxidoreductases [3]. CKOs commonly prefer isoprenoid cytokinins as substrates while aromatic cytokinins are oxidized only at low rates [18]. The reported crystal structures of plant CKOs show a two domain topology with a cofactor-binding domain and a substrate-binding domain [19,20]. Active site residues are highly conserved except for that one at the entrance to the active site (E381 in ZmCKO1), which is involved in substrate binding and influences sensitivity to competitive inhibitors based on phenylurea or benzylurea [21].

Amino acid sequences of maize, rice and Arabidopsis CKO isoenzymes show the presence of one to eight *N*-glycosylation tripeptide signals [17]. A glycosylation in ZmCKO1 was initially deduced from its binding to lectin affinity columns [13] and further confirmed by electrophoretic migration, which provided significantly higher molecular mass estimates than expected from sequence-based calculations [13–16].&& The published crystal structures have shown that at least six of the predicted *N*-glycosylation sites may be occupied by glycans attached at the residues Asn63, Asn89, Asn134, Asn294, Asn323 and Asn338 [19,21]. However, neither the composition and size of the carbohydrate chains, nor their contribution to the activity and stability of the enzyme, had been investigated yet.

Mass spectrometry (MS) has proven to be a reliable and invaluable tool for the analysis of *N*-glycosylation in plant proteins and elucidation of the corresponding *N*-glycan structures [22,23]. In this work, recombinant ZmCKO1 from *Y. lipolytica* was subjected to an enzymatic deglycosylation by endoglycosidase H under denaturing and non-denaturing conditions. The released *N*-glycans were analyzed by MALDI-TOF MS, ESI-Q-TOF MS and tandem MS (MS/MS). MALDI-TOF/TOF MS and MS/MS analyses were also performed directly on *N*-glycopeptides generated by tryptic digestion of recombinant ZmCKO1. The obtained results revealed the presence of high-mannose glycans and their importance for activity and stability of the enzyme.

2. Materials and methods

2.1. Chemicals

High-quality solvents for liquid chromatography/mass spectrometry were from Sigma-Aldrich Chemie (Steinheim, Germany). MALDI matrices were from Bruker Daltonik (Bremen, Germany), except for ferulic acid, 6-aza-2-thiothymine and 3-aminoquinoline supplied by Sigma-Aldrich Chemie. All other chemicals were of analytical purity grade. Graphitized carbon material was obtained from Hypercarb SPE cartridges (Thermo Fisher Scientific, Waltham, MA, USA) and packed into GELoader pipette tips (Eppendorf, Hamburg, Germany) using C8 disc as a frit to retain the carbon sorbent. Similarly, POROS R3 Oligo particles (PerSeptive Biosystems, Framingham, MA, USA) were used for peptide fractionation in GELoader pipette tips. Polyimide-coated fused silica capillaries (360 μm o.d., 200 μm i.d.; and 360 μm o.d., 50 μm i.d.) were purchased from Agilent Technologies (Santa Clara, USA), Ascentis® Express Peptide ES-C18 2.7 μm fused-core particles were obtained from corresponding 4.6 mm i.d.×150 mm column (Sigma-Aldrich, Steinheim, Germany). A microtight union (5/16–24, 360 μm o.d., cat. no. P-772) was obtained from UpChurch Scientific (Oak Harbor, USA), FEP tubing (1/16 in.×0.25 mm i.d.) was from Vici AG International (Schenkon, Switzerland).

2.2. Enzymes

ZmCKO1 was produced by recombinant expression in *Y. lipolytica* (secretion into the culture medium) and subsequent

chromatographic purification as previously described [16]. Recombinant endoglycosidase H from *Streptomyces plicatus* (Cat. No. A0810) was from Sigma-Aldrich Chemie.

2.3. Enzyme activity and thermostability assay

CKO activity in the dehydrogenase mode was assayed by the DCPIP method [15]. Thermostability of the enzyme was evaluated by monitoring the changes in activity upon incubating enzyme aliquots (in the assay buffer, pH 7.0) at temperatures from 25 °C up to 70 °C for 30 min, followed by rapid cooling in water-ice bath. Protein content was estimated using a colorimetric assay with bicinchoninic acid; BSA served as a standard [24].

2.4. Enzymatic deglycosylation of ZmCKO1

Enzymatic deglycosylation was conducted using endoglycosidase H. The enzyme from *Streptomyces plicatus* is supplied as a buffered aqueous solution. A total volume of 150 μl in the vial represents 1 activity unit, which is defined as an amount releasing *N*-glycans from 60 μmol ribonuclease B per hour at 37 °C and pH 5.5. Three different protocols were followed in a comparative experiment: 1) the glycoprotein (200 μg) was denatured in 42.5 μl of 50 mM K-phosphate buffer, pH 5.5, containing 1% SDS and 60 mM 2-mercaptoethanol by heating at 100 °C for 5 min followed by the addition of 15% Triton X-100 (2.5 μl) and endoglycosidase H (1 μl–6.7 milliunits); the reaction mixture was then incubated at 37 °C for 3 h; 2) the same protocol was followed with omitting the denaturation step; the deglycosylation reaction proceeded at 37 °C for 3 h; 3) the denaturation step was omitted as well; the deglycosylation reaction proceeded at 23 °C overnight. The deglycosylated samples were subjected to ultrafiltration on a 10-kDa Microcon centrifugal filter device (Millipore, Bedford, MA, USA) and the *N*-glycans recovered in the filtrate were purified on graphitized carbon essentially as described [25].

2.5. Electrophoresis and in-gel digestion

SDS-PAGE separation (10% T/3.3% C resolving gels) was performed by a standard method [26]. Proteins were visualized by Bio-Safe™ Coomassie Stain (Bio-Rad, Hercules, CA, USA). Then in-gel tryptic digestion followed according to Shevchenko et al. [27].

2.6. MALDI-TOF mass spectrometry

MALDI-TOF MS of peptides from tryptic digests was performed on a Microflex LRF20 instrument (Bruker Daltonik, Bremen, Germany) equipped with a microScout ion source and a 337-nm nitrogen laser pulsing at a repetition rate of 60 Hz. The experimental setup with an α-cyano-4-hydroxycinnamic acid (CHCA) matrix was the same as described [28]. Purified *N*-glycans were measured with 6-azathiothymine (ATT) [29] and 3-aminoquinoline (3AQ) [30] as matrices. Large tryptic *N*-glycopeptides were analyzed using ferulic acid as a matrix, 10 mg ml^{-1} in acetonitrile (ACN):0.1% v/v trifluoroacetic acid (TFA), 7:3, v/v, at a high relative laser energy of 60% (increased by 200% with respect to that routinely used for measuring common peptides using CHCA). MALDI probes were prepared by a standard dried-droplet technique on an MSP AnchorChip™ 600/96 target plate (Bruker Daltonik). Parameters of the instrument for measurements with ferulic acid were as follows: an acceleration voltage of 19 kV, an extraction voltage of 16.1 kV, a lens voltage of 9.4 kV, a reflectron voltage of 20 kV and a delayed extraction time of 300 ns. Mass spectra were accumulated from up to 400 laser shots; a mixture of standard peptides (Bruker Daltonik) was used for external calibration. Mass spectra were processed using flexAnalysis 3.0 and BioTools 3.2 software (Bruker Daltonik). MALDI-TOF/TOF measurements in the positive reflectron mode were carried out on an ABI 4800 Proteomics Analyzer (Applied Biosystems, Framingham, MA, USA). The instrument was equipped with a neodymium-doped: yttrium aluminium garnet laser (355 nm) of 3–7 ns pulse and 200-Hz firing rate. Both MS and MS/MS spectra were acquired using dual-stage reflectron mirror. Accelerating voltages applied for MS and MS/MS measurements were 20 kV and 8 kV, respectively. In MS/MS mode, a potential of 1 kV was applied and fragmentation was achieved by post-source decay. For measurements of protein digests, the matrix solution was CHCA (5 mg ml^{-1}) dissolved in ACN/0.1% TFA (3:2, v/v); a mixture of six standard peptides was used for external calibration. Aliquots of in-solution digests (desalted and fractionated on stop-and-go extraction tips [31]) were mixed on the target with the matrix solution and left to dry. MS and MS/MS data were processed using 4000 Series Explorer (Applied Biosystems) and further manually interpreted using Data Explorer 4.8 (Applied Biosystems) software.

2.7. Desalting and on-tip fractionation of digests

For desalting of tryptic digests, GELoader tips (Eppendorf, Hamburg, Germany) filled with POROS R3 Oligo particles were used [32]. When lying on a flat surface, the outlet of a GELoader tip was carefully squeezed with a Combi Tip syringe and then 1 μl of POROS R3 Oligo suspension in ACN was loaded into the pipette tip. The tip was wetted with 10 μl 80% ACN/0.1% TFA (v/v) and equilibrated with 10 μl 2% ACN/0.1% TFA (v/v). A digest sample (40 μl) acidified with 5% (v/v) TFA (using a volume ratio of acid to sample of 1:10) was passed through the packed tip and washed with 10 μl of 2% ACN/0.1% TFA (v/v). Fractionation of the sample was done by sequential elution of the retained sample by 10%, 20%, 30%, 40% and 80% ACN/0.1% TFA solutions (v/v; 10 μl each). The eluate was evaporated in a vacuum centrifuge and dissolved in 0.1% (v/v) TFA. The fraction containing *N*-glycopeptides (80% ACN/0.1% TFA) was further subjected to MS profiling and separation using a microgradient device.

2.8. Preparation of capillary columns

A 150-mm long capillary (360 μm o.d., 200 μm i.d.) was inserted into a 15-mm long piece of FEP tubing (1/16 in. × 0.25 mm i.d.) that had previously been widened using a steel pin. To the opposite end of this FEP tubing, a short (20 mm) and narrower capillary (360 μm o.d., 50 μm i.d.) was inserted in the same way so that the capillaries touched each other in the middle. The tubing was carefully heated using a small flame torch and after

cooling down both capillaries were tightly connected. The selected stationary phase (Ascentis® Express Peptide ES-C18, 2.7 μm) was introduced into the 200 μm i.d. capillary in the form of a dense suspension from a 250-mm long FEP tubing connected to a plastic syringe (0.5 ml) with fixed metal needle. The suspension was pressed down by pushing the syringe plunger forward with occasional sonication of the tubing-to-capillary connection. After the capillary column was filled up to the desired length, the empty rest of the capillary was cut away.

2.9. RP-LC separation using simple microgradient device

A simple microgradient device was used for reversed-phase liquid chromatography (RP-LC) separation of tryptic peptides [33]. It consisted of a syringe infusion pump (Harvard Apparatus, Holliston, MA, USA) with a 100-μl microsyringe (SGE, Australia) connected to a 250-mm long capillary (360 μm o.d., 200 μm i.d.) using FEP tubing as described above. The capillary was further connected to the previously made C18 analytical capillary column (74 mm, see above), through a 360 μm microtight union. The whole system was first wetted with 40 μl of 80% ACN/0.1% TFA (v/v) and then equilibrated with 40 μl of 2% ACN/0.1% TFA (v/v) after aspiration of the appropriate solvent into the microsyringe through the capillary disconnected from the analytical column. The digest fraction containing *N*-glycopeptides (obtained using 80%ACN/0.1%TFA, v/v, during the on-tip separation; dried and dissolved in 40 μl of 0.1% v/v TFA) was aspirated into the syringe and loaded on the analytical column. Prior to sample separation, the microsyringe with connecting capillary was filled consecutively by four ACN/0.1%TFA mobile phases with gradually decreasing ACN content (80% ACN/0.1% TFA — 40 μl, 55% ACN/0.1% TFA — 10 μl, 40% ACN/0.1% TFA — 10 μl, 30% ACN/0.1% TFA — 18 μl; all v/v). An S-shaped gradient of ACN was formed inside the microsyringe as a result of turbulent mixing of the mobile phases during aspiration [34]. Finally, the microsyringe (with the attached capillary) placed in the syringe infusion pump was connected to the analytical column. After 20 min-long separation at a flow rate of 1 μl min^{-1} the eluate was manually deposited in 30 s intervals (representing 0.5 μl aliquots) on a MALDI target. Then 0.5 μl of CHCA (5 mg ml^{-1}) in 60% ACN/0.1%TFA (v/v) was on-target mixed with the eluate aliquots.

2.10. Electrospray ionization mass spectrometry

ESI-MS was carried out using a maXis ultra high resolution Q-TOF instrument (Bruker Daltonik). Positive ionization mode was used. ZmCKO1 digest samples (dissolved in 0.5% formic acid) were separated by nanocapillary liquid chromatography employing a double column system comprising a precolumn 75 μm × 30 mm (Gold C18, 5 μm particles, Dr. Maisch GmbH, Germany) and an analytical column 75 μm × 150 mm (Gold C18, 3 μm particles, Dr. Maisch GmbH, Germany) operating at a flow rate of 250 nl min^{-1}. Endoglycosidase H-released *N*-glycans were dissolved in 40% (v/v) ACN and introduced into the mass spectrometer via direct infusion from a syringe at a flow rate of 300 nl min^{-1}. Basic parameters of the nanoelectrospray source were as follows: a capillary voltage of 2200 kV, a dry gas flow of 2 l min^{-1} and a drying temperature of 150 °C. Full scan spectra were obtained by scanning over the *m/z* range of 350–2000 (1 s per scan). Collision-induced tandem mass spectrometry (CID-MS/MS; product ion scan mode) was done by scanning a mass range from *m/z* 50 to 2200 (0.5–2 s per scan according to precursor ion intensity). Nitrogen was used as a collision gas and collision cell energy was adapted according to the molecular mass and charge state of the selected precursor ion. Mass spectra were acquired and processed using Compass 1.4 and Data analysis 4.0 SP4 (both by Bruker Daltonik), respectively.

3. Results and discussion

3.1. Glycosylation of cytokinin oxidases/dehydrogenases

CKOs, enzymes participating in homeostasis of the plant hormones cytokinins, commonly comprise potential *N*-glycosylation signals (i.e. the sequons N-X-T/S) in their amino acid sequence. Table 1 shows summarizing data for CKO isoenzymes from maize and Arabidopsis that have been completed using sequence-processing and prediction software. The number of the potential *N*-glycosylation signals varies from one to eight. The glycosylation is most frequent in ZmCKO1 and AtCKO1, the former being the subject of this work. The presence of *N*-glycan chains in ZmCKO1 was demonstrated in many previous studies on native and recombinant proteins [13–16,19,21]. Nevertheless, both the structure and role of the bound carbohydrates have never been analyzed.

3.2. SDS-PAGE analyses of glycosylated and deglycosylated ZmCKO1

Recombinant ZmCKO1 produced in *Y. lipolytica* was chosen to perform such a study because of its availability as a pure protein in high amounts. When separated in SDS-PAGE gels, the recombinant enzyme shows a typical behavior of glycoproteins as it provides a blurred protein band upon staining (Fig. 1, panel A), which refers to a heterogeneity in the length of sugar chains and molecular mass values ranging from 65 to 80 kDa [16]. Fig. 1, panel B, displays results of deglycosylation experiments with endoglycosidase H, which were performed under different experimental conditions either involving or omitting ZmCKO1 sample denaturation. The complete deglycosylation of the protein, resulting in a molecular mass value of 58 kDa, was achieved only in the presence of SDS as a denaturing agent. Note that endoglycosidase H leaves one *N*-acetylglucosamine (GlcNAc) residue attached per each occupied glycosylation site. After removal of glycan chains under non-denaturing conditions at 23 or 37 °C, two bands of deglycosylated enzyme (63 and 61 kDa) were observed on stained gels.

3.3. MALDI-TOF MS of tryptic peptides from deglycosylated ZmCKO1

After SDS-PAGE separation, the enzyme deglycosylated under denaturing conditions was subjected to a tryptic in-gel digestion followed by a direct MALDI-TOF peptide mass fingerprinting (without desalting; all in comparative experiments with the untreated recombinant ZmCKO1). Peptide

Table 1 – Predicted glycosylation and cellular targeting of cytokinin oxidases/dehydrogenases.

Protein	DNA/mRNA sequence (accession codes)	Length (AA)	Potential N-glycosylation sites [a]	Identity (%) [b]	Predotar [c]	TargetP [c]
Originating from *Zea mays*						
ZmCKO1	Y18377	534	8/5	–	ER	S
ZmCKO2	AJ606942	519	3/3	45.0	ER	S
ZmCKO3	AJ606943	525	3/3	44.8	ER	S
ZmCKO4	GU160398	541	2/1	49.5	ER	S
ZmCKO4b	GU160399	534	2/1	49.3	ER	S
ZmCKO5	GU160400	582	2/2	53.1	ER	S
ZmCKO6	GU160401	542	2/0	40.4	ER	S
ZmCKO7	GRMZM2G162048_T01 [d]	534	2/1	51.9	ER	M
ZmCKO8	GU160402	539	4/4	52.9	ER	M
ZmCKO9	GRMZM2G303707_T01 [d]	568	2/2	53.4	PL	S
ZmCKO10	FJ269181	525	2/1	41.6	n.p.	n.p.
ZmCKO11	GRMZM2G122340_T01 [d]	267 (533*)	1/0	37.8 (43.6*)	ER	n.p. (S*)
ZmCKO12	GU160403	528	1/0	43.7	ER	S
Originating from *Arabidopsis thaliana*						
AtCKO1	NM_129714	575	8/5**	41.8	n.p.	M
AtCKO2	NM_127508	501	3/3	46.9	ER	S
AtCKO3	NM_125079	523	4/2	46.7	ER?	M
AtCKO4	NM_119120	524	4/4	48.6	ER	S
AtCKO5	NM_106199	540	3/2**	45.1	ER	S
AtCKO6	NM_116209	533	4/4	46.7	M	M
AtCKO7	NM_180532	524	6/6	39.8	n.p.	n.p.

*Value refers to an extended transcript as shown in [35], supplementary material.
**Including a sequon NPS; the presence of proline in or around NXS/T sequences has been known to obstruct N-glycosylation due to conformational hindrance.
[a] All NXT or NXS glycosylation sites versus those showing more than 50% probability of N-glycosylation; calculated with NetNGly (www.cbs.dtu.dk/services/NetNGlyc/).
[b] Identity of ZmCKO1 with other listed CKO proteins (in percents) was calculated by Lalign (http://www.ch.embnet.org/software/LALIGN_form.html).
[c] Subcellular localization predictions were obtained using Predotar (http://urgi.versailles.inra.fr/predotar/) or TargetP (http://www.cbs.dtu.dk/services/TargetP/): M — mitochondria, ER — endoplamatic reticulum, n.p. — no prediction, PL — plastid, S — secreted.
[d] Accession codes in the maize genome browser at http://archive.maizesequence.org/; all other codes refer to the database EMBL/GenBank/DDBJ.

mass spectra acquired on the Microflex instrument showed a clear difference as a few more peptide peaks were registered in consequence of deglycosylation (Fig. 2). Examination of the results was done by mass calculations taking into account the predicted length of N-glycopeptides generated by tryptic digestion of ZmCKO1. There was a peak observed (*m*/*z* 4871; average mass) consistent with the peptide 269-LTAPRPGGG-GASFGPMSYVEGSVFVNQSLATDLANTGFFTDADVAR-314 with a methionine oxidation and one remaining GlcNAc residue attached at Asn294 (numbering is based on the ZmCKO1 sequence deposited under the accession code Q9T0N8 in the UniProtKB database; the glycosylation sequon residues are underlined and the same is done for all glycopeptide and potential glycopeptide sequences throughout the text). Its cleavage variant without the N-terminal group LTAPR (representing a mass difference of 539 Da) was reflected in a peak with *m*/*z* 4332. Both peaks were accompanied by neighbors without oxidized methionine (*m*/*z* 4855 and 4316, respectively). The other N-glycopeptides with *m*/*z* 5136 and 5740 (average masses) then refer to the peptides 323–367 and 49–101 (including an amino acid substitution of Gly79 to Ala79 [36]), each with two remaining GlcNAc residues at their respective N-glycosylation sites. MALDI-TOF/TOF MS measurements revealed monoisotopic patterns of the mentioned peptide peaks with signal-to-noise ratios above 20 and mass accuracy less than 100 ppm with external calibration (not shown). Taken together, the fingerprinting results indicated that the following sites were occupied by sugar residues in the recombinant enzyme: Asn294, Asn323 and Asn338, and then a pair from the residues Asn52, Asn63 and Asn89.

3.4. *MS and MS/MS analyses of N-glycans released from ZmCKO1 by endoglycosidase H*

For further analysis, the released N-glycans were recovered from the reaction mixture of endoglycosidase H using ultrafiltration followed by a microscale adsorption chromatography on graphitized carbon. After elution, the purified glycans were subjected to MALDI-TOF MS. Two matrices were used in comparative experiments. When ATT matrix was employed in the reflectron positive mode, a series of potassium adduct peaks ($[M+K]^+$) was observed between *m*/*z* 1394.4 and 2690.8 (with a mass difference of 162 Da) referring to carbohydrate structures with GlcNAc and from 7 to 15 hexose residues. Sodium adduct peaks ($[M+Na]^+$) were less pronounced in this case (not shown). The use of 3AQ allowed recognizing even larger structures, which is documented in Fig. 3. The compound is known to form Schiff bases with the reducing end of sugars, which causes

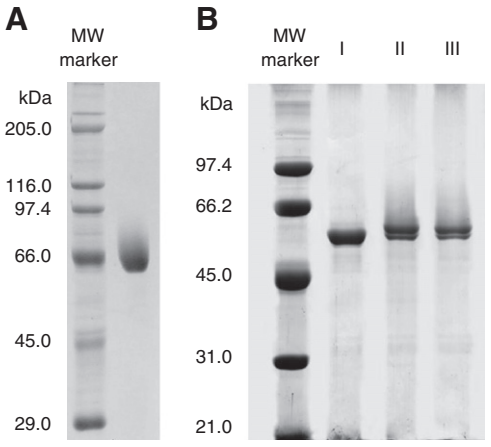

Fig. 1 – SDS-PAGE separation of untreated and endoglycosidase H-treated recombinant ZmCKO1. Panel A; from the left: protein standards with the indicated molecular mass, untreated recombinant ZmCKO1 (5 μg). Panel B; from the left: protein standards with the indicated molecular mass, lane I - recombinant ZmCKO1 after deglycosylation in the presence of SDS at 37 °C (5 μg), lane II — recombinant ZmCKO1 after deglycosylation without SDS at 23 °C (5 μg), lane III — recombinant ZmCKO1 after deglycosylation without SDS at 37 °C (4 μg). Proteins were visualized by staining with Coomassie Brilliant Blue R250.

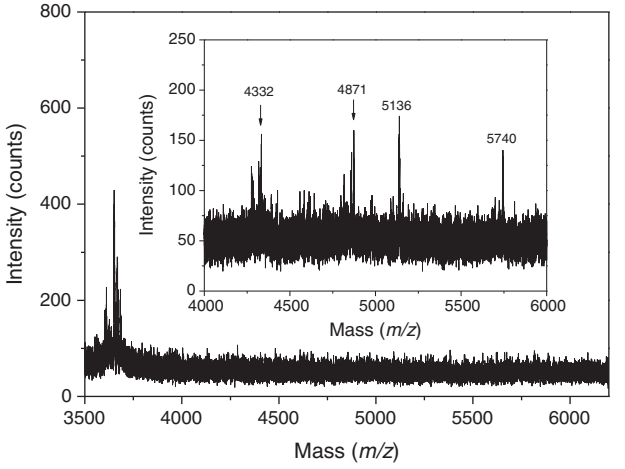

Fig. 2 – MALDI-TOF mass spectrometry of tryptic digests of ZmCKO1.Main panel shows the region of *m/z* 3500–6500 from a mass spectrum acquired using untreated recombinant ZmCKO1 after it had been digested with trypsin (without digest purification). Except for a very small glycopeptide peak with *m/z* 5812.9 (not labeled) and well pronounced signals with *m/z* 3649.8, 3665.8 and 3681.8 referring to a non-glycosylated peptide SMWDDGMSAATPSEDVFYAVSLLFSSVAPNDLAR and its variants with one or two oxidized methionines, respectively (not labeled), no other significant signal is visible at masses over *m/z* 3600. The inset shows a similar spectrum section acquired using the endoglycosidase H-treated enzyme. Several new peptide peaks appeared (see labeling), which refer to trimmed N-glycopeptides binding one residual GlcNAc at each N-glycosylation site. All spectra were measured on the Microflex LRF20 instrument operating in the reflectron mode for positive ions; CHCA was used as a matrix.

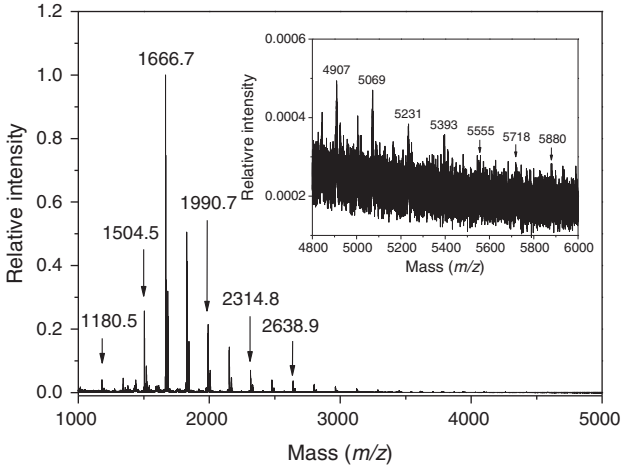

Fig. 3 – MALDI-TOF mass spectrum of neutral N-glycans released from recombinant ZmCKO1 by the treatment with endoglycosidase H. Main panel depicts the most intense glycan peaks from a series starting at *m/z* 1180 and going up to *m/z* 5880 with a regular mass difference of 162 Da (sodium adduct peaks $[M+Na]^+$). The inset provides a magnification of the signals in the region of *m/z* 4800–6000. The spectrum was acquired on the ABI 4800 Proteomics Analyzer operating in the reflectron mode for positive ions; 3-AQ was used as a matrix.

derivatization accompanied by a mass increase of 126.1 Da [30]. Sodium adduct peaks appeared in a series starting at *m/z* 1180.5 and going up to *m/z* 5880. This is consistent with derivatized glycan structures of the high-mannose type comprising from 5 to 34 mannose residues. The corresponding potassium adduct peaks were also observed. ESI-MS measurements on a Q-TOF instrument were performed with a glycan sample containing 0.1 mM sodium acetate to stimulate the preferential formation of sodium adduct peaks. The results showed a series of doubly charged ions $[M+2Na]^{2+}$ referring to glycan chains with one GlcNAc (reducing end) plus 7 to 19 Hex residues. The corresponding masses were between *m/z* 700.7 and 1673.1 (not shown). Without using sodium acetate, doubly charged ions $[M+H+K]^{2+}$ were predominant. They spanned the *m/z* interval from 697 to 1832 with a regular mass difference of 81 Da. From these, the peaks with *m/z* 778.7 and 859.7 were selected as precursors for CID-MS/MS analyses to evaluate the chemical structure of the glycans. Fig. 4 illustrates a tandem mass spectrum acquired for the precursor peak with *m/z* 859.7 showing predominant Y-ions according to the nomenclature by Domon and Costello [37,38]. The observed fragmentation pattern indicates the existence of high-mannose glycans in ZmCKO1 and may be considered the final evidence for their chemical composition.

3.5. *Activity and thermostability assays of deglycosylated ZmCKO1*

ZmCKO1 deglycosylated under non-denaturing conditions was subjected to activity assay with N^6-isopentenyladenine (iP) as a substrate. In addition, its thermostability was

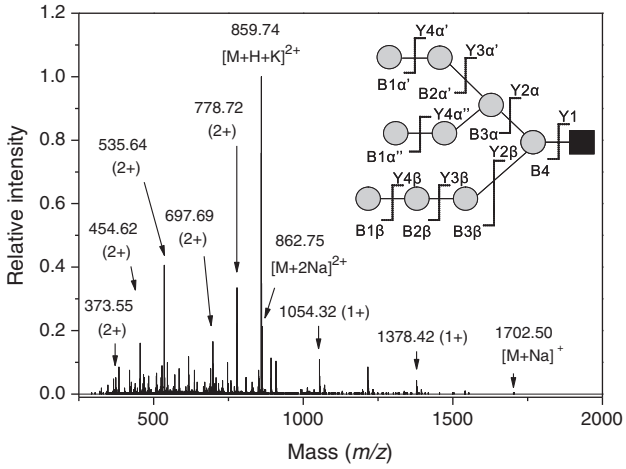

Fig. 4 – Positive ion electrospray CID-MS/MS spectrum of a glycan structure from recombinant ZmCKO1. The spectrum shows the fragmentation pattern of a doubly charged precursor ion with *m/z* 859.74. Reading mass differences allowed identifying a high-mannose glycan structure $Man_9GlcNAc$. The inset shows a typical fragmentation of such a glycan with the indicated nomenclature according to Domon and Costello [37]. The spectrum, which is dominated by glycosidic cleavages (namely Y ions) was measured on the maXis ultra high resolution Q-TOF instrument.

analyzed by incubating aliquots at temperatures from 25 °C to 70 °C, with subsequent measurement of its residual activity. The results were compared with those for untreated recombinant enzyme. The specific activity of the enzyme deglycosylated at 37 °C (3 h) was 300 nkat mg^{-1}, which represents a decrease by 30% with respect to the original value. Fig. 5 shows Michaelis–Menten saturation curves for ZmCKO1 measured prior to and after treatment with endoglycosidase H. From the corresponding Lineweaver–Burk plots, similar values of the K_m constant were deduced for the recombinant enzyme and its deglycosylated form (2.3 and 2.5 μM, respectively). Nevertheless, an interesting difference was observed: whereas recombinant ZmCKO1 displayed an excess substrate inhibition at iP concentrations exceeding 20 μM, the deglycosylated enzyme did not. As the determined K_m values are similar for both proteins, substrate binding at the active site is expected to be comparable. These data show that binding of a second iP molecule (at excessive substrate concentrations in the reaction mixture) in the glycosylated enzyme might be somehow easier. However, a mild structural change at the entrance to the active site that would occur in consequence of the treatment cannot be ruled out. The latter option is further supported by thermostability measurements that are summarized in Fig. 6. The untreated recombinant ZmCKO1 showed a T_{50} value of 57 °C (T_{50} is defined here as a temperature at which 50% of the activity is retained upon 30-min incubation). After the overnight non-denaturing deglycosylation performed at 23 °C, the observed T_{50} was only 49 °C. Anyway, the enzyme practically kept its original stability at temperatures up to 40 °C. In contrast, the other non-denaturing deglycosylation, which was performed at 37 °C (3 h), resulted in a significantly weakened thermostability between 20 and 50 °C. Such a behavior was not observed for a control sample of the recombinant enzyme, which was

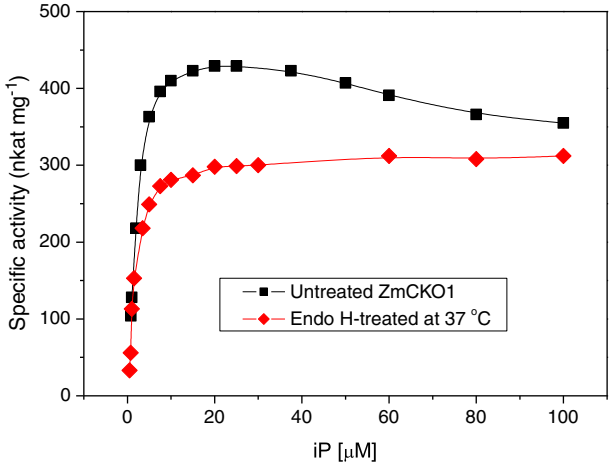

Fig. 5 – Michaelis-Menten kinetics of the deglycosylated recombinant ZmCKO1.Results for individual enzyme forms are color coded as follows: untreated recombinant ZmCKO1 — black squares, enzyme deglycosylated at 37 °C (no SDS) — red rhombi. A comparison of the saturation curves reveals that the deglycosylated enzyme does not undergo excess-substrate inhibition.

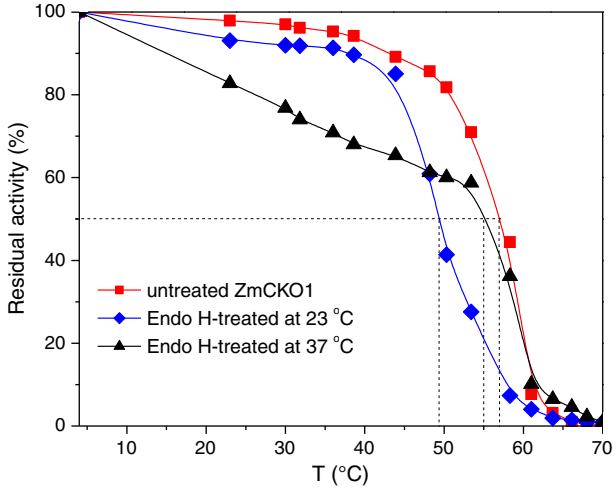

Fig. 6 – Thermostability of untreated and endoglycosidase H-treated recombinant ZmCKO1. Results for individual enzyme forms are color coded as follows: untreated recombinant ZmCKO1 — red squares, enzyme deglycosylated at 23 °C (no SDS) — blue rhombi, enzyme deglycosylated at 37 °C (no SDS) — black triangles. Enzyme samples were incubated at temperatures from 20 °C up to 75 °C for 30 min. After fast cooling of the samples in ice-cold water, they were assayed for residual activity at 37 °C. Dashed lines indicate subtraction of the corresponding T_{50} values.

incubated at 37 °C for the same time period (not shown). As there was no typical sigmoid activity-to-temperature dependence observed (like e.g. for ZmCKO1 after deglycosylation at 23 °C) but a relatively steep activity decrease with increasing temperature, the subtraction of T_{50} giving a value of 55 °C cannot be considered reliable in this case. Yet, the above kinetic experiments have clearly shown that the loss of *N*-glycosylation led to a destabilization of ZmCKO1 tertiary structure affecting only slightly the enzymatic activity.

3.6. *MALDI-TOF/TOF MS and MS/MS analyses of N-glycopeptides from ZmCKO1*

Thorough mass spectrometric analyses of tryptic digests of recombinant ZmCKO1 were carried out in order to gain information on the localization of glycan chains. After desalting, but without any gradient chromatographic separation of peptides from the digests, only large *N*-glycopeptides were observed in MALDI-TOF mass spectra as it is displayed in Fig. 7. Employing CHCA as a matrix, there were numerous glycopeptide peaks registered in the *m/z* region of 4500–6500. Many of the corresponding peptide ions were chosen as precursors and subjected to CID-MS/MS analysis on MALDI-TOF/TOF (see further). Using ferulic acid as a matrix and the Microflex LRF20 instrument, another group of *N*-glycopeptides was found. In this case, the corresponding signals appeared in the *m/z* region of 7900–12500 (Fig. 7, inset) in two distributions. Reading MS/MS spectra of precursor ions from the first group of *N*-glycopeptides, for example of those with *m/z* 6351.3, 5812.8 and 4735.2, allowed identification of three related series referring to the following amino acid sequences: P1 i.e. 269-LTAPRPGGGGASFGPMSY VEGSVFVNQSLATDLANTGFFTDADVAR-314, P2 i.e. 274-PGGG GASFGPMSYVEGSVFVNQSLATDLANTGFFTDADVAR-314 and P3 i.e. 285-SYVEGSVFVNQSLATDLANTGFFTDADVAR-314, respectively. This indicates one non-canonical tryptic cleavage (after Arg273 i. e. before a proline residue) plus one non-specific cleavage (after Met284). Non-specific peptides in tryptic digests are frequent and, as it has been shown recently based on statistical analysis of millions of tandem mass spectra, trypsin action before proline is not uncommon [39]. All sequenced *N*-glycopeptides from the first group were found to contain Asn294 as a glycosylation site. Simple mathematic calculations were used to assign the other peaks from the *m/z* region of 4500–6500. Taken together, the results were consistent with the presence of glycan structures from $Man_4GlcNAc_2$ up to $Man_{12}GlcNAc_2$ at the glycosylation site Asn294.

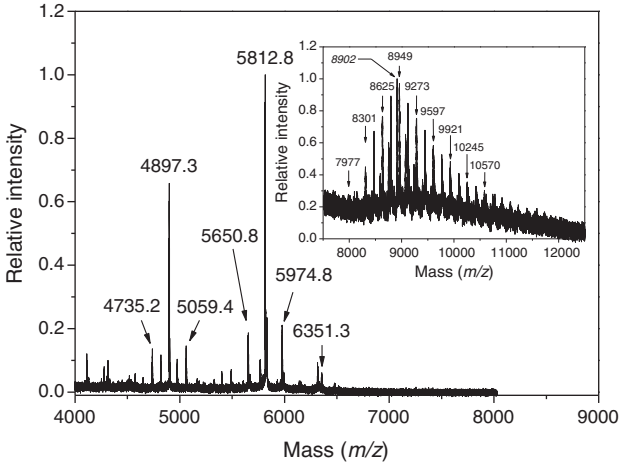

Fig. 7 – MALDI-TOF mass spectrometry of tryptic digests of ZmCKO1.Main panel shows the region of *m/z* 4500–8000 from a mass spectrum acquired using untreated recombinant ZmCKO1 after it had been digested with trypsin. There were a few series of *N*-glycopeptides observable. CID-MS/MS of selected precursor ions (e.g. *m/z* 4735.2, 4897.3, 5812.8 and 6351.3) allowed reading amino acid sequences with a confirmation of Asn294 as the site of glycosylation. The inset shows larger *N*-glycopeptides in two distributions. The labeled distribution refers to the glycopeptide 323–367 with glycans attached at Asn 323 and Asn338. The second distribution is indicated by labeling only the most abundant peak (in italics, *m/z* 8902) and refers to the peptide 49–101 with occupied Asn52 and Asn63. The main spectrum was acquired on the ABI 4800 Proteomics Analyzer operating in the reflectron mode for positive ions; CHCA was used as a matrix. The inset spectrum was acquired on the Microflex LRF20 instrument operating in the reflectron mode for positive ions; ferulic acid was used as a matrix.

3.7. *Microgradient separation of N-glycopeptides and their sequencing using MALDI-TOF/TOF MS/MS*

The large *N*-glycopeptides with molecular mass values over 8000 Da could not be analyzed by MALDI peptide sequencing without separation. A simple microgradient device with home-made capillary column was then used to optimize the separation of ZmCKO1 tryptic digests with subsequent MALDI-TOF/TOF MS and MS/MS analysis. This resulted in the detection of a glycopeptide series in the *m/z* range 1700–2900 that was identified as peptide 133-INVSADGR-140 with attached *N*-glycans $Man_3GlcNAc_2$–$Man_{10}GlcNAc_2$. Next to these glycopeptides, a nonglycosylated peptide 133-INVSADGR-140 with *m/z* 831.45 was also identified in this sample showing only partial glycosylation of Asn134. A similar detection of both nonglycosylated (*m/z* 831.46) and glycosylated (*m/z* 1034.54) forms of the peptide 133-INVSADGR-140 was done in MALDI-TOF MS analysis of the microgradient-separated tryptic digest of ZmCKO1 that had previously been treated with endoglycosidase H. The presence of sugars at this glycosylation site was additionally confirmed using reversed-phase gradient liquid chromatography of the ZmCKO1 digest coupled to ESI-Q-TOF MS. A doubly charged precursor ion with *m/z* 1267.53 was isolated and subjected to CID-MS/MS. The fragmentation pattern confirmed the presence of $Man_8GlcNAc_2$ attached to Asn134 (not shown).

Because the larger *N*-glycopeptides with molecular values exceeding 8000 Da were not eluted within the usual ACN gradient (2–35%), the ZmCKO1 tryptic digest was first fractionated in a GELoader tip containing POROS R3 Oligo particles and the peptide fraction eluting between 40 and 80% ACN/0.1% TFA was then dried, redissolved in 0.1% TFA and loaded on the C18 capillary column. Separation using ACN gradient between 30 and 80% ACN/0.1% TFA led to the detection of five distinct *N*-glycopeptide distributions. The first two distributions originated from the peptides P2 and P3 mentioned above. MS and MS/MS analyses of these series confirmed information about *N*-glycosylation of Asn294 already obtained

from the analysis of unseparated ZmCKO1 tryptic digest. The third glycopeptide series was observed in the *m/z* range of 8000–10600. MALDI-TOF/TOF MS/MS results on a precursor ion with *m/z* 8902.4 (Fig. 8) allowed to recognize a peptide 49-TDSNATAAASTDFGNITSALPAAVLYPSSTADLVALLSAANSTPGW-PYTIAFR-101, where Asn52 and Asn63 were found occupied with high-mannose glycan structures ($Man_8GlcNAc_2$ and $Man_9GlcNAc_2$, respectively). Almost complete y-ion series in the range y_4–y_{38} without any indication of attached glycan structures showed that Asn89 was not glycosylated in this glycopeptide. An abundant fragment ion with *m/z* 5930.4 was assigned to y_{41}-ion demonstrating a $Man_8GlcNAc_2$ attachment to Asn63. A fragment ion cluster in the *m/z* range 7030–7410 (losses of particular glycan structures from the precursor) and the presence of y_{51}-ion with *m/z* 8687.2 confirmed the existence of a glycosylation at Asn52 (with the most abundant attached form $Man_9GlcNAc_2$ for the analyzed precursor), which was unexpected in the light of previous reports [19,21]. This glycopeptide distribution had a summary composition ranging from $Man_{12}GlcNAc_4$ to $Man_{27}GlcNAc_4$, which appeared to be divided almost equally between the occupied Asn52 and Asn63. An analogous evaluation was done for the fourth glycopeptide distribution detected in the *m/z* range of 7900–12500. MALDI-TOF/TOF MS/MS analysis of a precursor ion with *m/z* 9110.9 resulted in the identification of a peptide 323-NATTVYSIEATLNYDNATAA-AAAVDQELASVLGTLSYVEGFAFQR-367 with doubled glycosylation at Asn323 and Asn338. Both sites were most abundantly occupied with $Man_{11}GlcNAc_2$ when a summary glycan composition ranged between $Man_{15}GlcNAc_4$ and $Man_{34}GlcNAc_4$. These results allowed the final identification of glycopeptide series detected by measuring on the Microflex LRF20 instrument with ferulic acid as a matrix (Fig. 7, inset), where even higher oligomers could be detected. Finally, the fifth glycopeptide distribution was found in the *m/z* range 5100–8800. MS/MS analysis of several precursors from this distribution (e.g. *m/z* 5622.2, 6267.6, 6755.9) identified glycopeptides originating from a semispecific tryptic peptide 329-SIEATLNYDNATAAAAAVDQE-LASVLGTLSYVEGFAFQR-367 (resulting from a cleavage after Tyr), where Asn338 was glycosylated with glycan structures ranging from $Man_4GlcNAc_2$ to $Man_{26}GlcNAc_2$. Thus Asn338 represents the possible site of ZmCKO1 hyperglycosylation detected by MALDI-TOF MS of *N*-glycans analysis using 3-AQ as a matrix as mentioned above (Fig. 3).

The last potential *N*-glycosylation site in ZmCKO1 is Asn434. During MALDI-TOF MS analysis of the fraction eluting between 40 and 80% ACN/0.1% TFA from GELoader tip with POROS R3 Oligo particles, only a non-glycosylated peptide 417-GILQGTDIVGPLIVYPLNK-435 with *m/z* 2010.25 was found. The same peptide was also observed after the microgradient separation of tryptic digest from endoglycosidase H-treated ZmCKO1. This is in agreement with previous results from the crystal structures demonstrating a vacancy of sugar residues at Asn434 [19,21]. Interestingly, MS/MS peptide sequencing on MALDI-TOF/TOF of a precursor ion with *m/z* 5939 from the separated tryptic digest of deglycosylated ZmCKO1 revealed one GlcNAc residue bound at Asn89 (besides its parallel binding at Asn52 and Asn63), which suggested the presence of an *N*-glycosylation (not shown). Unfortunately, no glycopeptide

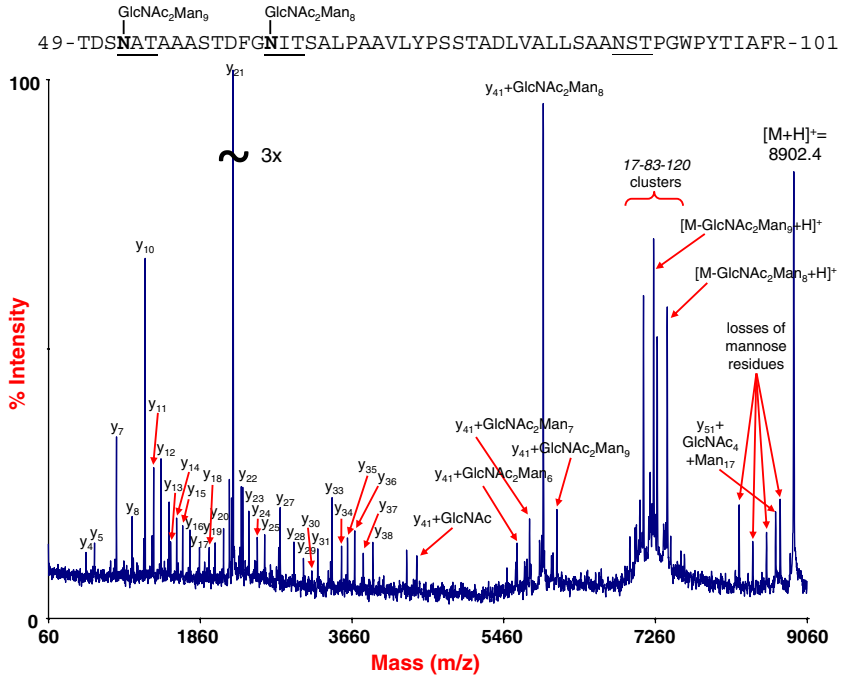

Fig. 8 – Positive ion MALDI-TOF/TOF CID-MS/MS spectrum of a glycopeptide from recombinant ZmCKO1. The spectrum shows the fragmentation pattern of a precursor ion with *m/z* 8902.4. Fragment masses are consistent with a ZmCKO1-derived tryptic peptide 49-TDSNATAAASTDFGNITSALPAAVLYPSSTADLVALLSAANSTPGWPYTIAFR-101 containing high-mannose glycan structures attached at Asn52 and Asn63. The results were obtained on the ABI 4800 Proteomics Analyzer operating in the reflectron mode for positive ions; CHCA was used as a matrix. Numbers shown in italics highlight the group with mass difference patterns of 17-83-120, which is typical for the fragmentation of *N*-glycopeptides.

Table 2 – An overview of ZmCKO1 N-glycosylation pattern from mass spectrometric results with glycopeptides.

N-glycosylation site	N-glycosylation type	Summary composition of N-glycan chains [a]	Note
Asn52 + Asn63	High mannose	$Man_{12}GlcNAc_4$–$Man_{27}GlcNAc_4$ [b]	–
Asn89	Unknown [c]	Unknown [c]	Partial glycosylation [d]
Asn134	High mannose	$Man_3GlcNAc_2$–$Man_{10}GlcNAc_2$	Partial glycosylation
Asn294	High mannose	$Man_4GlcNAc_2$–$Man_{12}GlcNAc_2$	–
Asn323 + Asn338	High mannose	$Man_{15}GlcNAc_4$–$Man_{34}GlcNAc_4$ [b]	–
Asn338	High mannose	$Man_4GlcNAc_2$–$Man_{26}GlcNAc_2$	Hyperglycosylation
Asn434	–	–	No glycosylation

[a] This was calculated from the observed mass ranges in the corresponding N-glycopeptide series.
[b] The summary composition is provided here in total for both glycosylation sites, which appeared in a single tryptic peptide.
[c] The possible glycosylation at Asn89 was demonstrated only by the presence of a bound GlcNAc residue after the enzymatic deglycosylation of ZmCKO1 with endoglycosidase H. No N-glycopeptide with glycan chains bound at Asn89 was registered in digests of recombinant ZmCKO1.
[d] A partial glycosylation was deduced when the above mentioned results with the deglycosylated and digested ZmCKO1 were combined with the observed absence of glycan chains at Asn89 in several N-glycopeptides analyzed by MALDI-TOF/TOF MS/MS.

bearing glycan chains at this site could be detected and sequenced from the digests of glycosylated ZmCKO1 to characterize the glycosylation type and extent.

4. Conclusions

Recombinant ZmCKO1 from *Y. lipolytica* contains N-glycan chains. In this work, their binding at the respective glycosylation sites and chemical structure were characterized for the first time in the group of cytokinin oxidases/dehydrogenases. Tandem mass spectrometry of enzymatically released carbohydrates confirmed their high-mannose type character. Glycopeptide sequencing on MALDI-TOF/TOF instrument demonstrated N-glycosylation at Asn52, 63, 134, 294, 323 and 338 (Table 2). The bound glycans contained 3–14 mannose residues. Interestingly, Asn134 was found only partially glycosylated. Asn338 was the sole site exhibiting large glycan chains exceeding 25 mannose residues. This feature could indicate some yet unknown significance of Asn338, which is located in a surface loop at the interconnection between an α-helix and a β-pleated sheet in the substrate binding domain. The reason for this peculiar glycosylation is unknown, as the couple Asn 294 and 323 has a similar solvent-exposed location [19,21]. The presence of an N-glycosylation at Asn89 could not be confirmed by glycopeptide analysis using the glycosylated protein as a starting material. It was demonstrated only by sequencing of an endoglycosidase-H trimmed glycopeptide, which contained one residual GlcNAc bound at this site. The enzyme subjected to an enzymatic deglycosylation under native conditions shows both decreased thermostability and lowered catalytic activity.

The second outcome of the present work has a more general biochemical significance. It resides in the first experimental evidence of the posttranslational formation of long sugar chains in recombinant proteins produced in *Y. lipolytica*. In contrast to mammals, lower eukaryotes such as yeasts are known to produce only high-mannose type N-glycans varying in length for endogenous and heterologous proteins [40,41]. When compared with *Saccharomyces cerevisiae* where they are typically of 50–150 residues (this extent is referred to as hyperglycosylation), *Pichia pastoris* and *Hansenula polymorpha* produce N-glycan chains consisting of only around 10 mannoses [42]. Previous results with *Y. lipolytica* as a host organism have shown no example of hyperglycosylation of recombinant proteins [42]. To our knowledge, the sole previous detailed study of oligosaccharidic chains in a recombinant protein produced in this yeast was performed on *Trichoderma reesei* endoglucanase I, and found them to exhibit sizes ranging from 8 to 12 mannoses [43]. Accordingly, a moderate glycosylation (reflected in molecular mass increases in the range of 10 kDa) has been emphasized as a typical feature of recombinant proteins produced in *Y. lipolytica*, which is advantageous as regards to their biological activity and antigenicity [42]. Recombinant ZmCKO1 does not represent an exception in this sense. Nevertheless, our results show that *Y. lipolytica* could hyperglycosylate some peculiar sites. Consequently, one should keep in mind that, despite a moderate overall glycosylation rate, individual glycan chains in recombinant protein products from *Y. lipolytica* may possess a bulky structure.

Acknowledgments

This work was supported by grant no. 522/08/0555 from the Czech Science Foundation, OP RD&I grant no. ED0007/01/01 (Centre of the Region Haná for Biotechnological and Agricultural Research), from the Ministry of Education Youth and Sports, Czech Republic and a long-term organization development plan no. 1011 from the Faculty of Military Health Sciences, University of Defence, Czech Republic.

REFERENCES

[1] Miller CO, Skoog F, von Saltza MH, Strong M. Kinetin, a cell division factor from deoxyribonucleic acid. J Am Chem Soc 1955;77:1329–34.
[2] Skoog F, Armstrong DJ. Cytokinins. Annu Rev Plant Physiol 1970;21:359–84.
[3] Mok MC, Martin RC, Mok DWS. Cytokinins: biosynthesis, metabolism and perception. In Vitro Cell Dev Biol-Plant, 36; 2000. p. 102–7.
[4] Frébort I, Kowalska M, Hluska T, Frébortová J, Galuszka P. Evolution of cytokinin biosynthesis and degradation. J Exp Bot 2011;62:2431–52.
[5] Pils B, Heyl A. Unraveling the evolution of cytokinin signaling. Plant Physiol 2009;151:782–91.

[6] Sakakibara H. Cytokinins: activity, biosynthesis, and translocation. Annu Rev Plant Biol 2006;57:431–49.
[7] Kakimoto T. Identification of plant cytokinin biosynthetic enzymes as dimethylallyl diphosphate: ATP/ADP isopentenyltransferases. Plant Cell Physiol 2001;42:677–85.
[8] Takei K, Sakakibara H, Sugiyama T. Identification of genes encoding adenylate isopentenyltransferase, a cytokinin biosynthesis enzyme, in *Arabidopsis thaliana*. J Biol Chem 2001;276:26405–10.
[9] Galuszka P, Frébort I, Šebela M, Sauer P, Jacobsen S, Peč P. Cytokinin oxidase or dehydrogenase? Mechanism of cytokinin degradation in cereals. Eur J Biochem 2001;268:450–61.
[10] Pačes V, Werstiuk E, Hall RH. Conversion of N^6-(Δ^2-isopentenyl) adenosine to adenosine by enzyme activity in tobacco tissue. Plant Physiol 1971;48:775–8.
[11] Whitty CD, Hall RH. A cytokinin oxidase in *Zea mays*. Can J Biochem 1974;52:789–99.
[12] Brownlee BG, Hall RH, Whitty CD. 3-Methyl-2-butenal: an enzymatic degradation product of the cytokinin N^6-(Δ^2-isopentenyl)adenine. Can J Biochem 1975;53:37–41.
[13] Houba-Hérin N, Pethe C, d'Alayer J, Laloue M. Cytokinin oxidase from *Zea mays*: purification, cDNA cloning and expression in moss protoplasts. Plant J 1999;17:615–26.
[14] Morris RO, Bilyeu KD, Laskey JG, Cheikh NN. Isolation of a gene encoding a glycosylated cytokinin oxidase from maize. Biochem Biophys Res Commun 1999;255:328–33.
[15] Bilyeu KD, Cole JL, Laskey JG, Riekhof WR, Esparza TJ, Kramer MD, et al. Molecular and biochemical characterization of a cytokinin oxidase from maize. Plant Physiol 2001;125:378–86.
[16] Kopečný D, Pethe C, Šebela M, Houba-Hérin N, Madzak C, Majira A, et al. High-level expression and characterization of *Zea mays* cytokinin oxidase/dehydrogenase in *Yarrowia lipolytica*. Biochimie 2005;87:1011–22.
[17] Schmülling T, Werner T, Riefler M, Krupková E, Bartrina y Manns I. Structure and function of cytokinin oxidase/dehydrogenase genes of maize, rice, Arabidopsis and other species. J Plant Res 2003;116:241–52.
[18] Galuszka P, Popelková H, Werner T, Frébortová J, Pospíšilová H, Mik V, et al. Biochemical characterization of cytokinin oxidases/dehydrogenases from *Arabidopsis thaliana* expressed in *Nicotiana tabacum* L. J Plant Growth Regul 2007;26:255–67.
[19] Malito E, Coda A, Bilyeu KD, Fraaije MW, Mattevi A. Structures of Michaelis and product complexes of plant cytokinin dehydrogenase: implications for flavoenzyme catalysis. J Mol Biol 2004;341:1237–49.
[20] Bae E, Bingman CA, Bitto E, Aceti DJ, Phillips GN. Crystal structure of *Arabidopsis thaliana* cytokinin dehydrogenase. Proteins 2008;70:303–6.
[21] Kopečný D, Briozzo P, Popelková H, Šebela M, Končitíková R, Spíchal L, et al. Phenyl- and benzylurea cytokinins as competitive inhibitors of cytokinin oxidase/dehydrogenase: a structural study. Biochimie 2010;92:1052–62.
[22] Rayon C, Cabanes-Macheteau M, Loutelier-Bourhis C, Salliot-Maire I, Lemoine J, Reiter WD, et al. Characterization of *N*-glycans from Arabidopsis. Application to a fucose-deficient mutant. Plant Physiol 1999;119:725–34.
[23] Séveno M, Cabrera G, Trigueroc A, Burel C, Leprince J, Rihouey C, et al. Plant *N*-glycan profiling of minute amounts of material. Anal Biochem 2008;379:66–72.
[24] Smith PK, Krohn RI, Hermanson GT, Mallia AK, Gartner FH, Provenzano MD, et al. Measurement of protein using bicinchoninic acid. Anal Biochem 1985;150:76–85.
[25] Packer NH, Lawson MA, Jardine DR, Redmond JW. A general approach to desalting oligosaccharides released from glycoproteins. Glycoconj J 1998;15:737–47.
[26] Laemmli UK. Cleavage of structural proteins during the assembly of the head of bacteriophage T4. Nature 1970;227:680–5.
[27] Shevchenko A, Tomas H, Havliš J, Olsen JV, Mann M. In-gel digestion for mass spectrometric characterization of proteins and proteomes. Nat Protoc 2006;1:2856–60.
[28] Kowalska M, Galuszka P, Frébortová J, Šebela M, Béres T, Hluska T, et al. Vacuolar and cytosolic cytokinin dehydrogenases of *Arabidopsis thaliana*: heterologous expression, purification and properties. Phytochemistry 2010;71:1970–8.
[29] Huang Y, Mechref Y, Novotny MV. N-Linked oligosaccharide structures in the diamine oxidase from porcine kidney. Carbohydr Res 2000;323:111–25.
[30] Rohmer M, Meyer B, Mank M, Stahl B, Bahr U, Karas M. 3-Aminoquinoline acting as matrix and derivatizing agent for MALDI MS analysis of oligosaccharides. Anal Chem 2010;82:3719–26.
[31] Rappsilber J, Mann M, Ishihama Y. Protocol for micro-purification, enrichment, pre-fractionation and storage of peptides for proteomics using StageTips. Nat Protoc 2007;2:1896–906.
[32] Kussmann M, Nordhoff E, Rahbek-Nielsen H, Haebel S, Rossel-Larsen M, Jakobsen L, et al. Matrix-assisted laser desorption/ionization mass spectrometry sample preparation techniques designed for various peptide and protein analytes. J Mass Spectrom 1997;32:593–601.
[33] Moravcová D, Kahle V, Řehulková H, Chmelík J, Řehulka P. Short monolithic columns for purification and fractionation of peptide samples for matrix-assisted laser desorption/ionization time-of-flight/time-of-flight mass spectrometry analysis in proteomics. J Chromatogr A 2009;1216:3629–36.
[34] Kahle V, Vázlerová M, Welsch T. Automated microgradient system for capillary electrochromatography. J Chromatogr A 2003;990:3–9.
[35] Vyroubalová Š, Václavíková K, Turečková V, Novák O, Šmehilová M, Hluska T, et al. Characterization of new maize genes putatively involved in cytokinin metabolism and their expression during osmotic stress in relation with cytokinin levels. Plant Physiol 2009;151:433–47.
[36] Kopečný D, Šebela M, Briozzo P, Spíchal L, Houba-Hérin N, Mašek V, et al. Mechanism-based inhibitors of cytokinin oxidase/dehydrogenase attack FAD cofactor. J Mol Biol 2008;380:886–99.
[37] Domon B, Costello CE. A systematic nomenclature for carbohydrate fragmentations in FAB-MS/MS spectra of glycoconjugates. Glycoconj J 1988;5:397–409.
[38] Harvey DJ. Electrospray mass spectrometry and fragmentation of N-linked carbohydrates derivatized at the reducing terminus. J Am Soc Mass Spectrom 2000;11:900–15.
[39] Rodriguez J, Gupta N, Smith RD, Pevzner PA. Does trypsin cut before proline? J Proteome Res 2007;7:300–5.
[40] Goochee CF, Gramer MJ, Andersen DC, Bahr JB, Rasmussen JR. The oligosaccharides of glycoproteins: bioprocess factors affecting oligosaccharide structure and their effect on glycoprotein properties. Biotechnology (N Y) 1991;9:1347–55.
[41] Byrd JC, Tarentino AL, Maley F, Atkinson PH, Trimble RB. Glycoprotein synthesis in yeast. Identification of $Man_8GlcNAc_2$ as an essential intermediate in oligosaccharide processing. J Biol Chem 1982;257:14657–66.
[42] Madzak C, Gaillardin C, Beckerich JM. Heterologous protein expression and secretion in the non-conventional yeast *Yarrowia lipolytica*: a review. J Biotechnol 2004;109:63–81.
[43] Song Y, Choi MH, Park JN, Kim MW, Kim EJ, Kang HA, et al. Engineering of the yeast *Yarrowia lipolytica* for the production of glycoproteins lacking the outer-chain mannose residues of N-glycans. Appl Environ Microbiol 2007;73:4446–54.

Article 2

Kinetic and structural investigation of the cytokinin oxidase/dehydrogenase active site

Kopečný[1*] D., Končitíková[1] R, Popelka[2] H., Briozzo[3] P., Vigouroux[4] A., Kopečná[1] M., Zalabák[5] D., Šebela[1] M., Ivo Frébort[5] I. and Moréra[4] S.

Manuscript

Kinetic and structural investigation of the cytokinin oxidase/dehydrogenase active site

David Kopečný[1*], Radka Končitíková[1], Hana Popelka[2], Pierre Briozzo[3], Armelle Vigouroux[4], Martina Kopečná[1], David Zalabák[5], Marek Šebela[1], Ivo Frébort[5] and Solange Moréra[4*]

[1]Department of Protein Biochemistry and Proteomics and [5]Department of Molecular Biology, Centre of the Region Haná for Biotechnological and Agricultural Research, Faculty of Science, Palacký University, Šlechtitelů 11, CZ-78371 Olomouc, Czech Republic; [2]Department of Molecular, Cellular and Developmental Biology, University of Michigan, Ann Arbor, MI 48109-1048, USA; [3]Institut Jean-Pierre Bourgin, UMR1318 INRA-AgroParisTech, Route de Saint-Cyr, F-78026 Versailles Cedex; [4]Institute for Integrative Biology of the Cell (I2BC), Department of Biophysics, Biochemistry and Structural Biology, CNRS CEA University Paris-Sud, F-91198 Gif-sur-Yvette Cedex, France.

Running head: Structure-function study on cytokinin oxidase/dehydrogenase

*Corresponding authors: david.kopecny@upol.cz, morera@i2bc.paris-saclay.fr; Tel.: +420 585634840 (D.K)/+33 1 69 82 34 70 (S.M.), Fax: +420 585634933 (D.K.)/+33 1 69 82 31 29 (S.M.)

Highlights

- Cytokinin oxidases/dehydrogenases (CKOs) regulate cytokinin levels in plants
- Function of active-site residues in CKOs was studied
- Crystal structures of CKOs and active-site mutants were analyzed
- The binding mode of cytokinin ribosides was structurally characterized
- Identification of critical active-site residues in catalysis and substrate specificity

Abstract

Cytokinins are hormones that regulate plant development and their environmental responses. Their levels are mainly controlled by the cytokinin oxidase/dehydrogenase (CKO), which oxidatively cleaves the cytokinins using redox-active electron acceptors. CKO belongs to the group of flavoproteins with an 8α-N(1)-histidyl FAD covalent linkage. Here, we investigated the role of seven active site residues: H105, D169, E288, V378, E381, P427 and L492, in substrate binding and catalysis of CKO1 from maize (*Zea mays*, ZmCKO1) combining side-directed mutagenesis with kinetic and X-ray crystallography. Here, we identify E381 as a key residue for enzyme specificity that restricts substrate binding as well as quinone electron acceptor binding. We show that D169 is important for catalysis and that H105 covalently linked to FAD maintains the enzyme's structural integrity, stability and high rates with electron acceptors. L492A mutation significantly modulates the cleavage of aromatic cytokinins and zeatin isomers. The high resolution X-ray structures of ZmCKO1 and the E381S mutant in complex with N^6-(2-isopentenyl)adenosine (iPR) reveal the binding mode of cytokinin ribosides. Those of ZmCKO2 and ZmCKO4a display a mobile domain, which might contribute to the substrate binding of the N9 substituted cytokinins.

Keywords:

Crystal structure; cytokinin oxidase/dehydrogenase; enzyme mechanism; flavoprotein; plant hormone; site-directed mutagenesis; *Zea mays*

Abbreviations: CKO/CKX, cytokinin oxidase/dehydrogenase; *c*Z, N^6-(*cis*-4-hydroxy-3-methyl-2-buten-1-yl)adenine i.e. *cis*-zeatin; DCPIP, 2,6-dichlorophenol indophenol; iP, N^6-(2-isopentenyl)adenine; iPR, N^6-(2-isopentenyl)adenosine; iP9G, N^6-isopentenyladenine-9-glucoside; MTT, 3-(4,5-dimethylthiazol-2-yl)-2,5-diphenyltetrazolium bromide; NQ, 1,4-naphthoquinone; PMS, phenazine methosulphate; Q_0, 2,3-dimethoxy-5-methyl-1,4-benzoquinone = coenzyme Q_0; WT, wild-type; *t*Z, *trans*-zeatin; *t*ZR, zeatin riboside; ZmCKO/ZmCKX, cytokinin oxidase/dehydrogenase from *Zea mays*

Introduction

Cytokinins are adenine-derived plant hormones that carry N^6-isoprenoid or N^6-aromatic side chain. They are key regulators of numerous processes in plant growth and development, such as cell division, shoot and root development, apical dominance and seed germination [1]. Irreversible degradation is mediated by cytokinin oxidase/dehydrogenase (CKO/CKX) which belongs to the flavoprotein oxidoreductases group including oxidases and dehydrogenases, containing either a covalently or a non-covalently bound FAD cofactor [2, 3]. CKO cleaves the isoprenoid side chain of N^6-(2-isopentenyl)adenine (iP), *trans*- and *cis*-zeatin (*t*Z, *c*Z) and their ribosides (iPR, *t*ZR, *c*ZR), leading to adenine/adenosine and the corresponding aldehyde [4, 5]. In higher plants, CKOs are encoded by small multigene families, including 7 genes in Arabidopsis (*AtCKOs*) [6], 11 genes in *Oryza sativa* (*OsCKOs*) and 13 putative CKO sequences in maize (*ZmCKOs*) [7, 8, 9, 10]. The *ZmCKO1* gene is strongly expressed in kernels, moderately in roots and sporadically distributed in other tissues [7, 11, 12, 13]. Its overexpression in *Arabidopsis thaliana* [14] causes the cytokinin deficiency phenotype represented by an increased root system, reduced size of aerial parts and defects in seed development, as previously observed for the *AtCKO* overexpressers [6]. *ZmCKO2* is preferentially expressed in old leaves and mature tassels, *ZmCKO3* in old leaves and *ZmCKO4a* in immature tassels [7]. Whereas the majority of CKOs are secreted to apoplast, AtCKO1 and AtCKO3 are most likely targeted to vacuoles [6] and only one CKO protein per plant devoid of signal peptide (e.g. ZmCKO10, AtCKO7 and OsCKO11) is always retained in the cell cytosol.

So far, the crystal structures of two CKO proteins, ZmCKO1 and AtCKO7 [15, 16], show that the enzyme is composed of two domains: the cofactor binding domain (residues 40-244 and 492-534) and the substrate binding domain (residues 245-491). Substrates, as well as inhibitors, do not induce any conformational changes upon binding in the active site [15, 9, 17]. A funnel-shaped passage from the protein surface leads to the active site that consists of an internal substrate cavity situated above the isoalloxazine ring (the *si*-face) of the FAD cofactor covalently linked to H105 *via* an 8α-*N*(1)-histidyl bond. The adenine ring of the bound substrate is wedged between two hydrophobic residues P427 and V378 and its N9 atom provides polar interactions with the carboxylate of E381. The isoprenoid/aromatic chain of the substrate points towards the FAD in the internal cavity formed by D169, W397, L458, S456, L492 and N399. Both highly conserved D169 and E288 residues are thought to polarize the N10 substrate amino group enabling the transfer of a proton and two electrons (hydride ion, Figure 1) from the C11 atom of the neighboring cytokinin side-chain to the N5 atom of the FAD cofactor [15]. Cytokinin substrate is oxidized to imine intermediate [17, 18] and further hydrolyzed. The reduced $FADH_2$ is then re-oxidized by either oxygen (oxidase mode) or quinone-like compounds (dehydrogenase mode), which is a rate-limiting step of the catalytic reaction. In the oxidase mode, CKO catalyzes the production of one molecule of H_2O_2 per one molecule of the cytokinin substrate [19], but in the dehydrogenase mode it behaves as a quinone reductase. While 2,6-dichlorophenol indophenol (DCPIP), phenazine methosulphate (PMS), 2,3-dimethoxy-5-methyl-1,4-

benzoquinone (coenzyme Q_0), and related compounds are known to function as efficient exogenous electron acceptors [20, 21] (Figure 1), other compounds such as 2,4-dihydroxy-7-methoxy-1,4-benzoxazin-one (DIMBOA), coniferron and free radicals originating from their oxidation have recently been shown to function as natural electron acceptors in maize phloem [22]. However, known crystal structures of CKOs did not reveal any specific tunnel or cavity suitable for electron acceptor binding in proximity to the FAD cofactor.

We investigated the role in substrate binding of seven active site residues of ZmCKO1, three of which are strictly conserved among all known CKOs, by site-directed mutagenesis followed by kinetic study. From liganded X-ray structures of ZmCKO1 reported here, we characterized the binding mode of cytokinin ribosides. In addition, the structures of ZmCKO2 and ZmCKO4a helped us to further understand the substrate specificity differences among CKO isoforms. Finally, we also investigated the role of these residues in electron acceptor preferences.

Results and discussion

Production of ZmCKO1 point mutants

Ten point mutants of eight active site residues in ZmCKO1 (H105A, D169E, D169N, E288Q, V378L, E381S, E381A, W397A, P427Q and L492A; Figure 2A) were constructed to define their role in substrate binding and catalysis. All ZmCKO1 variants were produced in yeast *Y. lipolytica* under the control of the recombinant promoter hp4d in the pINA6703 vector and directed into the culture medium. The yield of the secreted mutant proteins was determined by Western blotting with polyclonal anti-ZmCKO1 rabbit antibody (not shown). Seven mutant clones yielded an amount of CKO1 protein (50-100%) similar to that of wild type (WT), which was sufficient for further purification. Although H105A and D169N were poorly produced, a sufficient amount of pure protein could be obtained by repetitive purification. In contrast, W397A was no further studied due to unsuccessful protein production. The WT and mutant proteins were characterized by determining the specific activity using eight natural substrates (cytokinin bases, ribosides and glucosides) and two different electron acceptors DCPIP and PMS, respectively (Table 1 and Table S1). The kinetic data with both acceptors correlate well. The WT prefers the cytokinin bases iP and *t*Z (K_m = 1 μM and 9 μM) to their respective ribosides iPR and *t*ZR (K_m = 12 μM and 42 μM) using DCPIP as an electron acceptor as previously reported [19]. Structural and/or kinetic analysis allowed us to suggest a role for each of these seven residues in catalysis and/or substrate binding as presented below.

The conserved D169 and E288 residues and the structure of D169E in complex with iP

An oxygen atom of D169 side chain interacts with the site of the enzymatic oxidative attack, which is the N10 atom in any cytokinin substrate (Figure 1), while the other oxygen makes a hydrogen bond with the carboxylate of E288. Replacement of D169 by an asparagine results in very low

activity, 100-fold lower than that of the WT, with similar K_m values indicating that this strictly conserved aspartate is essential for catalysis (Table 1). N169 is, in principle, unable to abstract a proton from the N10 atom of substrate. Interestingly, a residual WT ZmCKO1 activity has been measured using a substrate analogue *N*-methyl-iP although the proton abstraction cannot occur due to the presence of a methyl group on the N10 atom. A possible deprotonation of the C11 atom of the isoprenoid side chain (positioned 3.2 Å in front of the flavin N5 atom) with the $FADH^-$ acting itself as the proton-abstracting base has been suggested [18] and can explain the residual activity for the D169N variant.

Replacement of D169 by a glutamate leads to a 60% decrease of the specific activity compared with the WT, as well as an increase in K_m values for all substrates (Table 1). D169E shows a higher activity with iP than with any other tested substrate. The structure of D169E in complex with iP shows that the presence of the glutamate imposes a 0.4 Å shift of the substrate adenine moiety compared with the WT structure in complex with iP (PDB ID: 1W1Q) preserving its interaction with the substrate amino group (N10 atom) (Figure 2B). This new substrate position causes a steric hindrance to accommodate substrates substituted on the N9 of the adenine ring, such as ribosides whose turnover is slowed down. Strikingly, the substrate molecule is bent while it is almost planar in the WT structure. The kinetic and structural data demonstrate that E169 can substitute D169. However, its longer side chain impacts its K_m value and substrate specificity resulting in a lower turnover rate

The catalytic efficiency of E288Q variant does not differ much from that of WT. Therefore E288, located in the second sphere of substrate interaction, only slightly affects the specific activity, showing that no proton abstraction occurs between D169 and E288 during catalysis. Slightly higher K_m values (Table 1) indicate that E288 maintains D169 in a rigid position to align N10 and C11 atoms of the substrate for the putative proton abstraction and hydride transfer. Indeed, CKO (FasE) from the bacterial phytopathogen *Rhodococcus fascians*, which carries a glutamine at the position of E288 residue, was found fully functional [23].

P427 and V378 residues and the structures of P427Q in complex with iP

The two non-polar residues P427 and V378 sandwich the substrate adenine moiety. Introducing a larger side chain through V378L and P427Q variants results in lower activities and higher K_m values for all tested substrates (except iP), as compared to WT (Table 1). Intriguingly, P427Q displays an even higher specific activity for iP. The structure of P427Q with iP reveals that the whole substrate molecule is flipped by 180° around its longitudinal axis formed by the isoprenoid side chain compared to that in the WT structure (PDB ID: 1W1Q) [15] shown in Figure 2C. The C11 atom is shifted by 0.3 Å away from the flavin N5 atom making the interaction between the N10 atom and the catalytic residue D169 shorter. This altered conformation has been previously observed in the structure of WT ZmCKO1 complexed with *t*Z (PDB ID: 1W1R) [15], where *t*Z adopts both conformations. Our structural and kinetic data with P427Q variant prove that the altered conformation of the substrate

forms a productive binding. Q427 contributes to the adenine base binding by fixing the E381 side chain (Figure 2C) and both residues thus interfere with the binding of riboside moiety in line with high K_m values observed for iPR and *t*ZR (Table 1).

The non-conserved E381 residue and its role in iPR binding

The non-conserved E381 residue appears in half of known CKO sequences and is replaced by Ser, Gly, Val or Ala in the other half. The interaction of the E381 carboxylate with the N9 atom of the substrate contributes to substrate binding. When it is replaced, as for example in the E381A and E381S variants, the activity decreases to 58% and 65%, respectively. In contrast to the WT enzyme, both E381A/S variants display an activity for all tested substrates including cytokinin glucosides such as N^6-isopentenyladenine-9-glucoside (iP9G) and *trans*-zeatin-9-glucoside (*t*Z9G) (Figure 3A and 3B) and their K_m values for cytokinin ribosides iPR and *t*ZR are comparable to those for cytokinin bases (iP and *t*Z) (Table 1). Indeed, the presence of E381 in WT enzyme increases K_m values for cytokinin ribosides and very low activity is detected with cytokinin glucosides iP9G and *t*Z9G.

To understand the role of E381 in cytokinin riboside binding, we determined the crystal structures of WT and E381S in complex with iPR (Figure 3C, 3E). The isopentenyladenine moiety of the bound iPR superimposes the bound iP (Figure 3D). However, due to the presence of the ribose in iPR, the side chain of E381, which can no longer form a hydrogen bond with the free N9 atom of the adenine ring, moves away and thus liberates room for the ribose. It should be noted that the E381 side chain is not well defined in the electron density map and is thus highly mobile. However, we can infer an interaction between the ribose and the E381 side chain. The ribose 5-hydroxyl group interacts with the R253 side chain and both 3- and 5-OH groups are in close contact with the main chain carbonyl of N303 and T304 (between 3.4-3.8 Å). Replacement of E381 by a serine, well defined in the electron density map, leads to an additional interaction with the ribose moiety of iPR. For both E381 variants, k_{cat} values are comparable between iPR and iP9G and their K_m values are four times lower compared with WT (Table 1). However, higher K_m values for iP9G make iPR a better substrate. Replacement of E381 by small residues clearly enlarges the entrance of the active site and facilitates the binding of bulkier substrates including cytokinin ribosides and glucosides. Thus, when present, this glutamate residue confers specificity for the enzyme by restricting ligand binding. This is emphasized with the kinetic analysis of four ZmCKO isoforms possessing a serine or an alanine at the equivalent position of E381 (Table 2). Indeed, unlike WT-ZmCKO1, ZmCKO2 and 3 (corresponding to the E381S variant) and ZmCKO4a and 4b (corresponding to the E381A variant) oxidize a wide range of substrates like E381A/S mutant variants. They display K_m values for iP derivatives ($K_{m(iP)}$ ~ 2 µM, $K_{m(iPR)}$ ~ 7 µM, $K_{m(iP9G)}$ ~ 17 µM) similar to those measured with both E381 mutants and show even much higher activities with cytokinin glucosides compared with WT-ZmCKO1. However, all these four ZmCKOs differ from E381A/S mutant variants in their high activity with iP9G.

The non-conserved E381 residue - ZmCKO2 and ZmCKO4a structures

To explain the above differences in substrate specificity including high rates with iP9G, we solved the crystal structures of ZmCKO4a and ZmCKO2, in two different space groups for each (Table S2 and Figure 4). The structures of ZmCKO2 and ZmCKO4a are very similar to that of ZmCKO1 with RMSD values of 1.2 Å (428 Cα atoms) and 1.1 Å (423 Cα atoms) respectively. The major difference concerns the residues region 294-325, composed of two helices and a loop, belonging to the substrate binding domain. This region, which is well defined in ZmCKO1 structure, is disordered in the high resolution structures of ZmCKO4a and ZmCKO2 and adopts a different conformation in the low resolution structure of ZmCKO2 (Figure 4A). The region delineating the substrate entrance comprises residues surrounding the ribose moiety of cytokinin substrate (N303 and T304 in ZmCKO1) and is most likely responsible for the kinetic differences between E381 variants and ZmCKO isoforms. Despite several attempts, we unfortunately did not succeed in obtaining a crystal structure of ZmCKO2 and ZmCKO4a in complex with iP9G. All known intracellular CKOs contain valine or serine at E381 position and some of them have recently been shown to oxidize iP9G and *t*Z9G in agreement with our data [24, 25]. Thus, the substrate specificity of CKOs appears related to their subcellular localization and corresponds to the presumed occurrence of particular cytokinin derivatives within intracellular compartments.

All studied ZmCKOs also show higher activities with *c*Z derivatives when compared with ZmCKO1 (differences in the active site is shown in Figure 4B and 4C). The preference of ZmCKO1 for *t*Z over *c*Z can be explained by a H-bond between the hydroxyl group of *t*Z and S456 residue (PDB ID: 1W1R) [15], while ZmCKO2, 3, 4a and 4b possess an alanine or a glycine at the equivalent position and share comparable activities with both zeatin isomers. Finally, E381 also affects the binding of urea inhibitors, as *N*-(2-chloro-pyridin-4-yl)-*N*′-phenylurea (CPPU) is found in alternate conformation in ZmCKO4a structure with chlorine only in the outside orientation (Figure S1), compared to that observed in ZmCKO1 structure with chlorine preferentially in the inside orientation [9].

L492 residue

The highly conserved L492 which is located in the internal part of the substrate cavity over the isoalloxazine ring (the *si*-face of FAD) points towards the end of the substrate side chain. The L492A variant is the only variant in this study to positively affect the degradation of aromatic cytokinins, which were found in poplar [26], while the WT enzyme has been shown to cleave these derivatives at low turnover rates [21]. The activity of WT-ZmCKO1 with *ortho*-, *meta*- and *para*-hydroxybenzyladenine (topolin) derivatives is about 0.5% of that with iP. In contrast, L492A variant cleaves *ortho*- and *meta*-topolin at much higher rates (15 and 22% compared to iP, respectively) using DCPIP. A model of a bound *ortho*- and *meta*-topolin based on the structure of ZmCKO1 with a bound benzyladenine (PDB ID: 1W1S) [15] shows that L492 points towards the *ortho*- and *meta*- group.

Therefore, an alanine at the position of the leucine will create space for both substrates to better accommodate them in the active site.

L492A shows higher catalytic efficiency for *c*Z compared with *t*Z, making this mutant particular (Table 1). Together with the kinetic data measured for ZmCKO2, 3, 4a and 4b, our results show that structural modification of the internal cavity volume and composition targeting for example residues L492, S456 or N399 could be used for construction of CKO variants to modulate the specificity towards aromatic cytokinins and zeatin isomers. Such variants could then be used for designing plants overexpressing CKO variant aimed at studying these cytokinins.

H105 residue and covalent FAD linkage

Although covalent linkage of FAD in flavoproteins is rather rare, it facilitates redox catalysis and enhances the oxidative power of flavin. H105A mutation prevents the formation of a covalent 8α-*N*(1)-histidyl bond leading to the CKO variant with a free FAD cofactor. The activity of the variant in culture media is around 1.1 nkat ml^{-1} compared to 14 nkat ml^{-1} for WT in agreement with the lower production yield observed for this variant. After purification, the specific activity ranges between 0.5 - 12 nkat mg^{-1} among various preparations, i.e. it is 1000-50 times lower than the specific activity of purified WT. The specific activity of H105 mutant is corrected in line with the flavin content (see text below). About 70% of the total activity is lost during the purification indicating that the mutant is unstable and sensitive to a high ionic strength during the ion exchange chromatography. Thermostability measurement confirms the instability of the H105A protein with a T_{50} value of ~ 31°C (a temperature at which 50% of the activity is retained after 30 min incubation), which is 25 degrees lower than that for WT (Figure S2A).

The FAD spectral characteristics at lower wavelengths reflect the change in the FAD binding (Figure S2B). While the maximum absorption at 443 nm is similar to that for WT (445 nm), a typical bathochromic shift of the near-UV maximum from 350 nm to 390 nm is observed in line with the fact that the flavin is no more covalently attached [27]. Almost identical spectra were obtained for analogous mutants of vanillyl-alcohol oxidase [28]. The absorbance ratio between 280 and 445 nm for WT enzyme and above mutants is about 7.0. It ranges from 17 to 30 for the H105A variant, indicating a loss of the FAD cofactor. Although the substrate specificity of the H105A variant is similar to WT, saturation curves significantly differ resulting in slightly higher K_m values (Figure S2C, Table 1). Both k_{cat} and k_{cat}/K_m values are more than 100-fold lower.

Electron acceptor preferences and reaction mechanism

Oxygen is not the sole electron acceptor of flavoproteins and many of them evolved the ability to carry out redox reactions using different electron acceptors, such as the cytokinin oxidase/dehydrogenases. We analyzed preferences of active-site variants towards oxygen and four organic electron acceptors (Table 3 and Figure 5). The re-oxidation step of FAD with oxygen is very

slow and rate limiting [18]. Specific activity of WT, measured in the oxidase mode [29], is about 3 nkat mg^{-1}. This value corresponds to only 0.2% of the activity observed with DCPIP, i.e. the reaction with DCPIP is ~ 500 times faster than with oxygen. This is also valid for the majority of mutant proteins and the slight increase of relative oxidase activity appears for H105A, D169E and L492A variants. D169N variant is the most affected and the DCPIP reaction is only 13-fold higher than that with oxygen. While the specific activity with DCPIP is 100-fold lower than that of the WT, the activity with oxygen is only 3-fold lower (1 nkat mg^{-1}).

The best electron acceptor of the WT, using iP as a substrate, is the synthetic molecule PMS (k_{cat} = 590 s^{-1}, K_m = 62 μM), followed by DCPIP (k_{cat} = 158 s^{-1}, K_m = 129 μM), NQ (k_{cat} = 105 s^{-1}, K_m = 290 μM) and Q_0 (k_{cat} = 81 s^{-1}, K_m = 840 μM) (Figure 5A). PMS is the most robust electron acceptor. It provides the highest rates and catalytic efficiencies for all variants (Table 3) but in all cases an inhibition effect is observed with an excess of PMS. Electron acceptor preferences and the shape of saturation curves of both E288Q and D169N variants were very similar to the WT (not shown). Accordingly, the K_m values of E288Q were similar and values of D169N were even lower than those for the WT. E381S and E381A variants exhibit higher relative rates and catalytic efficiencies with both quinones Q_0 and NQ compared with WT. Interestingly, activities with all four studied electron acceptors became almost equal at higher concentrations (Figure 5B). In contrast, P427Q mutant shows even higher rates with PMS and DCPIP than the WT itself but almost no activity with both quinones, which display high K_m values (1.2 mM for NQ and 2.2 mM for Q_0). These results further show that the presence/absence of non-conserved residues E381 and P427 at the entrance of the active site significantly affects both substrate and electron acceptor specificities. Therefore, the nature of these two residues may play a crucial role in functional differences between naturally occurring CKO isoforms. H105A variant also prefers PMS (k_{cat} = 1.8 s^{-1}, K_m = 16 μM) but does not differentiate between the three other acceptors (k_{cat} ~ 0.9 s^{-1}, K_m ~ 30-60 μM) (Figure S2D). The k_{cat}/K_m values are more than 100 times lower than those of WT pointing out the importance of the covalent 8α-*N*(1)-histidyl bond of FAD for the CKO activity.

Previous X-ray analyses revealed that upon binding, substrates seal the tunnel that leads to the catalytic site, leaving no space for electron acceptor entry except for the oxygen [15] and discourage previously proposed mechanism involving the formation of a ternary complex based on the measurements of enzyme kinetics with Q_0 [21]. When the ping-pong (double displacement) mechanism is considered, any electron acceptor might access the $FADH_2$ through the substrate tunnel after the imine intermediate release. Although we co-crystallized or soaked crystals with an electron acceptor, no electron density was observed for it. The kinetics of both D169E and L492A variants (Figure 6C and 6D) suggest that some electron acceptors might access the enzyme active site. Their saturation curves significantly differ from that of WT and other variants. Although the D169E variant has higher K_m values towards cytokinin substrates, K_m values for electron acceptors are lower (K_m ~ 56 μM for DCPIP, 330 μM for Q_0, 172 μM for NQ). The L492A variant also displays slightly lower K_m

values especially for NQ (K_m ~ 48 μM), which based on k_{cat}/K_m ratio becomes as efficient as DCPIP. Both mutations similarly lead to high activity (three times higher at 1 mM concentration) with the smallest electron acceptor - coenzyme Q_0.

We investigated the type of mechanism [30] used for the two synthetic electron acceptors (DCPIP and PMS) that we used for the study of cytokinin substrates binding (Table 1 and Table S1). Initial rates were plotted as a function of concentrations of cytokinin and electron acceptor (Figure S3). Data clearly show that the DCPIP-catalyzed reaction follows a double displacement (ping-pong mechanism), while that with PMS follows a single displacement meaning that PMS forms a ternary complex with the enzyme and the cytokinin substrate. Differing mechanisms may explain high versatility of PMS for various mutants. Although the catalytic mechanism and binding mode of DCPIP and PMS seem different, the activity comparison between the WT and mutants is relevant because use of both electron acceptors lead to similar kinetic parameters for the same cytokinin substrates. Above data show that active-site residues are linked to both substrate and electron acceptor preferences in CKOs.

Material and methods

Site-directed mutagenesis, screening and purification of CKO proteins

Recombinant ZmCKO1 was produced in *Yarrowia lipolytica* using the shuttle vector pINA6703 (9199 bp) [19]. However, the site-directed mutagenesis was carried out using a smaller 4766 bp-long vector pBS6703 (the pBluescript KS^- vector carrying *ZmCKO1* sequence) [11] with QuickChange II kit (Stratagene). The XL-10 Gold ultra-competent *E. coli* cells were transformed with the mutated gene constructs. The D169N mutant was obtained using phosphorylated primers with the mutation at the 5'end of one of them (tail-to-tail oriented, Table S3). The resulting pBS6703 clones were then sequenced. Finally, the *ZmCKO1* gene was cloned into the *Sfi*I-*Kpn*I digested-pINA1267 vector to obtain a mutated pINA6703 vector (mpINA6703). The plasmid mpINA6703 was linearized by *Spe*I to direct its integration into the pBR322 docking platform of the recipient *Y. lipolytica* Po1g strain (Leu^-, ΔAEP, ΔAXP, Suc^+, pBR322) [31,32]. Yeasts were transformed by the lithium acetate method [33] and Leu^+ transformants were selected on a minimal YNB medium. At least five *Y. lipolytica* transformants of each mutant line were screened for CKO activity in the supernatant of 5-day-old cultures in PPB medium (20 g l^{-1} sucrose, 1.32 g l^{-1} yeast extract, 1.32 g l^{-1} NH_4Cl, 0.32 g l^{-1} KH_2PO_4, 0.13 g l^{-1} $MgSO_4$ and 0.33 mg l^{-1} thiamine in 50 mM phosphate buffer, pH 6.8). The activity was tested in both the oxidase and dehydrogenase mode. Screening for protein production was performed by NuPAGE (Invitrogen). The proteins were then transferred to PVDF membrane (Millipore, USA) by semidry blotting. The membrane was incubated with polyclonal rabbit anti-ZmCKO1, treated with the goat anti-rabbit IgG alkaline phosphatase conjugate (Bio-Rad, USA) and stained with NBT/BCIP

(Roche Molecular Biochemicals, Germany). The WT-ZmCKO1 and mutant variants were purified as described previously [19].

Genes of *ZmCKO2*, *3*, *4a* and *4b* were cloned into pTYB12 vector under the *Nde*I and *EcoR*I restriction sites, expressed in *E. coli* BL21 STAR (DE3) cells for 16 hours at 18 °C. Proteins were purified by affinity chromatography on a column filled with a chitin resin. Enzymes were eluted using 50 mM Tris-HCl, pH 8.0, after intein tag removal by 50 mM DTT. The enzymes were further dialyzed, concentrated and purified by ion-exchange chromatography on HighQ column using a linear gradient of 0-1 M KCl. Pure fractions were subsequently pooled and concentrated by ultrafiltration [10].

.

Activity and protein assay

Cytokinin substrates were obtained from OlChemIm (Olomouc, Czech Republic); tritium-labeled substrates were from the Institute of Experimental Botany, Czech Academy of Sciences (Prague, Czech Republic). CKO activity in the oxidase mode was measured by the HPLC method that is based on the conversion of tritiated cytokinin substrate [29]. Activity of ZmCKO1 in the dehydrogenase mode was measured either by DCPIP or PMS/MTT initial rate assay at 30 °C [34, 20], or by 4-aminophenol end-point assay using DCPIP, Q_0, PMS or 1,4-naphthoquinone (NQ) dissolved in water as electron acceptors at 37°C [20]. Kinetic parameters were obtained after non-linear regression fitting of the Michaelis–Menten equation using GraphPad Prism 5 (GraphPad Software Inc., La Jolla, USA). The protein content was measured using the bicinchoninic acid method with BSA as a standard [35] and verified spectrophotometrically at 280 nm and 445 nm (ε_{280} = 82 mM^{-1} cm^{-1} and ε_{445} = 12 mM^{-1} cm^{-1}) [19].

Crystallization, structure solution and refinement of ZmCKO1, ZmCKO2 and ZmCKO4

Crystallization of WT-ZmCKO1 and mutants was made in PEG 1500 condition as described [36]. Crystals were soaked with 5-20 mM iP or iPR (dissolved in DMSO) for a few minutes before being transferred into a cryoprotectant solution (the reservoir solution supplemented with 20% (w/v) glycerol) and flash frozen in liquid nitrogen. Crystals of ZmCKO2 were grown in 100 mM sodium citrate pH 5.6, 20% 2-propanol and 20% PEG 4000. ZmCKO4a in the presence of 3 mM CPPU crystallized in either 22% ethylene-glycol or 100 mM HEPES pH 7.5 and 50% MPD. Diffraction data for ZmCKO1 crystals were collected at 100 K on BM30A-FIP, ID14-1 and ID14-2 beamlines at the European Synchrotron Radiation Facility (ESRF, Grenoble, France). Those for ZmCKO2 and ZmCKO4 were collected at 100 K on the PROXIMA 1 beamline at the SOLEIL synchrotron (Saint-Aubin, France). Diffraction intensities were integrated with the program XDS [37]. All structures were solved by molecular replacement with MOLREP [38] using the coordinates of ZmCKO1 structure (PDB ID: 1W1O) [15]. The four crystal structures of ZmCKO1: the WT-iPR complex (2.10 Å),

D169E-iP complex (2.00 Å), P427Q-iP complex (1.90 Å) and E381S-iPR (1.75 Å), the two different space group structures of ZmCKO2 (2.04 and 2.7 Å) and the two different space group structures of ZmCKO4 with CPPU (1.75 and 1.9 Å) were refined using BUSTER-TNT with autoncs and TLS options [39]. Electron density maps were evaluated using COOT [40]. Data collection and refinement statistics are given in Table S2. Data quality of ZmCKO2 and ZmCKO4a datasets was assessed using the correlation coefficient $CC_{1/2}$ [41]. Molecular graphics images were generated using PYMOL.

Accession numbers

The atomic coordinates and structure factors have been deposited in the Protein Data Bank (www.rcsb.org) under the accession codes 3S1C for WT-iPR, 3S1E for P427Q-iP, 3S1F for D169E-iP and 3S1D for E381S-iPR, 4ML8 and 4MLA for ZmCKO2 and 4O95 and 4OAL for ZmCKO4-CPPU complex.

Acknowledgements

This work was supported by grant 15-22322S from the Czech Science Foundation, grant LO1204 from the National Program of Sustainability I by the Ministry of Education, Youth and Sports, Czech Republic and partly supported by the CNRS for SM and AV, and by INRA for PB. We acknowledge SOLEIL for provision of synchrotron radiation facilities in using Proxima I beamline (proposal ID 20130869). We would like to acknowledge Nicole Houba-Hérin (INRA, Versailles) for her initial contribution to this project, the staff on BM30A-FIP, ID14-1 and ID14-2 beamlines (ESRF, Grenoble) and Roselyne Tâche (INRA-AgroparisTech, Versailles) for help in crystallization, and Catherine Madzak (INRA- AgroParisTech, Grignon, France) for yeast transformation.

Tables

Table 1. Effect of ZmCKO1 mutations on substrate specificity. Measurements were performed in triplicate in two independent runs with DCPIP as an electron acceptor in 100 mM phosphate buffer, pH 7.0 at 30 °C [34]. "–" stands for not determined.

ZmCKO1 variant	K_m **(µM)**						k_{cat}/K_m **(M^{-1} s^{-1})**					
	iP	iPR	iP9G	*t*Z	*t*ZR	*c*Z	iP	iPR	iP9G	*t*Z	*t*ZR	*c*Z
WT	1	12	151	9	42	47	4.2×10^7	2.9×10^6	6.8×10^3	6.0×10^6	3.1×10^5	4.6×10^5
H105A	13	19	–	22	53	–	6.9×10^4	1.4×10^4	–	2.4×10^4	2.5×10^3	–
D169N	2	13	–	8	39	–	2.0×10^5	2.6×10^4	–	6.0×10^4	1.6×10^3	–
D169E	24	74	–	144	310	–	9.2×10^5	4.7×10^4	–	5.3×10^4	5.3×10^3	–
E288Q	3	38	–	15	124	–	9.7×10^6	7.4×10^5	–	2.0×10^6	1.0×10^5	–
V378L	13	68	–	64	240	–	3.1×10^6	1.3×10^5	–	1.7×10^5	1.8×10^4	–
E381A	5	6	41	22	10	65	5.0×10^6	1.3×10^6	2.7×10^5	7.5×10^5	2.9×10^5	1.2×10^5
E381S	2	3	24	15	9	52	1.4×10^7	2.7×10^6	4.0×10^5	1.3×10^6	5.5×10^5	1.2×10^5
P427Q	5	97	–	23	280	–	1.2×10^7	3.3×10^5	–	2.0×10^6	8.9×10^4	–
L492A	7	50	–	65	78	31	3.0×10^6	1.3×10^5	–	1.7×10^5	2.8×10^4	2.5×10^5

Table 2. Relative activities of four maize CKOs with natural substrates. Relative activities were obtained with 30 μM substrates and DCPIP as an electron acceptor in 100 mM phosphate buffer, pH 7.0 [34].

	Relative activity to iP (%)							
	iP	iPR	iP9G	*t*Z	*t*ZR	*t*Z9G	*c*Z	*c*ZR
ZmCKO1	100	67	0.6	107	18	0.3	25	4
ZmCKO2	100	10	132	69	18	14	77	33
ZmCKO3	100	11	170	91	10	15	84	43
ZmCKO4a	100	8	166	61	14	4	88	9
ZmCKO4b	100	9	175	51	12	4	95	11

Table 3. Relative activities of ZmCKO1 mutants with different electron acceptors and iP as a substrate. Oxidase reaction was measured by HPLC method with [^{3}H]-iP in 20 mM Tris-HCl, pH 7.4 [29]. Dehydrogenase reaction was measured with 0.5 mM DCPIP, PMS, Q_0 and NQ by aminophenol method [20] using 150 μM iP in 75mM Tris-HCl, pH 8.0 (for DCPIP and PMS) or 75 mM imidazole-HCl, pH 6.5 (for Q_0 and NQ). First column shows specific activities (nkat mg^{-1}) measured with 0.5 mM DCPIP. Measurements were performed in triplicate in four independent runs.

ZmCKO1 variant	**Activity with DCPIP**	**DCPIP/O_2 ratio**	k_{cat}/K_m (relative to DCPIP)			
	(nmol s^{-1} mg^{-1})		DCPIP	PMS	Q_0	NQ
WT	1853	500	100	779	8	30
H105A	10	143	100	681	123	135
D169N	14	15	100	537	34	84
D169E	614	53	100	384	28	55
E288Q	1613	500	100	569	8	22
E381A	1501	500	100	337	19	73
E381S	1395	500	100	786	23	57
V378L	1408	500	100	370	20	53
P427Q	2399	500	100	686	2	4
L492A	825	77	100	808	29	96

REFERENCES

1. Mok, D. W. S. & Mok, M. C. (2001). Cytokinin metabolism and action. Annu. Rev. Plant Physiol. Plant Mol. Biol. 52, 89–118.

2. Schmülling, T., Werner, T., Riefler, M., Krupkova, E. & Bartrina y Manns, I. (2003). Structure and function of cytokinin oxidase/dehydrogenase genes of maize, rice, Arabidopsis and other species. J. Plant Res. 116, 241–252.

3. Fraaije, M.W., Benen, J.A.E., Visser, J., van Berkel, W.J.H. & Mattevi, A. (1998). A novel oxidoreductase family sharing a conserved FAD-binding domain. Trends Biochem. Sci. 23, 206-207.

4. Brownlee, B.G., Hall, R.H. & Whitty, C.D. (1975). 3-Methyl-2-butenal: an enzymatic degradation product of the cytokinin, N-6-(delta-2 isopentenyl) adenine. Can. J. Biochem. 53, 37-41.

5. Armstrong, D.J. (1994). Cytokinin oxidase and regulation of cytokinin degradation. In Cytokinins: Chemistry, Activity and Function (Mok, D.W.S. & Mok, M.C., eds.), pp. 139-154, CRC Press, Boca Raton.

6. Werner, T., Motyka, V., Laucou, V., Smets, R., Van Onckelen, H. & Schmulling, T. (2003). Cytokinin-deficient transgenic *Arabidopsis* plants show multiple developmental alterations indicating opposite functions of cytokinins in the regulation of shoot and root meristem activity. Plant Cell 15, 2532-2550.

7. Massonneau, A., Houba-Hérin N., Pethe, C., Madzak, C., Falque, M., Mercy, M., Kopečný, D., Majira, A., Rogowsky, P. & Laloue M. (2004). Maize cytokinin oxidase genes: differential expression and cloning of two new cDNAs. J. Exp. Bot. 55, 2549-2557.

8. Vyroubalová, S., Václavíková, K., Turečková, V., Novák, O., Šmehilová, M., Hluska, T., Ohnoutková, L., Frébort, I. & Galuszka, P. (2009). Characterization of new maize genes putatively involved in cytokinin metabolism and their expression during osmotic stress in relation to cytokinin levels. Plant Physiol. 151, 433-447.

9. Kopečný D, Briozzo P, Popelková H, Šebela M, Končitíková R, Spíchal L, Nisler J, Madzak C, Frébort I, Laloue M & Houba-Hérin N. (2010). Phenyl- and benzylurea cytokinins as competitive inhibitors of cytokinin oxidase/dehydrogenase: a structural study. Biochimie 92, 1052-1062.

10. Zalabák D, Galuszka P, Mrízová K, Podlešáková K, Gu R & Frébortová J. (2014). Biochemical characterization of the maize cytokinin dehydrogenase family and cytokinin profiling in developing maize plantlets in relation to the expression of cytokinin dehydrogenase genes. Plant Physiol. Biochem. 74, 283-293.

11. Houba-Hérin, N., Pethe, C., d'Alayer, J. & Laloue, M (1999). Cytokinin oxidase from *Zea mays*: purification, cDNA cloning and expression in moss protoplasts. Plant J. 17, 615–626.

12. Morris, R.O., Bilyeu, K.D., Laskey, J.G. & Cheikh, N.N. (1999). Isolation of a gene encoding a glycosylated cytokinin oxidase from maize. Biochem. Biophys. Res. Commun. 255, 328-333.

13. Brugière, N., Jiao, S., Hantke, S., Zinselmeier, Ch., Roessler, J.A., Niu, X., Jones, R.J., & Habben, J.E. (2003). Cytokinin oxidase gene expression in maize is localized to the vasculature, and is induced by cytokinins, abscisic acid, and abiotic stress. Plant Physiol. 132, 1228-1240.

14. Kopečný, D., Tarkowski, P., Majira, A., Bouchez-Mahiout, I., Nogué, F., Laurière, M., Sandberg, G., Laloue, M. & Houba-Hérin, N. (2006). Probing cytokinin homeostasis in *Arabidopsis thaliana* by constitutively overexpressing two forms of the maize cytokinin oxidase/dehydrogenase 1 gene. Plant Sci. 171, 114-122.

15. Malito, E., Coda, A., Bilyeu, K.D., Fraaije, M.W. & Mattevi A. (2004). Structures of Michaelis and product complexes of plant cytokinin dehydrogenase: implications for flavoenzyme catalysis. J. Mol. Biol. 341, 1237-1249.

16. Bae E., Bingman C.A., Bitto E., Aceti D.J. & Phillips G.N. (2008). Crystal structure of Arabidopsis thaliana cytokinin dehydrogenase. Proteins 7, 303-306.

17. Kopečný, D., Šebela, M., Briozzo, P., Spíchal, L., Houba-Hérin, N., Mašek, V., Joly, N., Madzak, C., Anzenbacher, P. & Laloue, M. (2008). Mechanism-based inhibitors of cytokinin oxidase/dehydrogenase attack FAD cofactor. J. Mol. Biol. 380, 886-899.

18. Popelková, H., Fraaije, M.W., Novák, O., Frébortová, J., Bilyeu, K.D. & Frébort, I. (2006). Kinetic and chemical analyses of the cytokinin dehydrogenase-catalysed reaction: correlations with the crystal structure. Biochem. J. 398, 113-124.

19. Kopečný, D., Pethe, C., Šebela, M., Houba-Hérin, N., Madzak, C., Majira, A. & Laloue, M. (2005). High-level expression and characterization of *Zea mays* cytokinin oxidase/dehydrogenase in *Yarrowia lipolytica*. Biochimie 87, 1011-1022.

20. Frébort, I., Šebela, M., Galuszka, P., Werner, T., Schmülling, T. & Peč P. (2002). Cytokinin oxidase/cytokinin dehydrogenase assay: optimized procedures and applications. Anal. Biochem. 306, 1-7.

21. Frébortová, J., Fraaije, M.W., Galuszka, P., Šebela, M., Peč, P., Hrbáč, J., Novák, O., Bilyeu, K.D., English, J.T. & Frébort, I. (2004). Catalytic reaction of cytokinin dehydrogenase: preference for quinones as electron acceptors. Biochem. J. 380, 121-130.

22. Frébortová, J., Novák, O., Frébort, I., Jorda, R. (2010). Degradation of cytokinins by maize cytokinin dehydrogenase is mediated by free radicals generated by enzymatic oxidation of natural benzoxazinones. Plant J. 61, 467-481.

23. Pertry, I., Václavíková, K., Gemrotová, M., Spíchal, L., Galuszka, P., Depuydt, S., Temmerman, W., Stes, E., De Keyser, A., Riefler, M., Biondi, S., Novák O., Schmülling, T., Strnad, M., Tarkowski, P., Holsters M., Vereecke D. (2010). *Rhodococcus fascians* impacts plant development through the dynamic fas-mediated production of a cytokinin mix. Mol. Plant Microbe Interact. 23, 1164-1174.

24. Šmehilová, M., Galuszka, P., Bilyeu, K.D., Jaworek, P., Kowalska, M., Šebela, M., Sedlářová, M., English, J.T. & Frébort, I. (2009). Subcellular localization and biochemical comparison of cytosolic and secreted cytokinin dehydrogenase enzymes from maize. J. Exp. Bot. 60, 2701-2712.

25. Kowalska M., Galuszka P., Frébortová J., Šebela M., Béres T., Hluska T., Šmehilová M., Bilyeu K.D. & Frébort I. (2010). Vacuolar and cytosolic cytokinin dehydrogenases of *Arabidopsis thaliana*: heterologous expression, purification and properties. Phytochemistry 71, 1970-1978.

26. Strnad, M. (1997). The aromatic cytokinins. Physiol. Plantarum 101, 674-688.

27. Kenney, W.C., Edmondson, D.E. & Seng, R.L. (1976). Identification of the covalently bound flavin of thiamin dehydrogenase. J. Biol. Chem. 251, 5386–5390.

28. Fraaije, M.W., van den Heuvel, R.H., van Berkel, W.J. **&** Mattevi, A. (1999). Covalent flavinylation is essential for efficient redox catalysis in vanillyl-alcohol oxidase. J Biol. Chem. 274, 35514-35520.

29. Laloue, M. & Fox, J.E. (1989). Cytokinin oxidase from wheat. Partial purification and general properties. Plant Physiol. 90, 899–906.

30. Segel, I. H. (1993). In Enzyme Kinetics: Behavior and analysis of rapid equilibrium and steady-state enzyme systems, pp. 320–329, J. Wiley and Sons, New York.

31. Madzak, C., Tréton, B. & Blanchin-Roland, S. (2000). Strong hybrid promoters and integrative expression/ secretion vectors for quasi-constitutive expression of heterologous proteins in the yeast *Yarrowia lipolytica*. J. Mol. Microbiol. Biotechnol. 2, 207-216.

32. Madzak, C., Gaillardin, C. & Beckerich J.-M. (2004). Heterologous protein expression and secretion in the non-conventional yeast *Yarrowia lipolytica*. J. Biotechnol. 109, 63–81.

33. Xuan, J.W., Fournier, P. & Gaillardin, C. (1988). Cloning of the LYS5 gene encoding saccharopine dehydrogenase from the yeast *Yarrowia lipolytica* by target integration. Curr. Genet. 14, 15–21.

34. Bilyeu, K.D., Cole, J.L., Laskey, J.G., Riekhof, W.R., Esparza, T.J., Kramer, M.D. & Morris, R.O. (2001). Molecular and biochemical characterization of a cytokinin oxidase from maize. Plant Physiol. 125, 378-386.

35. Smith, P.K., Krohn, R.I., Hermanson, G.T., Mallia, A.K., Gartner, F.H., Provenzano, M.D., Fujimoto, E.K., Goeke, N.M., Olson, B.J. & Klenk D.C. (1985). Measurement of protein using bicinchoninic acid. Anal. Biochem. 150, 76-85.

36. Kopečný, D., Briozzo, P., Joly, N., Houba-Hérin, N., Madzak, C., Pethe, C. & Laloue, M. (2004). Purification, crystallization and preliminary X-ray diffraction study of a recombinant cytokinin oxidase from *Zea mays*. Acta Crystallogr. Sect. D-Biol. Crystallogr. 60, 1500-1501.

37. Kabsch,W. (1993). Automatic processing of rotation diffraction data from crystals of initially unknown symmetry and cell constants. J. Appl. Crystallogr. 26, 795–800.

38. Vagin, A. & Teplyakov, A. (1997). MOLREP: an automated program for molecular replacement. J. Appl. Crystallogr. 30, 1022–1025.

39. Blanc, E., Roversi, P., Vonrhein, C., Flensburg, C., Lea, S.M. & Bricogne, G. (2004). Refinement of severely incomplete structures with maximum likelihood in BUSTER-TNT. Acta Crystallogr. Sect.D-Biol.Crystallogr. 60, 2210-2221.

40. Emsley, P. & Cowtan, K. (2004). Coot: model-building tools for molecular graphics. Acta Crystallogr. Sect.D-Biol.Crystallogr. 60, 2126-2132.

41. Karplus, P.A. & Diederichs, K. (2012). Linking crystallographic model and data quality. Science 336, 1030–1033.

FIGURE LEGENDS

Figure 1. Scheme of the CKO reaction mechanism with zeatin as a substrate. During the reductive half reaction, zeatin is oxidized to an imine intermediate. D169 (ZmCKO1 numbering) polarizes the secondary amino group of the substrate and facilitates the transfer of a proton and two electrons from the substrate to N5 atom of the FAD cofactor. E381 forms a hydrogen bond with the N9 atom of the substrate. The resulting imine undergoes hydrolysis to the corresponding aldehyde and adenine. Reduced FAD cofactor is re-oxidized either by oxygen with a subsequent release of H_2O_2 (oxidase mode) or by some other electron acceptor such as Q_0, DCPIP or PMS (dehydrogenase mode).

Figure 2. Active site of ZmCKO1. (A) Close-up view of ZmCKO1 active site with a bound substrate iP and residues studied by side-directed mutagenesis. The reactive part of the isoprenoid side chain of iP (in black) is sealed in the internal cavity over the FAD cofactor (in yellow). Its amino group is hydrogen bonded with D169 and the adenine N9 atom with E381. **(B) Interaction between active-site D169E mutant and bound substrate iP.** Side-chain residues are in light brown and labeled, iP substrate is in dark brown in its Fo-Fc omit map contoured at 2.5 σ. Mutation E169 is labeled in red. Superposed WT ZmCKO1 structure with iP (PDB ID: 1W1Q) [15] is shown in grey. **(C) Binding of iP substrate in the P427Q structure.** Side-chain residues are in light pink and labeled, iP is in magenta in its Fo-Fc omit map contoured at 2.5 σ. Mutation Q427 is labeled in red. Superposed WT structure with iP is shown in grey.

Figure 3. Binding of cytokinin ribosides. (A, B) Substrate specificity of WT-ZmCKO1and E381A variant. Data were measured with DCPIP as an electron acceptor (29) in 0.1 M potassium phosphate buffer, pH 7.0 at 30 °C. **(C) WT structure with bound iPR**. iPR (in brown) is shown in its Fo-Fc omit map contoured at 2.5 σ. Side-chain residues are in grey and labeled. FAD cofactor is shown in yellow and hydrogen bonds as dashed lines **(D) Superposition of bound cytokinin base iP (PDB ID: 1W1Q) [15] and cytokinin riboside iPR (PDB ID: 3S1C, this work) over the FAD cofactor.** E381 in both structures is indicated by the respective color corresponding to the color of cytokinin substrate.

(E) iPR binding in the active site of E381S. iPR molecule is shown in orange color and in the Fo-Fc omit map contoured at 2.5 σ.

Figure 4. Structural comparison between ZmCKO1 (in black), ZmCKO2 (in magenta) and ZmCKO4a (in sand yellow). (A) Superposition of their substrate binding domains. The helix-loop-helix region from residues 294 to 325 in ZmCKO1 (shown with red arrows) adopts a different conformation in ZmCKO2 and is disordered in ZmCKO4. **(B) Comparison of residues located at the active-site entrance. (C) Comparison of residues located in the internal cavity over the FAD cofactor**. H-bonds with substrate molecule *t*Z shown in green (PDB ID: 1W1R) [15] are indicated. Unconserved residues between ZmCKOs are labeled using the structure color. ZmCKO1 numbering is in black.

Figure 5. Saturation curves of WT and three ZmCKO1 mutants with four electron acceptors. Measured by aminophenol method using 150 μM iP (20) in 75 mM Tris-HCl, pH 8.0 (DCPIP and PMS) and in 75 mM imidazole-HCl, pH 6.5 (Q_0 and NQ) at 37 °C. For PMS and NQ, samples were measured at each concentration against the blank containing the electron acceptor at respective concentration.

Figure 1.

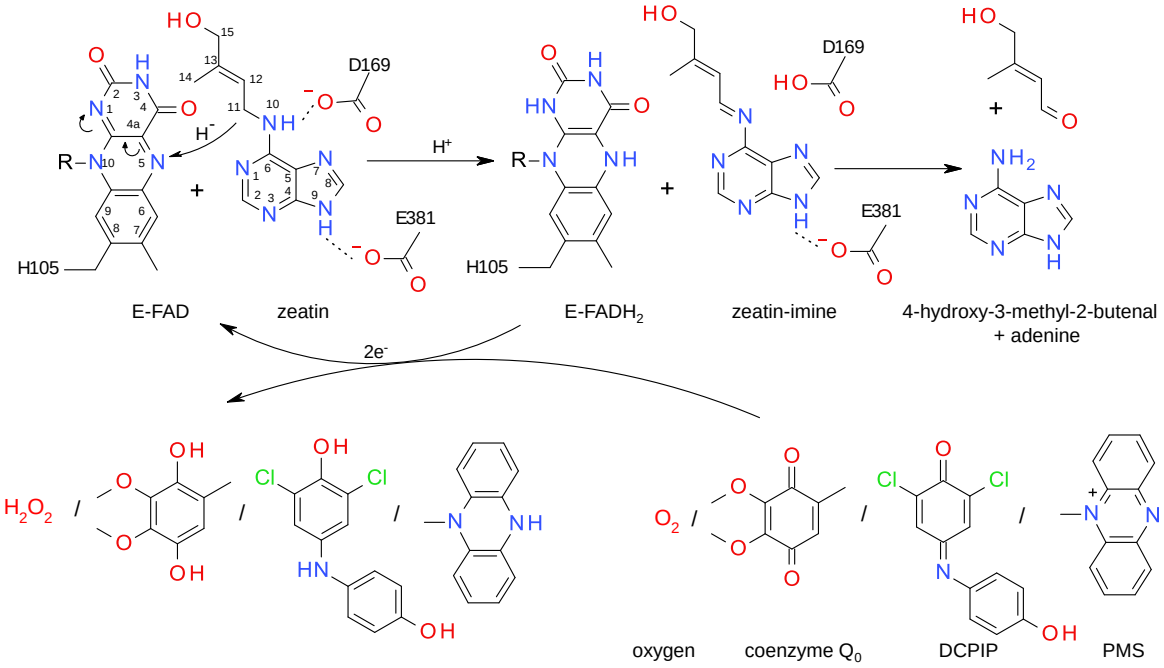
D169
E381
H105
H+
H-
2e-
E-FAD
zeatin
E-FADH2
zeatin-imine
4-hydroxy-3-methyl-2-butenal
+ adenine
H2O2
O2
oxygen
coenzyme Q0
DCPIP
PMS

Figure 2.

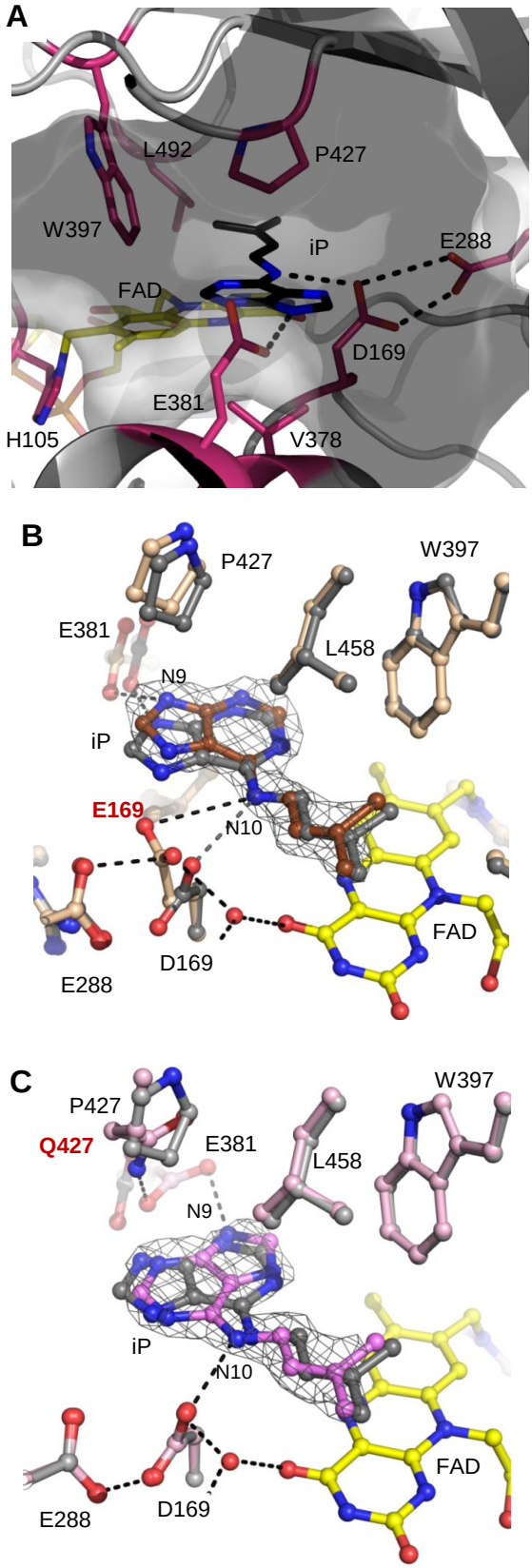
A
L492
P427
W397
iP
E288
FAD
D169
E381
H105
V378
B
P427
W397
E381
L458
N9
iP
E169
N10
FAD
D169
E288
C
P427
W397
Q427
E381
L458
N9
iP
N10
FAD
E288
D169

Figure 3.

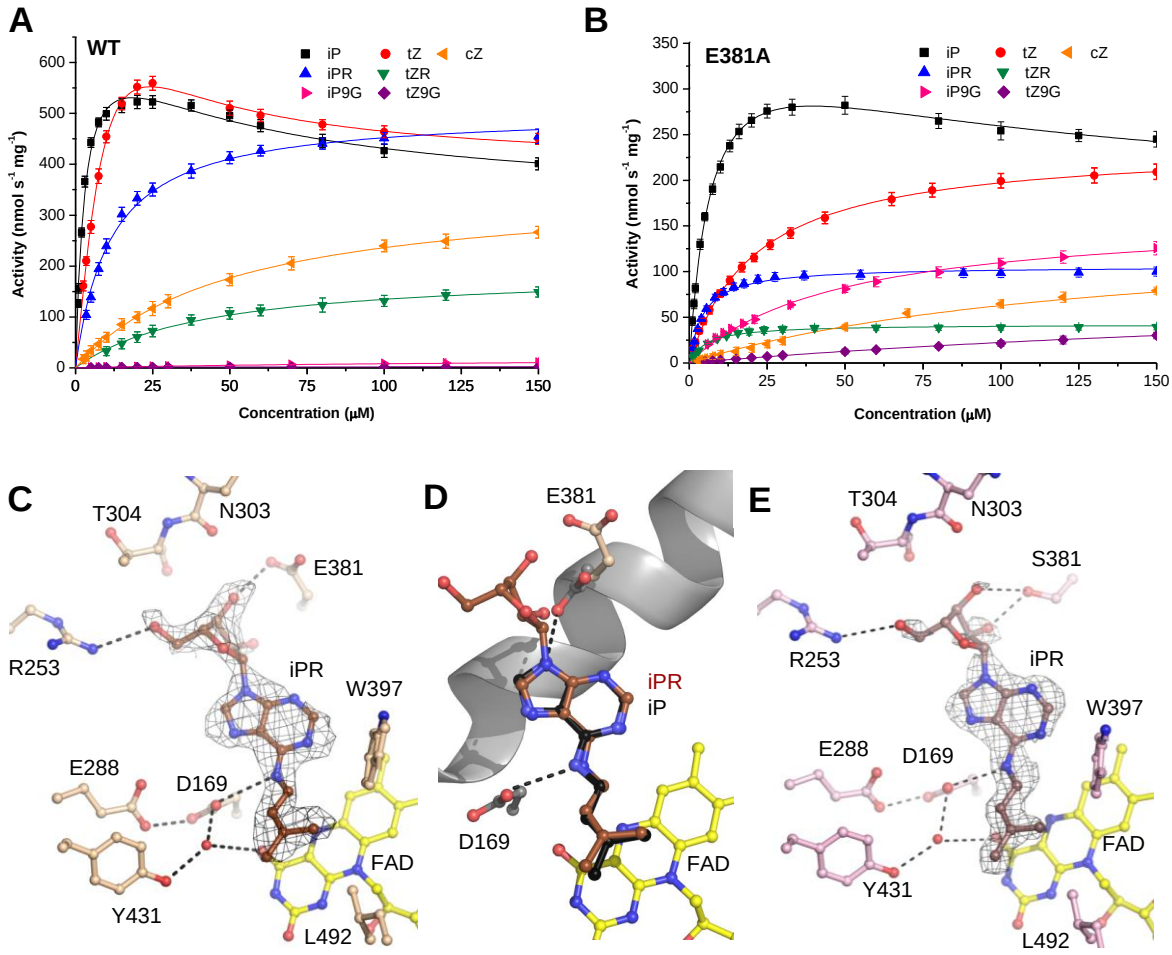
A
WT
iP
tZ
cZ
iPR
tZR
iP9G
tZ9G
Activity (nmol s-1 mg-1)
Concentration (μM)
B
E381A
C
T304
N303
E381
R253
iPR
W397
E288
D169
FAD
Y431
L492
D
E381
iPR
iP
D169
FAD
E
T304
N303
S381
R253
iPR
W397
E288
D169
FAD
Y431
L492

Figure 4.

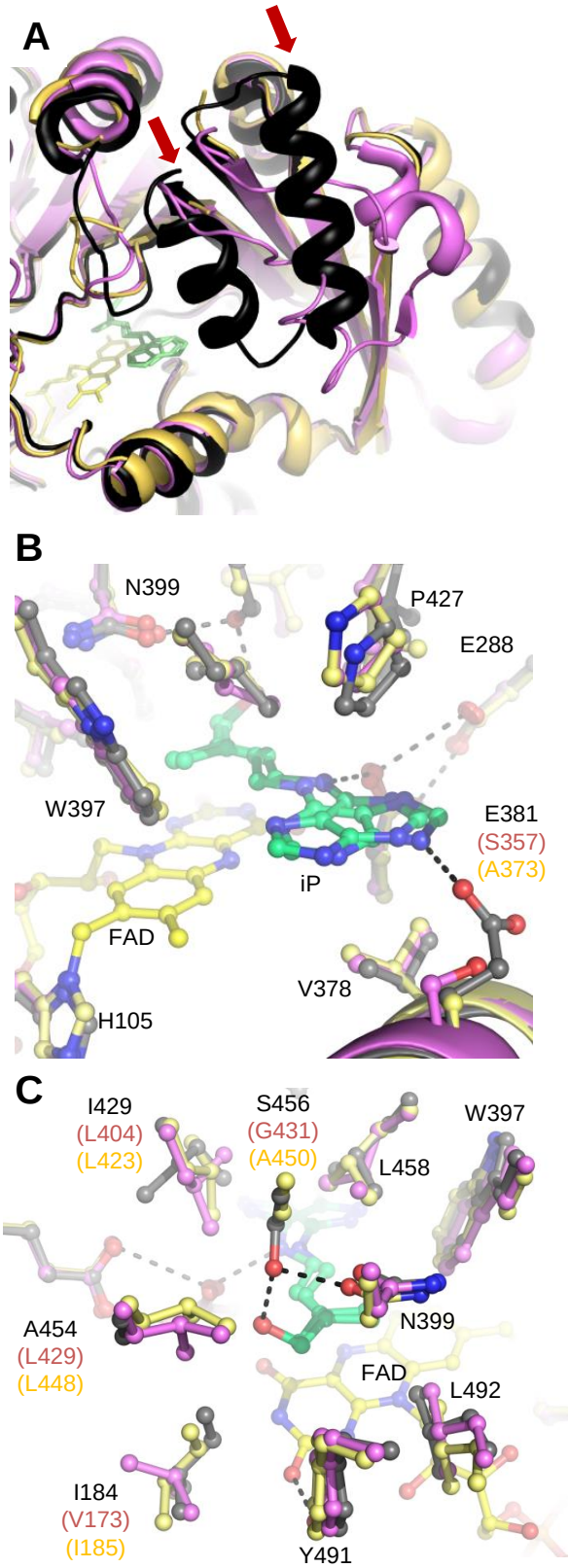
A
B
N399
P427
E288
W397
E381
(S357)
(A373)
iP
FAD
V378
H105
C
I429
(L404)
(L423)
S456
(G431)
(A450)
W397
L458
A454
(L429)
(L448)
N399
FAD
L492
I184
(V173)
(I185)
Y491

Figure 5.

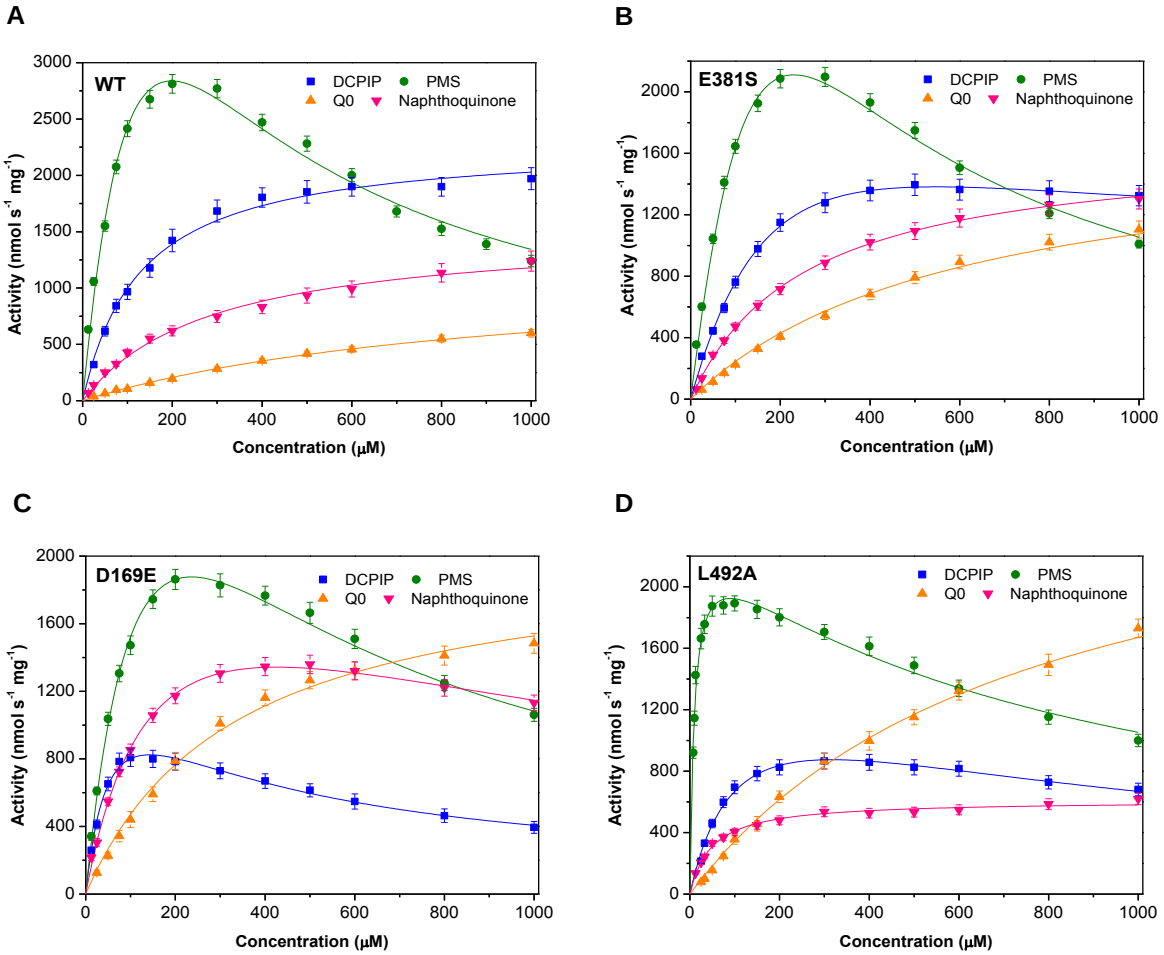
A
WT
DCPIP
PMS
Q0
Naphthoquinone
Activity (nmol s-1 mg-1)
Concentration (μM)
B
E381S
C
D169E
D
L492A

Table S1. Kinetic data for constructed mutant variants with six natural cytokinins and PMS as an electron acceptor. Measurements were performed in triplicate in two independent runs with 150 μM PMS as an electron acceptor by PMS/MTT method in 20 mM Tris-HCl, pH 8.0 at 30 °C [20]. "-" stands for not measured.

ZmCKO1 variant	K_m (μM)						k_{cat}/K_m (M^{-1} s^{-1})					
	iP	iPR	iP9G	*t*Z	*t*ZR	*c*Z	iP	iPR	iP9G	*t*Z	*t*ZR	*c*Z
WT	3	12	185	13	29	35	2.7×10^7	3.3×10^6	3.8×10^4	5.4×10^6	3.5×10^5	3.9×10^5
H105A	9	18	–	14	33	–	3.6×10^3	5.9×10^2	–	1.2×10^3	9.1×10^1	–
D169N	2	10	–	13	29	–	3.3×10^5	3.2×10^4	–	4.9×10^4	3.2×10^3	–
D169E	25	98	–	176	243	–	8.4×10^5	4.6×10^4	–	4.4×10^4	1.1×10^4	–
E288Q	7	55	–	33	140	–	1.4×10^7	7.1×10^5	–	1.5×10^6	9.8×10^4	–
V378L	16	112	–	142	190	–	5.3×10^6	1.2×10^5	–	1.1×10^5	1.4×10^4	–
E381A	7	4	20	14	7	22	4.5×10^6	1.3×10^6	2.8×10^5	1.2×10^6	3.5×10^5	6.9×10^4
E381S	5	5	21	18	7	25	7.9×10^6	1.8×10^6	3.1×10^5	1.4×10^6	4.3×10^5	1.2×10^5
P427Q	16	174	–	58	233	-	1.6×10^7	2.2×10^5	–	1.0×10^6	5.6×10^4	–
L492A	8	59	–	69	97	21	9.7×10^6	2.8×10^5	–	4.2×10^5	6.6×10^4	9.9×10^5

Table S2. Data collection and refinement statistics.

Data set Ligand	**WT-ZmCKO1** iPR	**D169E** iP	**P427Q** iP	**E381S** iPR	**ZmCKO2** none	**ZmCKO2** none	**ZmCKO4a** CPPU	**ZmCKO4a** CPPU
PDB ID	3S1C	3S1E	3S1F	3S1D	4MLA	4ML8	4O95	4OAL
Space group	C2	C2	C2	C2	$C222_1$	C2	$P4_32_12$	$C222_1$
Asymmetric unit	monomer	monomer	monomer	monomer	2 monomers	4 monomers	monomer	2 monomers
Unit cell (Å,°)								
a	251.0	250.2	250.1	252.3	75.7	183.2	74.5	112.7
b	50.6	50.7	50.1	50.5	181.9	76.7	74.5	112.6
c	51.4	51.2	51.2	51.5	197.0	201.0	208.3	203.0
α = γ	90.0	90.0	90.0	90.0	90.0	90.0	90.0	90.0
β	94.0	94.0	93.5	93.9	90.0	92.1	90.0	90.0
Resolution (Å)	32.5-2.10	32.4-2.00	48.3-1.90	41.7-1.75	23.6-2.04	38.4-2.70	42.7-1.75	1.90
Observed reflections	140563	168996	205494	225570	633807	264843	435663	758743
Unique reflections	35133	43223	48499	64971	85777	76884	58646	101537
Completeness (%)	91.1 (97.5)	99.0 (98.3)	96.5 (95.7)	99.3 (97.8)	99.2 (95.1)	99.6 (98.9)	97.5 (98.9)	99.7 (98.6)
I/σ(I)	16.9 (4.7)	15.6 (3.2)	15.7 (4.2)	16.0 (3.2)	14.0 (1.6)	9.8 (1.6)	13.1 (1.3)	11.4 (1.4)
R_{sym} (%)	5.8 (33.7)	6.3 (39.1)	6.0 (36.3)	5.1 (43.2)	8.6 (113.3)	11.1 (75.5)	7.1 (101.4)	13.0 (131.0)
$CC_{1/2}$	-	-	-	-	99.9 (79.7)	99.5 (65.0)	99.9 (84.3)	99.8 (59.8)
R_{cryst} (%)	21.3	17.8	19.8	21.5	18.2	18.1	18.7	20.7
R_{free} (%)	25.2	21.8	23.1	24.7	20.4	20.6	20.7	21.8
RMSD bond lengths (Å)	0.01	0.01	0.01	0.01	0.01	0.01	0.01	0.01
RMSD bond angles (°)	1.08	1.03	1.05	1.02	1.07	1.10	1.00	1.00
Mean B value ($Å^2$) protein	29.2	28.2	33.1	30.0	46.4	56.9	50.9	38.4
Mean B value ($Å^2$) ligand	38.4	29.4	33.6	42.5	-	-	37.3	29.7

Values in parenthesis are those for the last shell. $CC_{1/2}$ stands for a percentage of correlation between intensities from random half-dataset [41].

Table S3. Overview of the oligos used for site-directed mutagenesis of ZmCKO1.

Mutant variant	Primer pair
H105A	5’- GCCGCGGC**GCC**TCCCTCATGG-3’
	5’- CCATGAGGGA**GGC**GCCGCGGC-3’
D169E	5'-CGCTCCTGGACC**GAA**TACCTCTACCTCAC-3'
	5'-P-GTGAGGTAGAGGTA**TTC**GGTCCAGGAGCG-3'
D169N	5'-P-ACTACCTCTACCTCACCGTCGGCGG-3'
	5'-P-**T**GGTCCAGGAGCGCGGCGC-3'
E288Q	5'-CGATGAGCTACGTG**CAA**GGGTCGGTGTTC-3'
	5'-GAACACCGACCC**TTG**CACGTAGCTCATCG-3'
V378L	5'-TTCCTTGACCGG**TTG**CACGGCGAGGAG-3'
	5'-CTCCTCGCCGTG**CAA**CCGGTCAAGGAA-3'
E381A	5’-GTGCACGGC**GCG**GAGGTGGCG-3’
	5’-CGCCACCTC**CGC**GCCGTGCAC-3’
E381S	5’-GGTGCACGGC**TCG**GAGGTGGCG-3’
	5’-CGCCACCTC**CGA**GCCGTGCACC-3’
W397A	5'-GCCGCACCCG**GCG**CTCAACATGTTC-3'
	5'-GAACATGTTGAG**CGC**CGGGTGCGGC-3'
P427Q	5'-CGACATCGTCGGC**CAG**CTCATCGTCTACC-3'
	5'-GGTAGACGATGAG**CTG**GCCGACGATGTCG-3'
L492A	5'-AGTACAAGACCTAC**GCG**GCGCGGCACACG-3'
	5'-CGTGTGCCGCGC**CGC**GTAGGTCTTGTACT-3'

Figure S1. Superposition of CPPU in the active site of ZmCKO4a (yellow, this work) and ZmCKO1 (grey colored, PDB ID: 2QKN). Both urea nitrogens of CPPU molecule establish H-bonds to catalytic aspartate (D169 in ZmCKO1, D170 in ZmCKO4a).

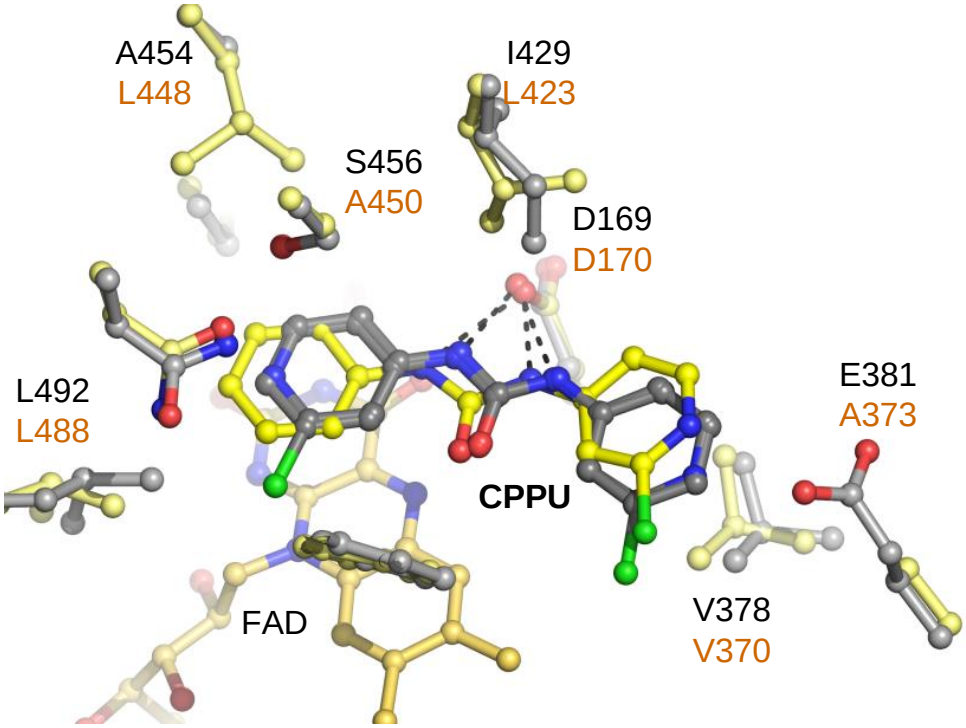

Figure S2. Properties of H105A variant. (A) Effect of the covalent 8α-*N*(1)-histidyl bond to FAD cofactor on the thermostability of the enzyme. **(B)** UV-Vis spectra of the free FAD and the FAD bound in the WT and the H105A variant. **(C)** Substrate specificity of H105A mutant. Measured with DCPIP as an electron acceptor (29) in 0.1 M potassium phosphate buffer, pH 7.0 at 30 °C. **(D)** Saturation curves of H105A with four electron acceptors, measured by aminophenol method using 150 μM iP (20) in 75 mM Tris-HCl, pH 8.0 (DCPIP and PMS) and in 75 mM imidazole-HCl, pH 6.5 (Q_0 and NQ). For PMS and NQ, samples were measured at each concentration against the blank containing the electron acceptor at respective concentration.

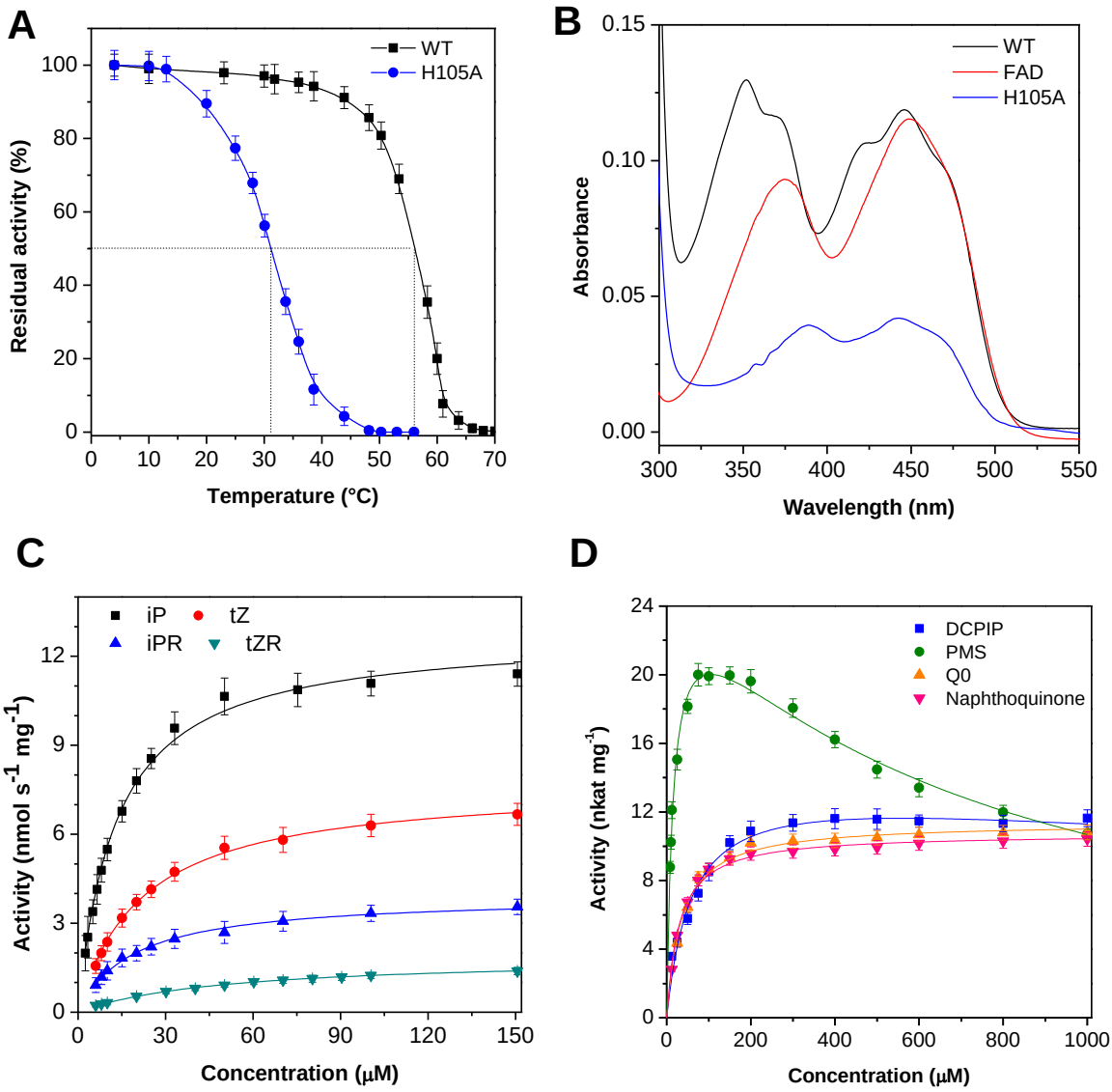

Figure S3. Double-reciprocal plots of ZmCKO1 activity with DCPIP and PMS and varying substrate concentration. Measurements were performed in triplicate in two independent runs with DCPIP and PMS as electron acceptors (29, 20).

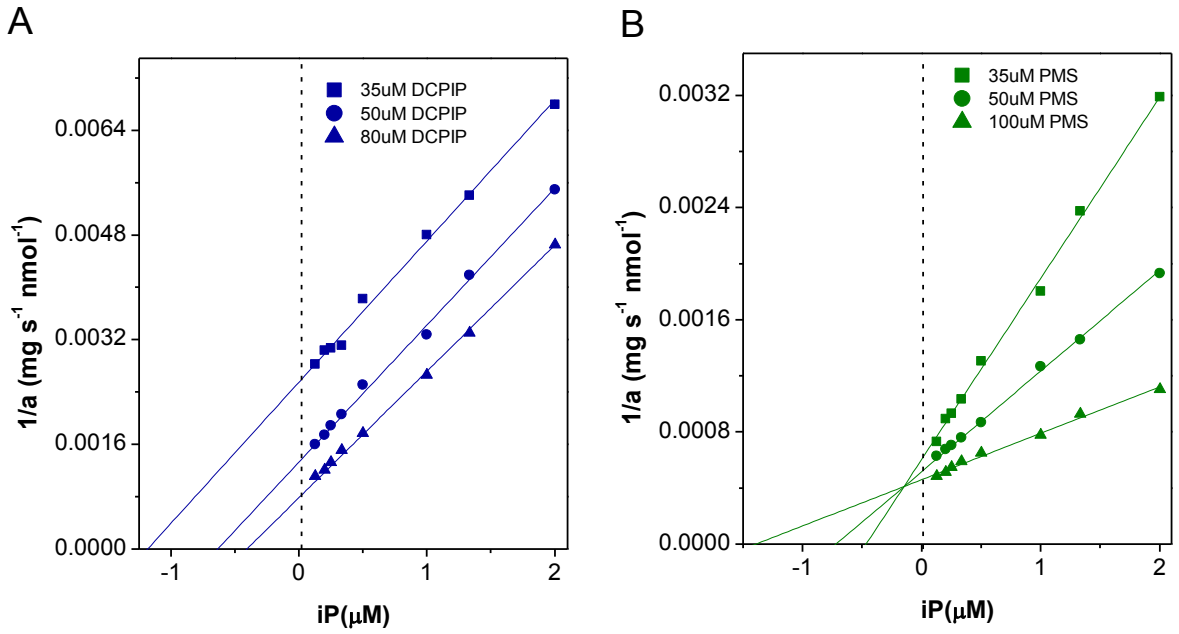

Article 3

Novel thidiazuron-derived inhibitors of cytokinin oxidase/dehydrogenase

Nisler J, Končitíková R, Zatloukal M, Kopečný D, Bazgie V, Berka K, , Zalabák D, Briozzo P, Strnad M, Spíchal L.

Manuscript

Novel thidiazuron-derived inhibitors of cytokinin oxidase/dehydrogenase

Jaroslav Nisler[1,*], Radka Končitíková[2], Marek Zatloukal[1], David Kopečný[2,*], Václav Bazgier[3,4], Karel Berka[4,5], David Zalabák[6], Pierre Briozzo[7], Miroslav Strnad[1], Lukáš Spíchal[1]

1) Laboratory of Growth Regulators, Institute of Experimental Botany, AS CR & Palacký University, Šlechtitelů 11, Olomouc 783 71, Czech Republic
2) Department of Protein Biochemistry and Proteomics, Centre of the Region Haná for Biotechnological and Agricultural Research, Faculty of Science, Palacký University, Šlechtitelů 11, CZ-783 71 Olomouc, Czech Republic
3) Centre of the Region Haná for Biotechnological and Agricultural Research, Department of Chemical Biology and Genetics, Faculty of Science, Palacký University, Šlechtitelů 11, Olomouc, CZ-78371, Czech Republic
4) Department of Physical Chemistry, Faculty of Science, Palacký University, 17. listopadu 1192/12, 771 46 Olomouc, Czech Republic
5) Regional Centre of Advanced Technologies and Materials, Faculty of Science, Palacký University, 17. listopadu 1192/12, 771 46 Olomouc, Czech Republic
6) Department of Molecular Biology, Centre of the Region Haná for Biotechnological and Agricultural Research
7) Institut Jean-Pierre Bourgin, UMR1318 INRA-AgroParisTech, Route de St-Cyr, F-78026 Versailles, France

Running head: Urea inhibitors of cytokinin oxidase/dehydrogenase

*Corresponding authors: jaroslav.nisler@gmail.com, david.kopecny@upol.cz; Tel.: +420 241062485 /+420 585634840 (D.K), Fax: +420 585634870 (J.N.)/+420 585634933 (D.K.)

Keywords

Cytokinin oxidase/dehydrogenase, crystal structure, molecular docking, organic synthesis, thidiazuron

Abbreviations

1-[1,2,3]thiadiazol-5-yl-3-(3-trifluoromethoxy-phenyl)urea, 3FMTDZ; 1-[2-(2-hydroxyethyl)phenyl]-3-(1,2,3-thiadiazol-5-yl)urea, HETDZ; 6-benzyladenine, BA; Arabidopsis response regulator 5, ARR5; N^6-(2-isopentenyl)adenine, iP; thidiazuron, TDZ; trans-zeatin, *t*Z, 1-phenyl-3-(2-chloro-pyridin-4-yl)urea, CPPU

Abstract

Cytokinins are plant hormones regulating wide range of essential processes in plants. Thidiazuron (*N*-phenyl-*N´*-1,2,3-thiadiazol-5-ylurea, TDZ), formerly registered as a cotton defoliant, is well known inhibitor of cytokinin oxidase/dehydrogenase (abbreviated as CKO or CKX) catalyzing the degradation of cytokinins. TDZ thus increases lifetime of cytokinins and their effects in plants. We have used *in silico* modelling to design, synthesize and characterize twenty new TDZ derivatives with improved inhibitory properties. Inhibitory strength of these compounds was analyzed using recombinant CKX2 from *Arabidopsis thaliana* (AtCKX2) and CKX1 and CKX4a from *Zea mays* (ZmCKX1 and ZmCKX4a). Two promising derivatives, namely 1-[1,2,3]thiadiazol-5-yl-3-(3-trifluoromethoxy-phenyl)urea (3FMTDZ) and 1-[2-(2-hydroxyethyl)phenyl]-3-(1,2,3-thiadiazol-5-yl)urea (HETDZ) were found and their IC_{50} values were at least by one fold lower compared with TDZ. Therefore, binding modes of 3FMTDZ and HETDZ were analyzed by X-ray crystallography. Crystal structure complexes, solved at 2.0 Å resolution, reveal that binding of HETDZ and 3FMTDZ in the active site of ZmCKX4a is different. The thiadiazolyl ring of 3FMTDZ is positioned over the isoalloxazine ring of FAD while that of HETDZ is in opposite orientation and points to entrance of the active site. The compounds were further tested for cytokinin activity in three classical cytokinin bioassays (wheat leaf senescence, tobacco callus and amaranth bioassays) as well as in *Arabidopsis ARR5::GUS* (*Arabidopsis* response regulator 5) reporter gene assay. None of derivatives possesses higher cytokinin activity than TDZ indicating their suitability for *in vivo* studies.

Introduction

Cytokinins are plant hormones which influence a wide range of essential processes in plants including cell division, shoot and root development, seed and fruit development, germination and senescence (Mok and Mok, 2001). They are adenine/adenosine derivatives with distinct N^6 side-chain. Nowadays, the use of plant growth regulators with cytokinin-like activity is a common practice in agricultural and horticultural fields and many efforts are devoted to the development of new compounds with improved cytokinin-like properties.

Thidiazuron (TDZ) is one of the most widely used synthetic compounds in agriculture with strong cytokinin effect, which is a combination of two characteristics. At first, the cytokinin activity of TDZ is comparable with that of *trans*-zeatin (*tZ*, Spíchal *et al*., 2004), which is a naturally occurring cytokinin with the highest cytokinin activity in most of higher plants. At second, TDZ inhibits cytokinin oxidase/dehydrogenase (CKO or CKX, EC 1.5.99.12). CKX catalyzes irreversible oxidative breakdown of Δ^2-isoprenoid cytokinins to form adenine/adenosine and the corresponding unsaturated aldehyde (Whitty and Hall, 1974, Brownlee *et al*., 1975, Chatfield and Armstrong, 1986). Therefore, TDZ increases levels of endogenous cytokinins in plants. Model plant *Arabidopsis thaliana* contains seven CKX isoforms, which are involved in the regulation of endogenous cytokinin levels (Werner *et*

al., 2003) and AtCKX2 is the most active and well-studied isoform (Galuszka *et al*., 2007). Model plant *Zea mays* contains 13 CKX isoforms and ZmCKX1 is the best studied CKX so far (Houba-Hérin *et al*., 1999, Morris *et al*., 1999, Massonneau *et al*., 2004, Frébortová *et al*. 2004, Zalabák *et al*. 2014). ZmCKX1 and AtCKX2 were expressed in yeast *Yarrowia lipolytica* and *Saccharomyces cerevisiae* (Kopečný *et al*., 2005, Frébortová *et al*., 2007) allowing for production of large amounts of recombinant CKX.

Up to date, several groups of compounds have been described to inhibit CKX. They include urea compounds TDZ and 1-phenyl-3-(2-chloro-pyridin-4-yl)urea (CPPU) and their derivatives (Laloue and Fox, 1989, Burch and Horgan, 1989, Hare and van Staden, 1994, Kopečný *et al*., 2010). Suicide substrates N^6-(buta-2,3-dienyl)adenine and N^6-(penta-2,3-dienyl)adenine were shown as strong CKX inhibitors with significant cytokinin activity (Suttle and Mornet, 2005, Kopečný *et al*., 2008). Anilinopurines can be stronger inhibitors than TDZ (Zatloukal *et al*., 2008). Synthesis of dienyl adenines as well as of anilinopurines is however more complicated. New urea derivatives, which would have increased CKX inhibitory strength and cover more CKO isoforms, have a potential in agriculture, horticulture and biotechnology.

To benefit from synthetic simplicity of TDZ, we used *in-silico* drug design to find new potent TDZ derivatives. Molecular docking technique was used to exploit the binding possibilities of new ligands in the active site of CKX. Designed derivatives were synthesized by condensation of 1,2,3-thiadiazol-5-isocyanate with corresponding amines and characterized using standard physical-chemical methods. Using molecular modelling approach, a model of AtCKX2 was constructed from the crystal structure of ZmCKX1 (PDB ID: 2QKN, Kopečný *et al*, 2010). Binding properties of TDZ derivatives obtained *in silico* were at first compared to IC_{50} values determined *in vitro* using AtCKX2. Subset of these derivatives was further screened using ZmCKX1 and ZmCKX4a. The latter significantly differs in substrate specificity compared with ZmCKX1 and AtCKX2. While iPRMP and iP9G are preferred substrates by ZmCKX4a (Zalabák *et al*., 2014), cytokinin bases and ribosides are preferred by ZmCKX1 (Frébortová *et al*. 2004, Kopečný *et al*., 2005) and AtCKX2 (Frébortová *et al*., 2007). New TDZ derivatives were also screened for cytokinin activity in three classical cytokinin bioassays - wheat leaf senescence, tobacco callus and Amaranthus bioassay (Holub *et al*., 1998). Finally, transgenic *Arabidopsis* plants harboring the *ARR5::GUS* reporter gene (D'Agostino *et al*. 2000) we used to gain complete information about the cytokinin activity of studied compounds in *Arabidopsis*. The *ARR5* is primary response gene with cytokinin-dependent promoter whose activation integrates the responses of several putative cytokinin signaling pathways and do not distinguish between the contribution of individual cytokinin receptors.

Results and discussion

Active sites in ZmCKX1 and AtCKX2

Active site of ZmCKX1 is composed of two pockets connected with a narrow tunnel surrounded by Asp169. The crystal structure in complex with CPPU (PDB ID: 2QKN, Kopečný *et al*., 2010) shows that Asp169 makes hydrogen bonds to both urea nitrogen atoms of CPPU. Smaller pocket is occupied by the isoalloxazine ring of FAD. Larger pocket is exposed to solvent and is guarded by Glu381. CPPU was found in two orientations either with phenyl ring or 2-chloropyridin-4-yl ring in direct π-stacking interaction with the isoalloxazine ring.

A homology model of AtCKX2, which was prepared based on ZmCKX1 structure, shares similar shape of the active site. Amino acids in the active site of AtCKX2 and ZmCKX1 are almost identical and include Asp150/Asp169, Leu461/Leu492, Tyr460/Tyr491, Asn366/Asn399, Trp358/Trp391, Glu348/Glu381 and Val345/Val378. A small difference represents Leu397 to Ile429 exchange. To verify the ligand binding, CPPU and TDZ were docked into the active site of ZmCKX1 and AtCKX2 with AutoDock Vina. The results were nearly mutually identical and matched. CPPU was found in two orientations with binding energies of -6.6 kcal mol^{-1} and -8.2 kcal mol^{-1}. The latter corresponds to preferred binding with phenyl ring in π-stacking interaction with the isoalloxazine ring. In case of TDZ, it is the thiadiazolyl ring, which is located over the isoalloxazine ring.

Design and chemistry of TDZ derivatives

Molecular docking to active site of AtCKX2 was performed side by side to the preparation of new N,N´-bis substituted urea derivatives possessing 1,2,3-thiadiazolyl ring TDZ derivatives. Twenty most promising compounds were selected and synthesized (Table 1 and Figure 1) based on obtained ligand conformations, their binding energies (Table 2) and availability of phenyl- and benzyl- amines for the synthesis. Commercially available 1,2,3-thiadiazol-5-ylamine was the starting compound for the synthesis of the intermediate 5-isocyanato-1,2,3-thiadiazole, which was prepared using diphosgene (Kurita *et al*., 1976). Although, many TDZ derivatives have been synthesized in past (DE 2214632 A1 19731004; DE 2506690 A1 19760902, Mok *et al*., 1982; Abad *et al*., 2004), so far the use of 5-isocyanato-1,2,3-thiadiazole has not yet been reported. Final compounds were prepared by mild heating of this isocyanate and the corresponding amine in the presence of catalytic amount of triethylamine in THF (Goldschmidt and Bardach, 1892). The compounds were characterized by HPLC, TLC, ES(+/-)-MS and ^{1}H NMR (Supplementary data).

Inhibition of AtCKX2 and correlation with molecular docking

TDZ derivatives were all docked in AtCKX2 model with the apparent preferred orientation of 1,2,3-thiadiazolyl ring towards the isoalloxazine ring and larger phenyl or benzyl rings pointing towards the entrance. Both urea nitrogen atoms bind to Asp150. The phenyl ring interacts with Glu348 at the entrance whereas the benzyl ring is too large to be accommodated easily in line with binding

energies, which were better for phenyl derivatives (ΔG from - 8.1 to - 9.3 kcal mol^{-1}) than those for benzyl derivatives (ΔG from - 6.3 to - 8.2 kcal mol^{-1}). These data correlate well with measured IC_{50} values and the comparison of binding energies obtained by docking and by *in vitro* testing with AtCKX2 is presented in Table 2.

The ability of the prepared derivatives to inhibit the activity of AtCKX2 was compared with that of TDZ (Figure 2). IC_{50} values (concentration at which the enzyme activity is inhibited by 50%) were determined using iP as a substrate (Table 2). The IC_{50} value of 62 μM was determined for TDZ. Similar IC_{50} values were determined for compounds 2 and 4, which are *ortho*- and *meta*- hydroxylated TDZ derivatives. No significant change was also observed for compounds **1** (*ortho*-methoxy), **7** (*ortho*-methyl, *meta*-hydroxy) and **11** (*meta*-trifluoromethyl). Lower IC_{50} values were observed for compounds **8** (IC_{50} = 18 μM) and **3** (IC_{50} = 22 μM) bearing *ortho*-methylhydroxy and *meta*-methoxy substituents, respectively. Compounds with IC_{50} values below 10 μM were compounds **5** (IC_{50} = 7.6 μM), **10** (3FMTDZ, IC_{50} = 5.5 μM) and **9** (HETDZ, IC_{50} = 3.9 μM) bearing 2,5-dimethoxy-, *meta*-trifluoro-methoxy- and *ortho*-ethylhydroxy groups. Compounds bearing dichloro-phenyl ring or substituted benzyl ring were less active or inactive. 3FMTDZ corresponds to the one of the two compounds with the best binding energy found by docking (ΔG = -9.3 kcal mol^{-1}) while the other one, compound **12**, was not effective at all. It is more hydrophobic due to the presence of chlorine atoms and it is very likely that lower solubility or non-specific binding can negatively affect its properties.

Inhibition of ZmCKX1 and ZmCKX4a

Based on results with AtCKX2, selected TDZ derivatives were further tested using ZmCKX1 and ZmCKX4a. Compounds 1-12 displayed similar properties towards ZmCKX1 as it has similar active site composition with AtCKX2. HETDZ and 3FMTDZ were the strongest inhibitors with IC_{50} value of 2.8 and 4.8 μM, respectively. On contrary, only compounds 7, 8, HETDZ and 3FMTDZ inhibited ZmCKX4a better than TDZ itself. The IC_{50} value for TDZ was slightly higher than 200 μM while that for compounds 7, 8 and HETDZ was 117, 91 and 120 μM, respectively. The best inhibitor was 3FMTDZ with IC_{50} value of 35 μM (Table 2 and Figure 2).

Although earlier work presented TDZ as a non-competitive inhibitor (Hare and Van Staden, 1994) more recent studies show that it is competitive inhibitor of CKX towards the substrate with 2,6-dichlorophenol indophenol (DCPIP) as an electron acceptor (Bilyeu *et al*., 2001; Kopečný *et al*., 2010). We have used method based on the coupled redox reaction of PMS and MTT (Frébort I. *et al*., 2002). Using this method TDZ and the two strongest inhibitors HETDZ and 3FMTDZ inhibit AtCKX2 as well as ZmCKX4a in a competitive manner (Figure 3). With AtCKX2, K_i values for HETDZ and 3FMTDZ were 1.25 and 1.8 μM, respectively while that for TDZ one fold higher (K_i = 21 μM). With ZmCKX4a, K_i values for TDZ and 3FMTDZ were 7.2 μM and 3.6 μM, respectively.

Crystal structures of ZmCKX4a in complex with HETDZ and 3FMTDZ

Two crystal structures of ZmCKX4a in complex with two urea inhibitors 3FMTDZ and (HETDZ) were solved at 2.0 Å resolution. A summary of the refinement results together with model statistics is given in Table 3. Crystal structure complexes reveal that HETDZ and 3FMTDZ occupy the same place in the active site as cytokinin substrates. Surprisingly, HETDZ and 3FMTDZ bind in opposite orientations (Figure 4). Their urea nitrogen atoms are at a distance from 2.7 Å to 3.1 Å from the side chain oxygen atom of D170 allowing hydrogen bond interactions. The urea's carbonyl oxygen is 3.3 Å far from the N5 atom of the cofactor isoalloxazine. The thiadiazolyl ring of 3FMTDZ is positioned over the flavin ring and one of its two nitrogen atoms can establish a hydrogen bond to N391 directly (3.3 Å distance) or via a water molecule. One of the urea nitrogens creates an H-bond to a water molecule, which is further bound to the side-chain oxygen atom of D170, O4 atom of isoalloxazine, hydroxyl group of Y425 and main-chain oxygen of I185. The 3-trifluoromethoxy group is oriented towards the hydrophobic pocket composed of side chains of W389, W383, F57, L377 and H387. In contrast, in case of HETDZ it is the 2-(2-hydroxyethyl)phenyl ring, which is positioned over the flavin ring. The oxygen atom of the hydroxyethyl side chain replaces a water molecule, observed in ZmCKX4a-3FMTDZ structure, and makes an H-bond to side-chain oxygen atom of D170 and hydroxyl group of Y425. The thiadiazolyl ring of HETDZ points to entrance of the active site.

Activity in classical cytokinin bioassays

Three classical cytokinin bioassays including tobacco callus assay, amaranth assay and wheat senescence assay were used to investigate cytokinin activity of new compounds using 6-benzylaminopurine (BAP) and TDZ for control (Table 4). TDZ is very potent cytokinin and none of the tested derivatives possessed higher activity than TDZ itself in any bioassay. In senescence assay, where the degradation of chlorophyll is assessed, eight compounds were completely inactive and only three had IC_{50} (concentration at which the chlorophyll degradation is inhibited by 50%) lower than 100 μM, although IC_{50} of TDZ in this assay is about 10 μM. The most active compounds were those bearing benzyl substituted in *meta*-position by fluorine or hydroxyl group (compounds 17 and 15). In amaranth assay, which is based on the dark induction of betacyanin synthesis in amaranth cotyledons by cytokinins, the EC_{50} values (concentration at which the activation response reaches 50%) were determined. Compound 8 was the most active in this assay, slightly exceeding the activity of BAP. This compound bears *meta*-methylhydroxy phenyl ring. Little less active were compounds 1, 2 and 3 which bear *ortho*-methoxy, *ortho*-hydroxy and *meta*-methoxy substituted phenyl ring, respectively and compound 17 which bears *meta*-fluorobenzyl group. In tobacco callus assay, where the growth of callus is cytokinin dependent, none of the compounds reached the TDZ activity. The most active compounds showed similar activity as BAP, namely compounds 8, 15 and 17. The same activity, at one fold lower concentration, reached substances: 3, 11, 14, 16 and 3FMTDZ.

Activation of cytokinin primary response gene *ARR5*

We employed transgenic Arabidopsis plants (*Arabidopsis thaliana*) harboring the *ARR5::GUS* reporter gene (D'Agostino *et al*. 2000) to monitor complex *in vivo* cytokinin activity of each compound. The *ARR5* is primary response gene with cytokinin-dependent promoter, which activation integrates the responses of several putative cytokinin signaling pathways as well as the contribution of individual cytokinin receptors. Compounds were tested at 0.5 μM, 1.0 and 10 μM concentrations (Figure 5) and their ability to activate the *ARR5::GUS* expression is shown in concentration, which is lower than the concentration at which the compound reaches its maximum. TDZ had highest activity in nanomolar range. The most active TDZ derivatives possess similar activity as BAP, namely compounds 1, 8 and HETDZ. Here the structure-activity relations are obvious and the activity is decreasing in following order: *ortho*-methoxy (1) > *ortho*-methylhydroxy (8) > *ortho*-ethylhydroxy (HETDZ). Little lower activity possess compounds 3, 4 and 10 (3FMTDZ), which bear methoxy-, hydroxy- and trifluoromethoxy- group in *meta* position on phenyl ring. Compounds 2, 5, 11, 12 and 15 caused maximal activation at 10 μM concentration. Other compounds, which do not activate the *ARR5::GUS* expression even in 10 μM concentration, can be assessed as very poor cytokinins. These include TDZ derivatives with substituted benzyl ring rather than phenyl ring. The exception is compound 15 bearing *meta*-hydroxybenzyl group and falls within the previous group.

Materials and methods

Molecular modelling and docking

A model of AtCKX2 was built in Modeller 9.10 (Eswar *et al*, 2006) by aligning the sequence (UNIPROT ID: Q9FUJ3) to template structure of ZmCKX1 (PDB ID: 2QKN, Kopečný *et al*, 2010). Ligands were constructed in Marvin 14.9.8 software (ChemAxon). Polar hydrogens were added to all ligands and proteins in the AutoDock Tools (ADT) software (Morris *et al*, 2009) prior to docking using Autodock Vina 1.05 (Trott *et al*, 2010). Grid box with size of 16 Å was centered on the active site around Asp150. Exhaustiveness parameter was set to 20 (default 8). After docking, the best docked ligand was selected and the best crystal-like poses of each ligand were analysed with Pymol 1.7.4 (The PyMOL Molecular Graphics System, Version 1.7.4 Schrödinger, LLC.) and Maestro 2014-4 (Schrödinger Release 2014-3: Maestro, version 9.9, Schrödinger, LLC, New York, NY, 2014).

Chemicals

1,2,3-Thiadiazol-5-ylamine was supplied by TCI Europe (Zwijndrecht, Belgium). TDZ, *t*Z and BA were supplied by Olchemim (Olomouc, Czech Republic). Other compounds including 2-methoxy-phenylamine, 2-amino-phenol, 3-methoxy-phenylamine, 3-amino-phenol, 2,5-dimethoxy-phenylamine, 2-hydroxy-3-methyl-phenylamine, (2-amino-phenyl)-methanol, (2-amino-phenyl)-ethanol, 3-trifluoromethoxy-phenylamine, 3-trifluormethyl-phenylamine, 2,4-dichloro-phenylamine,

2-hydroxy-benzylamine, 2-methyl-benzylamine, 3-hydroxy-benzylamine, 3-methoxy-benzylamine, 3-fluoro-benzylamine, 3-chloro-benzylamine, 2,5-dimethoxy-benzylamine and trimethyl-sillyl chloride were purchased from Sigma Aldrich (Germany). The other solvents and chemicals used were all of standard p.a. quality.

Synthesis of 5-isocyanato-1,2,3-thiadiazole and final products

The synthesis of isocyanates from amines was described elsewhere (Kurita *et al*., 1976). Briefly, 1,2,3-Thiadiazol-5-yl amine (1.01 g, 10 mmol) was dissolved in THF (40 mL) and added drop wise into a solution of diphosgene (2.6 g, 13 mmol) in THF (100 mL). Reaction mixture was stirred for 40 minutes at 0 °C and then the solvent and excess of diphosgene were evaporated. The yellow solid residue was 5-isocyanato-1,2,3-thiadiazole, which was re-suspended in diethyl ether and filtered off. Yield: 95%, ^{1}H NMR (δ, ppm, DMSO-d_6): 7.75(1H, s, CH).

All the prepared compounds were synthesized according to common protocols for the synthesis of di-substituted urea derivatives using amine and isocyanate as a starting material in the presence of catalytic amount of triethylamine (Goldschmidt and Bardach, 1892). In detail, 5-isocyanato-1,2,3-thiadiazole was mixed with THF (1:100) in high pressure tube. Then catalytic amount of triethylamine was added and the suspension was allowed to dissolve. Then starting amine was added in equimolar amount into the solution and the reaction mixture was stirred 5-12 hours at 60 °C. The conversion was monitored by TLC ($CHCl_3$:MeOH, 9:1). After reaction, the solvent was evaporated to a solid/semisolid residue, which was purified by flash silica column chromatography (mobile phase $CHCl_3$:MeOH, 9:1). Compounds were usually prepared in milligram quantities and yields varied between 30 and 80 %. When the starting amine contained free hydroxyl group, it was protected by trimethylsilyl chloride, prior the condensation with 5-isocyanato-1,2,3-thiadiazole and then de-protected in 2-propanolic HCl (Greene and Wuts, 1991). All products (Table 1) were characterized by ^{1}H NMR and HRMS (see Supplementary material for details).

General experimental procedures

The purity of synthesized compounds was confirmed by HPLC (Beckman Gold System) and was always above 97 %. Analytical thin-layer chromatography (TLC) was carried out using silica gel 60 WF254 plates (Merck). If necessary, compounds were separated on a flash chromatography column using 63 micron Chromatographic silica (Davisil) and eluted with a mobile phase containing $CHCl_3$/MeOH (9:1, v/v). Elemental composition of prepared compounds was confirmed by cap-LCHR-(ESI+) MS (Q-Tof micro™ Waters MS Technologies, Manchester, UK). Accurate masses were calculated and used for the determination of the elemental composition of analytes with fidelity better than 3 ppm. For the MS/MS experiments, the fragmentation was done in argon gas-filled collision cell with collision energies of 20, 25, 30 and 35 eV. NMR spectra were measured on a Jeol 500 SS spectrometer operating at a temperature of 300 K and a frequency of 500.13 MHz (^{1}H).

Samples were prepared by dissolving the compounds in DMSO-d_6 or $CDCL_3$. Tetramethylsilane (TMS) was used as the internal standard.

CKX inhibition measurements

The ability of the prepared compounds to inhibit AtCKX2, ZmCKX1 and ZmCKX4a was evaluated by determining their IC_{50} values in the PMS/MTT activity assay that had been previously adapted for screening in ELISA microtitre plates (Table 2, Frébort *et al*., 2002). Each well contained 100 μL of a reaction mixture consisting of 0.1 M KH_2PO_4 (pH adjusted to 7.4 with KOH), 1.5 mM phenazine methosulfate (PMS), 0.3 mM 3-(4,5-dimethylthiazol-2-yl)-2,5-diphenyltetrazolium bromide (MTT), the tested compound (at various concentrations) and 45 μM iP as a substrate for AtCKX2 and ZmCKX4a and 10 μM iP for ZmCKX1. Cell-free growth medium of *S. cerevisiae* strain 23344c ura- harbouring the plasmid pYES2-AtCKX2 (50 μL) was used directly as a source of AtCKX2 (Frébortová *et al*., 2007). Pure enzymes were used in case of ZmCKX1 and ZmCKX4a. ZmCKX1 was expressed in yeast *Yarrowia lipolytica* and purified according to a published protocol (Kopečný *et al*., 2005). *E. coli* BL21 STAR (DE3) cells carrying pTYB12-*ZmCKX4a* plasmid were grown for 16 hours at 18 °C to produce ZmCKX4a, which was further purified by affinity chromatography on a column filled with a chitin resin followed by ion-exchange chromatography (Zalabák *et al*. 2014). Plates were incubated in the dark for 20 min at 37 °C and the enzymatic reaction was monitored every 2 minutes by reading absorbance of the mixture in each well at 578 nm (spectrophotometer Synergy H4 Hybrid Reader). The absorbance of samples without substrate was subtracted. Compounds were tested in two replicates and the entire test was repeated at least twice. Using Gene 5 software we have calculated residual CKX activity for each compound and concentration. IC_{50} values for each compound were determined in Origin Pro software. The Lineweaver-Burk plots for K_i determination were constructed using iP as a substrate in the concentration range from 5 to 15 μM. The respective inhibitor concentrations were 7.5 μM and 15 μM in the case of TDZ and 1.5 μM and 3.0 μM for 3FMTDZ and HETDZ.

Crystallization and structure determination of 3FMTDZ and HETDZ complexes

Preliminary crystallization conditions were found in sitting drops using a screening kit Crystal Screen and Crystal Screen 2 (Hampton Research). ZmCKX4a was co-crystallized with 3FMTDZ in drops containing 100 mM HEPES pH 7.5, 80 % MPD, 0.16 mM ZmCKX4a and 10 mM 3FMTDZ in DMSO. Regarding HETDZ, the crystals of ZmCKX4a were grown in 22 % ethylene-glycol and then they were infiltrated by 5 mM HETDZ in DMSO for 1 hour. Crystals were directly flash frozen in liquid nitrogen. Diffraction data were collected at 100 K on the Proxima 1 beamline at the SOLEIL synchrotron (Saint-Aubin, France) at 2.0 Å resolution. Intensities were integrated using the XDS program (Kabsch, 2010) and data quality was assessed using the correlation coefficient $CC_{1/2}$ (Karplus and Diederichs, 2012). The crystal structures were determined by performing molecular replacement

with Phaser (Storoni *et al.*, 2004) using the monomer of ZmCKX1 (PDB 2QKN) as search models. Model refinement was performed with BUSTER-TNT (Bricogne *et al.*, 2011). Electron density maps were evaluated using COOT (Emsley and Cowtan, 2004). Refinement statistics are presented in Table 3. Molecular graphics images were generated using PYMOL (www.pymol.org).

Cytokinin bioassays and Arabidopsis *ARR5::GUS* reporter gene assay

Classical cytokinin bioassays including tobacco callus assay, Amaranthus assay and wheat senescence assay with excised wheat leaves in the dark) were performed as described in Holub *et al.* (1998). The tobacco callus bioassay was performed in 6-well microtiter plates (3 ml of MS medium in each well, into which 0.1 g of callus was placed). In the wheat leaf senescence and Amaranthus assays, IC_{50} values (concentration at which the chlorophyll degradation is inhibited by 50 %) and EC_{50} values (half maximal effective concentration) for each compound were determined (Table 4). In the tobacco callus bioassay the effect in optimal concentration was compared with the BAP activity (100 % is equal to 10^{-6} M BAP). The assay was done as described previously (Romanov *et al*., 2002). Quantitative determination of GUS activity was performed by measuring fluorescence on a Synergy H4 hybrid reader (Biotek, USA) at excitation and emission wavelengths of 365 and 445 nm, respectively. GUS specific activity was expressed in relative % and was calculated as RFU (relative fluorescence units) divided by protein content. Determination of protein content was done using the bicinchoninic acid assay (Smith *et al*., 1985).

Acknowledgments

The authors gratefully acknowledge support through the projects LO1204 and LO1305 from the Ministry of Education, Youth and Sports of the Czech Republic and the grant 15-22322S from the Czech Science Foundation. The work was also supported by student projects IGA_PrF_2015_027 and IGA_PrF_2015_021 of Palacký University Olomouc.

References

References

Abad, A., Agulló, C., Cuñat, A.C., Jiménez, R. & Vilanova, C. (2004) Preparation and promotion of fruit growth in kiwifruit of fluorinated N-phenyl-N'-1,2,3-thiadiazol-5-yl ureas. *J. Agric. Food Chem.* **52**, 4675-4683.

Bilyeu, K.D., Cole, J.L., Laskey, J.G., Riekhof, W.R., Esparza, T.J., Kramer, M.D. & Morris, R.O. (2001) Molecular and biochemical characterization of a cytokinin oxidase from maize. *Plant Physiol.* 125, 378-386.

Bricogne G., Blanc E., Brandl M., Flensburg C., Keller P., Paciorek W., Roversi P, Sharff A., Smart O.S., Vonrhein C. & Womack T.O. (2011) BUSTER version 2.1.0 Cambridge, United Kingdom: Global Phasing Ltd.

Brownlee, B.G., Hall, R.H. & Whitty, C.D. (1975) 3-Methyl-2-butenal: an enzymatic degradation product of the cytokinin, N-6-(delta-2 isopentenyl) adenine. *Can. J. Biochem.* **53**, 37-41.

Burch, L.R. & Horgan, R. (1989) The purification of cytokinin oxidase from *Zea mays* kernels. *Phytochemistry* **28**, 1313-1319.

Chatfield, J.M. and Armstrong, D.J. (1987) Cytokinin oxidase from *Phaseolus vulgaris* callus tissue. Enhanced *invitro* activity of the enzyme in the presence of copper-imidazole complexes. *Plant Physiol.* **84**, 726-731.

D'Agostino, I.B., Deruere, J. & Kieber, J.J. (2000) Characterization of the response of the *Arabidopsis* response regulator gene family to cytokinin. *Plant Physiol.* **124**, 1706–1717.

Frébort, I., Šebela, M., Galuszka, P., Werner, T., Schmülling, T., Peč, P. (2002) Cytokinin oxidase/cytokinin dehydrogenase assay: optimized procedures and applications. *Anal. Biochem.* **306**, 1–7.

Frébortová, J., Fraaije, M.W., Galuszka, P., Šebela, M., Peč, P., Hrbáč, J., Novák, O., Bilyeu, K.D., English, J.T. & Frébort, I. (2004) Catalytic reaction of cytokinin dehydrogenase: preference for quinones as electron acceptors, *Biochem. J.* **380**, 121-130.

Frébortová J, Galuszka P, Werner T, Schmülling T. & Frébort I. (2007) Functional expression and purification of cytokinin dehydrogenase from Arabidopsis thaliana (AtCKX2) in *Saccharomyces cerevisiae. Biologia Plantarum* **51**, 673-682.

Galuszka P., Popelková H., Werner T., Frébortová J., Pospíšilová H., Mik V., Köllmer I., Schmülling T., Frébort I. (2007) Biochemical characterization and histochemical localization of cytokinin oxidases/dehydrogenases from Arabidopsis thaliana expressed in *Nicotiana tabaccum* L. *J. Plant Growth Regul.* **26**, 255-267.

Goldschmidt H, Bardach B (1892) Zur Kenntniss der Diazoamidokörper. Chemische Berichte 25: 1347–1378.

Hare, P.D. & Van Staden, J. (1994) Inhibitory effect of thidiazuron on the activity of cytokinin oxidase isolated from soybean callus. *Plant Cell Physiol.* **35**, 1121-1125.

Holub, J. Hanuš, J. Hanke, D.E. & Strnad, M. (1998) Biological activity of cytokinins derived from ortho- and meta-hydroxybenzyladenine. *Plant Growth Regul.* **26**, 109-115.

Houba-Hérin, N., Pethe, C., d'Alayer, J. & Laloue, M (1999) Cytokinin oxidase from *Zea mays*: purification, cDNA cloning and expression in moss protoplasts. *Plant J.* **17**, 615–626.

Kabsch, W. (2010) XDS. *Acta Crystallogr D Biol Crystallogr.* **66**, 125-132.

Karplus, P.A. & Diederichs, K. (2012) Linking crystallographic model and data quality. *Science* **336**, 1030–1033.

Kopečný, D., Pethe, C., Šebela, M., Houba-Hérin, N., Madzak, C., Majira, A. & Laloue, M. (2005) High-level expression and characterization of *Zea mays* cytokinin oxidase/dehydrogenase in *Yarrowia lipolytica*. *Biochimie* **87**, 1011-1022.

Kopečný, D., Šebela, M., Briozzo, P., Spíchal, L., Houba-Hérin, N., Mašek, V., Joly, N., Madzak, C., Anzenbacher, P. & Laloue, M. (2008) Mechanism-based inhibitors of cytokinin oxidase/dehydrogenase attack FAD cofactor. *J. Mol. Biol.* **380**, 886-899.

Kopečný, D., Briozzo, P., Popelková, H., Šebela, M., Končitíková, R., Spíchal, L., Nisler, J., Madzak, C., Frébort, I., Laloue, M. & Houba-Hérin, N. (2010) Phenyl- and benzylurea cytokinins as competitive inhibitors of cytokinin oxidase/dehydrogenase: a structural study. *Biochimie* **92**, 1052-62

Kurita K, Matsumura T, Iwakura Y (1976) Trichloromethyl chloroformate. Reaction with amines, amino acids, and amino alcohols. J Org Chem 41: 2070-71.

Laloue, M. & Fox, J.E. (1989) Cytokinin oxidase from wheat: Partial purification and general properties. *Plant Physiol*. **90**, 899-906.

Massonneau, A., Houba-Hérin N., Pethe, C., Madzak, C., Falque, M., Mercy, M., Kopečný, D., Majira, A., Rogowsky, P. & Laloue M. (2004) Maize cytokinin oxidase genes: differential expression and cloning of two new cDNAs. *J. Exp. Bot.* **55**, 2549-2557.

Mok, D.W. & Mok, M.C. (2001) Cytokinin metabolism and action. *Annu. Rev. Plant Physiol. Plant Mol. Biol.* **52**, 89-118.

Mok, M.C. & Mok, D.W.S., Armstrong, D. J., Shudo, K., Isogai, Y. & Okamoto, T. (1982) Cytokinin activity of *N*-phenyl-*N′*-1,2,3-thiadiazol-5-ylurea (thidiazuron). *Phytochemistry* **21**, 1509-1511.

Morris, R.O., Bilyeu, K.D., Laskey, J.G. & Cheikh, N.N. (1999) Isolation of a gene encoding a glycosylated cytokinin oxidase from maize. *Biochem. Biophys. Res. Commun.* **255**, 328-333.

Morris, G. M., Huey, R., Lindstrom, W., Sanner, M. F., Belew, R. K., Goodsell, D. S. & Olson, A. J. (2009) Autodock4 and AutoDockTools4: automated docking with selective receptor flexibility. *J. Comput. Chem.* **16**, 2785-2791.

Wuts, P.G.M. & Greene, T.W. (1991) Greene's protective groups in organic synthesis, 4th edition, John Wiley & Sons, Inc. ISBN: 978-0-471-69754-1

Romanov, G.A., Kieber, J.J. & Schmülling, T. (2002) A rapid cytokinin response assay in *Arabidopsis* indicates a role for phospholipase D in cytokinin signalling. *FEBS Lett.* **515**, 39–43.

Schrödinger Release 2014-3: Maestro, version 9.9, Schrödinger, LLC, New York, NY, 2014.

Smith, P.K., Krohn, R.I., Hermanson, G.T., Mallia, A.K., Gartner, F.H., Provenzano, M.D., Fujimoto, E.K., Goeke, N.M., Olson, B.J. & Klenk, D.C. (1985) Measurement of protein using bicinchoninic acid. *Anal Biochem*. **150**, 76–85.

Spíchal, L., Rakova, N.Y., Riefler, M., Mizuno, T., Romanov, G.A., Strnad, M. & Schmülling, T. (2004) Two cytokinin receptors of *Arabidopsis thaliana*, CRE1/AHK4 and AHK3, differ in their ligand specificity in a bacterial assay. *Plant Cell Physiol.* **45**, 1299-1305.

Storoni, L.C., McCoy, A.J. & Read, R.J. (2004) Likelihood-enhanced fast rotation functions. *Acta Crystallogr D Biol Crystallogr*. **60**, 432–438.

Suttle, J.C. & Mornet, R. (2005) Mechanism-based irreversible inhibitors of cytokinin dehydrogenase. *J. Plant Physiol.* **162**, 1189-1196.

The PyMOL Molecular Graphics System, Version 1.7.4 Schrödinger, LLC.

Trott, O. & Olson, A. J. (2010) AutoDock Vina: improving the speed and accuracy of docking with a new scoring function, efficient optimization and multithreading, *J. Comput. Chem.* **31**, 455-461.

Webb, B. & Sali, A. (2014) Comparative protein structure modeling with MODELLER. *Curr. Protoc. Bioinformatics* **47**: 5.6.1-5.6.32.

Werner, T., Motyka, V., Strnad, M. & Schmülling, T. (2001) Regulation of plant growth by cytokinin. *Proc. Natl. Acad. Sci. U.S.A.* **98**, 10487–10492.

Whitty, C.D. & Hall, R.H. (1974) A cytokinin oxidase in *Zea mays*. *Can. J. Biochem.* **52**, 789-799.

Zalabák, D., Galuszka, P., Mrízová, K., Podlešáková, K., Gu, R. & Frébortová, J. (2014). Biochemical characterization of the maize cytokinin dehydrogenase family and cytokinin profiling in developing maize plantlets in relation to the expression of cytokinin dehydrogenase genes. *Plant Physiol. Biochem.* **74**, 283-293.

Zatloukal, M., Gemrotová, M., Doležal, K., Havlíček, L., Spíchal, L. & Strnad, M. (2008) Novel potent inhibitors of *A. thaliana* cytokinin oxidase/dehydrogenase. *Bioorg. Med. Chem.* **16**, 9268-9275.

Table 1. Structure and abbreviations of prepared compounds

Compounds of group I	**R1**	**R2**	**R3**	**R4**
TDZ	H	H	H	H
1	**OCH_3**	H	H	H
2	**OH**	H	H	H
3	H	**OCH_3**	H	H
4	H	**OH**	H	H
5	**OCH_3**	H	H	**OCH_3**
6	**OH**	H	H	**OH**
7	H	**OH**	**CH_3**	H
8	**CH_2OH**	H	H	H
9 - HETDZ	**CH_2CH_2OH**	H	H	H
10 - 3FMTDZ	H	**OCF_3**	H	H
11	H	**CF_3**	H	H
12	**Cl**	H	**Cl**	H

Compounds of group II	**R1**	**R2**	**R3**	**R4**
13	**OH**	H	H	H
14	**Me**	H	H	H
15	H	**OH**	H	H
16	H	**Cl**	H	H
17	H	**F**	H	H
18	H	**O-CH_3**	H	H
19	**OH**	**CH_3**	H	H
20	**O-CH_3**	H	H	**O-CH_3**

Table 2. Overview of binding energies of TDZ derivatives and their comparison to IC_{50} values measured with AtCKX2 and further with ZmCKX1 and ZmCKX4a. Binding energies (ΔG) of TDZ derivatives were obtained by the docking into the active site of AtCKX2. CKX activity was measured using PMS/MTT method. "n.a." means that the compound was not active as inhibitor and "– " means that IC_{50} was not determined.

Compound	**ΔG (*kcal/mol*)**	***IC*$_{50}$ (*μM*)**		
	AtCKX2	**AtCKX2**	**ZmCKX1**	**ZmCKX4a**
TDZ	-8.8	62 ± 6	40 ± 7	> 200
1	-8.4	36 ± 3	35 ± 5	> 200
2	-8.3	51 ± 5	37 ± 4	> 200
3	-8.8	22 ± 4	9 ± 3	> 200
4	-8.8	66 ± 5	43 ± 4	> 200
5	-8.9	7.6 ± 1	24 ± 4	> 200
6	-8.9	-	-	-
7	-9.2	33 ± 2	26 ± 3	117 ± 12
8	-8.3	18 ± 2	14 ± 2	91 ± 10
9 - HETDZ	-8.5	3.9 ± 0.6	2.8 ± 0.5	120 ± 15
10 - 3FMTDZ	-9.3	5.5 ± 0.6	4.8 ±0.3	35 ± 4
11	-8.1	45 ±7	48 ±5	> 200
12	-9.3	> 200	> 200	> 200
13	-	> 200	-	-
14	-6.9	n.a.	-	-
15	-7.2	106 ± 17	-	-
16	-6.3	> 200	-	-
17	-7.3	n.a.	-	-
18	-	n.a.	-	-
19	-6.3	n.a.	-	-
20	-8.2	n.a.	-	-

Table 3. Data collection and refinement statistics

	ZmCKO4a + 3FMTDZ	**ZmCKO4a + HETDZ**
Space group	$P4_32_12$	$P4_32_12$
Asymmetric unit	monomer	monomer
Unit cell (Å)		
a	79.7	74.5
b	79.7	74.5
c	203.7	208.1
$\alpha=\beta=\gamma$ (°)	90.0	90.0
Resolution (Å)	50.0-2.00	47.0-2.00
Observed reflections	325424 (52088)[a]	518187 (46997)
Unique reflections	45506 (7123)	40294 (6679)
Completeness (%)	99.7 (98.6)	99.6 (97.6)
$I/\sigma(I)$	14.7 (1.4)	22.9 (1.6)
$CC_{1/2}$[b]	99.9 (59.8)	100.0 (73.3)
R_{sym} (%)	8.6 (152.2)	7.8 (123.7)
R_{cryst} (%)	18.3	20.1
R_{free} (%)	20.8	22.4
RMSD bond lengths (Å)	0.010	0.010
RMSD bond angles (°)	0.99	1.02
B average value (Å^2)		
Protein	48.7	54.5

[a] Numbers in parentheses represent values in the highest resolution shell 2.00-2.12 Å.

[b] $CC_{1/2}$ stands for a percentage of correlation between intensities from random half-dataset (Karplus and Diederichs, 2012).

Table 4. Cytokinin activity of synthetized TDZ derivatives in classical cytokinin bioassays. In the tobacco callus bioassay the effect at optimal concentration is compared with the activity of BA and 100% stands for 10^{-6} M BA. . "n.a." means that the compound was not active "–" means that IC_{50} was not determined.

Compound	**Senescence bioassay** IC_{50} (μM)	***Amaranthus* bioassay** EC_{50} (μM)	**Tobacco callus bioassay** Optimal concentration (mol l^{-1})	Relative activity (%)
BA	155 ± 22	0.55 ± 0.13	10^{-6}	100
TDZ	12.8 ± 4	0.004 ± 0.0025	10^{-7}	102 ± 5
1	127 ± 13	1.5 ± 0.4	10^{-4}	103 ± 2
2	113 ± 14	3.5 ± 1.0	10^{-4}	94 ± 3
3	82 ± 7	3.3 ± 1.6	10^{-5}	93 ± 3
4	152 ± 12	29 ± 5.2	10^{-4}	108 ± 2
5	n.a.	>100	10^{-4}	75 ± 8
6	n.a.	>100	10^{-4}	15 ± 7
7	n.a.	n.a.	10^{-4}	48 ± 6
8	115 ± 12	0.42 ± 0.2	10^{-6}	105 ± 5
9 - HETDZ	127 ± 14	10.5 ± 2.1	-	-
10 - 3FMTDZ	n.a.	>100	10^{-5}	96 ± 4
11	n.a.	25 ± 8	10^{-5}	104 ± 6
12	105 ± 10	>100	10^{-5}	77 ± 4
13	n.a.	>100	10^{-4}	90 ± 4
14	157 ± 11	65 ± 7	10^{-5}	91 ± 3
15	65 ± 6	9.0 ± 1.2	10^{-6}	100 ± 4
16	n.a.	83 ± 7	10^{-5}	102 ± 2
17	32 ± 5	2.5 ± 0.8	10^{-6}	95 ± 7
18	n.a.	n.a.	n.a.	n.a.
19	n.a.	>100	10^{-4}	32 ± 5
20	160 ± 12	>100	-	-

Figure legends

Figure 1. Reaction scheme of synthesis of new TZD derivatives. In the first step, the 2,3-thiadiazol-5-yl amine was dissolved in THF and added drop-wise into a solution of diphosgene to form an intermediate 5-isocyanato-1,2,3-thiadiazole. The isocyanate was further reacted with phenyl- or benzylamine derivative in the presence of catalytic amount of triethylamine to form the final product.

Figure 2. Inhibitor strength of selected TDZ derivatives against AtCKX2, ZmCKX1 and ZmCKX4a. CKX activity was measured by PMS/MTT kinetic assay (Frébort *et al*., 2002) and the standard deviation did not exceed 10 %.

Figure 3. Inhibition of ZmCKX4a and AtCKX2 with selected TDZ derivatives. **(A)** Structures of the two best inhibitors HETDZ and 3FMTDZ. **(B, C)** Double-reciprocal plots of competitive inhibition of ZmCKX4a by TDZ and 3FMTDZ. The Lineweaver-Burk plots were constructed using iP as a substrate in the concentration range of 5 - 15 μM. The respective inhibitor concentrations were 0 μM (◊), 15 μM (■) and 30 μM (▲) for TDZ and 0 μM (◊), 4 μM (■) and 8 μM (▲) for 3FMTDZ. **(D, E, F)** Double-reciprocal plots showing competitive inhibition of AtCKX2 by TDZ, HETDZ and 3FMTDZ. The respective inhibitor concentrations were 0 μM (◊), 7.5 μM (■) and 15 μM (▲) for TDZ and 0 μM (◊), 1.5 μM (■) and 3 μM (▲) for HETDZ and 3FMTDZ. The insets show secondary plots of slopes against the inhibitor concentration, which were used for K_i determination.

Figure 4. Binding of two urea inhibitors 3FMTDZ and HETDZ in the active site of ZmCKX4a. (A) Binding of 3FMTDZ. The inhibitor is green colored and shown in Fo-Fc omit map, contoured at 4.0 σ. **(B)** Binding of UR15. The inhibitor is blue colored and shown in Fo-Fc omit map, contoured at 3.0 σ. **(C)** Superposition of bound 3FMOTDZ and HETDZ. Both ligands make hydrogen bond to the oxygen atom of D170 via two nitrogen atoms of urea backbone. Oxygen atom of the hydroxyethyl side chain of HETDZ replaces a water molecule observed in ZmCKX4a-3FMTDZ structure. FAD cofactor is yellow colored and neighboring residues are labelled.

Figure 5. Quantification of GUS activity in *ARR5::GUS* transgenics at 3 days after germination. The activity of compounds was compared to the activity of 1 μM BAP, which was set as 100% activation. 0.1% DMSO was used as a solvent control and its activity value was subtracted from the data. Measurements were done in triplicate and standard deviation did not exceed 10%.

Figure 1.

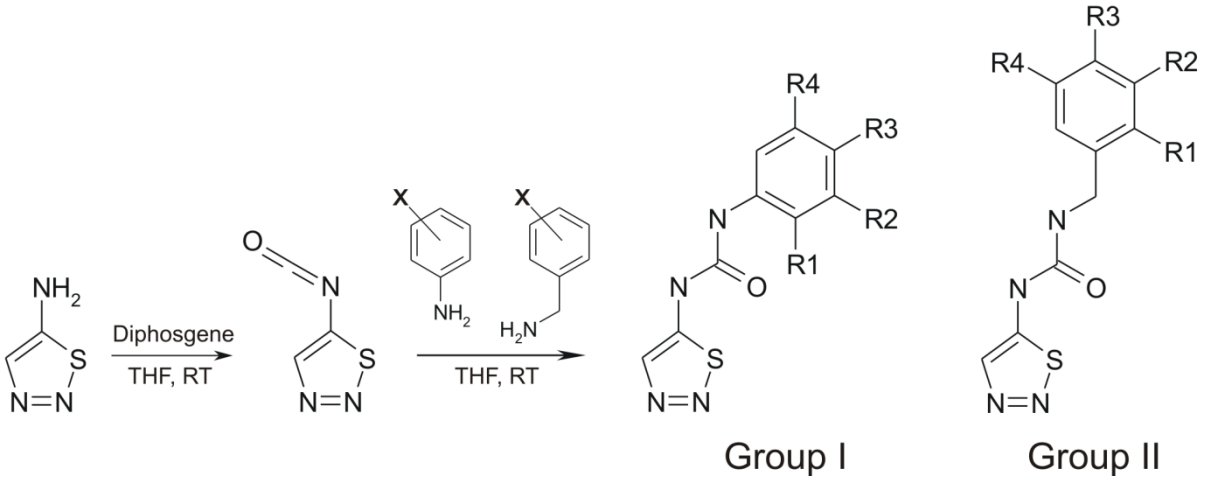

Figure 2.

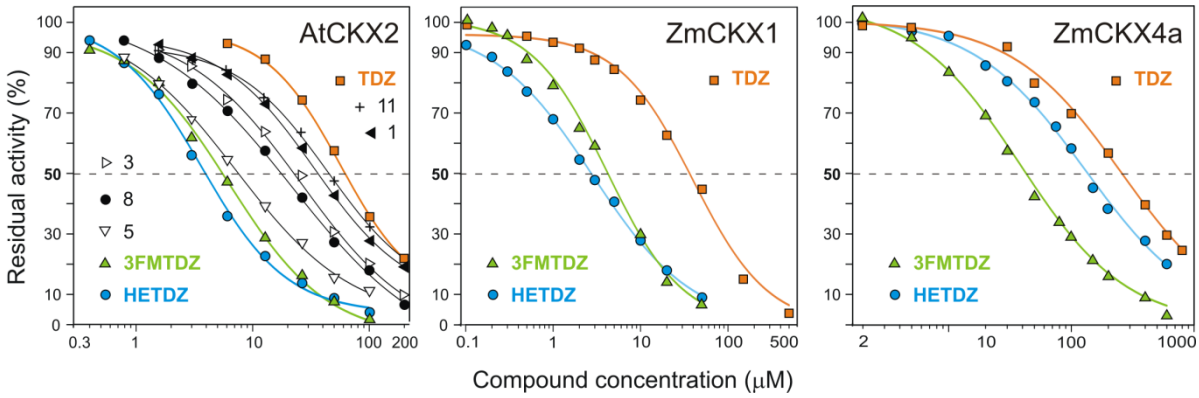

Figure 3.

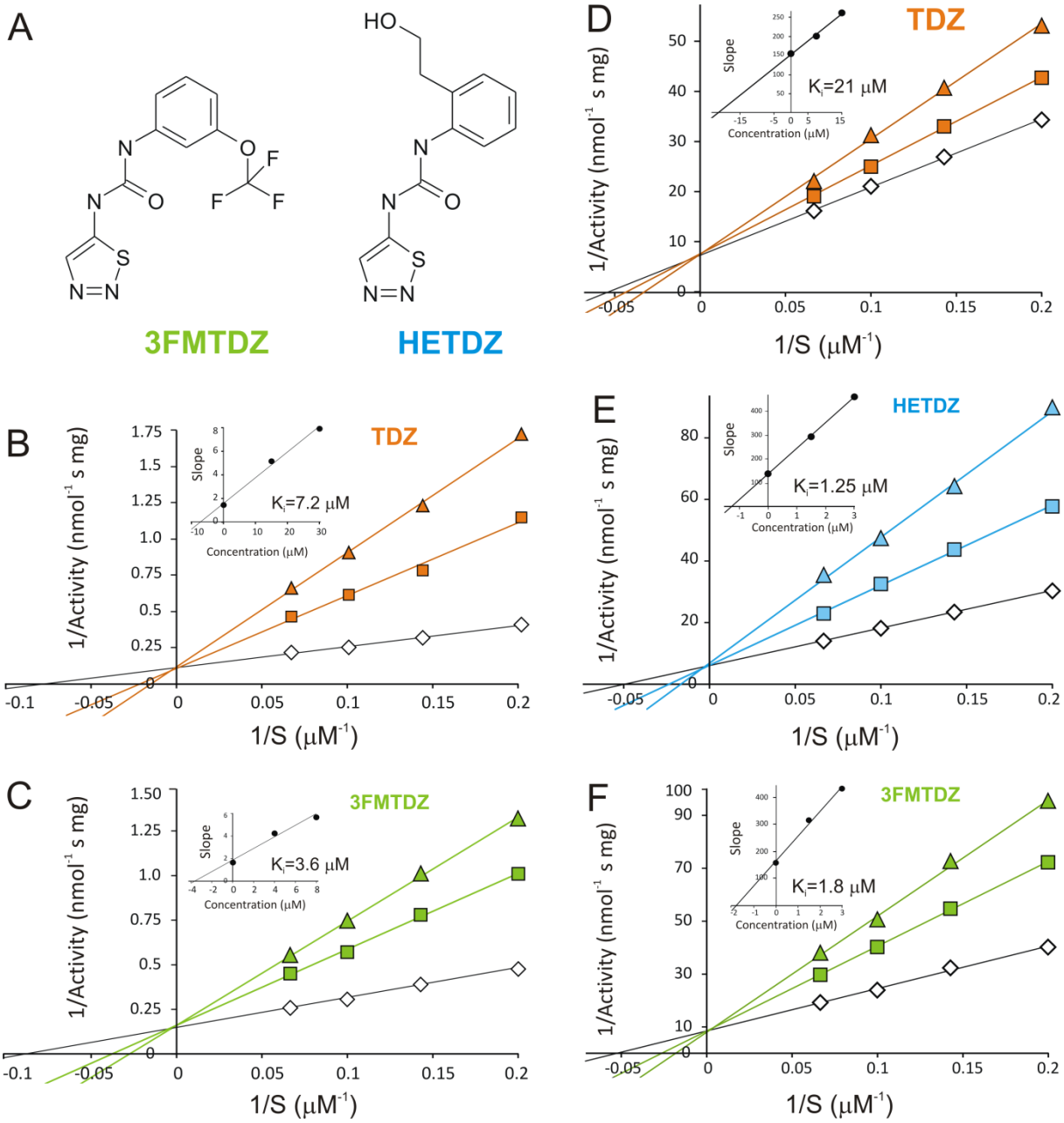
A
HO
N
O
F
F
F
N
O
S
N=N
3FMTDZ
HETDZ
B
TDZ
1/Activity (nmol^{-1} s mg)
1/S (μM^{-1})
Slope
Concentration (μM)
K_i=7.2 μM
C
3FMTDZ
K_i=3.6 μM
D
TDZ
K_i=21 μM
E
HETDZ
K_i=1.25 μM
F
3FMTDZ
K_i=1.8 μM

Figure 4.

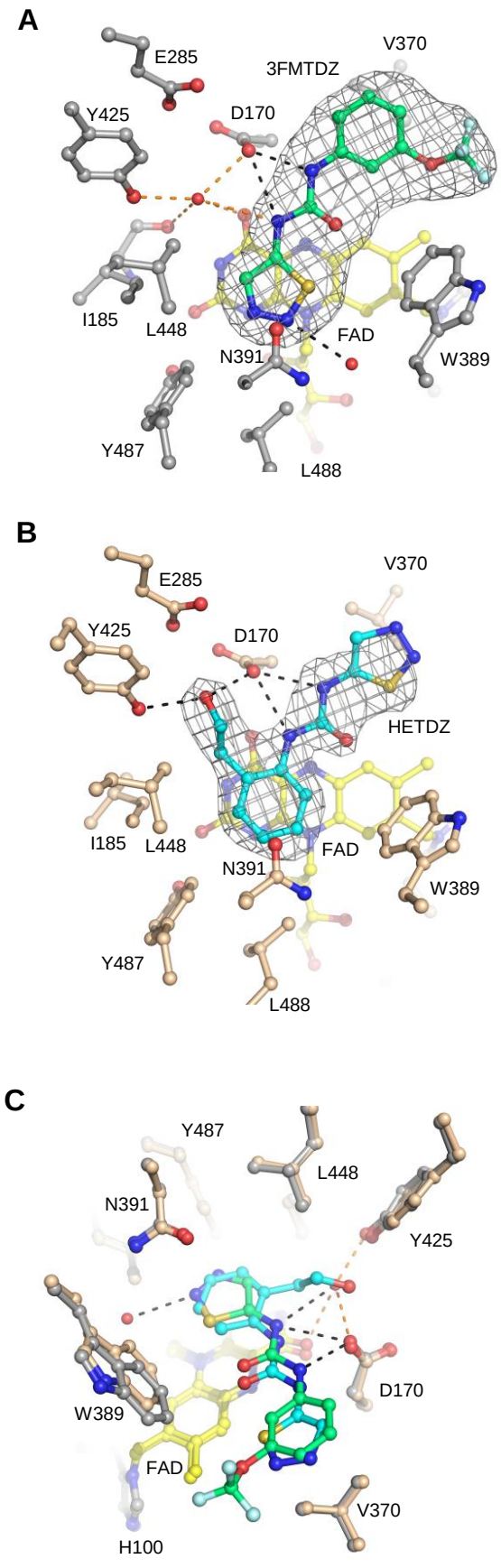
A
E285
V370
3FMTDZ
Y425
D170
I185
L448
FAD
N391
W389
Y487
L488
B
E285
V370
Y425
D170
HETDZ
I185
L448
FAD
N391
W389
Y487
L488
C
Y487
L448
N391
Y425
D170
W389
FAD
V370
H100

Figure 5.

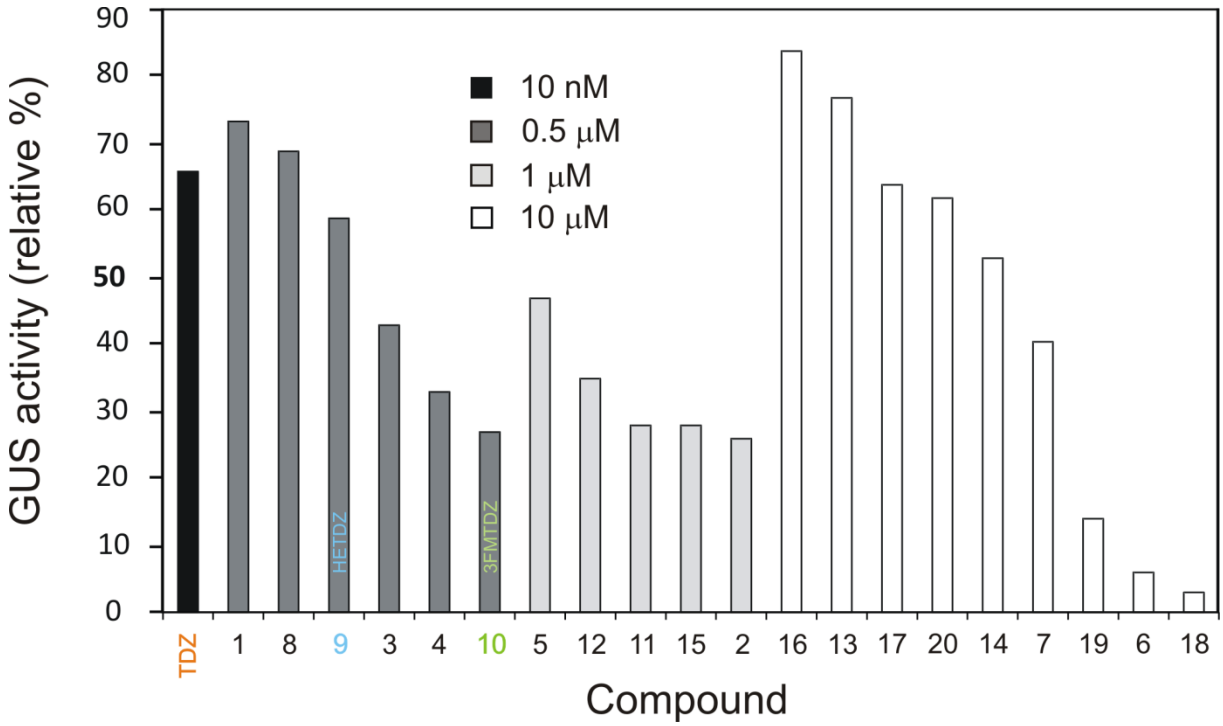
GUS activity (relative %)
90
80
70
60
50
40
30
20
10
0
10 nM
0.5 μM
1 μM
10 μM
HETDZ
3FMTDZ
TDZ
1
8
9
3
4
10
5
12
11
15
2
16
13
17
20
14
7
19
6
18
Compound

Article 4

Role and structural characterization of plant aldehyde dehydrogenases from family 2 and family 7.

Končitíková R, Vigouroux A, Kopečná M, Andree T, Bartoš J, Šebela M, Moréra S, Kopečný D.

Biochem J. 468(1): 109-23.*J* (2015)

Biochem. J. (2015) **468**, 109–123 doi:10.1042/BJ20150009

Role and structural characterization of plant aldehyde dehydrogenases from family 2 and family 7

Radka Končitíková*†, Armelle Vigouroux‡, Martina Kopečná*, Tomáš Andree†, Jan Bartoš§, Marek Šebela*, Solange Moréra‡[1] and David Kopečný*[1]

*Department of Protein Biochemistry and Proteomics, Centre of the Region Haná for Biotechnological and Agricultural Research, Faculty of Science, Palacký University, Šlechtitelů 11, Olomouc CZ-783 71, Czech Republic

†Department of Biochemistry, Faculty of Science, Palacký University, Šlechtitelů 11, Olomouc CZ-783 71, Czech Republic

‡Laboratoire d'Enzymologie et Biochimie Structurales, CNRS, Avenue de la Terrasse, Gif-sur-Yvette 91198, France

§Centre of Plant Structural and Functional Genomics, Centre of the Region Haná for Biotechnological and Agricultural Research, Institute of Experimental Botany, Šlechtitelů 31, Olomouc CZ-78371, Czech Republic

Aldehyde dehydrogenases (ALDHs) are responsible for oxidation of biogenic aldehyde intermediates as well as for cell detoxification of aldehydes generated during lipid peroxidation. So far, 13 ALDH families have been described in plants. In the present study, we provide a detailed biochemical characterization of plant ALDH2 and ALDH7 families by analysing maize and pea ALDH7 (ZmALDH7 and PsALDH7) and four maize cytosolic ALDH(cALDH)2 isoforms RF2C, RF2D, RF2E and RF2F [the first maize ALDH2 was discovered as a fertility restorer (RF2A)]. We report the crystal structures of ZmALDH7, RF2C and RF2F at high resolution. The ZmALDH7 structure shows that the three conserved residues Glu^{120}, Arg^{300} and Thr^{302} in the ALDH7 family are located in the substrate-binding site and are specific to this family. Our kinetic analysis demonstrates that α-aminoadipic semialdehyde, a lysine catabolism intermediate, is the preferred substrate for plant ALDH7. In contrast, aromatic aldehydes including benzaldehyde, anisaldehyde, cinnamaldehyde, coniferaldehyde and sinapaldehyde are the best substrates for cALDH2. In line with these results, the crystal structures of RF2C and RF2F reveal that their substrate-binding sites are similar and are formed by an aromatic cluster mainly composed of phenylalanine residues and several nonpolar residues. Gene expression studies indicate that the *RF2C* gene, which is strongly expressed in all organs, appears essential, suggesting that the crucial role of the enzyme would certainly be linked to the cell wall formation using aldehydes from phenylpropanoid pathway as substrates. Finally, plant ALDH7 may significantly contribute to osmoprotection because it oxidizes several aminoaldehydes leading to products known as osmolytes.

Key words: aldehyde dehydrogenase 2 (ALDH2), aldehyde dehydrogenase 7 (ALDH7), benzaldehyde, coniferaldehyde, cytokinin, fertility restorer.

INTRODUCTION

Aldehyde dehydrogenases (ALDHs) constitute a superfamily of $NAD(P)^+$-dependent enzymes that catalyse irreversible oxidation of aldehydes to the corresponding carboxylic acids. Aldehydes, which are highly reactive molecules, are toxic at high concentrations. Therefore, ALDHs play a crucial role in detoxifying aldehydes produced by various metabolic pathways. They also play a role during adaptation to various stress conditions such as salinity, drought, heat and cold [1]. ALDHs are classified according to their sequence identity. Those sharing more than 40 % sequence identity belong to the same family, whereas those with more than 60 % form a subfamily [2]. The superfamily of plant ALDHs currently contains 13 distinct families: ALDH2, ALDH3, ALDH5, ALDH6, ALDH7, ALDH10, ALDH11, ALDH12, ALDH18, ALDH21, ALDH22, ALDH23 and ALDH24 [3]. Only ALDH2, 3, 5, 6, 7 and 18 families possess mammalian orthologues.

The plant ALDH2 family (EC 1.2.1.-) comprises mitochondrial (mtALDH) and cytosolic (cALDH) isoforms split into ALDH2B and ALDH2C subfamilies respectively. They share ∼54 %–63 % amino-acid identity with human ALDH2 (hALDH2), which belongs to the ALDH2A subfamily. hALDH2 plays a role in ethanol metabolism by catalysing the oxidation of ethanol-derived acetaldehyde to acetate [4–6]. Its crystal structure is known (PDB 1CW3) [6]. The first maize (*Zea mays*) *ADLH2*

Abbreviations: ABAL, 4-aminobutyraldehyde; ALDH, aldehyde dehydrogenase; AMADH, aminoaldehyde dehydrogenase; APAL, 3-aminopropionaldehyde; AASAL, α-aminoadipate-semialdehyde; BAL, betaine aldehyde; cALDH, cytosolic aldehyde dehydrogenase; DAP, days after pollination; GABA, γ-aminobutyric acid; GBAL, 4-guanidinobutyraldehyde; hALDH2, human ALDH2; LKR, lysine-ketoglutarate reductase; MASAL, adipic semialdehyde methyl ester; mtALDH, mitochondrial aldehyde dehydrogenase; P6C, Δ^1-piperideine-6-carboxylate; PCAL, pyridine carboxaldehyde; PsALDH, ALDH from *Pisum sativum* (pea); RF, fertility restorer; TMABAL, 4-(trimethylamino)butyraldehyde; SDH, saccharopine dehydrogenase; TMAPAL, 3-(trimethylamino)propionaldehyde; ZmALDH, ALDH from *Zea mays* (maize).

[1] Correspondence may be addressed to either of these authors (email david.kopecny@upol.cz or morera@lebs.cnrs-gif.fr).

Sequence data can be found in the EMBL/GenBank data libraries under accession numbers KJ004509 for ZmALDH7, KJ004510 for RF2A, KJ004511 for RF2B, KJ004512 for RF2C, KM225857 for RF2D, KM225858 for RF2E and KJ004513 for RF2F.

The structure for ZmALDH2-3 (RF2C) complexed with NAD^+, ZmALDH2-6 (RF2F) complexed with NAD^+ and ZmALDH7 complexed with NAD^+ will appear in the PDB under accession code 4PXL, 4PZ2 and 4PXN respectively.

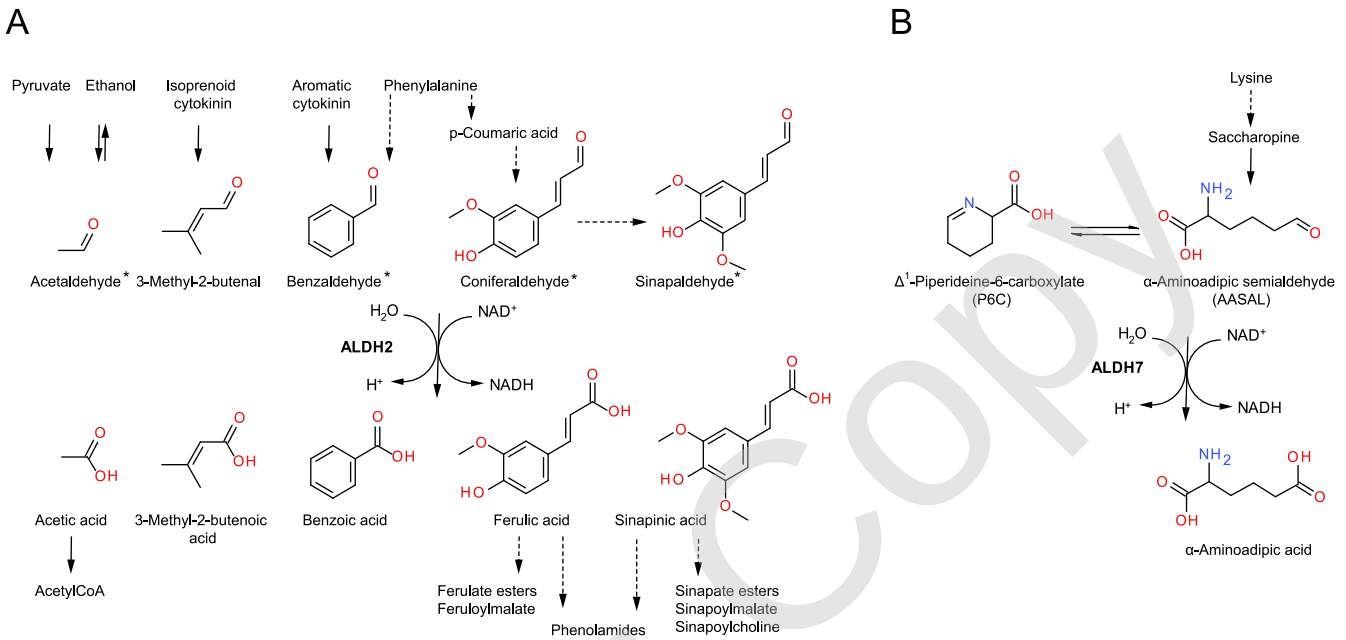

Figure 1 Possible reactions catalysed by plant ALDH2 and ALDH7

(**A**) Plant ALDH2 members catalyse conversion of acetaldehyde, 3-methyl-2-butenal, benzaldehyde, coniferaldehyde and sinapaldehyde. Confirmed *in vivo* substrates are marked with an asterisk [13–16]. (**B**) ALDH7 oxidizes AASAL to α-aminoadipic acid as confirmed *in vivo* for hALDH7 [18].

gene was identified as a male fertility restorer (*RF*)*2A* [7,8] followed by *RF2B* [9]. Both genes code for homotetrameric mtALDHs with an acetaldehyde activity. RF2A has a wide substrate specificity covering aliphatic and aromatic aldehydes, whereas RF2B oxidizes only short-chain aliphatic aldehydes. RF2A, which accumulates in tapetal cells, is required for normal another development. Two more maize genes, *RF2C* and *RF2D*, were identified, but not characterized further [10]. Two rice (*Oryza sativa*) mtALDHs are abundant in panicles [11] and two tobacco mtALDHs are abundant in reproductive tissues and play a role in pollen development [12]. All of the mtALDHs above along with those from *Arabidopsis* [10] produce acetate for acetyl-CoA biosynthesis from acetaldehyde generated via ethanolic fermentation, bypassing pyruvate dehydrogenase [11,13]. The recently characterized snapdragon benzaldehyde dehydrogenase [14] is indeed an mtALDH2. cALDH2 [reduced epidermal fluorescence 1 (REF1), ALDH2C4] isoforms from *Arabidopsis* and oilseed rape [15,16] oxidize sinapaldehyde and coniferaldehyde *in vivo* and play a major role in the formation of soluble and cell wall-linked ferulate and sinapate esters. A reaction scheme with possible *in vivo* substrates is shown in Figure 1A.

ALDH7 (EC 1.2.1.31) is also known as Δ^1-piperideine-6-carboxylate (P6C) dehydrogenase, α-aminoadipate-semialdehyde (AASAL) dehydrogenase or antiquitin. The *ALDH7* gene is highly conserved across species suggesting a conserved role within the cell using identical physiological substrates. Human ALDH7 (hALDH7 and ALDH7A1) shares ~60 % sequence identity with plant orthologues (ALDH7B subfamily) and its crystal structure is known (PDB 2J6L) [17]. The enzyme is primarily involved in the metabolism of lysine and catalyses the conversion of AASAL to α-aminoadipate (Figure 1B) [18]. P6C, which is the cyclic Schiff base of AASAL, is in equilibrium with AASAL in solution. Plant ALDH7 was first reported from pea (*Pisum sativum*) as a '26 g protein' involved in the regulation of turgor pressure. Its expression is induced by dehydration of leaves and the stem [19]. Later, *ADLH7* genes in oilseed rape (*btg-26*), *Arabidopsis*, rice and foxtail millet have also been reported to be induced by dehydration, high salinity, abscisic acid treatment or other stress conditions [20–23]. Soybean and *Arabidopsis* ALDH7 overexpressers confer tolerance to abiotic and oxidative stresses [24,25]. Stress tolerance is accompanied by a reduction of hydrogen peroxide and malondialdehyde derived from lipid peroxidation. ALDH7 was found to be important for seed viability and maturation in rice. Indeed, *osaldh7* mutants are more sensitive to various stresses and mutant seeds accumulate more malondialdehyde and melanoidin pigment, a product of a Maillard reaction between carbonyl and amino compounds [26].

We have previously kinetically and structurally characterized several ALDH10 [aminoaldehyde dehydrogenase (AMADH)] family members from pea, maize and tomato [27–29] linked to polyamine catabolism, osmoprotection, secondary metabolism (fragrance) and carnitine biosynthesis. In the present study, we investigate the structure–function relationship of plant ALDH2 and ALDH7 families by analysing the maize and pea ALDH7 families represented by a single member per plant species (ZmALDH7 and PsALDH7) as well as the maize ALDH2 family represented by six members with a special focus on four uncharacterized cALDH2 isoforms RF2C, RF2D, RF2E and RF2F (Table 1). To better understand substrate specificity, we solved the crystal structures of ZmALDH7 (systematic name ALDH7B6), RF2C (ZmALDH2-3, ALDH2C1) and RF2F (ZmALDH2-6, ALDH2C5) with NAD^+ at 2.94, 2.25 and 2.40 Å (1 Å = 0.1 nm) resolution respectively, and compared them with the human enzymes. Finally, we analysed the spatial and temporal

Table 1 Enzyme nomenclature and GenBank accession numbers of plant ALDH2 and 7 family members studied in the present work

The alternative and systematic names follow previous publications dealing with nomenclature of plant ALDHs [3,30]. Sequence identities (in %) of maize RF2C and maize ALDH7 with other ALDHs was calculated by Lalign [31].

Name	Alternative/systematic name	GenBank accession number	Maize chromosome	Exon #	AA #	Sequence identity (%)	
						RF2C	ZmALDH7
RF2A	ZmALDH2-1/ALDH2B2	KJ004510	9	11	549	59.1	29.5
RF2B	ZmALDH2-2/ALDH2B5	KJ004511	4	9	550	60.2	28.2
RF2C	ZmALDH2-3/ALDH2C1	KJ004512	3	7	502	–	27.5
RF2D	ZmALDH2-4/ALDH2C2	KM225857	3	8	511	73.8	29.7
RF2E	ZmALDH2-5/ALDH2C4	KM225858	8	10	501	71.1	29.1
RF2F	ZmALDH2-6/ALDH2C5	KJ004513	6	8	519	70.2	29.4
ZmALDH7	ALDH7B6	KJ004509	2	14	509	27.5	–
PsALDH7	ALDH7B1	X54359	–	–	508	28.4	78.2
hALDH7	ALDH7A1	AK312459	–	–	511	30.0	59.3

expression of *ALDH2* and *ALDH7* during the first 2 weeks in developing maize seedlings to assess their roles in early stages of development and also in various organs.

MATERIALS AND METHODS

Cloning, expression and purification of ALDHs from maize and pea

The total RNA from various maize organs (*Z. mays* cv. Cellux, Morseva) and apical meristem of pea seedlings (*P. sativum*) was extracted using the RNAqueous kit and plant RNA isolation aid (Ambion). The RNA was treated twice with the Turbo DNase-free kit (Ambion). The cDNA was synthesized using Superscript II RT (Life Technologies). Six *ZmALDH2* ORFs and three *ALDH7* ORFs, namely *ZmALDH7*, *PsALDH7* and *hALDH7*, were amplified using gene-specific primers and Accuprime *Pfx* polymerase (Life Technologies). Obtained maize sequences were submitted to GenBank. *ALDHs* were ligated into a pCDFDuet vector (Novagen), and then transformed into T7 expressing *Escherichia coli* cells (NEB). Cells were grown at 37 °C in LB media, at $D_{600} = 0.5$, the cultures were supplemented with 0.5 mM isopropyl-β-thiogalactopyranoside for protein expression and incubated at 20 °C overnight. Recombinant ALDHs were purified on HisPur Cobalt Spin Columns (Thermo Fisher Scientific) equilibrated with 20 mM Tris/HCl buffer, pH 8.0, containing 100 mM NaCl, 10 mM imidazole and 5 % glycerol. Elution was performed using 250 mM imidazole in the same buffer. Enzymes were concentrated using Amicon 30 kDa filters (Merck) and further purified by gel filtration chromatography on a HiLoad 26/60 Superdex 200 column in 50 mM Tris/HCl buffer, pH 8.0, 150 mM NaCl. Protein content was measured using Coomassie plus (Bradford) protein assay kit (Thermo Fisher Scientific) using BSA as a standard and using absorption coefficients calculated from sequences (http://web.expasy.org/protparam/). The purity of recombinant ALDHs was confirmed by SDS/PAGE using NuPAGE system (Life Technologies; Supplementary Figure S1). For activity measurements and storage, 5 % glycerol was added to the enzyme solution.

Enzyme kinetics

Activity was measured by monitoring the NADH formation ($\varepsilon_{340} = 6.62$ mM^{-1}·cm^{-1}) at 37 °C on a UV–Vis spectrophotometer 8453 (Agilent) in a cuvette and by monitoring fluorescence emission of NADH at 460 nm upon excitation at 365 nm on a FluoroLog-3 spectrofluorometer (Horiba). The reaction mixtures contained 150 mM Tris/HCl buffer, pH 8.0 (for RF2C and RF2F) or pH 7.5 (for RF2D and RF2E), 1 mM NAD^+ and ALDH2 or 100 mM sodium pyrophosphate buffer, pH 8.0, 2.5 mM NAD^+ and ALDH7. The enzyme reaction was started by the addition of aldehyde at a final 1 mM concentration. Kinetic constants for selected substrates (up to 6 mM concentration) were determined using GraphPad Prism 5.0 data analysis software (GraphPad Software). Elementary aliphatic and aromatic aldehydes, pyridine carboxaldehydes (PCALs), MASAL (methyl ester of adipic semialdehyde), BAL (betaine aldehyde) chloride together with APAL (3-aminopropionaldehyde) and ABAL (4-aminobutyraldehyde) diethylacetals were purchased from Sigma–Aldrich Chemie. AASAL ethylene acetal was purchased from Chiralix. Diethylacetals of 4-guanidinobutyraldehyde (GBAL), 3-guanidinopropionaldehyde (GPAL), 3-(trimethylamino)propionaldehyde (TMAPAL) and 4-(trimethylamino)butyraldehyde (TMABAL) were synthetic preparations [32,33]. Free aminoaldehydes were prepared by heating their acetals in a plugged test tube with 0.2 M HCl for 10 min [34].

Crystallization and structure determination

Crystallization conditions were screened using Qiagen kits. Crystals were obtained in hanging drops by mixing equal volumes of protein solution and a precipitant solution containing 30 % (w/v) PEG 400, 100 mM $CaCl_2$ and 100 mM sodium acetate, pH 4.5, for RF2C; 35 % 2-methyl-2,4-pentanediol (MPD), 100 mM 4-morpholineethanesulfonic acid (MES), pH 6.5, and 15 % (w/v) PEG 4000 for RF2F; 40 % MPD and 200 mM ammonium phosphate for ZmALDH7. Crystals were directly flash-frozen in liquid nitrogen. Diffraction data were collected at 100 K on the Proxima 1 beamline for RF2C and RF2F and on Proxima 2 beamline for ZmALDH7 at the SOLEIL synchrotron at 2.25, 2.40 and 2.94 Å resolution respectively. Intensities were integrated using the XDS program [35] and data quality was assessed using the correlation coefficient $CC_{1/2}$ [36,37]. The crystal structures were determined by performing molecular replacement with Phaser [38], using the monomers of hALDH2 (PDB codes 1CW3 and 1O05) and of seabream ALDH7 (PDB code 2JG7) as search models [6,39]. Both models were refined with NCS restraints and TLS using Buster 2.10 [40]. Electron density maps were evaluated using COOT [41]. Refinement statistics are presented in Table 2. Models of RF2D

Table 2 Data collection and refinement statistics

	RF2C (ZmALDH2-3)	RF2F (ZmALDH2-6)	ZmALDH7
PDB code	4PXL	4PZ2	4PXN
Space group	$P2_12_12$	$I4_1$	$I2_12_12_1$
Asymmetric unit	1 dimer	1 tetramer	2 monomers
Oligomeric state	Tetrameric	Tetrameric	Tetrameric
Unit cell (Å)			
a	109.9	233.9	79.2
b	126.1	233.9	162.5
c	78.3	82.9	188.6
$\alpha = \beta = \gamma$ (°)	90.0	90.0	90.0
Resolution (Å)	49.1–2.25	50.0–2.40	42.11–2.94
Observed reflections	381340 (59526)*	603883 (95778)	184717 (28407)
Unique reflections	52406 (8260)	87 611 (13838)	26085 (4014)
Completeness (%)	99.8 (99.0)	99.7 (98.3)	99.3 (95.7)
I/σ (I)	13.62 (2.1)	11.12 (1.2)	9.91 (1.8)
$CC_{1/2}$†	–	99.7 (58.4)	99.6 (58.3)
R_{sym} (%)	10.7 (78.9)	9.7 (155.7)	19.4 (153.3)
R_{cryst} (%)	17.1	19.0	18.8
R_{free} (%)	20.5	21.3	21.7
RMSD bond lengths (Å)	0.010	0.009	0.008
RMSD bond angles (°)	1.11	1.14	1.14
B average value (Å^2)			
Protein	41.9	83.7	80.4
NAD^+	55.9	85.2	100.5
Solvent	43.2	72.3	60.1

*Numbers in parentheses represent values in the highest resolution shell: 2.25–2.38 Å (ZmALDH2-3), 2.40–2.54 Å (ZmALDH2-6) and 2.94–3.12 Å (ZmALDH7).

†$CC_{1/2}$ stands for a percentage correlation between intensities from random half-datasets [36,37].

and RF2E were constructed using SWISS-MODEL server [42] with RF2C structure as a template. Molecular graphics images were generated using PYMOL (www.pymol.org).

qPCR analysis

The total RNA from 3- to 13-day-old and 3-month-old maize plants was isolated using the RNAqueous kit and plant RNA isolation aid (Ambion) and treated twice with a Turbo DNase-free kit (Ambion). First-strand cDNA was synthesized by RevertAid H Minus reverse transcriptase and oligo(dT) primers (Thermo Fisher Scientific). RNA from four biological replicates was transcribed in two independent reactions and PCR was performed in triplicate. Diluted cDNA samples were used as templates in real-time PCRs containing TaqMan Gene Expression Master Mix (Life Technologies), both primers at 300 nM concentrations and 250 nM TaqMan 6-FAM TAMRA probe on a StepOnePlus Real-Time PCR System. Primers and TaqMan probes were designed using Primer Express 3.0 software (Life Technologies) and are shown in Supplementary Table S1. Plasmid DNA carrying the ORF of the respective maize *ALDH2* or *ALDH7* gene was used as a template for a calibration curve to determine the PCR efficiencies of designed probes and primer pairs as well as to verify their specificity. Cycle threshold values were normalized with respect to elongation factor 1α and β-actin genes and amplification efficiency. Expression values were determined and statistically evaluated using the DataAssist v3.0 Software package (Life Technologies). Transcript abundance values are shown in Supplementary Table S2.

RESULTS AND DISCUSSION

Gene models and phylogenetic analysis of ALDH2 and ALDH7 families

The maize genome database (http://ensembl.gramene.org, AGPv3) indicates the existence of six putative ALDH2 genes and one ALDH7 gene. We cloned the complementary DNAs (cDNAs) of these seven ALDHs using gene-specific primers in order to identify the correct gene models in each case and to obtain the corresponding recombinant proteins. We deposited their sequences in GenBank. The unique ZmALDH7 gene composed of 14 exons lies on chromosome 2 (Table 1; Figure 2A). ZmALDH2 genes are composed of 7–11 exons with the last three conserved, except for *RF2E*, whose last exon is split into two by insertion of a CACTA-like DNA transposon. The first two exons are also conserved among the *ZmALDH2* gene family. Both *RF2A* and *RF2B* genes carry an additional exon at the 5′-end coding for a signal sequence towards the mitochondrion. The high variability in exon number rather than in total length appears in the middle section of the *ALDH2* genes. For example, although two exons (648 and 138 bp long) are found in *RF2C* gene, five exons (154, 230, 90, 174 and 138 bp long) are found in *RF2A* gene (Figure 2A). *RF2D* and *RF2E* are the most homologous, even though the third exon of *RF2D* is split into two in *RF2E* and separated by a long intron. This intron emerges with the insertion of a CACTA-like DNA transposon whose footprint (target site duplication) is unambiguously detectable in the gene/intron sequence. The intron contains at least eight other transposable elements mainly LTR retroelements. Currently, two ORFs (GRMZM2G380438 comprising the first three exons and GRMZM2G407949 comprising the remaining seven exons) represent *RF2E*, but the fact that the complete cDNA covering all 10 exons was cloned (Table 1; Figure 2A) shows that only one ORF exists and the gene is either incorrectly annotated or is different between the maize cultivar we used and the sequenced B73 line. The gene structures are similar to those in rice and *Arabidopsis* [22] with a high variability in exon/intron number in the middle part of the ALDH2 genes.

Phylogenetic analysis (Figure 2B) shows that both maize RF2A and RF2B belong to subfamily ALDH2B composed of mtALDH2 members from different plant species including the snapdragon (*Anrirrhinum majus*) benzaldehyde dehydrogenase [14], rice, tobacco and *Aradopsis* mtALDHs [10–12]. The remaining four uncharacterized enzymes RF2C, RF2D, RF2E and RF2F, which share about 70 % sequence identity (Table 1), belong to subfamily ALDH2C composed of cALDH2 members including *Arabidopsis* ALDH2C4, also named coniferaldehyde or sinapaldehyde dehydrogenase [15]. For comparison, rice, the other monocotyledonous plant, contains two genes, *ALDH2B5* and *ALDH2B1*, coding for mtALDH2 isoforms and three genes *ALDH2C1*, *ALDH2C2* and *ALDH2C3* coding for cALDH2 isoforms [11,22]. ZmALDH7, which shares 78 % sequence identity with PsALDH7, appears in the unique ALDH7B subfamily with other plant ALDH7s (Figure 2C). So far, *ALDH7* gene is absent from available algae genomes and exists in bryophytes like *Physcomitrella patens* or *Tortula ruralis* [46]. Angiosperms usually carry one *ALDH7* gene, but some species, for example poplar or soybean, can carry two or more *ALDH7* genes.

Substrate specificity and the role of the maize ALDH2 family

We purified four maize cALDH2 isoforms (ALDH2C subfamily), namely RF2C, RF2D, RF2E and RF2F (Supplementary Figure S1) and measured their enzyme kinetics using various

Table 3 Kinetic parameters of four ALDH2 family members from maize for selected substrates

K_m and k_{cat} values are given in μM and s^{-1} respectively. Kinetic constants were measured in 0.15 M Tris/HCl, pH 8.0 (for RF2C and RF2F) and pH 7.5 (for RF2D and RF2E), using 1.0 mM NAD^+. Specific activity values with 1 mM hexanal were 62 nkat mg^{-1} for RF2C, 12.2 nkat mg^{-1} for RF2D, 14.6 nkat mg^{-1} for RF2E and 8.9 nkat mg^{-1} for RF2F. The K_m value for NAD^+ and $NADP^+$ was measured at a fixed 1 mM concentration of hexanal. The symbol 'n.d.' stands for not determined.

	RF2C			RF2D			RF2E			RF2F		
Ligand	K_m (μM)	k_{cat} (s^{-1})	k_{cat}/K_m ($M^{-1}s^{-1}$)	K_m (μM)	k_{cat} (s^{-1})	k_{cat}/K_m ($M^{-1}s^{-1}$)	K_m (μM)	k_{cat} (s^{-1})	k_{cat}/K_m ($M^{-1}s^{-1}$)	K_m (μM)	k_{cat} (s^{-1})	k_{cat}/K_m ($M^{-1}s^{-1}$)
NAD^+	44 ± 3	3.46 ± 0.04	7.9×10^4	59 ± 7	0.85 ± 0.009	1.5×10^4	45 ± 2	0.86 ± 0.009	1.9×10^4	86 ± 8	0.55 ± 0.004	6.4×10^3
$NADP^+$	3012 ± 190	0.16 ± 0.01	5.4×10^1	1488 ± 78	0.21 ± 0.005	1.4×10^2	1364 ± 63	0.22 ± 0.004	1.6×10^2	1672 ± 113	0.14 ± 0.005	8.4×10^1
Acetaldehyde	2419 ± 170	0.59 ± 0.02	2.4×10^2	92 ± 9	0.37 ± 0.022	4.1×10^3	90 ± 8	0.59 ± 0.030	6.6×10^3	1090 ± 107	0.05 ± 0.001	4.5×10^1
Propionaldehyde	239 ± 22	2.12 ± 0.07	8.9×10^3	n.d.	n.d.	n.d.	50 ± 4	0.41 ± 0.009	8.1×10^3	944 ± 57	0.10 ± 0.001	1.0×10^2
Butyraldehyde	210 ± 20	3.54 ± 0.11	1.7×10^4	n.d.	n.d.	n.d.	30 ± 2	0.44 ± 0.005	1.5×10^4	291 ± 10	0.13 ± 0.002	4.4×10^2
Valeraldehyde	99 ± 5	3.20 ± 0.07	3.2×10^4	n.d.	n.d.	n.d.	31 ± 1	0.53 ± 0.004	1.7×10^4	142 ± 9	0.22 ± 0.004	1.5×10^3
Isovaleraldehyde	33 ± 3	2.32 ± 0.05	7.0×10^4	n.d.	n.d.	n.d.	52 ± 3	0.12 ± 0.002	2.4×10^3	269 ± 22	0.18 ± 0.004	6.9×10^2
3-Methyl-2-butenal	54 ± 11	0.24 ± 0.06	4.4×10^3	64 ± 3	0.08 ± 0.001	1.2×10^2	63 ± 5	0.06 ± 0.001	9.7×10^2	250 ± 9	0.14 ± 0.002	5.6×10^2
Hexanal	15 ± 1	4.54 ± 0.08	3.0×10^5	48 ± 4	0.91 ± 0.032	1.9×10^4	42 ± 5	0.85 ± 0.031	2.0×10^4	424 ± 21	0.72 ± 0.011	1.7×10^3
t-2-Hexenal	39 ± 5	0.35 ± 0.02	9.0×10^3	31 ± 1	0.08 ± 0.001	2.5×10^3	34 ± 2	0.06 ± 0.001	1.7×10^3	156 ± 11	0.014 ± 0.001	9.0×10^1
Heptanal	172 ± 11	0.77 ± 0.01	4.5×10^3	n.d.	n.d.	n.d.	130 ± 6	0.14 ± 0.002	1.0×10^3	1717 ± 99	0.007 ± 0.001	3.9
Octanal	312 ± 20	1.97 ± 0.04	6.3×10^3	n.d.	n.d.	n.d.	196 ± 30	0.18 ± 0.009	9.4×10^2	1852 ± 96	0.03 ± 0.001	1.5×10^1
Nonanal	51 ± 5	1.63 ± 0.06	3.2×10^4	159 ± 9	0.36 ± 0.009	2.3×10^3	143 ± 13	0.36 ± 0.010	2.5×10^3	181 ± 10	0.41 ± 0.013	2.3×10^3
t-2-Nonenal	19 ± 13	2.54 ± 0.30	1.3×10^5	89 ± 7	0.1 ± 0.004	1.1×10^3	79 ± 4	0.11 ± 0.001	1.4×10^3	177 ± 6	0.03 ± 0.001	1.6×10^2
Benzaldehyde	83 ± 9	1.21 ± 0.06	1.5×10^4	22 ± 2	1.49 ± 0.105	6.8×10^4	12 ± 1	0.99 ± 0.036	8.3×10^4	146 ± 7	0.29 ± 0.003	2.0×10^3
m-Anisaldehyde	203 ± 33	1.25 ± 0.14	6.2×10^3	17 ± 2	0.95 ± 0.037	$5{,}6 \times 10^4$	19 ± 3	0.65 ± 0.024	3.4×10^4	260 ± 29	0.35 ± 0.020	1.4×10^3
p-Anisaldehyde	299 ± 7	0.40 ± 0.03	1.3×10^3	6 ± 1	0.93 ± 0.020	1.5×10^5	13 ± 2	1.35 ± 0.078	1.0×10^5	536 ± 31	0.82 ± 0.016	1.6×10^3
Phenylacetaldehyde	480 ± 99	0.13 ± 0.02	2.8×10^2	196 ± 9	0.10 ± 0.002	5.3×10^2	195 ± 11	0.17 ± 0.003	8.9×10^2	1.8 ± 0.23	0.42 ± 0.014	2.3×10^5
Cinnamaldehyde	10 ± 1	2.95 ± 0.17	3.0×10^5	69 ± 7	0.31 ± 0.014	4.5×10^3	52 ± 2	0.65 ± 0.011	1.2×10^4	116 ± 7	0.17 ± 0.005	1.5×10^3
Hydrocinnamaldehyde	22 ± 3	2.41 ± 0.16	1.1×10^5	103 ± 10	0.60 ± 0.031	5.8×10^3	147 ± 35	1.00 ± 0.101	6.8×10^3	203 ± 17	0.17 ± 0.008	8.6×10^2
Coniferaldehyde	19 ± 3	2.65 ± 0.37	1.4×10^5	15 ± 3	0.37 ±0.055	2.5×10^4	14 ± 3	0.33 ± 0.027	2.4×10^4	10 ± 1	0.08 ± 0.006	7.8×10^4
Sinapaldehyde	14 ± 2	0.24 ± 0.02	2.4×10^4	26 ± 6	0.33 ± 0.088	1.3×10^4	23 ± 4	0.15 ± 0.010	6.6×10^3	7 ± 1	0.06 ± 0.006	8.8×10^4

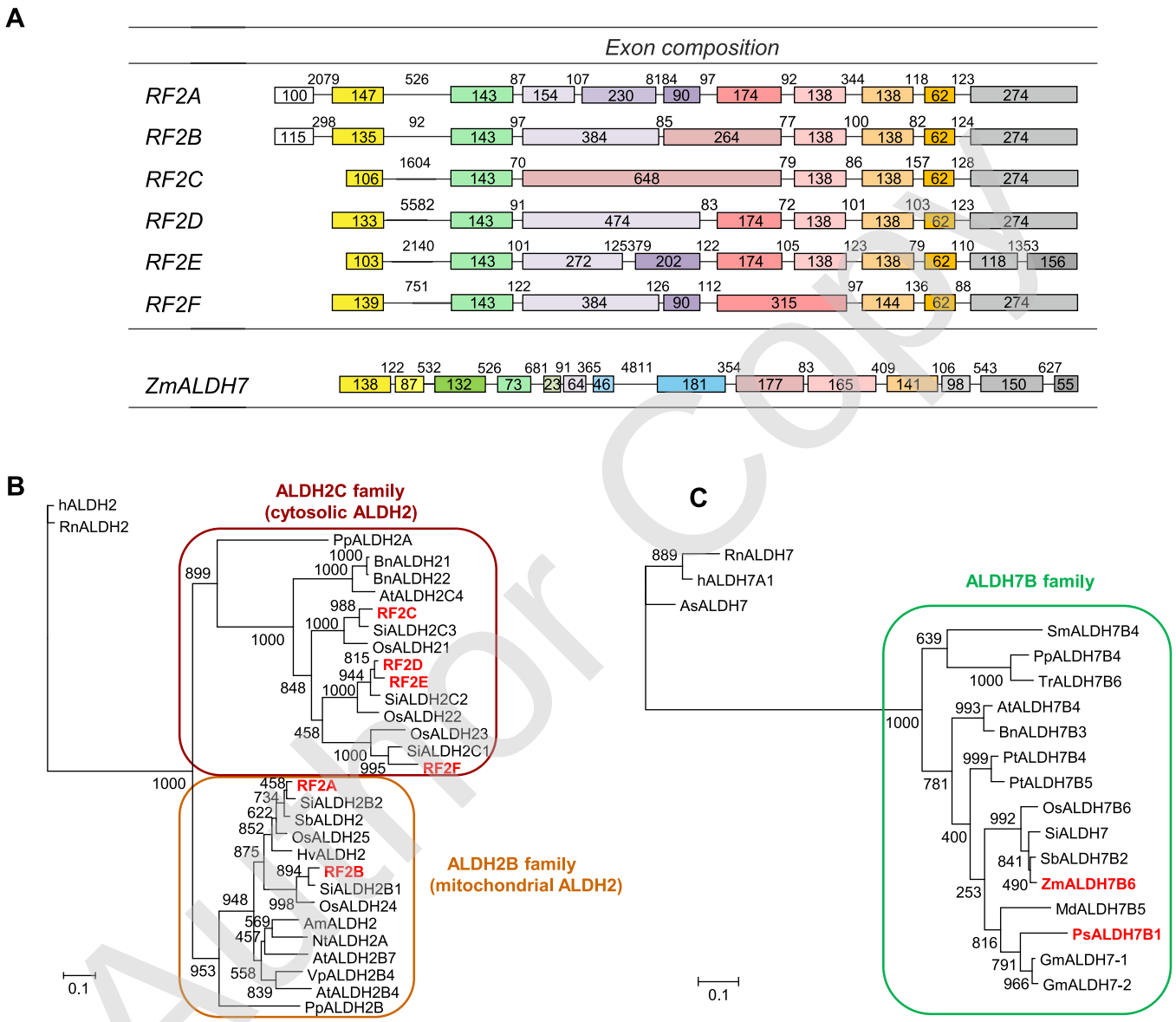

Figure 2 Phylogeny and gene models for studied plant ALDH2 and ALDH7 families

(**A**) Gene models for *Zea mays* ALDH2 and ALDH7 families. Gene models were constructed using cloned cDNA sequences (present work) and genomic DNA sequences obtained from maize genome (http://ensembl.gramene.org/Zea_mays/Info/Index). (**B** and **C**) Phylogenetic trees illustrating the relatedness of maize ALDH2 and ALDH7 to other ALDHs from the same families. Amino acid alignments were performed using MUSCLE v3.8 [43] followed by Gblocks [44]. A maximum likelihood phylogeny with bootstrap analysis was performed with PhyML v3.0 [45] using LG amino acid replacement matrix. Bootstrap values are given for the nodes. Only subset of known ALDHs was chosen, especially those that have been previously studied. ALDH2 sequences include those from *Antirrhinum majus* (FJ151199), *Arabidopsis thaliana* (At3g48000, At1g23800 and At3g24503), *Brassica napus* (FN995990 and FN995991), *Homo sapiens* (AY621070), *Hordeum vulgare* (BAB62757), *Nicotiana tabacum* (CAA71003), *Oryza sativa* (Os06g15990, Os02g49720, Os01g40860, Os01g40870 and Os06g39230), *Physcomitrella patens* (XP_001767457 and XP_001785650), *Rattus norvegicus* (P11884), *Sorghum bicolor* (BAB92019), *Vitis pseudoreticulata* (DQ150256), *Setaria italica* (XM_004953741, XM_004965148, XM_004965940, XM_004968994 and XM_004968990). ALDH7 sequences include those from *Acanthopagrus schlegelii* (AY847462), *Arabidopsis thaliana* (At1g54100), *Brassica napus* (Q41247), *Glycine max* (Glyma.15G178400 and Glyma.09G070300), *Homo sapiens* (AK312459), *Malus domestica* (BAA75633), *Oryza sativa* (Os09g26880), *Physcomitrella patens* (XP_001778351), *Pisum sativum* (X54359), *Populus trichocarpa* (Potri.003G067700 and Potri.001G167100), *Rattus norvegicus* (NP_001258034.1), *Selaginella moellendorffii* (XP_002961173), *Setaria italica* (XM_004956875), *Sorghum bicolor* (XP_002462451.1), *Tortula ruralis* (AY034889) and *Zea mays* (KJ004509).

aldehydes, ω-aminoaldehydes and AASAL at 1 mM concentration (Figure 3A). ALDH2C isoforms display a wide substrate preference for aliphatic and aromatic aldehydes, especially for hexanal, benzaldehyde and *p*-anisaldehyde. Other naturally occurring aldehydes, including AASAL, APAL, ABAL, citral and glycolaldehyde were weak substrates (all below the 10% rate compared with hexanal). Based on the catalytic efficiency values (k_{cat}/K_m ratios; Table 3), hexanal and cinnamaldehyde are the best substrates for RF2C, whereas RF2D and RF2E prefer *p*-anisaldehyde and benzaldehyde and RF2F preferentially oxidizes phenylacetaldehyde. Saturation curves for the RF2C, RF2E and RF2F show that a strong excess substrate inhibition appears at low concentrations for some aromatic aldehydes, such as for cinnamaldehyde with RF2C or phenylacetaldehyde with RF2F (Figure 3B).

The specific activity of all ZmALDH2 isoforms increases with the chain length of aliphatic aldehydes up to six carbons

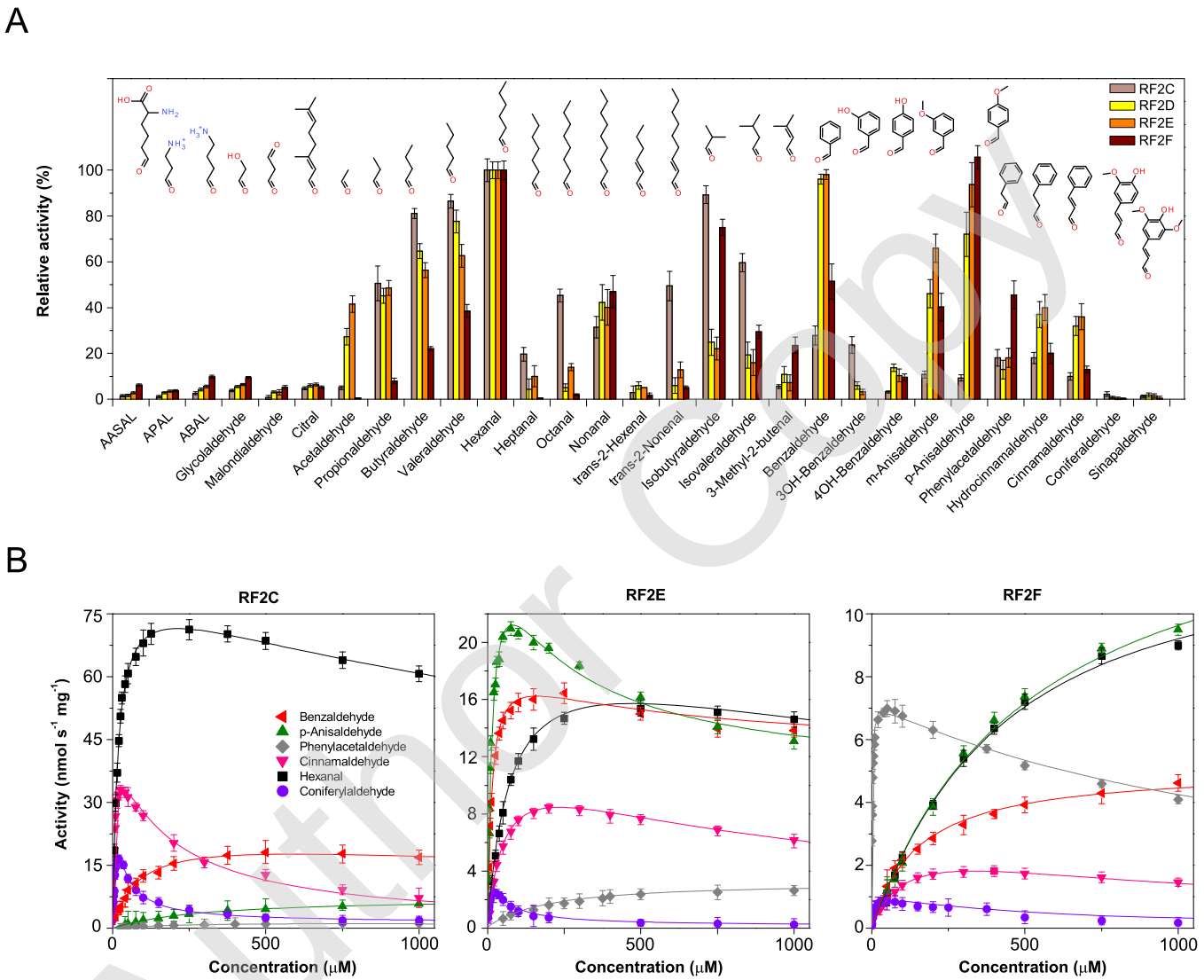

Figure 3 Screening of substrate specificity of maize ALDH2C isoforms

(**A**) Substrate specificity of four maize ALDH2 isoforms with aliphatic and aromatic aldehydes. Measurements were performed with 1 mM substrate in 0.15 M Tris/HCl buffer, pH 8.0 (for RF2C and RF2F) and pH 7.5 (for RF2D and RF2E), containing 1 mM NAD^+. Specific activity values with 1 mM hexanal were 62 nkat mg^{-1} for RF2C, 12.2 nkat mg^{-1} for RF2D, 14.6 nkat mg^{-1} for RF2E and 8.9 nkat mg^{-1} for RF2F. The activity with hexanal was arbitrarily taken as 100 %. Error bars stand for S.D. from four measurements. (**B**) Saturation curves for activity determination of maize RF2C, RF2E and RF2F. The data were measured as above and are shown for benzaldehyde, *p*-anisaldehyde, phenylacetaldehyde, cinnamaldehyde, hexanal and coniferaldehyde.

(hexanal). The activity with heptanal and octanal is much lower (except for RF2C and octanal) and increases again with nonanal (nine-carbon chain) up to 50 % activity compared with hexanal. The unsaturated C6 and C9 aldehydes, *t*-2-hexenal and *t*-2-nonenal respectively, are weaker substrates than the saturated ones. However, for RF2C isoform, *t*-2-nonenal is among the best substrates. Aliphatic C6 and C9 aldehydes and their unsaturated forms arise from linoleic or linolenic acids via the lipoxygenase pathway [47]. They belong to green leaf volatiles, which are synthesized in response to wounding and also provide fruits and vegetables with their aroma. Branched aliphatic C4 and C5 aldehydes are also good substrates. All isoforms display activity with 3-methyl-2-butenal (isopentenal), which is 8 %–25 % of that compared with hexanal. Isopentenal is formed by the oxidation of isoprenoid cytokinins by cytokinin oxidase/dehydrogenase [48].

The activity of ZmALDH2 isoforms toward aromatic aldehydes such as benzaldehyde, *m*- and *p*-anisaldehyde, phenylacetaldehyde, cinnamaldehyde and hydrocinnamaldehyde is variable. However, they are all good substrates. In plants, benzaldehyde originates either from phenylalanine via the non-β-oxidative pathway [49] or from the oxidation of aromatic cytokinins by cytokinin oxidase/dehydrogenase. Phenylacetaldehyde also originates from phenylalanine via several pathways [47]. ZmALDH2 isoforms display an activity with coniferaldehyde and sinapaldehyde (Table 3), which arise from the phenylpropanoid pathway and have been demonstrated as *in vivo* substrates for ALDH2C from *Arabidopsis* and oilseed rape [15,16].

Substrate specificity and the role of maize and pea ALDH7

A large screening study performed using 1 mM substrates proves that the three ALDH7 isoforms from maize, pea and human

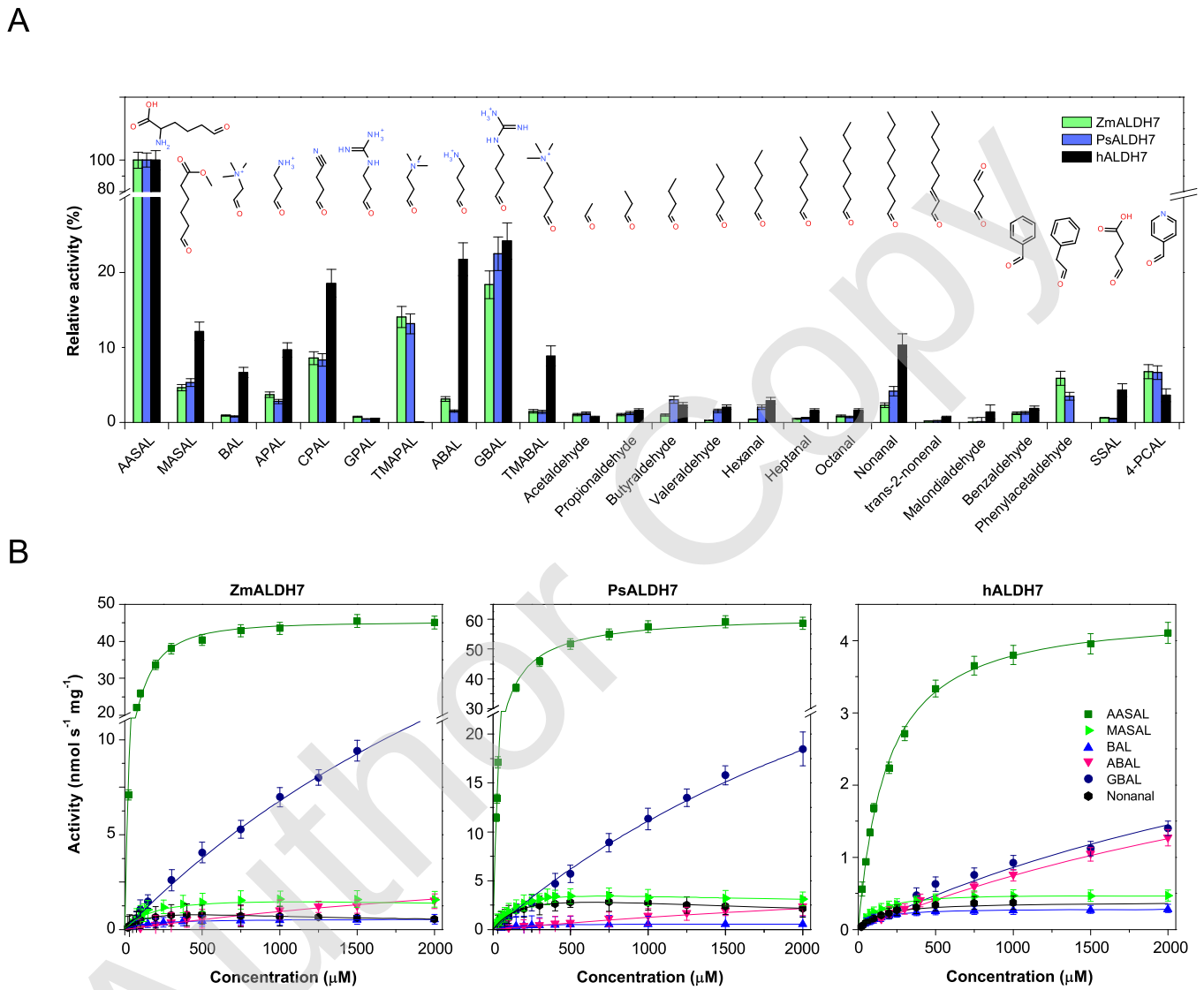

Figure 4 Screening of substrate specificity of ALDH7 isoforms

(**A**) Substrate specificity of maize, pea and human ALDH7. The measurements were performed with 1 mM substrates in 0.1 M sodium pyrophosphate buffer, pH 8.0, containing 2.5 mM NAD^+. The activity with AASAL was arbitrarily taken as 100 %. Error bars stand for S.D. Specific activity values measured with 1.0 mM AASAL as a substrate were 43.5, 57.5 and 3.8 nkat mg^{-1} for ZmALDH7, PsALDH7 and hALDH7 respectively. (**B**) Saturation curves for activity determination of ZmALDH7, PsALDH7 and hALDH7. The data were measured under the same conditions as above and are shown for selected substrates including α- AASAL, MASAL, ABAL, BAL, GBAL and nonanal.

preferentially oxidize AASAL (Figure 4A). The K_m values of 90 μM for ZmALDH7 and PsALDH7 and 170 μM for hALDH7 are in agreement with those previously found for seabream ALDH7 (67 μM) and hALDH7 (169 μM) [17,39]. MASAL is a much weaker substrate. Interestingly, both plant enzymes have narrower substrate specificity and higher specific activities compared with hALDH7 (45 compared with 4 nkat mg^{-1}). Indeed, natural ω-aminoaldehydes, such as BAL, APAL, ABAL, TMABAL and GBAL, are oxidized by hALDH7 with 10 %–25 % rates relative to that of AASAL, whereas only GBAL is similarly oxidized by plant enzymes. Aliphatic and aromatic aldehydes, as well as succinic semialdehyde (SSAL), are rather weak substrates. AASAL is clearly the best substrate for all ALDH7 isoforms as shown by the catalytic efficiency values (Table 4; Figure 4B).

Our kinetic analysis shows a very weak activity with lipid peroxidation products *t*-2-hexenal, *t*-2-nonenal and malondialdehyde (Table 4; Figure 4B). Decreased malondialdehyde levels have been observed in soybean and *Arabidopsis* ALDH7 overexpressers upon a stress treatment [24,25] suggesting a decreased oxidative stress *in vivo*. In line with these observations, *aldh7* mutant rice seeds accumulated more malondialdehyde and a melanoidin pigment in the endosperm during seed storage and desiccation [26]. Later it was shown that the dark yellow pigment corresponds to oryzamutaic acids, which are products of AASAL polymerization [50–52]. Plant ADLH7 from rice and *Arabidopsis* are confined to the cytosol [25,26], in agreement with the cytosolic localization of a bifunctional lysine-ketoglutarate reductase/saccharopine dehydrogenase (LKR/SDH) [53,54], which catalyses the first reaction of the lysine catabolism pathway (saccharopine pathway) leading to AASAL and glutamate. In contrast, hALDH7 was found in the mitochondria, cytoplasm and nucleus [17,55] in line with the existence of two lysine catabolism pathways in humans: the saccharopine pathway localized in mitochondria and the pipecolate pathway predominantly

Table 4 Kinetic parameters of maize and pea ALDH7 for selected substrates

All K_m and k_{cat} values are given in μM and s^{-1} respectively. Kinetic constants were measured in 0.1 M sodium pyrophosphate buffer, pH 8.0, using saturating 2.5 mM NAD^+ concentration. The K_m value for NAD^+ and $NADP^+$ was measured at a fixed 1.5 mM concentration of AASAL. The symbol 'n.d.' stands for not determined.

	ZmALDH7			PsALDH7			hALDH7		
Ligand	K_m (μM)	k_{cat} (s^{-1})	k_{cat}/K_m ($M^{-1}s^{-1}$)	K_m (μM)	k_{cat} (s^{-1})	k_{cat}/K_m ($M^{-1}s^{-1}$)	K_m (μM)	k_{cat} (s^{-1})	k_{cat}/K_m ($M^{-1}s^{-1}$)
NAD^+	358 ± 24	2.68 ± 0.030	7.5×10^3	393 ± 21	3.46 ± 0.046	8.8×10^3	224 ± 28	0.256 ± 0.011	1.2×10^3
$NADP^+$	14017 ± 758	0.27 ± 0.008	2.0×10^1	12834 ± 988	0.17 ± 0.009	1.3×10^1	10645 ± 623	0.233 ± 0.009	2.2×10^1
AASAL	97 ± 7	2.56 ± 0.043	2.6×10^4	89 ± 3	3.32 ± 0.027	3.7×10^4	170 ± 9	0.242 ± 0.003	1.4×10^3
MASAL	126 ± 21	0.09 ± 0.004	7.1×10^2	147 ± 17	0.26 ± 0.009	1.8×10^3	127 ± 8	0.030 ± 0.001	2.4×10^2
GBAL	2767 ± 146	1.43 ± 0.029	5.2×10^2	2551 ± 159	2.22 ± 0.071	8.7×10^2	3103 ± 119	0.218 ± 0.004	7.0×10^1
BAL	120 ± 3	0.03 ± 0.001	2.5×10^2	111 ± 7	0.03 ± 0.001	2.9×10^2	105 ± 5	0.016 ± 0.001	1.6×10^2
ABAL	4371 ± 116	0.27 ± 0.005	6.3×10^1	5167 ± 162	0.46 ± 0.007	9.0×10^1	4339 ± 331	0.220 ± 0.016	5.0×10^1
APAL	1280 ± 59	0.15 ± 0.002	1.1×10^2	1698 ± 81	0.34 ± 0.007	2.0×10^2	1007 ± 81	0.038 ± 0.001	3.7×10^1
Hexanal	1805 ± 186	0.11 ± 0.005	6.1×10^1	1672 ± 61	0.14 ± 0.002	8.3×10^1	1477 ± 123	0.013 ± 0.002	8.5
t-2-Hexenal	1652 ± 96	0.09 ± 0.002	5.4×10^1	1580 ± 57	0.10 ± 0.002	6.6×10^1	1145 ± 55	0.010 ± 0.002	9.0
Nonanal	174 ± 14	0.07 ± 0.006	4.3×10^2	198 ± 15	0.25 ± 0.010	1.2×10^3	257 ± 12	0.030 ± 0.001	1.2×10^2
t-2-Nonenal	953 ± 89	0.008 ± 0.001	8.4	974 ± 74	0.009 ± 0.001	9.5	993 ± 103	0.003 ± 0.001	3.5
TMAPAL	4820 ± 334	1.54 ± 0.096	3.2×10^2	4656 ± 260	1.57 ± 0.049	3.4×10^2	n.d.	n.d.	n.d.
3-PCAL	437 ± 46	0.14 ± 0.005	3.2×10^2	231 ± 13	0.29 ± 0.004	1.3×10^3	n.d.	n.d.	n.d.
4-PCAL	537 ± 51	0.22 ± 0.007	4.1×10^2	321 ± 10	0.27 ± 0.005	8.3×10^2	n.d.	n.d.	n.d.

peroxisomal/cytosolic [56]. A mutation in *hALDH7* gene results in the accumulation of P6C (cyclic form of AASAL) inactivating pyridoxal 5′-phosphate (PLP) and leading to acute depletion of vitamin B6 [18].

A recent study on hALDH7 pointed out the importance of BAL activity for possible protection from hyperosmotic stress [17]. The oxidation of BAL, which originates from choline, leads to glycine betaine, a well-known osmolyte. In the present study, we demonstrate kinetically for the first time that the plant ALDH7 family possesses a significant AMADH activity as the enzymes oxidize GBAL, APAL and ABAL providing directly (or after a further conversion) the cytosolic osmoprotectants 4-guanidinobutyrate, β-alanine and γ-aminobutyric acid (GABA) respectively. GBAL is an intermediate in arginine catabolism and the released 4-guanidinobutyrate may be further hydrolysed by ureohydrolase to urea and GABA.

Crystal structures of ZmALDH2 and ZmALDH7

To understand the substrate specificity differences within and between ALDH2 and ALDH7 family members, we solved the crystal structures of RF2C (ZmALDH2-3), RF2F (ZmALDH2-6) and ZmALDH7 (Table 2). The asymmetric unit of RF2F crystal contains a tetramer, whereas those of RF2C and ZmALDH7 contain a dimer and two monomers, respectively. However, using the crystallographic symmetry, both RF2C and ZmALDH7 form a tetramer which is the active form in solution in accordance with results from gel permeation chromatography (molecular mass values of 214, 226 and 181 kDa for RF2C, RF2F and ZmALDH7 respectively). Each subunit within the tetramer adopts the characteristic ALDH fold consisting of a coenzyme-binding domain, a catalytic domain and an oligomerization domain. The entrances of the substrate channel and the coenzyme-binding site are located on opposite sides of the monomer. A conserved sodium ion, probably having a structural role, binds in the cavity close to the coenzyme-binding site. Monomers of RF2C and RF2F are very similar to each other (average RMSD of 0.7 Å) and a structural comparison using PDBeFold (http://www.ebi.ac.uk/msd-srv/ssm/) shows that they both resemble the mitochondrialhALDH2 with the lowest RMSD of 0.80–0.85 Å for PDB codes 1O02, 1NZZ, 1NZX and others [57] (Supplementary Figure S1). Both RF2C and RF2F tetramers are very similar to hALDH2 tetramer with average RMSD values of 1.2 and 1.0 Å for 1940 Cα atoms respectively. Subtle differences in the oligomerization arrangement can be observed.

A comparison of substrate channel residues in RF2C and RF2F however indicates significant differences as shown in Figures 5A and 5B. The substrate-binding site of RF2C is narrow and formed by an aromatic cluster composed of Tyr^{171}, Phe^{178}, Phe^{458}, Phe^{460} and Phe^{466} and also by several mainly nonpolar residues including Ile^{302}, Val^{304}, Thr^{174}, Met^{175} and Thr^{297}. In contrast, that of RF2F is much wider because of the presence of Val^{192} and Met^{477} at the position of the two aromatic residues Phe^{178} and Phe^{460} in RF2C. Indeed, Met^{477} side chain, which is shifted outwards by 3 Å, opens the cavity. Two more residues Ala^{316} and Glu^{495} (Ile^{302} and Met^{478} in RF2C) also contribute to the substrate channel broadening. The cavity width of RF2F clearly correlates with high K_m values for various substrates most probably due to weaker nonpolar interactions except for phenylacetaldehyde. RF2D and RF2E, which share 95 % sequence identity, do not differ in active site residues and thus have similar kinetic properties. A model of RF2E was made using RF2C structure as a template (Figure 5C). The substrate-binding site of RF2E contains Phe^{459} (Phe^{460} in RF2C) making the cavity as narrow as in RF2C. Nevertheless, the cavity is slightly wider in the opposite direction because of the presence of Leu^{177} at the position of Phe^{178} in RF2C. Finally, only RF2C contains a threonine at position 297, whereas the other three maize isoforms contain a phenylalanine at the equivalent position. This threonine, which occupies less space, might have a role in substrate-binding plasticity and specificity by allowing the side chain of Tyr^{171} (equivalent to a phenylalanine in other maize isoforms) to move and facilitate substrate accommodation.

A sequence alignment of substrate channel residues in ALDH2C members (Figure 5D) reveals a high variability that allows various isoforms within one species oxidizing several different substrates from multiple pathways. Recently, maize *RF2C* gene was found to be induced in elongating internodes containing cells which exhibit primary cell wall biosynthesis, compared with non-elongating internodes with cells depositing

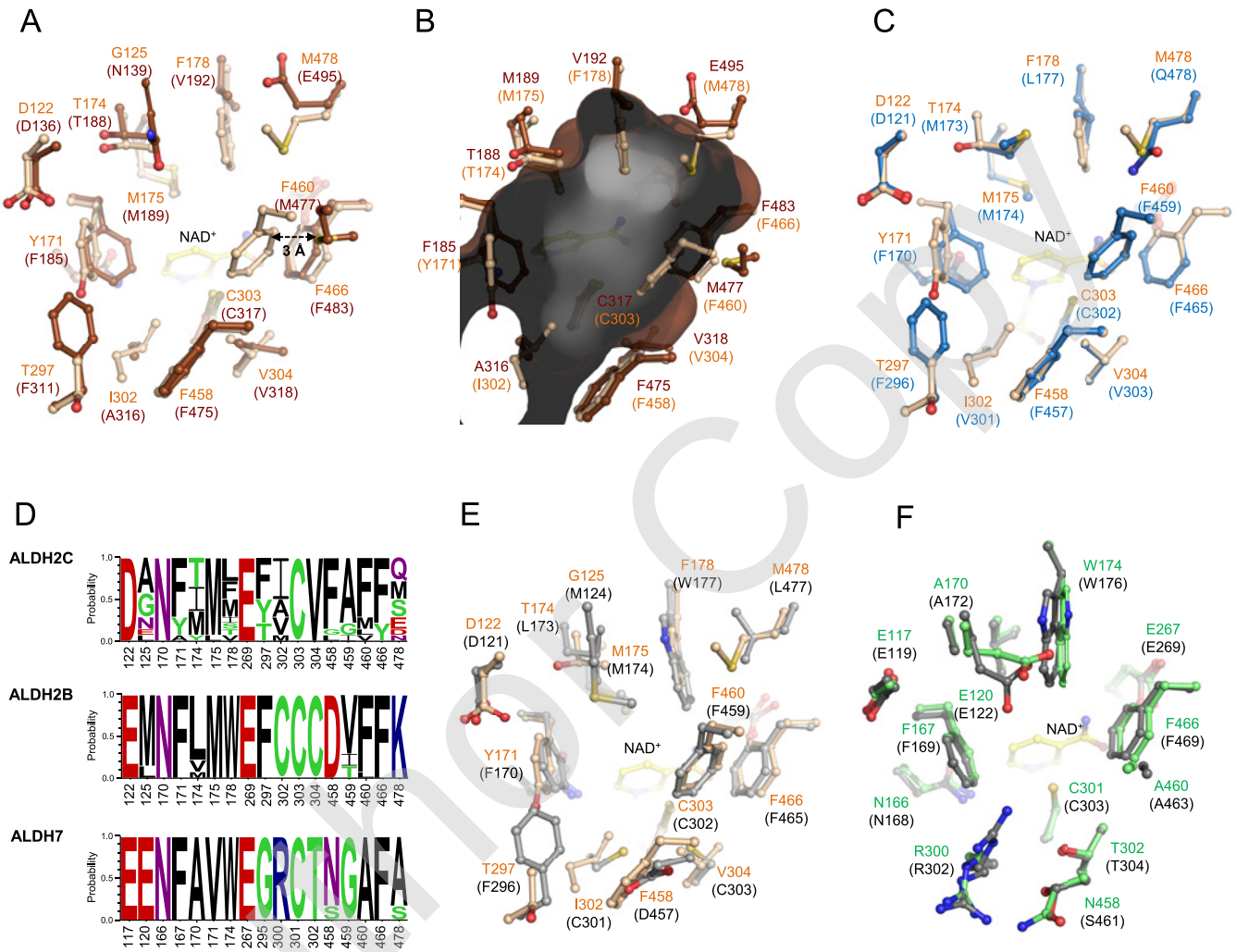

Figure 5 Composition of maize ALDH2 and ALDH7 active sites

(**A**) A view from the top on substrate channels of maize RF2C (light brown, present work) and RF2F (dark brown, present work). Residues of RF2C labelled in orange and those of RF2F are shown in brackets. (**B**) A transversal section of the substrate channel of RF2F. The inner surface is grey coloured (foreground is dark grey, background is light grey) and was calculated using Hollow with a 0.7 Å grid spacing and 1.2 Å interior probe. Residues are coloured in dark brown and labelled. Residues of RF2C (in light brown) are shown for comparison to indicate differences affecting diameter of the substrate channel. (**C**) Composition of the substrate channel in RF2E (blue). The model was made using SWISS-MODEL (http://swissmodel.expasy.org) and RF2C as a template. (**D**) An overview of conservation of amino acid residues forming the substrate channel in ALDH2 and ALDH7 families. Residues are numbered according to maize RF2C for ALDH2C and ALDH2B subfamilies and maize ALDH7 for ALDH7 family. Sequence logos were made using WebLogo (http://weblogo.threeplusone.com). (**E**) Superposition of the substrate channels of maize RF2C (light brown) and hALDH2 (grey, PDB code 1NZX) used as a reference. Residues of hALDH2 are shown in brackets. (**F**) Superposition of the substrate channels of ZmAMADH7 (green, present work) and hALDH7 (grey, PDB code 2J6L) used as a reference. Residues of hALDH7 are shown in brackets.

secondary cell wall material [58]. In line with our kinetic results, all four maize cALDH2 isoforms seem to be involved in the oxidation of coniferaldehyde and sinapaldehyde and formation of ferulic and sinapinic acids and their cell wall-linked esters similarly to ALDH2C in *Arabidopsis* and oilseed rape [15,16]. However, in the phenylpropanoid pathway, there are several other aldehydes involved including for example cinnamaldehyde, *p*-coumaryladehyde, caffeyaldehyde or 5-hydroxyconiferaldehyde. Because the last three hydroxy derivatives are not available, they could not be analysed although they probably belong to *in vivo* substrates.

In contrast, plant mtALDH2 isoforms including RF2A and RF2B share a conserved active site and are highly similar to hALDH2 (Figure 5D). Their sequences contain a triple cysteine motif including the catalytic cysteine. Although *in vivo* the preferred substrate of hALDH2 is acetaldehyde, the enzyme has been shown to oxidize various aliphatic and aromatic aldehydes, especially hexanal, phenylacetaldehyde or benzaldehyde [4]. Likewise, RF2A, but not RF2B, is in addition to acetaldehyde also highly active with benzaldehyde and cinnamaldehyde [9]. MtALDH2 from snapdragon was found to have the highest catalytic efficiency with acetaldehyde but *in vivo* it has been linked to oxidation of benzaldehyde to benzoate in flowers leading to emission of high levels of methylbenzoate and benzylbenzoate in floral scent [14].

ZmALDH7 monomer resembles that of humans and seabream (PDB codes 2J6L and 2JG7) with RMSDs of 0.72 and 0.74 Å respectively (Supplementary Figure S1). The major difference between ZmADLH7 and ZmALDH2 monomers (RMSD of 1.3–1.4 Å for 465 Cα atoms) comes from a slight shift in the oligomerization domain and the presence of an N-terminal helix in ZmALDH7 (Supplementary Figure S1). The tetramer

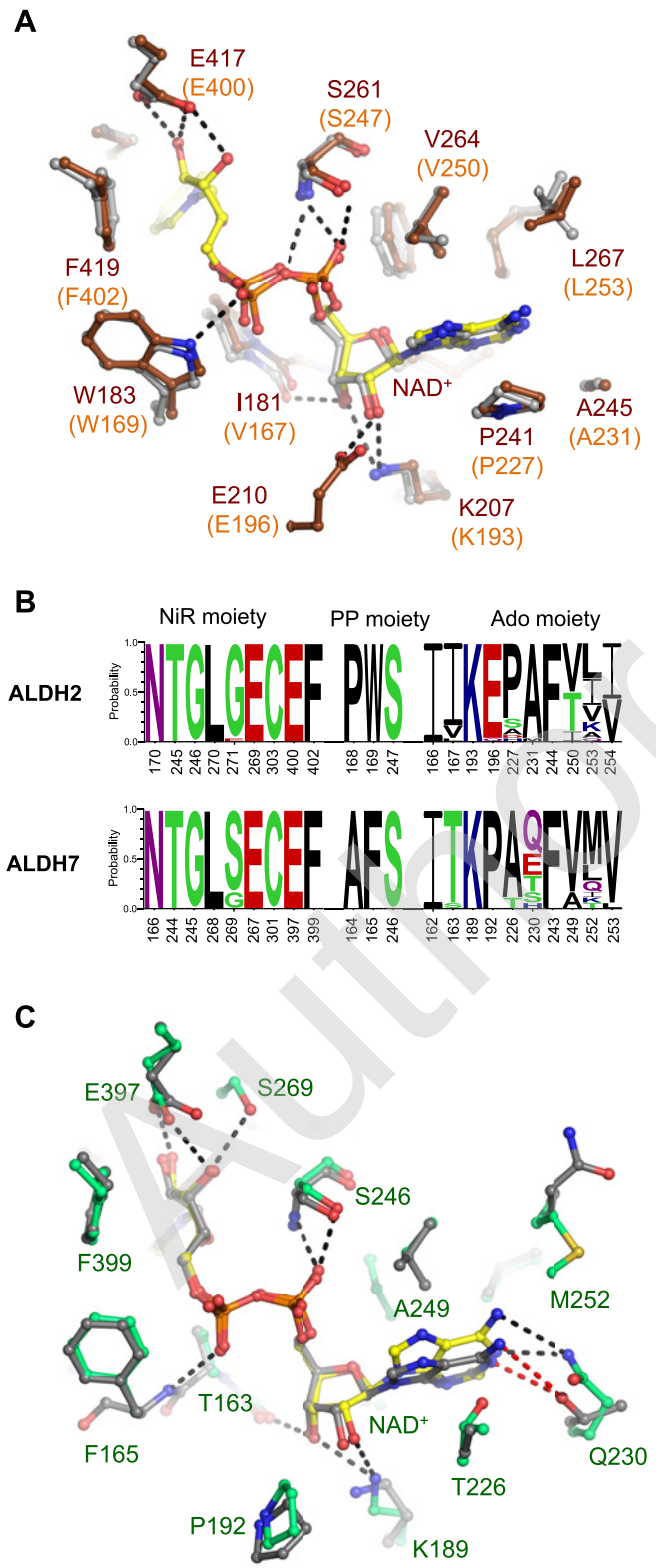

Figure 6 NAD$^+$ binding in ALDH2 and ALDH7 family

(**A**) Superposition of NAD$^+$-binding sites of maize RF2F (ZmALDH2-6, dark brown colour, present work) and hALDH2 (grey colour). Residues are labelled and numbered according to RF2F sequence; those of RF2C are shown in orange and brackets. (**B**) An overview of conservation of amino acid residues relevant for NAD$^+$ binding in ALDH2 and ALDH7 families. Residues are split into three clusters for NiR, diphosphate and Ado moiety of NAD$^+$ molecule and are numbered according to maize RF2C and ALDH7 sequence respectively. Sequence logos were made using WebLogo (http://weblogo.threeplusone.com). (**C**) Superposition of NAD$^+$-binding sites of maize ALDH7 (green colour, present work) and hALDH7 (grey colour). Residues in the vicinity of NAD$^+$ are labelled and numbered according to ZmALDH7 sequence. Those in human enzymes are grey coloured as a reference. NAD$^+$ molecules adopting the extended conformation are shown in yellow and atom-coded colour sticks.

of ZmALDH7 slightly differs from both ZmALDH2 tetramers with an average RMSD value of 2.4 Å. Their active site residues are almost identical indicating that these enzymes have the same cellular role in plants, mammals or fish using AASAL as the preferred substrate confirmed by our kinetic data. The three residues Glu^{120}, Arg^{300} and Thr^{302} located in the substrate-binding site of ZmALDH7 are conserved and specific to the ALDH7 family (Figure 5F). The role of Glu^{120} and Arg^{300} has been validated by mutagenesis studies on seabream ALDH7 and hALDH7 [39,59] suggesting that Glu^{120} binds the α-amino group of AASAL, whereas Arg^{300} binds its carboxylate group. The role of Thr^{302} has not been investigated by mutagenesis yet. However, visual inspection of ZmALDH7 active site together with manual modelling shows that this residue may interact with Arg^{300} in the binding of AASAL carboxylate side chain. Our kinetic analysis shows that AASAL and MASAL have similar K_m values but the k_{cat} value for MASAL is about 2-fold lower indicating that protonated amino group of the substrate (and interaction with Glu^{120}) is needed to achieve a high reaction rate. High K_m values for aminoaldehydes GBAL (~2.5 mM) and ABAL (~4.5 mM) indicate that the carboxy group (and interaction with Arg^{300} and Thr^{302}) is necessary to maintain low K_m values.

Coenzyme-binding sites in ZmALDH2 and ZmALDH7

In all ZmALDH2 monomers, a NAD$^+$ molecule is well defined in the electron density maps (Supplementary Figure S1). In RF2F structure, the coenzyme adopts an extended conformation typically observed for oxidized NAD$^+$ and the catalytic cysteine Cys^{317} is oriented towards the substrate channel (attacking conformation). In RF2C structure, it adopts a contracted conformation most probably due to the high concentration of calcium ions present in the crystallization conditions. A calcium ion binds to the pyrophosphate oxygen atoms O1N and O2A of the NAD$^+$ molecule in subunit A. An equivalent magnesium ion bound to the contracted coenzyme was previously observed in the hALDH2 structure (PDB code 1NZZ) [57] and it was shown that the presence of magnesium ions may select particular conformations of the coenzyme. The catalytic cysteine Cys^{303} is again in the attacking conformation and in subunit A it is oxidized into sulfenic acid [*S*-(hydroxy)cysteine].

The adenine moiety of NAD$^+$ lies in a hydrophobic pocket flanked by two helices with no polar contacts. In contrast, the ribose, both α and β-phosphates and the nicotinamide riboside (NiR) moiety of NAD$^+$ make several protein interactions identical to those observed for NAD$^+$ binding in hALDH2 (Figure 6A) as well as in plant ALDH10. Therefore, RF2C, RF2D, RF2E, RF2F, hALDH2 and ALDH10 display similar K_m values for NAD$^+$ (~10^{-5} μM) [27,29,60]. These enzymes are NAD$^+$ specific because they possess a conserved glutamate (Glu^{196} in RF2C, Glu^{210} in RF2F) preventing the binding of the 2′-phosphate group of NADP$^+$. Indeed, K_m values of 3.0, 1.5, 1.4 and 1.7 mM for NADP$^+$ with RF2C, RF2D, RF2E and RF2F respectively are ~20–70 times higher than those for NAD$^+$ and the reaction rates appear between 0.5 %–9 % of those with NAD$^+$. Catalytic efficiency values for NADP$^+$ are about 2-fold lower (with RF2C more than 3-fold lower) than those for NAD$^+$. Thus, NADP$^+$

does not function as an effective coenzyme in the plant ALDH2 family. A recent mutagenesis study on this conserved glutamate residue confirmed its importance for NAD^+ specificity in the plant ALDH3 family [61]. Figure 6B presents an overview of residues forming the NAD^+-binding site and their frequency. Notably, the residues involved in adenosine moiety (Ado) binding of NAD^+ are highly variable.

Although the coenzyme-binding site in ZmALDH7 slightly differs in residue composition from that of ALDH2 family and of hALDH7, a NAD^+ molecule present in each ZmALDH7 monomer adopts the extended conformation with the catalytic Cys^{301} in the attacking conformation and most of the important protein interactions conserved. Indeed, Phe^{165} in ZmALDH7 equivalent to Phe^{167} in hALDH7 is bound to the β-phosphate oxygen atom via its main chain NH atom restoring the direct interaction between the side chain of the tryptophan residue and the β-phosphate in both ALDH2 and ALDH10 families (Trp^{169} and Trp^{183} in RF2C and RF2F; Figure 6C). Ser^{269} in ZmALDH7 (glycine in ZmALDH2) makes an additional interaction with the O3D atom of the NiR moiety whereas hALDH7 and ALDH2 enzymes possess a glycine at the equivalent position. The conserved glutamate in ALDH2 (Glu^{196} in RF2C) and ALDH10, which prevents binding of the 2′-phosphate group of $NADP^+$, is replaced by a proline in ALDH7 family (Pro^{192} in ZmALDH7). This proline also makes a steric hindrance to 2′-phosphate of $NADP^+$ as reflected in the K_m value of 14 mM (40 times higher than that for NAD^+) and the reaction rate, which is only 0.5 % of that measured with NAD^+ and ZmALDH7. The major difference between ZmALDH7 and hALDH7 or ALDH2 concerns the adenine position of NAD^+. Indeed, the adenine adopts a different position in ZmALDH7 because of the presence of Thr^{226} side chain (alanine in hALDH7 and proline in ALDH2), which pushes the adenine ring up to 1 Å towards Ala^{249} (Figure 6C). The presence of the couple Tre^{226}–Ala^{249} appears only in a small subgroup of monocots including maize, whereas most ALDH7 family members carry a conserved alanine–valine couple (Ala–Val^{250} in hALDH7) at the corresponding positions. In ALDH7 family, adenine makes one polar interaction between its N1 atom and a glutamate, glutamine, serine, threonine or histidine. All the above differences contribute by one order of magnitude to the higher K_m values for NAD^+ of ZmALDH7 and PsALDH7 compared with those of ALDH2 and ALDH10 family members. Consequently, a higher saturating concentration of NAD^+ was used for kinetic measurements.

Expression of *ALDH2* and *ALDH7* genes in maize

First we analysed the expression pattern of ALDH2 and ALDH7 genes in developing maize seedlings (stem, roots and leaves) during the first two weeks after germination (Figure 7). *RF2C* is highly expressed compared with the five other *ALDH2* genes with a strong and comparable transcript levels in leaves and roots but lower in stem. *RF2A* was preferentially expressed in leaves, whereas *RF2B* was preferentially expressed in roots and less in leaves. Transcripts of *RF2D* and *RF2E* were the most abundant in roots, but almost absent from the stem, whereas *RF2F* transcripts appeared especially in the stem of 2-week-old seedlings. The highest levels of *ZmALDH7* transcripts were found in leaves.

The pattern of gene expression in older plants, in tassels, silks and kernels was also analysed. Again, *RF2C* is the most expressed *ALDH2* gene in maize. *RF2B*, *RF2C* and *ZmALDH7* are highly abundant in tassels at 5 days before pollination (DBP) and 0 days after pollination (DAP) suggesting their important role in pollen development. In silks, gene expression was lower compared with that in tassels. Relatively high levels of *RF2A*, *RF2B*, *RF2C* and *RF2F* transcripts appear in silks at 6 DAP. In kernel, we detected a strong expression of *RF2B* and *RF2C* followed by *RF2D* and *RF2F*. *RF2A* expression was highest in silks at 6 DAP and kernels at 20 DAP, whereas those of *RF2B*, *RF2C* and *ZmALDH7* were strongest in tassels. The *RF2D* transcripts accumulated in mature leaves, whereas the *RF2E* gene was significantly expressed only in the embryo. The *FR2F* gene was strongly expressed in the stem and main root. The strong expression of *ZmALDH7* in kernel, tassels and silks correlates well with a strong expression of *LKR/SDH* gene observed in maize endosperm [53] and in floral organs of *Arabidopsis* [62] suggesting an active saccharopine pathway in developing seeds and in reproductive organs containing actively dividing cells.

Several expression studies on the plant *ALDH* gene superfamily, including rice and foxtail millet, show that many *ALDH2* genes are induced by abiotic stressors, but some may also be down-regulated [22,23]. Indeed, *OsALDH2B5* gene was found up-regulated by submergence, drought and salinity stresses, whereas the *OsALDH2C2* gene is down-regulated by drought and salinity stresses [11,22]. Interestingly, a gene coding for mtALDH2 in Chinese wild grapevine *Vitis pseudoreticulata* (VpALDH2B4) [63] is induced by pathogens. Transgenic *35S:VpALDH2B4* plants are more resistant to a downy mildew, powdery mildew and salt stress. This all indicates that in addition to *in vivo* acetaldehyde, benzaldehyde and coniferaldehyde/sinapaldehyde dehydrogenase activities, plant ALDH2 members might be involved in the detoxification of aldehydes produced upon stress like *t*-2-hexenal and *t*-2-nonenal. Indeed, hexanal and *t*-2-nonenal, lipid peroxidation products [64], are among the best substrates for RF2C and when comparing k_{cat}/K_m values, ALDH2C isoforms show much higher catalytic efficiencies with these aldehydes than ALDH7 (Tables 3 and 4).

Phenolamides (hydroxycinnamic acid amides), known to contribute to cell-wall cross-linking, are composed of coumaric, caffeic and ferulic acids fused to either aryl monoamines (tyramine, tryptamine or others) or polyamines (putrescine and spermidine) [65,66]. They accumulate in reproductive organs of many plants, as well as during stress, in order to function as inducible defence against insect herbivory [67]. The accumulation is mainly associated with flower initiation and development and di- and tri-substituted hydroxycinnamoyl conjugates are found in pollen grains in anthers. Male sterility was previously linked to the absence of phenolamides in maize anthers [68]. In *Arabidopsis*, several genes involved in phenolamide biosynthesis are highly expressed in tapetal cells of anthers and major metabolites in pollen coat were identified as N^1,N^5,N^{10}-trihydroxyferuloyl spermidine and N^1,N^5-di(hydroxyferuloyl)-N^{10}-sinapoyl spermidine [69–71]. The *RF2A* gene, originally found to restore fertility to Texas cytoplasmic male sterility maize lines, is highly abundant in tapetal cells and important for the anther development [7,8]. We may hypothesize that fertility restoration linked to RF2A is because of the changes in phenolamide biosynthesis. As other cALDH2 isoforms also oxidize coniferaldehyde and sinapaldehyde, they might contribute to the biosynthesis of phenolamides in various plant organs as well as during stress conditions.

CONCLUSIONS

In the present work, we studied maize and pea ALDH7 and compared their kinetics with that of human ALDH7. Based on our kinetic and structural results, we can conclude now that a high conservation of the *ALDH7* gene during evolution is linked to the substrate preference of ALDH7 for AASAL in accordance

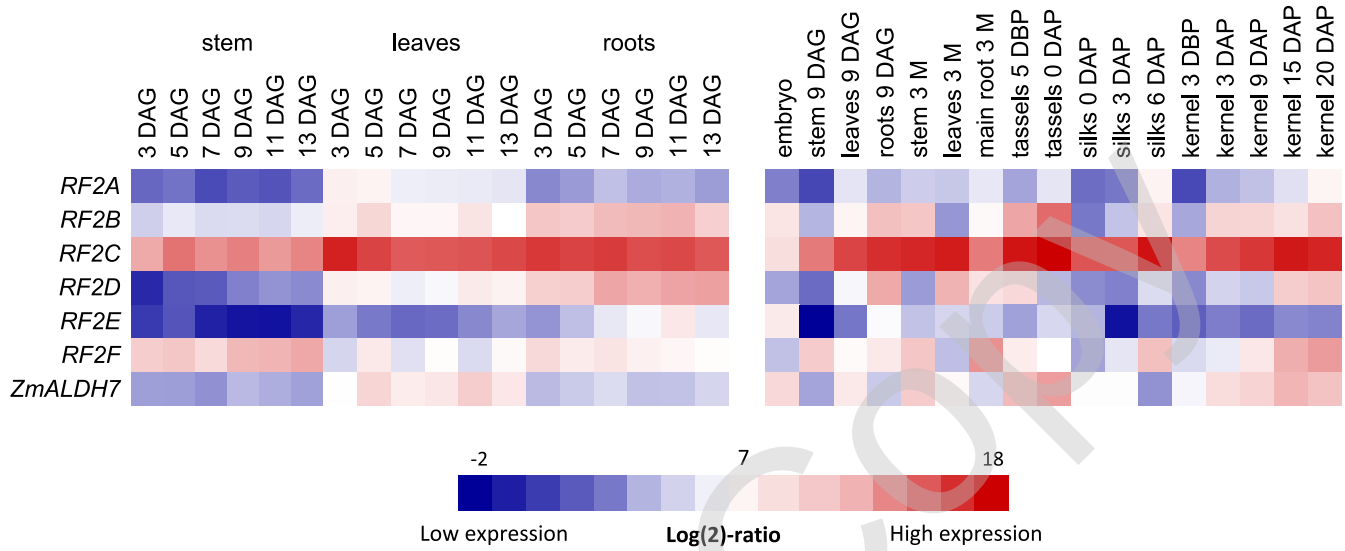

Figure 7 Expression profiles of *ZmALDH2* and *ZmALDH7* genes

Gene expression was studied in stem, leaves and roots during 2 weeks after germination (left side) and in various organs during the lifespan of maize plants (right side). The heat map illustrates transcript levels detected in 1 ng of total RNA. All values are expressed as $\log_2$-ratios and are colour-coded from blue to red (the lowest and highest detected transcript numbers, respectively). DAG, days after germination; M, months.

with conservation of the active site of ADLH7 across species. In contrast, maize ALDH2C isoforms show high preferences for benzenoid and phenylpropanoid aldehydes arising via the non-β-oxidative pathway from phenylalanine or via the phenylpropanoid pathway. The latter pathway is very complex and is a starting point for the production of many secondary metabolites, such as flavonoids, coumarins, monolignols (building blocks of lignin), phenolamides and others. Therefore, the ALDH2C subfamily displays a high variability in composition of the active site containing mainly aromatic and nonpolar residues in accordance with differences in phenylpropanoid pathway across species and different hydroxy and methoxy phenylpropanoid aldehydes arising from this pathway. Finally, ALDH2C isoforms may also contribute to the oxidation of 'lipid peroxidation' aldehydes, as well as to oxidation of aliphatic and aromatic aldehydes released after the oxidation of plant hormones cytokinins.

AUTHOR CONTRIBUTION

David Kopečný, Solange Moréra and Marek Šebela designed the research. Radka Končitíková, Tomáš Andree and David Kopečný analysed enzyme kinetics. Armelle Vigouroux and Solange Moréra performed the crystallographic study and contributed material and tools for crystallography. Radka Končitíková, Martina Kopečná and Jan Bartoš analysed gene expression. Solange Moréra and David Kopečný analysed the crystal structures. David Kopečný and Solange Moréra wrote the manuscript.

ACKNOWLEDGEMENTS

We acknowledge SOLEIL for provision of synchrotron radiation facilities (proposal ID 20130869) in using beamlines Proxima 1 and Proxima 2. The present work benefitted from IMAGIF platform facilities (http://www.imagif.cnrs.fr) at the Centre de Recherche de Gif-sur-Yvette (FRC3115, CNRS) for crystallization work. We thank William Shepard for a critical reading of the manuscript.

FUNDING

This work was supported by the Czech Science Foundation [grant number 15-22322S]; the National Program of Sustainability I (the Ministry of Education, Youth and Sports, Czech Republic) [grant number LO1204]; and the CNRS (to S.M. and A.V)].

REFERENCES

1 Yoshida, A., Rzhetsky, A., Hsu, L. C. and Chang, C. (1998) Human aldehyde dehydrogenase gene family. Eur. J. Biochem. **251**, 549–557 CrossRef PubMed
2 Vasiliou, V., Bairoch, A., Tipton, K. F. and Nebert, D. W. (1999) Eukaryotic aldehyde dehydrogenase (ALDH) genes: human polymorphism, and recommended nomenclature based on divergent evolution and chromosomal mapping. Pharmacogenetics **9**, 421–434 CrossRef PubMed
3 Brocker, C., Vasiliou, M., Carpenter, S., Carpenter, C., Zhang, Y., Wang, X., Kotchoni, S. O., Wood, A. J., Kirch, H. H., Kopečný, D. et al. (2013) Aldehyde dehydrogenase (ALDH) superfamily in plants: gene nomenclature and comparative genomics. Planta **237**, 189–210 CrossRef PubMed
4 Klyosov, A. A. (1996) Kinetics and specificity of human liver aldehyde dehydrogenases toward aliphatic, aromatic, and fused polycyclic aldehydes. Biochemistry **35**, 4457–4467 CrossRef PubMed
5 Steinmetz, C. G., Xie, P., Weiner, H. and Hurley, T. D. (1997) Structure of mitochondrial aldehyde dehydrogenase: the genetic component of ethanol aversion. Structure **5**, 701–711 CrossRef PubMed
6 Ni, L., Zhou, J., Hurley, T. D. and Weiner, H. (1999) Human liver mitochondrial aldehyde dehydrogenase: three-dimensional structure and the restoration of solubility and activity of chimeric forms. Protein Sci. **8**, 2784–2790 CrossRef PubMed
7 Cui, X., Wise, R. P. and Schnable, P. S. (1996) The rf2 nuclear restorer gene of male-sterile T-cytoplasm maize. Science **272**, 1334–1336 CrossRef PubMed
8 Liu, F., Cui, X., Horner, H. T., Weiner, H. and Schnable, P. S. (2001) Mitochondrial aldehyde dehydrogenase activity is required for male fertility in maize. Plant Cell **13**, 1063–1078 CrossRef PubMed
9 Liu, F. and Schnable, P. S. (2002) Functional specialization of maize mitochondrial aldehyde dehydrogenases. Plant Physiol. **130**, 1657–1674 CrossRef PubMed
10 Skibbe, D. S., Liu, F., Wen, T. J., Yandeau, M. D., Cui, X., Cao, J., Simmons, C. R. and Schnable, P. S. (2002) Characterization of the aldehyde dehydrogenase gene families of *Zea mays* and *Arabidopsis*. Plant Mol. Biol. **48**, 751–764 CrossRef PubMed
11 Nakazono, M., Tsuji, H., Li, Y., Saisho, D., Arimura, S., Tsutsumi, N. and Hirai, A. (2000) Expression of a gene encoding mitochondrial aldehyde dehydrogenase in rice increases under submerged conditions. Plant Physiol. **124**, 587–598 CrossRef PubMed
12 op den Camp, R. G. and Kuhlemeier, C. (1997) Aldehyde dehydrogenase in tobacco pollen. Plant Mol. Biol. **35**, 355–365 CrossRef PubMed
13 Wei, Y., Lin, M., Oliver, D. J. and Schnable, P. S. (2009) The roles of aldehyde dehydrogenases (ALDHs) in the PDH bypass of *Arabidopsis*. BMC Biochem. **10**, 7 CrossRef PubMed

14 Long, M. C., Nagegowda, D. A., Kaminaga, Y., Ho, K. K., Kish, C. M., Schnepp, J., Sherman, D., Weiner, H., Rhodes, D. and Dudareva, N. (2009) Involvement of snapdragon benzaldehyde dehydrogenase in benzoic acid biosynthesis. Plant J. **59**, 256–265 CrossRef PubMed

15 Nair, R. B., Bastress, K. L., Ruegger, M. O., Denault, J. W. and Chapple, C. (2004) The *Arabidopsis thaliana* REDUCED EPIDERMAL FLUORESCENCE1 gene encodes an aldehyde dehydrogenase involved in ferulic acid and sinapic acid biosynthesis. Plant Cell **16**, 544–554 CrossRef PubMed

16 Mittasch, J., Böttcher, C., Frolov, A., Strack, D. and Milkowski, C. (2013) Reprogramming the phenylpropanoid metabolism in seeds of oilseed rape by suppressing the orthologs of reduced epidermal fluorescence1. Plant Physiol. **161**, 1656–1669 CrossRef PubMed

17 Brocker, C., Lassen, N., Estey, T., Pappa, A., Cantore, M., Orlova, V., Chavakis, T., Kavanagh, K. L., Oppermann, U. and Vasiliou, V. (2010) Aldehyde dehydrogenase 7A1 (ALDH7A1) is a novel enzyme involved in cellular defense against hyperosmotic stress. J. Biol. Chem. **285**, 18452–18463 PubMed

18 Mills, P. B., Struys, E., Jakobs, C., Plecko, B., Baxter, P., Baumgartner, M., Willemsen, M. A., Omran, H., Tacke, U., Uhlenberg, B., Weschke, B. and Clayton, P. T. (2006) Mutations in antiquitin in individuals with pyridoxine-dependent seizures. Nat. Med. **12**, 307–309 CrossRef PubMed

19 Guerrero, F. D., Jones, J. T. and Mullet, J. E. (1990) Turgor-responsive gene transcription and RNA levels increase rapidly when pea shoots are wilted. Sequence and expression of three inducible genes. Plant Mol. Biol. **15**, 11–26 CrossRef PubMed

20 Stroeher, V. L., Boothe, J. G. and Good, A. G. (1995) Molecular cloning and expression of a turgor-responsive gene in *Brassica napus*. Plant Mol. Biol. **27**, 541–551 CrossRef PubMed

21 Kirch, H. H., Schlingensiepen, S., Kotchoni, S., Sunkar, R. and Bartels, D. (2005) Detailed expression analysis of selected genes of the aldehyde dehydrogenase (ALDH) gene superfamily in *Arabidopsis thaliana*. Plant Mol. Biol. **57**, 315–332 CrossRef PubMed

22 Gao, C. and Han, B. (2009) Evolutionary and expression study of the aldehyde dehydrogenase (ALDH) gene superfamily in rice (*Oryza sativa*). Gene **431**, 86–94 CrossRef PubMed

23 Zhu, C., Ming, C., Zhao-Shi, X., Lian-Cheng, L., Xue-Ping, C. and You-Zhi, M. (2014) Characteristics and expression patterns of the aldehyde dehydrogenase (ALDH) gene superfamily of foxtail millet (*Setaria italica* L.). PLoS One **9**, e101136 CrossRef PubMed

24 Rodrigues, S. M., Andrade, M. O., Gomes, A. P., Damatta, F. M., Baracat-Pereira, M. C. and Fontes, E. P. (2006) Arabidopsis and tobacco plants ectopically expressing the soybean antiquitin-like ALDH7 gene display enhanced tolerance to drought, salinity, and oxidative stress. J. Exp. Bot. **57**, 1909–1918 CrossRef PubMed

25 Kotchoni, S. O., Kuhns, C., Ditzer, A., Kirch, H. H. and Bartels, D. (2006) Over-expression of different aldehyde dehydrogenase genes in *Arabidopsis thaliana* confers tolerance to abiotic stress and protects plants against lipid peroxidation and oxidative stress. Plant Cell Environ. **29**, 1033–1048 CrossRef PubMed

26 Shin, J. H., Kim, S. R. and An, G. (2009) Rice aldehyde dehydrogenase 7 is needed for seed maturation and viability. Plant Physiol. **149**, 905–915 CrossRef PubMed

27 Tylichová, M., Kopečný, D., Moréra, S., Briozzo, P., Lenobel, R., Snégaroff, J. and Šebela, M. (2010) Structural and functional characterization of plant aminoaldehyde dehydrogenase from *Pisum sativum* with a broad specificity for natural and synthetic aminoaldehydes. J. Mol. Biol. **396**, 870–882 CrossRef PubMed

28 Kopečný, D., Tylichová, M., Snegaroff, J., Popelková, H. and Šebela, M. (2011) Carboxylate and aromatic active-site residues are determinants of high-affinity binding of ω-aminoaldehydes to plant aminoaldehyde dehydrogenases. FEBS J. **278**, 3130–3139 CrossRef PubMed

29 Kopečný, D., Končitíková, R., Tylichová, M., Vigouroux, A., Moskalíková, H., Soural, M., Šebela, M. and Moréra, S. (2013) Plant ALDH10 family: identifying critical residues for substrate specificity and trapping a thiohemiacetal intermediate. J. Biol. Chem. **288**, 9491–9507 CrossRef PubMed

30 Sophos, N. A., Pappa, A., Ziegler, T. L. and Vasiliou, V. (2001) Aldehyde dehydrogenase gene superfamily: the 2000 update. Chem.-Biol. Interact. **130–132**, 323–337 CrossRef

31 Huang, X. and Miller, W. (1991) A time-efficient linear-space local similarity algorithm. Adv. Appl. Math. **12**, 337–357 CrossRef

32 Šebela, M., Brauner, F., Radová, A., Jacobsen, S., Havliš, J., Galuszka, P. and Peč, P. (2000) Characterisation of a homogeneous plant aminoaldehyde dehydrogenase. Biochim. Biophys. Acta **1480**, 329–341 PubMed

33 Vaz, F. M., Fouchier, S. W., Ofman, R., Sommer, M. and Wanders, R. J. (2000) Molecular and biochemical characterization of rat γ-trimethylaminobutyraldehyde dehydrogenase and evidence for the involvement of human aldehyde dehydrogenase 9 in carnitine biosynthesis. J. Biol. Chem. **275**, 7390–7394 CrossRef PubMed

34 Trossat, C., Rathinasabapathi, B. and Hanson, A. D. (1997) Transgenically expressed betaine aldehyde dehydrogenase efficiently catalyzes oxidation of dimethylsulfoniopropionaldehyde and -aminoaldehydes. Plant Physiol. **113**, 1457–1461 PubMed

35 Kabsch, W. (2010) XDS. Acta Crystallogr. D Biol. Crystallogr. **66**, 125–132 CrossRef

36 Karplus, P. A. and Diederichs, K. (2012) Linking crystallographic model and data quality. Science **336**, 1030–1033 CrossRef PubMed

37 Diederichs, K. and Karplus, P. A. (2013) Better models by discarding data? Acta Crystallogr. D Biol. Crystallogr. **69**, 1215–1222 CrossRef

38 Storoni, L. C., McCoy, A. J. and Read, R. J. (2004) Likelihood-enhanced fast rotation functions. Acta Crystallogr. D Biol. Crystallogr. **60**, 432–438 CrossRef

39 Tang, W. K., Wong, K. B., Lam, Y. M., Cha, S. S., Cheng, C. H. and Fong, W. P. (2008) The crystal structure of seabream antiquitin reveals the structural basis of its substrate specificity. FEBS Lett. **582**, 3090–3096 CrossRef PubMed

40 Bricogne, G., Blanc, E., Brandl, M., Flensburg, C., Keller, P., Paciorek, W., Roversi, P, Sharff, A., Smart, O. S., Vonrhein, C. and Womack, T. O. (2011), In BUSTER version 2.1.0. Global Phasing Ltd., Cambridge, United Kingdom

41 Emsley, P. and Cowtan, K. (2004) Coot: model-building tools for molecular graphics. Acta Crystallogr. D Biol. Crystallogr. **60**, 2126–2132 CrossRef PubMed

42 Arnold, K., Bordoli, L., Kopp, J. and Schwede, T. (2006) The SWISS-MODEL Workspace: a web-based environment for protein structure homology modelling. Bioinformatics **22**, 195–201 CrossRef PubMed

43 Edgar, R. C. (2004) MUSCLE: multiple sequence alignment with high accuracy and high throughput. Nucleic Acids Res. **32**, 1792–1797 CrossRef PubMed

44 Castresana, J. (2000) Selection of conserved blocks from multiple alignments for their use in phylogenetic analysis. Mol. Biol. Evol. **17**, 540–552 CrossRef PubMed

45 Guindon, S. and Gascuel, O. (2003) A simple, fast, and accurate algorithm to estimate large phylogenies by maximum likelihood. Syst. Biol. **52**, 696–704 CrossRef PubMed

46 Chen, X., Zeng, Q. and Wood, A. J. (2002) Aldh7B6 encodes a turgor-responsive aldehyde dehydrogenase homologue that is constitutively expressed in *Tortula ruralis* gametophytes. Bryologist **105**, 177–184 CrossRef

47 Dudareva, N., Klempien, A., Muhlemann, J. K. and Kaplan, I. (2013) Biosynthesis, function and metabolic engineering of plant volatile organic compounds. New Phytol. **198**, 16–32 CrossRef PubMed

48 Kopečný, D., Pethe, C., Šebela, M., Houba-Hérin, N., Madzak, C., Majira, A. and Laloue, M. (2005) High-level expression and characterization of *Zea mays* cytokinin oxidase/dehydrogenase in *Yarrowia lipolytica*. Biochimie **87**, 1011–1022 CrossRef PubMed

49 Boatright, J., Negre, F., Chen, X., Kish, C. M., Wood, B., Peel, G., Orlova, I., Gang, D., Rhodes, D. and Dudareva, N. (2004) Understanding *in vivo* benzenoid metabolism in petunia petal tissue. Plant Physiol. **135**, 1993–2011 CrossRef PubMed

50 Shen, Y., Zhang, Y., Yang, C., Lan, Y., Liu, L., Liu, S., Chen, Z., Ren, G. and Wan, J. (2012) Mutation of OsALDH7 causes a yellow-colored endosperm associated with accumulation of oryzamutaic acid A in rice. Planta **235**, 433–441 CrossRef PubMed

51 Nakano, H., Kosemura, S., Suzuki, T., Hirose, K., Kaji, R. and Sakai, M. (2009) Oryzamutaic acid A, a novel yellow pigment from an *Oryza sativa* mutant with yellow endosperm. Tetrahedron Lett. **50**, 2003–2005 CrossRef

52 Nakano, H., Kosemura, S., Yoshida, M., Suzuki, T., Iwaura, R., Kaji, R., Sakai, M. and Hirose, K. (2010) Oryzamutaic acids B-G, new alkaloids from an *Oryza sativa* mutant with yellow endosperm. Tetrahedron Lett. **51**, 49–53 CrossRef

53 Kemper, E. L., Neto, G. C., Papes, F., Moraes, K. C., Leite, A. and Arruda, P. (1999) The role of opaque2 in the control of lysine-degrading activities in developing maize endosperm. Plant Cell **11**, 1981–1994 CrossRef PubMed

54 Zhu, X., Tang, G. and Galili, G. (2000) Characterization of the two saccharopine dehydrogenase isozymes of lysine catabolism encoded by the single composite AtLKR=AtLKR/SDH locus of Arabidopsis. Plant Physiol. **124**, 1363–1372 CrossRef PubMed

55 Wong, J. W., Chan, C. L., Tang, W. K., Cheng, C. H. and Fong, W. P. (2010) Is antiquitin a mitochondrial enzyme? J. Cell. Biochem. **109**, 74–81 PubMed

56 Hallen, A., Jamie, J. F. and Cooper, A. J. (2013) Lysine metabolism in mammalian brain: an update on the importance of recent discoveries. Amino Acids. **45**, 1249–1272 CrossRef PubMed

57 Perez-Miller, S. J. and Hurley, T. D. (2003) Coenzyme isomerization is integral to catalysis in aldehyde dehydrogenase. Biochemistry **42**, 7100–7109 CrossRef PubMed

58 Bosch, M., Mayer, C. D., Cookson, A. and Donnison, I. S. (2011) Identification of genes involved in cell wall biogenesis in grasses by differential gene expression profiling of elongating and non-elongating maize internodes. J. Exp. Bot. **62**, 3545–3561 CrossRef PubMed

59 Chan, C. L., Wong, J. W., Wong, C. P., Chan, M. K. and Fong, W. P. (2011) Human antiquitin: structural and functional studies. Chem. Biol. Interact. **191**, 165–170 CrossRef PubMed

60 Farrés, J., Wang, X., Takahashi, K., Cunningham, S. J., Wang, T. T. and Weiner, H. (1994) Effects of changing glutamate 487 to lysine in rat and human liver mitochondrial aldehyde dehydrogenase. A model to study human (Oriental type) class 2 aldehyde dehydrogenase. J. Biol. Chem. **269**, 13854–13860 PubMed

61 Stiti, N., Podgórska, K. and Bartels, D. (2014) Aldehyde dehydrogenase enzyme ALDH3H1 from Arabidopsis thaliana: Identification of amino acid residues critical for cofactor specificity. Biochim. Biophys. Acta **1844**, 681–693 CrossRef PubMed

62 Tang, G., Miron, D., Zhu-Shimoni, J. X. and Galili, G. (1997) Regulation of lysine catabolism through lysine-ketoglutarate reductase and saccharopine dehydrogenase in Arabidopsis. Plant Cell **9**, 1305–1316 PubMed
63 Wen, Y., Wang, X., Xiao, S. and Wang, Y. (2012) Ectopic expression of VpALDH2B4, a novel aldehyde dehydrogenase gene from Chinese wild grapevine (*Vitis pseudoreticulata*), enhances resistance to mildew pathogens and salt stress in Arabidopsis. Planta **236**, 525–539 CrossRef PubMed
64 Esterbauer, H. and Zollner, H. (1989) Methods for determination of aldehydic lipid peroxidation products. Free Radic. Biol. Med. **7**, 197–203 CrossRef PubMed
65 Bassard, J. E., Ullmann, P., Bernier, F. and Werck-Reichhart, D. (2010) Phenolamides: bridging polyamines to the phenolic metabolism. Phytochemistry **71**, 1808–1824 CrossRef PubMed
66 Gaquerel, E., Gulati, J. and Baldwin, I. T. (2014) Revealing insect herbivory-induced phenolamide metabolism: from single genes to metabolic network plasticity analysis. Plant J. **79**, 679–692 CrossRef PubMed
67 Onkokesung, N., Gaquerel, E., Kotkar, H., Kaur, H., Baldwin, I. T. and Galis, I. (2012) MYB8 controls inducible phenolamide levels by activating three novel hydroxycinnamoyl coenzyme A: polyamine transferases in *Nicotiana attenuata*. Plant Physiol. **158**, 389–407 CrossRef PubMed
68 Martin-Tanguy, J., Perdrizet, E., Prevost, J. and Martin, C. (1982) Hydroxycinnamic acid amides in fertile and cytoplasmic male sterile lines of maize. Phytochemistry **21**, 1939–1945 CrossRef
69 Grienenberger, E., Besseau, S., Geoffroy, P., Debayle, D., Heintz, D., Lapierre, C., Pollet, B., Heitz, T. and Legrand, M. (2009) A BAHD acyltransferase is expressed in the tapetum of Arabidopsis anthers and is involved in the synthesis of hydroxycinnamoyl spermidines. Plant J. **58**, 246–259 CrossRef PubMed
70 Fellenberg, C., Milkowski, C., Hause, B., Lange, P. R., Böttcher, C., Schmidt, J. and Vogt, T. (2008) Tapetum-specific location of a cation-dependent O-methyltransferase in *Arabidopsis thaliana*. Plant J. **56**, 132–145 CrossRef PubMed
71 Fellenberg, C., Böttcher, C. and Vogt, T. (2009) Phenylpropanoid polyamine conjugate biosynthesis in *Arabidopsis thaliana* flower buds. Phytochemistry **70**, 1392–1400 CrossRef PubMed

Received 5 January 2015/23 February 2015; accepted 3 March 2015
Published as BJ Immediate Publication 3 March 2015, doi:10.1042/BJ20150009

Article 5

Plant ALDH10 family: identifying critical residues for substrate specificity and trapping a thiohemiacetal intermediate.

Kopečny D*, Končitíková R*, Tylichová M, Vigouroux A, Moskalíková H, Soural M, Šebela M, Moréra S.

J Biol Chem, 13, 9491-507 (2013)

THE JOURNAL OF BIOLOGICAL CHEMISTRY VOL. 288, NO. 13, pp. 9491–9507, March 29, 2013

Plant ALDH10 Family

*IDENTIFYING CRITICAL RESIDUES FOR SUBSTRATE SPECIFICITY AND TRAPPING A THIOHEMIACETAL INTERMEDIATE**

Received for publication, December 10, 2012, and in revised form, February 4, 2013 Published, JBC Papers in Press, February 13, 2013, DOI 10.1074/jbc.M112.443952

David Kopečný[‡1,2], Radka Končitíková[‡§1], Martina Tylichová[‡], Armelle Vigouroux[¶], Hana Moskalíková[§], Miroslav Soural[‖], Marek Šebela[‡§3], and Solange Moréra[¶4]

From the [‡]Department of Protein Biochemistry and Proteomics, Centre of the Region Haná for Biotechnological and Agricultural Research, and the [§]Department of Biochemistry, Faculty of Science, Palacký University, Šlechtitelů 11, CZ-783 71 Olomouc, Czech Republic, the [¶]Laboratoire d'Enzymologie et Biochimie Structurales, CNRS, Avenue de la Terrasse, 91198 Gif-sur-Yvette, France, and the [‖]Department of Organic Chemistry, Faculty of Science, Palacký University, 17 Listopadu 12, 771 46 Olomouc, Czech Republic

Background: Plant aminoaldehyde dehydrogenases (AMADHs) detoxify ω-aminoaldehydes from several metabolic pathways.
Results: Two of five new AMADHs exhibit unusual kinetic properties. A thiohemiacetal intermediate was trapped in a crystal structure.
Conclusion: Five critical residues can modulate substrate specificity, and a new substrate was identified.
Significance: The present findings allow sequence-based predictions of AMADH substrate specificity linked with the production of individual osmoprotectants in plants.

Plant ALDH10 family members are aminoaldehyde dehydrogenases (AMADHs), which oxidize ω-aminoaldehydes to the corresponding acids. They have been linked to polyamine catabolism, osmoprotection, secondary metabolism (fragrance), and carnitine biosynthesis. Plants commonly contain two AMADH isoenzymes. We previously studied the substrate specificity of two AMADH isoforms from peas (PsAMADHs). Here, two isoenzymes from tomato (*Solanum lycopersicum*), SlAMADHs, and three AMADHs from maize (*Zea mays*), ZmAMADHs, were kinetically investigated to obtain further clues to the catalytic mechanism and the substrate specificity. We also solved the high resolution crystal structures of SlAMADH1 and ZmAMADH1a because these enzymes stand out from the others regarding their activity. From the structural and kinetic analysis, we can state that five residues at positions 163, 288, 289, 444, and 454 (PsAMADHs numbering) can, directly or not, significantly modulate AMADH substrate specificity. In the SlAMADH1 structure, a PEG aldehyde derived from the precipitant forms a thiohemiacetal intermediate, never observed so far. Its absence in the SlAMADH1-E260A structure suggests that Glu-260 can activate the catalytic cysteine as a nucleophile. We show that the five AMADHs studied here are capable of oxidizing 3-dimethylsulfoniopropionaldehyde to the cryo- and osmoprotectant 3-dimethylsulfoniopropionate. For the first time, we also show that 3-acetamidopropionaldehyde, the third aminoaldehyde besides 3-aminopropionaldehyde and 4-aminobutyraldehyde, is generally oxidized by AMADHs, meaning that these enzymes are unique in metabolizing and detoxifying aldehyde products of polyamine degradation to nontoxic amino acids. Finally, gene expression profiles in maize indicate that AMADHs might be important for controlling ω-aminoaldehyde levels during early stages of the seed development.

In plants, polyamines like spermine, spermidine, and putrescine are involved in various developmental processes and stress responses (1). Polyamines are degraded by copper diamine oxidases (EC 1.4.3.22, formerly 1.4.3.6) and FAD-containing polyamine oxidases (PAOs[5]; EC 1.5.3.14 and 1.5.3.17), leading to the production of reactive and cytotoxic ω-aminoaldehydes, such as 3-aminopropionaldehyde (APAL) or 4-aminobutyraldehyde (ABAL; in equilibrium with Δ^1-pyrroline) plus hydrogen peroxide (2, 3). The oxidation of ω-aminoaldehydes by aminoaldehyde dehydrogenase (AMADH) ends up with the formation of the nontoxic metabolites β-alanine and γ-aminobutyric acid (GABA), respectively (4, 5).

Studying the physiological aspects of plant AMADHs (EC 1.2.1.19) has become attractive for economic reasons. It has been shown that an *AMADH* gene mutation leads to the acetylation of free ABAL (or its cyclic form Δ^1-pyrroline) and accumulation of 2-acetyl-Δ^1-pyrroline, a potent flavor component

* This work was supported by Czech Science Foundation Grants P501/11/1591 and 522/08/0555 and OP RD&I Grant ED0007/01/01 (Centre of the Region Haná for Biotechnological and Agricultural Research) and supported in part by CNRS (to S. M. and A.V.).

The atomic coordinates and structure factors (codes 4I9B, 4I8Q, and 4I8P) have been deposited in the Protein Data Bank (http://wwpdb.org/).

[1] These authors contributed equally to this work.
[2] To whom correspondence may be addressed. Tel.: 420-585634927; Fax: 420-585634933; E-mail: kopecny_david@yahoo.co.uk.
[3] To whom correspondence may be addressed. Tel.: 420-585634927; Fax: 420-585634933; E-mail: marek.sebela@upol.cz.
[4] To whom correspondence may be addressed. Tel.: 33-1-69-82-34-70; Fax: 33-1-69-82-31-29; E-mail: morera@lebs.cnrs-gif.fr.

[5] The abbreviations used are: PAO, polyamine oxidase; ABAL, 4-aminobutyraldehyde; ACAPAL, 3-acetamidopropionaldehyde; ALDH, aldehyde dehydrogenase; hALDH, human ALDH; AMADH, aminoaldehyde dehydrogenase; APAL, 3-aminopropionaldehyde; BADH, betaine aldehyde dehydrogenase; BAL, betaine aldehyde; DMSP, 3-dimethylsulfoniopropionate; DMSPAL, 3-dimethylsulfoniopropionaldehyde; GBAL, 4-guanidinobutyraldehyde; PCAL, pyridine carboxaldehyde; TMABAL, *N,N,N*-trimethyl-4-aminobutyraldehyde; GB, glycine betaine; NiR, nicotinamide riboside; qPCR, quantitative PCR; GABA, γ-aminobutyric acid.

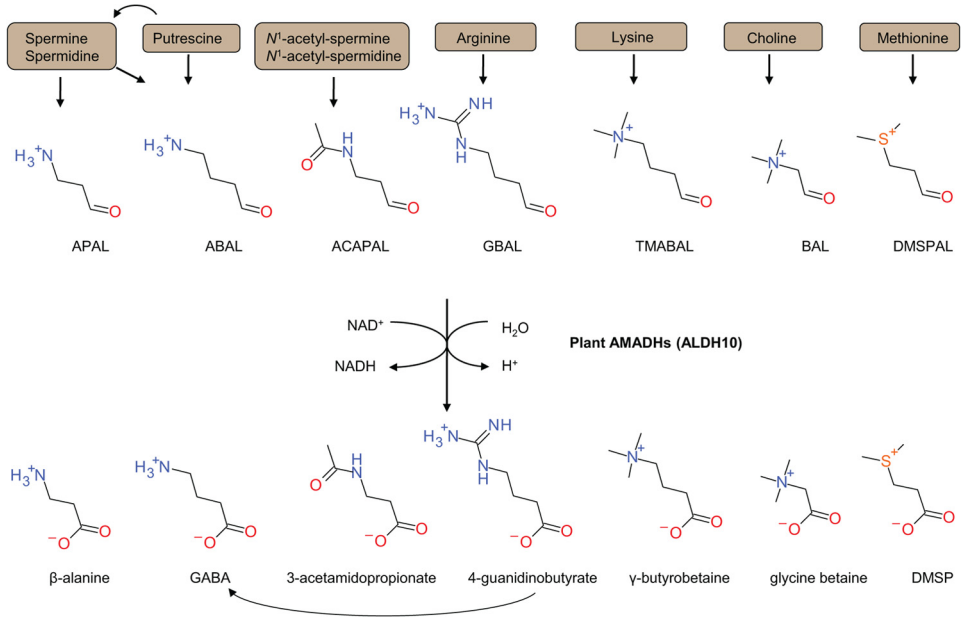

FIGURE 1. **An overview of possible natural substrates oxidized by plant members of the ALDH10 family (AMADHs).** APAL is converted to β-alanine, ABAL to GABA, ACAPAL to 3-acetamidopropionate, GBAL to 4-guanidinobutyrate, TMABAL to γ-butyrobetaine, BAL to glycine betaine, and DMSPAL to DMSP. A nomenclature derived from well characterized substrates has been frequently used for individual enzymes: 4-aminobutyraldehyde dehydrogenase (EC 1.2.1.19), 4-trimethylaminobutyraldehyde dehydrogenase (EC 1.2.1.47), 4-guanidinobutyraldehyde dehydrogenase (EC 1.2.1.54), and BADH (EC 1.2.1.8).

conferring a fragrance to several rice varieties like jasmine and basmati or to soybean (6, 7). Plant AMADHs have also been studied for their role in stress responses and in the production of the osmoprotectants glycine betaine (GB) and dimethylsulfoniopropionate (DMSP) by the oxidation of betaine aldehyde (BAL) and 3-dimethylsulfoniopropionaldehyde (DMSPAL), respectively (8, 9, 10).

AMADHs are classified in different aldehyde dehydrogenase (ALDH) families because of the established criteria stating that ALDH sequences have to be 40% identical to create a family. Because plant AMADHs display between 35 and 39% sequence identity with bacterial, fungal, fish, or mammalian AMADHs, they have recently been classified in the separate family ALDH10 (11). Several enzymes of the ALDH9 family covering mammalian AMADHs (12) and of the ALDH10 family from various species have been independently shown to oxidize a wide range of aminoaldehydes and other aldehydes (Fig. 1). Therefore, they have been also called 4-aminobutyraldehyde dehydrogenases (EC 1.2.1.19), 4-guanidinobutyraldehyde dehydrogenases (EC 1.2.1.54), betaine aldehyde dehydrogenases (BADHs; EC 1.2.1.8), and 4-trimethylaminobutyraldehyde dehydrogenases (EC 1.2.1.47).

Plant AMADHs share around 70–80% sequence identity. One complete AMADH sequence is usually known for many plant species. However, ongoing genome analyses have gradually shown the presence of two genes coding for two homologous proteins of at least 80% sequence identity. Interestingly, most plant AMADHs carry the C-terminal peroxisomal targeting signal S(A)KL and are found in peroxisomes (13, 14). We have previously identified two pea AMADHs (*Pisum sativum*; PsAMADH1 and PsAMADH2) and analyzed their crystal structures (4). Plant AMADHs are dimeric and possess a 14-Å-long substrate channel in each monomer. There are three strictly conserved residues essential for the catalysis, Asn-162, Cys-294, and Glu-260, which lie in PWNYP, GQI(V)CSATSR, and ELGGKSP consensus motifs. The three catalytic residues (Asn, Cys, and Glu) lie at the substrate channel bottom and together form the active site. The catalytic mechanism follows the well described sequential binding model valid for the ALDH superfamily (15, 16). Aminoaldehyde substrates undergo a nucleophilic attack by the catalytic cysteine, leading to a thioester formation (*i.e.* a covalent intermediate) and the subsequent hydride transfer to NAD^+. The conserved glutamate residue functions as a general base activating a water molecule. Such a molecule performs a nucleophilic attack at the thioester acyl-sulfur bond, resulting in the release of the amino acid.

Using site-directed mutagenesis performed on PsAMADH2 (17), we showed that two totally conserved aspartate residues located at the entrance of the substrate channel (Asp-110 and -113) are essential for high affinity binding of ω-aminoaldehydes (APAL is the best substrate). We also noticed that the activity on several aminoaldehyde substrates is affected by Trp-288. In order to predict the substrate specificity differences in AMADH pairs from a single species and between species and because only a few plant AMADH pairs were reported and studied (4, 6, 18), we cloned and biochemically characterized five ALDH10 members (19) (Table 1): two tomato (*Solanum lycopersicum*) isoenzymes SlAMADH1 and SlAMADH2 and three maize (*Zea mays*) isoenzymes ZmAMADH1a, ZmAMADH1b, and ZmAMADH2. Both tomato AMADHs share 80% sequence identity. ZmAMADH1a and -1b differ in 13 amino acids only (97% sequence identity). *ZmAMADH2* and both ZmAMADH1a/1b are 75% sequence identical.

Based on kinetic results, we decided to co-crystallize SlAMADH1 and ZmAMADH1a with NAD^+. The dimeric structures were determined at 1.90 and 1.95 Å resolution, respectively. Although both soaking and co-crystallization with substrates were attempted and despite using the active-site

TABLE 1

Enzyme nomenclature and GenBank™ accession numbers of the five studied ALDH10 family members (AMADHs)

The nomenclature of *Z. mays* ALDH10 family has been recently published (19). Because both tomato enzymes, SlAMADH1 and SlAMADH2, are not clustering (see "Phylogenetic Analysis") too close to the sequences with established ALDH10 nomenclature (11), we named them ALDH10A12 and ALDH10A13.

Source	Common name	Systematic name	GenBank™ accession
Z. mays	ZmAMADH1a	ALDH10A8	GQ184593
	ZmAMADH1b	ALDH10A9	JN635700
	ZmAMADH2	ALDH10A5	GQ184594
S. lycopersicum	SlAMADH1	ALDH10A12	AY796114
	SlAMADH2	ALDH10A13	FJ228482

base mutant SlAMADH1-E260A for this purpose, obtaining AMADH in such a complex was unsuccessful. However, ethylene glycol and polyethylene glycol (PEG) aldehyde molecules from the crystallization solution were found to mimic a substrate bound at the substrate binding site in ZmAMADH1a and SlAMADH1 structures, respectively. Moreover, we obtained the first crystal structure of a thiohemiacetal intermediate in AMADH family; a PEG aldehyde bound covalently to the catalytic cysteine forms an intermediate in one subunit of the SlAMADH1 structure in which only ADP moiety of NAD^+ is ordered. The whole NAD^+ is ordered in ZmAMADH1a and SlAMADH1-E260A structures and adopts the common conformation observed in ALDH structures. Combining structural analysis and kinetics, we can state that five residues at positions 163, 288, 289, 444, and 454 (PsAMADH numbering) can significantly modulate AMADH substrate specificity. Trp-288 and Tyr-163 are essential for the high affinity to ω-aminoaldehyde substrates. The absence of this Trp in addition to the presence of a Thr (instead of Cys in other enzymes) in SlAMADH1 leads to a broader substrate specificity due to an enlargement of its substrate channel. We can predict that AMADHs containing Ile-444 have only a negligible activity with BAL. Conversely, those containing an Asn at position 289 may display BAL activity. For the first time, we identify a new and common substrate for plant AMADHs.

EXPERIMENTAL PROCEDURES

Cloning, Expression, and Purification of AMADHs from Tomato and Maize—The total RNA from apical meristems and leaves of 7-day-old tomato seedlings (*S. lycopersicum* cv. Amateur) and 5-day-old maize seedlings (*Z. mays* cv. Sachara) was extracted using the Midi spin column kit (Macherey-Nagel, Düren, Germany), and the cDNA was synthesized using Superscript II reverse transcriptase (Invitrogen). *SlAMADH1* and *-2* and *ZmAMADH1a*, *-1b*, and *-2* cDNA sequences were originally obtained in this work and submitted to the EMBL/GenBank™ database. The *SlAMADH1* ORF (1515 bp; EMBL/GenBank™ accession number AY796114) was amplified using a primer pair with a BamHI (5′-CAGGGATCCGGCAAATCGTAATGTACCA-3′) and XhoI site (5′-CGTCTCGAGCTAATTCTTTGAAGGTGACTTAT-3′). For the *SlAMADH2* ORF (1518 bp; FJ228482), an upstream primer with the EcoRI site (5′-CATGAATTCGGCGATTCCTAATATACGGAT-3′) and a downstream primer with the KpnI site (5′-AGTGGTACCTTACAGCTTTGAAGGAGACT-3′) were used. All three maize genes were cloned with primer pairs containing EcoRI and XhoI sites. *ZmAMADH1*a ORF (1518 bp; GQ184593) was amplified using the following primers: 5′-ATTGAATTCTGCCTCGCCAGCGATGGTCCCG-3′ and 5′-CGTCTCGAGTTCGTCTTGCCAGTTTACAGC-3′. ZmAMADH1b ORF (1518 bp; JN635700) was amplified using the primer pair 5′-ATTGAATTCTGCCTCGCAAGCGATGGTACCG-3′ and 5′-CGTCTCGAGTTCGTCTTGCCAGTTTACAGC-3′, and *ZmAMADH2* ORF (1521 bp; GQ184594) was cloned using the primer pair 5′-ATAGAATTCAGCGCCGCCGCAGACGAT-3′ and 5′-ATACTCGAGTCACAGCTTAGATGGAGGCTGGT-3′.

The amplified sequences were inserted into a pCDFDuet vector (Novagen, La Jolla, CA), sequenced, and transformed into T7 express *Escherichia coli* cells for expression as N-terminal His_6 tag proteins. Enzymes were produced and purified on a column filled with Co(II)-charged IDA-Sepharose 6B (Sigma-Aldrich) as described previously (20). The complete purification from a 600-ml culture yielded about 20 mg of recombinant SlAMADHs. Specific activity values measured with 1 mM APAL as a substrate were 3.1 units mg^{-1} for SlAMADH1, 3.6 units mg^{-1} for SlAMADH2, 2.6 units mg^{-1} for ZmAMADH1a, 1.9 units mg^{-1} for ZmAMADH1b, 4.1 units mg^{-1} for ZmAMADH2.

For crystallization, the plasmid was transformed into *E. coli* BL21 pLysS (Novagen). The cells were grown in 2YT medium at 37 °C to an $A_{600} = 0.6$, the temperature was reduced to 20 °C, and expression was induced with 0.5 mM isopropyl 1-thio-β-D-galactopyranoside overnight. The cells were suspended in buffer A (50 mM Tris-HCl buffer, pH 8, 20 mM imidazole, and 500 mM NaCl) and disrupted by sonication. The lysate was cleared by centrifugation at 20,000 × *g* at 4 °C for 30 min. The supernatant was filtered through a 0.22-μm membrane (Millipore) and loaded on a 5-ml nickel-nitriloacetic acid-agarose column (GE Healthcare). After washing with 10% buffer B (50 mM Tris-HCl, pH 8, 300 mM imidazole, and 500 mM NaCl), elution was performed with 100% buffer B. Fractions containing AMADH were pooled, and the buffer exchange was performed on a HiLoad 26/60 Superdex 200 prep grade (GE Healthcare), using 50 mM Tris-HCl, pH 8, 150 mM NaCl. Fractions were analyzed by SDS-PAGE, and those containing AMADH were pooled, concentrated using Vivaspin-10kDa (Sartorius) at 14 mg/ml, and stored at −20 °C. The identity of the purified proteins was confirmed by peptide mass fingerprinting on a Microflex LRF20 MALDI-TOF mass spectrometer (Bruker Daltonik, Bremen, Germany) after SDS-PAGE and in-gel digestion (21).

Substrates, Activity Assays, and pH Optimum Determination—Elementary aliphatic aldehydes, pyridine carboxaldehydes, BAL chloride together with *N,N*-dimethyl-4-aminobutyraldehyde, APAL, and ABAL diethylacetals were purchased from Sigma-Aldrich. DMSPAL and diethylacetals of 4-amino-2-hydroxybutyraldehyde, 4-guanidinobutyraldehyde (GBAL), 4-guanidino-2-hydroxybutyraldehyde, and 3-guanidinopropionaldehyde were all synthetic preparations (9, 22). Diethyl acetal iodides of *N,N,N*-trimethyl-3-aminopropionaldehyde and TMA-BAL were synthesized according to a protocol described for the latter compound (23). 3-Acetamidopropionaldehyde (ACA-PAL) diethylacetal was synthesized as described (24); pyridine, acetic acid, and acetic anhydride were removed from the reac-

TABLE 2
Data collection and refinement statistics

	SlAMADH1	E260A mutant of SlAMADH1	ZmAMADH1a
Protein Data Bank code	4I9B	4I8Q	4I8P
Space group	$P2_12_12_1$	$I2_12_12_1$	C121
Asymmetric unit	1 dimer	1 monomer	1 dimer
Unit cell (Å)			
a	84.15	94.04	181.19
b	94.79	118.07	49.89
c	118.17	128.21	154.53
α (degrees)	90.0	90.0	90.0
β (degrees)	90.0	90.0	124.15
γ (degrees)	90.0	90.0	90.0
Resolution (Å)	43.9-1.90	50.0-2.65	45.0-1.95
Observed reflections	405,447 (45,398)[a]	142,957 (22,300)	338,559 (52,896)
Unique reflections	75,000 (11,743)	21,922 (3441)	83,412 (13,238)
Completeness (%)	99.2 (97.2)	99.2 (98.5)	99.1 (98.2)
$I/\sigma(I)$	12.2 (1.93)	15.3 (2.36)	10.71 (2.29)
R_{sym} (%)	9.8 (76.3)	12.0 (78.4)	10.9 (62.2)
R_{cryst} (%)	17.4	20.8	17.6
R_{free} (%)	21.2	28.2	21.0
Root mean square deviation			
Bond lengths (Å)	0.010	0.010	0.010
Bond angles (degrees)	1.12	1.23	1.07
Mean *B* value (Å²)			
Protein	26.0	45.1	27.6
NAD^+		37.4	23.3
ADP part	31.5		
PEG aldehyde intermediate	35.7		
Solvent	35.3	44.2	34.8

[a] Numbers in parentheses represent values in the highest resolution shell: 1.90–2.01 Å (SlAMADH1), 2.65–2.81 Å (E260A mutant of SlAMADH1), and 1.95–2.07 Å (ZmAMADH1a).

tion mixture in a lyophilizer; ^{1}H NMR (300 MHz, DMSO-d_6), δ (ppm): 1.10 (t, J = 7.04 Hz, 6 H) 1.63 (q, J = 6.65 Hz, 2 H) 1.77 (s, 3 H) 3.03 (q, J = 6.71 Hz, 2 H) 3.29–3.62 (m, 4 H) 4.48 (t, J = 5.58 Hz, 1 H) 7.80 (br. s., 1 H). ^{13}C NMR (75 MHz, DMSO-d_6), δ (ppm): 15.8, 23.1, 33.9, 35.3, 61.2, 101.0, 169.5. If necessary, free aminoaldehydes were prepared by heating their acetals in a plugged test tube with 0.2 M HCl for 10 min (10). NAD^+ and NAD analogs were purchased from Sigma-Aldrich.

Activity was measured spectrophotometrically by monitoring the formation of NADH (ϵ_{340} = 6.62 mM^{-1} cm^{-1}) at 37 °C. The reaction mixture in a cuvette contained 0.15 M Tris-HCl buffer, pH 9.0, 1 mM NAD^+, and appropriate amounts of AMADH. The enzyme reaction was started by the addition of APAL (or another aminoaldehyde) at a final 1 mM concentration. NAD^+ analogs were assayed at 0.5 mM concentration with 1 mM APAL as described previously (4). Tris-HCl buffers (150 mM) in the pH range from 7.0 to 9.0 and 150 mM glycine-NaOH buffers in the pH range from 8.8 to 10.6 were used to determine pH optima using 1 mM APAL and 0.5 mM NAD^+. Kinetic constants were determined with GraphPad Prism 5.0 data analysis software (GraphPad Software, Inc., La Jolla, CA). In those cases where no substrate inhibition was observed, the data were fitted to the Michaelis-Menten equation. The data were analyzed by a nonlinear regression using the Michaelis-Menten equation that includes terms in the numerator and denominator to account for partial substrate inhibition (25),

$$V = V_{max} \cdot [S]/(K_m \cdot (1/(1 + \beta \cdot [S]/K_i)) + [S] \cdot ((1 + [S]/K_i)/(1 + \beta \cdot [S]/K_i))) \quad \text{(Eq. 1)}$$

where v represents the determined initial velocity, V_{max} is the maximal velocity, [S] is the concentration of the substrate, K_m is the substrate concentration at half-maximal velocity, K_i is the substrate inhibition constant, and β is the factor that describes the effect of substrate inhibition on V_{max}.

Plant AMADHs share a similar pH optimum The pH optima of ZmAMADH1a, ZmAMADH2, and SlAMADH2 fall within the pH range of 9.4–9.8 (*i.e.* similarly to that of pea or rice AMADHs) (4, 6). The pH optima of SlAMADH1 and ZmAMADH1b are slightly more basic (pH ~10.2).

Crystallization and Data Collection—Crystallization conditions using commercial kits (Classics, PEGs II, and JCSG I suites from Qiagen) were screened in sitting-drop vapor diffusion experiments using a Cartesian nanodrop robot (Genomic Solutions) on IMAGIF (CNRS, Gif sur Yvette, France). SlAMADH1 with 5 mM NAD^+ was crystallized over reservoirs containing 23% PEG 1000, 0.1 M HEPES, pH 7.5. ZmAMADH1a with 5 mM NAD^+ was crystallized over reservoirs containing 16% PEG 4000, 0.1 M HEPES, pH 7.5, and 10% isopropyl alcohol. The E260A mutant of SlAMADH1 with 5 mM NAD^+ was crystallized over reservoirs containing 15% PEG 1500, 0.1 M imidazole, pH 7.0, and 10% glycerol. Crystals were transferred to a cryoprotectant solution (mother liquor supplemented with 25% PEG 400 for SlAMADH1 or 20% glycerol for the E260A mutant and ZmAMADH1a) and flash-frozen in liquid nitrogen. Diffraction data were collected at 100 K on the PROXIMA 1 beamline (SOLEIL Synchrotron, Saint-Aubin, France). Diffraction intensities were integrated with the program XDS (26). Data collection and processing statistics are given in Table 2.

Molecular Replacement, Refinement, and Final Model—The structures of SlAMADH1 and of ZmAMADH1a were solved by molecular replacement with Phaser (27) using the dimer structure of PsAMADH2 (Protein Data Bank code 3IWJ) as a search model. The structure of the SlAMADH1-E260A mutant was also solved with Phaser using a monomer of the WT structure

as a search model. Model refinement was performed with BUSTER-TNT (28). Electron density maps were evaluated using COOT (29) for manual refinement. In the SlAMADH1 structure, the maps revealed clear density for the ADP moiety of the NAD^+ coenzyme. In contrast, the side chain of the active-site base Glu-260 is disordered. For this reason, we set the occupancy of each atom forming the carboxylate at 0. In the ZmAMADH1a and SlAMADH1-E260A structures, the electron density of the whole NAD^+ molecule was observed. Glu-262 (equivalent to Glu-260) is well defined in the maize structure. Refinement details of the three structures are shown in Table 2. Molecular graphics images were generated using PyMOL (Schroedinger, LLC, New York).

qPCR Analysis—The total RNA from 10-day-old and 2 month-old tomato plants (cv. Amateur) for reverse transcription was isolated using the RNAqueous kit and Plant RNA Isolation Aid solutions from Ambion (Austin, TX). Isolated RNA was treated twice by the TURBO DNase-free kit (Ambion) to remove all traces of genomic DNA contamination and to minimize bias in qPCR data. First-strand cDNA was synthesized by RevertAid H Minus Moloney murine leukemia virus reverse transcriptase and oligo(dT) primers (Fermentas, Vilnius, Lithuania). Diluted cDNA samples were used as templates in real-time PCRs containing TaqMan Gene Expression Master Mix (Applied Biosystems), both primers at 300 nM concentrations, and 250 nM TaqMan 6-FAM MGB probe. For the *SlAMADH1* gene, the primer pair 5′-TGGACGTGATCTAGGGAAATGG-3′ plus 5′-CCAATGGTTCAGCAGAAGTATACTCT-3′ and a probe (5′-AATTTCTTGAACATTAAGCAGGMGB-3′) were used. For the *SlAMADH2* gene, the following primer pair and probe were used: 5′-GTAGTGGTTTTGGACGTGAGCTT-3′, 5′-TCGTCCGGAGTCACATACTGAGT-3′, and 5′-FAM-AATGGAGTCTCGAGAACT-3′, respectively. Expression of *ZmAMADH1* genes was analyzed using the following primer pairs and probes. 5′-CCAGAGGTTATCTGAGGAGATTGAC-3′, 5′-CCAAATCCACTGCGCTTGTT-3′, and 5′-FAM-TGGGTAAACTGCTCGCAACCCTGC-MGB-3′, respectively, were used for *ZmAMADH1a*; 5′-TGAGCGCTGCCAGAGATTATC-3′, 5′-AGCAGGGCTGTGAGCAGTTT-3′, and 5′-FAM-ATGCTGGAATTATCTGGG-MGB-3′, respectively, were used for *ZmAMADH1b*; and 5′-AGGTGTGAGCGCATTTCAAAG-3′, 5′-AAAACCGCTCCGCTTGTTC-3′, and 5′-FAM-TTCCCAACCATGCTTCGTTCAAGCTC-Tamra-3′, respectively, were used for *ZmAMADH2*.

The TaqMan probes together with the corresponding primers were designed by Applied Biosystems customer service. RNA from every biological replicate was at least transcribed in two independent reactions, and each cDNA sample was run in at least two technical replications on a StepOne-Plus real-time PCR system using a default program (Applied Biosystems). For each primer pair, plasmid DNA was used as a template to generate a calibration curve for determining the PCR efficiency. Cycle threshold values were normalized with respect to the elongation factor 1α of tomato (SlEF1α; primer pair 5′-GGTCATCATCATGAACCATCC-3′ and 5′-CATACCAGCATCACCGTTCTT-3′) or maize (ZmEF1α; primer pair 5′-TGATACCCACCAAGCCTATGGT-3′ and 5′-CATGTCGCGGACAGCAAAC-3′) and the efficiency of amplification.

Phylogenetic Analysis—Amino acid alignment was performed with MUSCLE version 3.8 (30), and then the maximum likelihood phylogeny with bootstrap analysis was performed with PhyML version 3.0 (31), using an LG amino acid replacement matrix. *AMADH* sequences were obtained from the EMBL/GenBank™ database, TGI database (tentative consensus numbers), or Phytozome version 8.0 database: *Amaranthus hypochondriacus* 1 and 2 (AF017150/O04895); *Avicennia marina* 1/2 (mangrove, AF170094, and AB043540); *Arabidopsis thaliana* 1/2 (AY093071/AF370333); *Beta vulgaris* (sugar beet, AB221006); *Brassica napus* 1/2 (rapeseed, AY351634/TC111063); *Glycine max* 1/2 (soybean, AB333793/AB333794); *Gossypium hirsutum* (cotton, AY461804); *Hordeum vulgare* 1/2 (barley, AB063179/AB063178); *Lycium barbarum* (wolfberry, FJ514799); *Leymus chinensis* 1/2 (wild rye, AB183715/AB183716); *Medicago truncatula* 1/2 (barrel medic, TC151999/BT053176); *Oryza sativa* 1/2 (rice, AB001348/AB096083); *Physcomitrella patens* (moss, EDQ78577); *Picea sitchensis* (spruce, BT070941); *Pinus sylvestris* (pine, TC133801); *P. sativum* 1/2 (pea, AJ315852/AJ315853); *Populus trichocarpa* 1/2 (poplar, XM_002322111/DR448910); *Prunus persica* 1/2 (peach, PPA004563M/PPA022568M); *S. lycopersicum* 1/2 (tomato, this work); *Solanum tuberosum* 1/2 (potato, PGSC0003DMC400055759/PGSC0003DMC400042549); *Sorghum bicolor* (sorghum, XM_002444312); *Spinacia oleracea* (spinach, M31480); *Triticum aestivum* 1/2 (wheat, AY050316/TC389888 + AK332255); *Z. mays* 1a/1b/2 (maize, this work); *Vitis vinifera* 1/2 (grapevine, XM_002283654/XM_002281948); and *Zoysia tenuifolia* 1/2 (velvetgrass, AB161712/AB161702).

Accession Numbers—The atomic coordinates and structure factors have been deposited in the Protein Data Bank with the following accession codes: 4I9B for SlAMADH1 in complex with NAD^+ and a thiohemiacetal intermediate, 4I8Q for the Glu-260 mutant of SlAMADH1 in complex with NAD^+, and 4I8P for ZmAMADH1a in complex with NAD^+.

RESULTS AND DISCUSSION

Crystal Structures of SlAMADH1, ZmAMADH1a, and SlAMADH1-E260A—Because SlAMADH1 and ZmAMADH1a differ in terms of activity from the other new studied AMADHs from tomato (*S. lycopersicum*) and maize (*Z. mays*) as well as those from peas (see "Substrate Catalysis and Specificity"), their crystal structures were solved at high resolution (Table 2). We also crystallized SlAMADH1-E260A mutant to trap an intermediate or a bound substrate, but these attempts were unsuccessful. However, we have been able to trap an intermediate in the SlAMADH1 structure, thanks to the PEG solution used as precipitant in the crystallization condition.

The asymmetric unit of SlAMADH1 and ZmAMADH1a crystals contains a dimer, which is the active form in solution in accordance with results from gel permeation chromatography (molecular mass estimates between 106 and 112 kDa). The asymmetric unit of SlAMADH1-E260A is composed of one molecule, which forms a dimer by the crystallographic symmetry. The dimers of tomato, maize, and pea (*P. sativum*) AMADHs are very similar, sharing the same oligomerization interface, folding, and topology. A major difference is that

TABLE 3

Kinetic parameters of ALDH10 family from tomato for selected substrates and the coenzyme NAD^+

All K_m and k_{cat} values are given in μM and s^{-1}, respectively, and k_{cat}/K_m ratios are expressed in $M^{-1}\,s^{-1}$. Activities were measured in 0.15 M Tris-HCl buffer, pH 9.0. Specific activity values with 1 mM APAL were 3.1 units mg^{-1} for SlAMADH1 and 3.6 units mg^{-1} for SlAMADH2. Kinetic constants were measured using a saturating NAD^+ concentration of 500 μM. The K_m value for NAD^+ was measured at a fixed 1 mM concentration of APAL. The data were further analyzed by a nonlinear regression using either a simpler equation for substrate inhibition, $v = V_{max}\cdot[S]/(K_m + [S]\cdot(1 + [S]/K_i))$, or an equation for partial substrate inhibition, $v = V_{max}\cdot[S]/(K_m\cdot(1/(1 + \beta\cdot[S]/K_i)) + [S]\cdot((1 + [S]/K_i)/(1 + \beta\cdot[S]/K_i)))$, where v is the determined initial velocity, V_{max} is the maximal velocity, [S] is the concentration of the substrate, K_m is the substrate concentration at half-maximal velocity, K_i is the substrate inhibition constant, and β is the factor that describes the effect of substrate inhibition on V_{max}. In cases where substrate inhibition was observed, K_i values are given in μM. −, not determined (very weak substrates); None, no substrate inhibition observed in the measured range.

Ligand	SlAMADH1					SlAMADH2				
	K_m	k_{cat}	k_{cat}/K_m	K_i	β	K_m	k_{cat}	k_{cat}/K_m	K_i	β
	μM	s^{-1}	$M^{-1}\,s^{-1}$	μM		μM	s^{-1}	$M^{-1}\,s^{-1}$	μM	
NAD^+	72 ± 7	–	–	–	–	89 ± 3	–	–	–	–
TMABAL	17 ± 1.4	3.6 ± 0.2	2.1 × 105	90 ± 14	0.22	141 ± 17	2.0 ± 0.1	1.4 × 104	1560 ± 108	0.04
GBAL	85 ± 13	4.5 ± 0.4	5.3 × 104	581 ± 74	–	22 ± 3	3.9 ± 0.3	1.8 × 105	211 ± 40	–
APAL	41 ± 5	6.0 ± 0.4	1.5 × 105	914 ± 84	–	9 ± 1.4	8.2 ± 0.7	9.1 × 105	111 ± 18	0.36
ABAL	278 ± 19	5.2 ± 0.4	1.9 × 104	None	–	54 ± 5	2.5 ± 0.1	4.6 × 104	858 ± 81	–
BAL	2051 ± 83	1.0 ± 0.02	4.6 × 102	None	–	–	–	–	–	–
3-PCAL	316 ± 14	2.2 ± 0.03	6.9 × 103	None	–	–	–	–	–	–
4-PCAL	50 ± 4	1.4 ± 0.03	2.8 × 104	None	–	–	–	–	–	–

TABLE 4

Kinetic parameters of ALDH10 family from maize for selected substrates and the coenzyme NAD^+

All K_m and k_{cat} values are given in μM and s^{-1}, respectively, and k_{cat}/K_m ratios are expressed in $M^{-1}\,s^{-1}$. Activities were measured in 0.15 M Tris-HCl buffer, pH 9.0. Specific activity values with 1 mM APAL were 2.6 units mg^{-1} for ZmAMADH1a, 1.9 units mg^{-1} for ZmAMADH1b, and 4.1 units mg^{-1} for ZmAMADH2. Kinetic constants were measured using a saturating NAD^+ concentration of 500 μM. The K_m value for NAD^+ was measured at a fixed 1 mM concentration of APAL. The data were further analyzed by a nonlinear regression using either a simpler equation for substrate inhibition, $v = V_{max}\cdot[S]/(K_m + [S]\cdot(1 + [S]/K_i))$, or an equation for partial substrate inhibition, $v = V_{max}\cdot[S]/(K_m\cdot(1/(1 + \beta\cdot[S]/K_i)) + [S]\cdot((1 + [S]/K_i)/(1 + \beta\cdot[S]/K_i)))$, where v is the determined initial velocity, V_{max} is the maximal velocity, [S] is the concentration of the substrate, K_m is the substrate concentration at half-maximal velocity, K_i is the substrate inhibition constant, and β is the factor that describes the effect of substrate inhibition on V_{max}. In cases where substrate inhibition was observed, K_i values are given in μM. −, not determined (very weak substrates); None, no substrate inhibition observed in the measured range.

Ligand	ZmAMADH1a					ZmAMADH1b					ZmAMADH2				
	K_m	k_{cat}	k_{cat}/K_m	K_i	β	K_m	k_{cat}	k_{cat}/K_m	K_i	β	K_m	k_{cat}	k_{cat}/K_m	K_i	β
	μM	s^{-1}	$M^{-1}\,s^{-1}$	μM		μM	s^{-1}	$M^{-1}\,s^{-1}$	μM		μM	s^{-1}	$M^{-1}\,s^{-1}$	μM	
NAD^+	91 ± 4	–	–	–	–	79 ± 6	–	–	–	–	86 ± 3	–	–	–	
TMABAL	6 ± 0.8	5.1 ± 0.3	8.4 × 10^5	66 ± 7	0.1	10 ± 2	5.7 ± 0.5	5.7 × 10^5	89 ± 11	–	16 ± 1.1	10.8 ± 0.7	6.8 × 10^5	38 ± 8	0.06
GBAL	3 ± 0.7	1.6 ± 0.2	5.2 × 10^5	21 ± 3	0.04	5 ± 1	1.7 ± 0.2	3.5 × 10^5	18 ± 4	0.04	11 ± 1.2	5.0 ± 0.4	4.5 × 10^5	29 ± 4	0.07
APAL	9 ± 2	11.8 ± 0.5	1.3 × 10^6	182 ± 31	0.09	11 ± 2	11.1 ± 0.4	1.0 × 10^6	109 ± 8	0.1	98 ± 8	10.3 ± 0.5	1.1 × 10^5	505 ± 28	0.07
ABAL	28 ± 3	1.2 ± 0.1	4.2 × 10^4	1214 ± 102	–	26 ± 4	1.7 ± 0.2	6.5 × 10^4	108 ± 17	–	59 ± 2	4.3 ± 0.1	7.2 × 10^4	652 ± 72	0.11
BAL	14 ± 1.6	0.6 ± 0.02	4.5 × 10^4	None	–	29 ± 4	0.07 ± 0.01	2.3 × 10^3	None	–	–	–	–	–	–
3-PCAL	–	–	–	–	–	–	–	–	–	–	–	–	–	–	–
4-PCAL	–	–	–	–	–	–	–	–	–	–	–	–	–	–	–

SlAMADH1 is shorter by three residues in the loop from residue 63 to 70 when compared with ZmAMADH1a and PsAMADHs.

All monomers are identical, with root mean square deviations for 494 Cα atoms between 0.6 and 0.8 Å. They adopt the characteristic ALDH fold, consisting of an $NAD(P)^+$ coenzyme binding domain (residues 1–131, 152–261, and 456–480), a catalytic domain (residues 262–455), and an oligomerization domain (132–151 and 481 at the C terminus). They all contain a monovalent cation present in a conserved intrasubunit cavity close to the coenzyme binding site. The cation cavity in SlAMADH1 (and also in ZmAMADH1a) is formed by the three equivalent carbonyl groups of Ile-31 (Val-30), Asp-99 (Asp-101), and Leu-189 (Leu-191) and the carboxyl group of Asp-99 (Asp-101). The nature of the protein ligands and the distances of around 2.4–2.6 Å are typical for a bound sodium ion (32). This ion probably allows maintenance of the protein structural integrity and/or stabilizes the position of a loop involved in NAD^+ binding (15).

The oligomerization domains connect both monomers by protruding over the surface of the neighboring subunits around substrate channel entrances, whereas the NAD^+ binding sites reside on the opposite side of the dimer. The catalytic cysteine lies between the NAD^+ and the substrate binding sites. All enzymes were co-crystallized with NAD^+. Whereas the whole well defined NAD^+ molecule adopts an extended conformation typical for oxidized NAD^+ (15) in ZmAMADH1a and SlAMADH1-E260A structures, the nicotinamide riboside (NiR) moiety is disordered in the SlAMADH1 structure, as frequently observed in structures of $NAD(P)^+$-dependent ALDHs, including PsAMADH2 (4, 33, 34). With the bound coenzyme fully observed in electron density maps, the catalytic cysteine points toward the substrate channel (attacking conformation), allowing the nicotinamide ring to interact with the active-site base Glu. In contrast, when the NiR moiety is mobile, the catalytic cysteine adopts the resting conformation by pointing toward the NAD^+ cavity and prevents the NiR moiety from being in the vicinity of the active-site base glutamate. In this state, mixed conformations of NAD^+ and NADH coenzyme are observed.

Coenzyme Binding Site—The coenzyme binding site is highly conserved in the plant AMADH family. The adenine moiety of NAD^+ inserted in a hydrophobic pocket flanked by two helices (αD and αE) makes no polar contact with the enzyme, so that the free amino group is exposed to the solvent. The O2B and O3B oxygen atoms of the ribose and both α- and β-phosphate oxygen atoms establish identical hydrogen bonds with the enzyme as described for PsAMADH2 (4). All five AMADHs

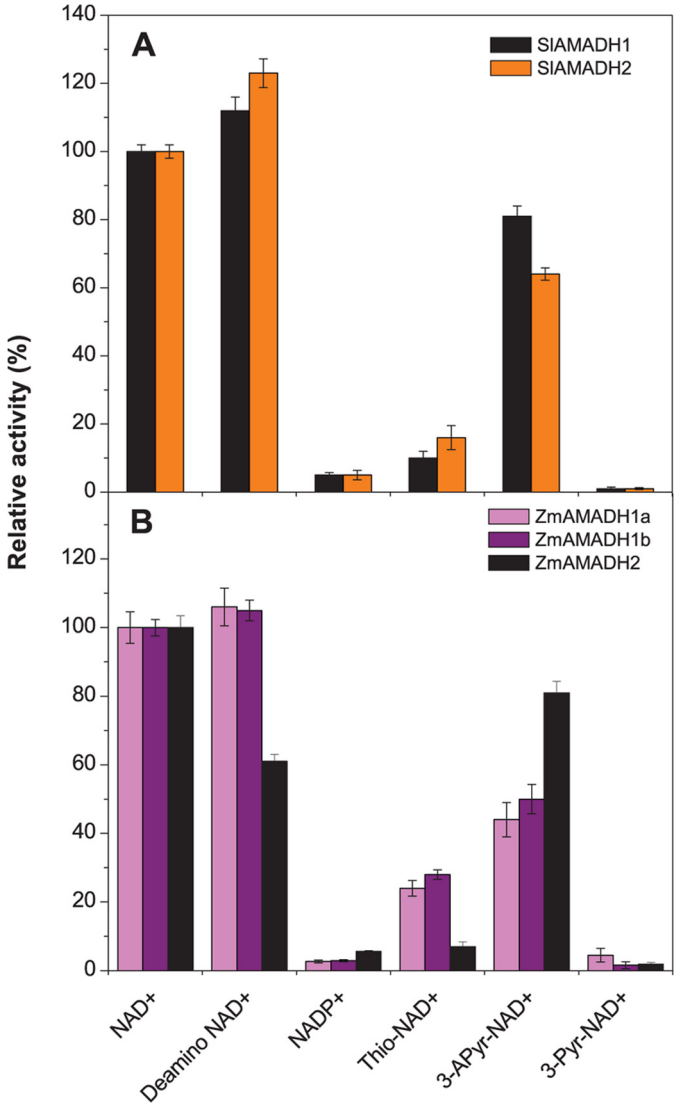

FIGURE 2. **Relative activities of tomato (*A*) and maize (*B*) AMADHs with NAD$^+$ analogs.** Coenzyme efficiency was measured with 1 mM APAL as a substrate and 500 μM NAD$^+$ analogs, in 0.15 M Tris-HCl buffer, pH 9.0. The rate of the NAD$^+$-mediated reaction was arbitrarily taken as 100%. *Error bars*, S.D.

display similar reaction rates and affinity for NAD$^+$ (K_m values are in the range of 10^{-5} μM; Tables 3 and 4). These enzymes are NAD$^+$-specific because they possess a conserved glutamate (Glu-188 in PsAMADH2 numbering), preventing the binding of the 2′-phosphate group of NADP$^+$, as described previously (4). Thus, their activity with NADP$^+$ is very low (Fig. 2).

A screening test using NAD$^+$ analogs with substitutions at the nicotinamide ring in the presence of APAL as a substrate shows that these compounds are less efficient as coenzymes (Fig. 2). 3-Acetylpyridine-NAD$^+$ is the best electron acceptor and leads to ~45% activity for ZmAMADH1a and ZmAMADH1b (as well as for both PsAMADHs) and ~75% activity for both SlAMADHs and ZmAMADH2 compared with that with NAD$^+$. Thio-NAD$^+$ drastically decreases AMADH activity (between 4.5 and 25%), especially that of ZmAMADH2 and PsAMADH1. 3-Pyridinealdehyde-NAD$^+$ is generally not accepted as a coenzyme for our studied AMADHs. To our knowledge, there is so far only one detailed analysis of the coenzyme binding site using various NAD$^+$ analogs performed on human ALDH1 (ALDH1A1), ALDH2, and AMADH (ALDH9A1) (35). The human ALDHs (hALDHs) significantly differ in their activity with nicotinamide analogs, and these differences are rather difficult to interpret in terms of interactions with the conserved catalytic residues. For example, thio-NAD$^+$, which is inactive with hALDH2 (reduced V_{max} and unaffected K_m), is a good coenzyme of hAMADH and a weak coenzyme for hALDH1. Similarly, 3-pyridinealdehyde-NAD$^+$, which is a coenzyme for hALDH1 and hALDH2, is inactive for hAMADH as well as for plant AMADHs. Indeed, 3-pyridinealdehyde-NAD$^+$ acts as a strong competitive inhibitor of hAMADH and might form a thiohemiacetal linkage with the catalytic cysteine, preventing its reduction (36).

Substrate Catalysis and Specificity—A large screening study performed using 1 mM substrates, such as natural ω-aminoaldehydes, including APAL, ABAL, GBAL, TMABAL, and BAL (Fig. 1), proves that all five plant AMADHs from tomato and maize most readily oxidize propionaldehyde and butyraldehyde natural and synthetic aminoaldehydes (Fig. 3). The highest reaction rates are obtained with APAL for all maize enzymes and SlAMADH2. Only SlAMADH1 displays the highest activity for ABAL. Methyl and guanidine derivatives of APAL and ABAL are also well oxidized, with 10–60% rates on average (relative to that of the best substrate), whereas hydroxylated derivatives are oxidized more slowly. Taken together, the three ZmAMADHs and SlAMADH2 resemble both PsAMADHs with respect to their substrate preference. Unexpectedly, SlAMADH1 exhibits much broader substrate specificity than SlAMADH2 and the other studied AMADHs. This enzyme oxidizes much better not only the guanidine derivatives 3-guanidinopropionaldehyde and GBAL but also 3- and 4-pyridine carboxaldehydes (3- and 4-PCAL; ~40% of the rate with ABAL) and several *n*-alkyl aldehydes like valeraldehyde and capronaldehyde (~15% of the rate with ABAL). One more unexpected result is that ZmAMADH1a shows a high activity with BAL, comparable with ABAL oxidation (~16% compared with APAL). To shed light on these surprising results, we focused on SlAMADH1 and ZmAMADH1a for a crystallographic study.

SlAMADH1 structure reveals well defined electron density maps in the substrate binding site of both subunits despite the absence of a co-crystallized or soaked substrate. The only compound considered as a potential ligand comes from the PEG solution used as a precipitant for crystallization. A di(hydroxyethyl)ether molecule was straightforward modeled. A continuous electron density between the SG atom of the catalytic cysteine Cys-295 and the C1 atom of the di(hydroxyethyl)ether molecule suggests a 1.7-Å-long covalent bond in subunit A (Fig. 4*A*). The density shape at C1 is not flat and satisfies an sp^3 hybridization expected for a thiohemiacetal intermediate. The oxygen atom of the hydroxyl group at C1 is hydrogen-bonded to the Cys-295 amide nitrogen (2.9 Å) and to the ND2 atom of Asn-162 (2.8 Å), two groups formerly postulated to be involved in the formation of the oxyanion hole and to stabilize the thiohemiacetal and thioacyl intermediates (37) (Fig. 4*B*). So far, the only reported intermediate in the ALDH family corresponding to the E268A glyceraldehyde-3-phosphate dehydrogenase mutant (38) is a thioester intermediate due to the

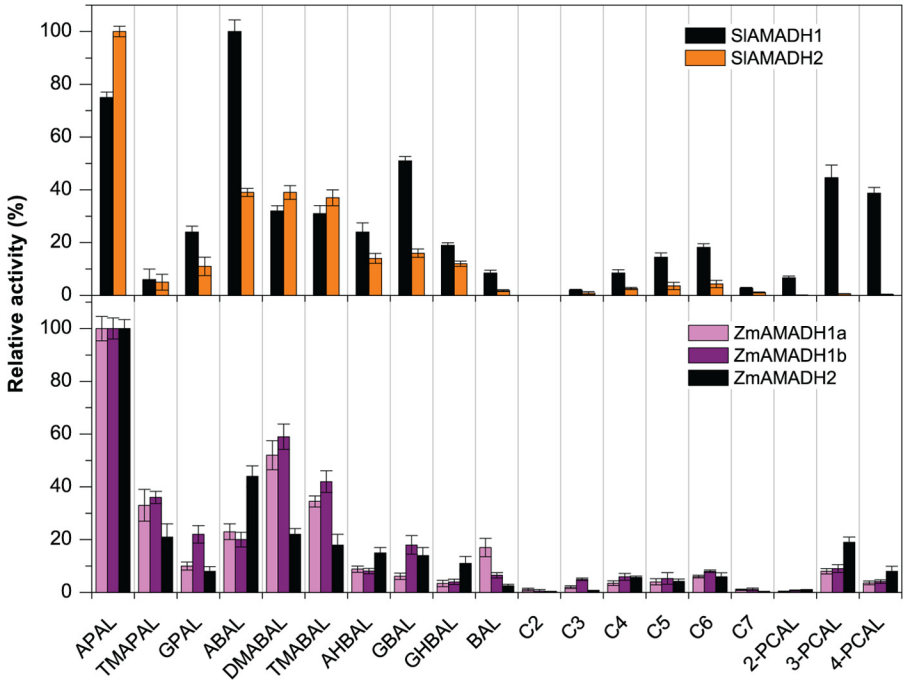

FIGURE 3. **Substrate specificity of ALDH10 isoenzymes from tomato (*top*) and maize (*bottom*).** The activity of each AMADH isoenzyme with the best substrate was arbitrarily taken as 100%. The measurements were performed with 1 mM substrates in 0.15 M Tris-HCl buffer, pH 9.0, containing 1 mM NAD^+. The following substrates were tested: APAL, *N,N,N*-trimethyl-3-aminopropionaldehyde (*TMAPAL*), 3-guanidinopropionaldehyde (*GPAL*), ABAL, *N,N*-dimethyl-4-aminobutyraldehyde (*DMABAL*), TMABAL, 4-amino-2-hydroxybutyraldehyde (*AHBAL*), GBAL, 4-guanidino-2-hydroxybutyraldehyde (*GHBAL*), BAL, acetaldehyde (*C2*), propionaldehyde (*C3*), butyraldehyde (*C4*), valeraldehyde (*C5*), capronaldehyde (*C6*), enanthaldehyde (*C7*), and pyridine carboxaldehydes (*PCAL*). Specific activity values with 1 mM APAL were 3.1 units mg^{-1} for SlAMADH1, 3.6 units mg^{-1} for SlAMADH2, 2.6 units mg^{-1} for ZmAMADH1a, 1.9 units mg^{-1} for ZmAMADH1b, and 4.1 units mg^{-1} for ZmAMADH2. *Error bars*, S.D.

flat density observed at the C1 atom, corresponding to a sp^2 hybridization.

The existence of the covalent bond and the disordered Glu-260 side chain strongly suggests that the enzyme is turning over in the crystal with a highly mobile Glu-260. Kinetic measurements with PEG solutions (PEG 1000 and 1500) used for crystallization confirm the presence of aldehydes and show an activity of about a 1% rate compared with that with capronaldehyde (data not shown). The presence of an aldehyde in PEG solution was also mentioned in an hALDH2 crystallographic study, where we believe that the soaked crotonaldehyde substrate forms an intermediate (Protein Data Bank code 1O01) (15). In consequence, instead of a di(hydroxyethyl)ether molecule, we modeled a 2-(hydroxyethoxy)acetaldehyde molecule in two conformations in subunit B of the SlAMADH1 structure because there was no continuous electron density proving the absence of a covalent bond (Fig. 4*C*). Indeed, the catalytic cysteine points toward the coenzyme cavity. However, we cannot rule out the presence of a carboxylate product because the NiR moiety of the coenzyme molecule is disordered in both subunits, indicating the presence of an NAD^+/NADH mixture in the crystals as previously shown in the hALDH2 study (15). The extended conformation typical for oxidized NAD^+ in the SlAMADH1-E260A structure proves that no turnover occurs in the crystal, although PEG was used as a precipitant. We verified that this mutant is inactive with the aldehyde in PEG solutions and capronaldehyde, at pH 7.0 and in the same buffer used in the crystallization solution, explaining the unsuccessful attempts at obtaining intermediate or bound substrates by soaking methods. At this pH, the catalytic cysteine (pK_a ~8.0) (39) should carry a thiol group and needs to be deprotonated to the nucleophilic thiolate to function properly. Because an intermediate was trapped in the WT enzyme, the acylation reaction is slow enough to observe the intermediate accumulation in the crystal (*i.e.* the nucleophilic activation is faster). Therefore, the absence of an intermediate formation in the mutant structure suggests that Glu-260 was required to activate the catalytic cysteine in the WT structure. The same function has been shown for the equivalent glutamate in hALDH2 (40, 41). However, under physiological conditions occurring in plant peroxisomes (a basic pH), we believe that the role of this glutamate is rather for proton abstraction from the hydrolytic water.

The presence of either intermediate or product/substrate in the active site does not induce conformational changes. The finding of a thiohemiacetal intermediate in only one subunit (subunit A) and the presence of either a substrate or carboxylate product in the other subunit would imply that in the context of dimer and the ALDH10 family, the hydride transfer (from NAD^+ to NADH followed by thioester formation) occurs in each subunit in turn. Otherwise, the covalent bond (between the catalytic cysteine Cys-295 in attacking conformation and a substrate molecule) would be randomly observed in both subunits. At the moment, we cannot conclude whether this property would be unique for the ALDH10 family or also apply for other ALDHs. Indeed, in the only other known case of the *Streptococcus* E268A-glyceraldehyde-3-phosphate dehydrogenase mutant (38), a thioester intermediate in all four subunits of the tetramer was observed due to a very slow deacylation rate allowing the accumulation of the intermediate in each subunit.

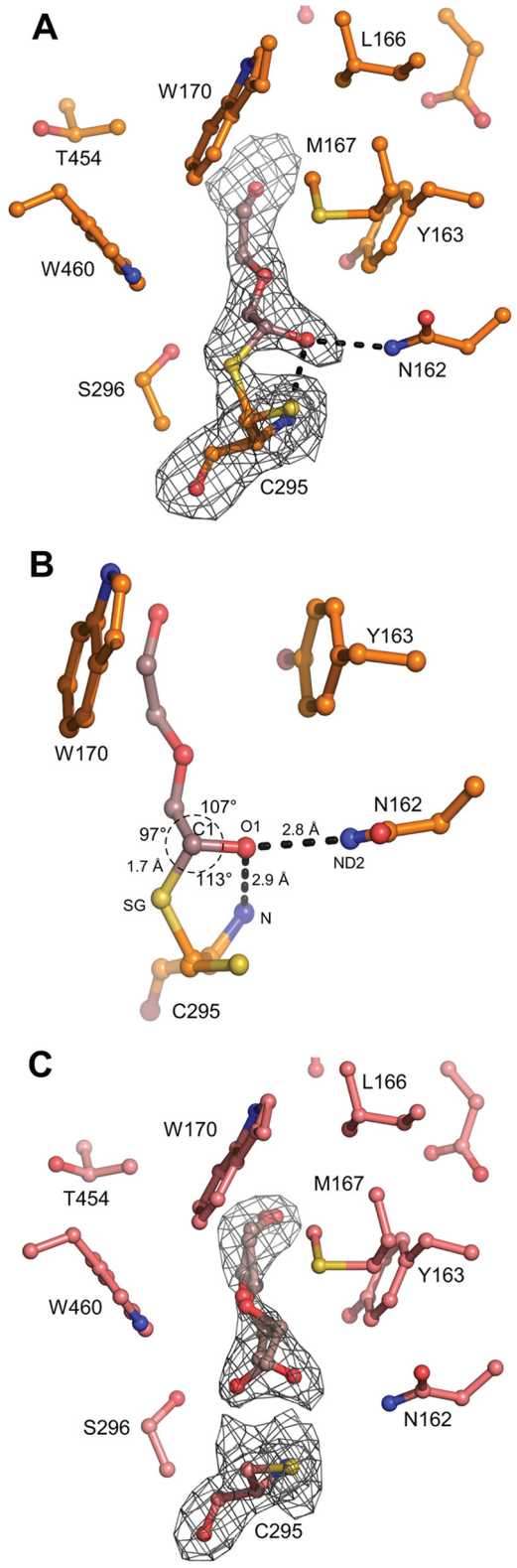

FIGURE 4. **SlAMADH1 substrate channel with a bound intermediate.** *A*, a *close-up view* of the active site in subunit A showing a continuous electron density from the $F_o - F_c$ omit map contoured at 3σ between the catalytic Cys-295 and the PEG aldehyde, which forms a thiohemiacetal intermediate. *B*, a covalent bond is formed between the SG atom of Cys-295 and the C1 atom of the PEG aldehyde. Hydrogen bonds between the intermediate and enzyme residues (Cys-295 and Asn-162) are shown as *dashed lines*. The angle geometry of this intermediate is shown. *C*, a *close-up view* of the active site in subunit B showing a discontinuous electron density map between the catalytic cysteine and the PEG aldehyde. Residues are *labeled*.

Role of Trp-288 and Tyr-163 in Catalysis of Aliphatic and Aromatic Aminoaldehydes—A comparison of the substrate channel residues in tomato, maize, and pea AMADHs shows that almost all residues are evolutionarily highly conserved (Table 5). Noticeably, two residues at positions 288 and 453 (PsAMADH numbering) are less preserved. Trp-288 could be substituted by Ala, Phe, or Ser, and Cys-453 could be substituted by Ser or Thr.

The five studied AMADHs exhibit the highest k_{cat} value with APAL (Tables 3 and 4). However, based on the k_{cat}/K_m ratio, APAL is the best substrate only for three of them (SlAMADH2, ZmAMADH1a, and ZmAMADH1b) as well as for PsAMADH2 (4), which all possess Trp-288 (Trp-289 in SlAMADH numbering, Trp-290 or -291 in ZmAMADHs). SlAMADH1 and ZmAMADH2, which contain an Ala at this position, prefer TMABAL as the best substrate, accented by the increased K_m values for APAL and ABAL. PsAMADH1 containing a phenylalanine also prefers TMABAL (4). Saturation curves for the five enzymes show that a strong excess substrate inhibition appears at relatively low substrate concentrations (Fig. 5, *A–E*). The inhibition appears at higher substrate concentrations for SlAMADH1 and ZmAMADH2 lacking Trp-288. This is in line with the behavior of the PsAMADH2-W288A mutant showing K_m values for APAL and ABAL 2–3-fold higher than those for the WT enzyme (17). The preference of TMABAL for Trp-288-absent AMADHs appears either directly due to the increase in the substrate channel diameter and the loss of possible π-electron stacking interaction with the electrophilic protonated amino group of the substrate or indirectly by affecting the position of the Tyr-163 side chain (see "BADH Activity of ZmAMADH1a and SlAMADH1; Role of Cys-446 and Asn-290"). Similar kinetic results have been reported for two rice (OsAMADHs) and barley (HvAMADHs) isoenzymes (6, 18). OsAMADH2 and HvAMADH2, which contain the Trp-288 residue, display significantly lower K_m values for APAL or ABAL than OsAMADH1 and HvAMADH1 lacking this tryptophan.

The five studied AMADHs oxidize 3- and 4-PCAL, representing heterocyclic aminoaldehydes with a tertiary nitrogen atom (Fig. 3). Interestingly, the product of 3-PCAL oxidation, named nicotinic acid, is methylated to the alkaloid trigonelline in plants, which acts among others as an osmoprotectant. AMADHs lacking the Trp-288 residue, such as SlAMADH1, ZmAMADH2, and PsAMADH1, should be more efficient, as demonstrated by the PsAMADH2-W288A mutant showing a 4 times higher rate with 3-PCAL than the WT enzyme (17). However, the activity of ZmAMADH2 and PsAMADH1 is not as high as that of SlAMADH1, which displays similar K_m and k_{cat} values for 3- and 4-PCAL as for the best aminoaldehyde substrates (Tables 3 and 4). Therefore, it becomes clear that such a change in SlAMADH1 kinetics does not only result from the Trp-288 absence.

Broad Substrate Specificity of SlAMADH1; Role of Thr-454—SlAMADH1 is unique among the studied enzymes in that it has a threonine at position 454 instead of a highly conserved cysteine or serine (Cys-453 in PsAMADHs). The substrate channel volume differs between SlAMADH1 and PsAMADH2, as is shown in Fig. 6*A*. A structural comparison of the substrate binding site

TABLE 5

A comparison of active-site residues in ALDH10 family from several plant species

Shown are active-site residues and C-terminal motifs of AMADHs from pea (PsAMADH) (4), tomato (SlAMADH), and maize (ZmAMADH). The numbering used follows the sequence of PsAMADH2, of which the substrate channel was previously analyzed by site-directed mutagenesis (17). Rice (OsAMADHs, UniProtKB numbers O24174 and Q84LK3) and barley enzymes (HvAMADHs, UniProtKB numbers Q94IC0 and Q94IC1) analyzed by other groups (6, 18) are shown for comparison and indicated by an asterisk. Enzymes accepting BAL as an efficient substrate are labeled with a cross.

	W109	D110	D113	N162	Y163	L166	M167	W170	E260	F284	W288	I293	C294	S295	I444	Q451	P452	C453	W459	C-term
PsAMADH2	W	D	D	N	Y	L	M	W	E	F	W	I	C	S	I	Q	P	C	W	AKL
PsAMADH1	A	D	D	N	Y	L	M	W	E	F	F	I	C	S	I	Q	P	S	W	SKL
SlAMADH1	A	D	D	N	Y	L	M	W	E	F	A	V	C	S	I	Q	P	T	W	SKN
SlAMADH2	S	D	D	N	Y	L	M	W	E	F	W	I	C	S	I	Q	P	C	W	SKL
ZmAMADH1a†	W	D	D	N	Y	L	M	W	E	F	W	I	C	S	C	Q	P	C	W	SKL
ZmAMADH1b	W	D	D	N	Y	L	M	W	E	F	W	I	C	S	I	Q	P	C	W	SKL
ZmAMADH2	G	D	D	N	Y	L	M	W	E	F	A	V	C	S	I	Q	P	C	W	SKL
*OsAMADH1	G	D	D	N	Y	L	M	W	E	F	A	V	C	S	I	Q	P	C	W	SKL
*OsAMADH2†	W	D	D	N	Y	L	M	W	E	F	W	I	C	S	I	Q	P	C	W	SKL
*HvAMADH1	A	D	D	N	Y	L	M	W	E	F	F	V	C	S	I	Q	P	T	W	SKL
*HvAMADH2†	W	D	D	N	Y	L	M	W	E	F	W	I	C	S	C	Q	P	C	W	AN–

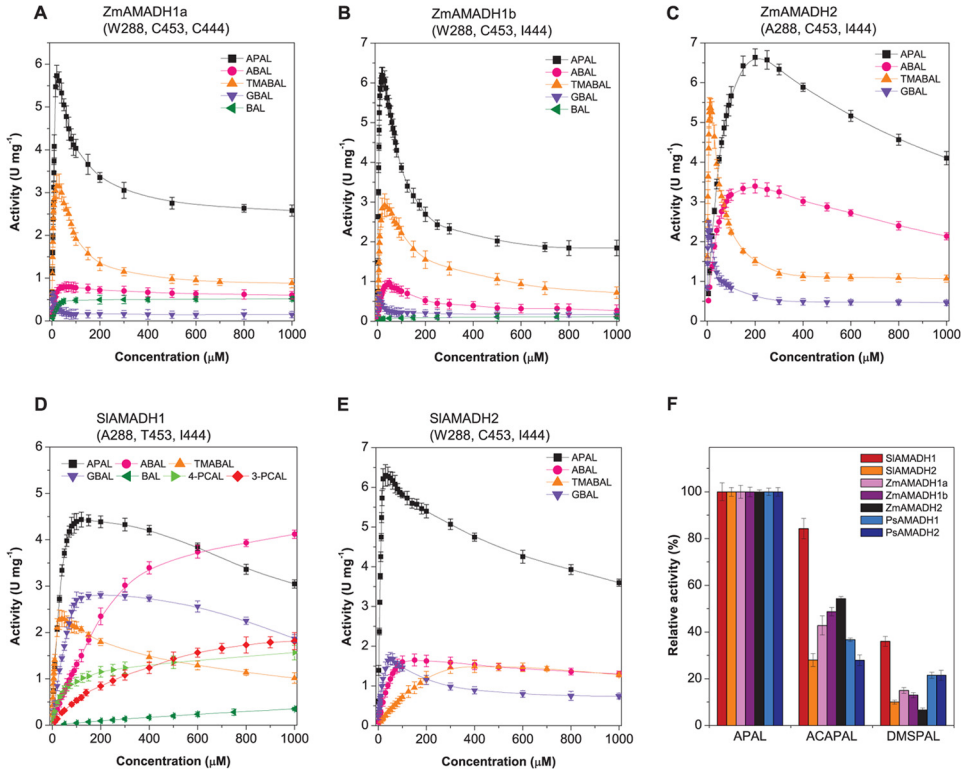

FIGURE 5. **Broad substrate specificity of plant AMADHs (ALDH10 family).** *A–E*, saturation curves for activity determination of ZmAMADHs and SlAMADHs. Data were measured in 0.15 M Tris-HCl buffer, pH 9.0, with APAL, ABAL, TMABAL, GBAL, BAL, 3-PCAL, and 4-PCAL as substrates in the presence of 1 mM NAD^+. *F*, relative activity values for all studied AMADHs with ACAPAL and DMSPAL. The data were measured in 0.15 M Tris-HCl, pH 9.0, using 1 mM substrate and in the presence of 1 mM NAD^+. The activity with APAL was taken as 100%. *Error bars*, S.D.

between SlAMADH1 and known plant AMADH structures reveals a displacement of four residues (from Thr-454 to Asp-457), which open the channel cavity in SlAMADH1. Thr-454, the most affected residue, is shifted by 1.8 Å away from the active site, allowing its side chain to make a hydrogen bond with the conserved Gln-485 NE1 atom from the oligomerization domain of the other subunit (Fig. 6*B*). Thr-454 is thus directly involved in the dimer interface interaction. The position of the Thr-454 side chain leads to a large and less polar channel interior, resulting in high rates of oxidation of aliphatic and aromatic aldehydes by SlAMADH1 compared with SlAMADH2 and both PsAMADHs (Figs. 3 and 5, *D* and *E*). Indeed, in PsAMADH1/2, the side chains of Ser-453/Cys-453 make the channel interior smaller by pointing inward and polar for substrate interaction (Fig. 6*C*). Therefore, the combination of the two residues, Ala-289 and Thr-454, distinguishes SlAMADH1 for its broad substrate specificity. The role of Thr-454 is emphasized by the PsAMADH2-C453A mutant, which does not display any significant differences from the WT enzyme (17).

BADH Activity of ZmAMADH1a and SlAMADH1; Role of Cys-446 and Asn-290—BAL, formed by choline monooxygenase (42) in plants, is oxidized by AMADH/BADH to the osmoprotectant GB. Under stress conditions, high levels of GB have been found in leaves of diverse families of dicots and monocots, including barley, wheat, and rye (43). In contrast, maize culti-

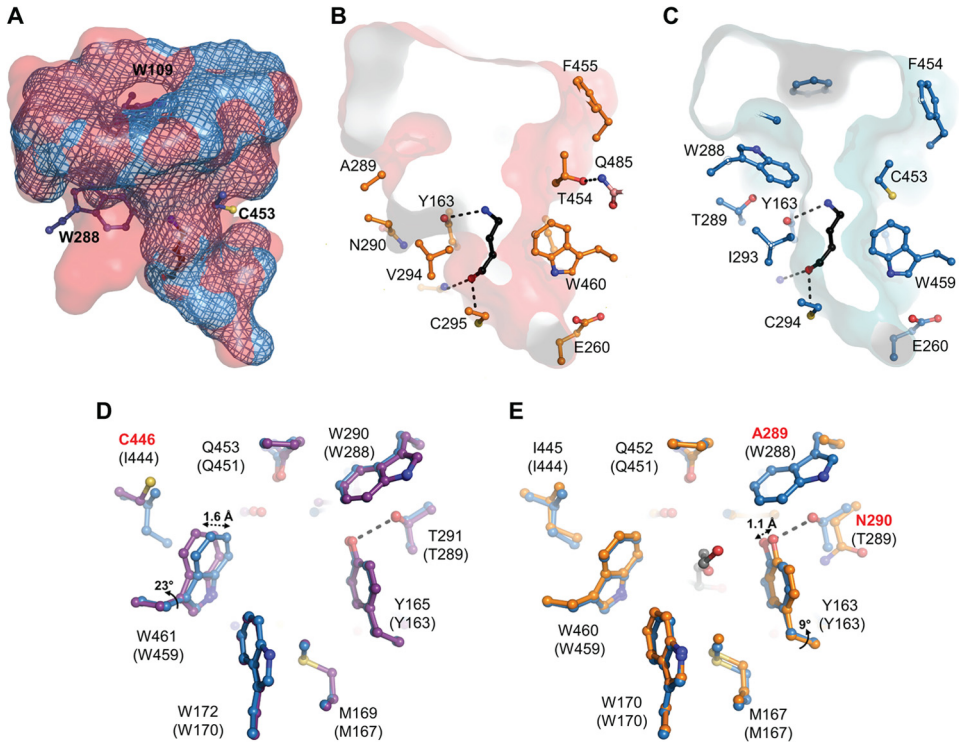

FIGURE 6. **Substrate channels of SlAMADH1, ZmAMADH1a, and PsAMADH2.** *A*, a comparison between the substrate channel volumes of SlAMADH1 (in *red*) and PsAMADH2 (in *blue mesh*; Protein Data Bank code 3IWJ). The enlarged volume of SlAMADH1 comes from the absence of Trp-109 and Trp-288 and a displacement at position 453; *B* and *C*, a transversal volume section of substrate channel of SlAMADH1 (in *red*) and PsAMADH2 (in *blue*), both with a docked ABAL ligand. These images show the enlarged middle section of the substrate channel of SlAMADH1, which occurs due to the presence of Ala-289 and Thr-454 residues compared with the presence of Trp-288 and Cys-453 in PsAMADH2. Thr-454 is hydrogen-bonded to Gln-485 from the other subunit and thus is involved in the dimer interface. Amino acid residues are shown as *sticks* and *labeled*. The total surface of the cavities was calculated using Hollow with 0.5-Å grid spacing and a 1.4-Å interior probe. The ABAL molecule (in *black*) is shown for illustration. It was docked into the active site using AutoDock, and its carbonyl oxygen atom establishes a hydrogen bond to the catalytic cysteine Cys-295/Cys-294, whereas the amino group is hydrogen-bonded to Tyr-163/Tyr-163; *D* and *E*, a substrate channel structural comparison of ZmAMADH1a (in *purple*) and SlAMADH1 (in *orange*) with PsAMADH2 (in *blue*, used as the reference for residue numbering shown in *parentheses*). Cys-446 in ZmAMADH1a allows a conserved Trp to move away from Tyr-165, thus opening the channel for a bulkier BAL molecule. Asn-290 in SlAMADH1 could have a similar role on the opposite side, allowing Tyr-163 to move toward Asn-290, thus opening the channel. Residues labeled in *red* are not totally conserved in plant AMADHs.

vars synthesize considerably lower levels of GB, and naturally occurring GB-deficient inbred lines have also been identified (44). Moreover, certain maize varieties with tomato and pea do not accumulate GB due to the loss of a functional *CMO* (choline monooxygenase) gene (45–47), correlated with the very low activity of ZmAMADH1b, ZmAMADH2, SlAMADH2, and PsAMADHs with BAL (below 1.5% compared with that with APAL; Fig. 3) (4). Interestingly, ZmAMADH1a exhibits a good activity with BAL (K_m = 14 μM, k_{cat} = 0.6 s^{-1}). SlAMADH1 oxidizes BAL significantly only at high concentrations, as indicated by the corresponding K_m value (Tables 3 and 4).

Based on AMADH structures, four strictly conserved residues, Tyr-163, Trp-170, Trp-288, and Trp-459 (Tyr-165, Trp-172, Trp-290, and Trp-461 in ZmAMADH1a), seem to be arranged suitably for cation-π interactions with the trimethylammonium group of BAL, which becomes sandwiched between Tyr-163 and Trp-459 upon binding. A structural comparison of the four plant AMADH structures (ZmAMADH1a, SlAMADH1, and PsAMADH1/2) reveals a difference between the position of Trp-461 in ZmAMADH1a and those of the equivalent tryptophans in the other three structures. Indeed, its side chain is shifted by 1.6 Å (corresponding to a rotation of 23° along the Cβ-Cγ axis) away from Tyr-163, leading to an enlargement of the substrate channel favorable for binding of the bulky trimethylammonium group (Fig. 6*D*). Ile-444 in PsAMADHs (Ile-445 in SlAMADH1) prevents Trp-459 from adopting the observed position in ZmAMADH1a due to a steric hindrance. Thus, the equivalent cysteine (Cys-446) in ZmAMADH1a, located in the second sphere of the substrate interaction, is responsible for the high activity with BAL, as shown in spinach AMADH/BADH (SoBADH; Protein Data Bank code 4A0M) (48). Notably, the concerned tryptophan and cysteine residues adopt the same position in ZmAMADH1a and SoBADH structures. HvAMADH2, which also contains a cysteine, exhibits a good BAL activity (18). Moreover, AMADHs from members of the Amaranthaceae family (amaranth, spinach, and sugarbeet), from several monocots like barley or wheat, and from several grasses like sorghum or velvetgrass, known for their high BADH activity, possess such a cysteine (or an alanine) (49, 50, 10, 51). The low or negligible BADH activity of ZmAMADH1b, ZmAMADH2, SlAMADH2, and PsAMADHs correlates with the presence of Ile-444 (Table 5). However, despite the presence of Ile-445 in SlAMADH1, its activity with BAL resembles that of the mutant Y163A from PsAMADH2 (17). Here the structural comparison shows that Tyr-163, in SlAMADH1, has no hydrogen bond involving its hydroxyl group (conversely, there is a hydrogen bond with the Thr-289 side chain in PsAMADH, which is

replaced by Asn-290 in SlAMADH1). Asn-290 does not interact with Tyr-163, which could move toward Asn-290 and away from the channel substrate. The flexibility of Tyr-163 in SlAMADH1 would allow bulkier BAL to pass to the catalytic cysteine. Thus, Asn-290 in SlAMADH1, located in the second sphere of substrate interaction, might have a similar role like that of Cys-446 in ZmAMADH1a, in terms of the channel widening, acting on the opposite side on the substrate channel. Another interesting different movement of Tyr-163 is observed in SlAMADH1 and PsAMADH2 structures compared with the two others. Its hydroxyl group can move 1.1 Å (corresponding to a rotation of 9° along the Cα-Cβ axis) toward Ala-289 and the equivalent Phe-288 residue, respectively, which is only possible due to the absence of Trp-288 at this position (Fig. 6*E*). Consequently, the nature of the residue at position 288 will have a significant effect on the interaction between the Tyr-163 side chain and the substrate.

Interestingly, human ALDH9 (ALDH9A1, also called E3 isoenzyme) has been shown to prefer TMABAL (K_m = 1.4 μM) over ABAL (K_m = 8–14 μM) and BAL (K_m = 120 μM) (23). The low K_m value for ABAL indicates that this enzyme is involved in GABA formation (reviewed in Ref. 53). So far, APAL and GBAL have not been tested with this enzyme. The other well studied ALDH9 from rat liver also shows a high preference for TMABAL. Fish ALDH9 from cod liver (Protein Data Bank codes 1A4S and 1BPW) (54) shows a higher k_{cat}/K_m ratio for BAL over aliphatic and aromatic aldehydes, and this is why the enzyme is called BADH (55). To our knowledge, other ω-aminoaldehydes have not yet been tested, but the active site preserves aromatic residues responsible for AMADH activity, typical for the ALDH10 family, namely Tyr-167 (Tyr-163 in ALDH10), Trp-174 (Trp-170), and Phe-466 (Trp-459). The variable Trp-288 in ALDH10 is replaced by Leu-291.

ACAPAL and DMSPAL Dehydrogenase Activities—Besides the two natural compounds APAL and ABAL, known to be among the best substrates of all plant AMADHs studied so far, we show for the first time that ACAPAL may also be generally oxidized (Fig. 5*F*). Therefore, these enzymes are unique in metabolizing and detoxifying characteristic aldehyde products of polyamine degradation to nontoxic acids. SlAMADH1 shows 85% activity with ACAPAL compared with that with APAL, whereas SlAMADH2 displays only 30% activity. For ZmAMADHs, the activity is between 43 and 55%, and for PsAMADHs, it is between 28 and 35%. With respect to ACAPAL oxidation by AMADH isoenzymes in a single species, the activity of the Trp-288-absent AMADH isoenzyme is higher. APAL mainly originates from the "polyamine back-conversion pathway" via the oxidation of spermine (to spermidine) and spermidine (to putrescine) on the *exo*-side of N^4-nitrogen by plant PAOs (56, 57). Likewise, the oxidation of N^1-acetylspermine and N^1-acetylspermidine ends up with ACAPAL. APAL or ACAPAL is oxidized by AMADH to β-alanine and 3-acetamidopropionate, respectively. β-Alanine can subsequently be methylated to the osmoprotectant β-alanine betaine (58). It is notable that three of five *Arabidopsis* PAOs are localized in peroxisomes (57, 59, 60). Another part of polyamine catabolism is localized outside peroxisomes because the existence of apoplastic and symplastic PAOs has also been reported (56, 57). These PAOs also oxidize polyamines on the *endo*-side of N^4-nitrogen, producing 1,3-propanediamine (from spermine) and ABAL (from spermidine). Because plant PAOs seem to have no activity or negligible activity with putrescine (57, 59), ABAL apparently originates from putrescine oxidation by plant copper diamine oxidases. It is then oxidized by AMADHs to GABA.

DMSPAL accumulates in many marine algae and a few higher plant species, including the Asteraceae and Poaceae families (9, 61). So far, DMSPAL has been shown to be oxidized by sugar beet and amaranth AMADHs/BADHs (10). Here we show that all studied AMADHs are capable of oxidizing it to the cryo- and osmoprotectant DMSP sharing similar properties with betaines (8, 61) (Fig. 5*F*). Indeed, SlAMADH1 and SlAMADH2 oxidize this compound at a 36 and 10% rate, respectively, compared with that with their best substrate. Likewise, ZmAMADHs display rates between 8 and 16% compared with those with APAL and both PsAMADHs at a 22% rate. The universal ability of AMADHs to convert DMSPAL seems related to its stable positive charge at the dimethylsulfonio group and its structural similarity with APAL, which is protonated at the primary amino group under physiological conditions. As well as ω-aminoaldehydes, DMSPAL is trapped into a nucleophilic cage formed by the carboxylic and aromatic residues at the active site of AMADH.

AMADH Gene Expression and Subcellular Localization—qPCR analysis shows that the expression of both tomato *AMADH* genes is relatively different. In contrast to the *SlAMADH1* gene, the *SlAMADH2* gene is highly and ubiquitously expressed in all analyzed tissues (Fig. 7). Whereas *SlAMADH2* is well expressed in roots at 10 days after germination and at 6 weeks, *SlAMADH1* is not expressed at all and expressed at a low extent (by 2 orders of magnitude), respectively. Both genes are expressed in cotyledons at 10 days after germination and later in flower organs (petals, carpel, and stamens) and senescent leaves. These data indicate that SlAMADH2 is playing a major role in all tomato organs in detoxifying toxic ω-aminoaldehydes. The observed high activity of both SlAMADHs with APAL and ABAL is in a good agreement with previous data obtained from *in vivo* experiments on tomatoes, where the formation of β-alanine and GABA was observed as a result of polyamine degradation (62).

Because of the incomplete knowledge of tomato genome, it was impossible to localize the tomato genes, whereas those for maize could be mapped. The paralogs *ZmAMADH1a* and *ZmAMADH1b* are located on chromosomes 4 and 1, respectively. The gene of *ZmAMADH2* is located on chromosome 10. The three maize genes are expressed differently (Fig. 7). A major difference concerns the *ZmAMADH2* gene, which is markedly less expressed than the others. Transcript abundance of *ZmAMADH2* is higher in silks at 0 and 5 days after pollination and in the kernel at 5 days after pollination. *ZmAMADH1a* (coding for the AMADH isoform with higher BADH activity) is highly expressed in young and mature leaves as well as in roots of younger plants. Transcript abundance of Z*mAMADH1b* is weaker in leaves but higher in roots compared with that of *ZmAMADH1a*. *ZmAMADH1b* is also highly expressed in silks at 0 days after pollination and in the kernel at 5 days after pol-

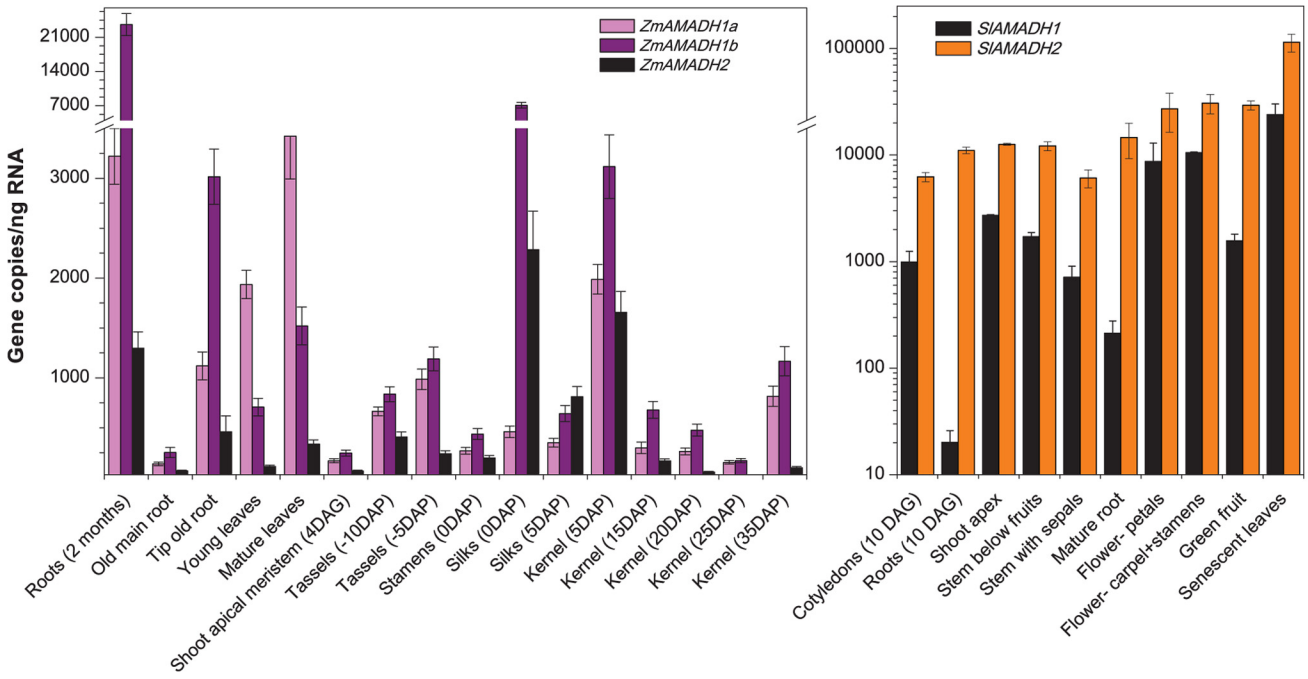

FIGURE 7. **Expression profiles of two *SlAMADH* and three *ZmAMADH* genes in various organs as evaluated by qPCR.** Transcript abundance is expressed as gene copy number in 1 ng of total RNA amplified by qPCR, normalized to *EF1α*, and recalculated as primer pair efficiency. Tomato samples, including roots and cotyledons, were collected at 10 days after germination (*DAG*); shoot apices (stem plus leaves), stems below flowers (including sepals), stems below fruits, petals, reproductive organs, green fruit, roots, and senescent leaves were collected from 6-week-old plants grown on a soil/peat mixture (2:1, v/v). Maize samples were collected from 3-month-old plants unless indicated otherwise. Tassels, silks, and kernels were collected at several days before, during, and after pollination (*DAP*). *Error bars*, S.D.

lination. Both *ZmAMADH1* genes are well expressed in tassels. These data indicate that AMADHs might be important for controlling ω-aminoaldehyde levels during early stages of the seed development.

Recently, several studies have shown that *AMADH2* gene mutation, naturally occurring in several rice varieties, is responsible for their fragrance (6, 63, 64). *AMADH2* was found to be transcribed constitutively in all tissues tested except for roots. The fragrance appears due to high abundance and subsequent acetylation of free ABAL and accumulation of 2-acetyl-Δ^1-pyrroline. Traditional aromatic cultivars often have undesirable properties, including poor crop yield, susceptibility to pests and diseases, and strong shedding. Although their causes have not been analyzed so far, based on our results, these will be a combination of accumulation of toxic aminoaldehydes and lower content of zwitterionic products (β-alanine betaine, GABA, and others) having osmo-, cryo-, and heat-protecting properties.

Most plant AMADHs, including rice AMADHs and HvAMADH1, carry the SKL C-terminal peroxisomal targeting signal (PTS-1) (14, 65). All of our studied AMADHs except for SlAMADH1 contain PTS-1. Indeed, SlAMADH1 ends with a tripeptide SKN, which is not a peroxisomal targeting signal, making SlAMADH1 probably localized in the cytosol. The loss of the peroxisomal signal in one of the two AMADH isoforms has been observed in many plant species. For example, in *Arabidopsis*, one isoform (with SKL signal) is localized in peroxisomes, whereas the other (KSPN motif at the C terminus) is targeted to leucoplasts (66). Similarly, in barley, one isoform was demonstrated to be localized in peroxisomes, whereas the second appears to reside in the cytosol (65). The exact subcellular localization of SlAMADH1 remains unclear.

The phylogenetic analysis of numerous AMADH/BADH sequences from monocots and dicots shows that there are two homologous sequences per species among flowering plants and an additional one for maize. Thus, we believe this number can be higher in species with genome duplications. Among monocots, including maize, rice, and barley, two orthologous AMADH subgroups can be identified (Fig. 8). One subgroup contains a cluster of the Triticeae (Poaceae family) predictable as wide substrate-specific AMADHs (due to the presence of Phe-288 and Thr-454 in PsAMADH numbering; Fig. 8, *highlighted* in *yellow*). Moreover, the presence of Asn-289 implies that Tyr-163 is mobile, affecting the substrate binding. A similar cluster is found in dicots from the Solanaceae family. The majority of members in the other monocot subgroup display significant BADH activity due to the presence of an Ala-444 or Cys-444 residue favoring BAL binding (48). They also possess the Trp-288 residue. Interestingly, higher BAL activity correlates in part with nonperoxisomal targeting. For example, HvAMADH2, wild rye AMADH2, and wheat AMADH1 miss the SKL targeting signal and carry a C-terminal KAPAN motif instead. In the dicots, such a clustering only exists among closely related species. Here again, sequences of AMADHs with BADH activity from the Amaranthaceae, Acanthaceae, and Salicaceae families carry the KSP C-terminal signal as well as Ala-444 and Trp-288. Such a variable targeting indicates that *AMADH* genes might be differently responsive to, for example, stress conditions in various plants. The differential subcellular localization of AMADHs may arise from the interconnection of

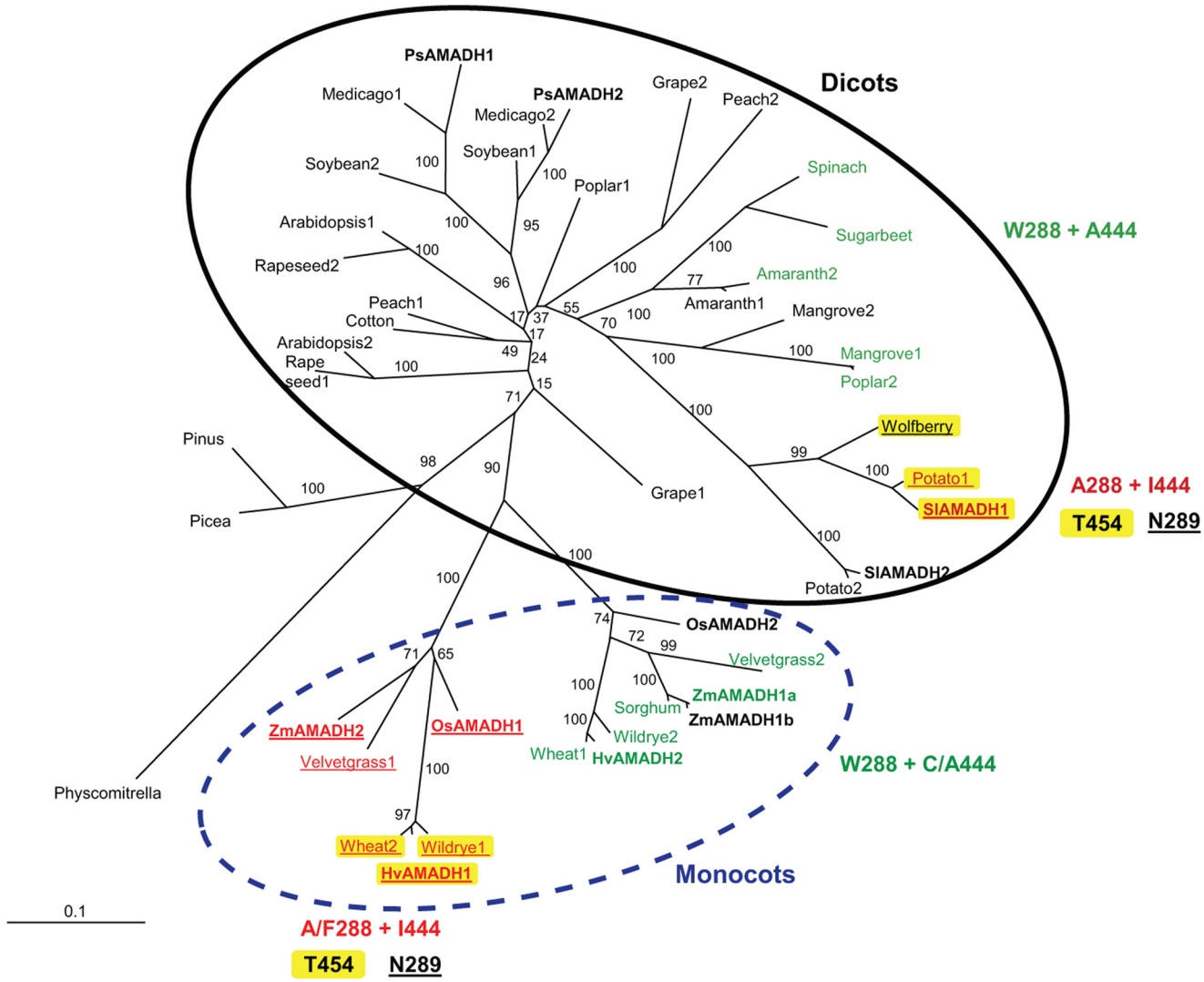

FIGURE 8. **Phylogenetic analysis of the plant ALDH10 family (AMADHs).** The unrooted phylogenetic consensus tree shows two distinct groups of AMADHs, one from dicots (*solid line*) and the other from monocots (*dashed line*). PsAMADH numbering is used to point out crucial residues modulating substrate specificity. AMADHs exhibiting a significant BADH activity are *highlighted* in *green*. AMADHs predictable as broad substrate specific enzymes are *highlighted* in *yellow* due to the presence of Thr-454. The presence of Asn-289 implies that Tyr-163 is mobile, affecting the substrate binding. The enzymes from maize (ZmAMADHs) and tomato (SlAMADHs) analyzed in this work are shown in *boldface type*, as are the previously characterized reference enzymes from peas (PsAMADHs) (4), rice (OsAMADHs) (6), and barley (HvAMADHs) (18). The *internal labels* give bootstrap frequencies for each clade. See "Experimental Procedures" for the corresponding GenBank™ accession numbers.

several metabolic pathways. Several PAOs are targeted to peroxisomes, where they generate APAL and ACAPAL from polyamines, which are detoxified by peroxisomal AMADHs. Other PAOs as well as copper diamine oxidases are localized in the cytoplasm. Copper diamine oxidases produce ABAL from putrescine, which is oxidized to GABA. In species accumulating GB, AMADHs are often found in chloroplasts (as well as choline monooxygenase), where they convert BAL to GB.

CONCLUSIONS

In this work, we continued studies on substrate specificity of plant AMADHs. After previous analysis of two PsAMADHs, we now cloned five more genes: two from tomato and three from maize. We produced and purified the corresponding enzymes (SlAMADH1, SlAMADH2, ZmAMADH1a, ZMAMADH1b, and ZmAMADH2) to characterize them kinetically. Because two of them stand out from the others in terms of substrate specificity, SlAMADH1 having the broadest range of substrates and ZmAMADH1a having high BADH activity, we determined their crystal structures. From structural comparisons, we observe that SlAMADH1 is distinguished by its large and less polar substrate channel due to residues at positions 289 and 454 (288 and 453 in PsAMADHs), which are responsible for this large specificity. We can also predict that AMADHs containing Ile-444 (PsAMADH numbering) have a negligible BADH activity, and those containing Asn-289 may display some BADH activity. The wide substrate specificity of SlAMADH1 allowed us to trap a thiohemiacetal intermediate in the structure, never observed before, which, in addition to the SlAMADH1-E260A structure, suggests a bifunctional role of the active-site base glutamate. In addition to its known role for the activation of the hydrolytic water, it can activate the protonated catalytic cysteine.

Based on results of the entire study, we can now state that a tryptophan (Trp-288 in PsAMADHs), which is found in more than three-quarters of AMADH sequences, together with the conserved cluster of Tyr-163, Trp-170, and Trp-459, is responsible for the high affinity to ω-aminoaldehydes with APAL as the best substrate. AMADHs devoid of this tryptophan prefer TMABAL either directly due to the increase in the substrate channel diameter (and consequent loss of possible π-electron stacking interaction with the electrophilic protonated amino group of the substrate) or indirectly by affecting the position of the Tyr-163 side chain involved in substrate interaction. For the first time, we identified ACAPAL as a possible common substrate for all plant AMADHs. We also showed that the enzymes are capable of oxidizing DMSPAL to form the cryo- and osmoprotectant DMSP.

It becomes now obvious that AMADHs, depending on the plant species, are capable of oxidizing a wide range of naturally occurring ω-aminoaldehydes, resulting in the production of various amino acids that may directly or after a further conversion function as osmoprotectants. Thus, in plants, AMADHs control levels of ω-aminoaldehydes, which are produced under normal and stress conditions. Current transgenic studies on the overexpression of *AMADH*/*BADH* in plants conferring increased abiotic stress tolerance are aimed especially at GB production. Related engineering of GB synthesis in species with nonfunctional choline monooxygenase is also targeted rather narrowly. In the context of the present work, the wide substrate specificity of plant AMADHs indicates that there is a possibility of altered production of β-alanine betaine, GABA, or γ-butyrobetaine, which is worthy of consideration for the development and analysis of stress-tolerant transgenic crops. The latter compound may also be involved in the biosynthetic pathway of L-carnitine in plants, which shares similar features with pathways in mammals and fungi. In addition to its role in the mitochondrial transport of fatty acids, L-carnitine was also shown to confer tolerance to abiotic stress (52, 67).

Acknowledgments—We are grateful to Beatriz Guimaraes for help in data collection on PROXIMA 1 at the SOLEIL synchrotron and to Dr. Jacques Snégaroff (Institut Jean-Pierre Bourgin, INRA Versailles) and Prof. Thomas D. Hurley (Indiana University School of Medicine) for helpful discussion during manuscript preparation. This work benefited from IMAGIF platform facilities at the Centre de Recherche de Gif-sur-Yvette (FRC3115, CNRS, France) for crystallization work at the Structural Biology and Proteomic Unit in the Laboratoire d'Enzymologie et Biochimie Structurales.

REFERENCES

1. Bouchereau, A., Aziz, A., Larher, F., and Martin-Tanguy, J. (1999) Polyamines and environmental challenges. Recent development. *Plant Sci.* **140,** 103–125
2. Šebela, M., Frébort, I., Petřivalský, M., and Peč, P. (2002) Copper/topa quinone-containing amine oxidases. Recent research developments. in *Studies in Natural Products Chemistry*, Vol. 26, *Bioactive Natural Products*, Part G (Atta-ur-Rahman, ed) pp. 1259–1299, Elsevier, Amsterdam
3. Li, W., Yuan, X. M., Ivanova, S., Tracey, K. J., Eaton, J. W., and Brunk, U. T. (2003) 3-Aminopropanal, formed during cerebral ischaemia, is a potent lysosomotropic neurotoxin. *Biochem. J.* **371,** 429–436
4. Tylichová, M., Kopečný, D., Moréra, S., Briozzo, P., Lenobel, R., Snégaroff, J., and Šebela, M. (2010) Structural and functional characterization of plant aminoaldehyde dehydrogenase from *Pisum sativum* with a broad specificity for natural and synthetic aminoaldehydes. *J. Mol. Biol.* **396,** 870–882
5. Bouché, N., and Fromm, H. (2004) GABA in plants. Just a metabolite? *Trends Plant Sci.* **9,** 110–115
6. Bradbury, L. M., Gillies, S. A., Brushett, D. J., Waters, D. L., and Henry, R. J. (2008) Inactivation of an aminoaldehyde dehydrogenase is responsible for fragrance in rice. *Plant Mol. Biol.* **68,** 439–449
7. Arikit, S., Yoshihashi, T., Wanchana, S., Uyen, T. T., Huong, N. T., Wongpornchai, S., and Vanavichit, A. (2011) Deficiency in the amino aldehyde dehydrogenase encoded by GmAMADH2, the homologue of rice Os2AP, enhances 2-acetyl-1-pyrroline biosynthesis in soybeans (*Glycine max* L.). *Plant Biotechnol. J.* **9,** 75–87
8. Rhodes, D., and Hanson, A. D. (1993) Quaternary ammonium and tertiary sulfonium compounds in higher plants. *Annu. Rev. Plant Physiol. Plant Mol. Biol.* **44,** 357–384
9. James, F., Paquet, L., Sparace, S. A., Gage, D. A., and Hanson, A. D. (1995) Evidence implicating dimethylsulfoniopropionaldehyde as an intermediate in dimethylsulfoniopropionate biosynthesis. *Plant Physiol.* **108,** 1439–1448
10. Trossat, C., Rathinasabapathi, B., and Hanson, A. D. (1997) Transgenically expressed betaine aldehyde dehydrogenase efficiently catalyzes oxidation of dimethylsulfoniopropionaldehyde and ω-aminoaldehydes. *Plant Physiol.* **113,** 1457–1461
11. Kirch, H. H., Bartels, D., Wei, Y., Schnable, P. S., and Wood, A. J. (2004) The ALDH gene superfamily of *Arabidopsis*. *Trends Plant Sci.* **9,** 371–377
12. Sophos, N. A., Vasiliou, V. (2003) Aldehyde dehydrogenase gene superfamily. The 2002 update. *Chem. Biol. Interact.* **143,** 5–22
13. Nakamura, T., Yokota, S., Muramoto, Y., Tsutsui, K., Oguri, Y., Fukui, K., and Takabe, T. (1997) Expression of a betaine aldehyde dehydrogenase gene in rice, a glycinebetaine nonaccumulator, and possible localization of its protein in peroxisomes. *Plant J.* **11,** 1115–1120
14. Reumann, S., Babujee, L., Ma, C., Wienkoop, S., Siemsen, T., Antonicelli, G. E., Rasche, N., Lüder, F., Weckwerth, W., and Jahn, O. (2007) Proteome analysis of *Arabidopsis* leaf peroxisomes reveals novel targeting peptides, metabolic pathways, and defense mechanisms. *Plant Cell* **19,** 3170–3193
15. Perez-Miller, S. J., and Hurley, T. D. (2003) Coenzyme isomerization is integral to catalysis in aldehyde dehydrogenase. *Biochemistry* **42,** 7100–7109
16. Wymore, T., Hempel, J., Cho, S. S., Mackerell, A. D., Jr., Nicholas, H. B., Jr., and Deerfield, D. W., 2nd (2004) Molecular recognition of aldehydes by aldehyde dehydrogenase and mechanism of nucleophile activation. *Proteins* **57,** 758–771
17. Kopečný, D., Tylichová, M., Snegaroff, J., Popelková, H., and Šebela, M. (2011) Carboxylate and aromatic active-site residues are determinants of high-affinity binding of ω-aminoaldehydes to plant aminoaldehyde dehydrogenases. *FEBS J.* **278,** 3130–3139
18. Fujiwara, T., Hori, K., Ozaki, K., Yokota, Y., Mitsuya, S., Ichiyanagi, T., Hattori, T., and Takabe, T. (2008) Enzymatic characterization of peroxisomal and cytosolic betaine aldehyde dehydrogenases in barley. *Physiol. Plant* **134,** 22–30
19. Brocker, C., Vasiliou, M., Carpenter, S., Carpenter, C., Zhang, Y., Wang, X., Kotchoni, S. O., Wood, A. J., Kirch, H. H., Kopečný, D., Nebert, D. W, and Vasiliou, V. (2013) Aldehyde dehydrogenase (ALDH) superfamily in plants. Gene nomenclature and comparative genomics. *Planta* **237,** 189–210
20. Tylichová, M., Briozzo, P., Kopečný, D., Ferrero, J., Moréra, S., Joly, N., Snégaroff, J., and Šebela, M. (2008) Purification, crystallization and preliminary crystallographic study of a recombinant plant aminoaldehyde dehydrogenase from *Pisum sativum*. *Acta Crystallogr. Sect. F Struct. Biol. Cryst. Commun.* **64,** 88–90
21. Šebela, M., Štosová, T., Havlis, J., Wielsch, N., Thomas, H., Zdráhal, Z., and Shevchenko, A. (2006) Thermostable trypsin conjugates for high-throughput proteomics. Synthesis and performance evaluation. *Proteomics* **6,** 2959–2963
22. Sebela, M., Brauner, F., Radová, A., Jacobsen, S., Havlis, J., Galuszka, P., and Pec, P. (2000) Characterisation of a homogeneous plant aminoalde-

hyde dehydrogenase. *Biochim. Biophys. Acta.* **1480,** 329–341
23. Vaz, F. M., Fouchier, S. W., Ofman, R., Sommer, M., and Wanders, R. J. (2000) Molecular and biochemical characterization of rat γ-trimethylaminobutyraldehyde dehydrogenase and evidence for the involvement of human aldehyde dehydrogenase 9 in carnitine biosynthesis. *J. Biol. Chem.* **275,** 7390–7394
24. Wood, P. L., Khan, M. A., and Moskal, J. R. (2007) The concept of "aldehyde load" in neurodegenerative mechanisms. Cytotoxicity of the polyamine degradation products hydrogen peroxide, acrolein, 3-aminopropanal, 3-acetamidopropanal and 4-aminobutanal in a retinal ganglion cell line. *Brain Res.* **1145,** 150–156
25. Holt, A., Degenhardt, O. S., Berry, P. D., Kapty, J. S., Mithani, S., Smith, D. J., and Di Paolo, M. L. (2007) The effects of buffer cations on interactions between mammalian copper-containing amine oxidases and their substrates. *J. Neural Transm.* **114,** 733–741
26. Kabsch, W. (2010) XDS. *Acta Crystallogr. D Biol. Crystallogr.* **66,** 125–132
27. McCoy, A. J., Grosse-Kunstleve, R. W., Adams, P. D., Winn, M. D., Storoni, L. C., Read, R. J. (2007) Phaser crystallographic software. *J. Appl. Crystallogr.* **40,** 658–674
28. Blanc, E., Roversi, P., Vonrhein, C., Flensburg, C., Lea, S. M., and Bricogne, G. (2004) Refinement of severely incomplete structures with maximum likelihood in BUSTER-TNT. *Acta Crystallogr. D Biol. Crystallogr.* **60,** 2210–2221
29. Emsley, P., Cowtan, K. (2004) Coot. Model-building tools for molecular graphics. *Acta Crystallogr. D Biol. Crystallogr.* **60,** 2126–2132
30. Edgar, R. C. (2004) MUSCLE. Multiple sequence alignment with high accuracy and high throughput. *Nucleic Acids Res.* **32,** 1792–1797
31. Guindon, S., and Gascuel, O. (2003) A simple, fast, and accurate algorithm to estimate large phylogenies by maximum likelihood. *Syst. Biol.* **52,** 696–704
32. Zheng, H., Chruszcz, M., Lasota, P., Lebioda, L., and Minor, W. (2008) Data mining of metal ion environments present in protein structures. *J. Inorg. Biochem.* **102,** 1765–1776
33. Lamb, A. L., and Newcomer, M. E. (1999) The structure of retinal dehydrogenase type II at 2.7 Å resolution. Implications for retinal specificity. *Biochemistry* **38,** 6003–6011
34. González-Segura, L., Rudiño-Piñera, E., Muñoz-Clares, R. A., and Horjales, E. (2009) The crystal structure of a ternary complex of betaine aldehyde dehydrogenase from *Pseudomonas aeruginosa* provides new insight into the reaction mechanism and shows a novel binding mode of the 2′-phosphate of $NADP^+$ and a novel cation binding site. *J. Mol. Biol.* **385,** 542–557
35. Izaguirre, G., Pietruszko, R., Cho, S., and MacKerell, A. Jr. (2001) Human aldehyde dehydrogenase catalytic activity and structural interactions with coenzyme analogs. *J. Biomol. Struct. Dyn.* **19,** 429–447
36. Hill, E. J., Chou, T. H., Shih, M. C., and Park, J. H. (1975) Covalent binding of 3-pyridinealdehyde nicotinamide adenine dinucleotide and substrate to glyceraldehyde 3-phosphate dehydrogenase. *J. Biol. Chem.* **250,** 1734–1740
37. Steinmetz, C. G., Xie, P., Weiner, H., and Hurley, T. D. (1997) Structure of mitochondrial aldehyde dehydrogenase. The genetic component of ethanol aversion. *Structure* **5,** 701–711
38. D'Ambrosio, K., Pailot, A., Talfournier, F., Didierjean, C., Benedetti, E., Aubry, A., Branlant, G., and Corbier, C. (2006) The first crystal structure of a thioacylenzyme intermediate in the ALDH family. New coenzyme conformation and relevance to catalysis. *Biochemistry* **45,** 2978–2986
39. Brauner, F., Šebela, M., Snégaroff, J., Peč, P., and Meunier, J. C. (2003) Pea seedling aminoaldehyde dehydrogenase. Primary structure and active site residues. *Plant Physiol. Biochem.* **41,** 1–10
40. Wang, X., and Weiner, H. (1995) Involvement of glutamate 268 in the active site of human liver mitochondrial (class 2) aldehyde dehydrogenase as probed by site-directed mutagenesis. *Biochemistry* **34,** 237–243
41. Mann, C. J., and Weiner, H. (1999) Differences in the roles of conserved glutamic acid residues in the active site of human class 3 and class 2 aldehyde dehydrogenases. *Protein Sci.* **8,** 1922–1929
42. Brouquisse, R., Weigel, P., Rhodes, D., Yocum, C. F., and Hanson, A. D. (1989) Evidence for a ferredoxin-dependent choline monooxygenase from spinach chloroplast stroma. *Plant Physiol.* **90,** 322–329
43. Ishitani, M., Arakawa, K., Mizuno, K., Kishitani, S., and Takabe, T. (1993) Betaine aldehyde dehydrogenase in the Gramineae. Levels in leaves of both betaine-accumulating and non-accumulating cereal plants. *Plant Cell Physiol.* **34,** 493–495
44. Brunk, D. G., Rich, P. J., and Rhodes, D. (1989) Genotypic variation for glycinebetaine among public inbreds of maize. *Plant Physiol.* **91,** 1122–1125
45. Lerma, C., Rich, P. J., Ju, G. C., Yang, W.-J., Hanson, A. D., and Rhodes, D. (1991) Betaine deficiency in maize. Complementation tests and metabolic basis. *Plant Physiol.* **95,** 1113–1119
46. Mäkelä, P., Jokinen, K., Kontturi, M., Peltonen-Sainio, P., Pheu, E., and Somersalo, S. (1998) Foliar application of glycinebetaine, a novel product from sugar beet, as an approach to increase tomato yield. *Ind. Crop. Prod.* **7,** 139–148
47. Charlton, A. J., Donarski, J. A., Harrison, M., Jones, S. A., Godward, J., Oehlschlager, S., Arques, J. L., Ambrose, M., Chinoy, C., Mullineaux, P. M., and Domoney, C. (2008) Responses of the pea (*Pisum sativum* L.) leaf metabolome to drought stress assessed by nuclear magnetic resonance spectroscopy. *Metabolomics* **4,** 312–327
48. Díaz-Sánchez, Á. G., González-Segura, L., Mújica-Jiménez, C., Rudiño-Piñera, E., Montiel, C., Martínez-Castilla, L. P., Muñoz-Clares, R. A. (2012) Amino acid residues critical for the specificity for betaine aldehyde of the plant ALDH10 isoenzyme involved in the synthesis of glycine betaine. *Plant Physiol.* **158,** 1570–1582
49. Weigel, P., Weretilnyk, E. A., and Hanson, A. D. (1986) Betaine aldehyde oxidation by spinach chloroplasts. *Plant Physiol.* **82,** 753–759
50. Hibino, T., Meng, Y. L., Kawamitsu, Y., Uehara, N., Matsuda, N., Tanaka, Y., Ishikawa, H., Baba, S., Takabe, T., Wada, K., Ishii, T., and Takabe, T. (2001) Molecular cloning and functional characterization of two kinds of betaine-aldehyde dehydrogenase in betaine-accumulating mangrove *Avicennia marina* (Forsk.) Vierh. *Plant Mol. Biol.* **45,** 353–363
51. Valenzuela-Soto, E. M., and Muñoz-Clares, R. A. (1994) Purification and properties of betaine aldehyde dehydrogenase extracted from detached leaves of *Amaranthus hypochondriacus* L. subjected to water deficit. *J. Plant Physiol.* **143,** 145–152
52. Rippa, S., Zhao, Y., Merlier, F., Charrier, A., and Perrin, Y. (2012) The carnitine biosynthetic pathway in *Arabidopsis thaliana* shares similar features with the pathway of mammals and fungi. *Plant Physiol. Biochem.* **60,** 109–114
53. Marchitti, S. A., Brocker, C., Stagos, D., and Vasiliou, V. (2008) Non-P450 aldehyde oxidizing enzymes: the aldehyde dehydrogenase superfamily. *Expert Opin. Drug Metab. Toxicol.* **4,** 697–720
54. Johansson, K., El-Ahmad, M., Ramaswamy, S., Hjelmqvist, L., Jörnvall, H., and Eklund, H. (1998) Structure of betaine aldehyde dehydrogenase at 2.1 Å resolution. *Protein Sci.* **7,** 2106–2117
55. Hjelmqvist, L., Norin, A., El-Ahmad, M., Griffiths, W., and Jörnvall, H. (2003) Distinct but parallel evolutionary patterns between alcohol and aldehyde dehydrogenases. Addition of fish/human betaine aldehyde dehydrogenase divergence. *Cell Mol. Life Sci.* **60,** 2009–2016
56. Tavladoraki, P., Rossi, M. N., Saccuti, G., Perez-Amador, M. A., Polticelli, F., Angelini, R., and Federico, R. (2006) Heterologous expression and biochemical characterization of a polyamine oxidase from Arabidopsis involved in polyamine back conversion. *Plant Physiol.* **141,** 1519–1532
57. Takahashi, Y., Cong, R., Sagor, G. H., Niitsu, M., Berberich, T., and Kusano, T. (2010) Characterization of five polyamine oxidase isoforms in *Arabidopsis thaliana*. *Plant Cell Rep.* **29,** 955–965
58. Raman, S. B., and Rathinasabapathi, B. (2003) β-Alanine *N*-methyltransferase of *Limonium latifolium*. cDNA cloning and functional expression of a novel *N*-methyltransferase implicated in the synthesis of the osmoprotectant β-alanine betaine. *Plant Physiol.* **132,** 1642–1651
59. Moschou, P. N., Sanmartin, M., Andriopoulou, A. H., Rojo, E., Sanchez-Serrano, J. J., and Roubelakis-Angelakis, K. A. (2008) Bridging the gap between plant and mammalian polyamine catabolism. A novel peroxisomal polyamine oxidase responsible for a full back-conversion pathway in *Arabidopsis*. *Plant Physiol.* **147,** 1845–1857
60. Kamada-Nobusada, T., Hayashi, M., Fukazawa, M., Sakakibara, H., and Nishimura, M. (2008) A putative peroxisomal polyamine oxidase, AtPAO4, is involved in polyamine catabolism in *Arabidopsis thaliana*.

Plant Cell Physiol. **49,** 1272–1282
61. Paquet, L., Rathinasabapathi, B., Saini, H., Zamir, L., Gage, D. A., Huang, Z.-H., and Hanson, A. D. (1994) Accumulation of the compatible solute 3-dimethylsulfoniopropionate in sugarcane and its relatives, but not other gramineous crops. *Aust. J. Plant Physiol.* **21,** 37–48
62. Rastogi, R., and Davies, P. J. (1990) Polyamine metabolism in ripening tomato fruit. I. Identification of metabolites of putrescine and spermidine. *Plant Physiol.* **94,** 1449–1455
63. Chen, S., Yang, Y., Shi, W., Ji, Q., He, F., Zhang, Z., Cheng, Z., Liu, X., and Xu, M. (2008) Badh2, encoding betaine aldehyde dehydrogenase, inhibits the biosynthesis of 2-acetyl-1-pyrroline, a major component in rice fragrance. *Plant Cell* **20,** 1850–1861
64. Niu, X., Tang, W., Huang, W., Ren, G., Wang, Q., Luo, D., Xiao, Y., Yang, S., Wang, F., Lu, B. R., Gao, F., Lu, T., and Liu, Y. (2008) RNAi-directed down regulation of OsBADH2 results in aroma (2-acetyl-1-pyrroline) production in rice (*Oryza sativa* L.). *BMC Plant Biol.* **8,** 100
65. Nakamura, T., Nomura, M., Mori, H., Jagendorf, A. T., Ueda, A., and Takabe, T. (2001) An isozyme of betaine aldehyde dehydrogenase in barley. *Plant Cell Physiol.* **42,** 1088–1092
66. Missihoun, T. D., Schmitz, J., Klug, R., Kirch, H. H., and Bartels, D. (2011) Betaine aldehyde dehydrogenase genes from *Arabidopsis* with different sub-cellular localization affect stress responses. *Planta* **233,** 369–382
67. Charrier, A., Rippa, S., Yu, A., Nguyen, P. J., Renou, J. P., and Perrin, Y. (2012) The effect of carnitine on *Arabidopsis* development and recovery in salt stress conditions. *Planta* **235,** 123–135

Article 6

Structure and function of nucleoside hydrolases from Physcomitrella patens and maize catalyzing the hydrolysis of purine, pyrimidine, and cytokinin ribosides.

Kopečná M, Blaschke H, Kopečný D, Vigouroux A, Končitíková R, Novák O, Kotland O, Strnad M, Moréra S, von Schwartzenberg K.

Plant Physiol. (4), 1568-83 (2013)

Structure and Function of Nucleoside Hydrolases from *Physcomitrella patens* and Maize Catalyzing the Hydrolysis of Purine, Pyrimidine, and Cytokinin Ribosides[1][W]

Martina Kopečná, Hanna Blaschke, David Kopečný*, Armelle Vigouroux, Radka Končitíková, Ondřej Novák, Ondřej Kotland, Miroslav Strnad, Solange Moréra*, and Klaus von Schwartzenberg*

Department of Protein Biochemistry and Proteomics, Center of the Region Haná for Biotechnological and Agricultural Research (M.K., D.K., R.K.), Department of Biochemistry (R.K., O.K.), Faculty of Science, Palacký University, CZ–783 71 Olomouc, Czech Republic; Laboratory of Growth Regulators, Palacký University and Institute of Experimental Botany, Academy of Sciences of the Czech Republic, CZ–783 71 Olomouc, Czech Republic (O.N., O.K., M.S.); Biozentrum Klein Flottbek und Botanischer Garten, Universität Hamburg, D–22609 Hamburg, Germany (H.B., K.v.S.); and Laboratoire d'Enzymologie et Biochimie Structurales, CNRS, F–91198 Gif-sur-Yvette cedex, France (A.V., S.M.)

We present a comprehensive characterization of the nucleoside *N*-ribohydrolase (NRH) family in two model plants, *Physcomitrella patens* (PpNRH) and maize (*Zea mays*; ZmNRH), using in vitro and in planta approaches. We identified two NRH subclasses in the plant kingdom; one preferentially targets the purine ribosides inosine and xanthosine, while the other is more active toward uridine and xanthosine. Both subclasses can hydrolyze plant hormones such as cytokinin ribosides. We also solved the crystal structures of two purine NRHs, PpNRH1 and ZmNRH3. Structural analyses, site-directed mutagenesis experiments, and phylogenetic studies were conducted to identify the residues responsible for the observed differences in substrate specificity between the NRH isoforms. The presence of a tyrosine at position 249 (PpNRH1 numbering) confers high hydrolase activity for purine ribosides, while an aspartate residue in this position confers high activity for uridine. Bud formation is delayed by knocking out single NRH genes in *P. patens*, and under conditions of nitrogen shortage, PpNRH1-deficient plants cannot salvage adenosine-bound nitrogen. All PpNRH knockout plants display elevated levels of certain purine and pyrimidine ribosides and cytokinins that reflect the substrate preferences of the knocked out enzymes. NRH enzymes thus have functions in cytokinin conversion and activation as well as in purine and pyrimidine metabolism.

Nucleoside hydrolases or nucleoside *N*-ribohydrolases (NRHs; EC 3.2.2.-) are glycosidases that catalyze the cleavage of the *N*-glycosidic bond in nucleosides to enable the recycling of the nucleobases and Rib (Fig. 1A). The process by which nucleosides and nucleobases are recycled is also known as salvaging and is a way of conserving energy, which would otherwise be needed for the de novo synthesis of purine- and pyrimidine-containing compounds. During the salvage, bases and nucleosides can be converted into nucleoside monophosphates by the action of phosphoribosyltransferases and nucleoside kinases, respectively, and further phosphorylated into nucleoside diphosphates and triphosphates (Moffatt et al., 2002; Zrenner et al., 2006; Fig. 1B). Uridine kinase and uracil phosphoribosyl transferase are key enzymes in the pyrimidine-salvaging pathway in plants (Mainguet et al., 2009; Chen and Thelen, 2011). Adenine phosphoribosyltransferase and adenosine kinase (ADK) are important in purine salvaging (Moffatt and Somerville, 1988; Moffatt et al., 2002), and their mutants cause reductions in fertility or sterility, changes in transmethylation, and the formation of abnormal cell walls. In addition, both enzymes were also reported to play roles in cytokinin metabolism (Moffatt et al., 1991, 2000; von Schwartzenberg et al., 1998; Schoor et al., 2011). Cytokinins (N^6-substituted adenine derivatives) are plant hormones that regulate

[1] This work was supported by the Czech Science Foundation (grant no. P501/11/1591), the Ministry of Education, Youth, and Sports of the Czech Republic (grant no. MSM 6198959215), Palacký University (grant no. PrF_2013_037), Operational Programme Research and Development for Innovation (grant no. ED0007/01/01), the Centre National de la Recherche Scientifique (to S.M. and A.V.), the Deutsch Forschungsgemeinschaft (grant no. SCHW687/6 to K.v.S. and H.B.), and the Appuhn Foundation (Hamburg). M.K. was a Federation of European Microbiological Societies fellow.

* Address correspondence to david.kopecny@upol.cz, morera@lebs.cnrs-gif.fr, and klaus.von.schwartzenberg@uni-hamburg.de.

The author responsible for distribution of materials integral to the findings presented in this article in accordance with the policy described in the Instructions for Authors (www.plantphysiol.org) is: David Kopečný (david.kopecny@upol.cz).

D.K., S.M., and K.v.S. designed the research; M.T., H.B., D.K., and R.K. analyzed enzyme kinetics; A.V. and S.M. performed the crystallographic study and contributed material and tools for crystallography; S.M. and D.K. analyzed the crystal structures; H.B. and K.v.S. generated and analyzed *P. patens* mutants, and O.N., O.K., and M.S. analyzed the metabolite levels. D.K., S.M., and K.v.S. wrote the paper.

[W] The online version of this article contains Web-only data.
www.plantphysiol.org/cgi/doi/10.1104/pp.113.228775

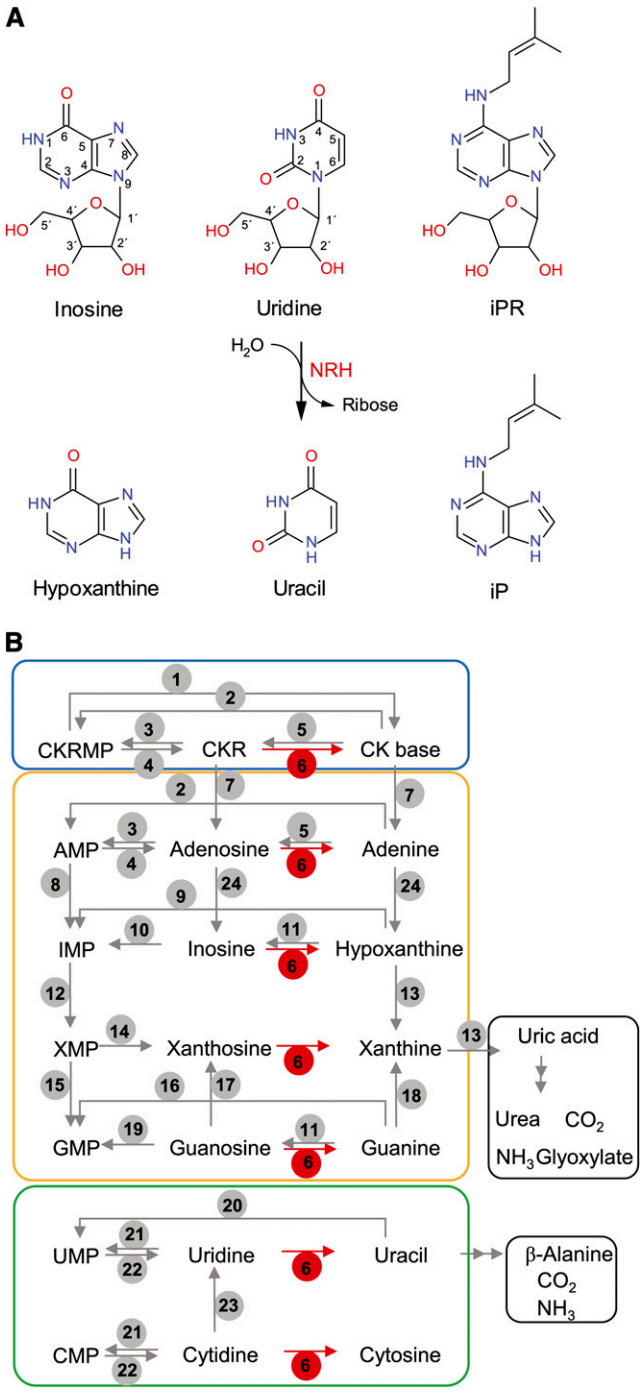

Figure 1. A, Scheme of the reactions catalyzed by plant NRHs when using purine (inosine), pyrimidine (uridine), and cytokinin (iPR) ribosides as the substrates. B, Simplified schematic overview of cytokinin, purine, and pyrimidine metabolism in plants. The diagram is adapted from the work of Stasolla et al. (2003) and Zrenner et al. (2006) with modifications. The metabolic components shown are as follows: 1, cytokinin nucleotide phosphoribohydrolase; 2, adenine phosphoribosyltransferase; 3, adenosine kinase; 4, 5′-nucleotidase; 5, adenosine phosphorylase; 6, purine/pyrimidine nucleoside ribohydrolase; 7, cytokinin oxidase/dehydrogenase; 8, AMP deaminase; 9, hypoxanthine phosphoribosyltransferase; 10, inosine kinase; 11, inosine-guanosine phosphorylase; 12, IMP dehydrogenase; 13, xanthine dehydrogenase; 14, 5′-nucleotidase; 15, GMP synthase; 16, hypoxanthine-guanine phosphoribosyltransferase; 17, guanosine deaminase; 18, guanine deaminase; 19, guanosine kinase; 20, uracil phosphoribosyltransferase; 21, uridine cytidine kinase; 22, pyrimidine 5′-nucleotidase; 23, cytidine deaminase; 24, adenosine/adenine deaminase. CK, Cytokinin; CKR, cytokinin riboside; CKRMP, cytokinin riboside monophosphate.

cell division and numerous developmental events (Mok and Mok, 2001; Sakakibara, 2006). Cytokinin ribosides are considered to be transport forms and have little or no activity.

NRHs are metalloproteins first identified and characterized in parasitic protozoa such as *Trypanosoma*, *Crithidia*, and *Leishmania* species that rely on the import and salvage of nucleotide derivatives. They have since been characterized in other organisms such as bacteria, yeast, and insects (Versées and Steyaert, 2003) but never in mammals (Parkin et al., 1991). They have been divided into four classes based on their substrate specificity: nonspecific NRHs, which hydrolyze inosine and uridine (IU-NRHs; Parkin et al., 1991; Shi et al., 1999); purine-specific inosine/adenosine/guanosine NRHs (Parkin, 1996); the 6-oxopurine-specific guanosine/inosine NRHs (Estupiñán and Schramm, 1994); and the pyrimidine nucleoside-specific cytidine/uridine NRHs (CU-NRHs; Giabbai and Degano, 2004). All NRHs exhibit a stringent specificity for the Rib moiety and differ in their preferences regarding the nature of the nucleobase. Crystal structures are available for empty NRH or in complex with inhibitors from *Crithidia fasciculata* (CfNRH; Degano et al., 1998), *Leishmania major* (LmNRH; Shi et al., 1999), and *Trypanosoma vivax* (TvNRH; Versées et al., 2001, 2002). The structures of two CU-NRHs from *Escherichia coli*, namely YeiK (Iovane et al., 2008) and YbeK (rihA; Muzzolini et al., 2006; Garau et al., 2010), are also available. NRHs are believed to catalyze *N*-glycosidic bond cleavage by a direct displacement mechanism. An Asp from a conserved motif acts as a general base and abstracts a proton from a catalytic water molecule, which then attacks the C1′ atom of the Rib moiety of the nucleoside. Kinetic isotope-effect studies on CfNRH (Horenstein et al., 1991) showed that the substrate's hydrolysis proceeds via an oxocarbenium ion-like transition state and is preceded by protonation at the N7 atom of the purine ring, which lowers the electron density on the purine ring and destabilizes the *N*-glycosidic bond. A conserved active-site His is a likely candidate for this role in IU-NRHs and CU-NRHs. In the transition state, the C1′-N9 glycosidic bond is almost 2 Å long, with the C1′ atom being sp^2 hybridized while the C3′ atom adopts an exo-conformation, and the whole ribosyl moiety carries a substantial positive charge (Horenstein et al., 1991).

Several NRH enzymes have been identified in plants, including a uridine-specific NRH from mung bean (*Phaseolus radiatus*; Achar and Vaidyanathan, 1967), an inosine-specific NRH (EC 3.2.2.2) and a guanosine-inosine-specific NRH, both from yellow lupine (*Lupinus luteus*; Guranowski, 1982; Szuwart et al., 2006), and an adenosine-specific NRH (EC 3.2.2.7) from coffee

(*Coffea arabica*), barley (*Hordeum vulgare*), and wheat (*Triticum aestivum*; Guranowski and Schneider, 1977; Chen and Kristopeit, 1981; Campos et al., 2005). However, their amino acid sequences have not been reported so far. A detailed study of the *NRH* gene family from Arabidopsis (*Arabidopsis thaliana*) has recently been reported (Jung et al., 2009, 2011). The AtNRH1 enzyme exhibits highest hydrolase activity toward uridine and xanthosine. It can also hydrolyze the cytokinin riboside N^6-(2-isopentenyl)adenosine (iPR), which suggests that it may also play a role in cytokinin homeostasis. However, Riegler et al. (2011) analyzed the phenotypes of homozygous *nrh1* and *nrh2* single mutants along with the homozygous double mutants and concluded that AtNRHs are probably unimportant in cytokinin metabolism.

Here, we identify and characterize plant IU-NRHs from two different model organisms, *Physcomitrella patens* and maize (*Zea mays*), combining structural, enzymatic, and in planta functional approaches. The moss *P. patens* was chosen to represent the bryophytes, which can be regarded as being evolutionarily basal terrestrial plants, and is suitable for use in developmental and metabolic studies (Cove et al., 2006; von Schwartzenberg, 2009), while maize is an important model system for cereal crops. We report the crystal structures of NRH enzymes from the two plant species, PpNRH1 and ZmNRH3. Based on these structures, we performed site-directed mutagenesis experiments and kinetic analyses of point mutants of PpNRH1 in order to identify key residues involved in nucleobase interactions and catalysis. To analyze the physiological role of the PpNRHs, single knockout mutants were generated. NRH deficiency caused significant changes in the levels of purine, pyrimidine, and cytokinin metabolites relative to those seen in the wild type, illustrating the importance of these enzymes in nucleoside and cytokinin metabolism.

RESULTS AND DISCUSSION

Gene Models of NRHs from *P. patens* and Maize

Ongoing genomic analyses suggest that most plant genomes contain at least two genes coding for NRHs. Several plant genomes, such as those of moss (*P. patens*), maize, Arabidopsis, rice (*Oryza sativa*), tomato (*Solanum lycopersicum*), and wheat, appear to contain several *NRHs*. We focused on two model plant organisms, the moss *P. patens* and maize, due to the availability of detailed information on cytokinin metabolism in both species (Massonneau et al., 2004; von Schwartzenberg, 2009; Vyroubalová et al., 2009). The genome databases for the moss *P. patens* (www.phytozome.net, version 9.1) and maize (www.maizesequence.org, version 5b.60) indicate that these species contain three and five *NRH* genes, respectively. In order to identify the correct gene models in each case and obtain the corresponding recombinant proteins, we cloned the complementary DNAs (cDNAs) of these eight *NRHs* using gene-specific primers and deposited their sequences to GenBank (see "Materials and Methods").

The cDNA sequence obtained for *PpNRH1* corresponds to the predicted gene model (Pp1s357_22V6.1), those obtained for *PpNRH2* and *PpNRH3* do not match the predicted gene models in the genome annotation version 6.1 (Pp1s140_172V6.1 and Pp1s5_276V6.1; see "Materials and Methods"; Supplemental Fig. S1). The two paralogous genes *ZmNRH1a* and *ZmNRH1b* are localized on chromosomes 8 and 3 (GRMZM2G029845 and GRMZM2G134149), respectively. The two other paralogs, *ZmNRH2a* and *ZmNRH2b*, lie on chromosomes 4 and 1 (GRMZM2G085960 and GRMZM2G015344), respectively. The last *ZmNRH3* gene (GRMZM2G104999) is localized on chromosome 2. These genes encode proteins of between 315 and 341 residues. All plant NRHs exhibit a conserved sequence motif, DTDPGIDD, at the N terminus (Fig. 2), which is involved in the binding of a calcium ion and the Rib moiety of the substrate (Versées and Steyaert, 2003). Another group of extracellular NRHs with two domains was recently identified in Arabidopsis (At5g18860; Jung et al., 2011). The authors suggested that these NRHs could correspond with the extracellular adenosine hydrolase activity found in potato (*Solanum tuberosum*) tubers (Riewe et al., 2008). Although the first domain carries a DTDVDTDD motif, the second contains an unconserved DMDMSXGD motif. Analogous sequences are also present in the genomes of other

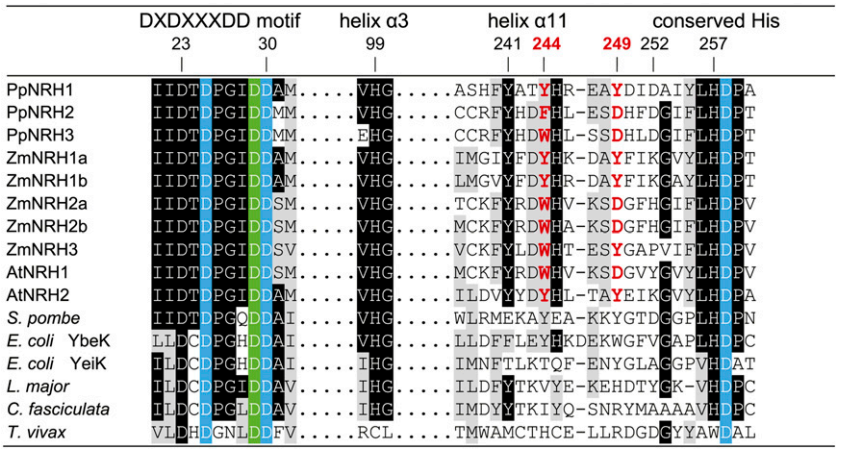

Figure 2. Multiple alignment of the amino acid sequences of NRHs from plants, yeast, bacteria, and protozoa, focusing on the DXDXXXDD motif and the α3 and α11 helix regions. Asp residues involved in calcium ion coordination are highlighted in blue. The Asp-binding 2-OH group of Rib is highlighted in green. Crucial residues involved in substrate binding in plant NRHs are highlighted in red. Residues are numbered according to the PpNRH1 sequence. Accession numbers for the sequences shown are listed in "Materials and Methods."

plants such as maize (GRMZM2G386229) and rice (Os05g33644 and Os05g33630).

Substrate Specificity of Plant NRHs

The pH effect on the specific activity of PpNRH1 (Supplemental Fig. S2) was analyzed, and high activity was found between pH 7.0 and 9.0. All subsequent kinetic analyses, therefore, were performed at pH 7.5. PpNRH1, ZmNRH2a, ZmNRH2b, and ZmNRH3 were obtained active and in high yield in soluble form. In contrast, the production of PpNRH2, ZmNRH1a, and ZmNRH1b primarily resulted in the formation of inclusion bodies, and refolding attempts did not lead to restoration of the enzymatic activity. Only very small quantities of these enzymes could be obtained in soluble form. We thus were only able to briefly screen the three NRHs with possible natural substrates, including purine, pyrimidine, and cytokinin ribosides, at 200 μM concentration (Table I). It was possible to analyze the substrate preferences for PpNRH2, whereas ZmNRH1a and ZmNRH1b show only negligible activity. However, cytidine and adenosine could be substrates of the two maize enzymes, but we cannot rule out that untested ribosides can be more suitable substrates. So far, the production of recombinant protein was not observed for any of the four splicing variants of PpNRH3, in contrast to the studied NRHs.

PpNRH1 is most active toward the two purine ribosides xanthosine and inosine and exhibits weaker activity with adenosine, uridine, and guanosine. In contrast, PpNRH2 prefers the pyrimidine riboside uridine and is less active toward xanthosine and inosine. ZmNRH2a and ZmNRH2b are also most active toward uridine. The activity of ZmNRH2b is 10 and 200 times higher than that of ZmNRH2a and PpNRH2, respectively. The comparatively low activity of PpNRH2 is likely due to being poorly expressed in *E. coli* and its low stability. ZmNRH3 preferentially hydrolyzes inosine and xanthosine, while the remaining nucleosides are weaker substrates. PpNRH1 and ZmNRH3 exhibit similar substrate preferences. However, subtle differences between these two enzymes are shown in Figure 3.

PpNRH1, ZmNRH2a, ZmNRH2b, and ZmNRH3 were further analyzed to determine their K_m and catalytic constant (k_{cat}) values (Table II) and confirmed the results discussed above. Both PpNRH1 and ZmNRH3 show the highest catalytic efficiency with inosine and xanthosine, while ZmNRH2a and ZmNRH2b display the highest catalytic efficiency for uridine and xanthosine. Although ZmNRH2a and ZmNRH2b have relatively high K_m values for uridine, it is also the substrate for which they have the highest k_{cat} values. Based on these kinetic values and the current system of classification, the investigated plant NRHs belong to the nonspecific IU-NRH class (Parkin et al., 1991; Shi et al., 1999). However, both PpNRH1 and ZmNRH3 (which prefer inosine and xanthosine) are apparently kinetically different from ZmNRH2a, ZmNRH2b, and PpNRH2 (all of which prefer uridine and xanthosine) and the AtNRH1 from Arabidopsis (Jung et al., 2009, 2011). Therefore, it seems that there are at least two subclasses of IU-NRHs in plants. Details of the sequences of these two subclasses are discussed below.

Inosine, xanthosine, and guanosine are all intermediates in the purine catabolic pathway (Fig. 1B) that starts with AMP (Zrenner et al., 2006). The xanthine and hypoxanthine nucleobases are formed by the action of nucleoside hydrolases and are further processed by xanthine dehydrogenase to give uric acid. Adenosine and adenine are by-products of the cytokinin degradation reactions catalyzed by cytokinin oxidase/dehydrogenase (EC 1.5.99.12; Houba-Hérin et al., 1999). In contrast to the two known bacterial CU-NRHs, the five plant IU-NRHs exhibit very weak activity toward cytidine (Table I). This is consistent with the fact that plants preferentially convert cytidine to uridine via cytidine deaminase (EC 3.5.4.5; Stasolla et al., 2003). To analyze the conversion of cytokinin ribosides, we first determined the extinction coefficients of iPR and trans-zeatin riboside (tZR) by spectrometric measurement according to Parkin (1996). All of the studied plant IU-NRHs have only weak activity toward iPR and tZR, between 1% and 0.1% of that toward their best substrates (Table I). ZmNRH2b and ZmNRH3 exhibit catalytic efficiencies between 1.7 and 5.3 $\times$ 10^2 M^{-1} s^{-1} (Table II). The

Table I. *Substrate specificity of NRHs from P. patens and maize*

Relative reaction rates (%) were measured at 200 μM substrate concentration. Activities were measured in 200 mM Tris-HCl buffer (pH 7.5) containing 400 mM KCl and 1 mM DTT. The specific activities for PpNRH1 and ZmNRH3 with 200 μM xanthosine were 135 and 61 nkat mg^{-1}, respectively. The specific activities for PpNRH2, ZmNRH2a, and ZmNRH2b with 200 μM uridine were 1.3, 26, and 226 nkat mg^{-1}, respectively. + indicates very low activity.

Substrate	Relative Rate				
	PpNRH1	PpNRH2	ZmNRH2a	ZmNRH2b	ZmNRH3
Inosine	87	22	9.3	9.5	100
Xanthosine	100	61	53	34	70
Adenosine	6.1	1.6	15	3.5	2
Guanosine	1.7	0	0.1	0.5	1.5
Uridine	5.7	100	100	100	5
Cytidine	0.1	3.9	5.0	0.9	0.1
iPR	0.1	+	0.03	0.3	1.4
tZR	0.1	+	0.03	0.3	1.5

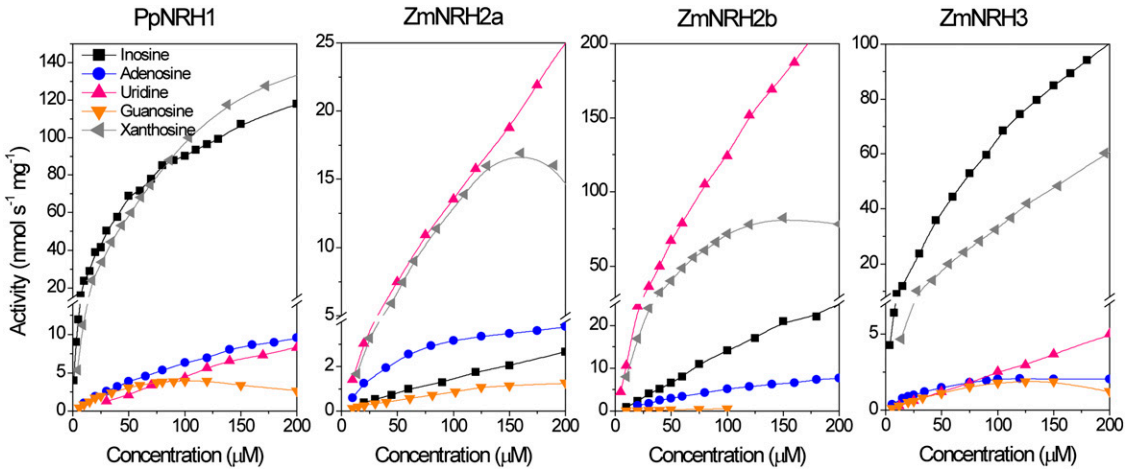

Figure 3. Saturation curves of activity for PpNRH1, ZmNRH2a, ZmNRH2b, and ZmNRH3. Data were measured with five substrates (inosine, xanthosine, adenosine, guanosine, and uridine) in 200 mM Tris-HCl buffer (pH 7.5) containing 400 mM KCl and 2 mM DTT.

conversion of the substrates by PpNRH1 and PpNRH2 was further confirmed by HPLC analysis using tritiated iPR and by HPLC-UV analysis for PpNRH1, ZmNRH2b, and ZmNRH3 (Supplemental Fig. S3).

Crystal Structure and Substrate Binding in Plant NRHs

The crystal structures of PpNRH1 and ZmNRH3 are, to our knowledge, the first reported crystal structures for any plant NRH. The asymmetric unit of the PpNRH1 crystal contains four very similar dimers with an average root mean square deviation (RMSD) of 0.75 Å for all Cα atoms. The asymmetric unit of the ZmNRH3 crystal contains only one dimer (Fig. 4A; Supplemental Table S1). This is consistent with the results from gel filtration chromatography showing that the active form in solution is a dimer (Supplemental Fig. S4). PpNRH1 and ZmNRH3 monomers and dimers are very similar to each other, with average RMSD values of 0.9 and 1.2 Å for all Cα atoms, respectively. Each monomer possesses a typical NRH fold containing 12 β-strands and 13 α-helices. Indeed, a structural comparison of the plant NRH monomer with all entries in the Protein Data Bank (PDB) using Secondary Structure Matching-program (European Bioinformatics Institute) revealed that it resembles numerous NRH structures from protozoa and bacteria, such as TvNRH, CfNRH, LmNRH, YeiK, and YbeK, with RMSD values ranging from 1.4 to 1.8 Å over 283 to 338 Cα atoms, corresponding to a sequence identity of 31% to 34% (Supplemental Fig. S5). The major structural difference concerns the loop region 278 to 294 (PpNRH1 numbering) involved in dimer contact, which is longer in plant NRHs than in all other known NRHs. All of the NRHs studied to date are homotetramers, except for TvNRH, which is a homodimer (Versées et al., 2001). Although PpNRH1 and ZmNRH3 are dimeric, their dimer is different from that of TvNRH. The ZmNRH3 and PpNRH1 dimer interfaces, which cover 1,262 and 1,278 Å^2 per subunit, respectively, involve three regions (residues 156–164, 228–223, and 263–289) that form hydrophobic interactions and are complemented by 10 hydrogen bonds.

A conserved Ca^{2+} ion in the active site is tightly bound to the Asp-25, Asp-30, and Asp-258 (Asp-8, Asp-13, and Asp-240) and to the main-chain carbonyl group of Leu-141 (Leu-123) in PpNRH1 (ZmNRH3 numbering). Its octahedral coordination can be completed either by three water molecules or by a catalytic

Table II. *Kinetic parameters for PpNRH1, ZmNRH2a, ZmNRH2b, and ZmNRH3*

Activities were measured in 200 mM Tris-HCl buffer (pH 7.5) containing 400 mM KCl and 1 mM DTT and using substrates up to 600 μM concentration. Kinetic constants were determined with GraphPad Prism 5.0 data-analysis software. –, Not determined.

Substrate	PpNRH1			ZmNRH2a			ZmNRH2b			ZmNRH3		
	K_m	k_{cat}	k_{cat}/K_m	K_m	k_{cat}	k_{cat}/K_m	K_m	k_{cat}	k_{cat}/K_m	K_m	k_{cat}	k_{cat}/K_m
	μM	s^{-1}	$s^{-1}\ M^{-1}$	μM	s^{-1}	$s^{-1}\ M^{-1}$	μM	s^{-1}	$s^{-1}\ M^{-1}$	μM	s^{-1}	$s^{-1}\ M^{-1}$
Inosine	78 ± 5	6.0 ± 0.3	7.7×10^4	1,013 ± 115	0.61 ± 0.05	6.0×10^2	713 ± 62	4.1 ± 0.3	5.7×10^3	201 ± 7	7.2 ± 0.2	3.6×10^4
Xanthosine	116 ± 9	7.0 ± 0.4	6.1×10^4	178 ± 28	1.3 ± 0.25	7.5×10^3	109 ± 19	4.6 ± 0.6	4.2×10^4	396 ± 50	6.2 ± 0.7	1.6×10^4
Adenosine	113 ± 7	0.6 ± 0.03	5.4×10^3	60 ± 4	0.18 ± 0.03	3.0×10^3	111 ± 17	0.4 ± 0.03	3.5×10^3	39 ± 4	0.12 ± 0.01	3.0×10^3
Guanosine	61 ± 6	0.2 ± 0.01	3.5×10^3	121 ± 14	0.07 ± 0.01	5.7×10^2	60 ± 13	0.03 ± 0.01	3.9×10^2	104 ± 18	0.12 ± 0.01	1.2×10^3
Uridine	890 ± 102	1.4 ± 0.2	1.5×10^3	468 ± 66	3.0 ± 0.24	6.4×10^3	514 ± 41	23.8 ± 1.5	4.6×10^4	1030 ± 180	1.1 ± 0.1	1.1×10^3
iPR	–	–	–	–	–	–	402 ± 53	0.07 ± 0.01	1.8×10^2	196 ± 20	0.10 ± 0.01	5.3×10^2
tZR	–	–	–	–	–	–	412 ± 36	0.07 ± 0.01	1.7×10^2	428 ± 48	0.17 ± 0.01	4.0×10^2

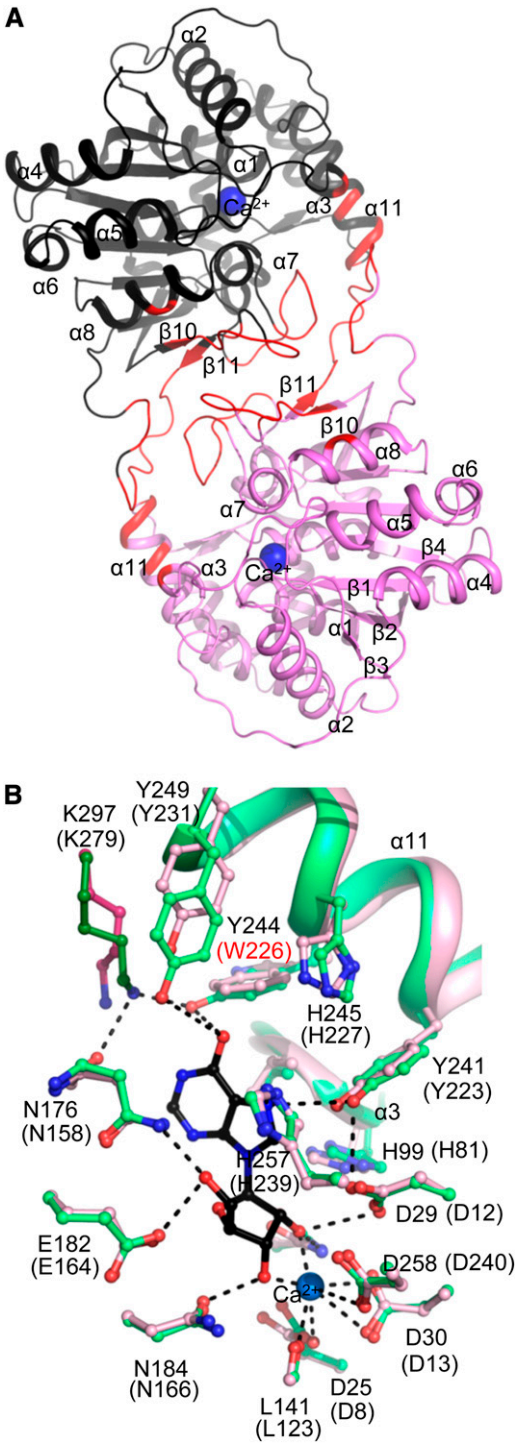

Figure 4. Crystal structure of plant NRHs. A, Dimeric structure of PpNRH1. One subunit is colored in black and the other in violet. The calcium ion in the active site is shown as a blue sphere. Intersubunit contacts are shown in red. B, Substrate-binding sites of PpNRH1 (in green) and ZmNRH3 (in pink). A molecule of inosine (in black) was docked into the active site. Amino acid residues are labeled and H-bonds, and calcium ion coordination are shown as dashed lines. Differences in the sequences of the two NRHs are labeled in red.

water molecule and the 2′- and 3′-hydroxyl groups of the substrate Rib moiety. The catalytic water molecule in turn interacts with the catalytic base, which is believed to increase the nucleophilicity of the water molecule attacking the C1′-N9 bond of the substrate. The calcium ion is believed to lower the pK_a of the catalytic water molecule prior to proton transfer to the active site base (Degano et al., 1998). Based on the sequence similarity and structural comparisons with protozoan NRHs (Versées et al., 2001), we designed and produced D25A and D8A mutants of PpNRH1 and ZmNRH3, respectively, to verify the roles of the targeted Asp residues as catalytic bases. Both mutants exhibit 10^4-fold lower activity than the wild-type proteins (Table III). These results confirm that the second Asp of the DTDPGIDD conserved motif functions as the active site base in plant NRHs. A similar result was reported for the equivalent D10A mutant in TvNRH (Versées et al., 2002), which was between 10^3 and 10^4 times less active than the wild-type enzyme but has an identical K_m value.

Soaking or cocrystallization of WT-PpNRH1 and D25A-PpNRH1, as well as of WT-ZmNRH3 and D8A-ZmNRH3, with nucleosides or inhibitors was unsuccessful. Therefore, we resorted to modeling and docking studies to understand the determinants for the substrate specificities of plant NRHs. We used the structure of YeiK in complex with inosine (PDB 3B9X) to model a substrate into the active sites of PpNRH1 and ZmNRH3 by structural superposition. The Rib moiety is tightly bound to conserved residues among the NRH family corresponding to Asn-176, Glu-182, Asp-258, Asn-184, Asp-29, Asp-30, and Asn-54 in PpNRH1 (Asn-158, Glu-164, Asp-240, Asn-166, Asp-12, Asp-13, and Asn-37 in ZmNRH3). In contrast, the nucleobase is surrounded by more variable residues (PpNRH1 numbering): Val-98 and His-99 from helix α3; aromatic residues Tyr-241, Tyr-244, His-245, and Tyr-249 from helix α11; His-257 in helix α12; Asn-176 in the β5-α7 loop; the adjacent side chain of Lys-297, which protrudes into the active site from the other subunit and is hydrogen bonded to Tyr-244; and the main-chain oxygen of Asn-176. A structural comparison of the substrate-binding sites of PpNRH1 and ZmNRH3 (Fig. 4B) shows that only one residue is different around the nucleobase, Tyr-244 in PpNRH1 is replaced by a Trp in ZmNRH3.

IU-NRHs such as CfNRH (Parkin et al., 1991; Degano et al., 1996) are characterized by a catalytic triad that consists of one His and two Tyr residues. These residues belong to a particular α9 helix (equivalent to the α11 helix in plant NRHs) that is known to move upon substrate binding in CU-NRHs from *E. coli* (Giabbai and Degano, 2004; Muzzolini et al., 2006; Iovane et al., 2008; Garau et al., 2010). This triad binds the substrate and allows the efficient protonation of the N7 atom of the purine base (the leaving group). Intriguingly, no such triad is present in the CU-NRHs, suggesting that the residues required for leaving group activation when protonating pyrimidine bases are different from those required for purines. In CfNRH, the triad consists of Tyr-229, Tyr-225, and His-241; His-241 is the residue

Table III. *Kinetic parameters for PpNRH1 and mutant proteins with the potential natural substrates inosine and xanthosine*

Relative reaction rates (%) were measured at 200 μM substrate concentration in 200 mM Tris-HCl buffer (pH 7.5) containing 400 mM KCl and 1 mM DTT. The concentration was chosen to avoid a substrate inhibition effect as observed with xanthosine. Kinetic constants K_m and k_{cat} were determined using GraphPad Prism 5.0 software. n.d., Not determined due to negligible activity.

Enzyme	Relative Rate Inosine/Xanthosine	Inosine			Xanthosine		
		K_m	k_{cat}	k_{cat}/K_m	K_m	k_{cat}	k_{cat}/K_m
	%	μM	s^{-1}	$s^{-1}\ M^{-1}$	μM	s^{-1}	$s^{-1}\ M^{-1}$
WT-PpNRH1	100/115	78	6.0	7.7×10^4	116	7.0	6.1×10^4
D25A	100/106	n.d.	5.4×10^{-4}	n.d.	n.d.	5.8×10^{-4}	n.d.
H99A	n.d.	n.d.	n.d.	n.d.	n.d.	n.d.	n.d.
Y241A	100/340	630	0.06	1.0×10^2	487	0.19	4.0×10^2
Y244A	100/188	1,208	1.4	1.2×10^3	206	0.58	2.8×10^3
H245A	100/240	1,090	1.1	1.0×10^3	356	1.3	3.6×10^3
E247A	100/124	94	5.7	6.1×10^4	140	7.2	5.1×10^4
Y249A	100/270	1,390	0.7	5.2×10^2	596	1.1	1.8×10^3
D250A	100/108	134	7.2	5.3×10^4	171	8.4	4.9×10^4
D252A	100/115	301	3.0	1.0×10^4	232	2.5	1.1×10^4
Y255A	100/190	760	0.47	6.2×10^2	367	0.43	1.2×10^3

that protonates the N7 atom (Fig. 5A; Gopaul et al., 1996). PpNRH1, which is an IU-NRH, possesses an equivalent triad consisting of His-245, Tyr-241, and His-257, in which His-257 is expected to protonate the leaving group. However, in this work, we mutated His-99 into Ala in PpNRH1 and found this mutant inactive with any riboside tested as a substrate. His-99 is conserved in all NRHs except for TvNRH. In our docking experiments (see below), His-99 is only 3.2 to 3.5 Å away from the N9 atom of the purine ring as well as the N1 and O2 atoms of a docked pyrimidine ring, indicating that it is another potential proton donor. Interestingly, Giabbai and Degano (2004) concluded from their mutagenesis analysis on two potential catalytic acids in bacterial YeiK (His-82 and His-239, equivalent to His-99 and His-257 in PpNRH1) that other active-site residues can function as alternative proton donors that could contribute to the *N*-glycosidic bond cleavage in this CU-NRH. The PpNRH1 substrate-binding site involves two additional residues, Tyr-244 and Tyr-249, which point toward the nucleobase compared with their equivalent residues Ile-228 and Tyr-234 in CfNRH. In CfNRH, the substrate-binding site is completed by the Arg-233 residue, which is located in the loop following the mobile α9 helix. Interestingly, the side chain of Lys-297 (from the neighboring subunit in PpNRH1) occupies a position similar to that of Arg-233 (Fig. 5A), suggesting that the dimer formation has an important role in enzymatic function of plant NRHs.

Docking Analysis and Site-Directed Mutagenesis of PpNRH1

Xanthosine and inosine show similar binding modes when docked into the PpNRH1 active site (Fig. 5B), with conserved interactions between the 6-oxo group and the side chains of Tyr-244 and Tyr-249 (and possibly the side chain of Lys-297) as well as between the N7 atom (protonated during catalysis) and the side chain of Tyr-241 (3.5-Å distance). Both the 2-oxo group and the N1 atom of xanthosine can form additional hydrogen bonds to the main chain carbonyl group of Asn-176. Docking experiments with uridine revealed that the 4-oxo group can interact with the hydroxyl groups of Tyr-244 and Tyr-249. The 2-oxo group points toward a cluster formed by four residues: the two imidazole rings of His-99 and His-257, the hydroxyl of Tyr-241, and the carboxyl group of Asp-29 (Fig. 5C).

To verify the results of our docking studies on substrate binding based on the PpNRH1 structure, we performed site-directed mutagenesis of Tyr-241, Tyr-244, His-245, and Tyr-249 from the mobile helix α11 and replaced them with Ala. We also mutated another residue from the α11 helix, Glu-247, whose side chain does not project into the substrate-binding site. Three other residues, Asp-250 and Asp-252, both positioned in the loop between helix α11 and strand β5, and Tyr-255, were also targeted in order to determine if more mobile regions are involved in substrate binding, as shown previously for TvNRH (Versées et al., 2002). Circular dichroism spectroscopy measurements indicate that the folding in solution of each mutant variant resembles that of WT-PpNRH1 (Supplemental Fig. S6).

The kinetic constants determined for each of the mutant variants using xanthosine and inosine as substrates are shown in Table III. The Y241A, Y244A, H245A, and Y249A mutants exhibit lower turnover rates (approximately 100-, 16-, 10-, and 22-fold lower k_{cat} values for inosine), which is consistent with their predicted role in nucleobase binding. The three mutants Y244A, H245A, and Y249A have higher K_m values (in the millimolar range) for inosine than for xanthosine, indicating a loss of interaction with the 6-oxo group of the inosine base. Because xanthosine has one more oxygen atom, the effect on K_m values is less pronounced because this additional oxygen, the 2-oxo group, could make an additional hydrogen bond to the main chain oxygen of

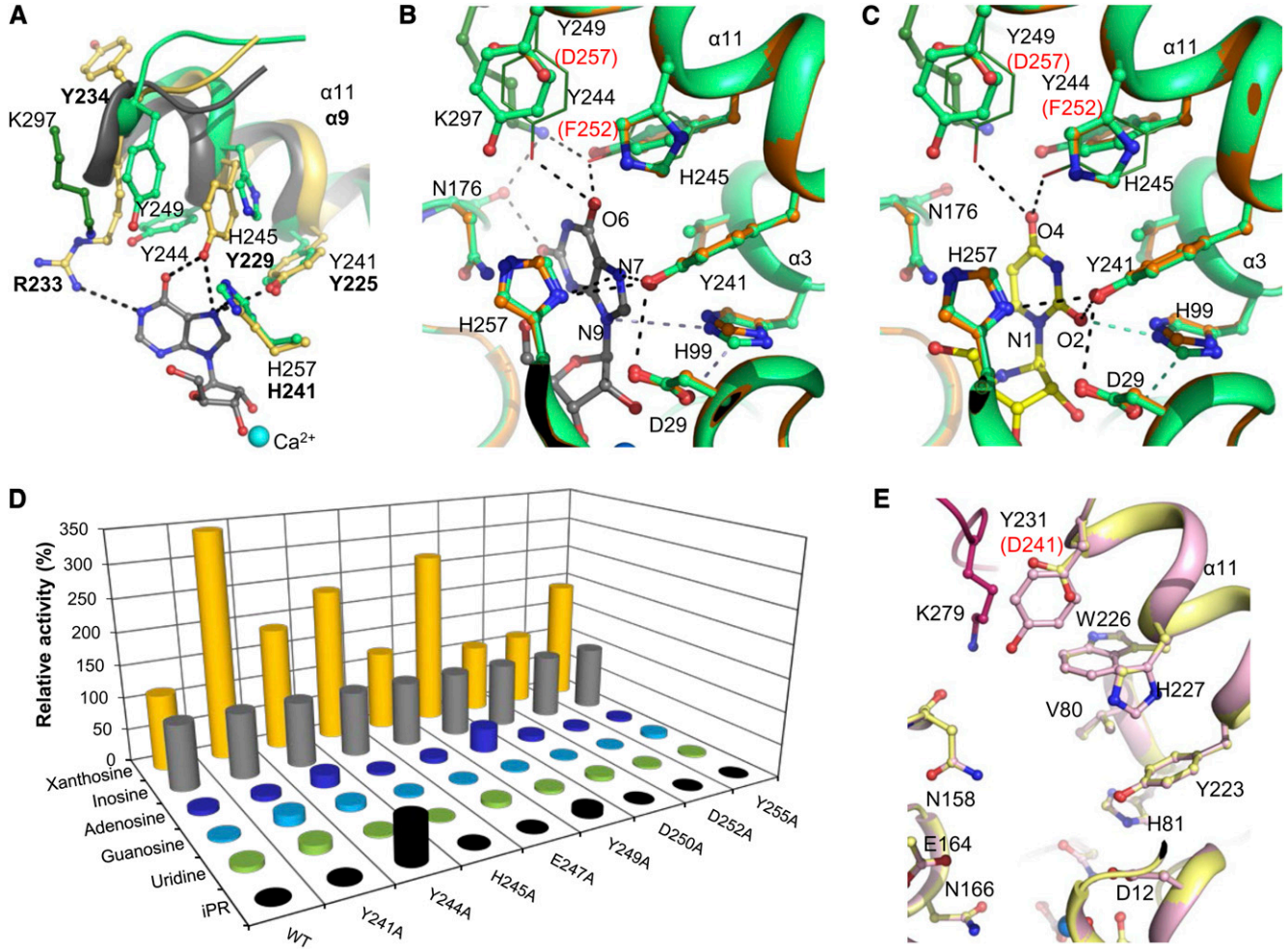

Figure 5. A, Comparison of the substrate-binding sites of PpNRH1 (green) and the IU-NRH from *C. fasciculata* (yellow; PDB 2MAS). The shift of helix α9 (in dark gray and equivalent to helix α11 in plant NRHs) that occurs upon substrate binding in the active site of YeiK is shown together with the observed position of the inosine substrate (shown in gray; PDB 3B9X). Dashed lines represent potential hydrogen bonds between the CfNRH residues and the purine base. B and C, Binding of the nucleobases of xanthosine and uridine in the active site of PpNRH1. The substrate molecules were docked into the active site of PpNRH1 (in green) using AutoDock 4.2. The rearrangements of the Tyr-249 and Tyr-244 side chains upon substrate binding are shown as lines. A model of PpNRH2 is shown in orange for comparison. Hydrogen bonds are shown as dashed lines, and those that depend on the orientation of the imidazole ring of His-99 are shown in light blue. Differences in sequence between the two NRHs are labeled in red. D, Substrate specificity of PpNRH1 proteins with six riboside substrates. Data were measured in 200 mM Tris-HCl buffer (pH 7.5) containing 400 mM KCl and 1 mM DTT and using 200 μM substrates. The activity toward inosine, as the best substrate for the wild-type enzyme, was arbitrarily taken as 100%. Using xanthosine as the substrate, a specific activity of 137 nkat mg^{-1} was measured for WT-PpNRH1, 1.2 nkat mg^{-1} for Y241A, 8.4 nkat mg^{-1} for Y244A, 14 nkat mg^{-1} for H245A, 135 nkat mg^{-1} for E247A, 6 nkat mg^{-1} for Y249A, 155 nkat mg^{-1} D250A, 66 nkat mg^{-1} for D252A, and 4.3 nkat mg^{-1} for Y255A. The D25A and H99A proteins exhibited no or negligible activity. E, Comparison of the active-site composition between ZmNRH3 (pink) and ZmNRH2b (model; light yellow). Differences in the sequences of the two NRHs are indicated by red labels.

Asn-176 (Fig. 5B). In addition, xanthosine, which is negatively charged at the studied pH, may be further stabilized by an interaction with Lys-297. In contrast, inosine exists predominantly as a neutral species at physiological pH. His-245 is fully conserved among plant NRHs, and the docking studies indicate that it does not interact with the nucleobase. However, a slight shift of helix α11, such as that observed on substrate binding in bacterial NRHs (Fig. 5A; Iovane et al., 2008), could bring its imidazole side chain into direct contact with the nucleobase, which is supported by mutagenesis results. The K_m values for the Y241A variant are higher but not as much as for the three mutants above. The residual activity of Y241A is not in favor of the catalytic acid function of this residue. However, the strongly reduced turnover rate is probably

a consequence of ineffective stabilization of the negative charge in the leaving group, leading to an increased energy barrier to reach the transition state. Because Tyr-241 is fully conserved among plant NRHs, it is most likely involved in this process and in line with similar findings on the equivalent residue in YeiK from *E. coli* and CfNRH (Iovane et al., 2008).

As expected from the structure, the E247A variant resembles the wild-type enzyme regarding activity. Both D250A and D252A also behave similarly to the wild-type enzyme, meaning that no more conformational change occurs upon substrate binding, and these residues are not in interaction with the substrate. A puzzling result was obtained with Y255A, which exhibits a 30-fold decrease in k_{cat} and a 10-fold increase in K_m values for inosine (Table III). This residue is not in direct contact with the substrate, based on docking models, but it lies in the vicinity of His-245 and His-257. Thus, it seems that the mutation has an indirect effect on catalysis by influencing the function of at least one of the two His residues.

Substrate specificity differences measured for all PpNRH1 variants with six various substrates are shown in Figure 5D. Two significant changes appear in the substrate specificity of the Y244A and Y249A proteins. First, both of the corresponding mutants have substantially higher reaction rates with adenosine (20% and 38%, respectively) compared with inosine (Fig. 5D), while WT-PpNRH1 hydrolyzes adenosine at only an 8% rate. Second, they also show higher relative rates with the cytokinin riboside iPR compared with inosine (62% and 10%, respectively), while the wild type shows only 0.1% activity. Therefore, it appears that Tyr-244 and Tyr-249 are both essential for the enzyme's activity but also have negative effects on the binding of the 6-amino group of the purine ring (in the case of adenosine) and that of the isoprenoid side chain (in the case of cytokinin ribosides).

All kinetic data correlate well with the docking experiments and highlight the essential roles of two residues, Tyr-244 and Tyr-249, in the binding of purine ribosides in PpNRH1. Notably, even though ZmNRH3 contains a Trp (Trp-226) at a position equivalent to Tyr-244 in PpNRH1, both PpNRH1 and ZmNRH3 are kinetically very similar. This suggests that the conserved Tyr-249 (Tyr-231) may be very important in determining their substrate specificity. PpNRH2, ZmNRH2a, and ZmNRH2b, which are all highly active toward uridine and xanthosine, carry an Asp residue at position 249 (Fig. 2), while all the other active-site residues remain identical (Fig. 5, B, C, and E). The Tyr replacement by an Asp is accompanied by three to five times higher K_m values for inosine and about one-half lower K_m values for uridine (Table II). This may imply that the uncharacterized PpNRH3, which also possesses an Asp, will preferentially catalyze the hydrolysis of uridine. ZmNRH1a and ZmNRH1b should behave similarly to ZmNRH3 and PpNRH1. Interestingly, AtNRH1, which exhibits higher activity toward uridine (Jung et al., 2009), also has an Asp residue at this position. We believe that the other Arabidopsis enzyme, AtNRH2, so far not kinetically characterized, should behave as ZmNRH3 and PpNRH1.

Phenotypes and Growth of *P. patens* NRH Knockout Mutants in Medium with Nucleosides as the Sole Nitrogen Source

To obtain in planta information on the function of PpNRH1, PpNRH2, and PpNRH3, we performed gene targeting and achieved a functional gene knockout by inserting a resistance cassette into each of the corresponding loci (Schaefer and Zrÿd, 1997). Three single knockout lines were selected for phenotypic analysis: d|PpNRH1#29, d|PpNRH2#56, and d|PpNRH3#7. Each of these lines satisfies all of the targeted gene knockout criteria, including the absence of detectable transcripts. When grown on full medium, all of the knockout lines had the wild-type phenotype in terms of protonema cell size and growth. When protonema suspensions were used to inoculate agar dishes, it became apparent during the first 4 weeks that all three mutant lines are delayed in bud formation (Fig. 6A). The strongest reduction in early budding is observed for d|PpNRH1#29, which exhibits only 4% of the number of buds compared with the wild type. The other mutants were less severely affected. Supplemental Figure S7 shows the significant reduction in early budding for two individual mutants for each of the PpNRH genes. The stronger phenotype of the d|PpNRH1#29 line suggests that PpNRH1 plays a more important role in cytokinin-mediated budding control in planta than do the other two PpNRHs.

We investigated the roles of each PpNRH gene product in the recycling of nucleoside-bound nitrogen by performing growth assays in which inosine, xanthosine, and adenosine were the sole nitrogen sources for nitrogen-starved tissues. The observed growth rates were compared with those achieved on a medium containing either KNO_3 or urea (Fig. 6A). All of the knockout lines perform similarly when fed with inosine and grow slightly better than on a nitrogen-free medium. However, they take on a brown color, which is indicative of nitrogen starvation in *P. patens*. Inosine has growth-inhibiting effects, which prevents the formation of gametophores. Because there are no apparent differences between the wild type and the knockout lines, we can deduce that at least two of the PpNRHs are capable of hydrolyzing inosine. The recombinant PpNRH1 and PpNRH2 proteins both hydrolyze inosine to hypoxanthine, which can be further converted to xanthine and thus act as a nitrogen source via purine degradation (Fig. 1B). Plants grown on medium containing xanthosine as the sole nitrogen source have green-colored filaments and are able to form gametophores. Again, the knockout lines have very similar phenotypes to the wild type, meaning that at least two of the three studied enzymes can convert xanthosine to xanthine and thereby enable nitrogen recycling. Both recombinant PpNRH1 and PpNRH2 hydrolyze

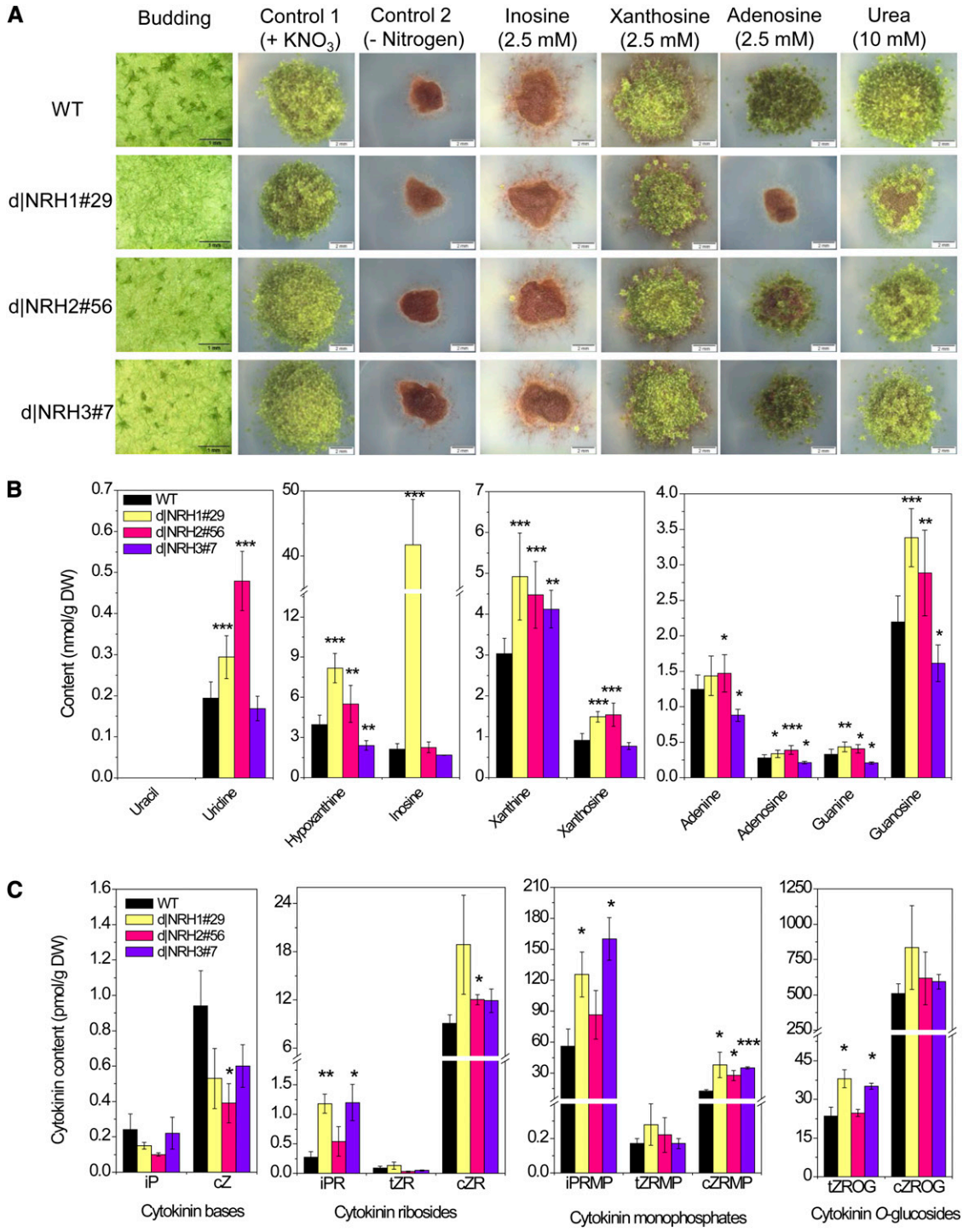

Figure 6. Phenotypic analysis of wild-type *P. patens* and three NRH knockout strains. A, Wild-type *P. patens* (WT) and the knockout strains d|PpNRH1#29, d|PpNRH2#56, and d|PpNRH3#7 were cultivated on agar medium under different conditions. The first column shows the extent of delayed budding in the mutants after 4 weeks of cultivation following aerial inoculation with a suspension of protonema cells. The second and third columns (controls 1 and 2) show cultures grown on medium containing either 10 mM KNO_3 as the sole nitrogen source or under nitrogen starvation. The remaining columns show cultures grown on medium containing 2.5 mM inosine, 2.5 mM xanthosine, or 2.5 mM adenosine as the sole nitrogen sources and an additional positive control with urea as the sole nitrogen source. Unlike the wild type, the knockout strain d|PpNRH1#29 is unable to recycle adenosine-bound nitrogen. Photographs were taken after 8 weeks. B, Levels of selected purine and pyrimidine metabolites in 21-d-old liquid-cultured protonema. The values shown represent mean values for four individual cultures per genotype; UPLC-mass spectrometry measurements were conducted in triplicate for each culture. C, Levels of selected

xanthosine (Table I). A remarkable result was obtained with medium containing adenosine as the sole nitrogen source: while the d | PpNRH2#56 and d | PpNRH3#7 knockout lines exhibited similar levels of growth to the wild type, no growth was observed for the d | PpNRH1#29 knockout line. Although recombinant PpNRH2 is weakly active toward adenosine (Table I), this finding strongly suggests that PpNRH1 is the only *P. patens* NRH that is capable of effectively recycling nitrogen from adenosine in vivo. This result clearly demonstrates that, together with xanthine dehydrogenase, NRHs play a central role in purine degradation and the recycling of nucleoside-bound nitrogen.

Changes in the Levels of Purine, Pyrimidine, and Cytokinin Metabolites in d | PpNRH Knockout Mutants

As expected from the kinetic data (Tables I and II), we observe accumulations of inosine (20-fold), uridine (1.4-fold), and xanthosine (1.5-fold) in the d | PpNRH1#29 mutant line relative to the wild type (Fig. 6B). The levels of uracil and cytidine in this mutant line are below the limit of detection. Similar accumulation is observed for uridine (2.5-fold) and xanthosine (1.6-fold) in d | PpNRH2#56 plants. Surprisingly, the level of hypoxanthine (which is produced by the hydrolysis of inosine) in the d | PpNRH1 plants is twice that in the wild type, indicating that purine metabolism is modified in this knockout. Because inosine has been found to cause growth inhibition in *P. patens* (Fig. 6A), we may assume that a harmful excess of inosine in the d | PpNRH1 mutant is eliminated by (unspecified) alternative pathways. It should be noted that Riegler et al. (2011) did not observe an accumulation of inosine over the detection limit in any of their *nrh1* and *nrh2* single and double mutants in Arabidopsis. In contrast, the AtNRH1 knockout mutant accumulates high levels of uridine in roots, which is consistent with the preferential activity of this NRH toward this substrate.

Although the xanthosine levels in the d | PpNRH1 and d | PpNRH2 plants are only slightly higher than those in the wild type, the difference is statistically significant ($P < 0.001$) and is consistent with the observation that both of the corresponding recombinant enzymes can hydrolyze this riboside. Overall, these data indicate that *P. patens* produces at least two NRHs hydrolyzing xanthosine. The levels of xanthine (a product of xanthosine hydrolysis) are increased significantly in all three knockout lines, which again suggests that they have abnormal purine metabolism due to deficiencies in NRH activity. Interestingly, the far less pronounced accumulation of xanthosine in d | PpNRH1#29 and d | PpNRH2#56 compared with that seen in the *nrh1* (*urh1*) Arabidopsis mutant (Riegler et al., 2011) suggests that bryophytes and seed plants differ in terms of xanthosine homeostasis. A comparable result (i.e. a relatively low but statistically significant increase in d | PpNRH1#29 and d | PpNRH2#56) is also found for the other purine nucleosides adenosine and guanosine. Conversely, the levels of these metabolites in the d | PpNRH3#7 plants are slightly lower than in the wild type. The finding that the levels of both the bases and the ribosides are altered indicates that their endogenous levels are regulated by both the NRHs and by enzymes that are active in other metabolic pathways, which will presumably respond to changes in the abundance of the various purine derivatives. The absence of an accumulation of uridine, inosine, and xanthosine in the d | PpNRH3#7 plants indicates that PpNRH3 probably plays a minor role in their in vivo hydrolysis, either due to low expression of the functional *PpNRH3* or because *PpNRH3* expression is specific to some developmental stage other than those examined in this work.

The first report on the functionality of AtNRH1 (Jung et al., 2009) demonstrated that recombinant enzyme is capable of hydrolyzing iPR. To date, no in planta experiments have been published showing the relevance of NRHs in cytokinin activation. The major pathway for cytokinin activation is that involving phosphoribohydrolase (LONELY GUY; Kurakawa et al., 2007), which releases cytokinin bases from the corresponding nucleotides. In mosses, N^6-(2-isopentenyl)adenine (iP) is an important cytokinin base that has significant effects on development because it induces bud formation in protonema (von Schwartzenberg et al., 2007). Our enzymatic study reveals that PpNRH1 and PpNRH2 are capable of releasing iP from the corresponding iPR, albeit at low rates (Table I). The kinetic data for ZmNRH2b and ZmNRH3 indicate that their K_m values for iPR and tZR are similar to those for other purine substrates, but their turnover rates for these substrates are much lower.

Cytokinin analyses demonstrate that the levels of endogenous iP and cis-zeatin in all three of the d | PpNRH mutant lines are slightly lower than in the wild type (the trans-zeatin levels are below the limit of detection). This is consistent with the observed hydrolysis of these cytokinin ribosides in vitro by the various PpNRH enzymes. The lower iP levels seen in our mutant lines are also consistent with their reduced levels of early bud formation. The ribosides iPR and cis-zeatin riboside as well as the ribonucleotides

Figure 6. (*Continued.*)
cytokinins in 21-d-old liquid-cultured protonema as determined by UPLC-mass spectrometry (three cultures per genotype). Asterisks indicate significant differences between the mutant lines and the wild type at *P* value thresholds of 0.05 (*), 0.01 (**), and 0.001 (***), according to Student's *t* test. Error bars indicate SD. cZ, cis-Zeatin; DW, dry weight; cZRMP, cis-zeatin riboside 5′-monophosphate; cZROG, cis-zeatin riboside-*O*-glucoside; iPRMP, isopentenyladenosine 5′-monophosphate; tZROG, trans-zeatin riboside-*O*-glucoside.

isopentenyladenosine 5′-monophosphate and cis-zeatin riboside 5′-monophosphate accumulate in all three mutant genotypes (Fig. 6C), whereas the accumulation of trans-zeatin derivatives is less pronounced. A significant accumulation of trans-zeatin riboside-*O*-glucoside is observed in d|PpNRH1#29 and d|PpNRH3#7 knockout plants. However, the levels of the cis-zeatin riboside-*O*-glucoside are only slightly elevated in d|PpNRH1#29. These observations indicate that an excess of zeatin-type ribosides is glucosylated by zeatin-*O*-glucosyltransferases. Cytokinin *O*-glucosides are generally assumed to be storage products that can be activated through hydrolysis by β-glucosidases. In summary, we can state that all three PpNRHs have an impact on cytokinin homeostasis, although we cannot rule out that some of the effects might be due to indirect or unspecific responses of the whole cytokinin homeostatic system involving other pathways in addition to NRHs.

Taken together, changes in the metabolite profiles are generally compatible with the substrate preferences determined for the recombinant PpNRHs. Unexpectedly, the increased levels of hypoxanthine, xanthine, or adenine can be possibly attributed to the activity of near pathways, including up-regulation of cytokinin oxidase/dehydrogenase, adenine deaminase, or xanthine oxidase, which might compensate the levels of these metabolites. Moreover, Jung et al. (2011) reported that the accumulation of nucleosides in the *nrh1* Arabidopsis mutant was strongly increased under conditions of prolonged darkness, when salvage pathways are more important than the biosynthetic routes. The metabolite profiling for the *P. patens* single knockout mutants was undertaken under standard conditions. In the case of ADK, another purine/cytokinin-interconverting enzyme, the expected decrease of AMP was not observed in ADK-silenced Arabidopsis plants, which was also explained by the activity of related metabolic pathways leading to AMP production (Schoor et al., 2011). NRH, ADK, and adenine phosphoribosyltransferase are similar in that the cytokinins are not their major substrates in vitro (Moffatt et al., 2000; Allen et al., 2002). Nevertheless, it was shown for the Arabidopsis ADK knockdown plants (Schoor et al., 2011) as well as for *adenine phosphoribosyltransferase1-1* mutants (Zhang et al., 2013) that the levels of endogenous cytokinins are significantly changed, revealing an impact of these enzymes on the cytokinin interconversion.

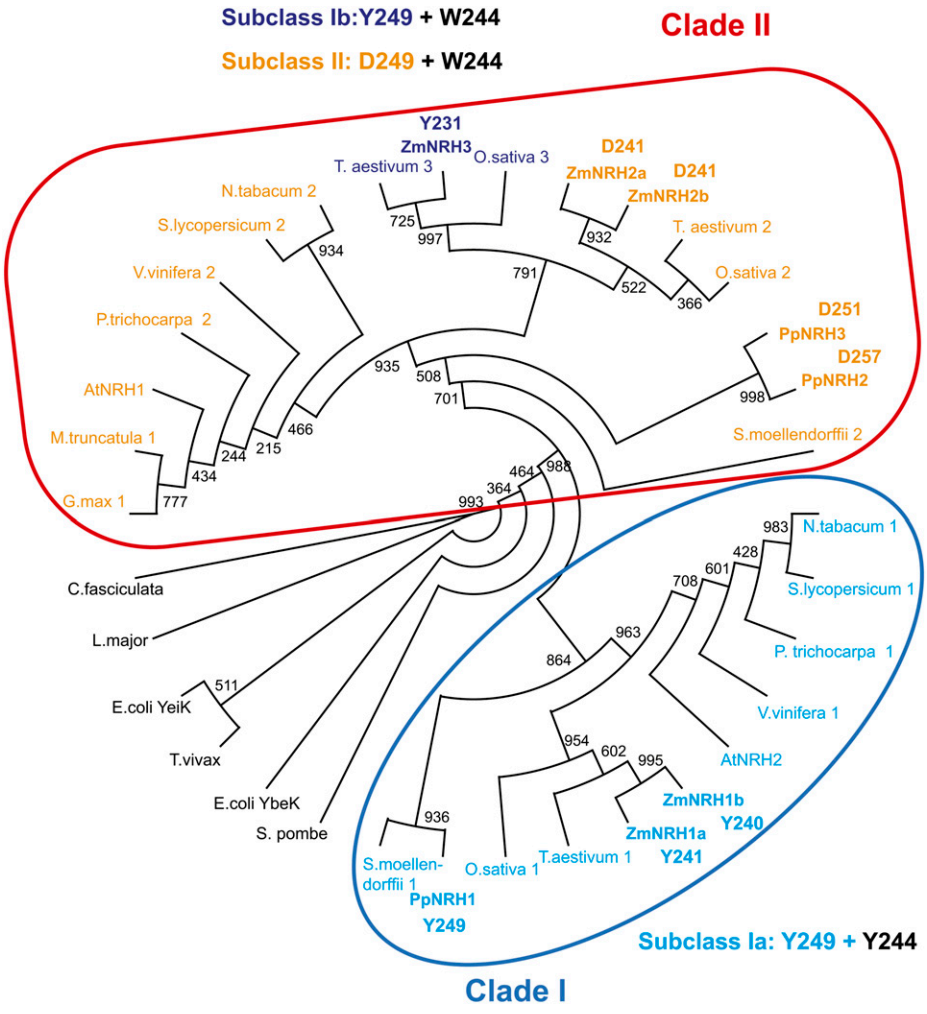

Figure 7. Cladogram of selected NRH proteins. The figure shows the clustering of plant IU-NRHs into two distinct clades (clade I and II) in the phylogenetic consensus tree. Internal labels give bootstrap frequencies for each clade. For the corresponding accession numbers, see "Materials and Methods." Subclass I (in light blue) comprises NRHs carrying a Tyr residue at position 249 (PpNRH1 numbering), which indicates preferential activity toward inosine/xanthosine. Subclass I occurs also in clade II. Subclass II (in orange) comprises NRHs carrying an Asp at position 249, which indicates preferential activity toward uridine/xanthosine.

Phylogeny of Plant IU-NRHs

Phylogenetic analysis (Fig. 7) shows clustering of plant IU-NRHs (Supplemental Fig. S8) into two clades. The outgroup comprising NRHs from *L. major*, *C. fasciculata*, *T. vivax*, *Schizosaccharomyces pombe*, and *E. coli* are, as expected, distant to the plant IU-NRHs. PpNRHs and ZmNRHs share 49% to 75% sequence identity with other plant NRHs (Supplemental Table S2). PpNRH1 is in the same branch (clade I) as ZmNRH1a and ZmNRH1b, while ZmNRH3 is in the same branch as ZmNRH2a, ZmNRH2b, PpNRH2, and PpNRH3 (clade II). It seems that early divergent land plants such as *P. patens* and *Selaginella moellendorffii* already had two NRH isoforms, which in most cases were preserved during the evolution of the seed plant line leading to two NRH isoforms, with one in each branch, in higher plants. The apparent duplication in *P. patens* resulted in *PpNRH2* and *PpNRH3* (clade II), probably due to a whole-genome duplication (Rensing et al., 2007). The Poaceae species maize, rice, and wheat display apparent diversification, leading to at least two isoforms in clade II. In the case of maize, a further diversification led to ZmNRH2a and ZmNRH2b.

There is a clear correlation between the clustering of the NRH genes and their enzymatic properties. Clade I comprises subclass 1a NRHs carrying Tyr-249 and Tyr-244 (using the PpNRH1 numbering), indicative of inosine and xanthosine preference. Clade II comprises mainly subclass II NRHs carrying an Asp at the same position (together with Trp-244), indicative of uridine/xanthosine preference. Interestingly, enzymes in clade II from the Poaceae family are also functionally diversified (Fig. 7). Although ZmNRH3 and ZmNRH2a/ZmNRH2b share 74.2% and 75.8% sequence identity (Supplemental Table S2), ZmNRH3 functionally belongs to subclass Ib (with Tyr-249 and Trp-244) and prefers the substrates inosine and xanthosine.

In the current classification, plant NRHs analyzed in this work (excluding two-domain NRHs) belong to nonspecific IU-NRHs. Our data show that assigning names of the plant IU-NRHs based on their in vitro substrate preferences can be misleading. For example, PpNRH1, which has a xanthosine/inosine preference, shows uridine as a weak substrate in vitro. However, in planta, the d|PpNRH1 line accumulates significant quantities of uridine, demonstrating that PpNRH1 is important for uridine conversion. This was the case for AtNRH1, which was initially named as uridine ribohydrolase (AtURH1; Jung et al., 2009). Plant IU-NRHs are obviously able to act on a wide range of ribosides, including cytokinin ribosides, and cannot be classified as having an exclusive preference for either purines or pyrimidines.

CONCLUSION

This work provides a comprehensive analysis of IU-NRHs from two plant species, maize and *P. patens*. It reveals the presence of several *NRH* genes per plant species, leading to the existence of at least two enzyme groups differing in substrate specificity, either preferring xanthosine/inosine (subclass I) or uridine/xanthosine (subclass II). Structural analysis combined with site-directed mutagenesis identified several residues responsible for nucleoside binding and catalysis. The single knockout mutants in *P. patens* show changes in the levels of purine, pyrimidine, and cytokinin metabolites and point out the importance of NRHs for nucleoside and cytokinin metabolism. Here, we prove the participation of plant IU-NRHs from both subclasses in cytokinin activation in vivo.

MATERIALS AND METHODS

Plant Material and Culture Conditions

The wild-type *Physcomitrella patens* (Funariaceae) strain used in this work was derived from the 'Gransden 2004' strain. Photoautotrophic growth was induced by keeping cultures under axenic conditions in growth chambers (RUMED 1602) at 25°C, illuminated with white light under a 16/8-h light/dark regime, with a flux of 50 μmol m^{-2} s^{-1}. For metabolite content analysis, tissue was cultivated in liquid medium (Wang et al., 1980) containing 0.359 mM $Ca(NO_3)_2$, 0.035 mM $FeSO_4$, 1.01 mM $MgSO_4$, 1.84 mM KH_2PO_4, and 10 mM KNO_3, to which 1 mL of Hoagland trace element solution was added (Ashton and Cove, 1977).

Cloning, Expression, and Gene Models of NRHs from *P. patens* and Maize

Total RNA for reverse transcription was isolated from *P. patens* (at the protonema stage) and from 5-d-old maize (*Zea mays* var *saccharata*) seedlings using the Plant RNA Isolation Aid solutions from Ambion. The RNA was treated twice with the TURBO DNase-free kit (Ambion). The cDNA was then synthesized using the SuperScript II reverse transcriptase (Invitrogen) and the RevertAid H Minus reverse transcriptase (Fermentas). Sequences coding for the *PpNRH1* (999 bp), *PpNRH2* (1,026 bp), and *PpNRH3* (1,017 bp) genes were amplified using gene-specific primers and the Accuprime *Pfx* polymerase (Invitrogen; Supplemental Table S3) and then cloned into a pCDFDuet His-tag vector (Novagen). In the case of PpNRH3, four splicing variants were obtained. In addition, five *NRH* coding sequences from maize were cloned (the primers used are shown in Supplemental Table S3) and submitted to GenBank. These sequences were as follows: *ZmNRH1a* (981 bp), *ZmNRH1b* (978 bp), *ZmNRH2a* (978 bp), *ZmNRH2b* (978 bp), and *ZmNRH3* open reading frame (ORF; 948 bp). The plasmids were transformed into T7 express cells (New England Biolabs). Protein expression was induced with 0.5 mM isopropyl-β-thiogalactopyranoside, after which the cultures were incubated at 20°C overnight.

Except for splicing variants of *PpNRH3_v3* and *PpNRH3_v4*, all of the analyzed *NRH* sequences consist of nine exons (Supplemental Fig. S1), with exons 2, 3, 6, and 7 all having the same length. Four variants of *PpNRH3* were identified due to alternative splicing at the 3′ ends of the fifth and eighth exons, none of which matches the current *PpNRH3* model. The eighth exon leads to a protein either with a FIAT C-terminal sequence (variants 3 and 4) or an SRLK C terminus (variants 1 and 2), in case the exon is spliced into two, meaning nine exons in total like all other NRH genes. The fifth exon, longer by 36 bp, introduces the VSLKRQKSHSRN peptide into the final protein (variants 2 and 4). Based on an alignment of plant NRH sequences, variant 1 most likely corresponds to the active form of PpNRH3. All five of the genes identified in maize also contain nine exons (Supplemental Fig. S1).

Site-Directed Mutagenesis of PpNRH1

Site-directed mutagenesis was performed on *PpNRH1* ORF in a pCDFDuet vector. The mutant H245A was prepared using two complementary primers containing the desired mutation (Supplemental Table S3). All of the other mutants were cloned using tail-to-tail-oriented phosphorylated primers, with the mutation being located at the 5′ end of one of the primers. PCR was performed using Accuprime *Pfx* polymerase (Invitrogen) in 30 cycles. The products were treated with *Dpn*I, gel purified, and ligated using the T4 DNA

ligase (Promega). The sequenced clones were transformed into T7 express competent cells (New England Biolabs). Mutant proteins were screened for the expression of the His-tagged protein by SDS-PAGE and using activity measurements.

Circular Dichroism Spectroscopy

The far-UV circular dichroism spectra of WT-PpNRH1 and its mutant variants were recorded on a J-815 spectropolarimeter (JASCO) at a concentration of 0.5 mg mL^{-1} in 20 mM Tris-HCl (pH 9.0) using a 0.1-cm quartz cell.

Phylogenetic Analysis

Amino acid alignments were performed using MUSCLE version 3.8 (Edgar, 2004). A maximum likelihood phylogeny with bootstrap analysis was performed with PhyML version 3.0 (Guindon et al., 2010) using the LG amino acid replacement matrix. *NRH* sequences from the following species were obtained from the National Center for Biotechnology Information, Phytozome, The Gene Index Project (http://compbio.dfci.harvard.edu/tgi/plant.html; Tentative Consensus accessions), or The Institute for Genomic Research (http://blast.jcvi.org/euk-blast/plantta_blast.cgi; Transcript Assembly accessions) databases: *Schizosaccharomyces pombe* (CAB91168), *Escherichia coli* YbeK (AAN79208), *E. coli* YeiK (AAA60514), *Leishmania major* (AY533501), *Crithidia fasciculata* (CFU43371), and *Trypanosoma vivax* (AF311701). Further complete plant NRH sequences were used: *P. patens* PpNRH1 (JQ649322), PpNRH2 (JX861385), and PpNRH3 (JX861386); maize ZmNRH1a (HQ825159), ZmNRH1b (HQ825160), ZmNRH2a (HQ825161), ZmNRH2b (JQ594984), and ZmNRH3 (HQ825162); Arabidopsis AtNRH1 (At2g36310) and AtNRH2 (At1g05620); soybean (*Glycine max 1*; BT097166), *Medicago truncatula 1* (XM_003625740), tobacco (*Nicotiana tabacum 1/2*; TC91311 and TC81540), rice (*Oryza sativa 1/2/3*; Os03g31170.1, Os08g44370.1, and Os09g39440.1), *Populus trichocarpa 1/2* (XM_002310348 and XM_002309011), *Selaginella moellendorffii 1/2* (XM_002974764 and XM_002984237), tomato (*Solanum lycopersicum 1/2*; AK325443 and AK322170), wheat (*Triticum aestivum 1/2/3*; TA56209_4565, TA76228_4565, and TA76014_4565), and grape (*Vitis vinifera 1/2*; XM_002280235 and XM_002283117).

Activity Measurement

Purine and pyrimidine ribosides were purchased from Sigma-Aldrich. The NRH activity was measured spectrophotometrically at 30°C according to a method described by Parkin (1996). The reaction in 200 mM Tris-HCl buffer, pH 7.5, 400 mM KCl, 1 mM dithiothreitol (DTT), and a riboside substrate was initiated by adding an appropriate amount of the enzyme (up to 50 μg for WT-PpNRH1 and 100–500 μg for the mutants). Kinetic constants were determined using the GraphPad Prism 5.0 software (GraphPad Software) by monitoring the absorption decrease of adenosine ($\Delta\varepsilon_{276} = -1.4$ mM^{-1} cm^{-1}), inosine ($\Delta\varepsilon_{280} = -0.92$ mM^{-1} cm^{-1}), uridine ($\Delta\varepsilon_{280} = -1.8$ mM^{-1} cm^{-1}), cytidine ($\Delta\varepsilon_{280} = -3.42$ mM^{-1} cm^{-1}), and thymidine ($\Delta\varepsilon_{265} = -1.7$ mM^{-1} cm^{-1}; Parkin, 1996). The differential extinction coefficients for xanthosine and guanosine were determined to be $\Delta\varepsilon_{248} = -3.7$ and -4.1 mM^{-1} cm^{-1}, respectively. Similarly, $\Delta\varepsilon_{289}$ values of -1.37 and -1.48 mM^{-1} cm^{-1} were determined for iPR and tZR, respectively.

Purification, Crystallization, and Structure Determination

All NRHs were purified on Co-Sepharose columns, and both PpNRH1 and ZmNRH3 were further purified by gel filtration chromatography on a HiLoad 26/60 Superdex 200 column using 50 mM Tris-HCl buffer (pH 8.0) and 150 mM NaCl. The purified PpNRH1 and ZmNRH3 fractions were concentrated to 30 to 35 mg mL^{-1}. Crystallization conditions for both NRHs were screened using Qiagen kits (Valencia) with a Cartesian nanodrop robot (Genomic Solutions). Crystals were obtained in hanging drops by mixing equal volumes of protein solution and a precipitant solution containing 0.1 M HEPES (pH 7.5), 100 mM sodium acetate, 10% (w/v) polyethylene glycol (PEG) 4000, and 10% ethylene glycol for PpNRH1 and containing 50 mM Tris-HCl (pH 8.0), 150 mM NaCl, and 20% (w/v) PEG 2000 monomethyl ether for ZmNRH3. Crystals were transferred to a cryoprotectant solution (the mother liquor supplemented with 25% PEG 400) and flash frozen in liquid nitrogen. Diffraction data for the PpNRH1 and ZmNRH3 crystals were collected at 100 K on the Proxima 1 beamline at the SOLEIL synchrotron at resolutions of 3.35 and 2.49 Å, respectively. Intensities were integrated using the XDS program (Kabsch, 2010; Supplemental Table S1).

The crystal structures of ZmNRH3 and PpNRH1 were determined by performing molecular replacement with Phaser (Storoni et al., 2004), using the monomer of YbeK (PDB 1YOE) and the dimer of ZmNRH3 as search models, respectively. Both models were refined with strong non-crystallographic symmetry restraints using Buster 2.10 (Bricogne et al., 2011). One translation/libration/screw-motion group was assigned for the dimer in the 2.49-Å structure and the four dimers in the lower resolution structure. Electron density maps were evaluated using COOT (Emsley and Cowtan, 2004). Refinement statistics are presented in Supplemental Table S1. No electron density was observed for residues 230 to 234 in subunit B of the ZmNRH3 structure. In subunit A, the electron density map was poorly defined for the side chains in the region comprising residues 228 to 337. Only two dimers (AB and CD) of the four were well defined in the electron density maps of the PpNRH1 structure. The dimer GH and mostly the molecule H present many disordered side chains and poor electron density maps in a few regions. Molecular graphics images were generated using PYMOL (www.pymol.org).

Substrate Docking into the Active Sites of PpNRH1 and ZmNRH3

The AutoDock suite 4.2.5.1 (Morris et al., 2009) was used for docking experiments. Both target active sites were kept rigid, while Tyr-241, Tyr-244, and Tyr-249 in PpNRH1 (Tyr-223, Trp-226, and Tyr-231 in ZmNRH3) were kept flexible. Hydrogen atoms were added and Gasteiger partial charges were computed. Calcium atom charges were added manually. Coordinates for inosine were taken from the structure of a YeiK complex (PDB 3B9X), while xanthosine and uridine were built in Avogadro 1.0.0 (http://avogadro.openmolecules.net/). The Rib moiety was constrained to maintain the C4′-endo puckered conformation, as commonly found in ribosides bound to NRHs. Docking calculations were performed using a Lamarckian genetic algorithm and a maximum of 100 conformers.

Generation of *P. patens* NRH Knockout Mutants

Functional gene knockouts of *PpNRH1*, *PpNRH2*, and *PpNRH3* were prepared using three gene-replacement vectors. The vectors were all designed using a resistance cassette flanked by 800- to 1,000-bp-long genomic fragments from the 5′ and 3′ regions of the corresponding genomic *NRH* locus. Details of the construction of the replacement vectors are provided in Supplemental Methods S1, and primer sequences are given in Supplemental Table S4. The transformation of *P. patens* protoplasts was carried out according to Schaefer et al. (1991) with minor modifications. Each transformation assay was performed using 25 μg of vector DNA. Between 15 and 20 stable moss lines were obtained after three rounds of selection using the appropriate antibiotic for each knockout construct. The haploid status of the transformants was verified, and eight to 10 transgenic lines for each mutant were arbitrarily chosen. These were then analyzed by PCR for recombination events at the corresponding loci and by reverse transcription-PCR for the absence of the transcript. Three knockout lines, d|PpNRH1#29, d|PpNRH2#56, and d|PpNRH3#7, were chosen for biochemical and phenotypic characterization.

Extraction and Determination of Purine, Pyrimidine, and Cytokinin Metabolites

P. patens wild-type and mutant lines were collected, freeze dried, and purified in triplicate (10 mg dry weight per sample). For quantification of the purine/pyrimidine bases and ribosides, the samples were homogenized, extracted in cold water with 25% ammonia (ratio, 4:1), and purified by solid-phase extraction with the addition of the stable-labeled internal standards. All samples were further purified on mixed-mode anion-exchange sorbent Oasis MAX cartridges (Waters) and analyzed using an Acquity ultra-performance liquid chromatography (UPLC) system connected to a triple quadrupole mass spectrometer (Xevo TQ MS; Waters MS Technologies). Further details are given in Supplemental Methods S1. Ultra-performance liquid chromatography-tandem mass spectrometry analysis was used to determine the cytokinin content of each sample (von Schwartzenberg et al., 2007) using a modified procedure of Novák et al. (2008).

Sequence data can be found in the GenBank/EMBL data libraries under accession numbers JQ649322 (*PpNRH1*), JX861385 (*PpNRH2*), JX861386 to JX861389 (the four splicing variants of *PpNRH3*), HQ825159 (*ZmNRH1a*), HQ825160 (*ZmNRH1b*), HQ825161 (*ZmNRH2a*), JQ594984 (*ZmNRH2b*), and HQ825162 (the *ZmNRH3* ORF). The atomic coordinates and structure factors have been deposited in the PDB under accession codes 4KPN (*PpNRH1*) and 4KPO (*ZmNRH3*).

Supplemental Data

The following materials are available in the online version of this article.

Supplemental Figure S1. *NRH* gene models for *P. patens*, maize, and Arabidopsis.

Supplemental Figure S2. Influence of pH and temperature on catalytic activity of recombinant PpNRH1.

Supplemental Figure S3. Confirmation of cytokinin riboside conversion by ZmNRH3, ZmNRH2b, and PpNRH1.

Supplemental Figure S4. Gel permeation chromatography of PpNRH1 and ZmNRH3.

Supplemental Figure S5. Structural comparison of plant NRH (ZmNRH3, this article) with NRH from *E. coli* (YeiK, PDB 3B9X).

Supplemental Figure S6. Production of PpNRH1 protein variants.

Supplemental Figure S7. Delayed bud development within 4 weeks after aerial inoculation with protonema suspension.

Supplemental Figure S8. Alignment of plant NHR sequences.

Supplemental Table S1. Data collection and refinement statistics of plant NRHs.

Supplemental Table S2. Identities of ZmNRH3 and PpNRH1 with other NRHs from maize and *P. patens* and from other species.

Supplemental Table S3. Primer pairs used for the cloning of NRHs and for the site-directed mutagenesis of PpNRH1.

Supplemental Table S4. Primers used for generation of gene replacement vectors and genetic analysis of *P. patens* knockout mutants.

Supplemental Methods S1. Generation of *P. patens* knockout mutants and quantification of ribosides.

ACKNOWLEDGMENTS

The pBZRF vector was provided by the courtesy of Fabien Nogué (Institut National de la Recherche Agronomique, Versailles). We thank Barbara Moffatt and Katja Engel (University of Waterloo) for contributions to enzyme assays in an early phase of the project, Jeanette Klein (Charité Berlin) for initial purine and pyrimidine measurements, Dr. Petr Tarkowski (University of Olomouc) for HPLC measurement, Vera Schwekendiek and Susanne Bringe (University of Hamburg) for excellent technical support, Beatriz Guimaraes for help in data collection on Proxima 1 at the SOLEIL synchrotron, Pierre Legrand (Synchrotron SOLEIL) and Gérard Bricogne (Global Phasing Ltd) for help in data processing and refinement strategy, and Andrew Thompson for help with manuscript preparation. This work benefited from the IMAGIF platform facilities (www.imagif.cnrs.fr) at the Centre de Recherche de Gif-sur-Yvette.

Received September 18, 2013; accepted October 28, 2013; published October 29, 2013.

LITERATURE CITED

Achar BS, Vaidyanathan CS (1967) Purification and properties of uridine hydrolase from mung-bean (*Phaseolus radiatus*) seedlings. Arch Biochem Biophys **119:** 356–362

Allen M, Qin W, Moreau F, Moffatt B (2002) Adenine phosphoribosyltransferase isoforms of Arabidopsis and their potential contributions to adenine and cytokinin metabolism. Physiol Plant **115:** 56–68

Ashton NW, Cove DJ (1977) The isolation and preliminary characterisation of auxotrophic and analogue resistant mutants of the moss, Physcomitrella patens. Mol Gen Genet **154:** 87–95

Bricogne G, Blanc E, Brandl M, Flensburg C, Keller P, Paciorek W, Roversi P, Sharff A, Smart OS, Vonrhein C, et al (2011) BUSTER Version 2.1.0. Global Phasing, Cambridge, UK

Campos A, Rijo-Johansen MJ, Carneiro MF, Fevereiro P (2005) Purification and characterisation of adenosine nucleosidase from *Coffea arabica* young leaves. Phytochemistry **66:** 147–151

Chen CM, Kristopeit SM (1981) Metabolism of cytokinin: deribosylation of cytokinin ribonucleoside by adenosine nucleosidase from wheat germ cells. Plant Physiol **68:** 1020–1023

Chen M, Thelen JJ (2011) Plastid uridine salvage activity is required for photoassimilate allocation and partitioning in *Arabidopsis*. Plant Cell **23:** 2991–3006

Cove D, Bezanilla M, Harries P, Quatrano R (2006) Mosses as model systems for the study of metabolism and development. Annu Rev Plant Biol **57:** 497–520

Degano M, Almo SC, Sacchettini JC, Schramm VL (1998) Trypanosomal nucleoside hydrolase: a novel mechanism from the structure with a transition-state inhibitor. Biochemistry **37:** 6277–6285

Degano M, Gopaul DN, Scapin G, Schramm VL, Sacchettini JC (1996) Three-dimensional structure of the inosine-uridine nucleoside N-ribohydrolase from *Crithidia fasciculata*. Biochemistry **35:** 5971–5981

Edgar RC (2004) MUSCLE: multiple sequence alignment with high accuracy and high throughput. Nucleic Acids Res **32:** 1792–1797

Emsley P, Cowtan K (2004) Coot: model-building tools for molecular graphics. Acta Crystallogr D Biol Crystallogr **60:** 2126–2132

Estupiñán B, Schramm VL (1994) Guanosine-inosine-preferring nucleoside N-glycohydrolase from *Crithidia fasciculata*. J Biol Chem **269:** 23068–23073

Garau G, Muzzolini L, Tornaghi P, Degano M (2010) Active site plasticity revealed from the structure of the enterobacterial N-ribohydrolase RihA bound to a competitive inhibitor. BMC Struct Biol **10:** 14

Giabbai B, Degano M (2004) Crystal structure to 1.7 a of the Escherichia coli pyrimidine nucleoside hydrolase YeiK, a novel candidate for cancer gene therapy. Structure **12:** 739–749

Gopaul DN, Meyer SL, Degano M, Sacchettini JC, Schramm VL (1996) Inosine-uridine nucleoside hydrolase from *Crithidia fasciculata*: genetic characterization, crystallization, and identification of histidine 241 as a catalytic site residue. Biochemistry **35:** 5963–5970

Guindon S, Dufayard JF, Lefort V, Anisimova M, Hordijk W, Gascuel O (2010) New algorithms and methods to estimate maximum-likelihood phylogenies: assessing the performance of PhyML 3.0. Syst Biol **59:** 307–321

Guranowski A (1982) Purine catabolism in plants: purification and some properties of inosine nucleosidase from yellow lupin (*Lupinus luteus* L.) seeds. Plant Physiol **70:** 344–349

Guranowski A, Schneider Z (1977) Purification and characterization of adenosine nucleosidase from barley leaves. Biochim Biophys Acta **482:** 145–158

Horenstein BA, Parkin DW, Estupiñán B, Schramm VL (1991) Transition-state analysis of nucleoside hydrolase from *Crithidia fasciculata*. Biochemistry **30:** 10788–10795

Houba-Hérin N, Pethe C, d'Alayer J, Laloue M (1999) Cytokinin oxidase from *Zea* mays: purification, cDNA cloning and expression in moss protoplasts. Plant J **17:** 615–626

Iovane E, Giabbai B, Muzzolini L, Matafora V, Fornili A, Minici C, Giannese F, Degano M (2008) Structural basis for substrate specificity in group I nucleoside hydrolases. Biochemistry **47:** 4418–4426

Jung B, Flörchinger M, Kunz HH, Traub M, Wartenberg R, Jeblick W, Neuhaus HE, Möhlmann T (2009) Uridine-ribohydrolase is a key regulator in the uridine degradation pathway of *Arabidopsis*. Plant Cell **21:** 876–891

Jung B, Hoffmann C, Möhlmann T (2011) Arabidopsis nucleoside hydrolases involved in intracellular and extracellular degradation of purines. Plant J **65:** 703–711

Kabsch W (2010) XDS. Acta Crystallogr D Biol Crystallogr **66:** 125–132

Kurakawa T, Ueda N, Maekawa M, Kobayashi K, Kojima M, Nagato Y, Sakakibara H, Kyozuka J (2007) Direct control of shoot meristem activity by a cytokinin-activating enzyme. Nature **445:** 652–655

Mainguet SE, Gakière B, Majira A, Pelletier S, Bringel F, Guérard F, Caboche M, Berthomé R, Renou JP (2009) Uracil salvage is necessary for early Arabidopsis development. Plant J **60:** 280–291

Massonneau A, Houba-Hérin N, Pethe C, Madzak C, Falque M, Mercy M, Kopecny D, Majira A, Rogowsky P, Laloue M (2004) Maize cytokinin oxidase genes: differential expression and cloning of two new cDNAs. J Exp Bot **55:** 2549–2557

Moffatt B, Pethe C, Laloue M (1991) Metabolism of benzyladenine is impaired in a mutant of *Arabidopsis thaliana* lacking adenine phosphoribosyltransferase activity. Plant Physiol **95:** 900–908

Moffatt B, Somerville C (1988) Positive selection for male-sterile mutants of Arabidopsis lacking adenine phosphoribosyl transferase activity. Plant Physiol **86:** 1150–1154

Moffatt BA, Stevens YY, Allen MS, Snider JD, Pereira LA, Todorova MI, Summers PS, Weretilnyk EA, Martin-McCaffrey L, Wagner C (2002) Adenosine kinase deficiency is associated with developmental abnormalities and reduced transmethylation. Plant Physiol **128:** 812–821

Moffatt BA, Wang L, Allen MS, Stevens YY, Qin W, Snider J, von Schwartzenberg K (2000) Adenosine kinase of Arabidopsis: kinetic properties and gene expression. Plant Physiol **124:** 1775–1785

Mok DW, Mok MC (2001) Cytokinin metabolism and action. Annu Rev Plant Physiol Plant Mol Biol **52:** 89–118

Morris GM, Huey R, Lindstrom W, Sanner MF, Belew RK, Goodsell DS, Olson AJ (2009) AutoDock4 and AutoDockTools4: automated docking with selective receptor flexibility. J Comput Chem **30:** 2785–2791

Muzzolini L, Versées W, Tornaghi P, Van Holsbeke E, Steyaert J, Degano M (2006) New insights into the mechanism of nucleoside hydrolases from the crystal structure of the Escherichia coli YbeK protein bound to the reaction product. Biochemistry **45:** 773–782

Novák O, Hauserová E, Amakorová P, Doležal K, Strnad M (2008) Cytokinin profiling in plant tissues using ultra-performance liquid chromatography-electrospray tandem mass spectrometry. Phytochemistry **69:** 2214–2224

Parkin DW (1996) Purine-specific nucleoside N-ribohydrolase from *Trypanosoma brucei brucei*: purification, specificity, and kinetic mechanism. J Biol Chem **271:** 21713–21719

Parkin DW, Horenstein BA, Abdulah DR, Estupiñán B, Schramm VL (1991) Nucleoside hydrolase from *Crithidia fasciculata*: metabolic role, purification, specificity, and kinetic mechanism. J Biol Chem **266:** 20658–20665

Rensing SA, Ick J, Fawcett JA, Lang D, Zimmer A, Van de Peer Y, Reski R (2007) An ancient genome duplication contributed to the abundance of metabolic genes in the moss *Physcomitrella patens*. BMC Evol Biol **7:** 130

Riegler H, Geserick C, Zrenner R (2011) *Arabidopsis thaliana* nucleosidase mutants provide new insights into nucleoside degradation. New Phytol **191:** 349–359

Riewe D, Grosman L, Fernie AR, Zauber H, Wucke C, Geigenberger P (2008) A cell wall-bound adenosine nucleosidase is involved in the salvage of extracellular ATP in *Solanum tuberosum*. Plant Cell Physiol **49:** 1572–1579

Sakakibara H (2006) Cytokinins: activity, biosynthesis, and translocation. Annu Rev Plant Biol **57:** 431–449

Schaefer D, Zryd JP, Knight CD, Cove DJ (1991) Stable transformation of the moss *Physcomitrella patens*. Mol Gen Genet **226:** 418–424

Schaefer DG, Zrÿd JP (1997) Efficient gene targeting in the moss *Physcomitrella patens*. Plant J **11:** 1195–1206

Schoor S, Farrow S, Blaschke H, Lee S, Perry G, von Schwartzenberg K, Emery N, Moffatt B (2011) Adenosine kinase contributes to cytokinin interconversion in Arabidopsis. Plant Physiol **157:** 659–672

Shi W, Schramm VL, Almo SC (1999) Nucleoside hydrolase from Leishmania major: cloning, expression, catalytic properties, transition state inhibitors, and the 2.5-Å crystal structure. J Biol Chem **274:** 21114–21120

Stasolla C, Katahira R, Thorpe TA, Ashihara H (2003) Purine and pyrimidine nucleotide metabolism in higher plants. J Plant Physiol **160:** 1271–1295

Storoni LC, McCoy AJ, Read RJ (2004) Likelihood-enhanced fast rotation functions. Acta Crystallogr D Biol Crystallogr **60:** 432–438

Szuwart M, Starzynska E, Pietrowska-Borek M, Guranowski A (2006) Calcium-stimulated guanosine-inosine nucleosidase from yellow lupin (*Lupinus luteus*). Phytochemistry **67:** 1476–1485

Versées W, Decanniere K, Pellé R, Depoorter J, Brosens E, Parkin DW, Steyaert J (2001) Structure and function of a novel purine specific nucleoside hydrolase from *Trypanosoma vivax*. J Mol Biol **307:** 1363–1379

Versées W, Decanniere K, Van Holsbeke E, Devroede N, Steyaert J (2002) Enzyme-substrate interactions in the purine-specific nucleoside hydrolase from *Trypanosoma vivax*. J Biol Chem **277:** 15938–15946

Versées W, Steyaert J (2003) Catalysis by nucleoside hydrolases. Curr Opin Struct Biol **13:** 731–738

von Schwartzenberg K (2009) Hormonal regulation of development by auxin and cytokinin in moss. Annu Plant Rev **36:** 246-281

von Schwartzenberg K, Kruse S, Reski R, Moffatt B, Laloue M (1998) Cloning and characterization of an adenosine kinase from Physcomitrella involved in cytokinin metabolism. Plant J **13:** 249–257

von Schwartzenberg K, Núñez MF, Blaschke H, Dobrev PI, Novák O, Motyka V, Strnad M (2007) Cytokinins in the bryophyte Physcomitrella patens: analyses of activity, distribution, and cytokinin oxidase/dehydrogenase overexpression reveal the role of extracellular cytokinins. Plant Physiol **145:** 786–800

Vyroubalová S, Václavíková K, Turecková V, Novák O, Smehilová M, Hluska T, Ohnoutková L, Frébort I, Galuszka P (2009) Characterization of new maize genes putatively involved in cytokinin metabolism and their expression during osmotic stress in relation to cytokinin levels. Plant Physiol **151:** 433–447

Wang TL, Cove DJ, Beutelmann P, Hartmann E (1980) Isopentenyladenine from mutants of the moss, *Physcomitrella patens*. Phytochemistry **19:** 1103–1105

Zhang X, Chen Y, Lin X, Hong X, Zhu Y, Li W, He W, An F, Guo H (2013) Adenine phosphoribosyl transferase 1 is a key enzyme catalyzing cytokinin conversion from nucleobases to nucleotides in Arabidopsis. Mol Plant **6:** 1661–1672

Zrenner R, Stitt M, Sonnewald U, Boldt R (2006) Pyrimidine and purine biosynthesis and degradation in plants. Annu Rev Plant Biol **57:** 805–836

PALACKY UNIVERSITY OLOMOUC

Faculty of Science

Department of Biochemistry

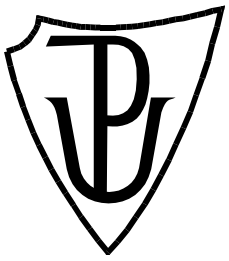

Mgr. Radka Končitíková

Enzymes linked to degradation pathway of cytokinins in maize

Ph.D. thesis summary

Biochemistry - P1406

Olomouc 2015

The Ph.D. Thesis was carried out at the Department of Biochemistry and Proteomics Centre of the Region Haná for Biotechnological and Agricultural Research, Faculty of Palacky University in Olomouc.

Candidate:
Mgr. Radka Končitíková
Department of Protein Biochemistry and Proteomics, Centre of the Region Haná for Biotechnological and Agricultural Research, Faculty of Science, Palacký University, Olomouc

Supervisor:
Mgr. David Kopečný, Ph.D.
Department of Protein Biochemistry and Proteomics, Centre of the Region Haná for Biotechnological and Agricultural Research, Faculty of Science, Palacký University, Olomouc

Consultant:
Prof. Mgr. Marek Šebela, Dr.
Department of Protein Biochemistry and Proteomics, Centre of the Region Haná for Biotechnological and Agricultural Research, Faculty of Science, Palacký University, Olomouc

Rewiewers:

Prof. RNDr. Michaela Wimmerová, Ph.D
National Centre for Biomolecular Research/ CEITEC/ Department of Biochemistry, Faculty of Science, Masaryk University, Brno

Prof. RNDr. Břetislav Brzobohatý, CSc.
Department of Molecular Biology and Radiobiology, CEITEC, Mendel University of Agriculture and Forestry, Brno / Institute of Biophysics, Academy of Sciences of the Czech Republic, Brno

Recommendation and statement of Ph.D. thesis was prepared by the Department of Biochemistry, Palacky University Olomouc.

The Ph.D. summary was sent on: _____

Defense of Ph.D.thesis will be performed on _____ at _____ in front of PhD committee for Faculty of Science postgradual study.

The Ph.D. thesis is availeble at the Department of Biochemistry, Faculty of Palacky University in Olomouc-Holice.

Head of the committee: **Doc. RNDr. Lenka Luhová, Ph.D**.

Contents

Summary

The presented Ph.D. thesis is focused on characterization of enzymes, which could be linked to degradation pathway of cytokinins in maize. Cytokinins are plant hormones, which play an important role in many developmental processes like regulation of cell proliferation and differentiation in root and shoot apical meristems, differentiation of plastids etc. Cytokinins negatively control root elongation and branching and the main naturally occurring cytokinins are N^6-prenylated adenine/adenosine derivatives, such as N^6-(Δ^2-isopentenyl)adenine (iP) and zeatin (Z) and their ribosides iPR and ZR. Cytokinin oxidase/dehydrogenase (CKO/CKX, EC 1.5.99.12) catalyzes irreversible degradation of above cytokinins to the corresponding adenine or adenosine and aldehyde.

The first aim of the work was to better understand substrate specificity differences among CKO isoforms and to search for more complex inhibitors. In consequence, new structures of CKO2 and CKO4a from maize as well as the binding mode of cytokinin ribosides were analyzed. New thidiazuron-derived inhibitors were tested and their binding was analyzed by X-ray crystallography. The importance of CKO glycosylation for the enzyme stability was studied using CKO1 from maize. The second aim of this work was to search for enzymes involved in possible interconversion of CKO reaction products. The search was focused on a superfamily of aldehyde dehydrogenases (ALDHs), which could metabolize the released aldehyde, and also on a family of nucleoside-N-ribohydrolases (NRH, EC 3.2.2.1), which could catalyze the interconversion of adenosine to adenine as well as the interconversion of cytokinin ribosides to bases.

Aldehydes are toxic, cancerogenic and mutagenic at higher concentrations and ALDHs are responsible for oxidation of biogenic aldehydes as well as for cell detoxification of aldehydes generated during lipid peroxidation. So far, 13 ALDH families have been described in plants. To get insight into their function, 10 maize genes covering three ALDH families (family 2, 7 and 10) were analyzed. Crystal structures of representatives of these three families were solved and their kinetics was characterized. It was found that ALDH2 family isoforms are able to oxidize aldehydes released from CKO reaction. NRHs catalyze a hydrolysis of nucleosides to nucleobase and ribose and the study was focused on purine nucleoside N-ribohydrolase, namely NRH3 from maize (ZmNRH3). Kinetic and structural study was performed and it was found that both adenosine and iPR/ZR can be metabolized to corresponding bases adenine and iP/Z.

Souhrn

Předkládaná disertační práce je zaměřena na charakterizaci enzymů, které by mohly být spojeny s degradací cytokininů v kukuřici. Cytokininy jsou rostlinné hormony, které hrají důležitou roli v mnoha vývojových procesech, jako je regulace buněčného dělení a vývoje kořene a prýtu, diferenciace plastidů atd. Cytokininy často kooperují s dalšími rostlinými hormony, zejména auxiny. Přirozeně se vyskytující cytokininy jsou N^6-prenylované deriváty adeninu / adenosinu, jako N^6- (Δ^2-isopentenyl) adeninu (iP) a zeatin (Z) a jejich ribosidy iPR a ZR. Cytokininoxidasa / dehydrogenasa (CKO / CKX, EC 1.5.99.12) katalyzuje ireverzibilní degradaci cytokininů na adeninu nebo adenosinu a odpovídající aldehyd.

Prvním cílem práce bylo lépe popsat rozdíly v substrátové specificitě mezi jednotlivými isoformami CKO a najít účinnější inhibitory. V důsledku toho, byly analyzovány nové struktury CKO2 a CKO4a z kukuřice, stejně jako vazebný způsob cytokininových ribosidů. Byly testovány nové inhibitory odvozené od thidiazuronu a pomocí rentgenové krystalografie analyzována jejich vazba. Vliv glykosylace na stabilitu enzymu byl studován na CKO1 z kukuřice. Druhým cílem této práce bylo hledání enzymů podílejících se na možné interkonverzi reakčních produktů metabolismu cytokininů. Hledání bylo zaměřeno na nadrodinu aldehyddehydrogenas (ALDHs), které by mohly metabolizovat uvolněný aldehyd, a také na rodiny nukleosid-N-ribohydrolas (NRH, EC 3.2.2.1), které mohou katalyzovat vzájemnou přeměnu adenosinu na adenin, stejně jako interkonverzi cytokininových ribosidů na odpovídající báze.

Aldehydy jsou při vyšších koncentracích toxické, kancerogenní a mutagenní. ALDHs jsou zodpovědné za oxidaci biogenních aldehydů, podobně i za detoxifikaci aldehydů vznikajících při peroxidaci lipidů. Dosud bylo popsáno 13 ALDH rodin v rostlinách. Pro bližší pochopení jejich funkcí, bylo analyzováno 10 kukuřičný genů ze tří ALDH rodin (rodina 2, 7 a 10). Byly řešeny krystalové struktury zástupců těchto tří rodin, a také charakterizovány jejich kinetické vlastnosti. Bylo zjištěno, že izoenzymy z ALDH2 rodiny jsou schopny oxidovat aldehydy produkované CKO. NRHs katalyzují hydrolýzu nukleosidů na odpovídající báze a ribózu. Byly studovány purinové nukleosid N-ribohydrolasy, a to NRH3 z kukuřice (ZmNRH3). Na základě provedených kinetických a strukturální studií bylo zjištěno, že jak adenosin tak i iPR / ZR mohou být metabolizovány na odpovídající báze adenin a iP / Z.

Aims of the work

1) Literature review about the degradation pathway of cytokinins focused on cytokinin oxidase/dehydrogenases, aldehydedehydrogenases and nucleoside-N-ribohydrolases

2) Cloning of maize genes, expression and protein purification

3) Characterization of molecular and kinetic properties with substrates and inhibitors

4) Crystallization studies

5) Gene expression studies in maize

1 Introduction

1.1 Cytokinin oxidases/dehydrogenases

The enzyme, which is responsible for cytokinin degradation, is known as a cytokinin oxidase/dehydrogenase (abbreviated as CKO or CKX, Chatfield and Armstrong 1987). CKO belongs to the group of oxidoreductases that contain a flavin cofactor (Fraaije *et al*., 1998). After it was shown that other compounds with reducing properties may act as a more efficient electron acceptors than oxygen, the enzyme was reclassified to cytokinin dehydrogenase in 2001 (EC 1.5.99.12; Morris *et al*., 1999; Galuszka *et al*. 2001). However, such a name is inaccurate because it excludes oxygen as the electron acceptor and the reaction simply occurs in both modes.

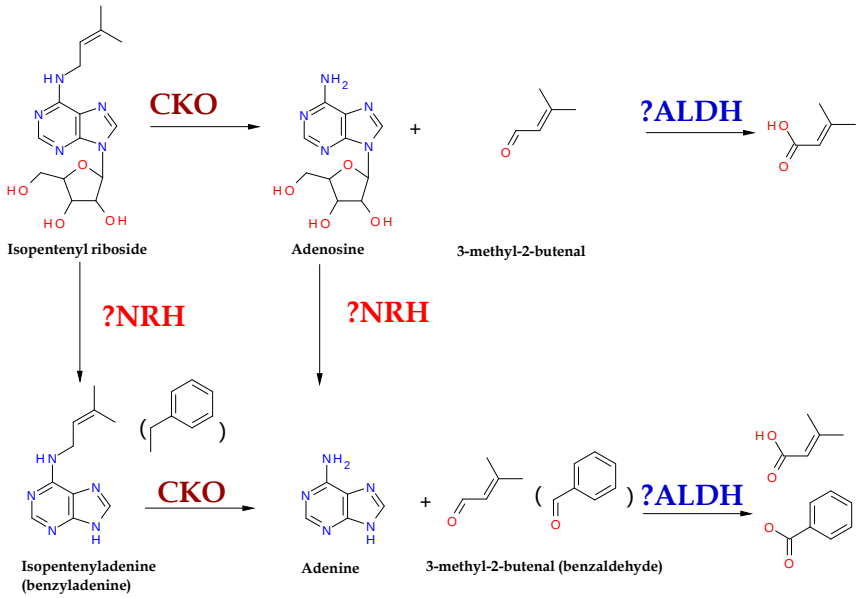

Figure 1. A scheme of CKO reaction with possible involvement of ALDH and NRH.

Cytokinins are inactivated by CKO by cleaving their isoprenyl or benzyl side-chain. FAD cofactor is reduced by two electrons transferred from substrate. An imine intermediate is formed and is further hydrolyzed to adenine and corresponding aldehyde (Mok and Mok 2001). $FADH_2$ is reoxidized by oxygen, which leads to production H_2O_2 (Kopečný *et al*., 2005) or other electron acceptor as for example by quinone (Frébortová *et al*., 2004). Flavin reduction is very fast but the reaction rate depends on the type and concentration of the used electron acceptor. If the flavin is reoxidized by molecular oxygen then the reaction rate reaches 0.5 s^{-1}. In case that highly efficient electron acceptor (as DCPIP or PMS) is used, the enzyme is able to degrade cytokinins at the reaction rate of 1000s^{-1} (Frébortová *et al*., 2004). A whole range of compounds have been tested as potential electron acceptors including caffeic acid, *p*-quinones, analogs of ubiquinone, coenzymes Q_0 (K_m = 210 μM) a Q_1, 1,4-naftoquinone (K_m =11 μM), phenazine methosulphate (PMS), 2,6- dichlorophenol indophenol

(DCPIP, K_m = 36 μM for ZmCKO1; Bilyeu *et al.*, 2001; Frébort *et al.*, 2002, Frébortová *et al.*, 2004). DCPIP is effective as electron acceptor in the neutral and slightly basic pH (7-9) while quinones are be predisposed to spontaneous oxidative side reactions in basic pH and thus they work at slightly acidic pH. CKOs are able to degrade aromatic cytokinins. Reaction rates are however rather low with no significant difference if using oxygen, Q_0 or DCPIP as the electron acceptor (Frébortová *et al.*, 2004). Precursor of natural electron acceptor could be 2,4-dihydroxy-7-methoxy-1,4-benzoxazin-3-on (DIMBOA) after reaction with polyphenol oxidase or peroxidase. DIMBOA is cleaved to 4-nitrosoresorcinol 1-monomethyl ether (coniferron). Coniferron is a functional electron acceptor but the affinity and reaction rates with CKO are very low compared with artificial acceptors DCPIP or PMS. The effective acceptor is formed upon subsequent oxidation of connifferon by laccase and peroxidase to the conifferon radical, which further forms the polymer. The process of polymerization is inhibited in presence of CKO. Increased cytokinin levels in plant tissues are followed by increased levels of laccase and peroxidase, which might be involved in the synthesis of radicals suitable as CKO electron acceptors (Frébortová *et al.*, 2010). ZmCKO1 (PDB 1W1Q, Malito *et al.*, 2004) is the best studied enzyme from CKO family. It is monomeric and glycosylated flavoenzyme. It comprises two domains, namely a FAD binding domain (residues 1 – 244 and 492 – 534) and a substrate binding domain (residues 245 – 491) which is very similar to other flavin oxidoreductases (Fraaije *et al.*, 1998). Isoalloxazine ring of FAD has a planar conformation and covalently bound to H105 via methyl- group in position 8. This H105 residue belongs to a GHS motif conserved among all CKOs. Covalent flavin binding facilitates reduction catalysis and increase oxidative power flavin (Fraaije *et al.*, 1999). Mutations leading to removal of covalent FAD generally results in a reduction in redox potential and the speed of flavin reduction. Therefore, it can be assumed that the covalent binding of the FAD in CKO facilitates the reduction of FAD during catalysis.

1.2 Aldehyde dehydrogenases

Aldehyde dehydrogenases (abbreviated as ALDHs) catalyze NAD(P)+-dependent oxidation of aldehydes to the corresponding carboxylic acid and NAD(P)H. These enzymes are present in many physiological metabolic pathways – carnitine biosynthesis, glycolysis, gluconeogenesis, amino acid metabolism (Marchitti et al., 2008; Sophos and Vasiliou 2003; Tylichová et al., 2010). They also participate in the detoxification of aldehydes generated during oxidative stress or during the metabolism of xenobiotics. ALDH enzymes play crucial role as "aldehyde scavengers" (Brocker et al., 2012) by oxidizing aldehydes which are toxic in higher concentrations. Aldehydes like 4-hydroxynonenal, 4-oxononenal and malondialdehyde originate from lipid peroxidation and act as electrophiles and thus easily build adducts with nucleic acids and proteins. Experiments performed on plants have shown that upregulation of *ALDH* is often a response to environmental stresses (Barclay and McKersie, 1994; Kirch *et al.*, 2001) such as drought, salinity etc. Depletion of water causes a

change in osmotic pressure on the membrane, thereby pushing the water out of the cell. One of the ways to prevent osmotic stress is the generation of osmoprotectants by ALDHs (Fong *et al*., 2006).

Family 2 ALDHs are mitochondrial or cytosolic homotetramers, which have been extensively studied not only in plants (Yoshida *et al.*, 1998, Navarro-Aviňo *et al*., 1999, Marchitti *et al*., 2008). Plant ALDH2 isoforms have been studied in maize (*Zea mays*), rice (*Oryza sativa*) and Arabidopsis thaliana (Skibbe *et al.*, 2002, Liu *et al.*, 2002 Nakazono *et al.*, 2000). Mitochondrial enzyme from rice (OsALDH2) is responsible for the efficient detoxification of acetaldehyde after the flooding and ethanol fermentation (Wei *et al*., 2009). Metabolism of acetaldehyde generates acetate, which is consecutively used for CoA synthesis *via* acetyl-CoA synthase, often described as the „pyruvate dehydrogenase pathway". In *Arabidopsis,* two *ALDH2* genes (*ALDH2B7* and *ALDH2B4*) code for isoforms with 75% similarity that accumulate in mitochondria. (Wei *et al* 2009). ALDH2B4 homologue in Chinese wild grapevine anticipates a mildew infection (Wen *et al.*, 2012). Nevertheless, the protection mechanism against pathogen infection is not well understood. A great progress in understanding the role of mitochondrial ALDH2 is linked to a discovery of *rf2a* (**r**estoration of **f**ertility) gene in maize, which codes for a mitochondrial ALDH (Liu *et al*., 2002) and its mutation is responsible for cytoplasmic male sterility (CMS). In general, male sterility is the failure of plants to produce functional anthers, pollen, or male gametes. Texas CMS maize is predisposed to the southern corn leaf blight disease caused by *Cochliobolus heterostrophus,* which produces a T-toxin (Hooker *et al*., 1970; Yoder, 1973). The *rf2a* is important for normal anther development in plants with normal cytoplasm (Liu *et al*., 2001). RF2A, but not RF2B, accumulates to high levels in the tapetal cells of anthers (Liu and Schnable, 2002) and the anther development halts in the lower florets of plants, which are homozygous for mutation in *rf2a* (Liu *et al*., 2001). There is an assumption that ALDH2 isoforms are involved in phenylpropanoid pathway *as REF1* gene, which codes for ALDH2 in Arabidopsis, plays a significant role in the synthesis of ferulic acid and sinapic acid. Esters of ferulic acid accumulate in a wide range of plants.

ALDHs from family 7 are known as antiquitins, α-aminoadipic semialdehyde dehydrogenases or Δ^1-piperideine-6-carboxylate dehydrogenases (P6CDH). The *ALDH7* gene family is one of the most conserved ALDH families across species and sequence identity of about 60% is observed on protein level among its members. These enzymes are involved in the lysine catabolism and oxidize α-aminoadipic semialdehyde to the corresponding acid (Brocker *et al*., 2010). The expression of *ALDH7* takes part in the protection against hyperosmotic stress and seed maturation (Kirch *et al*., 2005) in plant such as garden pea (Guerrero *et al*. 1990), apple (Yamada *et al*. 1999), *Tortula ruralis* (Chen *et al*. 2002), brassica (Stroeher *et al*. 1995), sorghum (Buchanan *et al*. 2005) and Arabidopsis (Kirch *et al*. 2005).

ALDH10 family members are known as aminoaldehyde dehydrogenases (AMADHs, EC 1.2.1.19), 4-aminobutyraldehyde dehydrogenases, 4-guanidinobutyraldehyde dehydrogenases (EC 1.2.1.54) and betaine aldehyde dehydrogenases (BADH; EC 1.2.1.8). ALDH10 family has been studied due to connection with polyamine metabolism, degradation of toxic and reactive ω-aminoaldehydes, such as 3-aminopropionaldehyde (APAL) or 4-aminobutyraldehyde (ABAL), which originate from different metabolic pathways. Oxidation of these aldehydes leads to formation of nontoxic compounds, such as β-alanine and γ-aminobutyric acid (GABA). Plant AMADHs share 70-80% sequence identity (Bradbury *et al*., 2008; Missihoun *et al*., 2011; Tylichová *et al*., 2010; Wei *et al*., 2009).

1.3 Nucleoside – N- ribohydrolases

Purine and pyrimidine metabolism is essential for growth and development because nucleotides represent building blocks of nucleic acids, major energy carrier components, essential coenzymes such as NAD^+ and alkaloid precursors and cytokinins. One of key enzymes associated with the catabolism of purines and pyrimidines is a nucleoside-N-ribohydrolase (NRH), also called simply a nucleosidase (NH). It catalyzes the hydrolytic cleavage of nucleosides to corresponding bases and ribose *via* oxocarbenium intermediate. (Horenstein and Schramm, 1993) NRH are widespread in nature, they are contained in bacteria (Petersen and Møller, 2001), yeast (Kurtz *et al.*, 2002), protozoans (Parkin, 1996) and in mesozoans (Versées *et al.*, 2003). Genes coding for NRH containing characteristic motif are also present in plants (Jung *et al.*, 2009) and insects (Ribeiro and Valenzuela, 2003). On the contrary, in mammals no NRHs have been found (Parkin *et al.*, 1991). NRHs have been well characterized in parasitic microorganisms as for example from *Trypanosoma, Leishmania*, and *Crithidia* but there is only little knowledge of their contribution in plant metabolism. These organisms rely on purine recycling (salvage pathway) because unlike most organisms they do not have the ability to synthesize *de novo* purine nucleotides. Plants contain ribosides and principle they can be either recycled or degraded. NRHs play a key role in these processes. Plant NRHs are localized in the cytosol. The distinctive feature of NRHs is the aspartate cluster sequence DXDXXXDD, which is located near the N -terminus and forms the active site (Versées and Steyaert, 2003). NRHs have Ca^{2+} ion in the active site coordinated to two aspartate residues from DXDXXXDD motif. The active site is highly specific for the ribose and the substrate binds *via* the ribosyl end to calcium ion and aspartate residue (Verseés *et al.*, 2001).

NRHs are classified into four classes based on their substrate specificity: nonspecific NRHs (Shi *et al.* 1999), NRH that preferred by inosine and uridine (IU - NRHs) (Parkin *et al*., 1991) and inosine and guanosine (IG-NRHs) (Estupiñán and Schramm, 1994) and purine-specific NRHs (Parkin *et al*, 1996) (IAG - NRHs). Dependence of nucleosidase activity on pH was determined for some of NRHs. NRH from *T. brucei* might be mentioned as an example (Parkin, 1996). The pH profile for the

inosine shows that three protonated groups contribute to full catalytic activity IAG - NRH. The loss of the proton from the most acidic group decreases V_{lim} ten times at pH 6.8 while the loss of two protons causes a complete inactivation of the IAG-NRH near pH 8.8. V_{lim} / K_m ratio shows that the catalytic activity does not change in the range of pH from 5 to 8.

Crystal structure of NRH is known for several microorganisms. *T. vivax* contains IAG - NRH, which has a dimeric structure (Verseés *et al.,* 2001). There are two independent active sites. The calcium ion is bound to to carboxyl group three aspartate residues at positions 10, 15 and 261 (first two aspartates belong to DXDXXXDD motif), the main chain oxygen of threonine 137, a water molecule and two –hydroxyl groups, which provides ribose of nucleoside substrate (Verseés *et al.,* 2001). IU-NRH from *C. fasciculata* has a tetrameric structure (Degano *et al.* 1996). Tetrameric structures have also YbeK (Muzzolini *et al.,* 2006) and YeiK (Giabbai B. and Degano M., 2004) proteins from *E. coli.* Novel insights into about catalytic mechanism provide two crystal structures of the purine-specific inosine-adenosine-guanosine NRH (IAG-NRH) and the pyrimidine-specific cytidine-uridine NRH (CU-NRH) from archaeon *Sulfolobus solfataricus.* Both isoenzymes are tetrameric. CU-NRH carries Na^+ instead of Ca^{2+} cation in the active site (Minici *et al*., 2012).

2 Methods

2.1 Cloning, expression and purification

ZmCKO1 was produced by recombinant expression in *Y. lipolytica* (secretion into the culture medium) and subsequent chromatographic purification form the supernatant of 5-day-old cultures grown in PPB medium (20 g l^{-1} sucrose, 1.32 g l^{-1} yeast extract, 1.32 g l^{-1} NH_4Cl, 0.32 g l^{-1} KH_2PO_4, 0.13 g l^{-1} $MgSO_4$ and 0.33 mg l^{-1} thiamine in 50 mM phosphate buffer, pH 6.8) as previously described (Kopečný *et al*., 2005).

The total RNA from apical meristems of 5-day-old maize seedlings (*Zea mays* var. *saccharata*) and pea seedlings (*Pisum sativum*) was extracted using the Plant RNA Isolation Aid solutions from Ambion (Austin, USA). The cDNA was synthesized using Superscript II reverse transcriptase (Invitrogen). ORFs were amplified using AccuPrime™ Pfx using gene specific primers shown in Table 2. The amplified sequences were double digested and ligated into a pCDFDuet vector (Novagen, La Jolla, CA), transformed into NEB 5 alpha *E. coli* cells (New England Biolabs, Hitchin, UK) and sequenced. Correct plasmids were transformed into T7 express *E. coli* cells (New England Biolabs, Hitchin, UK) for expression of N-terminal 6xHis-tagged ALDH proteins. Protein expression was induced with 0.5 mM isopropyl-β-thiogalactopyranoside (IPTG), after which the cultures were incubated at 20 °C overnight.

Total RNA for reverse transcription was isolated from 5-day old maize seedlings (*Zea mays* var. *saccharata*) using the Plant RNA Isolation Aid solutions from Ambion (Austin, USA). The RNA was treated twice with the TURBO DNase-free kit (Ambion). The cDNA was then synthesized using the Superscript II RT (Invitrogen, Carlsbad, USA) and the RevertAid H Minus RT (Fermentas, Vilnius, Lithuania). *ZmNRH3* ORF (948 bp) was amplified using AccuPrime™ Pfx. The plasmids were transformed into T7 express cells (New England Biolabs, Hitchin, UK). Protein expression was induced with 0.5 mM isopropyl-β-thiogalactopyranoside (IPTG), after which the cultures were incubated at 20 °C overnight.

The cells were re-suspended in buffer A (50 mM Tris-HCl buffer, pH 8.0, 10 mM imidazole and 500 mM NaCl with protease inhibitor cocktail and disrupted on a cell lyser (One Shot model, Constant systems, UK). The lysate was cleared by centrifugation at 20,000 *g* at 4 °C for 30 min. The supernatant was filtered through a 0.22-µm membrane (Millipore) and purified on a HisPur cobalt spin columns (Thermo Fisher Scientific, Waltham, MA, USA) equilibrated with 20 mM Tris-HCl buffer pH 8.0, containing 100 mM NaCl, 10 mM imidazole and 5% glycerol. Elution was performed using 250 mM imidazole in the same buffer. Fractions containing ALDH or NRH were pooled and were further purified on a Superdex 200 HR 10/300 column (GE Healthcare), using 50 mM Tris-HCl buffer, pH 8.0, 150 mM NaCl. Fractions were analyzed by SDS-PAGE, and those containing pure and active enzyme were pooled, concentrated using Amicon Ultra-4 centrifugal filter units (10kDa, Millipore) and stored at -20 °C.

2.2 Kinetic measurements

CKO activity was measured by DCPIP method (Bilyeu *et al*., 2001). The reaction was performed in a total volume of 1 ml at 30 ° C and contained 100 mM phosphate buffer, pH 7.0, 1 mM EDTA, 50 µM DCPIP, beef serum albumin (BSA, 1 mg mL^{-1}) and enzyme. The reaction was started adding the cytokinin substrate (iP) in the range of 1-100 µM. DCPIP reduction rate was monitored at 600 nm at 10 second intervals after addition of substrate. iP was dissolved in DMSO as a 100 mM stock solution. Accurate determination of iP concentration was performed spectrophotometrically using the extinction coefficient of ε_{270nm} = 19400 $M^{-1}cm^{-1}$. Aminophenol method (Frébort *et al*., 2002) was used for measurements with different electron acceptors. The method is based on the interaction of released aldehyde 3-methyl-2-butenal with 4-aminophenol under acidic conditions. Schiff base is formed and absorbs at 352 nm. The reaction mixture contained the enzyme on a suitable concentration, substrate (iP) and electron acceptors (0.5 mM DCPIP, 0.5 mM coenzyme Q_0, 0.5 mM 1,4-naphthoquinone and PMS) in 0.4M Tris-HCl buffer, pH8.5, for DCPIP and PMS or 0.4 M imidazole, pH 6.5, for Q_0 and 1,4-naphthoquinone. The mixture was incubated at 37 ° C for 30-50 minutes and then the reaction was stopped by adding 0.3 ml of 40% trichloroacetic acid. The mixture was centrifuged at 12000 g, for 5 min and then 0.2 ml of 2% of 4-aminophenol was added and spectra were

measured at 352 nm. Protein content was estimated using a colorimetric assay with bicinchoninic acid; BSA served as a standard (Smith *et al*., 1985).

.Activity was measured spectrophotometrically by monitoring the formation of NADH (ε_{340} = 6.62 mM^{-1} cm^{-1}) at 37 °C. The reaction mixture in a cuvette contained 0.15 M Tris-HCl buffer, pH 9.0, 1 mM NAD^+ and enzyme. The enzyme reaction was started by the addition of APAL (or another aminoaldehyde) at a final 1 mM concentration. Accurate aldehyde concentration was verified spectrophotometrically by the complete conversion of supposed 20 μM aldehyde using excess of enzyme and supposed release of 20 μM NADH. This amount corresponds to the absorbance change of 0.1324. Proteins were determined by Bradford method.

The NRH activity was measured spectrophotometrically at 30 °C according to a method described by Parkin (1996). The reaction was performed in 200 mM Tris-HCl buffer, pH 7.5, 400 mM KCl, 1 mM DTT, 200 μM riboside substrate and enzyme. Kinetic constants were determined by monitoring the absorption decrease of adenosine ($\Delta\varepsilon_{276}$ = -1.4 mM^{-1} cm^{-1}), inosine ($\Delta\varepsilon_{280}$ = -0.92 mM^{-1} cm^{-1}), uridine ($\Delta\varepsilon_{280}$ = -1.8 mM^{-1} cm^{-1}), cytidine ($\Delta\varepsilon_{280}$ = -3.42 mM^{-1} cm^{-1}) and thymidine ($\Delta\varepsilon_{265}$ = -1.7 mM^{-1} cm^{-1}) (Parkin, 1996). The differential extinction coefficients for xanthosine and guanosine were determined to be $\Delta\varepsilon_{248}$ = -3.7 mM^{-1} cm^{-1} and $\Delta\varepsilon_{253}$ = -4.1 mM^{-1} cm^{-1}, respectively. Similarly, $\Delta\varepsilon_{289}$ values of -1.37 mM^{-1} cm^{-1} and -1.48 mM^{-1} cm^{-1} were determined for iPR and trans-zeatin riboside (*t*ZR), respectively. Proteins were determined by Bradford method.

2.3 Crystallization and data collection

Crystallization conditions were screened using commercial kits Classics, PEGs II, and JCSG I suites from Qiagen and Crystal screen I and II from Hampton Research in sitting-drops using a Cartesian nanodrop robot (Genomic Solutions) or in hanging drops during manual optimization procedure (Kopečný *et al*., 2013; Končitíková *et al*., 2015; Kopečná *et al*., 2013).

Crystals were transferred to a cryoprotectant solution (the mother liquor supplemented with 25 % PEG 400 or glycerol) and flash frozen in liquid nitrogen. Diffraction data were collected at 100 K on the PROXIMA 1 and 2 beamlines (SOLEIL Synchrotron, Saint-Aubin, France). Diffraction intensities were integrated with the program XDS (Kabsch, 2010).

Diffraction data for ZmAMADH1a, RF2C, RF2F and ZmALDH7 were collected at resolutions of 1.95, 2.25, 2.40 and 2.80 Å, respectively. Diffraction data for the ZmNRH3 crystals were collected at resolutions of 2.49 Å. All structures were solved by molecular replacement with MOLREP (Vagin and Teplyakov 2010) or Phaser (Storoni *et al.*, 2004) using the monomer of human ALDH2 (PDB 1CW3 and 1O05) and of seabream ALDH7 (PDB 2JG7) as search models in case of RF2C, RF2F and ZmALDH7, using the coordinates of the YbeK monomer (PDB 1YOE) in case of ZmNRH3 and using the coordinates of ZmCKO1 (PDB 1W1O) in case of ZmCKO2 and ZmCKO4. The two different

space group structures of ZmCKO2 (at 2.04 and 2.7 Å) and the two different space group structures of ZmCKO4 with CPPU (at 1.75 and 1.9 Å) were refined. Complexes of ZmCKO4-3FMOTDZ and ZmCKO4-HETDZ were both resolved at 2.05 Å resolution. All structures were refined using BUSTER-TNT with autoncs and TLS options (Blanc *et al*., 2004). Electron density maps were evaluated using COOT (Emsley and Cowtan, 2004). Molecular graphics images were generated using PYMOL (www.pymol.org).

3 Results and discussion

3.1 List of publications

Results are divided into 3 sections in line with aims of the work and with the enzyme group that was studied:

1. Cytokinin oxidase/dehydrogenase
    - Franc V, Šebela M, Řehulka P, **Končitíková R**, Lenobel R, Madzak C, Kopečný D. (2012) Analysis of N-glycosylation in maize cytokinin oxidase/dehydrogenase 1 using a manual microgradient chromatographic separation coupled offline to MALDI-TOF/TOF mass spectrometry. *J Proteomics* 75(13): 4027-37. [**5.07 Impact Factor**]
    - Kopečný D*, **Končitíková R***, Popelková H, Briozzo P, Vigouroux A, Šebela M, Kopečná M, Zalabák D, Frébort I, Moréra S. (2015) Kinetic and structural investigation of the cytokinin oxidase/dehydrogenase active site by site directed-mutagenesis. *authors contributed equally to this work. Manuscript
    - Nisler J, **Končitíková R,** Zatloukal M, Kopečný D, Bazgier V, Berka K, Zalabák D, Briozzo P, Strnad M, Spíchal L (2015) Novel thidiazuron-derived inhibitors of cytokinin oxidase/dehydrogenase. Manuscript

2. Aldehyde dehydrogenase
    - **Končitíková R,** Vigouroux A, Kopečná M, Andree T, Bartoš J, Šebela M, Moréra S, Kopečný D (2015) Role and structural characterization of plant aldehyde dehydrogenases from family 2 and family 7. *Biochem J*. 468(1): 109-23. [**4.78 Impact Factor**]
    - Kopečný D*, **Končitíková R***, Tylichová M, Vigouroux A, Moskalíková H, Soural M, Šebela M, Moréra S. (2013) Plant ALDH10 family: identifying critical residues for substrate specificity and trapping a thiohemiacetal intermediate. *J Biol. Chem.* 288(13): 9491-507. [**4.60 Impact Factor**] *authors contributed equally to this work

3. Nucleoside-N-ribohydrolase
    - Kopečná M, Blaschke H, Kopečný D, Vigouroux A, **Končitíková R**, Novák O, Kotland O, Strnad M, Moréra S, von Schwartzenberg K. (2013) Structure and function of nucleoside hydrolases from Physcomitrella patens and maize catalyzing the hydrolysis of purine, pyrimidine, and cytokinin ribosides. *Plant Physiol*. 163(4): 1568-83. [**7.39 Impact Factor**]

3.2 Cytokinin oxidases/dehydrogenases

3.2.1 Role of glycosylation in ZmCKO1

The results of this chapter are published in Franc *et al.*, 2012. My contribution in this publication was a purification and preparation of the deglycosylated recombinant ZmCKO1 and all kinetics experiment.

Amino acid sequences of several CKOs clearly demonstrate the presence of one to eight *N*-glycosylation sites (Schmulling *et al.*, 2003). The glycosylation of ZmCKO1 was also proved by electrophoretic migration and estimated molecular mass was significantly higher than expected from sequence-based calculations (Houba-Hérin *et al.*, 1999; Morris *et al.*, 1999; Kopečný *et al.*, 2005). According to published crystal structures, six of predicted *N*-glycosylation sites comprising N63, N89, N134, N294, N323 and N338 residues may be occupied by glycans (Kopečný *et al.*, 2010; Malito *et al.*, 2004). Effect of glycosylation was investigated by activity assays with N^6-isopentenyladenine (iP) as a substrate. Figure 2 represents a comparison between the glycosylated and deglycosylated ZmCKO1 in terms of saturation curves and thermostability. Although determined K_m values were similar for both variants, there is no visible substrate inhibition for the deglycosylated ZmCKO1. Deglycosylation treatment might obviously cause a mild structural change at the entrance of the active site.

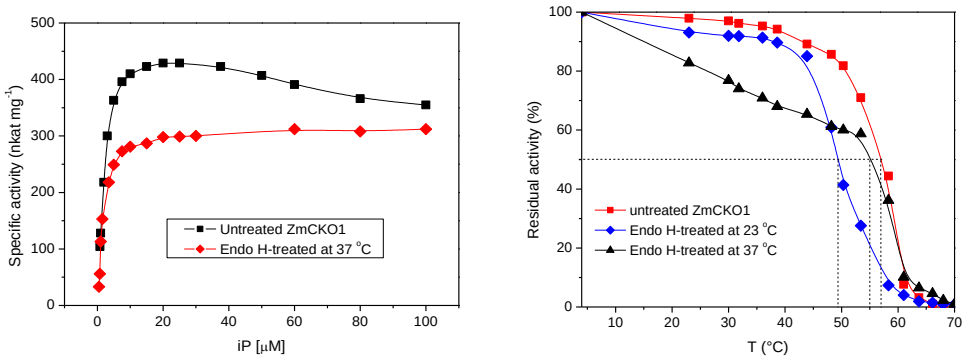

Figure 2. Left panel: Michaelis-Menten kinetics of the glycosylated (black colored curve) and the deglycosylated (colored red) ZmCKO1. Right panel: Thermostability of glycosylated (colored in red) and endoglycosidase H-treated ZmCKO1 (black and blue colored).

The thermostability of ZmCKO1 was analyzed by incubating aliquots at the temperature form 25 °C to 70 °C. The observed T_{50} value was 57 °C for untreated enzyme. After the deglycosylation step at 23 °C overnight, T_{50} value changed to 49 °C. Non-typical sigmoid curve was ascertained for recombinant ZmCKO1 deglycosylated at 37°C overnight with T_{50} value of 55 °C. Nevertheless, there is a significantly weaker activity between 20 - 50 °C in comparison with untreated enzyme. The

kinetic experiments illustrate that the loss of N-glycosylation resulted in a destabilization of ZmCKO1 tertiary structure without any strong effect on the enzyme activity.

3.2.2 Role of E381 - structures of ZmCKO2 and ZmCKO4a

The results of this chapter are part of submitted manuscript Kopečný *et al*. My contribution in this publication was a crystallization of ZmCKO2 and ZmCKO4a together with kinetic measurements of the isoforms and ZmCKO1 mutants.

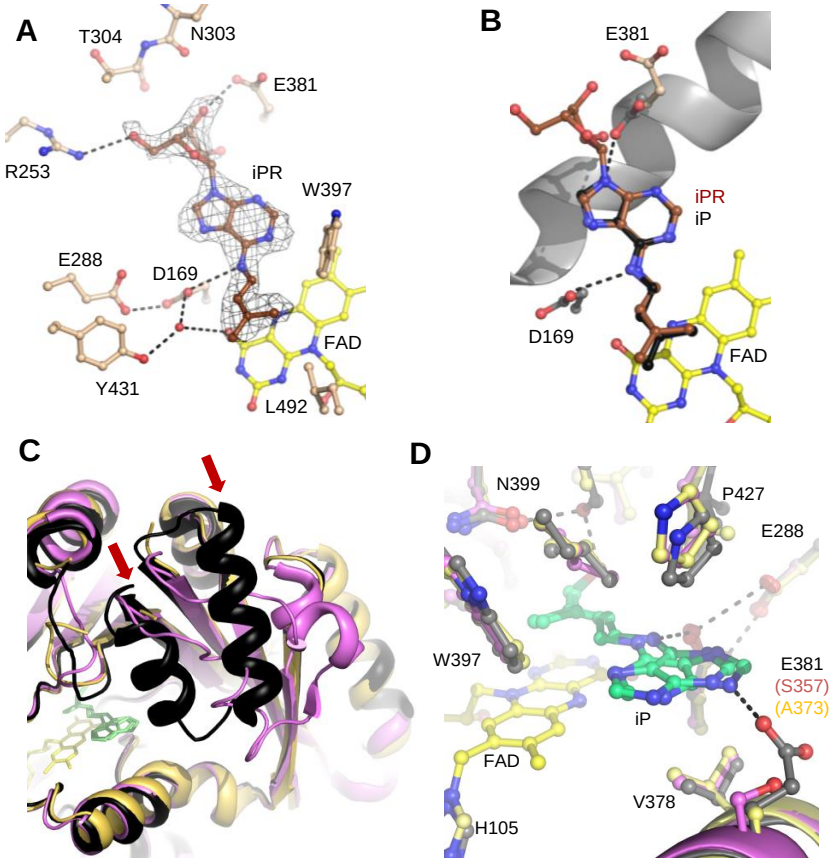

Figure 3. Binding of cytokinin ribosides in ZmCKO1 active site (A) WT ZmCKO1 structure. iPR (in brown) is shown in its Fo-Fc omit map contoured at 2.5 σ. Side-chain residues are in grey and labeled. FAD cofactor is shown in yellow and hydrogen bonds as dashed lines **(B)** Superposition of bound cytokinin base (iP, PDB 1W1Q, 15) and cytokinin riboside (iPR, PDB 3S1C, manuscript CKO) over the FAD cofactor. E381 in both structures is indicated by the respective color corresponding to the color of cytokinin substrate. **(C) Superposition of substrate binding domains between ZmCKO1 (in black), ZmCKO2 (in magenta) and ZmCKO4a (in sand yellow).** The helix-loop-helix region from residues 294 to 325 in ZmCKO1 (shown with red arrows) adopts a different conformation in ZmCKO2 and is disordered in ZmCKO4. **(D) Comparison of residues located at the active-site entrance in ZmCKO1 (in black), ZmCKO2 (in magenta) and ZmCKO4a (in sand yellow).**

Nonconserved residue E381 is present in half of known CKO sequences and participates in binding of the N9 atom of the cytokinin substrate. Presence of E381 residue in WT leads in higher K_m values for cytokinin ribosides and nearly no activity with cytokinin glucosides (iP9G and *t*Z9G). E381A and E381S mutants are highly active with all tested substrates including cytokinin glucosides such as N^6-isopentenyladenine-9-glucoside (iP9G) and *trans*-zeatin-9-glucoside (*t*Z9G). Crystal

structures in complex with iPR could help to understand the contribution of E381 in cytokinin riboside binding (Figure 3A, 3B).

Crystal structures of ZmCKO4a and ZmCKO2 were solved, in two different space groups for each (Figure 3) to explain differences in substrate specificity including high rates with iP9G. The structures of ZmCKO2 and ZmCKO4a are very similar to that of ZmCKO1 with RMSD values of 1.2 Å (428 Cα atoms) and 1.1 Å (423 Cα atoms) respectively. The major difference concerns the residues region 294-325, composed of two helices and a loop, belonging to the substrate binding domain. This region, which is well defined in ZmCKO1 structure, is disordered in the high resolution structures of ZmCKO4a and ZmCKO2 and adopts a different conformation in the low resolution structure of ZmCKO2 (Figure 3A). The region delineating the substrate entrance comprises residues surrounding the ribose moiety of cytokinin substrate (N303 and T304 in ZmCKO1) and is most likely responsible for the kinetic differences between E381 variants and ZmCKO isoforms. All known intracellular CKOs contain valine or serine at E381 position and some of them have recently been shown to oxidize iP9G and *t*Z9G in agreement with our data. Thus, the substrate specificity of CKOs appears related to their subcellular localization and corresponds to the presumed occurrence of particular cytokinin derivatives within intracellular compartments.

3.2.3 Novel thidiazuron-derived inhibitors of CKO

The results of this chapter are part of submitted manuscript Niesler *et al*. My contribution in this publication was a crystallization of ZmCKO4a with two inhibitors and kinetic measurements.

Two crystal structures of ZmCKO4a were solved in complex with two urea inhibitors derived from thidiazuron (1-phenyl-3-(1,2,3-thiadiazol-5-yl)urea, TDZ): 3-(1,2,3-thiadiazol-5-yl)-1-[3-(trifluoromethoxy)phenyl]urea (3FMTDZ) and 1-[2-(2-hydroxyethyl)phenyl]-3-(1,2,3-thiadiazol-5-yl)urea (HETDZ, Figure 4). Crystal structure complexes reveal that HETDZ and 3FMTDZ bind in the active site in two different orientations. Their urea nitrogens are H-bonded to D170. The thiadiazolyl ring of 3FMTDZ is oriented inside over the flavin ring. One of the urea nitrogens creates an H-bond to a water molecule close to D170 and one of two nitrogen atoms of thiadiazolyl ring is also bound to a water molecule close to N391. In contrast, the thiadiazolyl ring of HETDZ is oritented outside from the flavin ring and oxygen atom of the hydroxyethyl side chain of HETDZ makes an H-bond to oxygens of D170 and Y425 residues (Figure 4). HETDZ and 3FMTDZ both inhibit maize CKO1 (IC_{50} of 48 μM for TDZ, 5 μM for 3FMTDZ and 2 μM for HETDZ) and maize CKO4a (IC_{50} of 200 μM for TDZ, 30 μM for 3FMTDZ and 120 μM for HETDZ better than TDZ itself (Niesler *et al*., manuscript) and represent new possible inhibitors for *in vivo* studies.

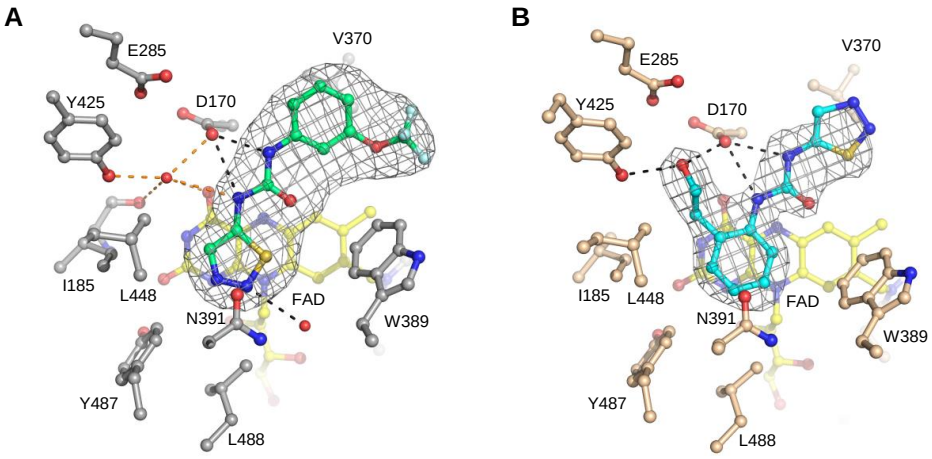

Figure 4. Binding of three urea inhibitors 3FMTDZ and HETDZ in the active site of ZmCKO4a. (A) Binding of 3FMTDZ. The inhibitor is green colored and shown in Fo-Fc omit map, contoured at 4.0 σ. **(B)** Binding of HETDZ. The inhibitor is blue colored and shown in Fo-Fc omit map, contoured at 3.0

3.3 ALDH2, ALDH7 and ALDH10 families

The results of this chapter are published in Kopečný *et al*., 2013 and Končitíková *et al*., 2015. My contribution in these publications was in cloning, expression, purification, kinetic measurments and crystallization of ZmAMADH1a, ZmALDH7 and all ZmALDH2 family members. I also performed qPCR measurements.

3.3.1 Kinetic properties of ZmALDH2 family

Four maize cytosolic ALDH2 isoforms (RF2C, RF2D, RF2E and RF2F) were purified and their kinetic parameters measured using wide range of aldehydes at 1 mM concentration. Specific activity values measured with 1.0 mM hexanal were 62 nkat mg^{-1} for RF2C, 12.2 nkat mg^{-1} for RF2D, 14.6 nkat mg^{-1} for RF2E and 8.9 nkat mg^{-1} for RF2F. ALDH2C isoforms exhibit a broad substrate preference for aliphatic and aromatic aldehydes, especially for hexanal, benzaldehyde and *p*-anisaldehyde. AASAL, 3-aminopropionaldehyde (APAL) and 4-aminobutyraldehyde (ABAL), citral, glycolaldehyde belong to naturally occurring substrates, which were found as weak substrates (all below 10% rate compared with hexanal). According to the catalytic efficiency values (Končitíková *et al.*, 2015) hexanal and cinnamaldehyde are the best substrates for RF2C (Table 1) while RF2D and RF2E preferentially oxidizes *p*-anisaldehyde and benzaldehyde and RF2F favors phenylacetaldehyde. A strong excess substrate inhibition is evident for especially aromatic aldehydes as for example for cinnamaldehyde with RF2C or phenylacetaldehyde with RF2F.

The specific activity of all ZmALDH2 isoforms is increasing with the length of linear carbon chain of aliphatic aldehyde up to six-carbon chain (hexanal). Much lower activities were described with heptanal and octanal (except for RF2C for octanal). A significant increase was evident for nonanal – up to 50% activity compared with hexanal. Both *t*-2-hexenal and *t*-2-nonenal are weak

substrates in comparison with the saturated analogues C6 and C9. Although *t*-2-nonenal represents one of the best substrate for RF2C isoform. Aliphatic C6 and C9 aldehydes and their unsaturated analogues belong to the green leaf volatiles. They are responsible for an aroma of fruits and vegetable, moreover, they are produced as a response to wounding. These aliphatic aldehydes are derived from linolenic acid originated from lipoxygenase pathway (reviewed in Dudareva *et al.*, 2013). Branched aliphatic C4 and C5 aldehydes represent good substrate as well. All ALDH2 isoforms oxidize 3-methyl-2-butenal (isopentenal) originating from isoprenoid cytokinins degradation pathway (Kopečný *et al.*, 2005). The activity of this unsaturated aldehyde is between 8 - 25% compared to hexanal. Aromatic aldehydes such as benzaldehyde, *m*- and *p*-anisaldehyde, phenylacetaldehyde, cinnamaldehyde and hydrocinnamaldehyde display differences in ZmALDH2 isoforms activity. Nevertheless, they are good substrates. Aromatic aldehydes originate from phenylalanine *via* several pathways (reviewed in Dudareva *et al.*, 2013). Benzaldehyde is formed *via* the non-*β*-oxidative pathway (Boatright *et al.*, 2004). Moreover, benzaldehyde is known as a product of oxidation of aromatic cytokinins by CKO. Coniferaldehyde and sinapaldehyde are produced *via* phenylpropanoid pathway. These two aldehydes are *in vivo* substrates for ALDH2C from Arabidopsis and oilseed rape (Nair *et al.*, 2004) and are also substrates for ZmALDH2 isoforms (Končitíková *et al*., 2015).

3.3.2 Kinetic properties of ZmALDH7

The maize ALDH7 isoform preferentially oxidizes AASAL as well as ALDH7 from pea (PsALDH7) and human (hALDH7). Specific activity measured with 1.0 mM AASAL was 45 nkat mg^{-1}. Substrate specificity study was performed using 1 mM substrates. K_m value of 90 μM for AASAL was measured with ZmALDH7 in agreement with previous studies on seabream ALDH7 (67 μM, Tang *et al.*, 2008) and on hALDH7 (169 μM, Brocker *et al.*, 2010). Methyl ester of adipic semialdehyde (MASAL) is oxidized with 5 % rate relative to that of AASAL. Natural *ω*-aminoaldehydes such as BAL, APAL, ABAL, 4-*N*-trimethylaminobutyraldehyde (TMABAL) and 4-guanidinobutyraldehyde (GBAL) are good substrates with up to 25 % rates relative to that of AASAL. Very weak activity was detected with aliphatic, aromatic aldehyde and succinic semialdehyde (SSAL). Very weak substrates are also *t*-2-hexenal, *t*-2-nonenal and malondialdehyde, which are products of lipid peroxidation (Končitíková *et al*., 2015). Plant ADLH7 from rice and Arabidopsis have been shown to be localized in cytosol (Shin *et al.*, 2009, Kotchoni *et al.*, 2006) in agreement with the presence of the bifunctional lysine-ketoglutarate reductase/saccharopine dehydrogenase (LKR/SDH, Kemper *et al.*, 1999; Zhu *et al.*, 2000), which catalyzes the first reaction of the lysine catabolism pathway (saccharopine pathway) leading to AASAL and glutamate. In contrast, hALDH7 was additionally found in mitochondria (Brocker *et al.*, 2010, Wong *et al.*, 2010) in line with the existence of two lysine catabolism pathways: the saccharopine pathway localized in mitochondria and the pipecolate pathway predominantly found in peroxisomal/cytosolic (reviewed in Hallen *et al.*, 2013). BAL activity is important for hyperosmotic stress protection. BAL originates from choline and is

oxidized to glycine betaine, which is an important osmolyte. It is clear that plant ALDH7 family is able to oxidize GBAL, APAL and ABAL (Table 1) results directly or after further conversion to osmoprotectants 4-guanidinobutyrate, β-alanine and γ-aminobutyric acid (GABA) in the cytosol. GBAL originates from arginine catabolism. 4-guanidinobutyrate, the product of the oxidation of GBAL, may be further hydrolyzed by ureohydrolase to urea and GABA.

Table 1. Kinetic parameters of maize ALDH7 and RF2C for selected substrates. All K_m and k_{cat} values are given in μM and s^{-1}, respectively.

	ZmALDH7				RF2C		
Ligand	K_m	k_{cat}	k_{cat}/K_m	Ligand	K_m	k_{cat}	k_{cat}/K_m
	μM	s^{-1}	$M^{-1}\ s^{-1}$		μM	s^{-1}	$M^{-1}\ s^{-1}$
AASAL	97 ± 7	2.56 ± 0.043	**2.6 x 10^4**	Acetaldehyde	2419 ± 170	0.59 ± 0.02	2.4 x 10^2
MASAL	126 ± 21	0.09 ± 0.004	7.1 x 10^2	Hexanal	15 ± 1	4.54 ± 0.08	**3.0 x 10^5**
GBAL	2767 ± 146	1.43 ± 0.029	5.2 x 10^2	*t*-2-Hexenal	39 ± 5	0.35 ± 0.02	9.0 x 10^3
BAL	120 ± 3	0.03 ± 0.001	2.5 x 10^2	Nonanal	51 ± 5	1.63 ± 0.06	3.2 x 10^4
APAL	1280 ± 59	0.15 ± 0.002	1.1 x 10^2	*t*-2-Nonenal	19 ± 13	2.54 ± 0.30	1.3 x 10^5
ABAL	4371 ± 116	0.27 ± 0.005	6.3 x 10^1	Benzaldehyde	83 ± 9	1.21 ± 0.06	1.5 x 10^4
Hexanal	1805 ± 186	0.11 ± 0.005	6.1 x 10^1	Cinnamaldehyde	10 ± 1	2.95 ± 0.17	**3.0 x 10^5**
Nonanal	174 ± 14	0.07 ± 0.006	4.3 x 10^2	Coniferaldehyde	19 ± 3	2.65 ± 0.37	1.4 x 10^5

3.3.3 Kinetic properties of ZmALDH10 family

In a large screening study 1 mM aldehydes were used (Figure 5). All three maize AMADHs most readily oxidize natural aminoaldehydes APAL, ABAL and TMABAL as well as synthetic aminoaldehydes (Figure 5).

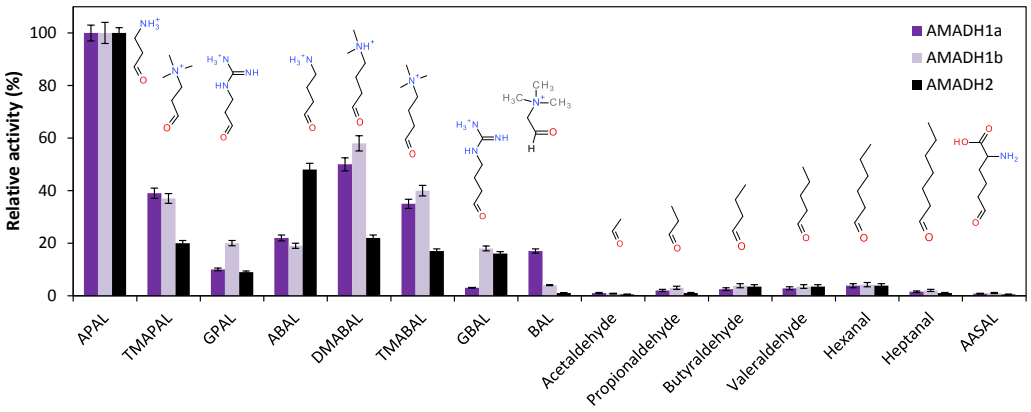

Figure 5. Substrate specificity of ALDH10 isoenzymes maize. The activity of each AMADH isoenzyme with the best substrate was arbitrarily taken as 100%. The measurements were performed with 1 mM substrates in 0.15 M Tris-HCl buffer, pH 9.0, containing 1 mM NAD. The following substrates were tested: APAL, N,N,N-trimethyl-3-aminopropionaldehyde (TMAPAL), 3-guanidinopropionaldehyde (GPAL), ABAL, TMABAL, GBAL, BAL, acetaldehyde (C2), propionaldehyde (C3), butyraldehyde (C4), valeraldehyde (C5), capronaldehyde (C6), enanthaldehyde (C7), and (AASAL). Specific activity values with 1 mM APAL were 2.6 units mg 1 for ZmAMADH1a, 1.9 units mg 1 for ZmAMADH1b, and 4.1 units mg 1 for ZmAMADH2.

Specific activity values measured with 1 mM APAL as a substrate 43 nkat mg^{-1} for ZmAMADH1a, 31 nkat mg^{-1} for ZmAMADH1b and 68 nkat mg^{-1} for ZmAMADH2. The highest reaction rates are achieved with APAL for all maize isoenzymes. Methyl and guanidine derivatives of APAL and ABAL are oxidized with 10 – 60% rates on average (relative to that of the best substrate). Hydroxylated derivatives as well as aliphatic aldehydes are oxidized more slowly. AASAL, the substrate of ALDH7 family is weak substrate, with 1 – 3 % rates on average. Only ZmAMADH1a exhibits a relatively high activity with BAL, comparable with ABAL oxidation (16% compared with APAL).

3.3.4 Overall fold of studied ALDHs

ZmAMADH1a, RF2C, RF2F and ZmALDH7 adopt the characteristic ALDH fold consisting of a coenzyme binding domain, a catalytic domain and an oligomerization domain. They all bind a conserved monovalent ion. The nature of the protein ligands and the distances of around 2.4 – 2.6 Å are typical for a bound sodium ion. This ion probably allows maintenance of the protein structural integrity and/or stabilizes the position of a loop involved in NAD^+ binding. The oligomerization domains connect both monomers by protruding over the surface of the neighboring subunits around substrate channel entrances while the NAD^+ binding sites reside on the opposite side of the dimer. The catalytic cysteine lies between the NAD^+ and the substrate binding sites. Monomers of RF2C and RF2F are very similar to each other (average RMSD of 0.7 Å) and a structural comparison using PDBeFold (http://www.ebi.ac.uk/msd-srv/ssm/) shows that they both resemble the mitochondrial hALDH2 with the lowest RMSD of 0.80 – 0.85 Å for PDB codes 1O02, 1NZZ, 1NZX and others (Perez-Miller and Hurley, 2003; Figure 6). Both RF2C and RF2F tetramers are very similar to hALDH2 tetramer with average RMSD values of 1.2 and 1.0 Å for 1940 Cα atoms, respectively. Subtle differences in the oligomerization arrangement can be observed. ZmALDH7 monomer is similar to that of human and seabream (PDB codes 2J6L and 2JG7) with RMSD of 0.72 and 0.74 Å, respectively. The major difference between ZmADLH7 and ZmALDH2 monomers (RMSD of 1.3-1.4 Å for 465 Cα atoms) comes from a slight shift in the oligomerization domain and the presence of an N-terminal helix in ZmALDH7.

3.3.5 Substrate channels of studied ALDHs

A sequence alignment of substrate channel residues in ALDH2C members (Figure 7) reveals a high variability that allows various isoforms within one species oxidizing several different substrates from multiple pathways. Recently, maize *RF2C* gene was found to be induced in elongating internodes containing cells, which exhibit primary cell wall biosynthesis, compared to non-elongating internodes with cells depositing secondary cell wall material Nair *et al.*, 2004. In contrast, plant mtALDH2 isoforms including RF2A and RF2B share a conserved active site and are highly similar to hALDH2 (Figure 7). Their sequences contain a triple cysteine motif including the catalytic cysteine. Although *in*

vivo preferred substrate of hALDH2 is acetaldehyde, the enzyme has been shown to oxidize various aliphatic and aromatic aldehydes especially hexanal, phenylacetaldehyde or benzaldehyde (Klyosov, 1996). Likewise, RF2A, but not RF2B, is in addition to acetaldehyde also highly active with benzaldehyde and cinnamaldehyde (Liu and Schnable, 2002).

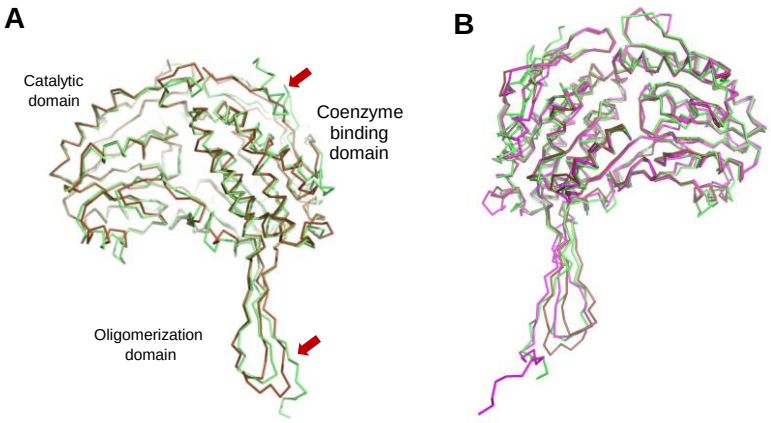

Figure 6. **ALDH fold in ZmALDHs**. **(A)** Superposition of maize RF2F monomer (brown, this work) and ZmALDH7 monomer (green, this work). Slight differences in the oligomerization domain and the presence of an N-terminal helix in maize ALDH7 are indicated by arrows. **(B)** Superposition of ALDH2 (brown), ALDH7 (green) and ALDH10 (violet) monomers.

Comparison of ZmALDH7 with human and seabream ALDH7 illustrates that their active site residues are almost identical indicating that these enzymes have the same cellular role in plants, mammals or fish using AASAL as the preferred substrate. The three residues E120, R300 and T302 located in the substrate binding site of ZmALDH7 are conserved and specific for ALDH7 family (Figure 7). The role of E120 and R300 has been validated by mutagenesis studies on seabream ALDH7 and hALDH7 (Tang *et al.*, 2008, Chan *et al.*, 2011). E120 binds the α-amino group of AASAL while R300 its carboxylate group. The role of T302 has not been studied by mutagenesis yet.

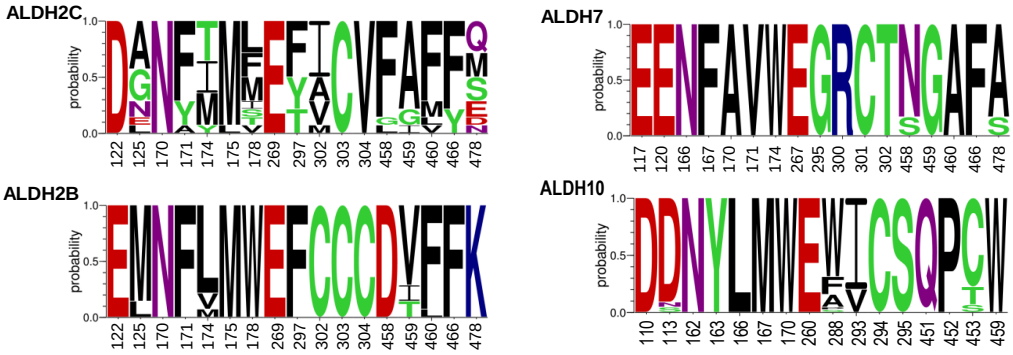

Figure 7. Composition of maize ALDH2, ALDH7 and ALDH10 active sites Conservation of amino acid residues forming the substrate channel in ALDH2 and ALDH7 families. Residues are numbered according to maize RF2C for ALDH2C and ALDH2B subfamilies and maize ALDH7 for ALDH7 family. Sequence logos were made using WebLogo (http://weblogo.threeplusone.com).

A comparison of the substrate channel residues in plant AMADHs show that almost all residues are evolutionarily highly conserved (Figure 7). Noticeably, two residues at the positions 288 and 453 (PsAMADH numbering) are less preserved. W288 could be substituted by Ala, Phe or Ser and C453 by Ser or Thr residue. Based on the k_{cat}/K_m ratio, APAL is the best substrate for ZmAMADH1a and ZmAMADH1b as well as for PsAMADH2 (Tylichová *et al*., 2010), which all possess W288 (W290 or W291 in ZmAMADH1s). ZmAMADH2, which contains an Ala at this position, prefers TMABAL as the best substrate accented by the increased K_m values for APAL and ABAL. PsAMADH1 containing a phenylalanine also prefers TMABAL (Tylichová *et al.*, 2010).

3.4 Purine riboside-preferring NRH from maize

The results of this chapter are published in Kopečná *et al*., 2013. My contribution in these publications was in cloning, expression, purification and kinetic measurements of ZmNRH3. I also performed qPCR measurements. These data are unpublished.

3.4.1 Substrate Specificity of ZmNRH3

The genome databases for the maize (www.maizesequence.org, v5b.60) indicate that it contains five *NRH* genes, respectively. The two paralogous genes *ZmNRH1a* and *ZmNRH1b* are localized on chromosomes 8 and 3, respectively. The two other paralogs, *ZmNRH2a* and *ZmNRH2b*, lie on chromosomes 4 and 1, respectively. The last *ZmNRH3* gene is localized on chromosome 2. In order to identify their function, I focused on analyzing ZmNRH3 isoform.

The specific activity of ZmNRH3 with 200 mM xanthosine was 61 nkat mg^{-1}. ZmNRH3 prefers inosine and xanthosine as the best substrates while adenosine, uridine, cytidine, iPR and tZR are weaker substrates. ZmNRH3 displays similar substrate preferences together with PpNRH1 (Kopečná et.al 2013). They both exhibit the highest catalytic efficiency with inosine and xanthosine. In line with our results and current system of classification, ZmNRH3 belongs to a nonspecific IU-NRH class with a preference towards purine ribosides (Parkin *et al*., 1991; Shi *et al*., 1999). The xanthine and hypoxanthine nucleobases are formed by the action of NRHs and are further processed by xanthine dehydrogenase to give uric acid. Adenosine and adenine are produced by the cytokinin degradation catalyzed by CKO (EC 1.5.99.12; Houba-Hérin *et al*., 1999).

3.4.2 Substrate binding in ZmNRH3

The asymmetric unit of the ZmNRH3 crystal includes one dimer and according to the results from gel filtration chromatography the active form in solution is a dimer (Kopečná *et al.*, 2013). The similar findings were obtained also for PpNRH1. PpNRH1 and ZmNRH3 crystal structures are the first reported crystal structures for plant NRHs (Figure 8). PpNRH1 and ZmNRH3 monomers and dimers share high similarity to each other, with average RMSD values of 0.9 and 1.2 Å for all Ca

atoms, respectively. Each monomer is composed from a typical NRH fold containing 12 β-strands and 13 α-helices.

A conserved Ca^{2+} ion in the active site is tightly bound to the D8, D13 and D240 and to the main-chain carbonyl group of L123 in ZmNRH3 (Figure 8). Its octahedral coordination can be completed either by three water molecules or by a catalytic water molecule and the 2´- and 3´-hydroxyl groups of the substrate ribose moiety. The catalytic water molecule in turn interacts with the catalytic base, which is believed to increase the nucleophilicity of the water molecule attacking the C1´-N9 bond of the substrate. The calcium ion is believed to lower the pK_a of the catalytic water molecule prior to proton transfer to the active site base (Degano *et al.*, 1998). The structure of YeiK in complex with inosine (PDB 3B9X) was used for modeling a substrate position in the active site of ZmNRH3 by structural superposition. The ribose moiety is tightly bound to conserved residues among NRHs family corresponding to N158, E164, D240, N166, D12, D13 and N37 in ZmNRH3. In contrast, the nucleobase is surrounded by more variable residues: V82 and H81 from helix α3, by the aromatic residues Y223, W226, H227 and Y231 from helix α11, by H239 in helix α12, by N158 in the β5-α7 loop and by the adjacent side chain of K279, which protrudes into the active site from the other subunit. A structural comparison of the substrate binding sites of PpNRH1 and ZmNRH3 (Figure 8) shows that only one residue is different around the nucleobase, tyrosine Y244 in PpNRH1 is replaced by a tryptophan in ZmNRH3.

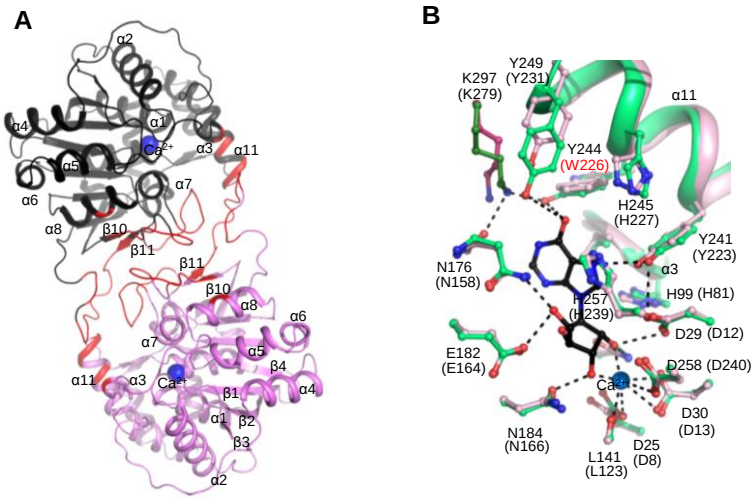

Figure 8. (A) Dimeric structure of plant NRH. One subunit is colored in black and the other in violet. The calcium ion in the active site is shown as a blue sphere. Inter-subunit contacts are shown in red. **(B) Substrate binding sites of PpNRH1 (in green) and ZmNRH3 (in pink).** A molecule of inosine (in black) was docked into the active site. Amino acid residues are labeled and H-bonds and calcium ion coordination are shown as dashed lines. Differences in the sequences of the two NRHs are red labeled

4 Conclusions

The most important outputs of this work can be summarized as follows:

1. The glycosylation of ZmCKO1 is important for the enzyme stability.

2. New structures of ZmCKO2 and ZmCKO4a were solved and both their structures surprisingly lack two helices and a loop from substrate binding domain. This change leads to more open substrate cavity and allows for binding larger substrates like cytokinin glucosides. The change in substrate preferences is also linked to nonconserved residue E381, which is present in half of known CKO sequences and participates in binding of the N9 atom of the cytokinin substrate. Presence of E381 residue in ZmCKO1 (but not in ZmCKO2 and ZmCKO4a) leads in higher K_m values for cytokinin ribosides and nearly no activity with cytokinin glucosides (iP9G and *t*Z9G).

3. Inhibitory strength and binding mode of two new thidiazuron derivatives 3-(1,2,3-thiadiazol-5-yl)-1-[3-(trifluoromethoxy)phenyl]urea (3FMTDZ) and 1-[2-(2-hydroxyethyl)phenyl]-3-(1,2,3-thiadiazol-5-yl)urea (HETDZ) was analyzed. Crystal structures reveal that they bind in the active site in two mutually opposite orientations - thiadiazolyl ring of 3FMTDZ is positioned over the isoalloxazine ring of FAD while that of HETDZ is in opposite orientation and points to entrance of the active site. The inhibitors are easy to synthetize; they are stronger inhibitors than thidiazuron itself and inhibit CKO in competitive manner.

4. Kinetic and structural studies were perfomed on maize ALDH2, ALDH7 and ALDH10 isoforms. Interestingly, ALDH2 and ALDH7 are tetrameric but ALDH10 is dimeric. While the active sites of ALDH7 and ALDH10 are quite conserved and determine the substrate specificity towards particular aldehydes, those of ALDH2 isoforms are highly variable and oxidize wide range of aliphatic and aromatic aldehydes including aldehydes released by CKO reaction and aldehydes released during the lipid peroxidation.

5. Kinetic and structural study was perofmed on maize NRH family especially on purine riboside-preferring ZmNRH3. The enzyme is dimeric and is able to hydrolyze adenosine and cytokinin ribosides in addition to preffered substrates inosine and xanthosine.

6. ALDH2 and NRH isoforms studied in this work are localized in cytosol as well as one of CKO isoforms indicating that a mutual interconnection of these pathways is possible (Figure 9).

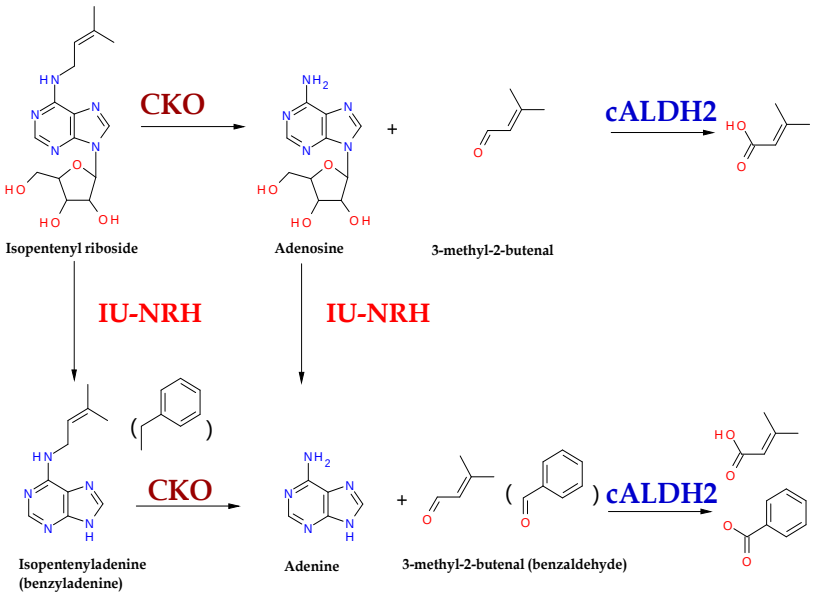

Figure 9. A scheme of possible reactions related to CKO. The scheme illustrates possible reactions in cytosol linked to action of cytosolic CKO including involvement of cytosolic ALDH2 and IU-NRHs

5 References

Barclay and McKersie (1994) *Lipids.* **29**, 877-882
Bilyeu *et al*. (2001) *Mol Plant Physiol.* **125**, 378-386.
Blanc *et al*. (2004) *Acta Crystallogr., Sect. D. Biol. Crystallogr.* **60**, 2210-2221.
Boatright *et al*. (2004) *Plant Physiol*. **135**, 1993–2011
Bradbury *et al*. (2008) *Plant Mol. Biol*. **68**, 439–449.
Brocker *et al*. (2010) *Journal of Biological Chemistry*. **285**, 18452-18463.
Brocker et al. (2012) *Biomol Concepts*. **3**(4), 345-364.
Buchanan *et al*. (2005) *Plant Mol Biol*. **58**, 699–720.
Degano *et al.* (1996) *Biochemistry.* **35**, 5971–5981.
Degano *et al.* (1998) *Biochemistry* **37**: 6277–6285.
Dudareva *et al.* (2013) *New phytologist*. **198**, 16-32.
Emsley and Cowtan (2004) *Acta Crystallogr. Sect.D-Biol.Crystallogr.* **60**, 2126-2132.
Estupiñán and Schramm (1994) *J Biol Chem.* **269**, 23068–23073.
Fraaije *et al*. (1998) *Trends Biochem. Sci.* **23**, 206–207.
Fraaije *et al*.. (1999) *J Biol. Chem.* **274**, 35514-35520.
Frébort *et al.*, (2002 *Anal. Biochem.* **306**, 1-7.
Frébortová *et al.* (2004) *Biochem. J.* **380**, 121-130.
Frébortová *et al.* (2010) *Plant J.* **61**, 467-481.
Fong *et al*. (2006) *Cellular and Molecular Life Sciences*. **63**, 2881-2885.
Fukuda, H., (2004) *Nature Reviews Molecular Cell Biology.* **5**, 379-391.
Galuszka *et al*. (2001) *Eur. J. Biochem.* **268**, 450–461.
Gan, S. and Amasino, R.M. (1995 *Science.* **270**, 1986-1988.
Chatfield and Armstrong (1987) *Plant Physiol.* **84**, 726-731.
Giabbai B. and Degano M. (2004) *Structure.* **12**, 739–749.
Guerrero *et al*. (1990) *Plant Molecular Biology*. **15**, 11-26.
Hallen *et al*., 2013 (2013) *Amino Acids.* **45**(6), 1249-72.
Hooker *et al*., (1970) *Plant Dis. Rep.* **54**, 708-712
Horenstein and Schramm (1993) *Biochemistry*. **32**, 7089-7097.
Houba-Hérin *et al*. (1999) *Plant J.* **17**, 615–626.
Chan *et al.* (2011) *Chemico-Biological Interactions.* **191** (2011), 165–170.
Chen *et al*. (2002) *Journal of Plant Physiology*. **159**, 677-684.
Inoue *et al*. (2001). *Nature.* **409**, 1060–1063.
Jung *et al.* (2009) *Plant Cell*. **21**, 876–891.
Kabsch (2010) *Acta Crystallogr D Biol Crystallogr.* **66**, 125-132.
Kemper *et al*. (1999) *Plant Cell.* 11(10)**,** 1981-94**.**
Kim *et al*, (1995) *J. Biol. Chem.* **270**, 31202-31209.
Kirch *et al*. (2001) *Plant Journal*. **28**, 544-554.
Kirch *et al.* (2005). *Plant Mol Biol.* **57**, 315–332.
Klyosov (1996) *Biochemistry.* **35,** 4457-4467.
Končitíková *et al*. (2015) *Biochem J.* **468**(1): 109-23.
Kopečný *et al*. (2005) *Biochimie.* **87**, 1011-1022.
Kopečný *et al*. (2013) *J Biol. Chem*. **288**(13), 9491-507.
Kopečná *et al*. (2013) *Plant Physiol*. **163**(4): 1568-83.
Kotchoni *et al.* (2006) *Plant Cell Environ.* **29**, 1033–1048.
Kurtz *et al.* (2002) *Curr Genet.* **41**(3), 132-41.
Liu *et al*. (2001) *Plant Cell.* **13**, 1063-1078.
Liu and Schnable (2002) *Plant Physiology*. **130**, 1657-1674.)
Mahonen *et al.* (2006) *Science.* **311**, 94-98.
Malito *et al.* (2004) *J. Mol. Biol.* **341**, 1237-1249.
Marchitti et al. (2008) *Expert Opin. Drug Metab. Toxicol.* **4**, 697–720.
Minici *et al*. (2012) *Biochemistry*. **51**(22):4590-9.
Missihoun *et al*. (2011) *Planta.* **233**, 369 –382.

Mok and Mok (2001) *Annu. Rev. Plant Physiol. Plant Mol. Biol*. **52**, 89–118.
Morris *et al*. (1999) *Biochem. Biophys. Res. Commun.* **255**, 328-333.
Muzzolini *et al.* (2006) *Biochemistry*. **45**, 773–782Nair *et al.*, 2004
Nakazono *et al.* (2000) *Plany Physiology*. **124**, 587-598.
Navarro-Aviño *et al*. (1999) *Yeast*. **15,** 829-842.
Parkin *et al.* (1996) *J Biol Chem*. **271**: 21713–21719.
Parkin *et al.* (1991) *J Biol Chem*. **266**, 20658–20665.
Perez-Miller and Hurley (2003) *Biochemistry*. **42**, 7100-710.
Petersen and Møller (2001) *J Biol Chem*. **276**(2):884-94.
Procházka *et al*. (1997), pp. 63-77, Academia, Praha
Ribeiro and Valenzuela (2003) *Insect Biochem Mol Biol*. **33**(1), 13-22.
Shi *et al*. (1999) *J Biol Chem*. **274**, 21114-21120.
Shin *et al* (2009) *Plant Physiology*. **149**, 905-915.
Schmulling *et al*. (2003) *J Plant Res*. **116**, 241–52.
Skibbe *et al.* (2002) *Plant Molecular Biology*. **48**, 751-764.
Skoog, F. and Armstrong, D.J. (1970) *Annu Rev Plant Physiol.* **21**, 359–84.
Smith *et al*. (1985) *Anal Biochem*.v**150**, 76–85.
Sophos and Vasiliou (2003) *Chem. Biol. Interact.* **143**, 5–22.
Storoni *et al.* (2004) *Acta Crystallogr D Biol Crystallogr*. **60**, 432–438.
Stroeher *et al*. (1995) *Plant Mol Biol*. **27**, 541–551.
Tang *et al.* (2008) *FEBS Lett.* **582**, 3090-3096.
Tanaka *et al.* (2006) *Plant J*. **45**, 1028-1036.
Tylichová M. *et al*. (2010) *J. Mol. Biol.* **396**, 870-882,
Vagin and Teplyakov (2010) *Acta Crystallogr D Biol Crystallogr*. **66**(Pt 1):22-5.
Versées *et al.* (2001) *J Mol Biol.* **307**, 1363–1379.
Versées *et al*. (2002) *J Biol Chem*. **277**, 15938–15946.
Versées and Steyaert (2003). *Curr Opin Struct Biol.* **13**, 731
Wei *et al*. (2009) *BMC Biochem.*, **10**:7.
Wen *et al.*, (2012) Planta. 236(2):525-39.
Wong *et al.* (2010) *J. Cell. Biochem.* **109**, 74-81.
Yamada *et al*. (1999) *Plant Cell Physiol.* **40**, 198–204.
Yoder *et al.* (1973) *Plant Physiol.* 52(6)**,** 513-7.
Yoshida *et al.* (1998) *European Journal of Biochemistry*. **251**, 549-557.
Zhu *et al.* (2000) *Biochem J.* **351**, 215–220.
Zalkin and Nygaard (1996) Cellular and Molecular Biology. Neidhardt, F.C. (ed.). Washington, DC: ASM Press, pp. 561–579.

6 Abstracts from conferences

1. **Končitíková R**, Kopečná M, Vigouroux A, Moréra S, Šebela M, Kopečný D. Structure-function study on plant aldehyde dehydrogenases from family 2 and family 7. G4G, Olomouc, June x-x, 2015. (Poster)

2. **Končitíková R**, Kopečná M, Vigouroux A, Moréra S, Šebela M, Kopečný D. Structure-function study on plant aldehyde dehydrogenases from family 2 and family 7. 13th Discussions in Structural Biology, Academic and University Center, Nové Hrady, March 19-21, 2015. (Poster)

3. **Končitíková R**, Kopečná M, Moréra S, Vigouroux A, Šebela M, Kopečný D. Structure-function study on enzymes linked to cytokinin metabolism - aldehyde dehydrogenases and nucleoside N-ribohydrolases. 12th Discussions in Structural Biology, Academic and University Center, Nové Hrady, March 13-15, 2014. (Poster)

4. **Končitíková R**, Kopečná M, Kopečný D, Moréra S, Vigouroux A, Frömmel J, Šebela M. Structural characterization of two maize aldehyde dehydrogenases from family 2. 11th Discussions in Structural Biology, Academic and University Center, Nové Hrady, March 14-16, 2013. (Poster)

5. Frömmel J., Kopečná M., Kopečný D., Soural M., **Končitíková R.,** Vinello F., Šebela M.: Aminoaldehyde dehydrogenase 1from tomato - enzyme structure and possible using as a tool to analyze aldehydes in beverages. 11th Discussion in Structural Molecular Biology, March 14-16, 2013, Nové Hrady, Czech Republic (Lecture)

6. **Končitíková R**, Tylichová M, Kopečný D, Moréra S, Vigouroux A, Frömmel J, Šebela M. Maize aledyhe dehydrogenases from the family 7 and 10. 10th Discussions in Structural Biology, Academic and University Center, Nové Hrady, March 22-24, 2012. (Lecture)

7. Šebela M, **Končitíková R**, Lenobel R, Franc V, Řehulka P, Tylichová M, Kopečný D, Madzak C. Analysis of N-glycosylation in maize cytokinin oxidase/dehydrogenase 1 using a manual micro gradient chromatographic separation coupled offline to MALDI-TOF/TOF mass spektrometry. Cytokinin metabolism, signaling and function, Freie Universität Berlin, Dahlem Centre of Plant Sciences (DCPS), July 6-8, 2012. (Poster)

8. Tylichová M., **Končitíková R.,** Kopečný D., Morera S., Vigouroux A., Frömmel J., Šebela M.: Newly charcterized aldehyde dehydrogenase from maize. 16th International Meeting - Enzymology and Molecular Biology of Carbonyl Metabolism, July 10-15, 2012, Plön, Germany. (Poster, Henry Weiner Prize for the best poster)

9. Šebela M, **Končitíková R**, Lenobel R, Franc V, Řehulka P, Tylichová M, Kopečný D. Structural and functional study on the glycosylation in maize cytokinin oxidase/dehydrogenase 1. 9th Discussions in Structural Biology, Academic and University Center, Nové Hrady, March 24-26, 2011. (Lecture)

10. **Končitíková R**., Kopečná M., Kopečný D., Moréra S., Vigouroux A., Frömmel J., Šebela M.: Structural characterization of two maize aldehyde dehydrogenases from family 2. 11th Discussion in Structural Molecular Biology, March 14-16, 2013, Nové Hrady, Czech Republic (Poster)

11. Šebela M, **Končitíková R**, Lenobel R, Franc V, Řehulka P, Tylichová M, Kopečný D. Mass spectrometric analysis of N-glycosylation in maize cytokinin oxidase/dehydrogenase 1. 5th Central and Eastern European Proteomic Conference, September 19-22, Conference Centre U Hájků, Prague, Czech Republic. (Poster)

12. Kopečný D, Tylichová M, Andree T, **Končitíková R**, Šebela M. Biochemical characterization of a recombinant plant aldehyde dehydrogenase 7 from *Pisum sativum* and *Zea mays*. 36th FEBS Congress, Biochemistry for Tomorrow's Medicine, Lingotto Conference Center, Torino, Italy, June 25-30, 2011. Poster

13. Šebela M, **Končitíková R**, Lenobel R, Franc V, Řehulka P, Tylichová M, Kopečný D. Structural and functional study on the glycosylation in maize cytokinin oxidase/dehydrogenase 1. 36th FEBS Congress, Biochemistry for Tomorrow's Medicine, Lingotto Conference Center, Torino, Italy, June 25-30, 2011. Poster